



**MODELLING AND TESTING OF A LOW
TEMPERATURE SOLAR ORGANIC RANKINE CYCLE
POWER PLANT**

Shadreck Mubiana Situmbeko

209542168

Supervisor: Prof. Freddie L. Inambao

Thesis submitted in fulfilment of the requirement for the degree of
DOCTOR OF PHILOSOPHY IN ENGINEERING (PhD)

(MECHANICAL ENGINEERING)

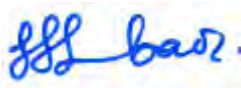
School of Engineering, University of KwaZulu-Natal, Durban, South
Africa

November, 2016

COLLEGE OF AGRICULTURE, ENGINEERING AND SCIENCE

As the candidate's Supervisor I agree/~~do not agree~~ to the submission of this thesis.

Signed



.....

Professor Dr. F.L. Inambao

DECLARATION 1 - PLAGIARISM

I, Shadreck Mubiana Situmbeko, declare that

1. The research reported in this thesis, except where otherwise indicated, is my original research.
2. This thesis has not been submitted for any degree or examination at any other university.
3. This thesis does not contain other persons' data, pictures, graphs or other information, unless specifically acknowledged as being sourced from other persons.
4. This thesis does not contain other persons' writing, unless specifically acknowledged as being sourced from other researchers. Where other written sources have been quoted, then:
 - a. Their words have been re-written but the general information attributed to them has been referenced
 - b. Where their exact words have been used, then their writing has been placed in italics and inside quotation marks, and referenced.
5. This thesis does not contain text, graphics or tables copied and pasted from the Internet, unless specifically acknowledged, and the source being detailed in the thesis and in the References sections.

Signed



.....

COLLEGE OF AGRICULTURE, ENGINEERING AND SCIENCE

DECLARATION 2 - PUBLICATIONS

Journal Papers

1. Situmbeko S.M. and Inambao F.L., Small Scale Axial Turbine Preliminary Design and Modelling, International Journal of Engineering Research & Technology (IJERT), ISSN: 2278-0181, Vol. 5 Issue 07, July-2016, pp 683-690
2. Situmbeko S.M. and Inambao F.L., Economic and environmental analyses of a 10 kWe low temperature solar thermal power plant, International Journal of Research in Engineering & Advanced Technology (IJREAT), ISSN: 2320 – 8791 (Impact Factor: 2.317), www.ijreat.org, Volume 3, Issue 6, Dec 2015 – Jan 2016, pp 1-12.
3. Situmbeko S.M. and Inambao F.L., ORC condenser heat exchanger design and modelling, International Journal of Engineering Research & Technology (IJERT), ISSN: 2278-0181, Vol. 4 Issue 08, August 2015, pp 279-286.
4. Situmbeko S.M. and Inambao F.L., Heat exchanger modelling for solar organic Rankine cycle, International Journal of Thermal and Environmental Engineering (IJTEE), Volume 9, No. 1, 2015, pp 7-16.
5. Situmbeko S.M., Kumar K.L. and Inambao F.L., Modeling of a solar air heater with sensible thermal storage and natural draft, International Journal of Engineering Research & Technology (IJERT), ISSN 2278-0181, Volume 3 Issue 09, September 2014, pp 624-634.
6. Situmbeko S.M. and Inambao F.L., System and component modelling of a low temperature solar thermal energy conversion cycle, Journal of Energy in Southern Africa, ISSN 1021 447X, Vol. 24 No 4, November 2013, pp 51-62.
7. Situmbeko S.M. and Inambao F.L., Low temperature solar thermal energy conversion, Energize, South Africa, June 2010, pp 21-24.

Conference Papers

1. Situmbeko S.M., Inambao F.L. (2016). Economic and Environmental Analysis of Renewable Energy Systems, Proceeding of the LeNSes Conference, September 28-30, 2016, Cape Town, South Africa, Paper ID 1095, pp 35-42
2. Situmbeko S.M. and Inambao F.L., Review of designs for low temperature organic Rankine cycle expanders, presented to the Botswana Institution of Engineers (BIE) 14th Biennial Conference, Gaborone, Botswana, October 2015.
3. Situmbeko S.M. and Inambao F.L., Low temperature thermal power concept case study, Botswana Institution of Engineers (BIE) 13th Biennial Conference, Gaborone, Botswana, October 2013.
4. Situmbeko S.M. and Kumar K.L., Solar air heater with sensible thermal storage, Botswana Institution of Engineers (BIE) 13th Biennial Conference, Gaborone, Botswana, October 2013.
5. Situmbeko S.M. and Inambao F.L., Mathematical modelling and computer simulation of a solar field for a low temperature organic Rankine cycle (ORC), 1st Southern African Solar Energy Conference (SASEC 2012) Stellenbosch, South Africa, 21-23 May 2012.
6. Situmbeko S.M. and Inambao F.L., Mathematical modeling and simulation of a low temperature solar thermal energy conversion system, International Solar Energy Society – Solar World Congress (ISES–SWC 2011), Kassel, Germany, 28 August - 2 September 2011.
7. Situmbeko S.M. and Inambao F.L., Low temperature solar thermal energy conversion, Domestic Use of Energy (DUE) Conference; Cape Peninsula University of Technology, Cape Town, South Africa, March 29 - 31, 2010.

Signed:



A handwritten signature in black ink, appearing to be 'A. L.', is written above a solid horizontal line.

.....

ACKNOWLEDGEMENTS

The researcher wishes to acknowledge the contributions of the research supervisor Professor Freddie L. Inambao and of several other colleagues from the University of KwaZulu-Natal (UKZN) who have tendered valuable suggestions and interacted with the researcher during the progress of the work. I wish also to thank my associates, Messieurs Kalaluka Mubiana, Peter Lungwa, Peter Banda, Khani Batshegi and Granton for their assistance in setting up and conducting the experimental phase. The invaluable contributions and advice rendered by colleagues from the Workshops, Messieurs Koch Roland, Harilall Sunpersadh and Styrn cannot go without a special mention.

Special acknowledgements are also in order to the Centre for Engineering Postgraduate Studies (CEPS), UKZN for providing a significant proportion of the research funding.

Shadreck M. Situmbeko,
March, 2016.

ABSTRACT

The post-apartheid era in South Africa has brought with it great challenges regarding electricity supply with demand far outstripping supply mainly due to the refocusing of the economy to foster industrialisation, the mass electrification programme, as well as several years of underinvestment in power generation and distribution infrastructure. Currently South Africa obtains about 77% of her electricity from coal, 6.5% from nuclear and the rest from a mix of diesel, gas and renewables. The government has adopted a diversification policy that encourages growth in electricity generation from renewable resources; this has led to renewed interest in renewables energies research and development as well as investment. By February 2015, government had procured 4 terawatts of renewable energy – electricity from IPP's while Eskom completed the grid-connected 100 megawatts Sere Wind farm. This current research is a response to the current energy scenario vis-à-vis supply challenges and research space.

The research investigated the technical, economic and environmental viability of a small to medium sized low temperature solar thermal organic Rankine cycle (ORC) power plant. Mathematical and computer models were developed for the ORC, and for the cycle components. The ORC model involved 14 working fluids and three plant configurations. The solar field model employed ethylene glycol water as the heat transfer fluid and involved a 9-collector solar field and a 180-collector solar field.

An evaporator model was developed based on a counter flow double pipe configuration and a flow boiling process incorporating both convective and nucleate boiling. Ethylene glycol water was placed on the shell side; the tube side fluid was modelled on four candidate working fluids.

The condenser model was based on a flow of vapour over a bundle of horizontal tubes. The working fluid was modelled from five organic fluids; the cooling liquid was ethylene glycol water and was placed on the tube side.

Preliminary turbine design models for both radial inflow and axial configurations were developed. The designs were presented in terms of geometric and thermodynamic parameters. The initial results have shown that small turbines for low temperature cycles are feasible.

The results of the economic and environmental analyses were a negative NPV value (ZAR -126 389.64), six years energy payback period (EPBP) and 426.9 days (1.17 years) carbon payback period (CPBP). Both the EPBP and CPBP values are comparable with similar technologies. A sensitive analysis based on locally designed and produced power block and solar field produced a positive NPV value.

The experimental set-up and experimental procedures were successively achieved but the experiments had to be postponed pending supply of a non-defective unit. The data obtained from the manufacturer show the ORC as a viable power supply.

The results of these models and simulations have been published in six peer-reviewed journal papers and six peer-reviewed conferences and conference proceedings. Overall, the research can be considered to have been a success judging by the quantity and quality of research output. A post-research proposal is being prepared and covers the outstanding tasks.

TABLE OF CONTENTS

DECLARATION 1 – PLAGIARISM	ii
DECLARATION 2 – PUBLICATIONS	iii
ACKNOWLEDGEMENTS	v
ABSTRACT.....	vi
TABLE OF CONTENTS.....	viii
LIST OF FIGURES	xi
LIST OF TABLES.....	xiii
CHAPTER 1 INTRODUCTION.....	1
1.1 Preamble.....	1
1.2 Background	1
1.3 Low Temperature Solar Energy	2
1.4 Organic Rankine Cycle Energy Conversion	3
1.5 Research Brief	4
1.6 Objectives	5
References.....	5
CHAPTER 2 RESEARCH METHODOLOGY	6
2.1 Introduction.....	6
2.2 Research Problem Formulation.....	6
2.3 Major Research Tasks	6
2.4 Time and Resources Planning.....	9
References.....	9
CHAPTER 3 FUNDAMENTALS OF LOW TEMPERATURE SOLAR ENERGY CONVERSION.....	11
3.1 Introduction.....	11
3.2 Low Temperature Solar Thermal Energy Technology.....	11
3.3 Working Fluids	13
3.4 Organic Rankine Cycle (ORC) Developers and Suppliers	18
3.5 Concept Plants.....	19
3.6 Conclusion	19
References.....	20
CHAPTER 4 SYSTEM DESIGN AND CYCLE COMPONENTS MODELLING	21
4.1 System Design and Modelling	21
4.2 Solar Field Design and Modelling	21

4.3	Evaporator Design and Modelling	22
4.4	Condenser Design and Modelling	22
CHAPTER 5 TURBINE DESIGN AND MODELLING		23
	Abstract	23
5.1	Introduction	23
5.2	Review of Organic Rankine Cycle Expanders	25
5.3	Theory of Turbomachinery	25
5.4	Radial Flow Turbine Model	27
5.4.1	Description of Turbine Arrangement	27
5.4.2	Mathematical Model	29
5.4.3	Computer Simulations	31
5.5	Axial Flow Turbine Model	37
5.5.1	Description	37
5.5.2	Mathematical Model	38
5.5.3	Computer Simulations	39
5.6	Discussion and Conclusions	43
5.7	Way Forward	44
	References	44
CHAPTER 6 ECONOMIC AND ENVIRONMENTAL ANALYSES		45
	Abstract	45
6.1	Results	45
CHAPTER 7 LABORATORY INVESTIGATIONS		46
	Preamble	46
7.1	Introduction	46
7.2	Description and Installation of the Heat Engine	47
7.3	Description and Installation of the Heater	48
7.4	Description and Installation of the Heat Sink	49
7.5	Measuring Equipment and Instruments	49
7.6	Testing Procedure/Methodology	50
7.6.1	Leakage Testing of ORC Unit before Charging with Refrigerant	51
7.6.2	Charging ORC unit with Refrigerant	52
7.6.3	Connecting the Heater Unit	53
7.6.4	Connecting the Cooling Cycle	53
7.6.5	Electrical Circuit (Load) for Measuring Power Output	54
7.6.6	Pump Settings	55
7.6.7	Running the Power Cycle	55

7.6.8	Problems Faced	55
7.7	System Experimental Results.....	57
7.8	Discussion and Conclusion	57
	References.....	58
CHAPTER 8	EVALUATION OF RESEARCH OBJECTIVES	59
8.1	Introduction.....	59
8.2	Analysis and Evaluation of Research Objectives.....	59
8.3	Discussion and Conclusion	62
	References.....	63
CHAPTER 9	CONCLUSIONS AND RECOMMENDATIONS.....	64
9.1	Introduction.....	64
9.2	Conclusions.....	64
9.3	Recommendations.....	67
9.4	Way Forward.....	67
	References.....	68
LIST OF APPENDIXES	69

LIST OF FIGURES

Figure 1.1: Solar thermal energy temperature ranges	3
Figure 1.2: Rankine cycle schematic layout	3
Figure 2.1: Preliminary model layout showing data recording points	8
Figure 2.2: Research Plan	10
Figure 3.1: Examples of low temperature solar thermal energy technologies	14
Figure 3.2: Three types of T-S expansion curves.....	16
Figure 3.3: IT10 Infinity Turbine ORC unit	19
Figure 5.1: Velocity diagram	26
Figure 5.2: Mollier diagram showing a typical expansion process.....	26
Figure 5.3: Cantilever radial turbine rotor (N=25).....	28
Figure 5.4: Cantilever turbine arrangement and velocity triangles	28
Figure 5.5: 90° IFR turbine rotor (N=15).....	29
Figure 5.6: 90° IFR turbine arrangement and velocity triangles	29
Figure 5.7: 90° IFR turbine enthalpy-entropy representation of the expansion process	30
Figure 5.8: Radial turbine blade geometry.....	32
Figure 5.9: radial turbine model rotor exit – temperature versus pressure.....	33
Figure 5.10: Radial turbine model total-to-total efficiency versus rotor exit pressure	33
Figure 5.11: Radial turbine model machine speed versus rotor diameter	34
Figure 5.12: Radial turbine model velocity triangles for R245fa and R134a	36
Figure 5.13: Radial turbine model velocity triangles for n-butane	36
Figure 5.14: Radial turbine model velocity triangles for isobutene	37
Figure 5.15: Axial turbine rotor (N = 5)	38
Figure 5.16: Axial turbine blade arrangement and velocity triangles	38
Figure 5.17: Mollier diagram for an axial turbine stage	39
Figure 5.18: Axial turbine model rotor exit – temperature versus pressure.....	40
Figure 5.19: Axial turbine model efficiency versus rotor exit pressure.....	41
Figure 5.20: Axial turbine model – machine speed versus rotor diameter.....	41
Figure 5.21: Axial turbine velocity triangles for R245fa.....	42
Figure 5.22: Axial turbine velocity triangles for R134a	42
Figure 5.23: Axial turbine velocity triangles for n-butane.....	43
Figure 5.24: Axial turbines velocity triangles for isobutene.....	43
Figure 7.1: 10 kWe ORC IT 10 unit [7.2].....	48
Figure 7.2: 450 litres vertical electric water heater unit [7.3].....	49
Figure 7.3: Test setup layout.....	50

Figure 7.4: Test setup photograph.....	51
Figure 7.5: System evacuation	52
Figure 7.6: Single port gravity or pump-assisted charging	52
Figure 7.7: Push-pull liquid transfer charging	53
Figure 7.8: rpm-volt characteristics of DC generator [7.5].....	54
Figure 7.9: Variable resistor load connection to DC generator.....	54
Figure 7.10: Circuit – parallel heating elements load connection to DC generator	55
Figure 7.11: Defective turbine exhaust unit.....	56
Figure 7.12: Extracts from the flange drawings.....	56
Figure 7.13: Replacement flange in process before fitting flexible hose.....	57

LIST OF TABLES

Table 3.1: Thermal efficiencies of the basic as well as modified ORCs for different working fluids [3.7]	17
Table 3.2: Results of the survey of suppliers for ORC expander.....	18
Table 3.3: Low temperature ORC concept plants	19
Table 5.1: Inlet conditions [5.8].....	32
Table 5.2: Radial turbine model simulation results.....	35
Table 5.3: Axial turbine model – revised inlet conditions	40
Table 5.4: Axial turbine model simulation results	42
Table 7.1: IT 10 specifications [7.2]	47
Table 8.1: Publication list for the models	59

CHAPTER 1 INTRODUCTION

1.1 Preamble

This thesis contains work undertaken to investigate the technical, economic, and environmental viability of producing electricity from low temperature solar thermal energy based on the organic Rankine cycle (ORC). The research has been conducted in fulfilment of a Doctor of Philosophy (PhD) degree at the University of KwaZulu-Natal. The major components of the research are mathematical modelling, computer simulations, and physical modelling; these are developed or performed on the system as a whole and separately on the major cycle components. The major cycle components are the solar field, the evaporator and condenser heat exchangers, and the turbine. Economic and environmental analyses have also been performed.

The thesis is broken down into nine chapters preceded by acknowledgements, abstract and a table of contents and followed by the appendices. The first chapter, Chapter 1, introduces the research topic, defines the scope and outlines the research objectives. Chapters 2 and 3 present the research methodology and fundamentals of low temperature solar energy conversion respectively. Chapter 4 presents the system design and modelling, and the design and modelling of the cycle components i.e. of the evaporator, condenser and solar field. Chapter 5 is devoted to the preliminary design and modelling of the single most critical component of a thermal conversion cycle, the turbine. The results of the economic and environmental analyses are presented in Chapter 6. Chapter 7 reports on the laboratory investigations. Chapter 8 provides an evaluation of the research objectives and Chapter 9 presents conclusions and recommendations.

The inception proposal, computer simulation codes, bulky research results, and a list of peer reviewed publications that were produced from this research are all included in the appendices.

1.2 Background

The energy problem in South Africa can be summed up into two aspects: the energy shortage resulting from several years of underinvestment in the electrical generation and distribution sector and the increase in demand due to the inclusion of previously discriminated majority (by 2015 there were still about 3.4 million households without electricity); and the need to change the energy mix away from over dependence on unsustainable generation methods and non-renewable energy resources (it is envisaged in the 20 year Integrated Resource Plan 2010 that about 42% of electricity generated must come from renewable resources). Presently South Africa obtains about 77% of her electricity from coal, 6.5% from nuclear and the rest from a mix of diesel, gas and renewables. The government has adopted a diversification policy that encourages growth in electricity generation from renewable resources. Current forecasts indicate a power supply deficit for South Africa of 19 TW by 2025[1.1].

The motivation behind enhanced and continuing research on new and renewable energy sources and resources is supported mainly by the following factors:

- Abundant availability of untapped low temperature solar energy and waste heat exhausted from most industrial processes possess immense potential for becoming a major complimentary energy resource for power generation [1.2].
- Low temperature energy technologies are less complex, less costly, and require low safety design considerations making them suitable for stand alone, remote area, and small-to-medium scale distributed applications [1.3].
- Development of small-to-medium, cost-effective energy technologies could contribute to improved global access to clean energy, reduced greenhouse gas emissions, encourage industrial development, and aid in meeting the Millennium Development Goals (MGD's), now Sustainable Development Goals (SDG's) [1.4].

1.3 Low Temperature Solar Energy

Most electrical energy generation systems involve conversion from naturally occurring energy to thermal energy; from thermal energy to mechanical energy; and then from mechanical energy to electrical energy. This conversion stream covers fossil fuels, biofuels, nuclear fuels and solar thermal energy (typically high temperature). Some other naturally occurring energy sources join the conversion stream midstream; for instance geothermal energy, being already in thermal form, enters the stream at the point of conversion to mechanical energy; whilst hydro-energy of rivers and oceans, wind energy and tidal energy are all already in mechanical form thus requiring only conversion to electrical energy; the same goes for the direct photovoltaic conversion of solar energy to electrical energy.

Similarly, the generation of electrical power from low temperature solar thermal energy using the ORC involves a multi-step energy conversion process starting with the harvesting of solar energy and its simultaneous conversion into heat energy by a collector system followed by the conversion of the heat energy into mechanical (motion) energy by a thermal engine, and further conversion to electrical energy by a generator.

Low temperature solar thermal energy refers mainly to a method of solar energy collection and conversion to heat energy without involving some form of concentrating the solar arrays or with only low concentration contribution. Thus maximum temperatures attained after conversion are restricted to lower values of the order of below 300°C [1.5]. This method mainly involves the use of flat solar collectors and solar ponds.

Sound thermodynamic principles dictate that higher operating temperatures must be used in a thermal energy cycle to ensure higher thermal efficiencies. However, technical and economic considerations, such as availability of large-surface, cost-efficient and sometimes naturally occurring solar energy collecting configurations, may sometimes justify operation of thermal cycles with relatively low upper temperature limits [1.6].

Figure 1.1 shows different temperature ranges for solar thermal energy from lower to higher temperatures.

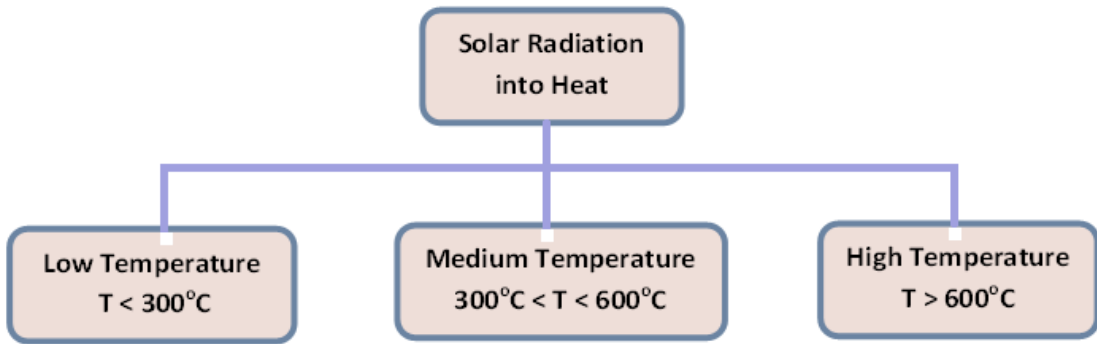


Figure 1.1: Solar thermal energy temperature ranges

1.4 Organic Rankine Cycle Energy Conversion

Approximately 80% of electrical energy used in the world is produced from medium to high temperature heat using a conventional thermodynamic conversion cycle known as the Rankine cycle [1.7]. In a Rankine cycle heat is applied externally to a closed cycle and water is used as the working fluid. A schematic representation of the Rankine cycle is shown in Figure 1.2.

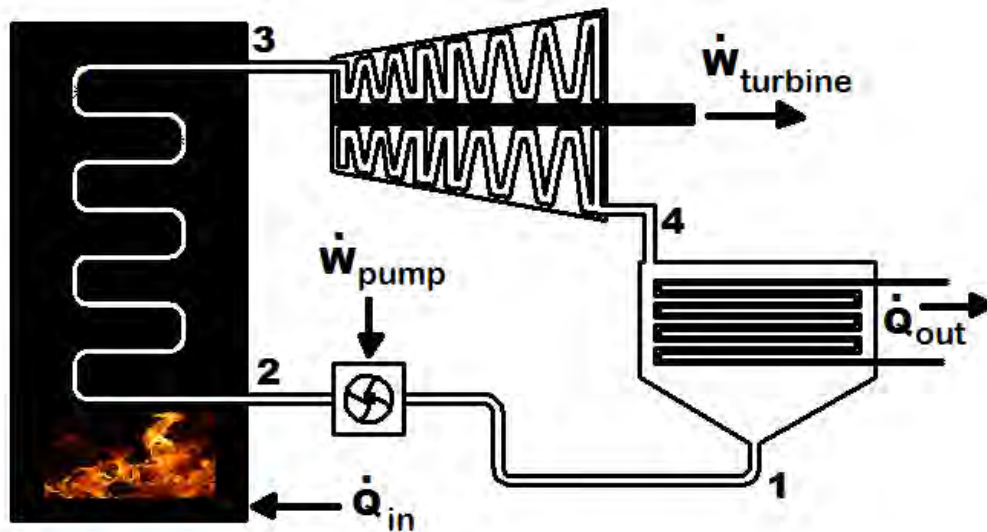


Figure 1.2: Rankine cycle schematic layout

In the conventional Rankine cycle the process starts with water being pumped from a lower pressure at point 1 to a higher pressure, point 2, by a pump; an external heat normally generated through the combustion of fossil fuels such as coal, diesel or natural gas is applied to the water thus producing a superheated steam, point 3; the high pressure and high temperature superheated steam is then expanded through a steam turbine to a lower pressure and lower temperature vapour, point 4; the expansion process converts the thermal energy into mechanical energy, shaft power, that normally drives a generator thus producing electrical energy. The

vapour at 4 is then cooled through a condenser to a liquid, point 1; the cycle is then repeated. Several versions of the Rankine cycle have been developed [1.8].

The ORC is an adaptation of the Rankine cycle and is operated with working fluids other than water, usually refrigerants or hydrocarbon fluids [1.9]. This project focuses on an ORC powered with low temperature solar thermal energy. Various working fluids have been investigated as part of this research. Detailed description of the ORC is included in Chapter 3, Information Research.

1.5 Research Brief

This research work investigates the viability of generating electrical power from low temperature solar thermal energy. Low temperature solar thermal energy technologies operate in temperature ranges below 300°C. The conversion system adopted for this work is that based on the ORC. The work involves development and optimization of scientific and mathematical models, computer simulated models and physical models of the power generation concept plant. Models are developed for the system as a whole as well as for separate cycle components. The main cycle components are the solar field, the two heat exchangers (the evaporator and the condenser), and the turbine.

1.6 Objectives

Objective 1: To develop and optimise mathematical models, computer simulations, and physical models of a low temperature solar thermal energy conversion system based on the Rankine cycle for conversion of low temperature solar energy to electrical energy. The mathematical and computer models will be used in the design of the physical models. Optimization will include thermodynamic, fluid mechanics and heat transfer analyses.

Objective 2: To undertake an extensive survey, through literature research, web-based search tools, and on-going research in other institutions, of low to medium temperature energy conversion concept plants and to evaluate their suitability as low temperature energy conversion cycles.

Objective 3: To carry out an extensive study of working fluids and evaluate their potential for use in a low temperature energy conversion cycle.

Objective 4: To install the developed physical model at a suitable site and carry out extensive evaluation of the model for a lengthy period of time (at least 12 months). Data recording will be accomplished via digital reading and storage modules.

Objective 5: To undertake overall economic and environmental performance evaluations of the developed and the proposed low temperature solar thermal energy conversion designs.

Objective 6: To publish the research results in peer reviewed conference papers, international journals and in a Research Thesis.

References

- [1.1] African Energy Resources Limited presentation accessed at [www.africanenergy](http://www.africanenergy.com), July 2015.
- [1.2] Weiss W., Solar thermal untapped potential: solar heat for industrial applications, *Renewable Energy World*, January-February 2006: pp 68-74, <http://www.aee-intec.at/0uploads/dateien238.pdf>.
- [1.3] Stine W.B. and Geyer M., Flat-Plate collectors, Chapter 6 in *Power from the sun*, 2001, <http://www.powerfromthesun.net/book.html>; accessed November, 2014.
- [1.4] World Bank, Energy in Africa: overview, June 2012, <http://go.worldbank.org/ZD42IOATZ0>
- [1.5] European Commission, Concentrated solar thermal energy, EUR 20898, European Communities, Luxembourg, 2004, ISBN 92-894-6353-8.
- [1.6] Kaltschmitt, M., Streicher W. and Wiese, A. (Eds), *Renewable Energy: Technology, Economics and Environment*, Springer Science & Business Media, 2007, ISBN 3540709495, 9783540709497, pp 171-224.
- [1.7] Rashid Muhammad H., *Alternative energy in power electronics*, Butterworth-Heinemann, 2014, ISBN 978-0-12-416714-8, pp 94-97.
- [1.8] Situmbeko S.M. and Inambao F.L., Low temperature solar thermal energy conversion, Domestic Use of Energy (DUE) Conference; Cape Peninsula University of Technology, Cape Town, South Africa, March 29 - 31, 2010.
- [1.9] Nishith B. D. and Santanu B., Process integration of organic Rankine cycle, *Energy Journal*, Vol 34, 2009, pp 1674-1686.

CHAPTER 2 RESEARCH METHODOLOGY

2.1 Introduction

In this chapter the research methodology used in carrying out this research is described. The research investigates the subject area of low temperature solar thermal energy conversion. The research comprises the following main tasks: information research, mathematical modelling, computer simulations, laboratory investigations, field investigations, data collection and data analysis.

2.2 Research Problem Formulation

The research investigates the technical, economic and environmental viability of a low temperature solar thermal energy conversion concept plant. The research undertook a systematic and scientific approach towards the design and development of soft and physical models of a low temperature solar thermal energy conversion system based on the ORC for conversion of low temperature solar energy to electrical energy. The soft models involved the development and optimization of mathematical models and their subsequent implementation on a suitable computerized software platform. Further, the results of these soft models were to be validated against physical prototypes initially on a laboratory scale and eventually on a real life field pilot plant. Technical, economic and environmental evaluations of the models were to be undertaken to ascertain the viability of the concept and of the developed models as a feasible power generation technology.

2.3 Major Research Tasks

The research consisted of six major tasks, namely: information research, mathematical model development, computer simulations, physical model development and validations, data collection and analysis, and economic and environmental analyses.

Task 1: Information Research

This involved an extensive review of energy conversion processes and systems with special emphasis on solar radiation collection and concentration, absorption and conversion to thermal energy, thermal energy transfer and storage, and conversion of thermal to mechanical energy. This entailed a study of thermodynamic cycles, especially the ORC, with regard to solar thermal technologies, thermal conversion cycle configurations, and heat transfer and working fluids; a review of thermodynamic laws, properties of states and processes, mollier diagrams; a review of heat transfer relations and modes of transfer, and of the laws of conservation of mass, momentum and energy and a review of the thermal and optical properties of materials. Another aspect was a review of cycle components such as turbines and pumps, heat exchangers, and solar collectors as well as a survey of suppliers of such components. An examination of modelling computer software with associated capabilities for analyses of thermodynamic, heat

transfer and fluid flow mathematical models was undertaken. A survey of concept plants and of on-going research as well as a search for intellectual properties and standards on the subject was conducted. Sources of information included general literature and web searches, records on international solar thermal energy projects and consultations with stakeholders in industry and academia.

Task 2: Mathematical Model Development

Two levels of modelling were accomplished: preliminary first pass models and detailed models. The first pass models of the system were based on the initial conceived concept plant and consisted of mathematical equations representing the thermodynamic states of the heat transfer and working fluids at the points separating the distinct thermodynamic processes in the cycle or system, such as points 1, 2, 3 and 4 in Figure 1.2. A number of assumptions were made regarding thermal and flow losses, and uniformity of state and flow properties. The mathematical formulations were based on generalized scientific theories and empirical correlations. The first pass model provided initial insights into the performance of the proposed energy conversion concept.

The detailed models consisted of more refined mathematical formulations of discrete models of the thermodynamic processes and involved selection and/or hybridization of the most fitting scientific theories and empirical correlations; detailed models are more likely to include time dependent variables in their formulations which provide a more detailed understanding of the different thermodynamic processes making up the system.

Task 3: Computer Simulations

This stage involved implementation of the mathematical models using computer programs which entailed generating equivalent computer models of the developed mathematical models. Simulations were processed for various working conditions. Software required for these purposes needed to have the capability of solving sets of mathematical equations, linear and non-linear equations, polynomial and optimization problems, ordinary and partial differential equations, logic, constraint and search algorithms; such software were also required to have advanced capabilities such as built-in databases of thermodynamic properties of various materials and built-in mathematical functions. The software needed to be able to simulate specific mass and heat transfer flow processes including 3D simulations such as in computational fluid dynamics (CFD).

Examples of software used in this research included Engineering Equation Solver (EES), Trnsys, and AxSTREAM. Other supporting software included Excel and SolidWorks [2.1, 2.2, 2.3].

Task 4: Physical Model Development and Validations

Field and/or laboratory validations were conducted on experimental models which were specifically designed and constructed; where standard components were readily available they were utilized in the construction process. Design specifications were based on the outcome of the information research and the mathematical and computer modelling.

Task 5: Data Collection and Analysis

Statistically adequate performance parameters/variables were to be measured and recorded during the validations; parameters to be recorded included pressure, temperature, flow rates, power output, power input, solar radiation (direct radiation, diffuse radiation, sun-hours) and other weather measurements (wind speed, ambient temperature), etc.; it was intended to use digital measuring and recording instruments. The preliminary model layout in Figure 2.1 shows some of the originally proposed data recording points.

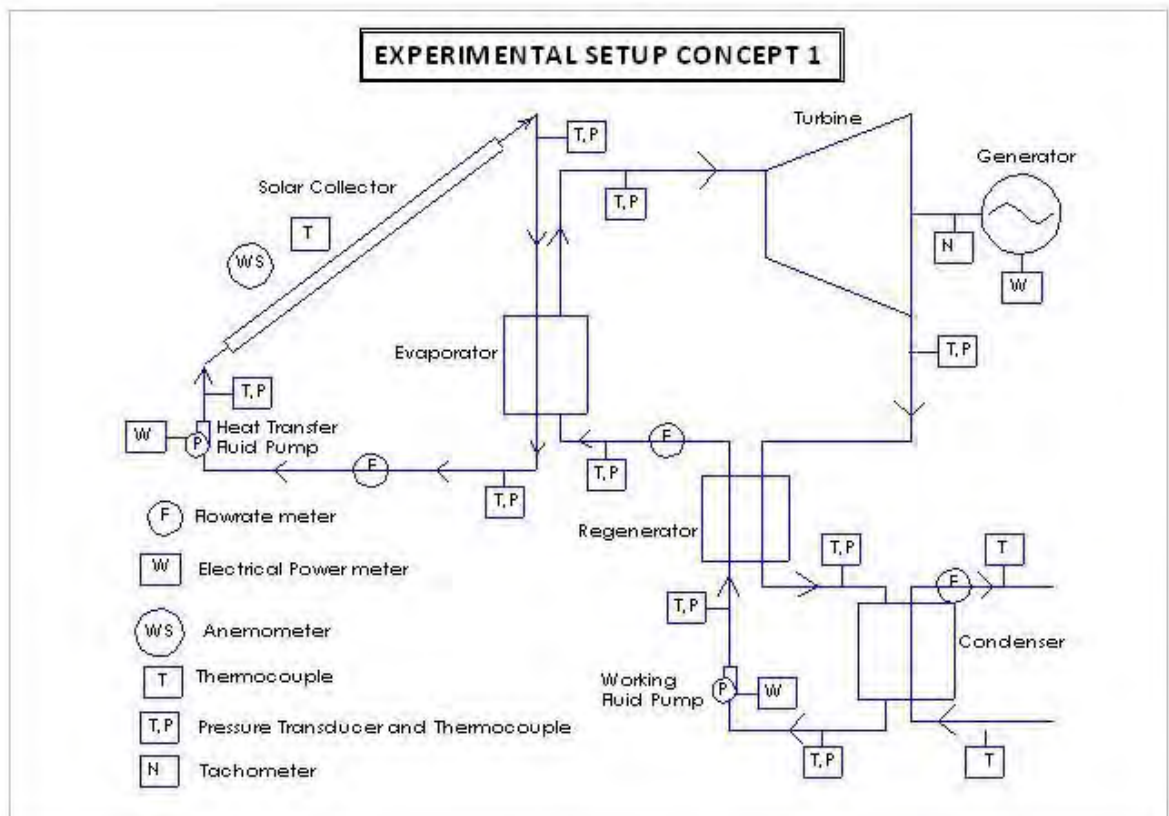


Figure 2.1: Preliminary model layout showing data recording points

Data analysis was to involve both quantitative and qualitative methods. Quantitative computations to establish performance indicators such as thermal conversion efficiencies, economic and environmental performance, etc. were performed; where possible these computations were to be contrasted with computer simulated data. Inferences formulated from

these investigations were to be evaluated against established and commonly accepted scientific truths as well as against results obtained by other researchers.

Task 6: Economic and Environmental Analysis

Economic analysis was conducted using the cost-benefit analysis metrics of benefit-cost ratio (BCR), return on investment (ROI), and net present value (NPV), [2.4].

The following metrics were used to assess the environmental performance of the low temperature solar thermal power generation concept plant: annual collector energy output, energy yield ratio, and avoided global warming impact [2.5].

2.4 Time and Resources Planning

The research plan is shown in Figure 2.2. Costs and other resources required are included in Chapters 6 and 7.

References

- [2.1] Klein S.A. and Alvarado F.L., EES, Engineering Equation Solver for Microsoft Windows Operating Systems, F-Chart Software, Middleton, WI 53562, USA, 1992-98.
- [2.2] <http://sel.me.wisc.edu/trnsys/index.html> accessed February, 2013
- [2.3] <http://www.softinway.com/> accessed September 17, 2014
- [2.4] <http://cbkb.org/toolkit/reporting-cost-benefit-results/> accessed June 17, 2014
- [2.5] http://www.swt-technologie.de/WP4-D2.8.b-final_report.pdf accessed October 14, 2014

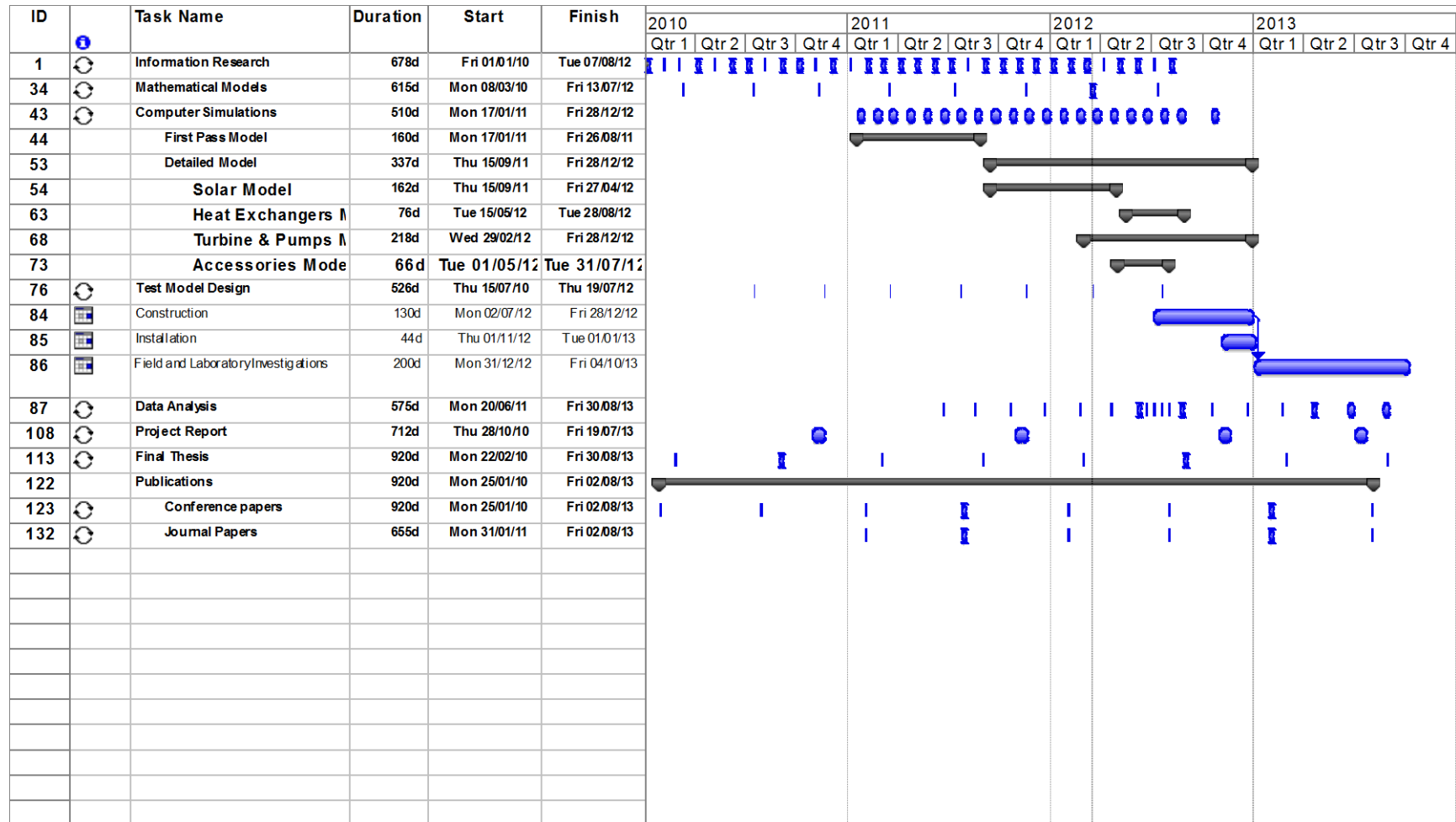


Figure 2.2: Research Plan

CHAPTER 3 FUNDAMENTALS OF LOW TEMPERATURE SOLAR ENERGY CONVERSION

3.1 Introduction

This chapter contains general information regarding low temperature solar thermal energy conversion systems, including a general description of low temperature solar thermal technologies, organic working fluids, ORC turbine developers and suppliers, and concept plants. Specific information regarding components of the low temperature solar thermal power cycle such as solar collectors, heat exchangers and turbines are included in respective chapters.

3.2 Low Temperature Solar Thermal Energy Technology

Most naturally occurring energies are present not in a readily usable form and sometimes difficult to transport in their natural form. Energy conversion systems transform natural energy to conveniently usable, storable and transportable forms.

Solar thermal energy (STE) technology refers to the conversion of shorter wavelength solar energy (400 nm – 700 nm) to longer wavelength (about 10 times as long) heat energy. The most important component of an STE technology is the collectors which absorb and convert solar energy into thermal energy from which we eventually derive electrical power.

Currently some high temperature solar thermal energy (HT-STE) technologies for electricity production have attained technical maturity and are only hindered by unfavourable market factors including lower tariffs, lack of appropriate environmental compensation, and high maintenance and operating costs. Examples of HT-STE technologies include parabolic dish, parabolic trough, and power tower systems [3.1].

Low temperature solar thermal energy (LT-STE) technologies have so far been restricted to water and space heating with little or no emphasis on power generation. Low temperature STEs operate within temperatures ranges below 300°C. Examples of applications include:

- Evaporation ponds for extraction of sea water salt;
- Concentrating brine solutions in leach mining and removing dissolved solids from waste streams;
- Domestic and process water heating;
- Preheating of ventilation air; and
- Crop drying as in drying of coffee beans and marigolds.

Low temperature heat sources are generally unattractive for power generation on account of the lower thermal density and hence lower conversion efficiencies. Low temperature heat is also

unable to produce steam of the desired quality to run in the conventional thermal conversion cycles. However, owing to their lower running costs and almost maintenance free operation, LT-STE technologies, although operating at lower efficiencies, may hold a key to future wider usage of solar energy. Such technology would make possible the harnessing and conversion to electrical power of naturally occurring low temperature thermal resources such as low temperature geothermal, oceanic and non-concentrated solar as well as industrial waste heat, a by-product of many industrial processes including high temperature power generation from fossils, nuclear and concentrated solar power.

Current research on LT-STE for power generation includes solar thermal ORC, solar thermal Kalina cycle, Solar Chimney and SNAP [3.1]; these are described briefly below; figure 3.1 shows schematic illustrations of the Solar Chimney, SNAP Plants, Organic Rankine and Kalina Cycles.

SNAP: the plant takes advantage of the continuous availability of hot dry air in mid-latitude, arid desert areas. A downward wind is created in a chimney by cooling the hot and dry air using a spray of water at the top. The cooled dense air descends inside the chimney creating a downward draft. Turbines at the bottom extract mechanical energy from the airflow and generate electricity. Suitable for locations with plenty of sea salty water as it also doubles as a desalination plant.

Solar Chimney: a solar chimney takes advantage of a large disused solar collecting ground surface by covering it with a transparent glass or plastic to create a greenhouse effect. The collector surface is slightly oriented upwards towards the centre where a chimney is placed. As air gets heated under the collector surface, it ascends towards the centre into the chimney base and gets accelerated upwards due to an upward draft effect induced by the chimney. Smaller horizontal axis turbines placed around the periphery of the chimney or one large vertical axis turbine placed inside the chimney extract mechanical energy from the airflow to generate electricity.

ORC: the low temperature solar organic Rankine cycle operates similarly to the conventional cycle with the exception that a fluid with a lower boiling temperature, usually a refrigerant, replaces water as the working fluid; this permits use of low grade heat. Heat addition is by means of a heat transfer fluid from a solar collecting system passing through an evaporator.

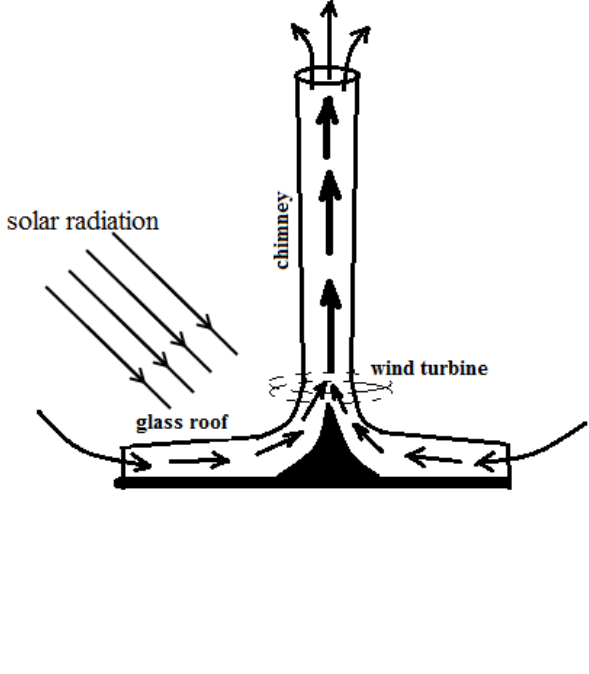
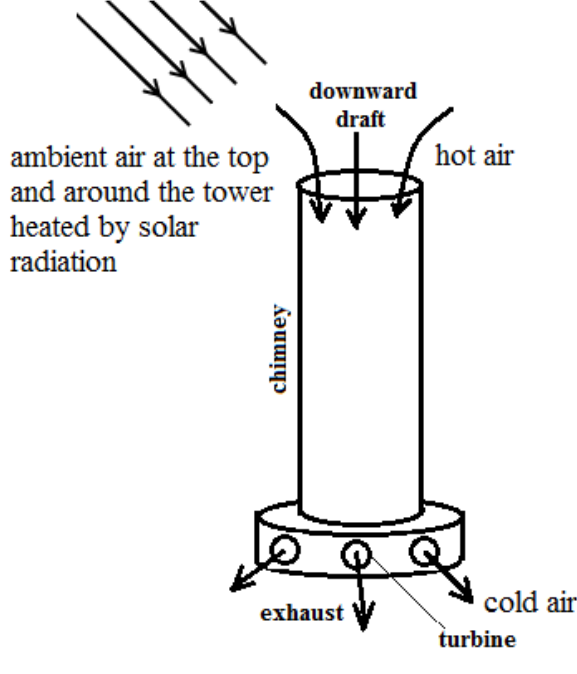
Kalina: the Kalina cycle, works on a similar concept as the conventional Rankine cycle, with the major difference being that it uses a mixture of two fluids, usually water and ammonia, as a working fluid. When operated as a solar thermal cycle, a heat transfer fluid transfers heat to the working fluid in the evaporator heat exchanger. Using a fluid mixture ensures that there is a temperature change during the phase transformation i.e. there is a temperature increase during heat addition and a temperature drop during heat rejection thus giving a relatively higher thermal efficiency. However it requires additional cycle components such as a separator to

separate a lean solution from the rich vapour, and a recuperator to recover some of the heat before rejection in the condenser.

3.3 Working Fluids

The selection of working fluid is of key importance in low temperature Rankine Cycles because in this case heat transfer inefficiencies have great influence on the overall cycle performance. These inefficiencies depend very strongly on the thermodynamic characteristics of the fluid and on the operating conditions. Two factors are important when selecting a working fluid for a solar thermal ORC power system:

- The working fluid selected should optimise cycle efficiency; and
- The working fluid thermodynamic state properties should match with those of the heat-transfer fluid.

Solar Chimney [3.2]	SNAP Plant
 <p>The diagram illustrates a Solar Chimney system. It features a central chimney with a glass roof at its base. Solar radiation enters from the left, heating the air inside the chimney. A wind turbine is located at the base of the chimney. Arrows indicate air rising in the chimney and being exhausted at the top.</p>	 <p>The diagram illustrates a SNAP Plant. It features a chimney with solar radiation heating the air around it. Ambient air is drawn in at the top, heated to become hot air, and then flows down the chimney. At the base, the hot air drives a turbine, and cold air is exhausted.</p>
<p>Organic Rankine Cycle [3.3](montaraventures.com)</p>	<p>Kalina Cycle [3.4]</p>

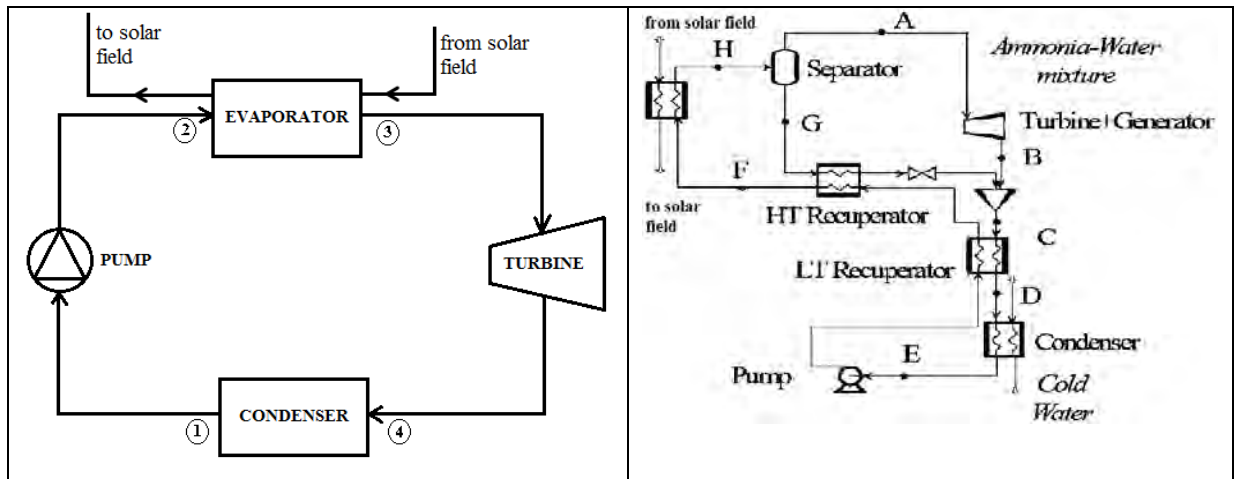


Figure 3.1: Examples of low temperature solar thermal energy technologies

A good candidate working fluid should have the following properties [3.5]:

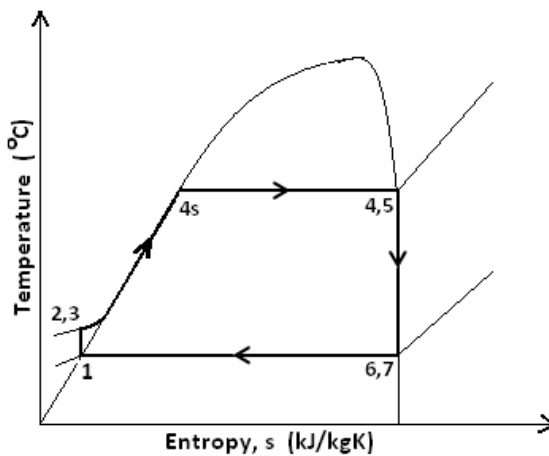
- Low specific heat capacity in the liquid phase so that most of the heat is added as latent heat;
- Critical point that is above the highest operating temperature to allow all heat to be added at the operating temperature;
- Moderate vapour pressure at the highest operating temperature for safety reasons and to reduce the cost of the equipment;
- Vapour pressure that is above atmospheric pressure, at the condensing temperature, to prevent air leakages into the system;
- Specific volume of the vapour at the exit of the turbine should be small to avoid large-diameter turbine blades and oversized heat exchangers;
- Vapour saturation curve on the temperature-entropy diagram should be isentropic to avoid expansion into the wet vapour or superheat regions (see Figure 3.2);
- High molecular weight to minimize rotational speed and/or number of turbine stages and to allow for reasonable mass flow rates and turbine nozzle areas;
- Should be liquid at atmospheric pressure and temperature for ease of handling and containment;
- Freezing point should be lower than the lowest ambient operating temperature; and
- Good heat-transfer properties, inexpensive, thermally stable at the highest operating temperature, non-flammable, noncorrosive and nontoxic.

Figure 3.2 shows three possible end states of a working fluid that is expanded from the saturated high pressure vapour. The end state after expansion may still lie on the saturated vapour line, or to the left (inside the T-s curve plot) or it may lie to the right. However, it is always desirable that the end state does not lie inside the T-s curve plot; in this state the fluid is a mixture of vapour and liquid droplets. These droplets have the undesirable effect of causing pitting and eroding of the turbine blade surfaces thus not only reducing the blade life but also altering the blade profile leading to increasing inefficiency of the turbine performance. To avoid this phenomenon, a liquid with a negative T-s vapour saturation curve is normally superheated thus compromising the thermal efficiency of the cycle and increasing capital costs. On the other hand

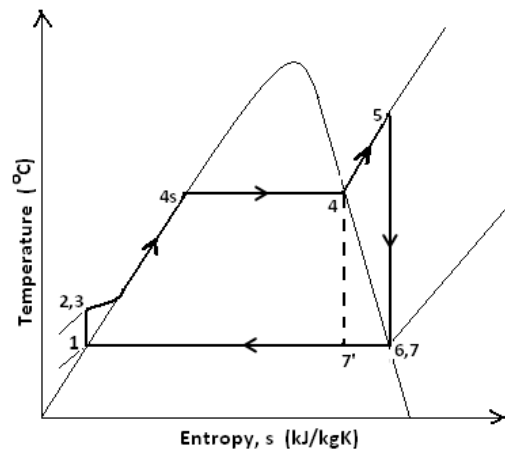
a positive T-s vapour saturation curve does not affect the blade profile but may lead to lower cycle efficiency due to the fluid entering the condenser in a superheated state thus requiring more cooling effort and possibly an oversized condenser; this may be overcome by incorporating a recuperator that uses some of the energy of the superheated low pressure vapour to preheat the fluid exiting the condenser before it is fed into the evaporator; this however is at the expense of losing the simplicity of the ORC and increasing initial investment costs.

Table 3.1 shows the usual types of working fluids that are used in low temperature Rankine cycles together with computer simulated performance results as well as environmental and safety information. Some of the parameters used in the table are explained below:

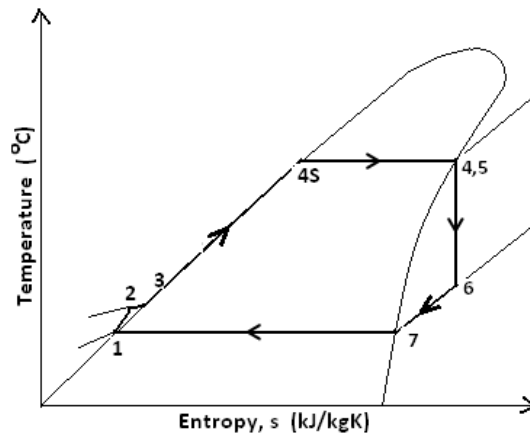
- $T_{critical}$: The temperature of the working fluid at the critical point;
- $P_{critical}$: The pressure of the working fluid at the critical point;
- Boiling Point: The boiling temperature of the working fluid at atmospheric pressure;
- Global Warming Potential: A measure of the global warming effect resulting from a given mass of a gas; this is usually calculated/measured over a 100 year period and uses carbon dioxide as the reference (i.e. GWP for $CO_2=1$) [3.6];
- P_{lower} : The pressure of the working fluid at the exit from the turbine and represents the lowest operating pressure in the thermal cycle;
- P_{higher} : The pressure of the working fluid at the entry to the turbine and represents the highest operating pressure in the thermal cycle;
- η : The thermal efficiency of the cycle with no regeneration and no bleeding;
- η_{reg} : The thermal efficiency of the cycle with regeneration;
- η_{bled} : The thermal efficiency of the cycle with bleeding; and
- $\eta_{bled-reg}$: The thermal efficiency of the cycle with regeneration and bleeding.



(a) Isentropic T-S Expansion



(b) Negative T-S Expansion



(c) Positive T-S Expansion

Figure 3.2: Three types of T-S expansion curves

Table 3.1: Thermal efficiencies of the basic as well as modified ORCs for different working fluids [3.7]

Working Fluid	Chemical Formula	T _{critical} (°C)	P _{critical} (MPa)	Boiling Point (°C)	Global Warming Potential	P _{power} (MPa)	P _{higher} (MPa)	η (%)	η _{reg} (%)	η _{hhd} (%)	η _{hhd-reg} (%)	Slope of Saturation Vapour line	Safety
n-pentane	C ₅ H ₁₂	196.6	3.37	36.1	Very low	0.1157	0.9067	12.6	13.9	13.9	14.7	Dry	Flammable
Benzene	C ₆ H ₆	288.9	4.894	80.1	Very low	0.0244	0.3002	14.1	14.3	15.1	15.2	Dry	Flammable
n-butane	C ₄ H ₁₀	152	3.796	-0.6	Very low	0.379	2.213	12.1	12.6	13.4	13.8		
n-hexane	C ₆ H ₁₄	234.7	3.034	68.7	Very low	0.0373	0.3998	12.8	14.4	14	15		
Isobutene	C ₄ H ₁₀	134.7	3.64	-11.7	Very low	0.531	2.84	11.3	11.5	12.7	12.8		
Isohexane	C ₆ H ₁₄	224.6	3.04	60.2	Very low	0.0507	0.4911	12.6	14.3	13.8	14.9		
Isopentane	C ₅ H ₁₂	187.2	3.396	27.8	Very low	0.1515	1.086	12.4	13.8	13.7	14.6	Dry	Flammable
n-perfluoropentane	C ₅ H ₁₂	147.4	2.045	29.8	8900	0.1459	1.192	9.9	12.9	11.4	13.3		
R 113	C ₂ Cl ₃ F ₃	214.1	3.392	47.6	6000	0.0783	0.6807	13	14.1	14.2	14.9	Dry	Non-flammable
R 123	C ₂ HCl ₂ F ₃	183.7	3.662	27.8	120	0.1545	1.199	13	13.4	14.2	14.5	Isentropic	Non-flammable
R141b	C ₃ H ₅ Cl ₂ F	204.4	4.212	32.1	700	0.1329	1.033	13.4	13.7	14.5	14.7		
R236ea	C ₃ H ₂ F ₆	139.3	3.502	6.2	1200	0.3377	2.357	11.4	12.2	12.9	13.4		
R245ca	C ₃ H ₃ F ₅	174.4	3.925	25.1	640	0.1735	1.435	12.5	13.3	13.8	14.3		
R245fa	C ₃ H ₃ F ₅	154	3.651	15.1	950	0.2505	1.928	12.1	12.7	13.5	13.9	Isentropic	Non-flammable
R365mfc	C ₄ H ₃ F ₅	186.9	3.271	40.3	890	0.1005	0.9324	12.4	13.8	13.7	14.6		
Toluene	C ₇ H ₈	318.6	4.126	110.6	Very low	0.0079	0.1314	14	14.6	15	15.3	Dry	Flammable

3.4 Organic Rankine Cycle (ORC) Developers and Suppliers

One major technical barrier to the maturation of low temperature power generation technology arising from this research is the unavailability of mass produced, appropriately priced, off-the-shelf small organic power cycle turbines. A number of developers and suppliers of turbines were contacted. The majority of them were well established in the development and supply of larger scale turbines in the Megawatt range; however, smaller version turbines suitable for organic fluids were either undergoing development and highly priced or were simply not available. Most suppliers have developed expanders based not on the turbine design but adapted mainly from positive displacement machines such as scroll type and screw type compressors and pumps. Table 3.2 shows the list of ORC suppliers in the small turbine market. Figure 3.3 shows the IT10 unit supplied by Infinity Turbine.

Table 3.2: Results of the survey of suppliers for ORC expander

Manufacturer	Company Website	Product Type	Minimum Expander	Prices
Infinity Turbine LLC USA	www.infinityturbine.com	Turbine expander	Model IT01 (1kWe) Model IT10 (10kWe)	IT10 ORC unit cost USD50,000
Green Energy, Australia	www.geaust.com.au	Turbine expander	Model SG10 (10kWe)	-
ORMAT Tech., Inc. USA	www.ormat.com	Screw expander	50kWe	-
ELECTRATHERM, USA	www.electratherm.com	Screw expander	50kWe	-
ENEFTECH, Switzerland	www.eneftech.com	Scroll expander	010GRE-01 (5kWe or 10kWe)	CHP unit cost €55,000
Freepower Ltd., England	www.freepower.co.uk	Scroll expander	6kWe	-
Turbolina® GmbH & Co. KG, Germany	www.turbolina.com	-	3.5kWe	-



Figure 3.3: IT10 Infinity Turbine ORC unit

3.5 Concept Plants

A detailed worldwide survey of existing ORC plants has been presented by Desai (2008); [3.15]. A computer model of a Regenerative Solar-Assisted Rankine Power Cycle has been presented by Lansing FL (1977) [3.16].

Solar pond power plants of electric capacities from a few ten kW up to a few MW have been built in Israel, the US (Texas), Australia (for process heat provision), among other countries as shown in Table 3.3 [3.17]. Pond collectors are either natural or artificial lakes, ponds or basins that act as a flat plate collector because of the different salt contents of water layers due to stratification.

Table 3.3: Low temperature ORC concept plants

	El Paso, Texas, USA	Beit Ha'Arava, Israel	Pyramid Hill, Australia
Capacity	300 kW _{th} 70 kW _e	5 MW _e (maximum) 570 kW _e (average)	60kW _{th}
Pond surface	3,350 m ²	250,000 m ²	3000 m ²

3.6 Conclusion

Description of low temperature solar thermal energy conversion technologies has been provided with examples. Their main differentiating factor from high temperature solar thermal energy conversion technologies is the limited temperature range of below 300°C. Working fluids for low temperature thermal cycles were investigated and the required salient features listed, most important among them being that the boiling temperature should be within the operating temperature range at the given operating pressures. The chapter has also indicated the unavailability of suitably developed small scale turbines for low temperature systems. Identified

current suppliers of expanders for small scale applications and some operational concept plants have been listed.

References

- [3.1] Groenendaal B.J., ECN project number 7.7372: Solar Thermal Power Technologies, 2002.
- [3.2] Schlaich J. and Robinson M., 1995: Principle of a Solar Chimney: Solar Chimney, Axel Menges GmbH, 1995, ISBN 3930698692,
- [3.3] montaraventures.com/energy/wp-content/uploads/2008/05/rankine-cycle-diagram.jpg.
- [3.4] www.eng.usf.edu/~hchen4/Kalina%20Cycle.htm accessed April 04, 2012.
- [3.5] Stine W.B. and Geyer M, Power cycles for electricity generation, Chapter 12 in Power from the sun, 2001, found at <http://www.powerfromthesun.net/book.html>; accessed October 15, 2014.
- [3.6] http://www.engineeringtoolbox.com/Refrigerants-Environment-Properties-d_1220.html accessed October 16, 2014.
- [3.7] Nishith B.D. and Santanu B., Process integration of organic Rankine cycle, Energy Journal, Vol 34, 2009, pp 1674-1686
- [3.8] www.infinityturbine.com accessed March 14, 2013
- [3.9] www.geaust.com.au accessed March 14, 2013
- [3.10] www.oramat.com accessed April 21, 2010
- [3.11] www.electrathern.com accessed March 14, 2013
- [3.12] www.eneftech.com accessed March 14, 2013
- [3.13] www.freepower.co.uk accessed March 14, 2013
- [3.14] www.turbolina.com accessed March 14, 2013
- [3.15] Desai N.B. Organic Rankine cycle. M.Tech. Dissertation, Indian Institute of Technology, Bombay, 2008.
- [3.16] Lansing F.L., Computer modelling of a regenerative solar-assisted Rankine power cycle; Technical Report: The Deep Space Network, pp 152-168; Jet Propulsion Lab., California Inst. of Tech., Pasadena, CA, United States, 1977, found at ipnpr.jpl.nasa.gov/progress_report2/42-37/37U.PDF, accessed February, 2015.
- [3.17] <http://www.cs.kumamoto-u.ac.jp/epslab/APSF/> accessed August 28, 2014

CHAPTER 4 SYSTEM DESIGN AND CYCLE COMPONENTS MODELLING

This chapter presents mathematical models and computer simulations of the following:

- organic Rankine cycle;
- solar field;
- evaporator; and
- condenser.

The models are presented in publications appended in Appendix A4.

4.1 System Design and Modelling

The system design and model was successfully developed and the write up is contained in the following three peer reviewed publications appended to this thesis under Appendix A4 Publications:

- A4.7 Situmbeko S.M. and Inambao F.L., Low temperature solar thermal energy conversion, Energize, South Africa, June 2010, pp 21-24.
- A4.13 Situmbeko S.M. and Inambao F.L., Mathematical modeling and simulation of a low temperature solar thermal energy conversion system, International Solar Energy Society – Solar World Congress (ISES–SWC 2011), Kassel, Germany, 28 August - 2 September 2011.
- A4.14 Situmbeko S.M. and Inambao F.L., Low temperature solar thermal energy conversion, Domestic Use of Energy (DUE) Conference; Cape Peninsula University of Technology, Cape Town, South Africa, March 29 - 31, 2010.

4.2 Solar Field Design and Modelling

The design and modelling of the solar field is contained in the following two peer reviewed publications appended to this thesis under Appendix A4 Publications:

- A4.6 Situmbeko S.M. and Inambao F.L., System and component modelling of a low temperature solar thermal energy conversion cycle, Journal of Energy in Southern Africa, ISSN 1021 447X, Vol. 24 No 4, November 2013, pp 51-62.
- A4.12 Situmbeko S.M. and Inambao F.L., Mathematical modelling and computer simulation of a solar field for a low temperature organic Rankine cycle (ORC), 1st Southern African Solar Energy Conference (SASEC 2012) Stellenbosch, South Africa, 21-23 May 2012.

4.3 Evaporator Design and Modelling

Design and modelling of the evaporator heat exchanger is presented in the following peer reviewed publication appended to this thesis under Appendix A4 Publications:

- A4.5 Situmbeko S.M. and Inambao F.L., Heat exchanger modelling for solar organic Rankine cycle, International Journal of Thermal and Environmental Engineering (IJTEE), Volume 9, No. 1, 2015, pp 7-16.

4.4 Condenser Design and Modelling

Design and modelling of the condenser heat exchanger is presented in the following peer reviewed journal publication appended to this thesis under Appendix A4 Publications:

- A4.3 Situmbeko S.M. and Inambao F.L., ORC condenser heat exchanger design and modelling, International Journal of Engineering Research & Technology (IJERT), ISSN: 2278-0181, Vol. 4 Issue 08, August 2015, pp 279-286.

CHAPTER 5 TURBINE DESIGN AND MODELLING

Abstract

There is not sufficient evidence to show that significant research and development work has been conducted with regard to turbomachinery design and development for small to medium size low temperature ORC systems. Most turbine manufacturers and developers place emphasis on larger scale models in the Megawatt (MW) ranges. Most researchers who have shown interest in micro-scale operations involving low temperature applications have concentrated their efforts on thermodynamic studies regarding the power cycle, and on the proper rules for the selection of the working fluids, with special attention to the power plant efficiency; and adaptation and modification of equipment, especially positive displacement machines, for use as ORC expanders. A turbine design suitable for small scale and low temperature operation based on the ORC thermodynamic cycle is required because the operating conditions such as speeds, flow rates, pressure ratios, etc. are quite different from those of conventional steam and gas turbines; also the properties of the organic fluids used as working fluids are different from those of the conventional steam or fossil-fuel-gas mixtures. This paper presents the preliminary design and modelling of a turbine suitable for use in a small to medium level low temperature solar thermal conversion cycle. The work involves thermodynamic and geometrical design and analyses. Empirical loss correlations are used to account for the different kinds of losses. The engineering equation solver (EES) is used to perform the thermodynamic analysis. 2D and 3D computational fluid dynamics (CFD) simulation and the aerofoil design are not done at this stage as they require specialized CFD software such as SoftInWay Inc.'s AxSTREAM, AutoDesk's CFD Simulation or SolidWorks Flow Simulation.

Keywords: ORC thermodynamic cycle, preliminary design and modelling, thermodynamic and geometrical design, EES

5.1 Introduction

In this paper we present work done on the research and development of a turbine suitable for a low temperature solar thermal conversion cycle based on the ORC. The turbine is the single most critical component in a thermal conversion cycle. The ideal solution should be characterized by maximum efficiency, small carbon footprint, and minimum shaft speed [5.1]. The developed device should be, essentially, based on one of the following architectures:

- Single stage radial turbine – cantilever type;
- Single stage radial turbine – ninety degree in-flow radial turbine (90° IFR); and
- Single stage axial turbine.

For micro operations, the radial turbine option seems more attractive as it allows a better performance in the lower size range which is also of special interest for distributed combined heat and power (CHP) units.

The turbine design process can be broken down into three stages:

- Preliminary design (PD);
- Mean-line/Streamline (1D/2D) analysis and optimization; and
- Profiling, 3D blade design, 3D modelling and analysis.

Preliminary design involves finding the optimal flow path, number of stages and distribution of geometrical parameters (heights and angles) based on the given thermodynamic conditions at turbine inlet and outlet. This process can further be subdivided into two tasks:

1. Initial enthalpy drop distribution: this entails determining the optimal number of stages and appropriately distributing the enthalpy drop between them and finding the first approximation of flow path geometry paths; and
2. Adjusting design calculations (inverse calculation task): this entails calculation of turbine main performance as well as exact thermodynamic and kinetic parameters basing on initial enthalpy drop distribution results.

Initial design parameters are the inlet working fluid conditions (pressure, temperature, and enthalpy), outlet pressure, mass flow rate and rotational speed. Initial enthalpy drop distribution consists of selection of optimal velocity ratios and outlet angles and recalculation of reaction degree from hub to mean section; and calculation of optimal number of stages, optimization of nozzle and blade heights as well as stage thermodynamic parameters. The results of initial enthalpy drop distribution are number of stages, flow path geometry (diameters and heights of stages), pressure ratio/drop between stages and outlet angles in the fixed and relative reference frames, σ and β values, respectively.

Adjusting design calculation is necessary for defining exactly the thermodynamic parameters and main performance characteristics such as efficiency and capacity using mean-line flow path analysis. These calculations are based on known values of inlet and outlet parameters such as stagnation enthalpy and rothalpy, stagnation pressure, outlet static pressure and reaction, and assumed values such as diameter, mass flow rate, rotational speed, initial velocity coefficient values (flow coefficient and stage blade-loading coefficient), and nozzle and blade heights. The results of adjusting design calculation are efficiency and capacity, angles based on selected reaction, thermodynamic and kinematic parameters distribution, and losses components.

Design point refers to the main operating mode of the turbine and equals 70% - 90% of the capacity of the maximum mode.

To fully develop a turbine model, the following factors are of paramount importance:

1. Manufacturing and material specifications of the rotor and nozzle;

2. Structural and aerodynamic design of the rotor and nozzle; and
3. Specifications of the inlet and outlet parameters such as pressures and temperatures.

5.2 Review of Organic Rankine Cycle Expanders

A review of available options of ORC expanders suitable for use in low temperature and small to medium level operations was undertaken and the write up on this subject is contained in a conference paper publication included in Appendix A4:

- A4.9 Situmbeko S. M. and Inambao F. L. (2015). Review of Designs for Low Temperature Organic Rankine Cycle Expanders, Proceedings of the Botswana Institution of Engineers (BIE) 14th Biennial Conference, Gaborone, Botswana, October 6 – 8, 2015, Paper ID C15-1025-2015, pp 1-7.

5.3 Theory of Turbomachinery

Fluid dynamics and hence turbomachinery theory is based on three fundamental principles of conservation of mass (continuity), conservation of momentum and conservation of energy, represented by the following equations:

$$\text{conservation of mass (continuity):} \quad \frac{\partial \rho}{\partial t} + \nabla \cdot (\rho \bar{U}) = 0 \quad (5.1)$$

$$\text{conservation of momentum:} \quad \frac{\partial \rho \bar{U}}{\partial t} + \nabla \cdot (\rho \bar{U} \bar{U} + P \bar{I} - \bar{\tau}) - \rho \bar{G} = 0 \quad (5.2)$$

$$\text{conservation of energy:} \quad \frac{\partial \rho(e+k)}{\partial t} + \nabla \cdot \left(\rho \bar{U} \left(e + \frac{P}{\rho} + k \right) - \bar{\tau} \cdot \bar{U} + \bar{Q} \right) - \rho \bar{G} \cdot \bar{U} = 0 \quad (5.3)$$

The work done by a turbomachine can be represented by the Euler turbine equation which can be written as [5.2]:

$$\dot{W}_t = \dot{m} \omega (r_2 \bar{V}_{\theta 2} - r_1 \bar{V}_{\theta 1}) \quad (5.4)$$

where \dot{m} is the mass flow rate, ω is the shaft angular velocity, r is the mean blade radius, \bar{V} is the working fluid flow velocity, while subscripts 1, 2 and θ represent the inlet and outlet to the machine, and tangential (circumferential) component respectively.

Velocity Triangles and Mollier diagrams are used to aid the analysis of the turbomachinery. Typically, the velocity triangle is a representation of the equation $\bar{V} = \bar{U} + \bar{W}$ at each station, that is, entry to nozzle, and entry and exit to rotor; where V is absolute fluid velocity, U is blade velocity and W is relative velocity of fluid flow to moving blades (Figure 5.1).

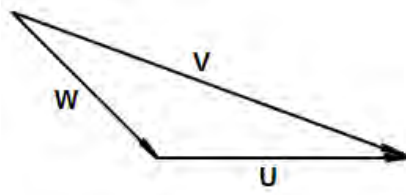


Figure 5.1: Velocity diagram

The Mollier diagram is a plot of enthalpy against entropy for a process in which one property (usually pressure or temperature) is kept constant [5.3]. Pertaining to turbine expansion processes, the mollier diagram aids in visualising the isentropic and real expansion processes as well as the stagnation and static states of the working fluid. Figure 5.2 shows a typical expansion process on a Mollier diagram.

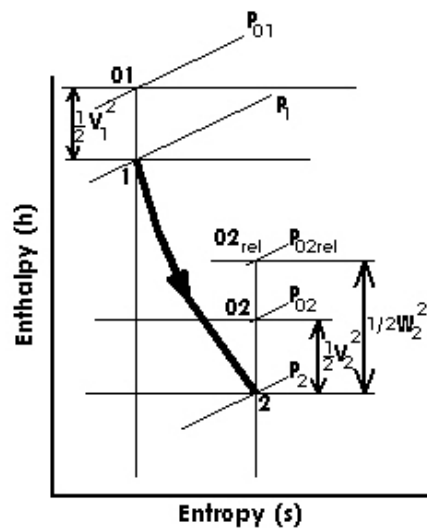


Figure 5.2: Mollier diagram showing a typical expansion process

Stagnation state is represented by state parameters designated as P_0 for stagnation pressure, T_0 for stagnation temperature, and h_0 for stagnation enthalpy. Stagnation pressure is the pressure at a state corresponding to zero velocity, a stagnation state which is representative of an adiabatic throttling process. The throttling process is a representation of flow through inlets, nozzles, and stationary turbomachinery blades, and the use of stagnation pressure as a measure of loss is a practice that has widespread application. Stagnation pressure is a key variable in propulsion and power systems.

The stagnation pressure at a given state is defined by the enthalpy equation:

$$h_0 = h + \frac{V^2}{2} \quad (5.5)$$

where: h_0 is the stagnation enthalpy (J/kg); h is the static enthalpy (J/kg); and V is the fluid speed (m/s).

Rothalpy is a function/property that remains constant throughout a rotating machine, that is, in an adiabatic irreversible process relative to the rotating component [5.4]. It is defined by the equation:

$$I = h + \frac{W^2}{2} - \frac{U^2}{2} \quad (5.6)$$

where h is static enthalpy, W is the relative velocity of the fluid, and U is the blade speed. Thus rothalpy (rotational enthalpy) is conserved between two stations in a rotating reference in any turbomachinery:

$$I_2 = I_3 \quad (5.7)$$

Stagnation enthalpy is conserved between two points in a fluid flow stream in a non-rotating reference system:

$$h_{01} = h_{02} \quad (5.8)$$

The degree of reaction is expressed as the relative pressure or enthalpy drop in the nozzle or rotor blades to that of the stage:

Rotor degree of reaction:
$$R_r = \frac{\text{static enthalpy drop in rotor}}{\text{stagnation enthalpy drop in stage}} \quad (5.9)$$

Nozzle degree of reaction:
$$R_n = \frac{\text{static enthalpy drop in nozzle}}{\text{stagnation enthalpy drop in stage}} \quad (5.10)$$

5.4 Radial Flow Turbine Model

5.4.1 Description of Turbine Arrangement

In a radial turbine the flow of the working fluid is substantially in the radial direction towards the turbine shaft axis. This configuration allows a radial turbine to be simpler, more robust, and more efficient especially for lower power ranges [5.5] when compared to an axial machine. The flow is generally inward, although there are newer designs with an outward flow such as the Euler turbine [5.6]. There are two types of inward flow radial turbines: Cantilever turbines and ninety degree in-flow radial (90°IFR) turbines.

The cantilever radial turbine is similar aerodynamically to the axial impulse type turbine and can be designed in a similar manner to axial turbines. Figure 5.3 shows a cantilever turbine rotor and Figure 5.4 shows the turbine blade arrangement and the corresponding rotor entry and exit velocity triangles.



Figure 5.3: Cantilever radial turbine rotor (N=25)

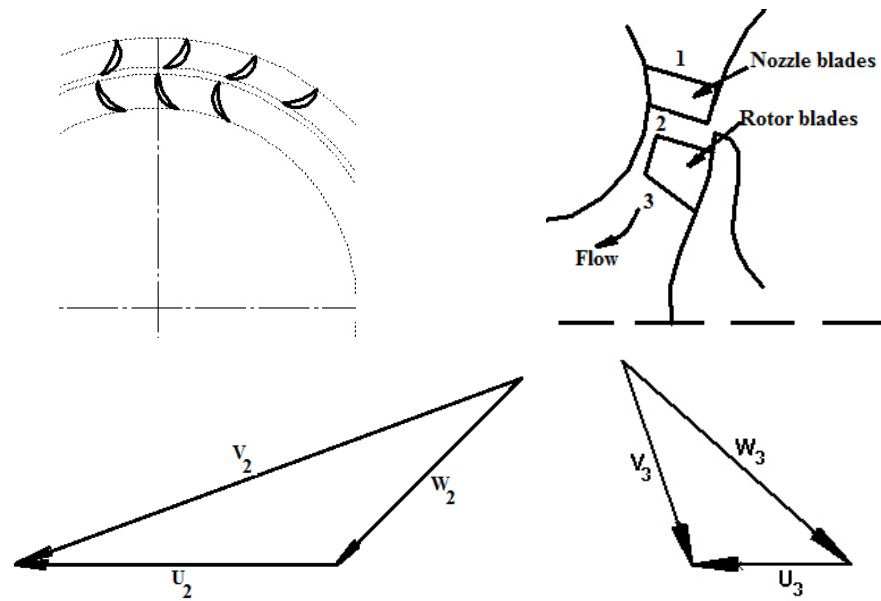


Figure 5.4: Cantilever turbine arrangement and velocity triangles

(where: V is absolute fluid velocity, U is blade velocity, and W is relative velocity of fluid flow to moving blades)

The 90° IFR turbine has a striking similarity with a centrifugal compressor with the flow direction and blade motion reversed. The flow enters the turbine radially and exits the turbine axially. Straight radial blades are generally preferred as curved blades would incur additional stresses. The rotor or impeller ends with an exducer. Usually the flow exiting the rotor passes through a diffuser to recover kinetic energy which would otherwise be wasted. The 90° IFR turbine rotor is shown in Figure 5.5 and the turbine blade arrangement and the corresponding rotor entry and exit velocity triangles are shown in Figure 5.6.



Figure 5.5: 90° IFR turbine rotor (N=15)

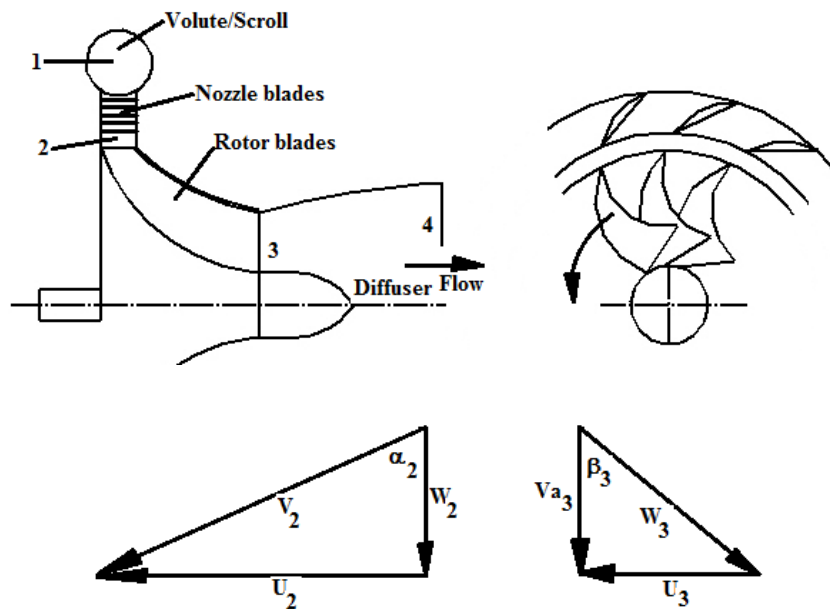


Figure 5.6: 90° IFR turbine arrangement and velocity triangles

5.4.2 Mathematical Model

The following figure is an enthalpy-entropy diagram (Mollier diagram) of the expansion process for a radial turbine with a diffuser where 1, 2, 3 and 4 represent the entry to the stator, entry to the rotor, exit from the rotor and exit from the diffuser respectively.

Total-to-Total expander efficiency is given by:

$$\eta_{tt} = \frac{h_{01} - h_{03}}{h_{01} - h_{03ss}} \quad (5.16)$$

Blade loading coefficient:

$$\Psi = \frac{\Delta h_{tt}}{U_2^2} = \frac{h_{01} - h_{03}}{U_2^2} \quad (5.17)$$

Flow coefficient:

$$\phi = \frac{V_{m2}}{U_2} \quad (5.18)$$

The effective degree of reaction is given by:

$$R_r = \frac{\Delta h_{RR}}{\Delta h_{Rstage}} \quad (5.19)$$

where: $\Delta h_{RR} = h_2 - h_3$, $\Delta h_{Rstage} = h_1 - h_3$

and the specific speed:

$$N_s = \frac{rpm}{60} \cdot \frac{Q_3^{0.5}}{\Delta h_{ostage}^{3/4}} \quad (5.20)$$

where: $\Delta h_{ostage} = h_{01} - h_{03ss}$

5.4.3 Computer Simulations

The following parameters as represented in Figure 5.8, together with the inlet conditions shown in Table 5.1, are used in the computer simulations. The simulations are performed on the EES (engineering equation solver) platform [5.7]:

- L_d = axial flow length of turbine;
- d1 = nozzle inlet diameter;
- d2 = rotor inlet diameter;
- d3 = rotor mean outlet diameter;
- d4 = diffuser outlet diameter;
- b1 = nozzle inlet blade height;
- b2 = rotor inlet blade height;
- b3 = rotor exit blade height;
- b4 = diffuser gap height;
- α_1 = nozzle inlet (absolute) flow angle;
- α_2 = rotor inlet absolute flow angle;
- α_3 = rotor exit absolute flow angle;
- β_2 = rotor inlet relative flow angle;
- β_3 = rotor exit relative flow angle; and
- α_4 = diffuser exit (absolute) flow angle.

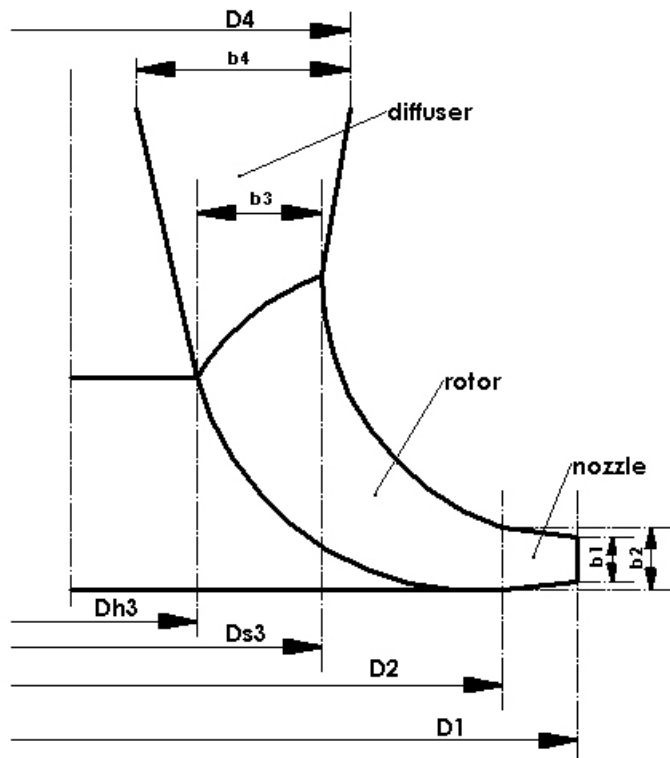


Figure 5.8: Radial turbine blade geometry

Table 5.1: Inlet conditions [5.8]

Working Fluid	Mass flow rate	Inlet Pressure	Inlet Temperature
	[kg/s]	[Pa]	[°C]
R245fa	0.396	810600	80.99
R134a	0.396	810600	80.99
n-butane	0.207	1010000	80.03
Isobutene	0.241	1010000	66.82

In the simulations that follow, the outlet pressure was varied from 130 kPa to 180 kPa and the rotor inlet diameter varied from 20 mm to 150 mm. R134a was included at a later stage, although it had previously not been considered favourable during the development stage of the evaporator model; the reason for this change of heart was mainly because it had now been established that since this was the working fluid that we were able to procure, this was the liquid we were going to use for the experimental model.

Three sets of simulations were conducted:

Simulation 1: rotor exit static pressure (P_3) was varied from 130 kPa to 180 kPa; the results are shown in plots of Figures 5.9 and 5.10.

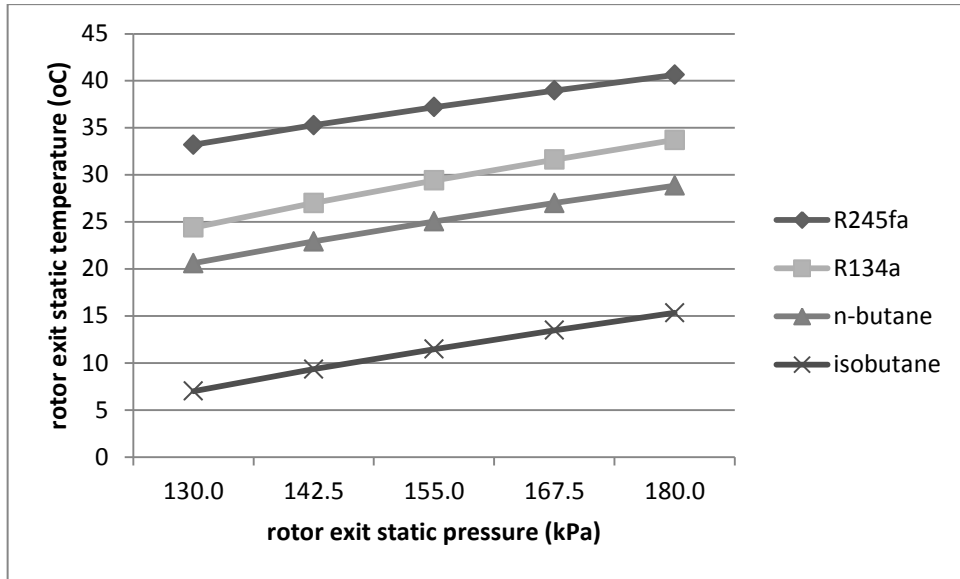


Figure 5.9: radial turbine model rotor exit – temperature versus pressure

The turbine (rotor) exit temperature is important in that it needs to be higher than the sink (usually ambient) temperature for the thermal cycle to meet requirements for thermodynamic functionality; from these simulations it is evident that given the current operating conditions only R245fa (and to a lesser extent R134a) satisfy this cycle temperature constraint; for n-butane and isobutene the cycle requires to operate at higher pressures for them to satisfy the temperature limits.

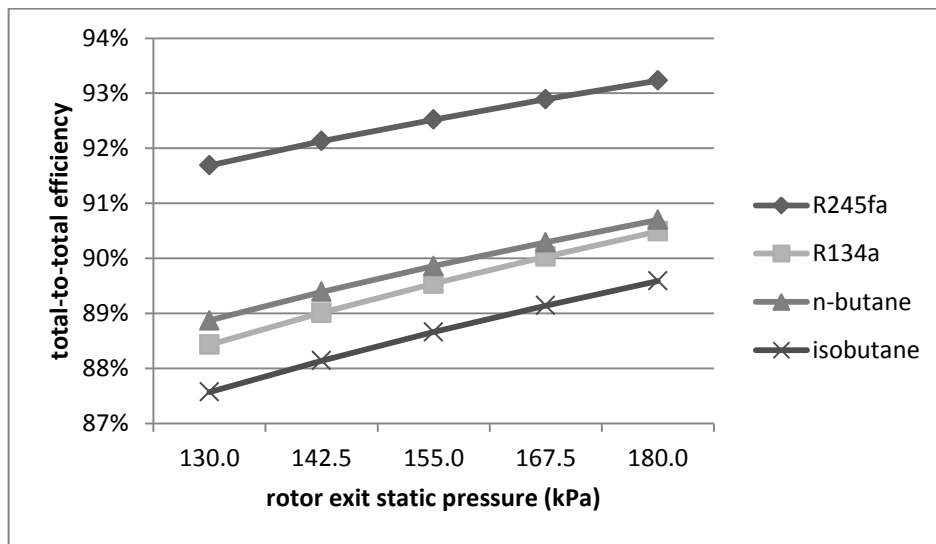


Figure 5.10: Radial turbine model total-to-total efficiency versus rotor exit pressure

In terms of the efficiency it is seen that all the four working fluids perform satisfactorily; R245fa has the highest efficiency followed by n-butane, R134a is third and isobutene has the lowest efficiency.

Simulation 2: rotor inlet diameter (D_2) was varied from 20 mm to 150 mm while keeping rotor exit pressure constant at 180 kPa by adjusting the machine rotational speed to achieve the desired power output. Results are shown in Figure 5.11.

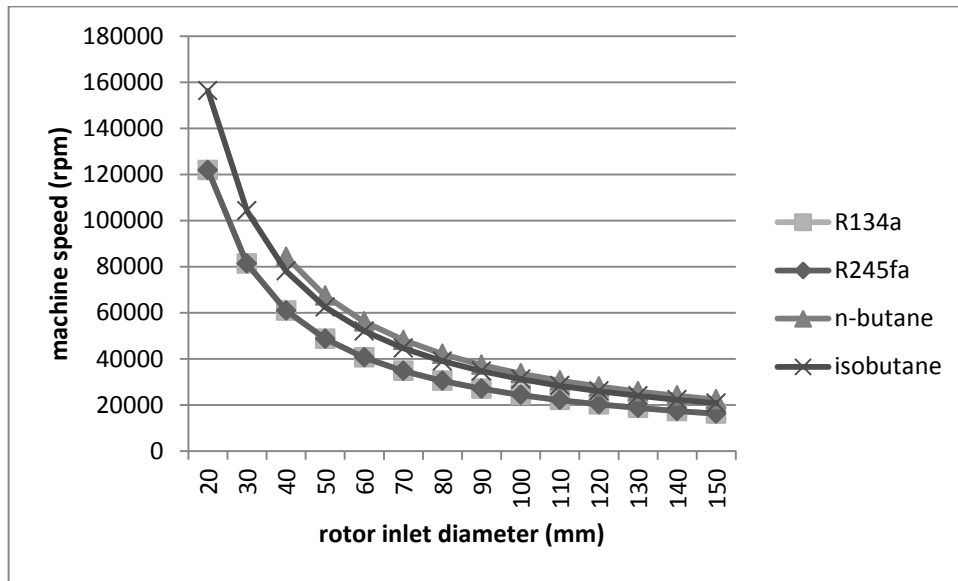


Figure 5.11: Radial turbine model machine speed versus rotor diameter

Simulation 3: machine speed was set constant at 20000 RPM. With the rotor exit pressure and machine speed set constant at 180 kPa and 20000 rpm, the final simulation was performed for the optimized results; the rotor outlet velocity triangle for R134a had to be reset to the ‘NO-swirl’ state thus giving a β_3 angle of 77.09° .

With the first simulations, the machine speed was not constrained and attained too high levels of 61000 rpm for both R245fa and R134a, 84500 rpm for n-butane and 78000 rpm for isobutene. Since it was desirable to limit the machine speed to lower values, another set of simulations was performed whereby the rotor exit pressure was kept at the higher optimum value of 180 kPa while the machine speed was varied by incrementally changing the rotor inlet diameter; all other dimensional characteristics of the turbomachine model were geometrically linked to the rotor inlet diameter. The objective of these simulations was to size the turbomachine such that it had an acceptable speed. From Figure 5.11 it can be seen that 20000 rpm is an acceptable optimal speed. The corresponding preliminary design parameters for the 10 kWe radial ORC turbine model are tabulated and plotted in the Table 5.2 and velocity triangles in Figures 5.12 to 5.14 respectively; the rest of the results are captured in Appendixes A3.4 - A3.7.

Table 5.2: Radial turbine model simulation results

Fluid\$	m_dot	P_1	P_2	P_3	PR	T_1	T_2	T_3	T_4	eta_tt
	[kg/s]	[Pa]	[Pa]	[Pa]		[C]	[C]	[C]	[C]	[-]
R245fa	0.396	810600	250080	180000	4.5	80.99	48.67	40.64	40.67	0.9324
R134a	0.396	810600	350969	180000	4.5	80.99	53.84	33.69	34.55	0.9051
n-butane	0.207	1010000	372911	180000	5.6	80.03	48.65	28.86	29.61	0.907
isobutene	0.241	1010000	412422	180000	5.6	66.82	38.13	15.33	16.29	0.896

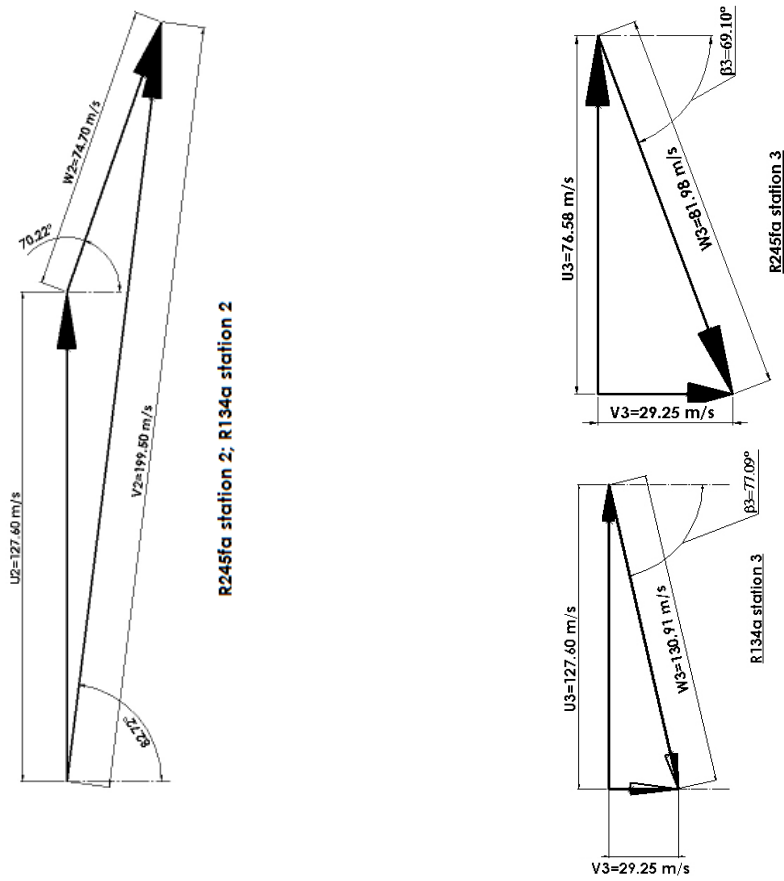


Figure 5.12: Radial turbine model velocity triangles for R245fa and R134a

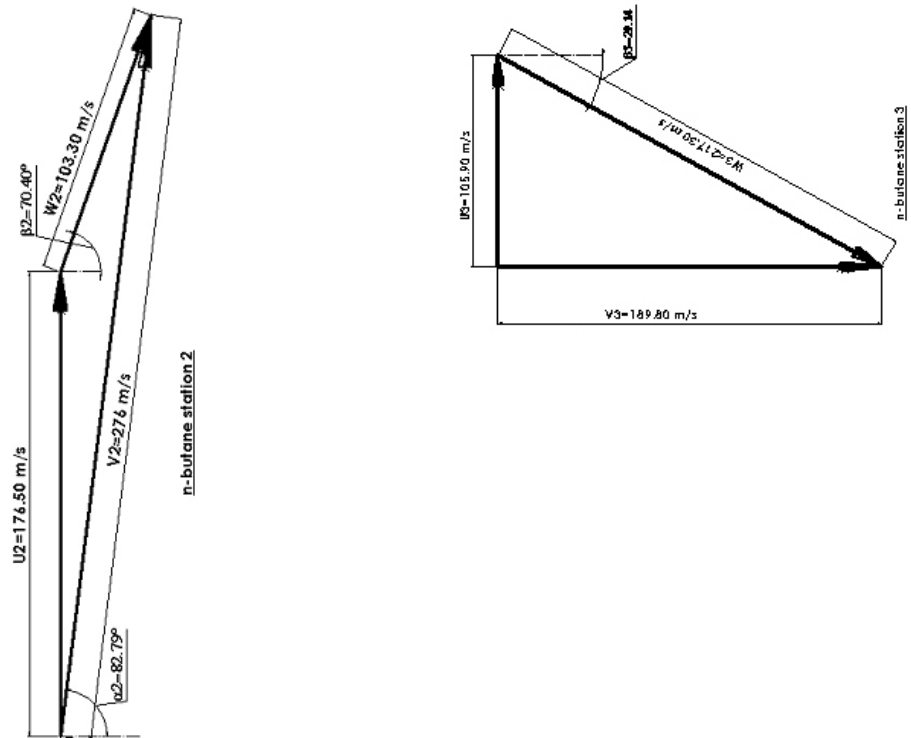


Figure 5.13: Radial turbine model velocity triangles for n-butane

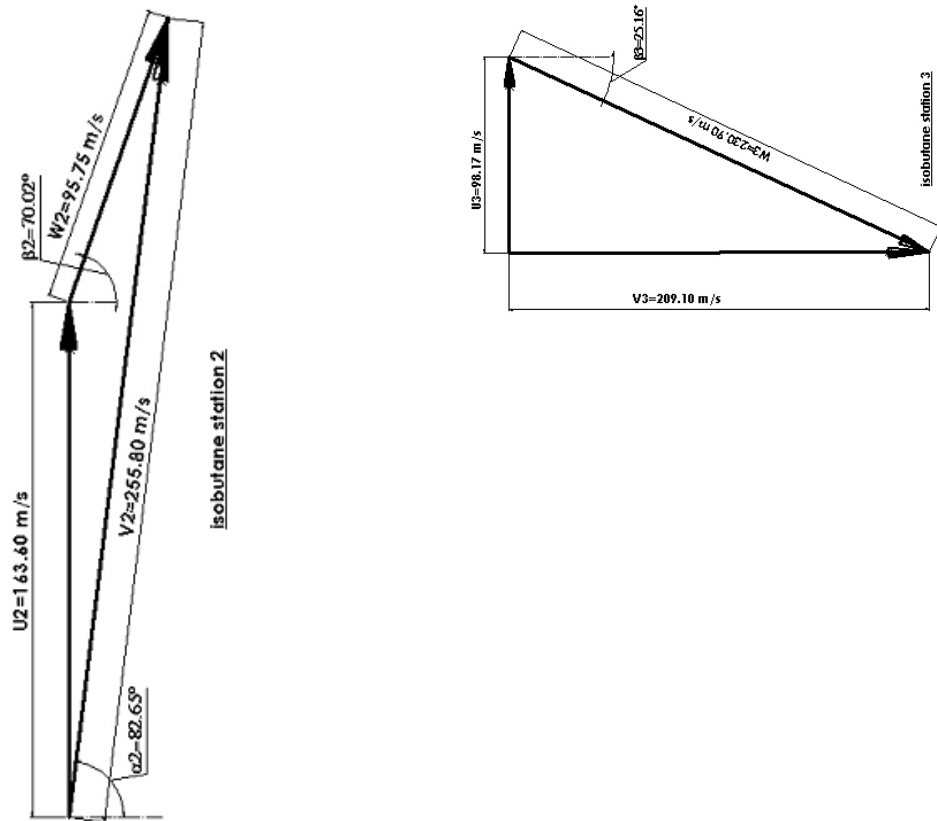


Figure 5.14: Radial turbine model velocity triangles for isobutene

5.5 Axial Flow Turbine Model

5.5.1 Description

The fluid flow in an axial turbine is essentially in a direction parallel to the axis of rotation of the machine. Axial turbines usually have several stages such that each stage only handles a moderate pressure or enthalpy drop. Figure 5.15 shows an axial turbine rotor.



Figure 5.15: Axial turbine rotor ($N = 15$)

For a single stage the diameter will usually be the same at the turbine inlet and outlet and as such the blade speed remains constant along a flow path; and a combined velocity triangle can be drawn as shown in Figure 5.16.

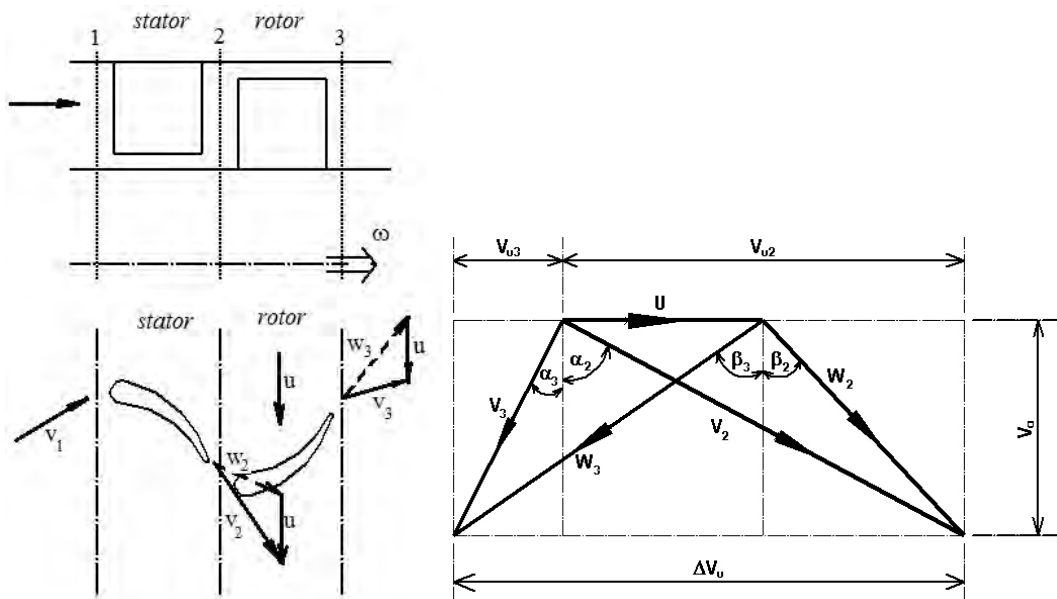


Figure 5.16: Axial turbine blade arrangement and velocity triangles

5.5.2 Mathematical Model

With reference to Figures 5.16 and 5.17 the following set of equations can be written for the single stage axial turbine:

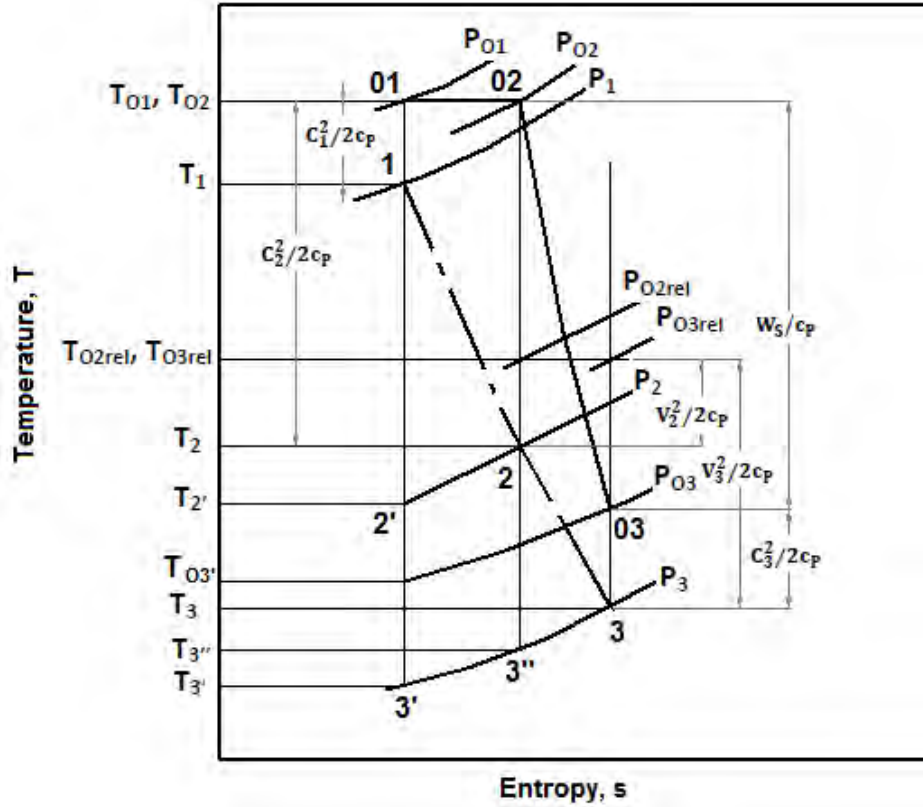


Figure 5.17: Mollier diagram for an axial turbine stage

The work output per unit mass flow is given by:

$$\dot{w} = U \cdot (V_{u2} + V_{u3}) = U \cdot V_a \cdot (\tan\alpha_2 + \tan\alpha_3) = U \cdot V_a \cdot (\tan\beta_2 + \tan\beta_3) \quad (5.21)$$

The blade-loading coefficient is used to express work capacity of the stage. It is defined as the ratio of the specific work of the stage to the square of the blade velocity:

$$\Psi = \frac{\dot{w}}{U^2} \quad (5.22)$$

The flow coefficient, ϕ , is the ratio of the axial component of the inlet flow velocity to the blade speed:

$$\phi = \frac{V_a}{U} \quad (5.23)$$

5.5.3 Computer Simulations

As no convergence could be attained with the given mass flow rates, the first simulation was to determine the lowest feasible mass flow rates for all the working fluids by varying the mass flow rates from 0.1 kg/s to 2 kg/s; the results showed 0.459 kg/s for isobutene, 0.420 kg/s for n-butane, 0.226 kg/s for R134a and 0.909 kg/s for R245fa. The results are shown in Appendix A3.8. Using these new figures, the input conditions were modified and then the simulations progressed as was the case with the radial turbine model. The revised inlet conditions are shown in the Table 5.3:

Table 5.3: Axial turbine model – revised inlet conditions

Working Fluid	Mass flow rate	Inlet Pressure	Inlet Temperature
	[kg/s]	[Pa]	[°C]
R245fa	0.909	810600	80.99
R134a	0.226	810600	80.99
n-butane	0.420	1010000	80.03
isobutene	0.459	1010000	66.82

Three sets of simulations were conducted:

Simulation 1: Rotor exit static pressure was varied within the feasible pressure range and the results are shown in Figures 5.18 and 5.19. Convergence for R245fa could only be attained for pressures 350 kPa to 360 kPa; however, since this range happened to yield higher total-to-total efficiencies, the rotor exit pressure was set at 355 kPa for the remainder of the simulations.

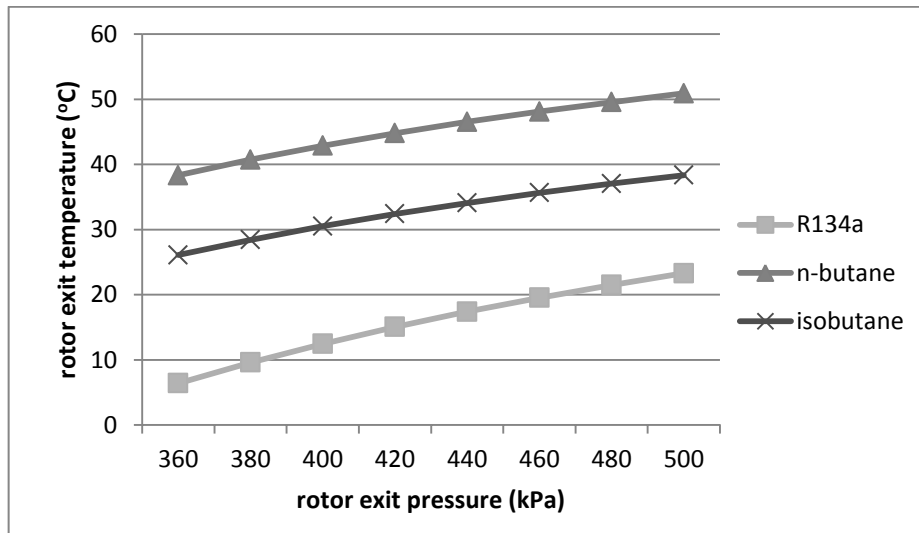


Figure 5.18: Axial turbine model rotor exit – temperature versus pressure

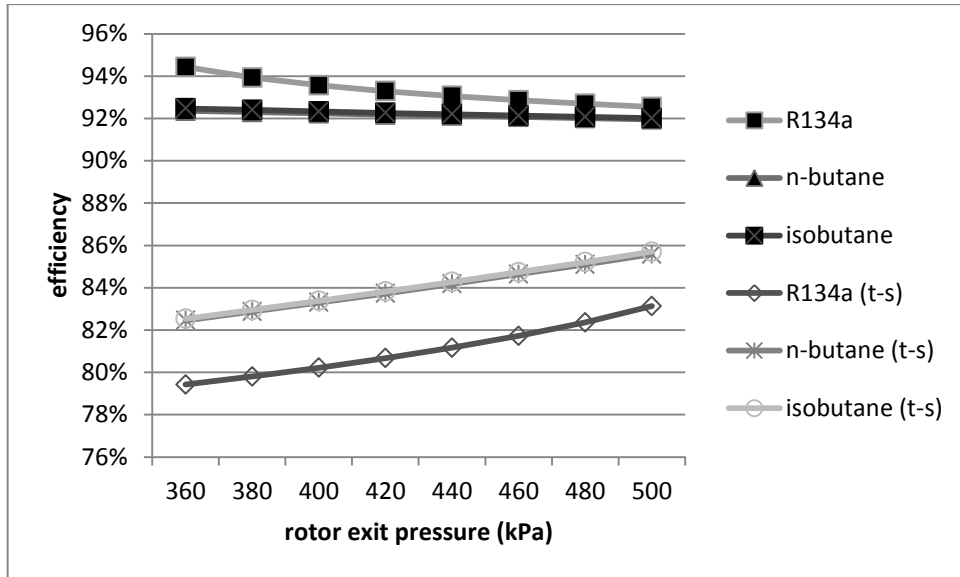


Figure 5.19: Axial turbine model efficiency versus rotor exit pressure
(t-s is for total-to-static; other series are for total-to-total)

Simulation 2: With the rotor exit pressure set constant at 355 kPa, the rotor diameter was varied from 26 mm to 160 mm as a way to optimize the machine speed at a lower acceptable level. Results of these simulations are shown in Figure 5.20. From the results it can be seen that any speed between 5000 rpm and 15000 rpm could be considered acceptable; however, the speed was set at 20000 rpm as had been done with the radial turbine model. The final optimal results are shown in Table 5.4 and velocity triangles in Figures 5.21 to 5.24. The remainder of the results are captured in Appendix A3.9.

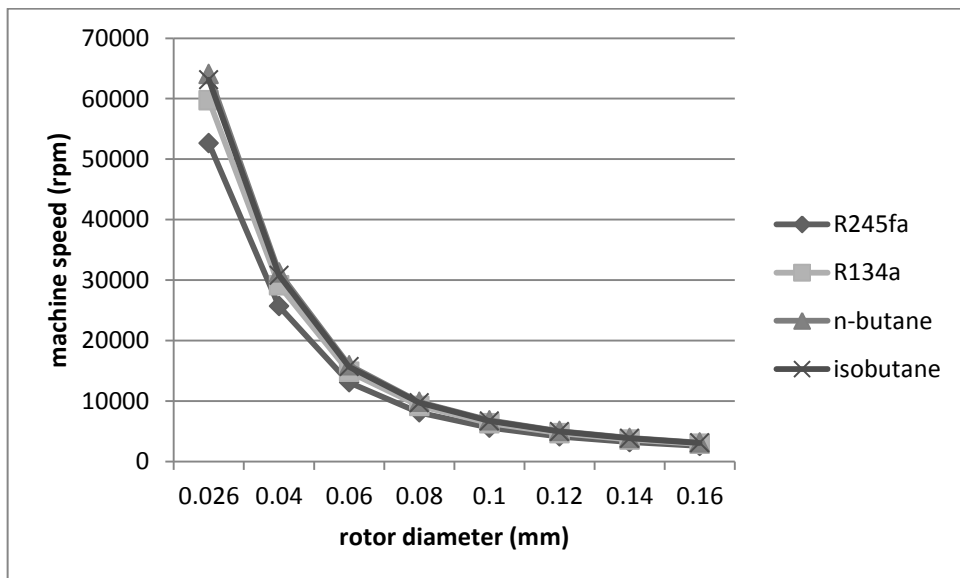


Figure 5.20: Axial turbine model – machine speed versus rotor diameter

Table 5.4: Axial turbine model simulation results

WF\$	m_dot	P_1	P_2	P_3	T_1	T_2	T_3	eta_ts	eta_tt	PR
	[kg/s]	[Pa]	[Pa]	[Pa]	[C]	[C]	[C]	[-]	[-]	
R245fa	2.061	810600	356544	355000	80.99	62.67	61.58	0.8397	0.92	1.777
R134a	1.77	810600	356633	355000	80.99	65.28	63.91	0.8348	0.9196	1.896
n-butane	1.627	1010000	355929	355000	80.03	59.83	59.11	0.863	0.9222	2.226
isobutene	1.657	1010000	355998	355000	66.82	46.23	45.48	0.8632	0.9223	2.211

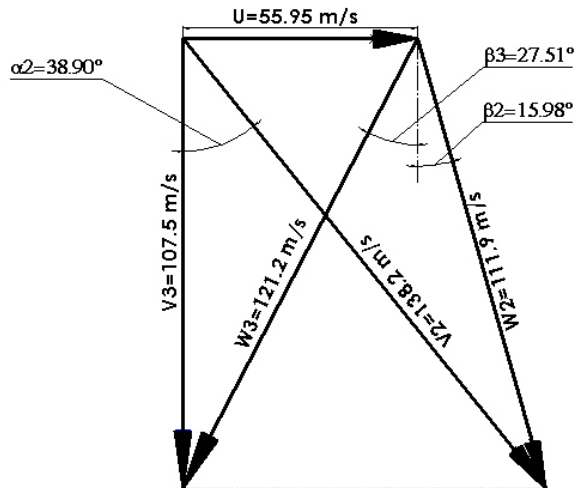


Figure 5.21: Axial turbine velocity triangles for R245fa

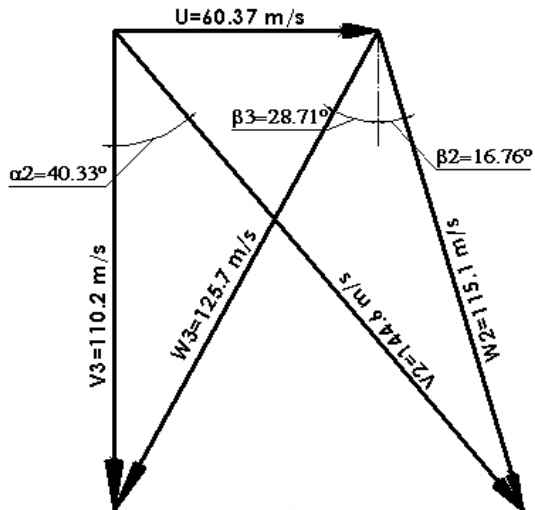


Figure 5.22: Axial turbine velocity triangles for R134a

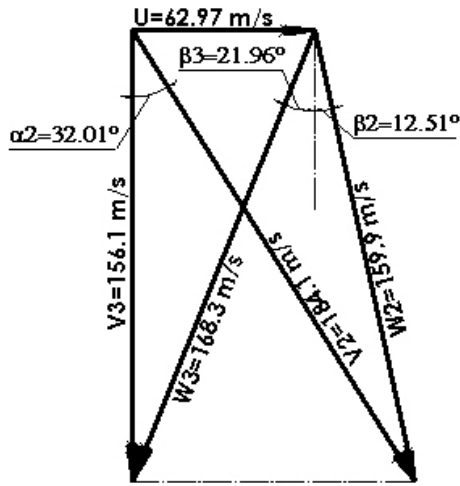


Figure 5.23: Axial turbine velocity triangles for n-butane

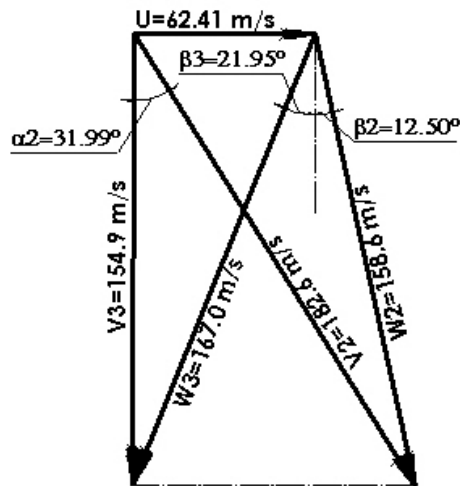


Figure 5.24: Axial turbines velocity triangles for isobutene

5.6 Discussion and Conclusions

This paper has presented the theory on the design of turbomachinery. It has also presented preliminary design models for both radial and axial turbines suitable for a 10 kWe low temperature ORC. The preliminary design has been presented in terms of geometric parameters of flow angles, blade diameters and heights. The preliminary design included thermodynamic parameters of stagnation and static pressures, temperatures and enthalpy's; the thermodynamic analyses were conducted within the cycle temperature ranges of the evaporator and condenser. Although the presented design models are not complete, this work has shown that small turbines for low temperature cycles are a feasible design option. The turbine preliminary design parameters for the 10 kWe turbine model after parametric optimization are listed in the Tables 5.1 and 5.3. From the results it is evident that for the same rotational speed the radial turbine requires less mass flow rates compared to the axial turbine. The radial turbine has a higher pressure ratio too as compared to the axial counterpart; on the other hand, the total-to-total expander efficiency tends to be the same for both turbine models with the axial turbine having a

slight edge over the radial turbine. In terms of size, the axial turbine also performs better by requiring a lesser diameter i.e. almost a quarter of that required by the radial turbine. The EES codes for the two models are included in Appendix A2.5.

5.7 Way Forward

To fully complete this task it is necessary to employ CFD and FEA analyses and modelling of the detailed blade and nozzle geometry and flow profile design. This would be followed by providing material and manufacturing specifications for prototype construction and testing; 3D printed physical prototypes could be produced and laboratory tested. AxSTREAM software suite by SoftInWay Inc. is a good package for turbine CFD modelling; AxSTREAM Lite, a lower version provided at no cost can be used for the preliminary CFD model, although it can only model axial turbines with air as the working fluid.

References

- [5.1] Cooper D., Baines N. and Sharp N., Organic Rankine cycle turbine for exhaust energy recovery in a heavy truck engine, 2010 Concepts ETI, Inc.
- [5.2] Ingram G., Basic concepts in turbomachinery, 2009 Ventus Publishing ApS, ISBN 978-87-7681-435-9.
- [5.3] <http://dictionary.reference.com/browse/mollier+diagram>; accessed February 10, 2015.
- [5.4] http://www.answers.com/Q/What_is_the_rothalpy; accessed February 10, 2015.
- [5.5] <http://en.wikipedia.org/w/index.php?oldid=605456316>; accessed February 10, 2015.
- [5.6] Welch P. and Boyle P., New turbines to enable efficient geothermal power plants, Energent Corporation; GRC Transactions, Vol. 33, 2009, http://www.energent.net/documents/Geothermal_Resources_Council_2009_Paper.pdf, accessed February 10, 2015.
- [5.7] Klein S.A. and Alvarado F.L. Engineering Equation Solver for Microsoft Windows Operating Systems, F-Chart Software, Middleton, USA. 2014.
- [5.8] Situmbeko S.M. and Inambao F.L., Heat exchanger modelling for solar organic Rankine cycle, International Journal of Thermal and Environmental Engineering (IJTEE), Volume 9, No. 1, 2015, pp 7-16.

CHAPTER 6 ECONOMIC AND ENVIRONMENTAL ANALYSES

Abstract

This aspect of the study evaluates the economic and environmental performance of the 10 kWe low temperature solar thermal energy conversion plant. It is part of an overall study to evaluate the feasibility of low temperature solar thermal energy conversion system based on the ORC as a viable means of generating clean and environmentally sustainable electricity. The study was conducted at University of KwaZulu-Natal (UKZN), Durban, South Africa. The study is presented in two sections – an economic analysis and an environmental analysis. The Cost-Benefit Analysis is used for the economic analysis and its output is in the form of Net Present Value (NPV) and Rate on Investment (ROI). The Life Cycle Analysis (LCA) method is used for the environmental analysis and its output is in the form of Carbon Pay Back Period (CPBP) and Carbon Intensity. Two other parameters are determined and may aid in assessing both the economic and the environmental performances and they are Energy Pay Back Period and Energy Intensity.

Keywords: organic Rankine cycle (ORC), cost-benefit analysis, net present value (NPV), rate on investment (ROI), life cycle analysis (LCA), carbon pay-back period (CPBP), carbon intensity, energy pay-back period, energy intensity

6.1 Results

Economic and environmental analyses for the 10 kWe low temperature solar thermal power plant were performed and the results are contained in a journal paper publication included in Appendix A4:

A4.2 Situmbeko S.M. and Inambao F.L., Economic and environmental analyses of a 10 kWe low temperature solar thermal power plant, International Journal of Research in Engineering & Advanced Technology (IJREAT), ISSN: 2320 – 8791 (Impact Factor: 2.317), www.ijreat.org, Volume 3, Issue 6, Dec 2015 – Jan 2016, pp 1-12.

CHAPTER 7 LABORATORY INVESTIGATIONS

Preamble

This chapter describes the experimental study that was carried out on a simulated heat recovery ORC. The laboratory experiments were carried out in the Mechanical Engineering Workshop at Howard College, University of KwaZulu-Natal, Durban, South Africa on dates: January 9, 21 and 25, 2016 and February 19 and 20, 2016. The objective was to evaluate the potential of a low temperature ORC in heat recovery, particularly its efficiency in thermal-to-electricity conversion, as well as to validate the theoretical models which had been developed and computer simulated earlier on in the research.

7.1 Introduction

The experiments conducted were physical simulations of a low temperature solar thermal energy conversion system. Due to financial limitations it was agreed to simulate the solar thermal input with an electrical heater. Shortcomings arising from this were that the solar input was not adequately simulated as the electrical heater used provided a near-constant thermal supply; however, through a thermostat the temperature was restricted to the low temperature range of below 80°C, which is characteristic of low temperature solar thermal systems.

A complete ORC unit consists of three cycles of fluid flows:

- Heat transfer fluid (HTF) flow: basically water (with an antifreeze additive) in this case, which collects the thermal energy from the source (such as solar thermal collectors) and transfers it to the working fluid through the evaporator heat exchanger;
- Working fluid (WF) flow: either R134a or R245fa refrigerant in this case, which facilitates the thermodynamic conversion of thermal energy collected from the evaporator to mechanical energy through expansion in the turbine; and
- Cooling fluid (CF) flow: mains water in this case, which extracts the waste heat from the thermal conversion cycle.

The experimental setup consisted of two major tangible units:

1. A 10 kWe complete ORC unit operating the WF cycle; and
2. A 450 litre electric water heater operating the HTF cycle.

The cooling fluid flow (CF) was provided through a connection to a mains water supply line.

The experimentation units are described in detail in the following sections.

7.2 Description and Installation of the Heat Engine

The heat engine comprises the 10 kWe, IT10 ORC unit supplied by Global Energy and Infinity Turbine LLC, Madison, Wisconsin, USA. This unit is supplied as a complete and assembled system requiring no special installation other than connecting to the heat source and to the heat sink as well as hooking up an electric load to the direct current (DC) generator on the unit.

The complete IT10 ORC unit, as supplied, consists of an evaporator, a turbine, a permanent magnet synchronous DC (PMDC) generator, a water cooled condenser, a feed pump and a storage cylinder for the working fluid, as shown in Figure 7.1. The evaporator and the condenser were flat plate heat exchangers while the turbine was a ninety degrees in-flow radial turbine (90° IFR). The feed pump was a 220 V direct current (DC), 2.24 kW, diaphragm pump. The feed pump was connected to the AC mains through a Titan C Series, micro single phase input, three phase output, sensor-less/ space vector control, constant torque, 0.5 to 3 HP, 200-230 VAC, inverter [7.1].

The operational and geometrical specifications of the ORC unit are shown in Table 7.1.

Table 7.1: IT 10 specifications [7.2]

Evaporator Flow – gallons per minute(gpm)/ litres per minute (lpm)	22 gpm @ 194°F less 25°F outlet (83 lpm @ 90°C less 4°C outlet)
Condenser Flow – gpm (lpm)	44 gpm @ 59°F plus 25°F outlet (166 lpm @ 15°C plus 4°C outlet)
Thermal Input	420000 btu/hr (123.08 kW)
Dimensions (uncrated) and Weight – Frame Version Only	610 mm x 610 mm x 1220 mm (181 kg)
Operating Sound (Depends on Working Fluid)	65dBA @ 10 m
Inlet and Outlet Pipe Sizes	2 inch (51 mm)

Although this type of working cycle can run on several working fluids the supplied unit is specified for R245fa (or R134a); we had challenges procuring the recommended R245fa so for the experiments we used R134a which was readily available; the quantity of working fluid required was estimated at 58 kg of liquid R245fa.

The flow of the working fluid is such that it is raised to a higher pressure by the feed pump and then heated from liquid to a vapour at the higher pressure in the evaporator; it then flows through the turbine where it expands to a lower pressure and lower temperature vapour thus having its thermal energy converted into mechanical energy or shaft power; it is then converted to a liquid in the condenser before being pressurized to the higher pressure again by the feed pump and then fed to the evaporator to repeat the cycle. The 10 kWe ORC unit is shown in Figure 7.1.

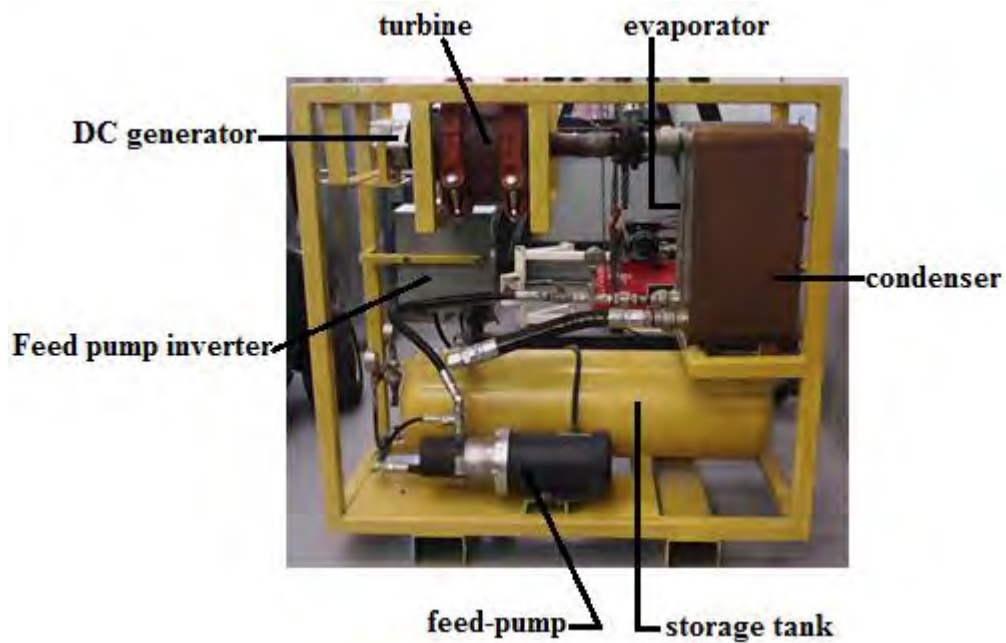


Figure 7.1: 10 kW ORC IT 10 unit [7.2]

7.3 Description and Installation of the Heater

The thermal load, heat transfer fluid cycle, was provided through an electric water heater unit supplied by Kwikot, Durban, South Africa [7.3]. The particular unit adopted for these experiments was a 450 litres vertical unit installed with 6 x 3 kW standard immersion elements, connected through a 3 phase isolator to a 3 phase circuit mains. For these experiments, the usual thermostat (graduated between 30°C and 70°C) was replaced with one that reaches a maximum temperature of 80°C, an 11 inch long thermostat supplied by WireOhms, Durban, South Africa [7.4]. The electric water heater was also supplied with a water circulation pump (with specifications: 220 V AC/DC electric power) with a required flow rate of 22 gallons per minute (83 litres per minute). The water heater unit is shown in Figure 7.2.

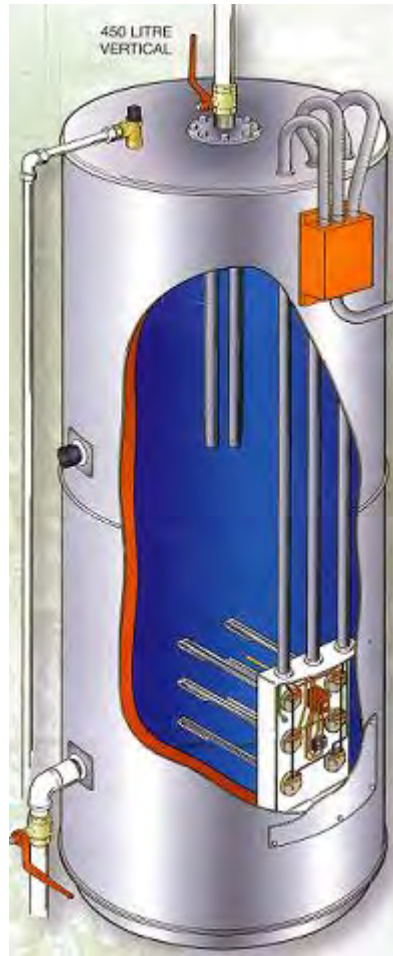


Figure 7.2: 450 litres vertical electric water heater unit [7.3]

The water heater was connected through heavy duty hoses to the evaporator heat exchanger of the ORC unit first before being filled up with 450 litres of heat transfer fluid.

7.4 Description and Installation of the Heat Sink

The cooling fluid (CF) cycle was an open water cooled circuit consisting of a hose delivering cooling water from an industrial water line to the inlet port of the condenser and another hose conveying the exhausted water from the outlet port of the condenser to an open field, 'the heat sink'. The cooling water temperature depended on the ambient conditions; in the theoretical models this was assumed to be ranging from 35°C to 50°C. The flow rate required was 44 gallons per minute (or 166 litres per minute).

7.5 Measuring Equipment and Instruments

The ORC unit was supplied with fitted analogy pressure gauges and these were used to record the pressure readings. The unit did not have measuring instrumentation for readings of temperatures and fluid flow rates, nor for energy, power and torque measurements. In order to

measure the temperature at different positions in the fluid circuit, an infrared digital thermometer was to be used. The energy output was to be determined by using a multimeter to measure current and voltage. A variable electrical load was connected to the generator to facilitate the amperage and voltage measurements.

It is proposed that adequate measuring instruments and data-logging equipment be installed for future experiments.

7.6 Testing Procedure/Methodology

The experimental set-up is shown in the schematic representation and photograph in Figures 7.3 and 7.4.

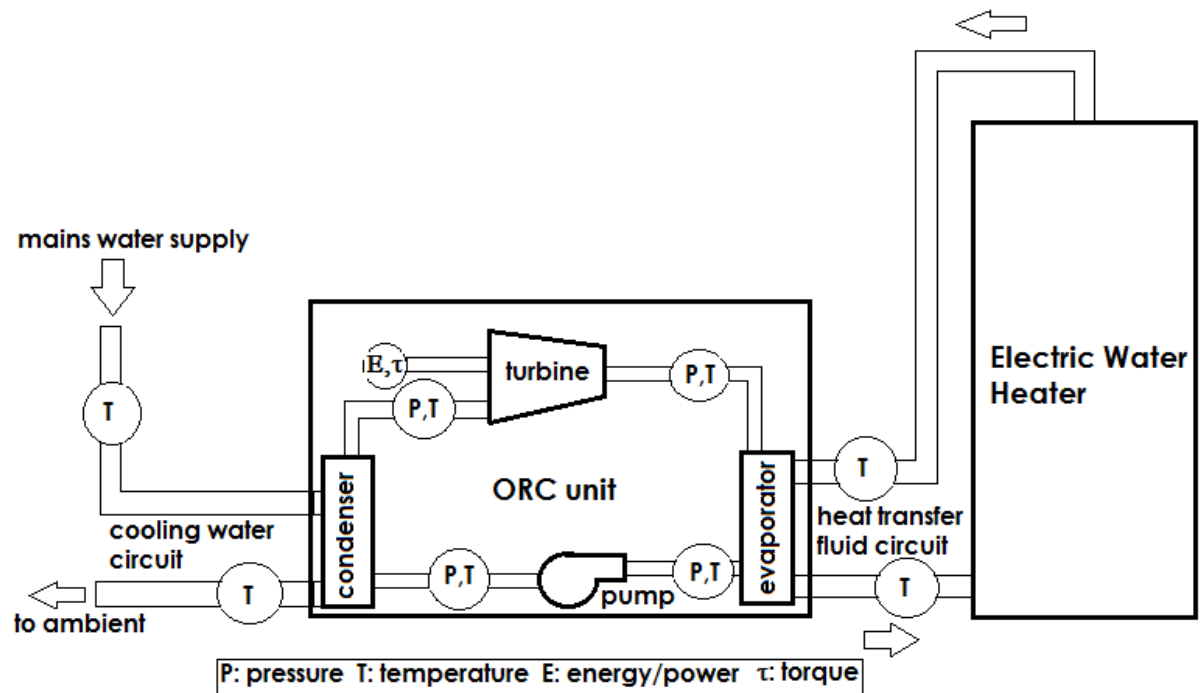


Figure 7.3: Test setup layout

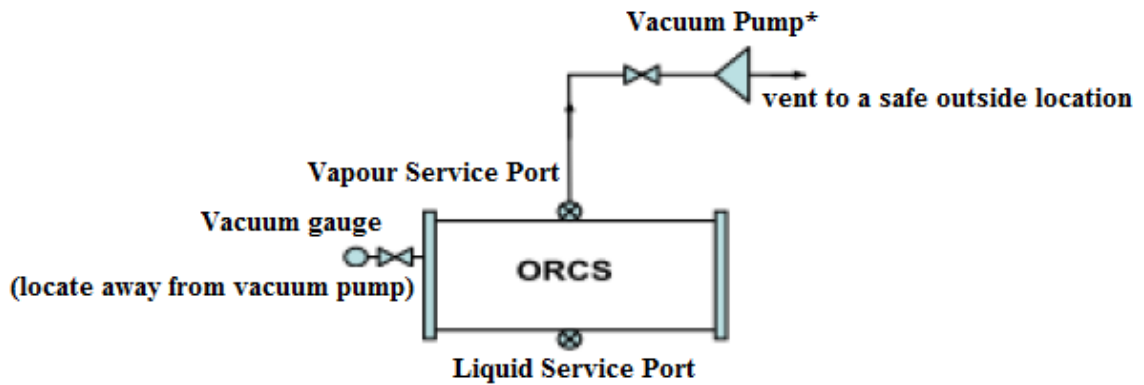


Figure 7.4: Test setup photograph

7.6.1 Leakage Testing of ORC Unit before Charging with Refrigerant

The following tests were conducted according to the IT10 manual before charging with the working fluid (maximum operating pressure 280 psi (1931 kPa)):

- Physical Inspection – to check for any damage to the hoses or joints;
- Air leakage test: fill ORC system with air to maximum 100 psi (689.5 kPa) for 3 hours and record pressure readings before and after 3 hours; if leaks are detected follow procedures in the manual to repair the leaking points.
- Nitrogen gas leakage test: fill ORC system to maximum 150 psi (1034 kPa) for 24 hours and record pressure readings before and after 24 hours; if leaks are detected follow procedures in the manual to repair the leaking points.
- Ultrasonic leak test: fill with dry nitrogen to 860 kPa and use an ultrasonic leak detector or use a trace gas leak detecting procedure; if leaks are detected follow procedures in the manual to repair the leaking points.
- Vacuum leakage test; evacuate the system to less than 500 microns (mercury) using a good vacuum gauge; if the vacuum pressure does not rise more than 300 microns in 10 minutes, the system is tight. If the pressure rises more than 300 microns and then becomes steady, there is still moisture in the system. If pressure rises continuously, there is still a leak in the system; follow procedures in the manual to repair the leaking points. Figure 7.5 shows the evacuation set-up.



***If a recovery/charging unit is used instead of a vacuum pump, consult the recovery equipment manufacturer for recommended evacuation connections and procedure**

Figure 7.5: System evacuation

7.6.2 Charging ORC unit with Refrigerant

Charging was conducted according to the IT10 manual; the system was to be charged with 58 kg on liquid R245fa (or R134a in our case). Charging may be accomplished using either the gravity method or the pump-assisted method from single-port source cylinders (Figure 7.6); or the push-pull liquid transfer method for source cylinders having separate liquid and vapour ports (Figure 7.7).

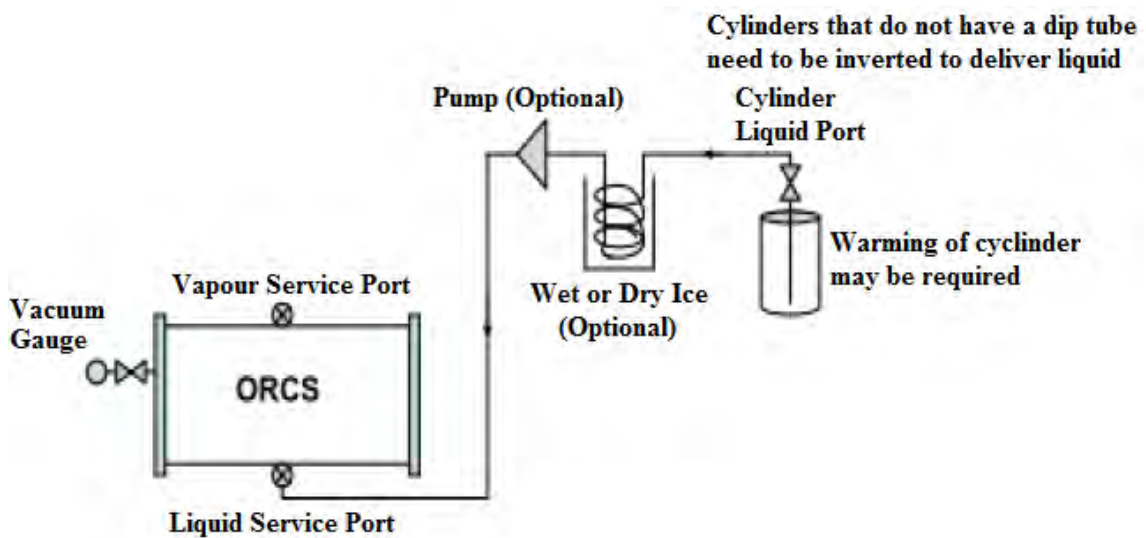
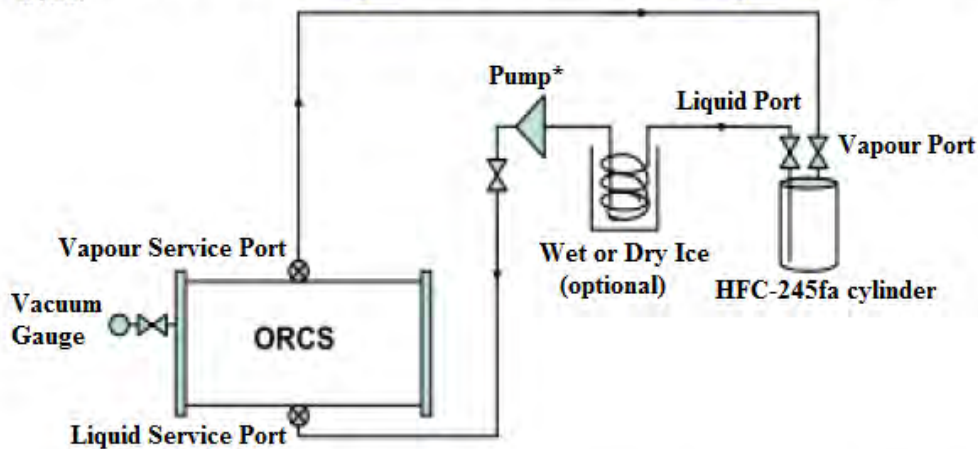


Figure 7.6: Single port gravity or pump-assisted charging

1. For large systems, break vacuum by first charging vapour to a system pressure of 11.0 inches mercury vacuum.
2. Open cylinder liquid port and valves along liquid transfer line, then start pump to begin charging liquid.



***If a recovery/charging unit is used instead of a pump, consult the recovery equipment manufacturer for recommended connections and charging/recovery procedures**

Figure 7.7: Push-pull liquid transfer charging

For these experiments, the single port gravity method was used for charging R134a into the system.

7.6.3 Connecting the Heater Unit

Two hose-lines connected the electric heater tank to the evaporator on the IT10, the hot water outlet of the heater tank was connected to the suction port of the circulation pump, and the discharge port of the circulation pump was connected to the hot water inlet port of the evaporator. The outlet port on the evaporator was connected to the inlet port of the heater unit. The hoses used were heavy duty rubber hoses of 2 inches (51 mm) internal diameter; appropriately selected (sized) galvanized metal pipe fittings and heavy duty clamps were used to secure the hoses to the various ports. Electrical and plumbing connections were made according to the Kwikot manual.

7.6.4 Connecting the Cooling Cycle

The cooling unit used in the test runs consisted of two hoses, one connected to the mains water supply and to the inlet port to the condenser and the other to the outlet port from the condenser and left to dump into the sink. This was considered adequate owing to the shorter experiment cycle times and hence less overall quantity of cooling water required or wasted, otherwise a cooling water reservoir would be required for a closed cooling fluid cycle.

7.6.5 Electrical Circuit (Load) for Measuring Power Output

Figure 7.8 shows the rotational speed (rpm) - output voltage characteristics of the permanent magnet DC generator in the IT10 unit.

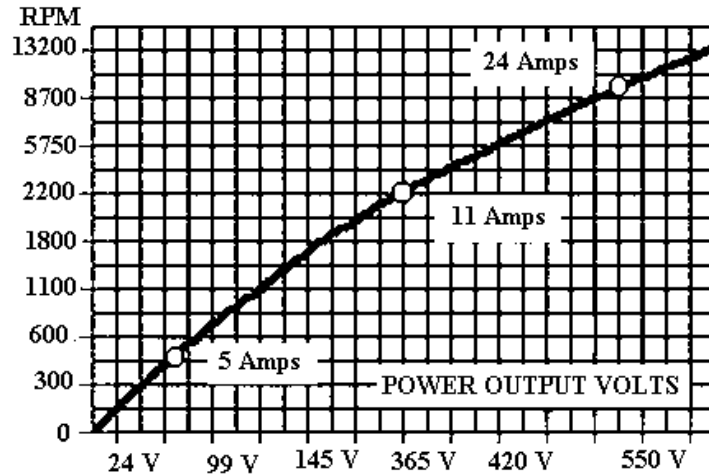


Figure 7.8: rpm-volt characteristics of DC generator [7.5]

In order to measure the power output of the generator at a given turbine speed, the generator needs to be loaded so as to enable measurements of the output voltage and current. The most appropriate way to achieve this would be to employ a variable resistor as shown in Figure 7.9. However, the required 20 ohms - 30 ohms variable resistor was not available for purchase locally; as such we opted to use heating elements connected in parallel as shown in the circuit of Figure 7.10 and the load would be varied by shutting off some of the parallel loads.

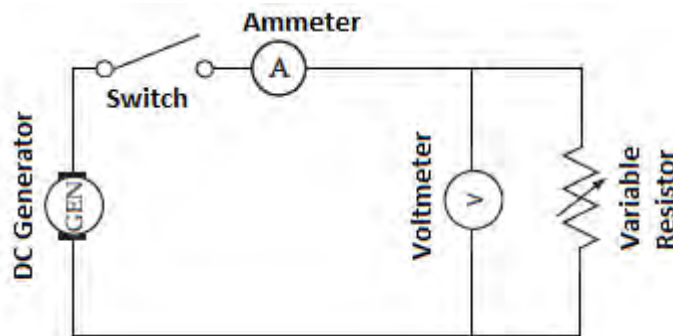


Figure 7.9: Variable resistor load connection to DC generator

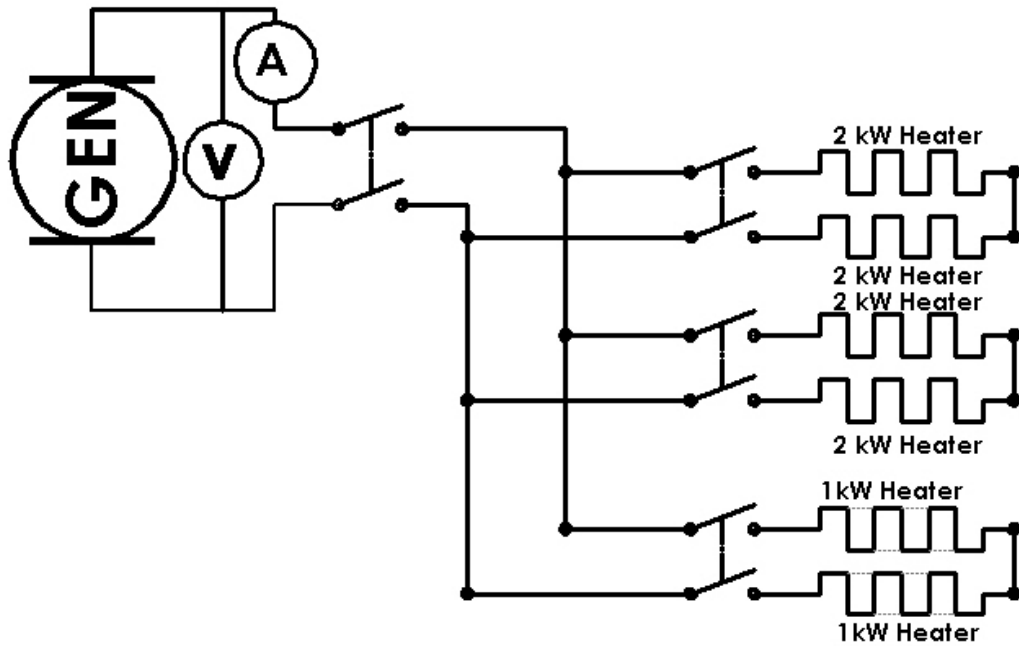


Figure 7.10: Circuit – parallel heating elements load connection to DC generator

7.6.6 Pump Settings

In order to run the pump at the various speeds the required settings were programmed onto the Titan C Series inverter according to the procedure in the inverter manual [7.1].

7.6.7 Running the Power Cycle

- Step 1 Switch on the electric heater and leave it on until the temperature attains 80°C. Record the temperature.
- Step 2 Switch on the heat transfer fluid circulation pump and wait for the heat transfer fluid temperature to stabilise. Record the temperature.
- Step 3 Switch on the cooling cycle (i.e. open the water tap).
- Step 4 Switch on the working fluid cycle pump; with all valves set to the open position.
- Step 5 Record pressure, temperature, current and voltage readings.
- Step 6 Repeat the recordings after two and half minutes and after 5 minutes (i.e. end of test run)
- Step 7 Repeat steps 1 to 6 above until a set of ten test runs has been attained.

7.6.8 Problems Faced

The biggest problem we faced before we could even perform trial runs were the major leakages experienced during the air-leakage tests. This was independently confirmed by research colleagues at the Laboratory for Solar Energy and Energy Savings, Burkina Faso. After several months of checking connecting pipes, joints and valves and attempting to seal all leakages detected and not getting anywhere close to solving the leakages, it was finally agreed that the

turbine exhaust unit (Figure 7.11) was defective and had to be replaced. Manufacturing drawings for the new exhaust piece were produced and the new unit was produced with assistance of two companies, Mendel Welding, Gaborone, Botswana [7.6] and Rubber, Gasket and Hose, Durban, South Africa [7.7], who specialise in flexible stainless steel reinforced hoses.



Figure 7.11: Defective turbine exhaust unit

Figures 7.12 and 7.13 show extracts from the drawings and a picture of the replacement part in process of being manufactured.

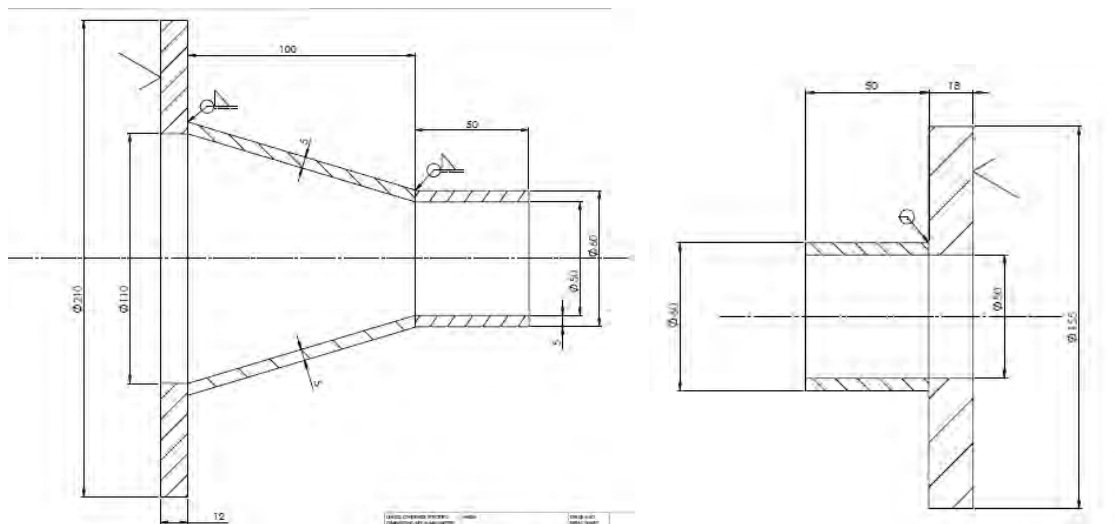


Figure 7.12: Extracts from the flange drawings



Figure 7.13: Replacement flange in process before fitting flexible hose

The second problem we encountered was procurement of services, such as hire of equipment for charging/recovery of nitrogen, system evacuation, and charging/recovery of refrigerant; and finding suppliers of materials, basically nitrogen and the refrigerants.

Another major problem was the scanty supplier's information regarding setting up of the ORC unit; this caused delays as we attempted to consult the supplier, sometimes in vain, and other experts available locally.

7.7 System Experimental Results

Having satisfied ourselves that the test set-up was satisfactory, we proceeded to run the first experiments on Saturday, January 9, 2016; however, the turbine was not turning and therefore there was not electrical power output. Following failure of the experiments several inspections were conducted on January 21 and 25, 2016 and February 19 and 20, 2016 on the electrical and flow pipe connections as well as on the pumps before a decision was made to defer any further experiments until a solution to the defective turbine unit has been found; the supplier has since agreed to exchange the defective unit with an advanced version currently under development.

7.8 Discussion and Conclusion

Adequate description of the test set-up, experimental procedure and remedial measures taken during the set-up has been provided. However, following failure of the experiments, the experimental stage has been postponed until another none defective and advanced IT10 unit is received. Nonetheless, the data provided by the supplier show the ORC unit as a viable power supply [7.8]; this will be corroborated after finalisation of the experiments.

References

- [7.1] Titan_C_Series_User_Manual, Cerus Industrial Corporation 3101 SW 153rd Drive Suite 318 Beaverton OR, 97006 1-800-962-3787 Get all the latest in motor controls ... 11/7/03 Document #0003M-00-03.
- [7.2] Infinity Turbine LCC. ORC Engine Generator Set IT10, 10 kWe Full Build Version 11 Installation Manuals; 2012.
- [7.3] Kwikot product brochures; Kwikot Kwa-Zulu Natal Division; 814 Peter Close, Springfield Park, Durban, South Africa,
www.kwikot.co.za/Contact/Contact%20Details.php accessed September 30, 2014
- [7.4] WireOhms, Durban, South Africa.
- [7.5] Global Energy and Infinity Turbine LLC, Madison, Wisconsin, USA.
- [7.6] Mendel Welding, Broadhurst Industrial, Gaborone, Botswana.
- [7.7] Rubber, Gasket and Hose, 166 Bluff Road, Jacobs Industrial Park, Jacobs, Durban, South Africa.
- [7.8] Giese G., President, Global Energy and Infinity Turbine LLC, Madison, Wisconsin, USA.

CHAPTER 8 EVALUATION OF RESEARCH OBJECTIVES

8.1 Introduction

This chapter examines the research objectives set out at the commencement of the study and evaluates to what extent each objective has been accomplished.

8.2 Analysis and Evaluation of Research Objectives

Objective 1: To develop and optimise mathematical models, computer simulations, and physical models of a low temperature solar thermal energy conversion system based on the Rankine cycle for conversion of low temperature solar energy to electrical energy. Mathematical and computer models will be used in the design of the physical models. Optimization will include thermodynamic, fluid mechanics and heat transfer analyses.

Result: mathematical models have been developed for the organic Rankine cycle (ORC), as well as for the components which include solar field, evaporator, condenser and turbine. All these mathematical models were computer simulated on the engineering equation solver (EES) platform. Physical models were proposed based on the mathematical and computer models. However, these could only be partially implemented due to technical and funding constraints; thus only a partial laboratory simulated model was implemented. The results of these models and simulations have been published in journals and conferences. Table 8.1 lists the developed models and the corresponding papers (which appear in the Appendix A4), and thesis chapters they have been published in:

Table 8.1: Publication list for the models

model	Publication reference in appendices
ORC system model	1. Conferences: A4.14, A4.13, A4.12, A4.10 2. Journals: A4.7, A4.6
Solar field model	1. Conferences: A4.12, A4.11 2. Journals: A4.6, A4.5
Evaporator model	1. Journal: A4.4
Condenser model	1. Journal: A4.3
Turbine model	1. Conferences: A4.9 2. Chapter 5 of thesis
Physical model	1. Chapter 7 of thesis (note: the experimental model failed)
Economic and Environmental model	1. Journal: A4.2

Also included in the appendices are the corresponding computer simulation codes and results for the models.

Objective 2: To undertake an extensive survey, through literature research, web-based search tools, and on-going research in other institutions, of low to medium temperature energy conversion concept plants and to evaluate their suitability as low temperature energy conversion cycles.

Result: A number of low temperature conversion cycles were identified and they include solar thermal ORC, solar thermal Kalina cycle, Solar Chimney and SNAP (a downdraft chimney system). In evaluating the sustainability of low temperature solar thermal cycles it was established that both the Solar Chimney and SNAP plants were not feasible until such a time that chimneys of much greater heights in the range of several hundreds of meters can be feasibly designed structurally and economically, possibly following development of ultra-light and lower cost structural materials and techniques. Kalina was considered a complicated cycle due to the dual phase working fluids of ammonia and water as well as due to requirements for various additional safety measures because of combustibility and toxicity of ammonia [8.1]. The organic Rankine cycle was considered to be suitable due to its simplicity of layout and lower operational and maintenance costs.

A number of ORC expander suppliers were identified including: Infinity Turbine LLC, USA; Green Energy, Australia; ORMAT Tech., Inc. USA; ELECTRATHERM, USA; ENEFTECH, Switzerland; Freepower Ltd., England; and Turbolina® GmbH & Co. KG, Germany.

A detailed survey of existing worldwide ORC plants has been presented by Desai (2008); [3.15]. A computer model of a Regenerative Solar-Assisted Rankine Power Cycle has been presented by Lansing FL (1977); [3.16]. Solar pond power plants of electric capacities from a few ten kW up to a few MW have been built in at Beit Ha'Arava, Israel; El Paso, Texas, USA; and Pyramid Hill, Australia.

A number of working fluids such as n-pentane, Benzene, n-butane, n-hexane, Isobutene, Isohexane, Isopentane, n-perfluoro-pentane, R113, R123, R141b, R236ea, R245ca, R245fa, R365mfc and Toluene were identified as possible candidate working fluids.

The above survey and research findings are contained in Chapter 3 of this report. Research on specific disciplines such as solar, heat exchangers, turbines, and economic and environmental analyses are reported in the corresponding chapters and publications.

Objective 3: To carry out an extensive study of working fluids and evaluate their potential for use in a low temperature energy conversion cycle.

Result: The study of working fluids revealed that the selection of the working fluid for an ORC is critical in that it should optimize cycle efficiency and match the thermodynamic properties of the heat transfer fluid while maintaining simplicity in cycle configuration. The working fluid

should also meet other operational or regulatory requirements such as lower global warming potential, lower ozone depletion potential, non-corrosiveness, safety requirements such as lower toxicity and lower inflammability; and preferably have a low purchasing cost. Sixteen fluids were identified as potential working fluids for this research and are listed in Table 3.1 of Chapter 3.

The system model analysed 14 fluids and categorized them on the basis of their temperature-entropy (T-s) characteristics during the expansion phase into negative T-s, positive T-s, and isentropic T-s. The results, (Table 2 in publication A4.6 in the appendices) showed that six working fluids (Benzene, n-butane, Isobutene, R141b, R245fa, and R123) had isentropic T-s, five working fluids (n-pentane, n-hexane, Isopentane, R113, and Toluene) had positive T-s, and three working fluids (R22, R134a, and Water) had negative T-s. Isentropic T-s is preferred in that no additional cycle components such as recuperators (for positive T-s) and superheaters (for negative T-s) are required. Table 4 in publication A4.6 in the appendices lists the Global Warming Potential (GWP) and the Ozone Depletion Potential (ODP) of the working fluids.

Four working fluids with an isentropic T-s (n-butane, isobutene, R245fa, R123) were further analysed in the subsequent component models of the evaporator, condenser and turbine; R134a was also included as it was a recommended working fluid from the supplier of the test power block, the IT10 Infinity Turbine unit. The results of the evaporator models showed that isobutene was the most optimal from four candidate working fluids (publication A4.3 in the appendices). The condenser model on the other hand showed n-butane giving the best performance with R123 and isobutene giving the worst performance (publication A4.2 in the appendices).

Two turbine models were developed: a single stage axial turbine and a 90° inflow radial turbine, both using four working fluids: n-butane, isobutene, R245fa and R134a. For the axial models Isobutene provided the best performance and R245fa the worst both in terms of total-to-total and total-to-static efficiencies, however, variations were minimal. For the radial models, R245fa provided the best performance and Isobutene the worst in terms of total-to-total efficiencies.

Objective 4: To install the developed physical model in a suitable site and carryout extensive evaluation of the model for a lengthy period of time (at least 12 months). Data recording will be accomplished via digital reading and storage modules.

Result: This was not achieved due to several factors. Firstly, the laboratory test unit, the turbine unit was defective and could not produce electrical power output. Secondly, due to funding limitations it was not possible to install a solar field. Thus, the only experiments that could be attempted were based on a simulated heat source, a 450 litres electric geyser. Other problems encountered were procurement of test materials such as nitrogen gas and refrigerant R134a, and we could not locally procure a 20 ohms - 30 ohms variable resistor for load measurements on the DC generator. We finally settled for a laboratory built load circuit consisting of 1000 W and 2000 W geyser elements wired through isolators and connector blocks to the DC generator; the

elements would be immersed in containers filled with water during the experiments to simulate a variable electric load.

The experiments have been put on hold until the supplier delivers another experimental model. However, supplier data was used to conclude, for now, the experimental aspect of the research.

Objective 5: To undertake overall economic and environmental performance evaluations of the developed and the proposed low temperature solar thermal energy conversion designs.

Result: This was undertaken and the outcome indicates that the 10kW low temperature solar thermal concept plant is economically not feasible, under the current scenario whereby the power block is imported at a high price and the price of the solar collector field remains as high as computed. The options include locally designing and manufacturing the turbine and solar collectors as well as sourcing all other cycle components locally. This is based on the negative net present value (NPV) (ZAR -126 389.64) obtained under the current scenario. When the other option of local procurement is assumed and the power block and the solar collectors are assumed at half price a positive NPV is obtained (ZAR +853 610.36).

The energy payback period (EPBP) was obtained as six years while the Carbon payback period (CPBP) was computed as 426.9 days (1.17 years); both figures viewed as comparable to other renewable energy systems.

The implications of these analyses indicate that the low temperature solar thermal concept plant has potential to be a cost effective and environmentally beneficial net clean energy producer.

Objective 6: To publish the research results in peer reviewed conference papers, international journals and in a research thesis.

Result: This has been achieved; seven peer reviewed journal papers have been published and seven peer reviewed papers presented to conferences and published in conference proceedings. Copies of the publications are included in Appendix A4.

8.3 Discussion and Conclusion

Most objectives have been achieved. However, the most critical ones to determine the technical feasibility of a small to medium sized, low temperature solar thermal power plant have not been satisfied. Overall, the research can be considered to have been a success judging by the quantity and quality of research output.

References

- [8.1] <http://www.google.com/patents/US5007240> accessed August 2015.

CHAPTER 9 CONCLUSIONS AND RECOMMENDATIONS

9.1 Introduction

The research intended to investigate the technical, economic and environmental viability of a small to medium sized (10 kWe), low temperature (below 300 °C) solar thermal organic Rankine cycle as a power generating plant. Such a concept plant would have the potential of improving access to clean energy, increasing plant energy efficiency and extending utilization of waste heat.

9.2 Conclusions

Extensive information research was conducted and it covered a number of books, journal papers, websites and consultations with other researchers and equipment suppliers. The research topics varied from low temperature thermal cycles, working fluids, solar collectors, heat exchangers, turbines, thermal storage, economic and environmental assessment, etc.

Preliminary small-scale concept plants of sizes 0.5 kWe and 2 kWe which were laboratory scale models and 10 kWe, a field model, were developed, modelled and computer-simulated (using the Engineering Equation Solver) with 14 different working fluids and three plant configurations. The thermal efficiencies varied from 10.38% for R245fa (conventional Rankine configuration) to 12.04% for n-pentane (Rankine with recuperator configuration).

Through initial pre-modelling analysis, it had been estimated that the 0.5 kWe model would require a 9-collector solar field (solar collector size 1840 mm x 1650 mm) and the 10 kWe model would require a 180-collector solar field. The solar field modelling was conducted with ethylene glycol water (50% concentration) as the heat transfer fluid. The model included simulations of hourly solar insolation values, and solar collector and storage tank energy balances. The absorber temperature increased from ambient temperature of 20°C to slightly over 100°C at noon while the ethylene glycol water attained a maximum of slightly below 100°C at the exit of the solar collector and about 90°C in the storage tank respectively. The transparent cover had a much lower temperature ranging from ambient temperature to about 40°C.

An evaporator heat exchanger model for a low temperature solar thermal organic Rankine cycle was developed and evaluated on the EES platform. Simulations were conducted for each of the four candidate working fluids and for each of the three thermal loads of 4.2 kWth, 16.8 kWth and 84.2 kWth respectively representing cycles with power outputs of 0.5 kWe, 2 kWe and 10 kWe. Parameters considered included heat exchanger size, pressure drop and fluid velocity on both the tube and shell sides. Reference values for pressure drop and velocity were based on the tubular exchanger manufacturers' association (TEMA) standards. The models developed satisfied the thermal loads, pressure drops and fluid velocities for the 4.2 kWth and 16.8 kWth loads; for these thermal loads the double pipe heat exchanger model was adequate in terms of

both material and manufacturing costs (size) and operational costs (pressure drop and velocity limits). On account of very high pressure drops and therefore costly pumping requirements it was proposed to redesign the heat exchanger model for the 84.2 kWth thermal load to a multi-tube, shell and tube or plate heat exchanger; assuming a tube length of 5m as acceptable a simple conversion to a single pass shell and single pass tube configuration was proposed. In terms of working fluid performance, the results showed that from the four candidate working fluids, models developed with isobutene as the working fluid were the most optimal, followed by n-butane, and then R245fa, and finally R123. The results showed that a glycol water mass flow rate of 2.5 kg/s was adequate for the two thermal loads of 4.2 kWth and 16.8 kWth for all four working fluids both in terms of shell side pressure drops and fluid velocities.

A condenser heat exchanger model suitable for incorporation into a low temperature solar thermal power cycle was developed. The model consisted of a flow of vapour over a bundle of horizontal tubes. The simulations showed the effect of condensate inundation in reducing the heat transfer capacity of tubes low down in a column of horizontal tubes. The simulations also showed that Nusselts correlations resulted in more conservative values compared to the Kerns method. All the working fluids depicted similar device thermal exchange characteristics; n-butane performed better than the other fluids and R123 and isobutene performed the worst. Sizing of the heat exchanger was determined by the number of tube rows and columns; in this case, the simulations showed that 8 rows by 6 columns would be adequate for the given heat exchanger configuration and thermal load. For all combinations of correlations two observations can be made: condensate heat transfer coefficient varies from maximum on the first tube to minimum on the last tube; and condensate heat transfer coefficients are highest with n-butane, followed by R134a, R245fa, and are lowest for R123 and isobutene. The Kerns method gives higher values of the condensate heat transfer coefficient, varying from about 900 W/m²°C to 1900 W/m²°C, compared to the Nusselts correlation, where corresponding values varied from about 700 W/m²°C to 1900 W/m²°C; the heat transfer coefficient for the first tube was almost the same regardless of whether the Nusselts or the Dhir and Lienhard correlation was used. In terms of thermal loads n-butane resulted in the highest value followed by R134a, R245fa, and R123, with the lowest being obtained with isobutene. The average outlet temperatures of the ethylene glycol cooling fluid for each of the working fluids showed a continuous decline with increases in cooling fluid mass flow rate, with n-butane resulting in the highest outlet temperatures. Outlet temperatures varied from a maximum of approximately 28.5°C to a minimum of approximately 25.8°C.

The turbine is the single most critical component in a thermal conversion cycle. Turbines for small scale applications should have few stages, preferably only a single stage. Review of available expander designs adapted for low temperature ORCs was undertaken and results published. The review examined positive displacement machines that can be adapted for use as expanders in small to medium scale ORC systems and described the required modifications; the machines included rotary vane type compressors, rotary screw compressors, scroll type compressors, piston type compressors and swash plate type compressors. The most common type of expander used in small scale ORC systems are those based on the positive displacement type due to their simplicity and low cost. Volumetric expanders are widely applied for large scale power generation systems and have achieved high turbine efficiency and high reliability. Factors that influence the type of expander adopted in a power generation cycle are shaft speed,

mass flow rate, nominal power range, specific cost and operating conditions in general. Operating conditions refer to inlet and outlet pressures (pressure ratio), temperatures and quality of working fluid at the end of the expansion process, mass and volumetric flow rates and nominal shaft speed. The two positive displacement expanders that have been successfully developed and widely applied are the scroll type and the twin-screw expanders; this is mainly due to their smooth and low noise operation with minimum vibrations and compactness, with minimum number of moving parts. The reciprocation motion in the other types such as the vane type, and the reciprocating piston and swash plate limits their applications to very low speeds. Scroll type expanders are mainly confined to light applications with lower pressure ratio, lower speed and lower power rating, typically below 30 kWe. In order to avoid excessive leakage the rotary twin screw type is adapted to handle relatively higher pressures, speeds and power ratings owing to their robustness.

Preliminary design models based on the velocity expander type for both radial inflow and axial configurations, and suitable for a 10 kWe low temperature organic Rankine cycle, were developed. The preliminary designs were presented in terms of geometric parameters of flow angles, blade diameters and heights; the preliminary design also includes thermodynamic parameters of stagnation and static pressure, temperature and enthalpy; the thermodynamic analyses were conducted within the cycle temperature ranges of the evaporator and condenser. Although the presented design models are not complete, this work has shown that small turbines for low temperature cycles are a feasible design option. Further, this work has shown that for the same rotational speed the radial turbine requires less mass flow rates compared to the axial turbine. The radial turbine has a higher pressure ratio too compared to the axial counterpart. The total-to-total expander efficiency tended to be the same for both turbine models with the axial turbine having a slight edge over the radial turbine. In terms of size, the axial turbine performed better by requiring a lesser diameter – almost a quarter of that required by the radial turbine. Economic and environmental analyses for the 10 kWe low temperature solar thermal power plant were performed and the results were published in a journal article. It was evident from the negative NPV value (ZAR -126 389.64) obtained that under the current scenario a 10 kW low temperature solar thermal concept power plant is not an attractive investment option, economically. This is mainly due to the higher initial capital requirements, resulting largely from the higher costs of the IT10 power block (ZAR 600 000), which is charged at research and development (R&D) rates, and the cost of the solar field (ZAR 1 260 000 solar collectors only). Under an assumed scenario, where the power block and the solar collectors are designed and produced locally their costs could drop by 50% or more, in which case the NPV realised becomes positive (ZAR +853 610.36). Commercially available larger turbine generators in the Megawatt range cost from USD 450 to USD 950 per kW.

The energy payback period (EPBP) obtained was six years which is comparable with other similar technologies. A typical solar power system is reported to payback after about four years, a photovoltaic system between one-and-half and three-and-half years, while a small wind turbine could take between fifteen to fifty years. Carbon payback period (CPBP) on the other hand was computed as 426.9 days (1.17 years); this figure too is comparable with what has been obtained by other researchers such as 2.21 years obtained for a solar water heater by Marimuthu C. and Kirubakaran V. [9.1], and CPBPs periods (excluding transport) obtained as 6.0, 2.2, and 1.9 years for PV system, solar thermal-individual and solar thermal-community respectively, by

Croxford Ben and Scott Kat [9.2]. The results obtained here are considered partial or conservative because the scrap and recycling values of the materials or components following decommissioning has not been taken into account; this would reduce the embodied energy and emissions. The implications of these analyses do, however, indicate that the low temperature solar thermal concept plant has potential to be a cost effective and environmentally beneficial net clean energy producer.

The experimental set-up and experimental procedures were successively achieved; several remedial measures were taken during the set-up but the experiments failed due to defective equipment. The experiments had to be postponed pending supply by the manufacturer of a non-defective and more advanced IT10 unit. The data provided by the manufacturer nonetheless did indicate that the ORC unit is a viable power supply; this will be validated when experiments have been concluded.

Seven peer reviewed journal papers have been published and seven peer reviewed papers presented to conferences and published in conference proceedings.

Overall, the research can be considered to have been a success judging by the quantity and quality of research output. Outstanding tasks will be undertaken in further research work as outlined under 'Recommendations' below.

9.3 Recommendations

A proposal is being drafted for further continuation of the research; at this stage, this is an expression of interest between the researcher and the supervisor to continue with the research in whatever possible format, whether as 'post-doctoral' or as 'collaborative research'. The draft document proposes:

1. To halt current efforts to repair the defective IT10 unit; the supplier has agreed to have it traded in for an advanced version on which further testing will be conducted.
2. To finalise the turbine designs by following through with the CFD modelling that will lead to the manufacture and testing of prototypes.
3. To produce a local low temperature ORC prototype for testing, with possibilities of commercial production.
4. All other concerns raised during the experimental stage covering: measuring instruments for flow and temperature, leakage repairs (on the cooling cycle, heating cycle and ORC cycle), pumps, electric load measurement and charging of refrigerant (R245fa/R134a) must be resolved before any experiments are undertaken.

9.4 Way Forward

Following successful completion of the experimental stage, follow through with:

1. Finalising the turbine designs by CFD modelling, leading to manufacture and testing of prototypes.
2. Producing a local low temperature ORC prototype for testing, with possibilities of commercial production.

References

- [9.1] Marimuthu C. and Kirubakaran V., Carbon payback period and energy payback period for solar water heater, *International Research Journal of Environment Sciences*, Vol. 3(2), 93-98, February 2014, ISSN 2319–1414, pp 93-98.
- [9.2] Croxford B. and Scott K., Can PV or solar thermal systems be cost effective ways of reducing CO₂ emissions for residential buildings, Bartlett School of Graduate Studies, University College London: *Renewable Energy - Key to Climate Recovery*, American Solar Energy Society, 2006, available at <http://www.cs.rug.nl/~pagani/publications/techRepBB.pdf>

LIST OF APPENDIXES

Appendix A1: Inception Proposal	70
Appendix A2: EES Codes	75
Appendix A3: Results	102
Appendix A4: Publications	172

APPENDIX A1 INCEPTION PROPOSAL

University of KwaZulu-Natal, Faculty of Engineering

Research Project Proposal

- 1.1 Name of student:** Shadreck Mubiana Situmbeko **1.2 Student no.** 209542168
- 1.3 Degree Programme:** PhD in Mechanical Engineering
- 1.4 Topic:** Low Temperature Solar Thermal Energy Conversion System
- 1.5 Supervisor:** Dr. F.L. Inambao
- 1.6 Co-supervisor(s):**

2 RESEARCH QUESTION:

Continuing growing environmental and climate change concerns as well as the current power supply deficits in Southern Africa call for urgent R&D work to attaining commercialization of alternative energy sources. Solar thermal energy is one such energy source whereby successful technology take-off is faced with several challenges. Solar thermal technical research challenges include the need for comprehensive resource mapping, performance competitiveness against conventional energy sources, and cost effectiveness on parts, operation and maintenance.

One way to address performance and economic competitiveness is to investigate ways of improving the solar thermal system efficiency; more specifically the optical efficiency of the collector materials, the thermal efficiency of the collector construction geometry as well as the process efficiency of the thermal-mechanical conversion.

This project will concentrate on the economic performance and process efficiency of a solar thermal energy conversion system by focusing on the development and optimization of a low temperature solar thermal system. This is one area that if successfully developed has potential for improving the energy efficiencies of plants, processes and buildings by being able to harness low temperature energy sources such as waste heat and non-concentrated solar radiation. Such a system typically operates in the temperature range below 300°C.

The demonstration prototype will be implemented on the basis of the Adapted Rankine cycle using an organic fluid as a working fluid and employing low to medium temperature solar thermal collectors. Development of new working fluids remains an active area of research; some fluids currently under active investigations include ammonia and carbon dioxide.

3 BACKGROUND INFORMATION

Solar thermal energy conversion for power generation is an active research area more so for low temperature systems. A number of high temperature thermal power generation concept power plants have been installed worldwide.

APPENDIX A1 INCEPTION PROPOSAL

Low temperature thermal energy conversion research is quickly gaining momentum owing to its immense potential for utilizing waste heat and thus raising plant efficiency as well as its viability for remote and small scale operations.

Low temperature solar thermal typically uses flat plate solar collectors; flat plate collectors are relatively cheaper and easier to operate; its use is currently mainly limited to water heating and space heating. Use of low temperature thermal for power generation requires modifications to the conventional energy conversion cycles to enable conversion at lower temperatures.

Several thermal-mechanical conversion cycles have been developed e.g. diesel, otto, Rankine, Brayton, Kalina. However, majority of these have been developed for high temperature systems. Research is currently on-going to develop low temperature thermal conversion technologies; examples would be the patented Kalina and the Organic Rankine cycles.

This project will focus on the Rankine cycle. The Rankine cycle will be modified to suit low temperature operation. One aspect will be to switch to a working fluid that attains phase change at low temperatures. Further considerations will be placed on aspects of heat transfer and fluid flow losses.

4 OBJECTIVES

- 4.1 To evaluate the suitability of various thermal-mechanical conversion cycles for low temperature solar thermal energy conversion applications.
- 4.2 To develop and optimize a hypothetical computer model of a solar thermal energy conversion adapted Rankine cycle based on thermodynamic, fluid mechanics and heat transfer principles.
- 4.3 To investigate the thermo-mechanical efficiency and overall economic and environmental performance of a low temperature solar thermal energy conversion system based on the adapted Rankine cycle.
- 4.4 To investigate the performance of various working fluids including their blends in an adapted Rankine cycle.
- 4.5 To review the design and performance of the major cycle components of a low temperature solar thermal energy conversion plant and carry out an optimization of their energy efficiencies, economic and environmental performances.
- 4.6 To design, construct and install a concept plant of a solar thermal energy conversion adapted Rankine cycle.
- 4.7 To propose a final working design suitable for a small scale power generating plant based on the findings of the project.

APPENDIX A1 INCEPTION PROPOSAL

5 METHODOLOGY

The research will consist of Information Research, Theoretical and Computer Simulations and Experimentation.

The information research stage will involve a review of literature, study of international solar thermal energy projects and consultations with stakeholders in industry and academia. Several thermal-mechanical conversion cycles will also be reviewed to evaluate their suitability (or potential for modification) for low temperature solar thermal application.

A Solar Thermal Energy Conversion Computer Model will be developed and simulated for various working conditions. The model development will be based on sound thermodynamic, heat transfer and fluid mechanics principles.

Field and Laboratory Validations will be conducted on Experimental Models to be specifically designed and constructed. Supplementary Validation based on physical simulations and laboratory testing will also be considered.

APPENDIX A1 INCEPTION PROPOSAL

6 PLAN OF ACTIVITIES

Tasks	Months	2	4	6	8	10	12	14	16	18	20	22	24
	Information Research		█	█	█	█	█	█	█	█	█	█	█
Theoretical and Computer Simulation and Modelling			█	█	█	█	█	█	█	█	█	█	█
Experimental Model – Design, Construction, Installation						█	█	█	█	█	█	█	█
Experimental Model – Field and Laboratory Investigations					█	█	█	█	█	█	█	█	█
Data Analysis					█	█	█	█	█	█	█	█	█
Reporting		█	█	█	█	█	█	█	█	█	█	█	█

APPENDIX A1 INCEPTION PROPOSAL

7 RESOURCES

- Materials to be purchased for this project include Solar Thermal Collector materials, materials for Heat Exchangers including piping and insulation and various organic fluids (to be determined).
- Equipment to be purchased include a Vapour Turbine-Generator (capacity to be determined), Digital Data Loggers, Storage Modules, Thermocouples, Fluid Flow Meters, Pressure Meters and Energy Meters.
- Radiation measuring instruments: Pyranometer and Pyrheliometer will also be required.
- The department will identify and avail a secured site for field tests.

REFERENCES

1. <http://www.warren.usyd.edu.au/bulletin/NO51/ed51art6.htm>
2. <http://www.shpegs.org/>
3. Nishith B.D. and Santanu B., Process integration of organic Rankine cycle, Energy Journal, Vol 34, 2009, pp 1674-1686.

Hazardous Materials Clearance:	Yes	<input type="checkbox"/>	No	<input checked="" type="checkbox"/>
Ethical Clearance required:	Yes	<input type="checkbox"/>	No	<input checked="" type="checkbox"/>
Confidentiality Agreement required:	Yes	<input type="checkbox"/>	No	<input checked="" type="checkbox"/>

Signature of candidate:



Date: October 15, 2009

Signature of Supervisor:

Date:

APPENDIX A2 EES CODES

- A2.1 Organic Rankine Cycle (ORC) System First Pass Model
- A2.2 Solar Field Model
- A2.3 Evaporator Model
- A2.4 Condenser Model
- A2.5 Radial Turbine and Axial Turbine Models

APPENDIX A2 EES CODES

Appendix 2.1: EES Codes

```
{ $DS. } "General EES Code"
PROCEDURE ModelType(s_high_s, s_low_s: s[5], ModelType$)
$COMMON WorkingFluid$, P[1], P[2]
  If (ABS((s_high_s-s_low_s)/(s_low_s))>0.05) and
(s_high_s>s_low_s) Then
    s[5]:=entropy(WorkingFluid$, P=P[2], x=1)
    "Q_dot_superheater:=0
    Q_dot_recu:=Q_dot_recu"
    ModelType$='Rankine with Recuperator No Superheater'
  Else
    If (ABS((s_high_s-s_low_s)/(s_low_s))>0.005) and
(s_high_s<s_low_s) Then
      s[5]:=entropy(WorkingFluid$, P=P[1], x=1)
      "Q_dot_superheater:=Q_dot_superheater
      Q_dot_recu:=0"
      ModelType$='Rankine with Superheater No Recuperator'
    Else
      s[5]:=entropy(WorkingFluid$, P=P[2], x=1)
      "Q_dot_superheater:=0
      Q_dot_recu:=0"
      ModelType$='Conventional Rankine No Recuperator No
Superheater'
    Endif
  Endif
End

PROCEDURE CondenserInlet(s_high_s, s_low_s: h[7])
$COMMON WorkingFluid$, P[1], h[6]
  If((s_high_s-s_low_s)>(0.05*s_low_s)) Then
    h[7]:=enthalpy(WorkingFluid$, P=P[1], x=1)
  Else
    h[7]:=h[6]
  Endif
End

PROCEDURE SuperheaterRecuperator(m_dot, h[5], h[4], h[6], h[7],
ModelType$: Q_dot_superheater, Q_dot_recu)
$COMMON WorkingFluid$, P[1], P[2]
  If (ModelType$='Rankine with Recuperator No Superheater')
Then
    Q_dot_superheater:=0
    Q_dot_recu:=m_dot*(h[6]-h[7])
  Else
    If (ModelType$='Rankine with Superheater No Recuperator')
Then
      Q_dot_recu:=0
      Q_dot_superheater:=m_dot*(h[5]-h[4])
    Else
      Q_dot_superheater:=0
      Q_dot_recu:=0
    Endif
  Endif
End

"Pump"
W_dot_pump/m_dot=h[2]-h[1]
```

APPENDIX A2 EES CODES

```
h[2]-h[1]=v[1]*(P[2]-P[1])/eta_pump
s[2]=entropy(WorkingFluid$,P=P[2],h=h[2])
T[2]=Temperature(WorkingFluid$, P=P[2], h=h[2])

"Evaporator"
Q_dot_evap/m_dot=h[4]-h[3]
rho_WF=density(WorkingFluid$,T=T_3_4, P=P[2])
T_3_4=(T[3]+T[4])/2
T[3]=Temperature(WorkingFluid$, P=P[2], h=h[3])
s[3]=entropy(WorkingFluid$,P=P[2],h=h[3])
V_dot_WF=m_dot*10^6/rho_WF

"Turbine"
W_dot_turbine/m_dot=h[5]-h[6]
h[5]-h[6]=(h[5]-h_6_s)*eta_turbine

"Condenser"
Q_dot_cond/m_dot=h[7]-h[1]

"Power Output and Efficiency"
eta_therm=(W_dot_turbine-
W_dot_pump)/(Q_dot_evap+Q_dot_superheater)*100
Power=W_dot_turbine

"Input Data"
P[2]=500[kPa]
P[1]=101.325[kPa] "standard atmospheric pressure"
m_dot=0.01[kg/s]
eta_pump=0.65
eta_turbine=0.85

"DUPLICATE vary the working fluids each state parameter will be 2D
i.e. Working Fluid + State No."
i=1
WorkingFluid$=Lookup$('ORC Working Fluids.lkt', i, 'WorkingFluid$')

"Also warning statement required for negative Recuperator or
Superheater Load"

"Equate Pressures"
P[1]=P[6]; P[1]=P[7]
P[2]=P[3]; P[2]=P[4]; P[2]=P[5]

"Known States"
"State 1- Wet Saturated"
h[1]=enthalpy(WorkingFluid$,P=P[1],x=0)
v[1]=volume(WorkingFluid$,P=P[1],x=0)
s[1]=entropy(WorkingFluid$,P=P[1],x=0)
T[1]=temperature(WorkingFluid$,P=P[1],x=0)

"State 4 - Dry Saturated"
h[4]=enthalpy(WorkingFluid$,P=P[2],x=1)
s[4]=entropy(WorkingFluid$,P=P[2],x=1)
T[4]=temperature(WorkingFluid$,P=P[2],x=1)

"Superheater"
"Q_dot_superheater/m_dot=h[5]-h[4]"
```

APPENDIX A2 EES CODES

```
"Recuperator"
h[6]-h[7]=h[3]-h[2]
"Q_dot_recu/m_dot=h[6]-h[7]"

"Model Type Selection"
s_high_s=entropy(WorkingFluid$,P=P[2],x=1)
s_low_s=entropy(WorkingFluid$,P=P[1],x=1)
Call ModelType(s_high_s, s_low_s: s[5], ModelType$)

"State 5 and 6_s"
h[5]=enthalpy(WorkingFluid$,P=P[2],s=s[5])
T[5]=temperature(WorkingFluid$,P=P[2],s=s[5])
h_6_s=enthalpy(WorkingFluid$, P=P[1], s=s[5])

CALL CondenserInlet(s_high_s, s_low_s: h[7])
s_1=(s_high_s-s_low_s)/s_low_s
s_2=(s_low_s-s_high_s)/s_low_s
CALL SuperheaterRecuperator(m_dot, h[5], h[4], h[6], h[7],
ModelType$: Q_dot_superheater, Q_dot_recu)
s[6]=entropy(WorkingFluid$,P=P[6],h=h[6])
T[6]=temperature(WorkingFluid$,P=P[6],h=h[6])
s[7]=entropy(WorkingFluid$,P=P[7],h=h[7])
T[7]=temperature(WorkingFluid$,P=P[7],h=h[7])
v[2]=volume(WorkingFluid$,P=P[2],h=h[2])
v[3]=volume(WorkingFluid$,P=P[3],h=h[3])
v[4]=volume(WorkingFluid$,P=P[4],h=h[5])
v[5]=volume(WorkingFluid$,P=P[5],h=h[5])
v[6]=volume(WorkingFluid$,P=P[6],h=h[6])
v[7]=volume(WorkingFluid$,P=P[7],h=h[7])
```

APPENDIX A2 EES CODES

Appendix 2.2: EES Codes

```
{ $DS. } "SEGMENTED MODEL 01 - SOLAR COLLECTOR"  
  
"Procedures to determine Nusselt numbers of air gap"  
  
Procedure NusseltNumber(Ra[1..5,1..30],beta_angle:Nup[1..5,1..30])  
  j1:=0  
  Repeat  
    j1:=j1+1  
    j2:=0  
    Repeat  
      j2:=j2+1  
      Term:=(1-  
(1708*(sin(1.8*(beta_angle)))^1.6)/(Ra[j1,j2]*cos(beta_angle)))  
      IF(Term>0) Then Term_1:=Term Else Term_1:=0  
      Term:=(1-1708/(Ra[j1,j2]*cos(beta_angle)))  
      IF(Term>0) Then Term_2:=Term Else Term_2:=0  
      IF((Ra[j1,j2]*(cos(beta_angle))/5830)>1) Then  
Term_3:=((Ra[j1,j2]*(cos(beta_angle))/5830)^(1/3)-1) Else Term_3:=0  
      Nup[j1,j2]:=1+1.44*Term_1*Term_2+Term_3  
    Until (j2>=30)  
  Until(j1>=5)  
End  
  
"ambient conditions"  
T_a=20[C] "ambient temperature"  
vel_wind=3.0[m/s] "wind speed"  
I_sol=360[W/m^2] "solar insolation"  
  
"geometrical properties of solar collector"  
Length_col=2.0[m] "length of collector"  
L_col=Length_col/N_sc "length of one segment of a collector"  
N_sc=10 "number of segments in one collector"  
W_col=1.0[m] "width of collector"  
N_p=8 "number of riser pipes in each collector"  
N_s=30 "number of segments in one model"  
N_c=3 "number of collectors in each bank"  
N_b=3 "number of banks in one solar array"  
N_h=24 "number of hours in one day for hourly change of  
Insolation data"  
d_p=0.006[m] "internal diameter of riser pipe"  
d_h=0.01[m] "internal diameter of header pipe"  
beta_angle=30[deg] "inclination angle of collector"  
L_p=0.025[m] "spacing between absorber plate and glass"  
L_ins=0.04[m] "insulation thickness"  
NCycle=5 "number of cycles in one hour"  
  
"thermal properties of collector"  
tau_c=0.9 "transmissivity of glass"  
alpha_p=0.9 "absorptivity of absorber plate"  
epsilon_p=0.1 "emissivity of absorber"  
epsilon_c=0.85 "emissivity of glass"  
k_ins=0.023[W/m-K] "insulation conductivity"  
  
"water-glycol properties"  
Cp_wg=4180[J/kg-K] "can be taken as constant - average between  
ethylene glycol & water"
```


APPENDIX A2 EES CODES

```
rho_wg=1000[kg/m^3]      "can be taken as constant - average between
ethylene glycol & water"
alpha_wg=k_wg/(Cp_wg*rho_wg) "thermal diffusivity      a=k/?c"
mu_wg=658E-06          "dynamic viscosity"
nu_wg=mu_wg/rho_wg      "kinematic viscosity"
k_wg=0.4335 [W/m-K]      "can be taken as constant - average between
ethylene glycol & water"
vol_dot_col=43E-06[m^3/s]

m_dot_wg=vol_dot_wg*rho_wg
vol_dot_wg=vol_dot_col/N_p

"Incident Radiation"
Q_dot_inc=I_sol*A_p

"Radiation absorbed by Absorber"
Q_dot_p=Q_dot_inc*tau_c*alpha_p

A_p=L_col*W_col/N_p

T_sky=0.0552*(T_a)^1.5
T_skyK=CONVERTTEMP('C', 'K', T_sky)
h_c_a=5.0[W/m^2-K]

h_p_b=k_ins/L_ins

Nud_wg=(h_p_wg*d_p)/k_wg
Nud_wg=(3.66+4.36)/2      "assume laminar flow"
Red_wg=vel_wg*d_p/mu_wg    "Reynold's number - check if laminar
flow"
vel_wg=vol_dot_wg/A_wg_c
A_wg_a=PI*d_p*L_col
A_wg_c=(PI*d_p^2)/4

T_wg_in[1,1]=T_a          "assume inlet temperature of water-glycol
equals ambient temperature"

DUPLICATE k=2,5
    T_wg_in[k,1]=T_tank[k-1]      "Set Inlet Temperature of Next
Cycle to last tank Temperature of last Cycle"
END

DUPLICATE k1=1,5
    DUPLICATE k2=2,30
        T_wg_in[k1,k2]=T_wg_out[k1,k2-1]      "Set Inlet
Temperature to Next Segment to Outlet Temperature of Current
Segment"
    END
END

"thermal efficiency of collector"
"eta_therm_col=Q_dot_wg/Q_dot_inc"

DUPLICATE i=1,5
    "Segment Models"
    "NEnergy=N_s"
    DUPLICATE j=1,30
        "Heat Lost to the Cover"
        Q_dot_conv[i,j]=h_p_c_conv[i,j]*A_p*(T_p[i,j]-T_c[i,j])
```

APPENDIX A2 EES CODES

```

Q_dot_rad[i,j]=h_p_c_rad[i,j]*A_p*(T_p[i,j]-T_c[i,j])

"Back Loss"
Q_dot_back[i,j]=h_p_b*A_p*(T_p[i,j]-T_a)

"Heat absorbed by Water-Glycol"
Q_dot_wg[i,j]=h_p_wg*A_wg_a*(T_p[i,j]-T_wg_m[i,j])
Q_dot_wg[i,j]=m_dot_wg*Cp_wg*(T_wg_out[i,j]-
T_wg_in[i,j])

T_wg_m[i,j]=(T_wg_in[i,j]+T_wg_out[i,j])/2

"Top Loss"
Q_dot_c_a[i,j]=h_c_a*A_p*(T_c[i,j]-T_a)
Q_dot_c_s[i,j]=epsilon_c*sigma#*A_p*((CONVERTTEMP('C',
'K', T_c[i,j]))^4-T_skyK^4)

"Heat Transfer Coefficients"

h_p_c_conv[i,j]=Nup[i,j]*L_p/k_air[i,j]

Ra[i,j]=g#*beta_air[i,j]*(T_p[i,j]-
T_c[i,j])*L_p^3/(alpha_air[i,j]*nu_air[i,j]) "RA IS THE RAYLEIGH
NUMBER"

h_p_c_rad[i,j]=sigma#*((CONVERTTEMP('C', 'K',
T_p[i,j]))^2+(CONVERTTEMP('C', 'K',
T_c[i,j]))^2)*((CONVERTTEMP('C', 'K', T_p[i,j]))+(CONVERTTEMP('C',
'K', T_c[i,j])))/(1/epsilon_p+1/epsilon_c-1)

"air gap thermal properties PROPERTIES"
T_m_airK[i,j]=CONVERTTEMP('C', 'K', T_m_air[i,j])
Cp_air[i,j]=Cp(Air, T=T_m_air[i,j])
rho_air[i,j]=density(Air, T=T_m_air[i,j], P=Po#)
alpha_air[i,j]=k_air[i,j]/(Cp_air[i,j]*rho_air[i,j])
"thermal diffusivity"
mu_air[i,j]=viscosity(Air, T=T_m_air[i,j]) "dynamic
viscosity"
nu_air[i,j]=mu_air[i,j]/rho_air[i,j] "kinematic
viscosity"
k_air[i,j]=conductivity(Air, T=T_m_air[i,j])
beta_air[i,j]=1/T_m_airK[i,j]
T_m_air[i,j]=(T_p[i,j]+T_c[i,j])/2

"energy balance"

Q_dot_p=Q_dot_conv[i,j]+Q_dot_rad[i,j]+Q_dot_back[i,j]+Q_dot_
wg[i,j]

Q_dot_conv[i,j]+Q_dot_rad[i,j]=Q_dot_c_a[i,j]+Q_dot_c_s[i,j]
END
END

CALL NusseltNumber(Ra[1..5,1..30],beta_angle:Nup[1..5,1..30])

```

APPENDIX A2 EES CODES

```
"Tank Model"  
Q_dot_tank[1]=m_dot_wg*Cp_wg*(T_wg_out[1,N_s]-T_tank[1])  
Q_dot_tank[1]=m_tank*Cp_wg*(T_tank[1]-T_a)/t_cycle  
  
DUPLICATE i_cycle3=2,NCycle  
    Q_dot_tank[i_cycle3]=m_dot_wg*Cp_wg*(T_wg_out[i_cycle3,N_s]-  
T_tank[i_cycle3])  
    Q_dot_tank[i_cycle3]=m_tank*Cp_wg*(T_tank[i_cycle3]-  
T_tank[i_cycle3-1])/t_cycle  
END  
  
t_cycle=N_s*L_col/vel_wg  
m_tank=Vol_tank*rho_wg/(N_p*N_c)  
Vol_tank=1[m^3]  
N_hr=3600/t_cycle      "number of cycles in one hour"82
```

APPENDIX A2 EES CODES

Appendix 2.3: EES Codes

```
{$DS.}Procedure NucleateBoilingCoefficient(pr,TWF2:nf) "tests if
fluid is a cryogen"
  IF(TWF2>-180) THEN
    nf:=0.8-0.1*exp(1.75*pr) "the expression is for all fluids
except cryogenes (nitrogen, oxygen, etc.)"
  ELSE
    nf:=0.7-0.13*exp(1.105*pr) "nucleate boiling exponent for
cryogenes such as nitrogen, oxygen, etc."
  ENDIF
END
```

```
PROCEDURE
FCB(N2,xWF2[1..N2],rhoWF2_L,rhoWF2_G,h_Lt,h_Gt:F_cb[1..N2])

  ifcb:=0
  REPEAT
    ifcb:=ifcb+1
    IF(xWF2[ifcb]=<0.6) THEN

      F_cb[ifcb]:=((1-
xWF2[ifcb])^1.5+1.9*xWF2[ifcb]^0.6*(rhoWF2_L/rhoWF2_G)^0.35)^1.1

    ELSE

      xWF2[ifcb]:=0.95 "..... procedure needs reworking so
that if xWF2[ifcb]>0.95 hi2=h_Gt .....CHECK"

      F_cb[ifcb]:=((1-xWF2[ifcb])^1.5+1.9*xWF2[ifcb]^0.6*(1-
xWF2[ifcb])^0.01*(rhoWF2_L/rhoWF2_G)^0.35)^(-
2.2)+((h_Gt/h_Lt)*xWF2[ifcb]^0.01*(1+8*(1-
xWF2[ifcb])^0.7)*(rhoWF2_L/rhoWF2_G)^0.67)^(-2))^(-5)

    ENDIF
  UNTIL(ifcb=>N2)

END
```

```
Procedure ONB(N2,q_ONB,
qi2[1..N2],hcb[1..N2],htb[1..N2]:hi2[1..N2]) "modify later
.....if x<0.5 then hi2[?]=hLt ::::::: if x>0.95 then
hi2[?]=h_Gt"

  ih2:=0
  REPEAT
    ih2:=ih2+1
    IF(qi2[ih2]<q_ONB) THEN
      hi2[ih2]:=hcb[ih2]
    ELSE
      hi2[ih2]:=htb[ih2]
    ENDIF
  UNTIL(ih2=>N2)

END
```

APPENDIX A2 EES CODES

```

"DATA"

D_o=0.023 [m]      "tube outer diameter"
D_i=0.020 [m]      "tube inner diameter"
"D_s=0.026 [m]"    "shell inner diameter"

HTF$='EG'         "Heat Transfer Fluid, Cooling Fluid"
"WF$='isobutane'" "Working Fluid"
WF$='R245fa'      "Working Fluid"
Material$='Copper' "tube material"

"m_dot_HTF=2.5 [kg/s]" "Heat Transfer Fluid mass flow rate"
"m_dot_WF=0.25 [kg/s]" "Working Fluid mass flow rate"
m_dot_CF=2 [kg/s] "Cooling Fluid mass flow rate"

"P_high=10*convert(atm,Pa)" "High cycle pressure"
P_high=8*convert(atm,Pa)    "High cycle pressure"
P_low=3.5*convert(atm,Pa)   "Low cycle pressure"

T_HTF_i=90 [C]    "Heat Transfer Fluid inlet temperature"
T_WF_i=40 [C]     "Working Fluid inlet temperature"
T_CF_i=25 [C]     "Cooling Fluid inlet temperature"
"
"
"PREHEATER HEAT EXCHANGER"
N1=1
DUPLICATE i1=1,N1
    Q1[i1]=Uo1[i1]*Ao1[i1]*deltaTLM1[i1]
    Q1[i1]=m_dot_HTF*CpHTF1[i1]*(THTF1[i1]-THTF1[i1-1])
    Q1[i1]=m_dot_WF*CpWF1[i1]*(TWF1[i1]-TWF1[i1-1])

    deltaTLM1[i1]=((THTF1[i1]-TWF1[i1])-(THTF1[i1-1]-TWF1[i1-1]))/LN((THTF1[i1]-TWF1[i1])/(THTF1[i1-1]-TWF1[i1-1]))
    CpHTF1[i1]=Cp(HTF$, T=THTF1[i1], C=50 [%])
    CpWF1[i1]=Cp(WF$, T=TWF1[i1], x=0)
    Ao1[i1]=pi*D_o*LSEG
    Ai1[i1]=pi*D_i*LSEG
    Uo1[i1]*Ao1[i1]=1/(1/(hi1[i1]*Ai1[i1])+R`_fi/Ai1[i1]+LN(D_o/D_i)/(2*pi*Kwall1[i1]*LSEG)+1/(ho1[i1]*Ao1[i1])+R`_fo/Ao1[i1])
    Uo1[i1]*Ao1[i1]=Ui1[i1]*Ai1[i1]

"Convective Coefficients"

    "Outside surface"
    rhoHTF1[i1]=Density(HTF$, T=THTF1[i1], C=50 [%])
    "kg/m^3.....density"
    kHTF1[i1]=Conductivity(HTF$, T=THTF1[i1], C=50 [%])
    "(W/m-C)...thermal conductivity"
    muHTF1[i1]=viscosity(HTF$, T=THTF1[i1], C=50 [%])
    "(kg/m-s)...dynamic viscosity"
    muHTF1_s[i1]=viscosity(HTF$, T=ToWall1[i1], C=50 [%])
    "(kg/m-s)...dynamic viscosity"
    PrHTF1[i1]=Prandtl(HTF$, T=THTF1[i1], C=50 [%])
    "Prandtl number"
    ReDHTF1[i1]=D_H*velHTF1[i1]*rhoHTF1[i1]/muHTF1[i1] "...>4000
is turbulent flow"

```

APPENDIX A2 EES CODES

```

"Using Dittus-Boelter equation to determine heat transfer
coefficient for outside surface"
NuDHTF1[i1]=0.023*ReDHTF1[i1]^0.8*PrHTF1[i1]^0.3 "Nusselt
number "
hol[i1]=NuDHTF1[i1]*kHTF1[i1]/D_H "... conductivity, k is for
liquid"

"Inside Fluid Convective Coefficients"

rhoWF1[i1]=Density(WF$, T=TWF1[i1], x=0)
"kg/m^3.....density"
kWF1[i1]=Conductivity(WF$, T=TWF1[i1], x=0) " (W/m-
C)...thermal conductivity"
muWF1[i1]=viscosity(WF$, T=TWF1[i1], x=0) " (kg/m-
s)...dynamic viscosity"
muWF1_s[i1]=viscosity(WF$, T=TiWall1[i1], x=0)
" (kg/m-s)...dynamic viscosity"
PrWF1[i1]=Prandtl(WF$, T=TWF1[i1], x=0) "Prandtl number"
ReDWF1[i1]=D_i*velWF1[i1]*rhoWF1[i1]/muWF1[i1]
"...>4000 is turbulent flow"

"Using Dittus-Boelter equation to determine heat transfer
coefficient for inside surface"
NuDWF1[i1]=0.023*ReDWF1[i1]^0.8*PrWF1[i1]^0.4 "Nusselt number
"
hil[i1]=NuDWF1[i1]*kWF1[i1]/D_i "... conductivity, k
is for liquid"

"Wall Thermal Conductivity"
Kwall1[i1]=Conductivity(Material$, T=TWall1[i1])
"conductivity of copper"

"wall surface temperatures - energy balance at the surface"
TWall1[i1]=(TiWall1[i1]+ToWall1[i1])/2
(THTF1[i1]-ToWall1[i1])/(1/(hol[i1]*Ao1[i1]))=(ToWall1[i1]-
TWF1[i1])/(1/(hil[i1]*Ai1[i1])+R` `_fi/Ai1[i1]+LN(D_o/D_i)/(2*pi*Kwa
ll1[i1]*LSEG)+R` `_fo/Ao1[i1])
(TiWall1[i1]-TWF1[i1])/(1/(hil[i1]*Ai1[i1]))=(THTF1[i1]-
TiWall1[i1])/(R` `_fi/Ai1[i1]+LN(D_o/D_i)/(2*pi*Kwall1[i1]*LSEG)+1/(
hol[i1]*Ao1[i1])+R` `_fo/Ao1[i1])

"Velocity and Pressure Drops"
velHTF1[i1]=4*m_dot_HTF/(rhoHTF1[i1]*pi*(D_s^2-D_o^2))
velWF1[i1]=4*m_dot_WF/(rhoWF1[i1]*pi*D_i^2)

deltaPWF1[i1]=(fWF1[i1]*GWF1[i1]^2*LSEG)/(2*g#*rhoWF1[i1]*D_i
*phiWF1[i1])

GWF1[i1]=velWF1[i1]*rhoWF1[i1]
fWF1[i1]=(0.7904*ln(ReDWF1[i1])-1.64)^(-2)
phiWF1[i1]=(muWF1[i1]/muWF1_s[i1])^0.14

deltaPHTF1[i1]=(fHTF1[i1]*GHTF1[i1]^2*LSEG)/(2*g#*rhoHTF1[i1]
*D_H*phiHTF1[i1])

GHTF1[i1]=velHTF1[i1]*rhoHTF1[i1]
fHTF1[i1]=(0.7904*ln(ReDHTF1[i1])-1.64)^(-2)
phiHTF1[i1]=(muHTF1[i1]/muHTF1_s[i1])^0.14

```

APPENDIX A2 EES CODES

END

"Segmentation of Sensible Section is on Equal HX lengths"
 "Segmentation of Latent Section is on Equal Quality Change"

L1=LSEG*N1

"VAPOURISER HEAT EXCHANGER"

N2=2

DUPLICATE i2=1,N2

Q2[i2]=Uo2[i2]*Ao2[i2]*deltaTLM2[i2]

deltaTLM2[i2]=(THTF2[i2]-THTF2[i2-1])/LN(ABS((THTF2[i2]-TWF2)/(THTF2[i2-1]-TWF2)))

Q2[i2]=m_dot_HTF*CpHTF2[i2]*(THTF2[i2]-THTF2[i2-1])

CpHTF2[i2]=Cp(HTF\$, T=THTF2[i2], C=50 [%])

Q2[i2]=m_dot_WF*HfWF2/N2

xWF2[i2]=xWF2[i2-1]+1/N2

Ao2[i2]=pi*D_o*L2[i2]

Ai2[i2]=pi*D_i*L2[i2]

Uo2[i2]*Ao2[i2]=1/(1/(hi2[i2]*Ai2[i2])+R` `_fi/Ai2[i2]+LN(D_o/D_i)/(2*pi*Kwall2[i2]*L2[i2])+1/(ho2[i2]*Ao2[i2])+R` `_fo/Ao2[i2])

Uo2[i2]*Ao2[i2]=Ui2[i2]*Ai2[i2]

"Convective Coefficients"

(ho2[i2]*D_H)/kHTF2[i2]=((fHTF2[i2]/8)*(ReDHTF2[i2]-1000)*PrHTF2[i2])/(1+12.7*(fHTF2[i2]/8)^(1/2)*(PrHTF2[i2]^(2/3)-1))
 "Gnielinski Correlation for HTF"

fHTF2[i2]=(0.7904*ln(ReDHTF2[i2])-1.64)^(-2)

"ManningFrictionFactor"

"Outside surface"

rhoHTF2[i2]=Density(HTF\$, T=THTF2[i2], C=50 [%])

"kg/m^3.....density"

kHTF2[i2]=Conductivity(HTF\$, T=THTF2[i2], C=50 [%]) "(W/m-C)...thermal conductivity"

muHTF2[i2]=viscosity(HTF\$, T=THTF2[i2], C=50 [%])

"(kg/m-s)...dynamic viscosity"

muHTF2_s[i2]=viscosity(HTF\$, T=ToWall12[i2], C=50 [%])

PrHTF2[i2]=Prandtl(HTF\$, T=THTF2[i2], C=50 [%])

"Prandtl number"

ReDHTF2[i2]=D_H*velHTF2[i2]*rhoHTF2[i2]/muHTF2[i2] "...>4000 is turbulent flow"

"Wall Thermal Conductivity"

APPENDIX A2 EES CODES

```

Kwall2[i2]=Conductivity(Material$, T=TWall2[i2])
"conductivity of copper"

"wall surface temperatures - energy balance at the surface"
TWall2[i2]=(TiWall2[i2]+ToWall2[i2])/2
(THTF2[i2]-ToWall2[i2])/(1/(ho2[i2]*Ao2[i2]))=(ToWall2[i2]-
TWF2)/(1/(hi2[i2]*Ai2[i2])+R`_fi/Ai2[i2]+LN(D_o/D_i)/(2*pi*Kwall2[
i2]*L2[i2])+R`_fo/Ao2[i2])
(TiWall2[i2]-TWF2)/(1/(hi2[i2]*Ai2[i2]))=(THTF2[i2]-
TiWall2[i2])/(R`_fi/Ai2[i2]+LN(D_o/D_i)/(2*pi*Kwall2[i2]*L2[i2])+1
/(ho2[i2]*Ao2[i2])+R`_fo/Ao2[i2])

velHTF2[i2]=4*m_dot_HTF/(rhoHTF2[i2]*pi*(D_s^2-D_o^2))

"Steiner and Taborek"

qi2[i2]=hi2[i2]*(TiWall2[i2]-TWF2)

htb[i2]=(hnb[i2]^3+hcb[i2]^3)^(1/3)

hnb[i2]=h_nb_o*F_nb[i2]

F_nb[i2]=F_pf*(qi2[i2]/q_nb_o)^nf*(D_i/D_nb_o)^(-
0.4)*(R_p/R_p_o)^0.133*FM

hcb[i2]=h_Lt*F_cb[i2]

"Pressure Drop for Two Phase Flow          ..... needs reworking
.....          CHECK"

deltaPWF2[i2]=(fWF2_L*GWF2_L^2*L2[i2])/(2*g#*rhoWF2_L*D_i*phi
WF2[i2])

phiWF2[i2]=(muWF2_L/muWF2_s[i2])^0.14

muWF2_s[i2]=viscosity(WF$, T=TiWall2[i2], x=0)

deltaPHTF2[i2]=(fHTF2[i2]*GHTF2[i2]^2*L2[i2])/(2*g#*rhoHTF2[i
2]*D_H*phiHTF2[i2])

GHTF2[i2]=velHTF2[i2]*rhoHTF2[i2]
{fHTF2[i2]=(0.7904*ln(ReDHTF2[i2])-1.64)^(-2)}
"already calculated above"
phiHTF2[i2]=(muHTF2[i2]/muHTF2_s[i2])^0.14

END

CALL ONB(N2,q_ONB, qi2[1..N2],hcb[1..N2],htb[1..N2]:hi2[1..N2])

"
_____
_____
_____
_____

```


APPENDIX A2 EES CODES

```

"
CALL FCB(N2,xWF2[1..N2],rhoWF2_L,rhoWF2_G,h_Lt,h_Gt:F_cb[1..N2])

"Constant Parameters and Boundary Conditions"
HfWF2=enthalpy_vaporization(WF$, T=TWF2)
TWF2=T_sat(WF$, P=P_high)
THTF2[N2]=90 [C]
TWF1[0]=40 [C]
Q=Q1+Q2
"Q=84200"
TWF1[N1]=TWF2
THTF1[N1]=THTF2[0]
xWF2[0]=0

"THTF2[0]=87.97 [C]"

R`_fi=FoulingFactor('Ethylene glycol solution')

R`_fo=FoulingFactor('Refrigerant liquids')

D_H=D_s-D_o "Define the hydraulic diameter for annulus ... D_H=4A/P"

"-----"
"-----"
"-----"

"EES Properties for Gnielinski Correlation for WF SATURATED
LIQUID"

kWF2_L=CONDUCTIVITY(WF$, T=TWF2, x=0) "liquid conductivity"

PrWF2_L=Prandtl(WF$, T=TWF2, x=0) "liquid Prandtl number"

muWF2_L=Viscosity(WF$, T=TWF2, x=0) "liquid viscosity"

rhoWF2_L=Density(WF$, T=TWF2, x=0) "liquid density"

ReWF2_L=(m_dot_WF*D_i)/(muWF2_L*A_i_flow) "liquid Reynolds
number"

velWF2_L=4*m_dot_WF/(rhoWF2_L*pi*D_i^2) "density based on
total flow as liquid???? check"

GWF2_L=velWF2_L*rhoWF2_L
{fWF2_L=(0.7904*ln(ReWF2_L)-1.64)^(-2)} "already calculated
below"

"EES Properties for Gnielinski Correlation for WF SATURATED
VAPOUR"
"....."
"....."

```

APPENDIX A2 EES CODES

```

.....
....."

kWf2_G=CONDUCTIVITY(WF$, T=TWF2, x=1)          "vapour conductivity"

PrWF2_G=Prandtl(WF$, T=TWF2, x=1)             "vapour Prandtl number"

muWF2_G=Viscosity(WF$, T=TWF2, x=1)           "vapour viscosity"

rhoWF2_G=Density(WF$, T=TWF2, x=1)            "vapour density"

ReWF2_G=(m_dot_WF*D_i)/(muWF2_G*A_i_flow)      "vapour Reynolds
number"

A_i_flow=(pi*D_i^2)/4

".....
.....
....."

(h_Lt*D_i)/kWf2_L=((fWF2_L/8)*(ReWF2_L-
1000)*PrWF2_L)/(1+12.7*(fWF2_L/8)^(1/2)*(PrWF2_L^(2/3)-1))

fWF2_L=(0.7904*ln(ReWF2_L)-1.64)^(-2)

(h_Gt*D_i)/kWf2_G=((fWF2_G/8)*(ReWF2_G-
1000)*PrWF2_G)/(1+12.7*(fWF2_G/8)^(1/2)*(PrWF2_G^(2/3)-1))

fWF2_G=(0.7904*ln(ReWF2_G)-1.64)^(-2)

"-----
-----
-----"

q_ONB=(2*sigma*T_satK*h_Lt)/(r_cr*rhoWF2_G*HfWF2)

T_satK=ConvertTemp('C', 'K', TWF2)

sigma=SURFACETENSION(WF$, T=TWF2)

D_nb_o=0.01 [m]
R_p=1*10^(-6) "equals 1 if unknown"
R_p_o= 1*10^(-6) "micro-meter"
r_cr=0.3*10^(-6) "critical nucleation radius"

F_M1=0.377+0.199*ln(M)+0.000028427*M^2

FM=min(F_M1,2.5)

M=molarmass(WF$)

Call NucleateBoilingCoefficient(pr,TWF2:nf) "tests if fluid is a
cryogen and returns the nucleate boiling exponent, nf, on the
normalised heat flux term"

pr=P_sat/P_crit

```

APPENDIX A2 EES CODES

```
P_sat=P_high  
P_crit=P_Crit(WF$)  
F_pf=2.816*pr^0.45+(3.4+(1.7/(1-pr^7)))*pr^3.7  
"q_nb_o=Lookup('Standard Nucleate Flow Boiling  
Coefficients.lkt',29,4)  
h_nb_o=Lookup('Standard Nucleate Flow Boiling  
Coefficients.lkt',29,5)"  
q_nb_o=20000  
h_nb_o=2744  
Q1=SUM(Q1[Q1i], Q1i=1,N1)  
Q2=SUM(Q2[Q2i], Q2i=1,N2)  
L2=SUM(L2[L2i], L2i=1,N2)  
Ao1=SUM(Ao1[A1i], A1i=1,N1)  
Ao2=SUM(Ao2[A2i], A2i=1,N2)  
ULV=muWF2_L/muWF2_G    "ratio for pressure drop multiplier  
correlation"
```

APPENDIX A2 EES CODES

Appendix 2.4: EES Codes

```
{ $DS. } Procedure NUD(N, NuD_Turb[1..N], NuD_Lam, ReD_CF[1..N]:
NuD[1..N])
    k:=0
    REPEAT
    k:=k+1
    IF(ReD_CF[k]>3000) THEN
    NuD[k]:=NuD_Turb[k] ELSE
    NuD[k]:=NuD_Lam
    ENDIF
    UNTIL(k>N)
END

"Data"
{WF$='R134a'}      "Working Fluid"

CF$='EG'      "Cooling Fluid"

D_i=0.0165 [m]
D_o=0.019 [m]
L_tube=2.85 [m]

Material$='Copper'      "tube material"

{m_dot_CF=2 [kg/s]}

T_CF_i=25 [C]
T_WF_sat=50 [C]

R`_fi=FoulingFactor('Ethylene glycol solution')
R`_fo=FoulingFactor('Refrigerant liquids')

NuD_Lam=(3.66+4.36)/2

" _____ "

A_o=pi*D_o*L_tube
A_i=pi*D_i*L_tube
m_dot_CF_tube=m_dot_CF/N

k_L=CONDUCTIVITY(WF$, T=T_WF_sat, x=0)      "liquid conductivity"
rho_L=Density(WF$, T=T_WF_sat, x=0)      "liquid density"
rho_G=Density(WF$, T=T_WF_sat, x=1)      "vapour density"
h_fg=enthalpy_vaporization(WF$, T=T_WF_sat)
mu_L=Viscosity(WF$, T=T_WF_sat, x=0)      "liquid viscosity"

N=8      "number of tubes in one column"
```

APPENDIX A2 EES CODES

```

M=6          "number of columns"

"
-----"

DUPLICATE i=1,N

Q[i]=A_o*U_o[i]*deltaTLM[i]

    U_o[i]*A_o=U_i[i]*A_i

    U_o[i]*A_o=1/(1/(h_CF[i]*A_i)+R`_fi/A_i+LN(D_o/D_i)/(2*pi*k_w[i]*L_tube)+1/(h_WF[i]*A_o)+R`_fo/A_o)

    deltaTLM[i]=((T_WF_sat-T_CF_i)-(T_WF_sat-T_CF_o[i]))/LN((T_WF_sat-T_CF_i)/(T_WF_sat-T_CF_o[i]))

Q[i]=m_dot_CF_tube*Cp[i]*(T_CF_o[i]-T_CF_i)

    Cp[i]=SpecHeat(CF$, T=T_CF[i], C=50 [%])

    T_CF[i]=(T_CF_o[i]+T_CF_i)/2

Q[i]= 2*L_tube*GAMMA_WF[i]*h_fg

NuD_Turb[i]=((f_CF[i]/8)*(ReD_CF[i]-1000)*Pr_CF[i])^(1/2)/(1+12.7*(f_CF[i]/8)^(1/2)*(Pr_CF[i]^(2/3)-1))
    "Gnielinski Correlation for CF"

NuD[i]=(h_CF[i]*D_i)/k_CF[i]

    f_CF[i]=(0.7904*ln(ReD_CF[i])-1.64)^(-2)
    "ManningFrictionFactor"

    k_CF[i]=Conductivity(CF$, T=T_CF[i], C=50[%])          "(W/m-
C)...thermal conductivity"

    ReD_CF[i]=(D_i*vel_CF[i]*rho_CF[i])/mu_CF[i]          "...>4000
is turbulent flow"

    vel_CF[i]=m_dot_CF_tube/(rho_CF[i]*pi*D_i^2/4)

    rho_CF[i]=Density(CF$, T=T_CF[i], C=50[%])
    "kg/m^3.....density"

    mu_CF[i]=viscosity(CF$, T=T_CF[i], C=50[%])          "(kg/m-
s)...dynamic viscosity"

    Pr_CF[i]=Prandtl(CF$, T=T_CF[i], C=50[%])            "Prandtl
number"

k_w[i]=Conductivity(Material$, T=T_w[i])

GAMMA[i]=1.924*(((D_o/2)^3*k_L^3*ABS(T_WF_sat-T_w_o[i])^3*(rho_L-
rho_G)*g#)/(h_fg^3*(mu_L/rho_L)))^(1/4)

```

APPENDIX A2 EES CODES

```
(T_WF_sat-T_w_o[i])/(1/(h_WF[i]*A_o))=(T_w_o[i]-
T_CF[i])/(1/(h_CF[i]*A_i)+R`_fi/A_i+LN(D_o/D_i)/(2*pi*K_w[i]*L_tub
e)+R`_fo/A_o) {apply energy balance at the wall}
```

```
(T_w_i[i]-T_CF[i])/(1/(h_CF[i]*A_i))=(T_WF_sat-
T_w_i[i])/(R`_fi/A_i+LN(D_o/D_i)/(2*pi*K_w[i]*L_tube)+1/(h_WF[i]*A
_o)+R`_fo/A_o) {apply energy balance at the wall}
```

```
T_w[i]=(T_w_i[i]+T_w_o[i])/2
```

```
END
```

```
" _____ "
```

```
{h_WF[1]=0.725*((k_L^3*rho_L*(rho_L-
rho_G)*g#*h_fg)/(mu_L*(ABS(T_WF_sat-T_w_o[1]))*D_o))^(1/4)}
"Nusselt's correlation"
```

```
h_WF[1]=0.729*((k_L^3*rho_L*(rho_L-
rho_G)*g#*h_fg)/(mu_L*(ABS(T_WF_sat-T_w_o[1]))*D_o))^(1/4)
"Dhir and Lienhard correlation"
```

```
DUPLICATE i2=2,N
```

```
{h_WF[i2]/h_WF[1]=i2^(3/4)-(i2-1)^(3/4)} "Nusselt's
correlation"
```

```
h_WF[i2]/h_WF[1]=i2^(5/6)-(i2-1)^(5/6) "Kern's method"
```

```
END
```

```
Q_column=SUM(Q[i3], i3=1,N)
```

```
Q_HX=Q_column*M
```

```
m_dot_WF_column=2*L_tube*SUM(GAMMA_WF[i4], i4=1,N)
```

```
m_dot_WF_HX=m_dot_WF_column*M
```

```
m_dot_CF_HX=m_dot_CF*M
```

```
Call NUD(N, NuD_Turb[1..N], NuD_Lam, ReD_CF[1..N]: NuD[1..N])93
```

APPENDIX A2 EES CODES

Appendix 2.5: EES Codes

```
{$DS.}"RADIAL TURBINE MODEL WITH PARAMETRIC TABLE ANALYSIS"
```

```
"Flow through Nozzle"
```

```
"_____"
```

```
"Geometrical Input Data"
```

```
d_1/d_2=1.4 "Nozzle geometry ratio"
```

```
d_3/d_2=0.60 "Rotor geometry ratio"
```

```
d_4/d_3=1.5 "diffuser geometry ratio"
```

```
b_2/d_2=0.15 "rotor aspect ratio"
```

```
b_1/b_2=1 "Nozzle height ratio"
```

```
L_d/d_3=2 "Rotor exit height-diameter ratio"
```

```
b_4=0.01343 [m]
```

```
d_2=0.04 [m]
```

```
d_3=(d_3h+d_3s)/2
```

```
b_3=(d_3s-d_3h)/2
```

```
d_3h/d_3s=0.48
```

```
"_____"
```

```
PSI=1.55 "blade loading coefficient"
```

```
PHI=0.20 "flow coefficient"
```

```
R_s=0.35 "reaction"
```

```
W_dot=10000 [J/s] "output power"
```

```
"_____"
```

```
h_01=h_1+0.5*c_1^2
```

```
h_1=enthalpy(Fluid$, P=P_1, T=T_1)
```

```
rho_1=density(Fluid$, P=P_1, T=T_1)
```

```
s_1=entropy(Fluid$, P=P_1, T=T_1)
```

```
m_dot=rho_1*c_m1*b_1*d_1*pi*(1-BK_1)
```

```
BK_1=0.05 "assumed"
```

```
c_1=c_m1
```

```
alpha_1=0
```

```
P_01=pressure(Fluid$, h=h_01, s=s_1)
```

```
"_____"
```

```
h_01=h_02
```

```
"Nozzle isentropic expansion"
```

```
s_2s=s_1
```

```
h_2s=enthalpy(Fluid$, P=P_2, s=s_2s)
```

```
zeta_N=0.08034 "assumed"
```

```
W_dot=m_dot*deltah_tt
```

APPENDIX A2 EES CODES

```
deltah_tt=h_01-h_03
u_2=SQRT(deltah_tt/PSI)
c_m2=PHI*u_2
u_2=(rpm*convert(min^-1,s^-1))*pi*d_2
m_dot=rho_2*c_m2*b_2*d_2*pi*(1-BK_2)
BK_2=0.05 "assumed"
W_dot=m_dot*(u_2*c_u2-u_3*c_u3)
c_m2=c_2*cos(alpha_2)
alpha_2=82.65 [deg] "set after parametric modeling"
h_02=h_2+0.5*c_2^2
h_2=h_2s+zeta_N*c_2^2/2
h_2=enthalpy(Fluid$, P=P_2, T=T_2)
s_2=entropy(Fluid$, h=h_2, T=T_2)
" _____ "
w_u2=w_2*sin(beta_2)
c_m2=w_2*cos(beta_2)
c_u2=u_2+w_u2
h_02rel=h_2+0.5*w_2^2
P_02=pressure(Fluid$, h=h_02, s=s_2)
P_02rel=pressure(Fluid$, h=h_02rel, s=s_2)
cos(alpha_2)^2=1/N_blades "N_blades is optimum number of blades
-from Whitfield's equation"
" _____ "
i_2=h_2+0.5*w_2^2-0.5*u_2^2
i_3=i_2
s_3s=s_2
u_3=rpm*convert(min^-1,s^-1)*pi*d_3
" _____ "
h_3s=enthalpy(Fluid$, P=P_3, s=s_3s)
```


APPENDIX A2 EES CODES

```
i_3=h_3+0.5*w_3^2-0.5*u_3^2
h_3=h_3s+0.5*zeta_R*w_3^2
zeta_R=0.08034    "assumed"

T_3=temperature(Fluid$, P=P_3, h=h_3)
s_3=entropy(Fluid$, P=P_3, h=h_3)

"
_____

h_03=h_3+0.5*c_3^2
h_03rel=h_3+0.5*w_3^2
P_03=pressure(Fluid$, h=h_03, s=s_3)
P_03rel=pressure(Fluid$, h=h_03rel, s=s_3)
c_m3=c_3*cos(alpha_3)
alpha_3=0
c_u3=c_3*sin(alpha_3)
w_u3=u_3+c_u3
w_u3=w_3*sin(beta_3)

"
_____

m_dot=rho_3*pi*((d_3s^2-d_3h^2)/4)*(1-BK_3)*c_m3
BK_3=0.05    "assumed"

"
_____

s_4s=s_3
h_4s=enthalpy(Fluid$, P=P_4, s=s_4s)
P_4=180000 [Pa]    "delete"
h_04=h_03
h_04=h_4+0.5*c_4^2
h_4=h_4s+0.5*zeta_d*c_4^2
zeta_d=0.08034    "assumed"

T_4=temperature(Fluid$, P=P_4, h=h_4)
s_4=entropy(Fluid$, P=P_4, h=h_4)
m_dot=rho_4*pi*((d_4^2-(d_4-2*b_4)^2)/4)*(1-BK_4)*c_m4
```

APPENDIX A2 EES CODES

```
BK_4=0.05 "assumed"

c_m4=c_4*cos(alpha_4)
c_u4=c_4*sin(alpha_4)

alpha_4=0

"
_____
"Efficiency"

eta_ts=(h_01-h_03)/(h_01-h_3ss)

eta_tt=(h_01-h_03)/(h_01-h_03ss)

h_03ss=enthalpy(Fluid$, P=P_03, s=s_1)

"Reaction"
Rr=deltah_RR/deltah_Rstage

deltah_RR=h_2-h_3

deltah_RN=h_1-h_2

deltah_Rstage=h_1-h_3

R_s=deltah_SR/deltah_SStage

deltah_SR=h_2s-h_3ss

deltah_SStage=h_1-h_3ss

"Specific Speed"
N_s=rpm/(1*convert(min,s))*Q_3^0.5/deltah_0stage^(3/4)
Q_3=m_dot/rho_3
deltah_0stage=h_01-h_03ss

"Mach Numbers"

Ma_1=c_1/(SoundSpeed(Fluid$,T=T_1,P=P_1))

Ma_2=c_2/(SoundSpeed(Fluid$,T=T_2,P=P_2))

Ma_2rel=w_2/(SoundSpeed(Fluid$,T=T_2,P=P_2))

Ma_3=c_3/(SoundSpeed(Fluid$,T=T_3,P=P_3))

Ma_3rel=w_3/(SoundSpeed(Fluid$,T=T_3,P=P_3))

Ma_4=c_4/(SoundSpeed(Fluid$,T=T_4,P=P_4))

C_s1=SoundSpeed(Fluid$,T=T_1,P=P_1)

C_s2=SoundSpeed(Fluid$,T=T_2,P=P_2)
```

APPENDIX A2 EES CODES

```
C_s3=SoundSpeed(Fluid$,T=T_3,P=P_3)
```

```
C_s4=SoundSpeed(Fluid$,T=T_4,P=P_4)
```

APPENDIX A2 EES CODES

```
{ $DS. } "AXIAL TURBINE MODEL WITH PARAMETRIC TABLE ANALYSIS"
```

```
"Flow through Nozzle"
```

```
"  
-----"  
"Geometrical Input Data"  
d_1=d_2  
d_3=d_2  
b_1=b_2  
b_3=b_2  
b_1/d_1=0.15  
"  
-----"
```

```
"Operational Input Data"
```

```
PSI=1.55
```

```
PHI=0.8 "assumed"
```

```
rpm=U/(pi*(d_1+b_1))*convert('-/s','-/min')
```

```
W_dot=m_dot*(h_01-h_03)
```

```
PSI=W_s/U^2
```

```
PHI=C_a1/U
```

```
"  
-----"
```

```
"station 1"
```

```
rho_1=density(WF$,P=P_1,T=T_1)
```

```
h_1=enthalpy(WF$,P=P_1,T=T_1)
```

```
s_1=entropy(WF$,P=P_1,T=T_1)
```

```
P_01=pressure(WF$,h=h_01,s=s_1)
```

```
T_01=Temperature(WF$,h=h_01,s=s_1)
```

```
"  
-----"
```

```
"station 2"
```

```
rho_2=density(WF$,P=P_2,T=T_2)
```

```
h_2=enthalpy(WF$,P=P_2,T=T_2)
```

```
s_2=entropy(WF$,P=P_2,T=T_2)
```

```
P_02=pressure(WF$,h=h_02,s=s_2)
```

```
T_02=Temperature(WF$,h=h_02,s=s_2)
```

```
"  
-----"
```

```
"station 3"
```

```
rho_3=density(WF$,P=P_3,T=T_3)
```

```
h_3=enthalpy(WF$,P=P_3,T=T_3)
```

```
s_3=entropy(WF$,P=P_3,T=T_3)
```

```
P_03=pressure(WF$,h=h_03,s=s_3)
```

```
T_03=Temperature(WF$,h=h_03,s=s_3)
```

```
"  
-----"
```

APPENDIX A2 EES CODES

"Continuity"

$$A_1 = \pi \cdot d_1 \cdot b_1$$

$$A_1 = A_2$$

$$A_3 = A_2$$

$$m_{\text{dot}} = A_1 \cdot C_{a1} \cdot \rho_{o1}$$

$$m_{\text{dot}} = A_2 \cdot C_{a2} \cdot \rho_{o2}$$

$$m_{\text{dot}} = A_3 \cdot C_{a3} \cdot \rho_{o3}$$

"

"Conservation of stagnation enthalpy"

$$h_{o1} = h_{o2}$$

$$h_{o1} = h_1 + 0.5 \cdot C_1^2$$

$$\alpha_1 = 0$$

$$\alpha_1 = \alpha_3 \quad \text{"assumed"}$$

$$C_{a1} = C_1 \cdot \cos(\alpha_1)$$

$$C_{a2} = C_2 \cdot \cos(\alpha_2)$$

$$C_{a3} = C_3 \cdot \cos(\alpha_3)$$

"

"Conservation of Rothalpy"

$$i_2 = i_3$$

$$i_2 = h_2 + 0.5 \cdot W_2^2 - 0.5 \cdot U^2$$

$$i_3 = h_3 + 0.5 \cdot W_3^2 - 0.5 \cdot U^2$$

$$C_{a3} = W_3 \cdot \cos(\beta_3)$$

$$U = W_3 \cdot \sin(\beta_3)$$

"

$$W_s = h_{o1} - h_{o3}$$

$$W_s = U \cdot (C_{u2} + C_{u3})$$

$$W_s = U \cdot (W_2 \cdot \sin(\beta_2) + U)$$

$$W_2 \cdot \cos(\beta_2) = W_3 \cdot \cos(\beta_3)$$

$$C_2 \cdot \cos(\alpha_2) = C_3 \cdot \cos(\alpha_3)$$

$$C_2 \cdot \sin(\alpha_2) + C_3 \cdot \sin(\alpha_3) = W_2 \cdot \sin(\beta_2) + W_3 \cdot \sin(\beta_3)$$

$$C_{u3} = C_3 \cdot \sin(\alpha_3)$$

APPENDIX A2 EES CODES

```
h_03=h_3+0.5*C_3^2

"
_____
"

"Soderbergs loss correlations"
h_2-h_2s=0.5*C_2^2*zeta_N

h_3-h_3s=0.5*W_3^2*zeta_R

zeta_N=0.04+0.06*(epsilon_N/100)^2

zeta_R=0.04+0.06*(epsilon_R/100)^2

epsilon_N=alpha_1+alpha_2      "fluid deflection assumed equal blade
deflection"

epsilon_R=beta_2+beta_3      "fluid deflection assumed equal blade
deflection"

"Reaction"
R_s=(h_2-h_3)/(h_1-h_3)

"Efficiencies"

h_03ss=enthalpy(WF$,P=P_03,s=s_1)

h_3ss=enthalpy(WF$,P=P_3,s=s_1)

eta_tt_2=(1+(zeta_R*W_3^2+zeta_N*C_2^2*(T_3/T_2))/(2*(h_1-h_3)))^(-1)

eta_ts_2=(1+(zeta_R*W_3^2+zeta_N*C_2^2*(T_3/T_2)+C_1^2)/(2*(h_1-
h_3)))^(-1)

PHI_T=PHI

2*Ratio*(tan(alpha_1)+tan(alpha_2))*cos(alpha_2)^2=PHI_T "optimum
ratio = s/b space-chord ratio"

PR=P_01/P_03      "pressure ratio"

"Mach Numbers"

Ma_1=C_1/(SoundSpeed(WF$,T=T_1,P=P_1))

Ma_2=C_2/(SoundSpeed(WF$,T=T_2,P=P_2))

Ma_2rel=W_2/(SoundSpeed(WF$,T=T_2,P=P_2))

Ma_3=C_3/(SoundSpeed(WF$,T=T_3,P=P_3))

Ma_3rel=W_3/(SoundSpeed(WF$,T=T_3,P=P_3))

C_s1=SoundSpeed(WF$,T=T_1,P=P_1)

C_s2=SoundSpeed(WF$,T=T_2,P=P_2)

C_s3=SoundSpeed(WF$,T=T_3,P=P_3)
```

APPENDIX A3 RESULTS

- A3.1 9-collector model
- A3.2 180-collector model
- A3.3 Condenser Model Parametric Analysis
- A3.4 Turbine Modeling and Design – Summarised Results
- A3.5 Radial Turbine Simulations No. 01
- A3.6 Radial Turbine Simulations No. 02
- A3.7 Radial Turbine Simulations No. 03
- A3.8 Axial Turbine Simulations
- A3.9 Axial Turbine Preliminary Simulations
- A3.10 Axial Turbine Simulations
- A3.11 Experimental Test Results Template

APPENDIX A3 RESULTS

A3.1 9 Collector Model

Segment No.	alpha_air[i]	beta_air[i]	Cp_air[i]	h_p_c_conv[i]	h_p_c_rad[i]	k_air[i]	mu_air[i]	nu_air[i]	Q_dot_back[i]	Q_dot_conv[i]	Q_dot_c_a[i]	Q_dot_c_s[i]
-	[m ² /s]	[1/K]	[J/kg-K]	[W/m ² -K]	[W/m ² -K]	[W/m-K]	[N-s/m ²]	[m ² /s]	[J/s]	[J/s]	[J/s]	[J/s]
1	0.00002093	0.003398	1004	2.471	0.5679	0.02522	0.0000183	0.00001526	0.08696	0.6117	-0.482	1.234
2	0.00002095	0.003397	1004	2.482	0.5689	0.02523	0.00001831	0.00001527	0.0908	0.6264	-0.473	1.242
3	0.00002097	0.003395	1004	2.492	0.5699	0.02524	0.00001832	0.00001529	0.09462	0.641	-0.463	1.251
4	0.000021	0.003393	1004	2.502	0.5709	0.02526	0.00001833	0.0000153	0.09844	0.6556	-0.454	1.259
5	0.00002102	0.003391	1004	2.512	0.5719	0.02527	0.00001834	0.00001532	0.1022	0.6702	-0.445	1.268
6	0.00002104	0.003389	1004	2.521	0.5728	0.02528	0.00001834	0.00001533	0.106	0.6847	-0.436	1.276
7	0.00002106	0.003387	1004	2.53	0.5738	0.02529	0.00001835	0.00001535	0.1098	0.6992	-0.427	1.285
8	0.00002108	0.003385	1004	2.539	0.5748	0.02531	0.00001836	0.00001536	0.1135	0.7137	-0.418	1.293
9	0.00002111	0.003383	1004	2.548	0.5758	0.02532	0.00001837	0.00001538	0.1173	0.7281	-0.409	1.302
10	0.00002113	0.003381	1005	2.556	0.5768	0.02533	0.00001838	0.0000154	0.121	0.7425	-0.4	1.31
11	0.00002115	0.003379	1005	2.564	0.5777	0.02534	0.00001838	0.00001541	0.1247	0.7569	-0.391	1.319
12	0.00002117	0.003377	1005	2.572	0.5787	0.02536	0.00001839	0.00001543	0.1285	0.7712	-0.382	1.327
13	0.00002119	0.003375	1005	2.58	0.5797	0.02537	0.0000184	0.00001544	0.1322	0.7855	-0.373	1.335
14	0.00002122	0.003374	1005	2.587	0.5806	0.02538	0.00001841	0.00001546	0.1358	0.7997	-0.365	1.344
15	0.00002124	0.003372	1005	2.594	0.5816	0.02539	0.00001841	0.00001547	0.1395	0.8139	-0.356	1.352

APPENDIX A3 RESULTS

A3.1 9 Collector Model

Segment No.	$\alpha_{air}[i]$	$\beta_{air}[i]$	$C_{p_air}[i]$	$h_{p_c_conv}[i]$	$h_{p_c_rad}[i]$	$k_{air}[i]$	$\mu_{air}[i]$	$\nu_{air}[i]$	$Q_{dot_back}[i]$	$Q_{dot_conv}[i]$	$Q_{dot_c_a}[i]$	$Q_{dot_c_s}[i]$
-	[m ² /s]	[1/K]	[J/kg-K]	[W/m ² -K]	[W/m ² -K]	[W/m-K]	[N-s/m ²]	[m ² /s]	[J/s]	[J/s]	[J/s]	[J/s]
16	0.00002126	0.00337	1005	2.601	0.5826	0.02541	0.00001842	0.00001549	0.1432	0.8281	-0.347	1.36
17	0.00002128	0.003368	1005	2.608	0.5835	0.02542	0.00001843	0.0000155	0.1468	0.8423	-0.338	1.369
18	0.0000213	0.003366	1005	2.615	0.5845	0.02543	0.00001844	0.00001551	0.1504	0.8563	-0.329	1.377
19	0.00002132	0.003364	1005	2.621	0.5855	0.02544	0.00001844	0.00001553	0.1541	0.8704	-0.321	1.385
20	0.00002134	0.003363	1005	2.628	0.5864	0.02545	0.00001845	0.00001554	0.1577	0.8844	-0.312	1.394
21	0.00002137	0.003361	1005	2.634	0.5874	0.02547	0.00001846	0.00001556	0.1613	0.8984	-0.303	1.402
22	0.00002139	0.003359	1005	2.64	0.5883	0.02548	0.00001847	0.00001557	0.1648	0.9123	-0.294	1.41
23	0.00002141	0.003357	1005	2.646	0.5893	0.02549	0.00001847	0.00001559	0.1684	0.9262	-0.286	1.418
24	0.00002143	0.003355	1005	2.652	0.5902	0.0255	0.00001848	0.0000156	0.172	0.9401	-0.277	1.426
25	0.00002145	0.003354	1005	2.658	0.5912	0.02551	0.00001849	0.00001562	0.1755	0.9539	-0.269	1.435
26	0.00002147	0.003352	1005	2.663	0.5921	0.02552	0.0000185	0.00001563	0.179	0.9677	-0.26	1.443
27	0.00002149	0.00335	1005	2.668	0.593	0.02554	0.0000185	0.00001565	0.1826	0.9814	-0.251	1.451
28	0.00002151	0.003348	1005	2.674	0.594	0.02555	0.00001851	0.00001566	0.1861	0.9951	-0.243	1.459
29	0.00002153	0.003347	1005	2.679	0.5949	0.02556	0.00001852	0.00001567	0.1896	1.009	-0.234	1.467
30	0.00002155	0.003345	1005	2.684	0.5959	0.02557	0.00001853	0.00001569	0.1931	1.022	-0.226	1.475

APPENDIX A3 RESULTS

A3.1 9 Collector Model

Segment No.	Q_dot_rad[i]	Q_dot_wg[i]	rho_air[i]	T_c[i]	T_m_air[i]	T_m_airK[i]	T_p[i]	T_wg_in[i]	T_wg_m[i]	T_wg_out[i]	Nup[i]	Ra[i]
-	[J/s]	[J/s]	[kg/m ³]	[C]	[C]	[K]	[C]	[C]	[C]	[C]	[-]	[-]
1	0.1406	6.451	1.2	16.15	21.1	294.2	26.05	20	20.14	20.29	2.493	16150
2	0.1436	6.429	1.199	16.22	21.27	294.4	26.32	20.29	20.43	20.57	2.505	16422
3	0.1466	6.408	1.198	16.29	21.44	294.6	26.58	20.57	20.72	20.86	2.516	16692
4	0.1496	6.386	1.198	16.37	21.61	294.8	26.85	20.86	21	21.14	2.528	16959
5	0.1526	6.365	1.197	16.44	21.78	294.9	27.11	21.14	21.28	21.43	2.539	17224
6	0.1556	6.344	1.196	16.51	21.94	295.1	27.38	21.43	21.57	21.71	2.55	17486
7	0.1586	6.322	1.196	16.58	22.11	295.3	27.64	21.71	21.85	21.99	2.56	17745
8	0.1616	6.301	1.195	16.66	22.28	295.4	27.9	21.99	22.13	22.27	2.57	18002
9	0.1646	6.28	1.194	16.73	22.44	295.6	28.16	22.27	22.41	22.55	2.58	18257
10	0.1676	6.259	1.194	16.8	22.61	295.8	28.42	22.55	22.69	22.83	2.59	18510
11	0.1705	6.238	1.193	16.87	22.77	295.9	28.68	22.83	22.97	23.11	2.599	18759
12	0.1735	6.217	1.192	16.94	22.94	296.1	28.94	23.11	23.24	23.38	2.609	19007
13	0.1765	6.196	1.192	17.01	23.1	296.3	29.19	23.38	23.52	23.66	2.618	19252
14	0.1795	6.175	1.191	17.08	23.27	296.4	29.45	23.66	23.8	23.93	2.626	19495
15	0.1825	6.154	1.19	17.15	23.43	296.6	29.7	23.93	24.07	24.21	2.635	19736

APPENDIX A3 RESULTS

A3.1 9 Collector Model

Segment No.	Q_dot_rad[i] [J/s]	Q_dot_wg[i] [J/s]	rho_air[i] [kg/m ³]	T_c[i] [C]	T_m_air[i] [C]	T_m_airK[i] [K]	T_p[i] [C]	T_wg_in[i] [C]	T_wg_m[i] [C]	T_wg_out[i] [C]	Nup[i] [-]	Ra[i] [-]
16	0.1855	6.133	1.19	17.23	23.59	296.7	29.96	24.21	24.34	24.48	2.643	19975
17	0.1884	6.113	1.189	17.3	23.75	296.9	30.21	24.48	24.62	24.75	2.652	20211
18	0.1914	6.092	1.188	17.37	23.92	297.1	30.47	24.75	24.89	25.02	2.66	20445
19	0.1944	6.071	1.188	17.44	24.08	297.2	30.72	25.02	25.16	25.29	2.668	20677
20	0.1974	6.051	1.187	17.51	24.24	297.4	30.97	25.29	25.43	25.56	2.676	20907
21	0.2003	6.03	1.186	17.58	24.4	297.5	31.22	25.56	25.7	25.83	2.683	21135
22	0.2033	6.01	1.186	17.64	24.56	297.7	31.47	25.83	25.97	26.1	2.691	21360
23	0.2063	5.989	1.185	17.71	24.71	297.9	31.72	26.1	26.23	26.37	2.698	21584
24	0.2092	5.969	1.185	17.78	24.87	298	31.96	26.37	26.5	26.63	2.705	21806
25	0.2122	5.948	1.184	17.85	25.03	298.2	32.21	26.63	26.76	26.9	2.712	22025
26	0.2152	5.928	1.183	17.92	25.19	298.3	32.46	26.9	27.03	27.16	2.719	22243
27	0.2181	5.908	1.183	17.99	25.34	298.5	32.7	27.16	27.29	27.42	2.726	22459
28	0.2211	5.888	1.182	18.06	25.5	298.7	32.94	27.42	27.55	27.68	2.732	22672
29	0.224	5.868	1.181	18.13	25.66	298.8	33.19	27.68	27.82	27.95	2.739	22884
30	0.227	5.848	1.181	18.19	25.81	299	33.43	27.95	28.08	28.21	2.745	23094

APPENDIX A3 RESULTS

A3.2 180 Collector Model

Segment No.	alpha_air[i]	beta_air[i]	Cp_air[i]	h_p_c_conv[i]	h_p_c_rad[i]	k_air[i]	mu_air[i]	nu_air[i]	Q_dot_back[i]	Q_dot_conv[i]	Q_dot_c_a[i]	Q_dot_c_s[i]
-	[m ² /s]	[1/K]	[J/kg-K]	[W/m ² -K]	[W/m ² -K]	[W/m-K]	[N-s/m ²]	[m ² /s]	[J/s]	[J/s]	[J/s]	[J/s]
1	0.00002093	0.003398	1004	2.471	0.5679	0.02522	0.0000183	0.00001526	0.087	0.6117	-0.4816	1.234
2	0.00002095	0.003397	1004	2.482	0.5689	0.02523	0.00001831	0.00001527	0.0908	0.6264	-0.4725	1.242
3	0.00002097	0.003395	1004	2.492	0.5699	0.02524	0.00001832	0.00001529	0.0946	0.641	-0.4633	1.251
4	0.000021	0.003393	1004	2.502	0.5709	0.02526	0.00001833	0.0000153	0.0984	0.6556	-0.4543	1.259
5	0.00002102	0.003391	1004	2.512	0.5719	0.02527	0.00001834	0.00001532	0.1022	0.6702	-0.4452	1.268
6	0.00002104	0.003389	1004	2.521	0.5728	0.02528	0.00001834	0.00001533	0.106	0.6847	-0.4361	1.276
7	0.00002106	0.003387	1004	2.53	0.5738	0.02529	0.00001835	0.00001535	0.1098	0.6992	-0.4271	1.285
8	0.00002108	0.003385	1004	2.539	0.5748	0.02531	0.00001836	0.00001536	0.1135	0.7137	-0.4181	1.293
9	0.00002111	0.003383	1004	2.548	0.5758	0.02532	0.00001837	0.00001538	0.1173	0.7281	-0.4091	1.302
10	0.00002113	0.003381	1005	2.556	0.5768	0.02533	0.00001838	0.0000154	0.121	0.7425	-0.4001	1.31
11	0.00002115	0.003379	1005	2.564	0.5777	0.02534	0.00001838	0.00001541	0.1247	0.7569	-0.3912	1.319
12	0.00002117	0.003377	1005	2.572	0.5787	0.02536	0.00001839	0.00001543	0.1285	0.7712	-0.3823	1.327
13	0.00002119	0.003375	1005	2.58	0.5797	0.02537	0.0000184	0.00001544	0.1322	0.7855	-0.3734	1.335
14	0.00002122	0.003374	1005	2.587	0.5806	0.02538	0.00001841	0.00001546	0.1358	0.7997	-0.3645	1.344
15	0.00002124	0.003372	1005	2.594	0.5816	0.02539	0.00001841	0.00001547	0.1395	0.8139	-0.3557	1.352
16	0.00002126	0.00337	1005	2.601	0.5826	0.02541	0.00001842	0.00001549	0.1432	0.8281	-0.3468	1.36
17	0.00002128	0.003368	1005	2.608	0.5835	0.02542	0.00001843	0.0000155	0.1468	0.8423	-0.338	1.369
18	0.0000213	0.003366	1005	2.615	0.5845	0.02543	0.00001844	0.00001551	0.1504	0.8563	-0.3293	1.377
19	0.00002132	0.003364	1005	2.621	0.5855	0.02544	0.00001844	0.00001553	0.1541	0.8704	-0.3205	1.385
20	0.00002134	0.003363	1005	2.628	0.5864	0.02545	0.00001845	0.00001554	0.1577	0.8844	-0.3118	1.394
21	0.00002137	0.003361	1005	2.634	0.5874	0.02547	0.00001846	0.00001556	0.1613	0.8984	-0.3031	1.402
22	0.00002139	0.003359	1005	2.64	0.5883	0.02548	0.00001847	0.00001557	0.1648	0.9123	-0.2944	1.41
23	0.00002141	0.003357	1005	2.646	0.5893	0.02549	0.00001847	0.00001559	0.1684	0.9262	-0.2857	1.418

APPENDIX A3 RESULTS

A3.2 180 Collector Model

Segment No.	$\alpha_{air}[i]$	$\beta_{air}[i]$	$Cp_{air}[i]$	$h_{p_c_conv}[i]$	$h_{p_c_rad}[i]$	$k_{air}[i]$	$\mu_{air}[i]$	$\nu_{air}[i]$	$Q_{dot_back}[i]$	$Q_{dot_conv}[i]$	$Q_{dot_c_a}[i]$	$Q_{dot_c_s}[i]$
-	[m ² /s]	[1/K]	[J/kg-K]	[W/m ² -K]	[W/m ² -K]	[W/m-K]	[N-s/m ²]	[m ² /s]	[J/s]	[J/s]	[J/s]	[J/s]
24	0.00002143	0.003355	1005	2.652	0.5902	0.0255	0.00001848	0.0000156	0.172	0.9401	-0.2771	1.426
25	0.00002145	0.003354	1005	2.658	0.5912	0.02551	0.00001849	0.00001562	0.1755	0.9539	-0.2685	1.435
26	0.00002147	0.003352	1005	2.663	0.5921	0.02552	0.0000185	0.00001563	0.179	0.9677	-0.2599	1.443
27	0.00002149	0.00335	1005	2.668	0.593	0.02554	0.0000185	0.00001565	0.1826	0.9814	-0.2514	1.451
28	0.00002151	0.003348	1005	2.674	0.594	0.02555	0.00001851	0.00001566	0.1861	0.9951	-0.2429	1.459
29	0.00002153	0.003347	1005	2.679	0.5949	0.02556	0.00001852	0.00001567	0.1896	1.009	-0.2344	1.467
30	0.00002155	0.003345	1005	2.684	0.5959	0.02557	0.00001853	0.00001569	0.1931	1.022	-0.2259	1.475
31	0.00002158	0.003343	1005	2.689	0.5968	0.02558	0.00001853	0.0000157	0.1966	1.036	-0.2173	1.483
32	0.0000216	0.003341	1005	2.694	0.5977	0.02559	0.00001854	0.00001572	0.2	1.05	-0.2089	1.491
33	0.00002162	0.00334	1005	2.698	0.5987	0.0256	0.00001855	0.00001573	0.2035	1.063	-0.2005	1.499
34	0.00002164	0.003338	1005	2.703	0.5996	0.02562	0.00001855	0.00001575	0.2069	1.077	-0.1921	1.507
35	0.00002166	0.003336	1005	2.707	0.6005	0.02563	0.00001856	0.00001576	0.2103	1.09	-0.1837	1.515
36	0.00002168	0.003335	1005	2.712	0.6014	0.02564	0.00001857	0.00001577	0.2138	1.103	-0.1754	1.523
37	0.0000217	0.003333	1005	2.716	0.6024	0.02565	0.00001858	0.00001579	0.2172	1.117	-0.1671	1.531
38	0.00002172	0.003331	1005	2.72	0.6033	0.02566	0.00001858	0.0000158	0.2205	1.13	-0.1589	1.539
39	0.00002174	0.00333	1005	2.724	0.6042	0.02567	0.00001859	0.00001582	0.2239	1.143	-0.1506	1.547
40	0.00002176	0.003328	1005	2.728	0.6051	0.02568	0.0000186	0.00001583	0.2273	1.156	-0.1424	1.555
41	0.00002178	0.003326	1005	2.732	0.606	0.02569	0.0000186	0.00001584	0.2306	1.169	-0.1342	1.563
42	0.0000218	0.003325	1005	2.736	0.6069	0.02571	0.00001861	0.00001586	0.234	1.182	-0.126	1.571
43	0.00002182	0.003323	1005	2.74	0.6078	0.02572	0.00001862	0.00001587	0.2373	1.195	-0.1179	1.579
44	0.00002184	0.003321	1005	2.744	0.6087	0.02573	0.00001862	0.00001588	0.2406	1.209	-0.1098	1.586
45	0.00002186	0.00332	1005	2.747	0.6096	0.02574	0.00001863	0.0000159	0.2439	1.221	-0.1017	1.594
46	0.00002188	0.003318	1005	2.751	0.6106	0.02575	0.00001864	0.00001591	0.2472	1.234	-0.09362	1.602

APPENDIX A3 RESULTS

A3.2 180 Collector Model

Segment No.	alpha_air[i]	beta_air[i]	Cp_air[i]	h_p_c_conv[i]	h_p_c_rad[i]	k_air[i]	mu_air[i]	nu_air[i]	Q_dot_back[i]	Q_dot_conv[i]	Q_dot_c_a[i]	Q_dot_c_s[i]
-	[m ² /s]	[1/K]	[J/kg-K]	[W/m ² -K]	[W/m ² -K]	[W/m-K]	[N-s/m ²]	[m ² /s]	[J/s]	[J/s]	[J/s]	[J/s]
47	0.0000219	0.003317	1005	2.755	0.6115	0.02576	0.00001864	0.00001593	0.2505	1.247	-0.08559	1.61
48	0.00002192	0.003315	1005	2.758	0.6123	0.02577	0.00001865	0.00001594	0.2538	1.26	-0.07758	1.617
49	0.00002194	0.003313	1005	2.761	0.6132	0.02578	0.00001866	0.00001595	0.2571	1.273	-0.06959	1.625
50	0.00002196	0.003312	1005	2.765	0.6141	0.02579	0.00001867	0.00001597	0.2603	1.286	-0.06163	1.633
51	0.00002198	0.00331	1005	2.768	0.615	0.0258	0.00001867	0.00001598	0.2635	1.298	-0.0537	1.64
52	0.000022	0.003309	1005	2.771	0.6159	0.02581	0.00001868	0.00001599	0.2668	1.311	-0.04579	1.648
53	0.00002202	0.003307	1005	2.774	0.6168	0.02582	0.00001869	0.00001601	0.27	1.324	-0.03791	1.656
54	0.00002203	0.003305	1005	2.777	0.6177	0.02584	0.00001869	0.00001602	0.2732	1.336	-0.03006	1.663
55	0.00002205	0.003304	1005	2.78	0.6186	0.02585	0.0000187	0.00001603	0.2764	1.349	-0.02223	1.671
56	0.00002207	0.003302	1005	2.783	0.6194	0.02586	0.0000187	0.00001605	0.2796	1.361	-0.01443	1.679
57	0.00002209	0.003301	1005	2.786	0.6203	0.02587	0.00001871	0.00001606	0.2827	1.374	-0.00665	1.686
58	0.00002211	0.003299	1005	2.789	0.6212	0.02588	0.00001872	0.00001607	0.2859	1.386	0.0011	1.694
59	0.00002213	0.003298	1005	2.792	0.6221	0.02589	0.00001872	0.00001608	0.289	1.398	0.00882	1.701
60	0.00002215	0.003296	1005	2.794	0.6229	0.0259	0.00001873	0.0000161	0.2922	1.411	0.01652	1.709
61	0.00002217	0.003295	1005	2.797	0.6238	0.02591	0.00001874	0.00001611	0.2954	1.423	0.02434	1.716
62	0.00002219	0.003293	1005	2.8	0.6247	0.02592	0.00001874	0.00001612	0.2985	1.435	0.03199	1.724
63	0.00002221	0.003292	1005	2.802	0.6256	0.02593	0.00001875	0.00001614	0.3016	1.448	0.03961	1.731
64	0.00002222	0.00329	1005	2.805	0.6264	0.02594	0.00001876	0.00001615	0.3047	1.46	0.0472	1.738
65	0.00002224	0.003289	1005	2.807	0.6273	0.02595	0.00001876	0.00001616	0.3078	1.472	0.05477	1.746
66	0.00002226	0.003287	1005	2.81	0.6282	0.02596	0.00001877	0.00001617	0.3108	1.484	0.06231	1.753
67	0.00002228	0.003286	1005	2.812	0.629	0.02597	0.00001878	0.00001619	0.3139	1.496	0.06983	1.761
68	0.0000223	0.003284	1005	2.814	0.6299	0.02598	0.00001878	0.0000162	0.317	1.508	0.07732	1.768
69	0.00002232	0.003283	1005	2.817	0.6307	0.02599	0.00001879	0.00001621	0.32	1.52	0.08479	1.775

APPENDIX A3 RESULTS

A3.2 180 Collector Model

Segment No.	$\alpha_{air}[i]$	$\beta_{air}[i]$	$Cp_{air}[i]$	$h_{p_c_conv}[i]$	$h_{p_c_rad}[i]$	$k_{air}[i]$	$\mu_{air}[i]$	$\nu_{air}[i]$	$Q_{dot_back}[i]$	$Q_{dot_conv}[i]$	$Q_{dot_c_a}[i]$	$Q_{dot_c_s}[i]$
-	[m ² /s]	[1/K]	[J/kg-K]	[W/m ² -K]	[W/m ² -K]	[W/m-K]	[N-s/m ²]	[m ² /s]	[J/s]	[J/s]	[J/s]	[J/s]
70	0.00002234	0.003281	1005	2.819	0.6316	0.026	0.00001879	0.00001623	0.323	1.532	0.09223	1.782
71	0.00002235	0.00328	1005	2.821	0.6324	0.02601	0.0000188	0.00001624	0.326	1.543	0.09965	1.79
72	0.00002237	0.003278	1005	2.823	0.6333	0.02602	0.00001881	0.00001625	0.3291	1.555	0.107	1.797
73	0.00002239	0.003277	1005	2.825	0.6341	0.02603	0.00001881	0.00001626	0.3321	1.567	0.1144	1.804
74	0.00002241	0.003276	1005	2.827	0.6349	0.02604	0.00001882	0.00001628	0.335	1.579	0.1217	1.811
75	0.00002243	0.003274	1005	2.829	0.6358	0.02605	0.00001883	0.00001629	0.338	1.59	0.1291	1.819
76	0.00002244	0.003273	1005	2.831	0.6366	0.02606	0.00001883	0.0000163	0.341	1.602	0.1363	1.826
77	0.00002246	0.003271	1005	2.833	0.6375	0.02607	0.00001884	0.00001631	0.3439	1.613	0.1436	1.833
78	0.00002248	0.00327	1005	2.835	0.6383	0.02608	0.00001884	0.00001632	0.3469	1.625	0.1509	1.84
79	0.0000225	0.003269	1005	2.837	0.6391	0.02609	0.00001885	0.00001634	0.3498	1.636	0.1581	1.847
80	0.00002252	0.003267	1005	2.839	0.64	0.0261	0.00001886	0.00001635	0.3528	1.648	0.1653	1.854
81	0.00002253	0.003266	1005	2.841	0.6408	0.02611	0.00001886	0.00001636	0.3557	1.659	0.1724	1.861
82	0.00002255	0.003264	1005	2.843	0.6416	0.02612	0.00001887	0.00001637	0.3586	1.671	0.1796	1.868
83	0.00002257	0.003263	1005	2.845	0.6424	0.02613	0.00001887	0.00001639	0.3615	1.682	0.1867	1.875
84	0.00002259	0.003262	1005	2.846	0.6432	0.02614	0.00001888	0.0000164	0.3644	1.693	0.1938	1.882
85	0.0000226	0.00326	1005	2.848	0.6441	0.02615	0.00001889	0.00001641	0.3672	1.705	0.2008	1.889
86	0.00002262	0.003259	1005	2.85	0.6449	0.02616	0.00001889	0.00001642	0.3701	1.716	0.2079	1.896
87	0.00002264	0.003258	1005	2.851	0.6457	0.02616	0.0000189	0.00001643	0.3729	1.727	0.2149	1.903
88	0.00002266	0.003256	1005	2.853	0.6465	0.02617	0.0000189	0.00001645	0.3758	1.738	0.2219	1.91
89	0.00002267	0.003255	1005	2.855	0.6473	0.02618	0.00001891	0.00001646	0.3786	1.749	0.2288	1.917
90	0.00002269	0.003254	1005	2.856	0.6481	0.02619	0.00001892	0.00001647	0.3814	1.76	0.2358	1.924
91	0.00002271	0.003252	1005	2.858	0.6489	0.0262	0.00001892	0.00001648	0.3842	1.771	0.2426	1.93
92	0.00002272	0.003251	1005	2.859	0.6497	0.02621	0.00001893	0.00001649	0.387	1.782	0.2495	1.937

APPENDIX A3 RESULTS

A3.2 180 Collector Model

Segment No.	alpha_air[i]	beta_air[i]	Cp_air[i]	h_p_c_conv[i]	h_p_c_rad[i]	k_air[i]	mu_air[i]	nu_air[i]	Q_dot_back[i]	Q_dot_conv[i]	Q_dot_c_a[i]	Q_dot_c_s[i]
-	[m ² /s]	[1/K]	[J/kg-K]	[W/m ² -K]	[W/m ² -K]	[W/m-K]	[N-s/m ²]	[m ² /s]	[J/s]	[J/s]	[J/s]	[J/s]
93	0.00002274	0.00325	1005	2.861	0.6505	0.02622	0.00001893	0.0000165	0.3898	1.793	0.2563	1.944
94	0.00002276	0.003248	1005	2.862	0.6513	0.02623	0.00001894	0.00001652	0.3926	1.804	0.2632	1.951
95	0.00002278	0.003247	1005	2.864	0.6521	0.02624	0.00001894	0.00001653	0.3954	1.815	0.27	1.958
96	0.00002279	0.003246	1005	2.865	0.6529	0.02625	0.00001895	0.00001654	0.3981	1.825	0.2768	1.964
97	0.00002281	0.003244	1005	2.867	0.6537	0.02626	0.00001896	0.00001655	0.4009	1.836	0.2836	1.971
98	0.00002283	0.003243	1005	2.868	0.6545	0.02627	0.00001896	0.00001656	0.4037	1.847	0.2903	1.978
99	0.00002284	0.003242	1005	2.869	0.6553	0.02628	0.00001897	0.00001657	0.4064	1.857	0.2971	1.985
100	0.00002286	0.00324	1005	2.871	0.6561	0.02628	0.00001897	0.00001659	0.4091	1.868	0.3038	1.991
101	0.00002288	0.003239	1005	2.872	0.6569	0.02629	0.00001898	0.0000166	0.4118	1.879	0.3104	1.998
102	0.00002289	0.003238	1005	2.873	0.6576	0.0263	0.00001898	0.00001661	0.4145	1.889	0.3171	2.005
103	0.00002291	0.003237	1005	2.874	0.6584	0.02631	0.00001899	0.00001662	0.4172	1.9	0.3237	2.011
104	0.00002293	0.003235	1005	2.876	0.6592	0.02632	0.00001899	0.00001663	0.4199	1.91	0.3303	2.018
105	0.00002294	0.003234	1005	2.877	0.66	0.02633	0.000019	0.00001664	0.4226	1.921	0.3369	2.024
106	0.00002296	0.003233	1005	2.878	0.6608	0.02634	0.00001901	0.00001665	0.4253	1.931	0.3435	2.031
107	0.00002297	0.003232	1005	2.879	0.6615	0.02635	0.00001901	0.00001666	0.4279	1.941	0.35	2.037
108	0.00002299	0.00323	1005	2.88	0.6623	0.02635	0.00001902	0.00001668	0.4306	1.952	0.3565	2.044
109	0.00002301	0.003229	1005	2.882	0.6631	0.02636	0.00001902	0.00001669	0.4332	1.962	0.363	2.05
110	0.00002302	0.003228	1005	2.883	0.6638	0.02637	0.00001903	0.0000167	0.4359	1.972	0.3695	2.057
111	0.00002304	0.003227	1005	2.884	0.6646	0.02638	0.00001903	0.00001671	0.4385	1.982	0.3759	2.063
112	0.00002306	0.003226	1005	2.885	0.6654	0.02639	0.00001904	0.00001672	0.4411	1.993	0.3823	2.07
113	0.00002307	0.003224	1005	2.886	0.6661	0.0264	0.00001904	0.00001673	0.4437	2.003	0.3887	2.076
114	0.00002309	0.003223	1005	2.887	0.6669	0.02641	0.00001905	0.00001674	0.4463	2.013	0.3951	2.083
115	0.0000231	0.003222	1005	2.888	0.6676	0.02642	0.00001905	0.00001675	0.4489	2.023	0.4015	2.089

APPENDIX A3 RESULTS

A3.2 180 Collector Model

Segment No.	alpha_air[i]	beta_air[i]	Cp_air[i]	h_p_c_conv[i]	h_p_c_rad[i]	k_air[i]	mu_air[i]	nu_air[i]	Q_dot_back[i]	Q_dot_conv[i]	Q_dot_c_a[i]	Q_dot_c_s[i]
-	[m ² /s]	[1/K]	[J/kg-K]	[W/m ² -K]	[W/m ² -K]	[W/m-K]	[N-s/m ²]	[m ² /s]	[J/s]	[J/s]	[J/s]	[J/s]
116	0.00002312	0.003221	1005	2.889	0.6684	0.02642	0.00001906	0.00001676	0.4515	2.033	0.4078	2.095
117	0.00002313	0.00322	1005	2.89	0.6691	0.02643	0.00001906	0.00001677	0.454	2.043	0.4141	2.102
118	0.00002315	0.003218	1005	2.891	0.6699	0.02644	0.00001907	0.00001678	0.4566	2.053	0.4204	2.108
119	0.00002317	0.003217	1005	2.892	0.6706	0.02645	0.00001907	0.0000168	0.4592	2.063	0.4266	2.114
120	0.00002318	0.003216	1005	2.893	0.6714	0.02646	0.00001908	0.00001681	0.4617	2.072	0.4329	2.12
121	0.0000232	0.003215	1005	2.894	0.6721	0.02647	0.00001909	0.00001682	0.4642	2.082	0.4391	2.127
122	0.00002321	0.003214	1005	2.895	0.6729	0.02647	0.00001909	0.00001683	0.4668	2.092	0.4453	2.133
123	0.00002323	0.003213	1005	2.896	0.6736	0.02648	0.0000191	0.00001684	0.4693	2.102	0.4515	2.139
124	0.00002324	0.003211	1005	2.897	0.6743	0.02649	0.0000191	0.00001685	0.4718	2.112	0.4577	2.145
125	0.00002326	0.00321	1005	2.897	0.6751	0.0265	0.00001911	0.00001686	0.4743	2.121	0.4638	2.152
126	0.00002327	0.003209	1005	2.898	0.6758	0.02651	0.00001911	0.00001687	0.4768	2.131	0.4699	2.158
127	0.00002329	0.003208	1005	2.899	0.6765	0.02651	0.00001912	0.00001688	0.4793	2.14	0.476	2.164
128	0.0000233	0.003207	1005	2.9	0.6773	0.02652	0.00001912	0.00001689	0.4817	2.15	0.482	2.17
129	0.00002332	0.003206	1005	2.901	0.678	0.02653	0.00001913	0.0000169	0.4842	2.159	0.4881	2.176
130	0.00002334	0.003205	1005	2.902	0.6787	0.02654	0.00001913	0.00001691	0.4866	2.169	0.4941	2.182
131	0.00002335	0.003203	1005	2.902	0.6795	0.02655	0.00001914	0.00001692	0.4891	2.178	0.5001	2.188
132	0.00002337	0.003202	1005	2.903	0.6802	0.02656	0.00001914	0.00001693	0.4915	2.188	0.5061	2.194
133	0.00002338	0.003201	1005	2.904	0.6809	0.02656	0.00001915	0.00001694	0.4939	2.197	0.512	2.2
134	0.0000234	0.0032	1005	2.905	0.6816	0.02657	0.00001915	0.00001695	0.4964	2.207	0.5179	2.206
135	0.00002341	0.003199	1005	2.905	0.6823	0.02658	0.00001916	0.00001696	0.4988	2.216	0.5239	2.212
136	0.00002342	0.003198	1005	2.906	0.683	0.02659	0.00001916	0.00001697	0.5012	2.225	0.5297	2.218
137	0.00002344	0.003197	1005	2.907	0.6837	0.02659	0.00001917	0.00001698	0.5036	2.234	0.5356	2.224
138	0.00002345	0.003196	1005	2.907	0.6845	0.0266	0.00001917	0.00001699	0.506	2.244	0.5415	2.23

APPENDIX A3 RESULTS

A3.2 180 Collector Model

Segment No.	alpha_air[i]	beta_air[i]	Cp_air[i]	h_p_c_conv[i]	h_p_c_rad[i]	k_air[i]	mu_air[i]	nu_air[i]	Q_dot_back[i]	Q_dot_conv[i]	Q_dot_c_a[i]	Q_dot_c_s[i]
-	[m ² /s]	[1/K]	[J/kg-K]	[W/m ² -K]	[W/m ² -K]	[W/m-K]	[N-s/m ²]	[m ² /s]	[J/s]	[J/s]	[J/s]	[J/s]
139	0.00002347	0.003195	1005	2.908	0.6852	0.02661	0.00001918	0.000017	0.5083	2.253	0.5473	2.236
140	0.00002348	0.003194	1005	2.909	0.6859	0.02662	0.00001918	0.00001701	0.5107	2.262	0.5531	2.242
141	0.0000235	0.003193	1005	2.909	0.6866	0.02663	0.00001918	0.00001702	0.5131	2.271	0.5589	2.248
142	0.00002351	0.003191	1005	2.91	0.6873	0.02663	0.00001919	0.00001703	0.5154	2.28	0.5646	2.254
143	0.00002353	0.00319	1005	2.911	0.688	0.02664	0.00001919	0.00001704	0.5178	2.289	0.5704	2.26
144	0.00002354	0.003189	1005	2.911	0.6887	0.02665	0.0000192	0.00001705	0.5201	2.298	0.5761	2.265
145	0.00002356	0.003188	1005	2.912	0.6894	0.02666	0.0000192	0.00001706	0.5224	2.307	0.5818	2.271
146	0.00002357	0.003187	1005	2.913	0.6901	0.02666	0.00001921	0.00001707	0.5247	2.316	0.5875	2.277
147	0.00002358	0.003186	1005	2.913	0.6908	0.02667	0.00001921	0.00001708	0.5271	2.325	0.5931	2.283
148	0.0000236	0.003185	1005	2.914	0.6914	0.02668	0.00001922	0.00001709	0.5294	2.334	0.5988	2.289
149	0.00002361	0.003184	1005	2.914	0.6921	0.02669	0.00001922	0.0000171	0.5316	2.342	0.6044	2.294
150	0.00002363	0.003183	1005	2.915	0.6928	0.02669	0.00001923	0.00001711	0.5339	2.351	0.61	2.3
151	0.00002364	0.003182	1005	2.916	0.6935	0.0267	0.00001923	0.00001712	0.5362	2.36	0.6157	2.306
152	0.00002366	0.003181	1005	2.916	0.6942	0.02671	0.00001924	0.00001713	0.5385	2.369	0.6212	2.311
153	0.00002367	0.00318	1005	2.917	0.6949	0.02672	0.00001924	0.00001714	0.5408	2.377	0.6268	2.317
154	0.00002368	0.003179	1005	2.917	0.6956	0.02672	0.00001925	0.00001715	0.543	2.386	0.6323	2.323
155	0.0000237	0.003178	1005	2.918	0.6962	0.02673	0.00001925	0.00001716	0.5453	2.395	0.6378	2.328
156	0.00002371	0.003177	1006	2.918	0.6969	0.02674	0.00001925	0.00001717	0.5475	2.403	0.6432	2.334
157	0.00002373	0.003176	1006	2.919	0.6976	0.02675	0.00001926	0.00001718	0.5497	2.412	0.6487	2.34
158	0.00002374	0.003175	1006	2.919	0.6982	0.02675	0.00001926	0.00001719	0.552	2.42	0.6541	2.345
159	0.00002375	0.003174	1006	2.92	0.6989	0.02676	0.00001927	0.0000172	0.5542	2.429	0.6596	2.351
160	0.00002377	0.003173	1006	2.92	0.6996	0.02677	0.00001927	0.00001721	0.5564	2.437	0.665	2.356
161	0.00002378	0.003172	1006	2.921	0.7002	0.02678	0.00001928	0.00001722	0.5586	2.446	0.6703	2.362

APPENDIX A3 RESULTS

A3.2 180 Collector Model

Segment No.	alpha_air[i]	beta_air[i]	Cp_air[i]	h_p_c_conv[i]	h_p_c_rad[i]	k_air[i]	mu_air[i]	nu_air[i]	Q_dot_back[i]	Q_dot_conv[i]	Q_dot_c_a[i]	Q_dot_c_s[i]
-	[m ² /s]	[1/K]	[J/kg-K]	[W/m ² -K]	[W/m ² -K]	[W/m-K]	[N-s/m ²]	[m ² /s]	[J/s]	[J/s]	[J/s]	[J/s]
162	0.00002379	0.003171	1006	2.921	0.7009	0.02678	0.00001928	0.00001723	0.5608	2.454	0.6757	2.367
163	0.00002381	0.00317	1006	2.921	0.7016	0.02679	0.00001929	0.00001723	0.563	2.462	0.681	2.373
164	0.00002382	0.003169	1006	2.922	0.7022	0.0268	0.00001929	0.00001724	0.5651	2.471	0.6864	2.378
165	0.00002383	0.003168	1006	2.922	0.7029	0.0268	0.0000193	0.00001725	0.5673	2.479	0.6917	2.384
166	0.00002385	0.003167	1006	2.923	0.7035	0.02681	0.0000193	0.00001726	0.5695	2.487	0.6969	2.389
167	0.00002386	0.003166	1006	2.923	0.7042	0.02682	0.0000193	0.00001727	0.5716	2.495	0.7022	2.394
168	0.00002387	0.003165	1006	2.924	0.7048	0.02683	0.00001931	0.00001728	0.5738	2.504	0.7074	2.4
169	0.00002389	0.003164	1006	2.924	0.7055	0.02683	0.00001931	0.00001729	0.5759	2.512	0.7127	2.405
170	0.0000239	0.003163	1006	2.924	0.7061	0.02684	0.00001932	0.0000173	0.578	2.52	0.7179	2.411
171	0.00002391	0.003162	1006	2.925	0.7068	0.02685	0.00001932	0.00001731	0.5802	2.528	0.7231	2.416
172	0.00002393	0.003161	1006	2.925	0.7074	0.02685	0.00001933	0.00001732	0.5823	2.536	0.7282	2.421
173	0.00002394	0.00316	1006	2.926	0.7081	0.02686	0.00001933	0.00001733	0.5844	2.544	0.7334	2.426
174	0.00002395	0.00316	1006	2.926	0.7087	0.02687	0.00001933	0.00001733	0.5865	2.552	0.7385	2.432
175	0.00002397	0.003159	1006	2.926	0.7093	0.02687	0.00001934	0.00001734	0.5886	2.56	0.7436	2.437
176	0.00002398	0.003158	1006	2.927	0.71	0.02688	0.00001934	0.00001735	0.5907	2.568	0.7487	2.442
177	0.00002399	0.003157	1006	2.927	0.7106	0.02689	0.00001935	0.00001736	0.5927	2.576	0.7538	2.448
178	0.00002401	0.003156	1006	2.927	0.7112	0.02689	0.00001935	0.00001737	0.5948	2.584	0.7588	2.453
179	0.00002402	0.003155	1006	2.928	0.7119	0.0269	0.00001936	0.00001738	0.5969	2.592	0.7639	2.458
180	0.00002403	0.003154	1006	2.928	0.7125	0.02691	0.00001936	0.00001739	0.5989	2.599	0.7689	2.463

APPENDIX A3 RESULTS

A3.2 180 Collector Model

Segment No.	Q_dot_rad[i]	Q_dot_wg[i]	rho_air[i]	T_c[i]	T_m_air[i]	T_m_airK[i]	T_p[i]	T_wg_in [i]	T_wg_m[i]	T_wg_out[i]	Nup[i]	Ra[i]
-	[J/s]	[J/s]	[kg/m^3]	[C]	[C]	[K]	[C]	[C]	[C]	[C]	[-]	[-]
1	0.1406	6.451	1.2	16.15	21.1	294.2	26.05	20	20.14	20.29	2.493	16150
2	0.1436	6.429	1.199	16.22	21.27	294.4	26.32	20.29	20.43	20.57	2.505	16422
3	0.1466	6.408	1.198	16.29	21.44	294.6	26.58	20.57	20.72	20.86	2.516	16692
4	0.1496	6.386	1.198	16.37	21.61	294.8	26.85	20.86	21	21.14	2.528	16959
5	0.1526	6.365	1.197	16.44	21.78	294.9	27.11	21.14	21.28	21.43	2.539	17224
6	0.1556	6.344	1.196	16.51	21.94	295.1	27.38	21.43	21.57	21.71	2.55	17486
7	0.1586	6.322	1.196	16.58	22.11	295.3	27.64	21.71	21.85	21.99	2.56	17745
8	0.1616	6.301	1.195	16.66	22.28	295.4	27.9	21.99	22.13	22.27	2.57	18002
9	0.1646	6.28	1.194	16.73	22.44	295.6	28.16	22.27	22.41	22.55	2.58	18257
10	0.1676	6.259	1.194	16.8	22.61	295.8	28.42	22.55	22.69	22.83	2.59	18510
11	0.1705	6.238	1.193	16.87	22.77	295.9	28.68	22.83	22.97	23.11	2.599	18759
12	0.1735	6.217	1.192	16.94	22.94	296.1	28.94	23.11	23.24	23.38	2.609	19007
13	0.1765	6.196	1.192	17.01	23.1	296.3	29.19	23.38	23.52	23.66	2.618	19252
14	0.1795	6.175	1.191	17.08	23.27	296.4	29.45	23.66	23.8	23.93	2.626	19495
15	0.1825	6.154	1.19	17.15	23.43	296.6	29.7	23.93	24.07	24.21	2.635	19736
16	0.1855	6.133	1.19	17.23	23.59	296.7	29.96	24.21	24.34	24.48	2.643	19975
17	0.1884	6.113	1.189	17.3	23.75	296.9	30.21	24.48	24.62	24.75	2.652	20211
18	0.1914	6.092	1.188	17.37	23.92	297.1	30.47	24.75	24.89	25.02	2.66	20445
19	0.1944	6.071	1.188	17.44	24.08	297.2	30.72	25.02	25.16	25.29	2.668	20677
20	0.1974	6.051	1.187	17.51	24.24	297.4	30.97	25.29	25.43	25.56	2.676	20907
21	0.2003	6.03	1.186	17.58	24.4	297.5	31.22	25.56	25.7	25.83	2.683	21135
22	0.2033	6.01	1.186	17.64	24.56	297.7	31.47	25.83	25.97	26.1	2.691	21360
23	0.2063	5.989	1.185	17.71	24.71	297.9	31.72	26.1	26.23	26.37	2.698	21584

APPENDIX A3 RESULTS

A3.2 180 Collector Model

Segment No.	Q_dot_rad[i]	Q_dot_wg[i]	rho_air[i]	T_c[i]	T_m_air[i]	T_m_airK[i]	T_p[i]	T_wg_in [i]	T_wg_m[i]	T_wg_out[i]	Nup[i]	Ra[i]
-	[J/s]	[J/s]	[kg/m^3]	[C]	[C]	[K]	[C]	[C]	[C]	[C]	[-]	[-]
24	0.2092	5.969	1.185	17.78	24.87	298	31.96	26.37	26.5	26.63	2.705	21806
25	0.2122	5.948	1.184	17.85	25.03	298.2	32.21	26.63	26.76	26.9	2.712	22025
26	0.2152	5.928	1.183	17.92	25.19	298.3	32.46	26.9	27.03	27.16	2.719	22243
27	0.2181	5.908	1.183	17.99	25.34	298.5	32.7	27.16	27.29	27.42	2.726	22459
28	0.2211	5.888	1.182	18.06	25.5	298.7	32.94	27.42	27.55	27.68	2.732	22672
29	0.224	5.868	1.181	18.13	25.66	298.8	33.19	27.68	27.82	27.95	2.739	22884
30	0.227	5.848	1.181	18.19	25.81	299	33.43	27.95	28.08	28.21	2.745	23094
31	0.23	5.827	1.18	18.26	25.97	299.1	33.67	28.21	28.34	28.47	2.751	23305
32	0.2329	5.807	1.18	18.33	26.12	299.3	33.92	28.47	28.6	28.73	2.758	23511
33	0.2359	5.788	1.179	18.4	26.28	299.4	34.16	28.73	28.86	28.99	2.764	23716
34	0.2388	5.768	1.178	18.46	26.43	299.6	34.39	28.99	29.11	29.24	2.77	23918
35	0.2417	5.748	1.178	18.53	26.58	299.7	34.63	29.24	29.37	29.5	2.775	24119
36	0.2447	5.728	1.177	18.6	26.73	299.9	34.87	29.5	29.63	29.75	2.781	24318
37	0.2476	5.709	1.177	18.66	26.88	300	35.11	29.75	29.88	30.01	2.787	24515
38	0.2506	5.689	1.176	18.73	27.04	300.2	35.34	30.01	30.13	30.26	2.792	24710
39	0.2535	5.67	1.175	18.8	27.19	300.3	35.58	30.26	30.39	30.51	2.798	24904
40	0.2564	5.65	1.175	18.86	27.34	300.5	35.81	30.51	30.64	30.76	2.803	25096
41	0.2593	5.631	1.174	18.93	27.49	300.6	36.04	30.76	30.89	31.01	2.808	25286
42	0.2623	5.611	1.174	18.99	27.63	300.8	36.28	31.01	31.14	31.26	2.814	25475
43	0.2652	5.592	1.173	19.06	27.78	300.9	36.51	31.26	31.39	31.51	2.819	25662
44	0.2681	5.573	1.172	19.12	27.93	301.1	36.74	31.51	31.64	31.76	2.824	25848
45	0.271	5.554	1.172	19.19	28.08	301.2	36.97	31.76	31.88	32.01	2.829	26031
46	0.274	5.534	1.171	19.25	28.22	301.4	37.2	32.01	32.13	32.25	2.834	26214

APPENDIX A3 RESULTS

A3.2 180 Collector Model

Segment No.	Q_dot_rad[i] [J/s]	Q_dot_wg[i] [J/s]	rho_air[i] [kg/m^3]	T_c[i] [C]	T_m_air[i] [C]	T_m_airK[i] [K]	T_p[i] [C]	T_wg_in [i] [C]	T_wg_m[i] [C]	T_wg_out[i] [C]	Nup[i] [-]	Ra[i] [-]
47	0.2769	5.515	1.171	19.32	28.37	301.5	37.43	32.25	32.38	32.5	2.838	26394
48	0.2798	5.496	1.17	19.38	28.52	301.7	37.65	32.5	32.62	32.74	2.843	26573
49	0.2827	5.477	1.17	19.44	28.66	301.8	37.88	32.74	32.87	32.99	2.848	26751
50	0.2856	5.459	1.169	19.51	28.81	302	38.11	32.99	33.11	33.23	2.852	26927
51	0.2885	5.44	1.169	19.57	28.95	302.1	38.33	33.23	33.35	33.47	2.857	27102
52	0.2914	5.421	1.168	19.63	29.1	302.2	38.56	33.47	33.59	33.72	2.861	27275
53	0.2943	5.402	1.167	19.7	29.24	302.4	38.78	33.72	33.84	33.96	2.866	27446
54	0.2972	5.383	1.167	19.76	29.38	302.5	39	33.96	34.08	34.2	2.87	27616
55	0.3001	5.365	1.166	19.82	29.52	302.7	39.23	34.2	34.31	34.43	2.874	27785
56	0.303	5.346	1.166	19.88	29.67	302.8	39.45	34.43	34.55	34.67	2.878	27952
57	0.3058	5.328	1.165	19.95	29.81	303	39.67	34.67	34.79	34.91	2.883	28118
58	0.3087	5.309	1.165	20.01	29.95	303.1	39.89	34.91	35.03	35.15	2.887	28282
59	0.3116	5.291	1.164	20.07	30.09	303.2	40.11	35.15	35.26	35.38	2.891	28445
60	0.3145	5.273	1.164	20.13	30.23	303.4	40.33	35.38	35.5	35.62	2.895	28607
61	0.3174	5.254	1.163	20.19	30.37	303.5	40.55	35.62	35.74	35.85	2.899	28770
62	0.3203	5.236	1.163	20.26	30.51	303.7	40.76	35.85	35.97	36.09	2.902	28929
63	0.3232	5.218	1.162	20.32	30.65	303.8	40.98	36.09	36.2	36.32	2.906	29087
64	0.326	5.2	1.161	20.38	30.79	303.9	41.2	36.32	36.43	36.55	2.91	29243
65	0.3289	5.182	1.161	20.44	30.92	304.1	41.41	36.55	36.67	36.78	2.914	29398
66	0.3317	5.164	1.16	20.5	31.06	304.2	41.62	36.78	36.9	37.01	2.917	29552
67	0.3346	5.146	1.16	20.56	31.2	304.3	41.84	37.01	37.13	37.24	2.921	29704
68	0.3375	5.128	1.159	20.62	31.33	304.5	42.05	37.24	37.35	37.47	2.925	29855
69	0.3403	5.11	1.159	20.68	31.47	304.6	42.26	37.47	37.58	37.7	2.928	30005

APPENDIX A3 RESULTS

A3.2 180 Collector Model

Segment No.	Q_dot_rad[i]	Q_dot_wg[i]	rho_air[i]	T_c[i]	T_m_air[i]	T_m_airK[i]	T_p[i]	T_wg_in [i]	T_wg_m[i]	T_wg_out[i]	Nup[i]	Ra[i]
-	[J/s]	[J/s]	[kg/m^3]	[C]	[C]	[K]	[C]	[C]	[C]	[C]	[-]	[-]
70	0.3432	5.092	1.158	20.74	31.6	304.8	42.47	37.7	37.81	37.92	2.932	30154
71	0.346	5.075	1.158	20.8	31.74	304.9	42.68	37.92	38.04	38.15	2.935	30301
72	0.3488	5.057	1.157	20.86	31.87	305	42.89	38.15	38.26	38.37	2.938	30448
73	0.3517	5.039	1.157	20.92	32.01	305.2	43.1	38.37	38.49	38.6	2.942	30593
74	0.3545	5.022	1.156	20.97	32.14	305.3	43.31	38.6	38.71	38.82	2.945	30736
75	0.3573	5.004	1.156	21.03	32.27	305.4	43.51	38.82	38.93	39.04	2.948	30879
76	0.3602	4.987	1.155	21.09	32.41	305.6	43.72	39.04	39.15	39.27	2.951	31021
77	0.363	4.97	1.155	21.15	32.54	305.7	43.93	39.27	39.38	39.49	2.955	31161
78	0.3658	4.952	1.154	21.21	32.67	305.8	44.13	39.49	39.6	39.71	2.958	31300
79	0.3686	4.935	1.154	21.26	32.8	306	44.34	39.71	39.82	39.93	2.961	31438
80	0.3714	4.918	1.153	21.32	32.93	306.1	44.54	39.93	40.04	40.15	2.964	31575
81	0.3743	4.901	1.153	21.38	33.06	306.2	44.74	40.15	40.26	40.36	2.967	31711
82	0.3771	4.884	1.152	21.44	33.19	306.3	44.94	40.36	40.47	40.58	2.97	31846
83	0.3799	4.867	1.152	21.49	33.32	306.5	45.15	40.58	40.69	40.8	2.973	31979
84	0.3827	4.85	1.151	21.55	33.45	306.6	45.35	40.8	40.91	41.01	2.976	32112
85	0.3855	4.833	1.151	21.61	33.58	306.7	45.55	41.01	41.12	41.23	2.979	32243
86	0.3883	4.816	1.15	21.66	33.7	306.9	45.75	41.23	41.34	41.44	2.982	32374
87	0.391	4.799	1.15	21.72	33.83	307	45.94	41.44	41.55	41.66	2.984	32503
88	0.3938	4.782	1.149	21.77	33.96	307.1	46.14	41.66	41.76	41.87	2.987	32632
89	0.3966	4.766	1.149	21.83	34.08	307.2	46.34	41.87	41.98	42.08	2.99	32759
90	0.3994	4.749	1.149	21.89	34.21	307.4	46.54	42.08	42.19	42.29	2.993	32885
91	0.4021	4.733	1.148	21.94	34.33	307.5	46.73	42.29	42.4	42.5	2.995	33009
92	0.4049	4.716	1.148	22	34.46	307.6	46.92	42.5	42.61	42.71	2.998	33133

APPENDIX A3 RESULTS

A3.2 180 Collector Model

Segment No.	Q_dot_rad[i]	Q_dot_wg[i]	rho_air[i]	T_c[i]	T_m_air[i]	T_m_airK[i]	T_p[i]	T_wg_in [i]	T_wg_m[i]	T_wg_out[i]	Nup[i]	Ra[i]
-	[J/s]	[J/s]	[kg/m^3]	[C]	[C]	[K]	[C]	[C]	[C]	[C]	[-]	[-]
93	0.4077	4.7	1.147	22.05	34.58	307.7	47.12	42.71	42.82	42.92	3	33256
94	0.4104	4.683	1.147	22.11	34.71	307.9	47.31	42.92	43.02	43.13	3.003	33379
95	0.4132	4.667	1.146	22.16	34.83	308	47.5	43.13	43.23	43.34	3.006	33500
96	0.416	4.651	1.146	22.21	34.96	308.1	47.7	43.34	43.44	43.54	3.008	33621
97	0.4187	4.634	1.145	22.27	35.08	308.2	47.89	43.54	43.65	43.75	3.011	33740
98	0.4215	4.618	1.145	22.32	35.2	308.4	48.08	43.75	43.85	43.95	3.013	33859
99	0.4242	4.602	1.144	22.38	35.32	308.5	48.27	43.95	44.06	44.16	3.016	33976
100	0.4269	4.586	1.144	22.43	35.45	308.6	48.46	44.16	44.26	44.36	3.018	34093
101	0.4297	4.57	1.143	22.48	35.57	308.7	48.65	44.36	44.47	44.57	3.02	34209
102	0.4324	4.554	1.143	22.54	35.69	308.8	48.84	44.57	44.67	44.77	3.023	34324
103	0.4351	4.538	1.143	22.59	35.81	309	49.03	44.77	44.87	44.97	3.025	34438
104	0.4379	4.522	1.142	22.64	35.93	309.1	49.21	44.97	45.07	45.17	3.028	34551
105	0.4406	4.506	1.142	22.7	36.05	309.2	49.4	45.17	45.27	45.37	3.03	34663
106	0.4433	4.49	1.141	22.75	36.17	309.3	49.58	45.37	45.47	45.57	3.032	34775
107	0.446	4.475	1.141	22.8	36.28	309.4	49.77	45.57	45.67	45.77	3.034	34885
108	0.4487	4.459	1.14	22.85	36.4	309.6	49.95	45.77	45.87	45.97	3.037	34995
109	0.4514	4.443	1.14	22.9	36.52	309.7	50.14	45.97	46.07	46.17	3.039	35104
110	0.4542	4.428	1.14	22.96	36.64	309.8	50.32	46.17	46.27	46.37	3.041	35211
111	0.4569	4.412	1.139	23.01	36.76	309.9	50.5	46.37	46.46	46.56	3.043	35319
112	0.4595	4.397	1.139	23.06	36.87	310	50.69	46.56	46.66	46.76	3.045	35425
113	0.4622	4.381	1.138	23.11	36.99	310.1	50.87	46.76	46.86	46.95	3.047	35530
114	0.4649	4.366	1.138	23.16	37.1	310.3	51.05	46.95	47.05	47.15	3.049	35635
115	0.4676	4.351	1.137	23.21	37.22	310.4	51.23	47.15	47.24	47.34	3.052	35739

APPENDIX A3 RESULTS

A3.2 180 Collector Model

Segment No.	Q_dot_rad[i] [J/s]	Q_dot_wg[i] [J/s]	rho_air[i] [kg/m^3]	T_c[i] [C]	T_m_air[i] [C]	T_m_airK[i] [K]	T_p[i] [C]	T_wg_in [i] [C]	T_wg_m[i] [C]	T_wg_out[i] [C]	Nup[i] [-]	Ra[i] [-]
116	0.4703	4.335	1.137	23.26	37.33	310.5	51.41	47.34	47.44	47.53	3.054	35842
117	0.473	4.32	1.137	23.31	37.45	310.6	51.59	47.53	47.63	47.73	3.056	35944
118	0.4756	4.305	1.136	23.36	37.56	310.7	51.76	47.73	47.82	47.92	3.058	36046
119	0.4783	4.29	1.136	23.41	37.68	310.8	51.94	47.92	48.01	48.11	3.06	36147
120	0.481	4.275	1.135	23.46	37.79	310.9	52.12	48.11	48.2	48.3	3.062	36247
121	0.4836	4.26	1.135	23.51	37.9	311.1	52.29	48.3	48.39	48.49	3.064	36346
122	0.4863	4.245	1.134	23.56	38.02	311.2	52.47	48.49	48.58	48.68	3.065	36445
123	0.4889	4.23	1.134	23.61	38.13	311.3	52.65	48.68	48.77	48.87	3.067	36543
124	0.4916	4.215	1.134	23.66	38.24	311.4	52.82	48.87	48.96	49.05	3.069	36640
125	0.4942	4.2	1.133	23.71	38.35	311.5	52.99	49.05	49.15	49.24	3.071	36736
126	0.4969	4.186	1.133	23.76	38.46	311.6	53.17	49.24	49.33	49.43	3.073	36831
127	0.4995	4.171	1.132	23.81	38.57	311.7	53.34	49.43	49.52	49.61	3.075	36926
128	0.5021	4.156	1.132	23.86	38.68	311.8	53.51	49.61	49.71	49.8	3.077	37020
129	0.5047	4.142	1.132	23.9	38.79	311.9	53.68	49.8	49.89	49.98	3.078	37114
130	0.5074	4.127	1.131	23.95	38.9	312.1	53.85	49.98	50.07	50.17	3.08	37207
131	0.51	4.113	1.131	24	39.01	312.2	54.02	50.17	50.26	50.35	3.082	37299
132	0.5126	4.098	1.13	24.05	39.12	312.3	54.19	50.35	50.44	50.53	3.084	37390
133	0.5152	4.084	1.13	24.1	39.23	312.4	54.36	50.53	50.62	50.71	3.085	37481
134	0.5178	4.069	1.13	24.14	39.34	312.5	54.53	50.71	50.8	50.89	3.087	37571
135	0.5204	4.055	1.129	24.19	39.44	312.6	54.7	50.89	50.98	51.08	3.089	37660
136	0.523	4.041	1.129	24.24	39.55	312.7	54.86	51.08	51.17	51.25	3.091	37748
137	0.5256	4.027	1.129	24.28	39.66	312.8	55.03	51.25	51.34	51.43	3.092	37837
138	0.5282	4.012	1.128	24.33	39.76	312.9	55.2	51.43	51.52	51.61	3.094	37924

APPENDIX A3 RESULTS

A3.2 180 Collector Model

Segment No.	Q_dot_rad[i] [J/s]	Q_dot_wg[i] [J/s]	rho_air[i] [kg/m^3]	T_c[i] [C]	T_m_air[i] [C]	T_m_airK[i] [K]	T_p[i] [C]	T_wg_in [i] [C]	T_wg_m[i] [C]	T_wg_out[i] [C]	Nup[i] [-]	Ra[i] [-]
-												
139	0.5307	3.998	1.128	24.38	39.87	313	55.36	51.61	51.7	51.79	3.096	38011
140	0.5333	3.984	1.127	24.42	39.98	313.1	55.53	51.79	51.88	51.97	3.097	38097
141	0.5359	3.97	1.127	24.47	40.08	313.2	55.69	51.97	52.06	52.14	3.099	38182
142	0.5384	3.956	1.127	24.52	40.19	313.3	55.85	52.14	52.23	52.32	3.1	38267
143	0.541	3.942	1.126	24.56	40.29	313.4	56.02	52.32	52.41	52.5	3.102	38351
144	0.5436	3.928	1.126	24.61	40.39	313.5	56.18	52.5	52.58	52.67	3.103	38435
145	0.5461	3.915	1.126	24.65	40.5	313.6	56.34	52.67	52.76	52.85	3.105	38518
146	0.5487	3.901	1.125	24.7	40.6	313.8	56.5	52.85	52.93	53.02	3.107	38600
147	0.5512	3.887	1.125	24.75	40.7	313.9	56.66	53.02	53.11	53.19	3.108	38682
148	0.5537	3.873	1.124	24.79	40.81	314	56.82	53.19	53.28	53.36	3.11	38763
149	0.5563	3.86	1.124	24.84	40.91	314.1	56.98	53.36	53.45	53.54	3.111	38844
150	0.5588	3.846	1.124	24.88	41.01	314.2	57.14	53.54	53.62	53.71	3.113	38924
151	0.5614	3.832	1.123	24.93	41.11	314.3	57.3	53.71	53.8	53.88	3.114	39004
152	0.5639	3.819	1.123	24.97	41.22	314.4	57.46	53.88	53.97	54.05	3.115	39083
153	0.5664	3.805	1.123	25.01	41.32	314.5	57.62	54.05	54.14	54.22	3.117	39161
154	0.5689	3.792	1.122	25.06	41.42	314.6	57.78	54.22	54.3	54.39	3.118	39239
155	0.5714	3.779	1.122	25.1	41.52	314.7	57.93	54.39	54.47	54.56	3.12	39316
156	0.5739	3.765	1.122	25.15	41.62	314.8	58.09	54.56	54.64	54.72	3.121	39393
157	0.5764	3.752	1.121	25.19	41.72	314.9	58.24	54.72	54.81	54.89	3.123	39469
158	0.5789	3.739	1.121	25.23	41.82	315	58.4	54.89	54.97	55.06	3.124	39544
159	0.5814	3.726	1.12	25.28	41.91	315.1	58.55	55.06	55.14	55.22	3.125	39619
160	0.5839	3.712	1.12	25.32	42.01	315.2	58.71	55.22	55.31	55.39	3.127	39694
161	0.5864	3.699	1.12	25.36	42.11	315.3	58.86	55.39	55.47	55.55	3.128	39767

APPENDIX A3 RESULTS

A3.2 180 Collector Model

Segment No.	Q_dot_rad[i] [J/s]	Q_dot_wg[i] [J/s]	rho_air[i] [kg/m^3]	T_c[i] [C]	T_m_air[i] [C]	T_m_airK[i] [K]	T_p[i] [C]	T_wg_in [i] [C]	T_wg_m[i] [C]	T_wg_out[i] [C]	Nup[i] [-]	Ra[i] [-]
162	0.5889	3.686	1.119	25.41	42.21	315.4	59.01	55.55	55.64	55.72	3.129	39841
163	0.5913	3.673	1.119	25.45	42.31	315.5	59.16	55.72	55.8	55.88	3.131	39914
164	0.5938	3.66	1.119	25.49	42.4	315.6	59.31	55.88	55.96	56.04	3.132	39986
165	0.5962	3.647	1.118	25.53	42.5	315.6	59.46	56.04	56.13	56.21	3.133	40058
166	0.5987	3.635	1.118	25.58	42.6	315.7	59.62	56.21	56.29	56.37	3.134	40129
167	0.6012	3.622	1.118	25.62	42.69	315.8	59.76	56.37	56.45	56.53	3.136	40200
168	0.6036	3.609	1.117	25.66	42.79	315.9	59.91	56.53	56.61	56.69	3.137	40270
169	0.606	3.596	1.117	25.7	42.88	316	60.06	56.69	56.77	56.85	3.138	40340
170	0.6085	3.584	1.117	25.74	42.98	316.1	60.21	56.85	56.93	57.01	3.139	40409
171	0.6109	3.571	1.116	25.78	43.07	316.2	60.36	57.01	57.09	57.17	3.141	40478
172	0.6133	3.558	1.116	25.83	43.17	316.3	60.51	57.17	57.25	57.33	3.142	40546
173	0.6158	3.546	1.116	25.87	43.26	316.4	60.65	57.33	57.41	57.48	3.143	40614
174	0.6182	3.533	1.115	25.91	43.35	316.5	60.8	57.48	57.56	57.64	3.144	40682
175	0.6206	3.521	1.115	25.95	43.45	316.6	60.94	57.64	57.72	57.8	3.146	40749
176	0.623	3.508	1.115	25.99	43.54	316.7	61.09	57.8	57.88	57.95	3.147	40815
177	0.6254	3.496	1.114	26.03	43.63	316.8	61.23	57.95	58.03	58.11	3.148	40881
178	0.6278	3.484	1.114	26.07	43.72	316.9	61.38	58.11	58.19	58.27	3.149	40947
179	0.6302	3.471	1.114	26.11	43.82	317	61.52	58.27	58.34	58.42	3.15	41012
180	0.6326	3.459	1.113	26.15	43.91	317.1	61.66	58.42	58.5	58.57	3.151	41076

APPENDIX A3 RESULTS

A3.3: Condenser Model Parametric Analysis

WF\$	h_WF [1]	h_WF [2]	h_WF [3]	h_WF [4]	h_WF [5]	h_WF [6]	h_WF [7]	h_WF [8]	m_dot_WF _HX	m_dot_CF _CF	m_dot_CF_ tube	m_dot_CF_ HX
	[W/m^ 2-C]	[W/m^ 2-C]	[W/m^ ^2-C]	[W/m^2 -C]	[W/m^2 -C]	[W/m^2 -C]	[W/m^ ^2-C]	[W/m^ 2-C]	[kg/s]	[kg/s]	[kg/s]	[kg/s]
R134a	1526	1193	1093	1033	990.2	957.5	931.2	909.2	0.7854	8	1	48
R134a	1544	1207	1106	1045	1001	968.4	941.7	919.5	0.7646	6	0.75	36
R134a	1577	1233	1129	1067	1023	989.2	962	939.2	0.7263	4	0.5	24
R134a	1671	1306	1197	1131	1084	1048	1020	995.5	0.6282	2	0.25	12
R134a	1860	1454	1332	1259	1207	1167	1135	1108	0.4744	1	0.125	6
R134a	1963	1535	1406	1329	1274	1232	1198	1169	0.4097	0.8	0.1	4.8
R134a	2165	1693	1551	1465	1405	1358	1321	1290	0.3121	0.6	0.075	3.6
R134a	2378	1859	1703	1609	1543	1492	1451	1417	0.2393	0.5	0.0625	3
R134a	2925	2287	2095	1980	1898	1835	1785	1743	0.1313	0.4	0.05	2.4
R134a	4068	3180	2914	2753	2639	2552	2482	2423	0.04946	0.35	0.04375	2.1
R123	1442	1127	1033	975.9	935.6	904.7	879.8	859	0.7191	8	1	48
R123	1458	1140	1044	986.6	945.9	914.7	889.5	868.5	0.7007	6	0.75	36
R123	1488	1164	1066	1007	965.7	933.8	908.1	886.6	0.6667	4	0.5	24
R123	1575	1231	1128	1066	1022	988.3	961	938.4	0.5793	2	0.25	12
R123	1750	1368	1253	1184	1135	1098	1068	1042	0.4404	1	0.125	6
R123	1845	1443	1322	1249	1197	1158	1126	1099	0.3814	0.8	0.1	4.8
R123	2033	1590	1456	1376	1319	1276	1240	1211	0.2918	0.6	0.075	3.6
R123	2231	1744	1598	1510	1448	1400	1361	1329	0.2243	0.5	0.0625	3
R123	2742	2144	1964	1856	1779	1720	1673	1633	0.1235	0.4	0.05	2.4
R123	3811	2979	2730	2579	2473	2391	2325	2270	0.04667	0.35	0.04375	2.1

APPENDIX A3 RESULTS

A3.3: Condenser Model Parametric Analysis

WF\$	h_WF [1]	h_WF [2]	h_WF [3]	h_WF [4]	h_WF [5]	h_WF [6]	h_WF [7]	h_WF [8]	m_dot_WF _HX	m_dot_CF	m_dot_CF_ tube	m_dot_CF_ HX
	[W/m^ 2-C]	[W/m^ 2-C]	[W/m ^2-C]	[W/m^2 -C]	[W/m^2 -C]	[W/m^2 -C]	[W/m ^2-C]	[W/m^ 2-C]	[kg/s]	[kg/s]	[kg/s]	[kg/s]
R245fa	1480	1157	1060	1001	960	928.3	902.7	881.4	0.671	8	1	48
R245fa	1496	1170	1072	1012	970.6	938.6	912.8	891.2	0.6536	6	0.75	36
R245fa	1528	1194	1094	1034	991.2	958.5	932.1	910.1	0.6214	4	0.5	24
R245fa	1618	1265	1159	1095	1050	1015	987.1	963.8	0.5388	2	0.25	12
R245fa	1799	1406	1288	1217	1167	1129	1097	1072	0.4084	1	0.125	6
R245fa	1898	1484	1359	1284	1231	1191	1158	1131	0.3532	0.8	0.1	4.8
R245fa	2092	1635	1498	1416	1357	1312	1276	1246	0.2697	0.6	0.075	3.6
R245fa	2297	1795	1645	1554	1490	1441	1401	1368	0.2071	0.5	0.0625	3
R245fa	2824	2207	2022	1911	1832	1772	1723	1682	0.1138	0.4	0.05	2.4
R245fa	3925	3069	2811	2656	2547	2463	2395	2338	0.04296	0.35	0.04375	2.1
n-butane	1723	1347	1234	1166	1118	1081	1051	1026	0.3813	8	1	48
n-butane	1743	1363	1249	1180	1131	1094	1064	1039	0.3705	6	0.75	36
n-butane	1783	1394	1277	1207	1157	1119	1088	1062	0.3505	4	0.5	24
n-butane	1896	1482	1358	1283	1230	1189	1157	1129	0.3003	2	0.25	12
n-butane	2119	1656	1518	1434	1375	1329	1293	1262	0.2236	1	0.125	6
n-butane	2240	1751	1604	1516	1453	1405	1367	1334	0.192	0.8	0.1	4.8
n-butane	2476	1935	1773	1675	1606	1553	1510	1475	0.1451	0.6	0.075	3.6
n-butane	2723	2129	1950	1843	1767	1708	1661	1622	0.1106	0.5	0.0625	3
n-butane	3356	2624	2404	2271	2177	2106	2048	1999	0.06019	0.4	0.05	2.4
n-butane	4673	3653	3347	3162	3032	2932	2851	2784	0.02257	0.35	0.04375	2.1

APPENDIX A3 RESULTS

A3.3: Condenser Model Parametric Analysis

WF\$	h_WF [1]	h_WF [2]	h_WF [3]	h_WF [4]	h_WF [5]	h_WF [6]	h_WF [7]	h_WF [8]	m_dot_WF _HX	m_dot_CF	m_dot_CF_ tube	m_dot_CF_ HX
	[W/m^ 2-C]	[W/m^ 2-C]	[W/m ^2-C]	[W/m^2 -C]	[W/m^2 -C]	[W/m^2 -C]	[W/m ^2-C]	[W/m^ 2-C]	[kg/s]	[kg/s]	[kg/s]	[kg/s]
isobutane	1440	1126	1031	974.3	934.1	903.3	878.4	857.6	0.3868	8	1	48
isobutane	1468	1148	1051	993.4	952.4	920.9	895.6	874.4	0.3694	5	0.625	30
isobutane	1538	1203	1102	1041	998.1	965.1	938.6	916.4	0.3293	2.5	0.3125	15
isobutane	1573	1229	1126	1064	1020	986.6	959.4	936.8	0.3116	2	0.25	12
isobutane	1747	1366	1251	1182	1133	1096	1066	1041	0.237	1	0.125	6
isobutane	1842	1440	1319	1247	1195	1156	1124	1097	0.2053	0.8	0.1	4.8
isobutane	2029	1587	1454	1373	1317	1273	1238	1209	0.157	0.6	0.075	3.6
isobutane	2227	1741	1595	1507	1445	1397	1359	1327	0.1207	0.5	0.0625	3
isobutane	2737	2140	1960	1852	1776	1717	1670	1630	0.0665	0.4	0.05	2.4
isobutane	3804	2974	2724	2574	2468	2386	2321	2266	0.02512	0.35	0.04375	2.1

APPENDIX A3 RESULTS

A3.3: Condenser Model Parametric Analysis

WF\$	Q[1]	Q[2]	Q[3]	Q[4]	Q[5]	Q[6]	Q[7]	Q[8]	Q_column	Q_HX	T_CF[1]	T_CF_i	T_CF_o[1]
	[W]	[W]	[W]	[W]	[W]	[W]	[W]	[W]	[W]	[W]	[C]	[C]	[C]
R134a	2977	2639	2519	2442	2384	2339	2302	2270	19871	119225	25.45	25	25.89
R134a	2878	2564	2451	2379	2325	2283	2247	2217	19344	116064	25.57	25	26.15
R134a	2699	2426	2327	2263	2215	2178	2146	2119	18374	110242	25.81	25	26.62
R134a	2266	2079	2010	1964	1930	1903	1880	1860	15893	95356	26.35	25	27.71
R134a	1641	1549	1513	1490	1472	1457	1445	1434	12001	72008	26.96	25	28.92
R134a	1395	1331	1305	1288	1276	1265	1256	1249	10365	62190	27.08	25	29.17
R134a	1040	1006	992.6	983.5	976.5	970.7	965.9	961.7	7897	47380	27.07	25	29.14
R134a	785.2	767.1	759.8	754.8	750.9	747.7	745	742.7	6053	36319	26.88	25	28.75
R134a	422.4	417.8	415.9	414.6	413.6	412.8	412.1	411.5	3321	19925	26.26	25	27.53
R134a	157.2	156.7	156.5	156.4	156.2	156.2	156.1	156	1251	7507	25.54	25	26.08
R123	2899	2561	2442	2365	2308	2263	2226	2195	19258	115550	25.43	25	25.87
R123	2805	2490	2378	2306	2253	2211	2176	2146	18766	112593	25.56	25	26.12
R123	2636	2361	2262	2198	2150	2113	2081	2054	17855	107133	25.79	25	26.58
R123	2222	2033	1962	1916	1882	1854	1831	1812	15513	93080	26.33	25	27.66
R123	1619	1524	1488	1464	1445	1430	1418	1407	11795	70769	26.93	25	28.87
R123	1380	1313	1287	1269	1256	1245	1236	1228	10215	61289	27.06	25	29.12
R123	1032	996.5	982.5	972.9	965.6	959.7	954.6	950.3	7814	46883	27.05	25	29.11
R123	780.9	761.8	754.1	748.9	744.8	741.5	738.7	736.2	6007	36041	26.87	25	28.73
R123	421.3	416.4	414.5	413.1	412	411.1	410.4	409.7	3309	19851	26.26	25	27.52
R123	157.1	156.5	156.3	156.2	156.1	156	155.9	155.8	1250	7499	25.54	25	26.07

APPENDIX A3 RESULTS

A3.3: Condenser Model Parametric Analysis

WF\$	Q[1]	Q[2]	Q[3]	Q[4]	Q[5]	Q[6]	Q[7]	Q[8]	Q_column	Q_HX	T_CF[1]	T_CF_i	T_CF_o[1]
	[W]	[W]	[W]	[W]	[W]	[W]	[W]	[W]	[W]	[W]	[C]	[C]	[C]
R245fa	2934	2596	2476	2399	2343	2298	2260	2229	19535	117210	25.44	25	25.88
R245fa	2838	2524	2411	2339	2286	2243	2208	2178	19027	114162	25.57	25	26.13
R245fa	2665	2390	2292	2227	2180	2142	2110	2084	18090	108540	25.8	25	26.59
R245fa	2242	2054	1984	1938	1904	1876	1853	1834	15685	94113	26.34	25	27.68
R245fa	1629	1536	1500	1476	1457	1443	1430	1419	11889	71334	26.95	25	28.89
R245fa	1387	1321	1295	1278	1265	1254	1245	1238	10283	61700	27.07	25	29.14
R245fa	1035	1001	987.1	977.8	970.6	964.8	959.8	955.5	7852	47111	27.06	25	29.12
R245fa	782.9	764.2	756.7	751.6	747.6	744.3	741.6	739.2	6028	36168	26.87	25	28.74
R245fa	421.8	417.1	415.1	413.8	412.8	411.9	411.2	410.5	3314	19885	26.26	25	27.52
R245fa	157.1	156.6	156.4	156.3	156.1	156.1	156	155.9	1250	7503	25.54	25	26.07
n-butane	3141	2805	2685	2607	2549	2503	2465	2433	21189	127132	25.47	25	25.94
n-butane	3030	2720	2607	2535	2481	2438	2402	2372	20584	123506	25.6	25	26.21
n-butane	2832	2564	2466	2402	2355	2317	2285	2258	19478	116867	25.85	25	26.69
n-butane	2355	2176	2109	2065	2032	2005	1982	1963	16688	100129	26.41	25	27.82
n-butane	1685	1599	1566	1543	1526	1513	1501	1491	12424	74541	27.01	25	29.02
n-butane	1425	1366	1343	1327	1315	1305	1297	1290	10669	64013	27.13	25	29.26
n-butane	1056	1025	1013	1005	998.1	992.9	988.4	984.5	8062	48373	27.1	25	29.2
n-butane	793.8	777.5	770.9	766.4	762.9	760	757.6	755.5	6145	36867	26.9	25	28.79
n-butane	424.5	420.5	418.8	417.7	416.8	416	415.4	414.9	3345	20068	26.27	25	27.54
n-butane	157.4	157	156.8	156.7	156.6	156.5	156.4	156.4	1254	7523	25.54	25	26.08

APPENDIX A3 RESULTS

A3.3: Condenser Model Parametric Analysis

WF\$	Q[1]	Q[2]	Q[3]	Q[4]	Q[5]	Q[6]	Q[7]	Q[8]	Q_column	Q_HX	T_CF[1]	T_CF_i	T_CF_o[1]
	[W]	[W]	[W]	[W]	[W]	[W]	[W]	[W]	[W]	[W]	[C]	[C]	[C]
isobutane	2897	2559	2439	2363	2306	2261	2224	2192	19241	115445	25.43	25	25.87
isobutane	2733	2435	2329	2260	2209	2168	2135	2106	18375	110251	25.65	25	26.31
isobutane	2373	2154	2074	2021	1982	1951	1925	1903	16383	98296	26.14	25	27.27
isobutane	2221	2031	1961	1915	1881	1853	1830	1810	15502	93014	26.33	25	27.66
isobutane	1618	1524	1487	1463	1444	1429	1417	1406	11789	70733	26.93	25	28.87
isobutane	1379	1312	1286	1269	1256	1245	1236	1228	10210	61263	27.06	25	29.12
isobutane	1031	996.2	982.2	972.6	965.3	959.4	954.3	949.9	7811	46869	27.05	25	29.11
isobutane	780.8	761.7	754	748.7	744.6	741.3	738.5	736	6005	36033	26.87	25	28.73
isobutane	421.3	416.4	414.4	413	412	411.1	410.3	409.7	3308	19849	26.26	25	27.52
isobutane	157.1	156.5	156.3	156.2	156.1	156	155.9	155.8	1250	7499	25.54	25	26.07

APPENDIX A3 RESULTS

A3.4: Turbine Modelling and Design – Summarised Results

Radial Turbine Geometric Specifications, Velocities and Mach Numbers

Fluid\$	L d	d 1	d 2	d 3	d 4	α 1	α 2	α 3	α 4	β 2	β 3	b 1	b 2	b 3	b 4
	[m]	[m]	[m]	[m]	[m]	[deg]	[deg]	[deg]	[deg]	[deg]	[deg]	[m]	[m]	[m]	[m]
R245fa	0.1463	0.1706	0.1219	0.07313	0.1097	0	82.65	0	0	70.02	69.38	0.01828	0.01828	0.0257	0.01343
R134a	0.1463	0.1706	0.1219	0.07313	0.1097	0	82.65	0	0	70.02	77.09	0.01828	0.01828	0.0257	0.01343
n-butane	0.2023	0.236	0.1686	0.1012	0.1517	0	82.65	0	0	70.02	29.18	0.02529	0.02529	0.03554	0.01343
Isobutene	0.1875	0.2187	0.1562	0.09375	0.1406	0	82.65	0	0	70.02	25.16	0.02344	0.02344	0.03294	0.01343

Fluid\$	V 1	V 2	V 3	V 4	U 2	U 3	W 2	W 3	Ma 1	Ma 2	Ma 2rel	Ma 3	Ma 3rel	Ma 4
	[m/s]	[m/s]	[m/s]	[m/s]	[m/s]	[m/s]	[m/s]	[m/s]	[-]	[-]	[-]	[-]	[-]	[-]
R245fa	0.9396	199.5	29.25	28.14	127.6	76.58	74.7	81.82	0.0073	1.453	0.5439	0.2125	0.5943	0.2044
R134a	1.374	199.5	142.1	136.7	127.6	76.58	74.7	161.3	0.008341	1.214	0.4546	0.8767	0.9955	0.8422
n-butane	0.4635	276	189.8	182.7	176.5	105.9	103.3	217.3	0.002422	1.338	0.5008	0.9142	1.046	0.8782
Isobutene	0.6007	255.8	209.1	201.2	163.6	98.17	95.75	230.9	0.003214	1.271	0.4757	1.029	1.136	0.9876

APPENDIX A3 RESULTS

A3.4: Turbine Modelling and Design – Summarised Results

Axial Turbine Geometric Specifications, Velocities and Mach Numbers

Fluid\$	rpm	d	b	R _s	alpha ₁	alpha ₂	alpha ₃	beta ₂	beta ₃
	[-/min]	[m]	[m]		[deg]	[deg]	[deg]	[deg]	[deg]
R245fa	20000	0.04646	0.006969	0.1133	0	38.88	0	15.97	27.49
R134a	20000	0.05013	0.00752	0.1204	0	40.33	0	16.76	28.71
n-butane	20000	0.05229	0.007843	0.08103	0	32.01	0	12.51	21.96
isobutane	20000	0.05182	0.007773	0.08094	0	31.99	0	12.5	21.95

Fluid\$	C ₁	C ₂	C ₃	U	W ₂	W ₃	Ma ₁	Ma ₂	Ma ₃	Ma _{2rel}	Ma _{3rel}
	[m/s]	[m/s]	[m/s]	[m/s]	[m/s]	[m/s]					
R245fa	44.76	138.2	107.5	55.95	111.9	121.2	0.3478	1.001	0.7809	0.8103	0.8803
R134a	48.3	144.6	110.2	60.37	115.1	125.7	0.2932	0.862	0.6586	0.6863	0.7509
n-butane	50.37	184.1	156.1	62.97	159.9	168.3	0.2633	0.8666	0.7358	0.7527	0.7934
isobutane	49.92	182.6	154.9	62.41	158.6	167	0.2671	0.8772	0.7451	0.7621	0.8033

APPENDIX A3 RESULTS

A3.4: Turbine Modelling and Design – Summarised Results

Axial Turbine Preliminary Simulations

Working Fluid	m_dot [kg/s]	P_3 [Pa]	T_3 [C]	T_1 [C]	P_1 [Pa]	rpm [-/min]	d_1 [m]
R245fa	2	354638	61.29	80.99	810600	20764	0.04543
R245fa	1.5	354638	58.32	80.99	810600	29749	0.03661
R245fa	1	354638	52.69	80.99	810600	49385	0.02701
R245fa	0.95	354638	51.83	80.99	810600	52655	0.02599
R245fa	0.925	354638	51.38	80.99	810600	54440	0.02548
R245fa	0.9125	354638	51.14	80.99	810600	55374	0.02522
R245fa	0.91	354638	51.09	80.99	810600	55564	0.02517
R245fa	0.909	354638	51.07	80.99	810600	55640	0.02515
R245fa	0.9085	NO CONVERGENCE BELOW THIS					
Working Fluid	m_dot [kg/s]	P_3 [Pa]	T_3 [C]	T_1 [C]	P_1 [Pa]	rpm [-/min]	d_1 [m]
R134a	2	354638	65.13	80.99	810600	17169	0.05494
R134a	1.5	354638	61.96	80.99	810600	24599	0.04428
R134a	1	354638	55.84	80.99	810600	40835	0.03267
R134a	0.9	354638	53.85	80.99	810600	46584	0.03018
R134a	0.8	354638	51.41	80.99	810600	53973	0.02763
R134a	0.7	354638	48.33	80.99	810600	63777	0.025
R134a	0.6	354638	44.33	80.99	810600	77330	0.02227
R134a	0.5	354638	38.91	80.99	810600	97123	0.01942
R134a	0.45	354638	35.43	80.99	810600	110795	0.01795
R134a	0.4	354638	31.19	80.99	810600	128369	0.01643
R134a	0.3	354638	19.32	80.99	810600	183922	0.01324
R134a	0.25	354638	10.66	80.99	810600	230999	0.01155
R134a	0.24	354638	8.603	80.99	810600	243092	0.0112
R134a	0.23	354638	6.425	80.99	810600	256375	0.01085
R134a	0.229	354638	6.2	80.99	810600	257775	0.01081
R134a	0.228	354638	5.973	80.99	810600	259189	0.01078
R134a	0.227	354638	5.745	80.99	810600	260617	0.01074
R134a	0.226	354638	5.516	80.99	810600	262060	0.01071
R134a	0.225	NO CONVERGENCE BELOW THIS					

APPENDIX A3 RESULTS

A3.4: Turbine Modelling and Design – Summarised Results

Working Fluid	m_dot [kg/s]	P_3 [Pa]	T_3 [C]	T_1 [C]	P_1 [Pa]	rpm [-/min]	d_1 [m]
n-butane	2	354638	60.66	80.03	1010000	15454	0.06104
n-butane	1.5	354638	58.38	80.03	1010000	22141	0.04919
n-butane	1	354638	53.98	80.03	1010000	36755	0.03629
n-butane	0.9	354638	52.56	80.03	1010000	41929	0.03354
n-butane	0.8	354638	50.8	80.03	1010000	48580	0.0307
n-butane	0.7	354638	48.6	80.03	1010000	57404	0.02777
n-butane	0.6	354638	45.73	80.03	1010000	69603	0.02474
n-butane	0.5	354638	41.87	80.03	1010000	87419	0.02158
n-butane	0.45	354638	39.38	80.03	1010000	99725	0.01994
n-butane	0.44	354638	38.83	80.03	1010000	102566	0.01961
n-butane	0.43	354638	38.25	80.03	1010000	105556	0.01927
n-butane	0.42	354638	37.65	80.03	1010000	108707	0.01893
	0.419	NO CONVERGENCE BELOW THIS					
Working Fluid	m_dot [kg/s]	P_3 [Pa]	T_3 [C]	T_1 [C]	P_1 [Pa]	rpm [-/min]	d_1 [m]
isobutane	2	354638	46.94	66.82	1010000	15804	0.05968
isobutane	1.5	354638	44.57	66.82	1010000	22644	0.0481
isobutane	1	354638	39.99	66.82	1010000	37589	0.03549
isobutane	0.9	354638	38.51	66.82	1010000	42880	0.03279
isobutane	0.8	354638	36.69	66.82	1010000	49682	0.03002
isobutane	0.7	354638	34.41	66.82	1010000	58707	0.02716
isobutane	0.6	354638	31.45	66.82	1010000	71182	0.02419
isobutane	0.5	354638	27.48	66.82	1010000	89402	0.0211
isobutane	0.49	354638	27.01	66.82	1010000	91688	0.02078
isobutane	0.48	354638	26.52	66.82	1010000	94082	0.02046
isobutane	0.47	354638	26.01	66.82	1010000	96591	0.02014
isobutane	0.46	354638	25.48	66.82	1010000	99223	0.01982
isobutane	0.459	354638	25.43	66.82	1010000	99493	0.01979
	0.458	NO CONVERGENCE BELOW THIS					

APPENDIX A3 RESULTS

A3.5: Radial Turbine Simulations No. 01

Fluid\$	m_dot	P_1	P_2	P_3	P_4	T_1	T_2	T_3	T_4	h_01	h_02	h_02rel	h_03
	[kg/s]	[kPa]	[Pa]	[kPa]	[kPa]	[C]	[C]	[C]	[C]	[J/kg]	[J/kg]	[J/kg]	[J/kg]
R245fa	0.396	810.6	250.594	130.0	180	80.99	48.72	33.2	41.12	462394	462394	445275	437142
R245fa	0.396	810.6	250.594	142.5	180	80.99	48.72	35.27	40.99	462394	462394	445275	437142
R245fa	0.396	810.6	250.594	155.0	180	80.99	48.72	37.19	40.88	462394	462394	445275	437142
R245fa	0.396	810.6	250.594	167.5	180	80.99	48.72	38.97	40.77	462394	462394	445275	437142
R245fa	0.396	810.6	250.594	180.0	180	80.99	48.72	40.64	40.68	462394	462394	445275	437142
R134a	0.396	810.6	352.096	130.0	180	80.99	53.94	24.4	35.22	317912	317912	300793	292659
R134a	0.396	810.6	352.096	142.5	180	80.99	53.94	27	35.03	317912	317912	300793	292659
R134a	0.396	810.6	352.096	155.0	180	80.99	53.94	29.4	34.86	317912	317912	300793	292659
R134a	0.396	810.6	352.096	167.5	180	80.99	53.94	31.62	34.71	317912	317912	300793	292659
R134a	0.396	810.6	352.096	180.0	180	80.99	53.94	33.7	34.56	317912	317912	300793	292659
n-butane	0.207	1.01E+03	373.215	130.0	180	80.03	48.67	20.61	30.16	696523	696523	663773	648214
n-butane	0.207	1.01E+03	373.215	142.5	180	80.03	48.67	22.91	30.00	696523	696523	663773	648214
n-butane	0.207	1.01E+03	373.215	155.0	180	80.03	48.67	25.04	29.86	696523	696523	663773	648214
n-butane	0.207	1.01E+03	373.215	167.5	180	80.03	48.67	27.01	29.73	696523	696523	663773	648214
n-butane	0.207	1.01E+03	373.215	180.0	180	80.03	48.67	28.86	29.61	696523	696523	663773	648214
isobutane	0.241	1.01E+03	412.856	130.0	180	66.82	38.16	7.005	16.85	642769	642769	614639	601275
isobutane	0.241	1.01E+03	412.856	142.5	180	66.82	38.16	9.329	16.69	642769	642769	614639	601275
isobutane	0.241	1.01E+03	412.856	155.0	180	66.82	38.16	11.47	16.55	642769	642769	614639	601275
isobutane	0.241	1.01E+03	412.856	167.5	180	66.82	38.16	13.47	16.41	642769	642769	614639	601275
isobutane	0.241	1.01E+03	412.856	180.0	180	66.82	38.16	15.33	16.29	642769	642769	614639	601275

APPENDIX A3 RESULTS

A3.5: Radial Turbine Simulations No. 01

Fluid\$	h_03rel	h_03ss	h_04	h_1	h_2	h_2s	h_3	h_3s	h_3ss	h_4	h_4s	P_01	P_02
	[J/kg]	[J/kg]	[J/kg]	[J/kg]	[J/kg]	[J/kg]	[J/kg]	[J/kg]	[J/kg]	[J/kg]	[J/kg]	[Pa]	[Pa]
R245fa	440062	434854	437142	462356	442485	440886	431208	430496	429324	437137	437137	812325	736857
R245fa	440062	434984	437142	462356	442485	440886	432744	432156	429324	437016	437006	812325	736857
R245fa	440062	435102	437142	462356	442485	440886	434156	433682	429324	436906	436887	812325	736857
R245fa	440062	435209	437142	462356	442485	440886	435463	435093	429324	436806	436779	812325	736857
R245fa	440062	435309	437142	462356	442485	440886	436679	436407	429324	436713	436679	812325	736857
R134a	295579	289357	292659	317831	298003	296403	275338	273712	284865	283832	283123	813123	761110
R134a	295579	289542	292659	317831	298003	296403	277337	275871	284865	283665	282943	813123	761116
R134a	295579	289710	292659	317831	298003	296403	279181	277864	284865	283514	282779	813123	761116
R134a	295579	289863	292659	317831	298003	296403	280894	279714	284865	283376	282630	813123	761116
R134a	295579	290005	292659	317831	298003	296403	282493	281442	284865	283249	282493	813123	761116
n-butane	653799	642166	648214	696489	658435	655375	617990	615113	633237	632489	631225	1.01E+06	930615
n-butane	653799	642478	648214	696489	658435	655375	621401	618798	633237	632207	630921	1.01E+06	930610
n-butane	653799	642761	648214	696489	658435	655375	624541	622190	633237	631951	630645	1.01E+06	930610
n-butane	653799	643021	648214	696489	658435	655375	627450	625333	633237	631718	630393	1.01E+06	930610
n-butane	653799	643259	648214	696489	658435	655375	630161	628262	633237	631503	630161	1.01E+06	930610
isobutane	606073	595385	601275	642727	610055	607427	567794	564719	588419	581961	580409	1.01E+06	939005
isobutane	606073	595691	601275	642727	610055	607427	571039	568225	588419	581688	580114	1.01E+06	939005
isobutane	606073	595968	601275	642727	610055	607427	574028	571454	588419	581441	579847	1.01E+06	939005
isobutane	606073	596222	601275	642727	610055	607427	576798	574446	588419	581215	579604	1.01E+06	939005
isobutane	606073	596455	601275	642727	610055	607427	579380	577235	588419	581008	579380	1.01E+06	939005

APPENDIX A3 RESULTS

A3.5: Radial Turbine Simulations No. 01

Fluid\$	P_02rel	P_03	P_03rel	Rr	R_s	c_1	c_2	c_3	c_4	eta_ts	eta_tt	Ma_1	Ma_2
	[Pa]	[Pa]	[Pa]	[-]	[-]	[m/s]	[m/s]	[m/s]	[m/s]	[-]	[-]	[-]	[-]
R245fa	291441	180049	211044	0.3621	0.35	8.724	199.5	108.9	3.074	76%	92%	0.06778	1.453
R245fa	291441	181340	212569	0.329	0.35	8.724	199.5	93.79	15.86	76%	92%	0.06778	1.453
R245fa	291441	182520	213962	0.2953	0.35	8.724	199.5	77.28	21.71	76%	93%	0.06778	1.453
R245fa	291441	183605	215245	0.2611	0.35	8.724	199.5	57.95	25.93	76%	93%	0.06778	1.453
R245fa	291441	184610	216432	0.2261	0.35	8.724	199.5	30.43	29.28	76%	93%	0.06778	1.453
R134a	393050	265220	297989	0.5334	0.35	12.76	199.5	186.1	132.9	76%	88%	0.07745	1.214
R134a	393053	267221	300246	0.5103	0.35	12.76	199.5	175.1	134.1	76%	89%	0.07745	1.214
R134a	393053	269048	302306	0.487	0.35	12.76	199.5	164.2	135.2	76%	90%	0.07745	1.214
R134a	393053	270729	304201	0.4632	0.35	12.76	199.5	153.4	136.3	76%	90%	0.07745	1.214
R134a	393053	272284	305956	0.4389	0.35	12.76	199.5	142.6	137.2	76%	90%	0.07745	1.214
n-butane	423957	271261	309983	0.5152	0.35	8.233	276	245.9	177.3	76%	89%	0.04303	1.338
n-butane	423955	273323	312359	0.4932	0.35	8.233	276	231.6	178.9	76%	89%	0.04303	1.338
n-butane	423955	275209	314531	0.4711	0.35	8.233	276	217.6	180.3	76%	90%	0.04303	1.338
n-butane	423955	276943	316529	0.4488	0.35	8.233	276	203.8	181.6	76%	90%	0.04303	1.338
n-butane	423955	278548	318379	0.4263	0.35	8.233	276	190	182.8	76%	91%	0.04303	1.338
isobutane	462941	304711	343398	0.564	0.35	9.165	255.8	258.8	196.5	76%	88%	0.04903	1.271
isobutane	462941	307080	346090	0.5442	0.35	9.165	255.8	245.9	197.9	76%	88%	0.04903	1.271
isobutane	462941	309244	348549	0.5244	0.35	9.165	255.8	233.4	199.2	76%	89%	0.04903	1.271
isobutane	462941	311234	350810	0.5044	0.35	9.165	255.8	221.3	200.3	76%	89%	0.04903	1.271
isobutane	462941	313076	352904	0.4842	0.35	9.165	255.8	209.3	201.3	76%	90%	0.04903	1.271

APPENDIX A3 RESULTS

A3.5: Radial Turbine Simulations No. 01

Fluid\$	Ma_2rel	Ma_3	Ma_3rel	Ma_4	N_blades	rpm	PSI	PHI	L_d	d_1	d_2	d_3	d_4
	[-]	[-]	[-]	[-]		[-/min]	[-]	[-]	[m]	[m]	[m]	[m]	[m]
R245fa	0.5439	0.7917	0.9671	0.02231	61.1	60944	1.55	0.2	0.048	0.056	0.04	0.024	0.036
R245fa	0.5439	0.6813	0.8788	0.1151	61.1	60944	1.55	0.2	0.048	0.056	0.04	0.024	0.036
R245fa	0.5439	0.5612	0.7893	0.1576	61.1	60944	1.55	0.2	0.048	0.056	0.04	0.024	0.036
R245fa	0.5439	0.4209	0.6965	0.1883	61.1	60944	1.55	0.2	0.048	0.056	0.04	0.024	0.036
R245fa	0.5439	0.2211	0.5974	0.2126	61.1	60944	1.55	0.2	0.048	0.056	0.04	0.024	0.036
R134a	0.4546	1.159	1.253	0.8177	61.1	60944	1.55	0.2	0.048	0.056	0.04	0.024	0.036
R134a	0.4546	1.087	1.186	0.8257	61.1	60944	1.55	0.2	0.048	0.056	0.04	0.024	0.036
R134a	0.4546	1.017	1.122	0.8329	61.1	60944	1.55	0.2	0.048	0.056	0.04	0.024	0.036
R134a	0.4546	0.9484	1.06	0.8394	61.1	60944	1.55	0.2	0.048	0.056	0.04	0.024	0.036
R134a	0.4546	0.88	0.9984	0.8453	61.1	60944	1.55	0.2	0.048	0.056	0.04	0.024	0.036
n-butane	0.5009	1.187	1.292	0.8516	61.1	84293	1.55	0.2	0.048	0.056	0.04	0.024	0.036
n-butane	0.5009	1.117	1.228	0.8595	61.1	84293	1.55	0.2	0.048	0.056	0.04	0.024	0.036
n-butane	0.5009	1.049	1.166	0.8666	61.1	84293	1.55	0.2	0.048	0.056	0.04	0.024	0.036
n-butane	0.5009	0.9816	1.106	0.873	61.1	84293	1.55	0.2	0.048	0.056	0.04	0.024	0.036
n-butane	0.5009	0.915	1.047	0.8789	61.1	84293	1.55	0.2	0.048	0.056	0.04	0.024	0.036
isobutane	0.4757	1.277	1.366	0.9638	61.1	78121	1.55	0.2	0.048	0.056	0.04	0.024	0.036
isobutane	0.4757	1.212	1.305	0.9709	61.1	78121	1.55	0.2	0.048	0.056	0.04	0.024	0.036
isobutane	0.4757	1.15	1.247	0.9773	61.1	78121	1.55	0.2	0.048	0.056	0.04	0.024	0.036
isobutane	0.4757	1.089	1.191	0.9832	61.1	78121	1.55	0.2	0.048	0.056	0.04	0.024	0.036
isobutane	0.4757	1.03	1.137	0.9885	61.1	78121	1.55	0.2	0.048	0.056	0.04	0.024	0.036

APPENDIX A3 RESULTS

A3.5: Radial Turbine Simulations No. 01

Fluid\$	alpha_1	alpha_2	alpha_3	alpha_4	beta_2	beta_3	b_1	b_2	b_3	b_4
	[deg]	[deg]	[deg]	[deg]	[deg]	[deg]	[m]	[m]	[m]	[m]
R245fa	0	82.65	0	0	70.02	35.14	0.006	0.006	0.008432	0.01343
R245fa	0	82.65	0	0	70.02	39.28	0.006	0.006	0.008432	0.01343
R245fa	0	82.65	0	0	70.02	44.8	0.006	0.006	0.008432	0.01343
R245fa	0	82.65	0	0	70.02	52.99	0.006	0.006	0.008432	0.01343
R245fa	0	82.65	0	0	70.02	68.61	0.006	0.006	0.008432	0.01343
R134a	0	82.65	0	0	70.02	22.37	0.006	0.006	0.008432	0.01343
R134a	0	82.65	0	0	70.02	23.64	0.006	0.006	0.008432	0.01343
R134a	0	82.65	0	0	70.02	25.02	0.006	0.006	0.008432	0.01343
R134a	0	82.65	0	0	70.02	26.54	0.006	0.006	0.008432	0.01343
R134a	0	82.65	0	0	70.02	28.25	0.006	0.006	0.008432	0.01343
n-butane	0	82.65	0	0	70.02	23.32	0.006	0.006	0.008432	0.01343
n-butane	0	82.65	0	0	70.02	24.59	0.006	0.006	0.008432	0.01343
n-butane	0	82.65	0	0	70.02	25.97	0.006	0.006	0.008432	0.01343
n-butane	0	82.65	0	0	70.02	27.48	0.006	0.006	0.008432	0.01343
n-butane	0	82.65	0	0	70.02	29.15	0.006	0.006	0.008432	0.01343
isobutane	0	82.65	0	0	70.02	20.78	0.006	0.006	0.008432	0.01343
isobutane	0	82.65	0	0	70.02	21.77	0.006	0.006	0.008432	0.01343
isobutane	0	82.65	0	0	70.02	22.82	0.006	0.006	0.008432	0.01343
isobutane	0	82.65	0	0	70.02	23.94	0.006	0.006	0.008432	0.01343
isobutane	0	82.65	0	0	70.02	25.14	0.006	0.006	0.008432	0.01343

APPENDIX A3 RESULTS

A3.6: Radial Turbine Simulations No. 02

Fluid\$	m_dot	P_1	P_2	P_3	P_4	T_1	T_2	T_3	T_4	h_01	h_02	h_02rel	h_03
	[kg/s]	[Pa]	[Pa]	[Pa]	[Pa]	[C]	[C]	[C]	[C]	[J/kg]	[J/kg]	[J/kg]	[J/kg]
R245fa	0.396	810600	250077	180000	180000	80.99	48.67	40.64	40.67	462357	462357	445237	437104
R245fa	0.396	810600	250078	180000	180000	80.99	48.67	40.64	40.67	462357	462357	445237	437104
R245fa	0.396	810600	250079	180000	180000	80.99	48.67	40.64	40.67	462357	462357	445237	437104
R245fa	0.396	810600	250081	180000	180000	80.99	48.67	40.64	40.67	462357	462357	445237	437104
R245fa	0.396	810600	250083	180000	180000	80.99	48.67	40.64	40.67	462357	462357	445238	437105
R245fa	0.396	810600	250088	180000	180000	80.99	48.67	40.64	40.67	462357	462357	445238	437105
R245fa	0.396	810600	250095	180000	180000	80.99	48.67	40.64	40.67	462358	462358	445238	437105
R245fa	0.396	810600	250107	180000	180000	80.99	48.67	40.64	40.67	462359	462359	445239	437106
R245fa	0.396	810600	250130	180000	180000	80.99	48.67	40.64	40.67	462360	462360	445241	437108
R245fa	0.396	810600	250177	180000	180000	80.99	48.68	40.64	40.67	462364	462364	445245	437111
R245fa	0.396	810600	250287	180000	180000	80.99	48.69	40.64	40.68	462372	462372	445253	437119
R245fa	0.396	810600	250594	180000	180000	80.99	48.72	40.64	40.68	462394	462394	445275	437142
R245fa	0.396	810600	251722	180000	180000	80.99	48.84	40.65	40.69	462477	462477	445357	437224
R245fa	0.396	810600	258522	180000	180000	80.99	49.52	40.68	40.76	462965	462965	445846	437713
R134a	0.396	810600	350961	180000	180000	80.99	53.84	33.69	34.55	317831	317831	300712	292578
R134a	0.396	810600	350963	180000	180000	80.99	53.84	33.69	34.55	317831	317831	300712	292579
R134a	0.396	810600	350966	180000	180000	80.99	53.84	33.69	34.55	317831	317831	300712	292579
R134a	0.396	810600	350970	180000	180000	80.99	53.84	33.69	34.55	317832	317832	300712	292579
R134a	0.396	810600	350975	180000	180000	80.99	53.84	33.69	34.55	317832	317832	300713	292579
R134a	0.396	810600	350985	180000	180000	80.99	53.84	33.69	34.55	317833	317833	300713	292580
R134a	0.396	810600	351000	180000	180000	80.99	53.84	33.69	34.55	317834	317834	300714	292581
R134a	0.396	810600	351027	180000	180000	80.99	53.84	33.69	34.55	317836	317836	300716	292583
R134a	0.396	810600	351077	180000	180000	80.99	53.85	33.69	34.55	317839	317839	300720	292587

APPENDIX A3 RESULTS

A3.6: Radial Turbine Simulations No. 02

Fluid\$	m_dot	P_1	P_2	P_3	P_4	T_1	T_2	T_3	T_4	h_01	h_02	h_02rel	h_03
	[kg/s]	[Pa]	[Pa]	[Pa]	[Pa]	[C]	[C]	[C]	[C]	[J/kg]	[J/kg]	[J/kg]	[J/kg]
R134a	0.396	810600	351181	180000	180000	80.99	53.86	33.7	34.55	317847	317847	300727	292594
R134a	0.396	810600	351422	180000	180000	80.99	53.88	33.7	34.55	317864	317864	300744	292611
R134a	0.396	810600	352096	180000	180000	80.99	53.94	33.7	34.56	317912	317912	300793	292659
R134a	0.396	810600	354571	180000	180000	80.99	54.17	33.71	34.59	318088	318088	300968	292835
R134a	0.396	810600	369618	180000	180000	80.99	55.54	33.8	34.75	319133	319133	302014	293881
n-butane	0.207	1.01E+06	372912	180000	180000	80.03	48.65	28.86	29.61	696489	696489	663739	648180
n-butane	0.207	1.01E+06	372912	180000	180000	80.03	48.65	28.86	29.61	696489	696489	663739	648180
n-butane	0.207	1.01E+06	372913	180000	180000	80.03	48.65	28.86	29.61	696489	696489	663739	648180
n-butane	0.207	1.01E+06	372914	180000	180000	80.03	48.65	28.86	29.61	696489	696489	663739	648180
n-butane	0.207	1.01E+06	372916	180000	180000	80.03	48.65	28.86	29.61	696489	696489	663739	648180
n-butane	0.207	1.01E+06	372918	180000	180000	80.03	48.65	28.86	29.61	696490	696490	663740	648181
n-butane	0.207	1.01E+06	372922	180000	180000	80.03	48.65	28.86	29.61	696490	696490	663740	648181
n-butane	0.207	1.01E+06	372929	180000	180000	80.03	48.65	28.86	29.61	696491	696491	663741	648182
n-butane	0.207	1.01E+06	372943	180000	180000	80.03	48.65	28.86	29.61	696492	696492	663742	648183
n-butane	0.207	1.01E+06	372970	180000	180000	80.03	48.65	28.86	29.61	696496	696496	663745	648186
n-butane	0.207	1.01E+06	373035	180000	180000	80.03	48.66	28.86	29.61	696503	696503	663753	648194
n-butane	0.207	1.01E+06	373215	180000	180000	80.03	48.67	28.86	29.61	696523	696523	663773	648214
n-butane	0.207	1.01E+06	373215	180000	180000	80.03	48.67	28.86	29.61	696523	696523	663773	648214
n-butane	0.207	1.01E+06	373215	180000	180000	80.03	48.67	28.86	29.61	696523	696523	663773	648214
isobutane	0.241	1.01E+06	412422	180000	180000	66.82	38.13	15.33	16.29	642727	642727	614597	601233
isobutane	0.241	1.01E+06	412423	180000	180000	66.82	38.13	15.33	16.29	642727	642727	614598	601234
isobutane	0.241	1.01E+06	412424	180000	180000	66.82	38.13	15.33	16.29	642727	642727	614598	601234
isobutane	0.241	1.01E+06	412426	180000	180000	66.82	38.13	15.33	16.29	642728	642728	614598	601234

APPENDIX A3 RESULTS

A3.6: Radial Turbine Simulations No. 02

Fluid\$	m_dot	P_1	P_2	P_3	P_4	T_1	T_2	T_3	T_4	h_01	h_02	h_02rel	h_03
	[kg/s]	[Pa]	[Pa]	[Pa]	[Pa]	[C]	[C]	[C]	[C]	[J/kg]	[J/kg]	[J/kg]	[J/kg]
Isobutene	0.241	1.01E+06	412428	180000	180000	66.82	38.13	15.33	16.29	642728	642728	614598	601234
isobutane	0.241	1.01E+06	412431	180000	180000	66.82	38.13	15.33	16.29	642728	642728	614598	601234
isobutane	0.241	1.01E+06	412437	180000	180000	66.82	38.13	15.33	16.29	642729	642729	614599	601235
isobutane	0.241	1.01E+06	412447	180000	180000	66.82	38.13	15.33	16.29	642730	642730	614600	601236
isobutane	0.241	1.01E+06	412467	180000	180000	66.82	38.13	15.33	16.29	642732	642732	614602	601238
isobutane	0.241	1.01E+06	412506	180000	180000	66.82	38.14	15.33	16.29	642735	642735	614606	601242
isobutane	0.241	1.01E+06	412599	180000	180000	66.82	38.14	15.33	16.29	642744	642744	614614	601250
isobutane	0.241	1.01E+06	412856	180000	180000	66.82	38.16	15.33	16.29	642769	642769	614639	601275
isobutane	0.241	1.01E+06	413799	180000	180000	66.82	38.23	15.33	16.3	642860	642860	614730	601366
isobutane	0.241	1.01E+06	419449	180000	180000	66.82	38.64	15.36	16.34	643399	643399	615269	601905

APPENDIX A3 RESULTS

A3.6: Radial Turbine Simulations No. 02

Fluid\$	h_03rel	h_03ss	h_04	h_1	h_2	h_2s	h_3	h_3s	h_3ss	h_4	h_4s	P_01	P_02
	[J/kg]	[J/kg]	[J/kg]	[J/kg]	[J/kg]	[J/kg]	[J/kg]	[J/kg]	[J/kg]	[J/kg]	[J/kg]	[Pa]	[Pa]
R245fa	440024	435274	437104	462356	442447	440848	436676	436407	429266	436708	436676	810608	735313
R245fa	440024	435274	437104	462356	442447	440848	436676	436407	429266	436708	436676	810611	735316
R245fa	440024	435274	437104	462356	442447	440848	436676	436407	429266	436708	436676	810615	735319
R245fa	440024	435274	437104	462356	442447	440848	436676	436407	429266	436708	436676	810621	735324
R245fa	440024	435274	437105	462356	442448	440848	436676	436407	429267	436708	436676	810630	735332
R245fa	440025	435274	437105	462356	442448	440848	436676	436407	429267	436708	436676	810644	735345
R245fa	440025	435275	437105	462356	442448	440849	436676	436407	429268	436708	436676	810667	735366
R245fa	440026	435276	437106	462356	442449	440850	436677	436407	429269	436708	436677	810707	735402
R245fa	440028	435277	437108	462356	442451	440852	436677	436407	429272	436709	436677	810783	735471
R245fa	440031	435280	437111	462356	442455	440855	436677	436407	429277	436709	436677	810940	735611
R245fa	440039	435288	437119	462356	442463	440863	436677	436407	429290	436710	436677	811306	735940
R245fa	440062	435309	437142	462356	442485	440886	436679	436407	429324	436713	436679	812325	736857
R245fa	440144	435385	437224	462356	442567	440968	436685	436407	429451	436725	436685	816065	740220
R245fa	440632	435836	437713	462356	443056	441456	436718	436403	430203	436792	436718	838682	760547
R134a	295498	289930	292578	317831	297922	296322	282488	281442	284741	283238	282488	810613	758756
R134a	295498	289930	292579	317831	297922	296322	282487	281442	284741	283238	282487	810617	758764
R134a	295498	289931	292579	317831	297922	296322	282487	281442	284741	283238	282487	810623	758769
R134a	295499	289931	292579	317831	297922	296323	282487	281442	284741	283238	282487	810631	758777
R134a	295499	289931	292579	317831	297923	296323	282487	281442	284742	283238	282487	810644	758789
R134a	295500	289932	292580	317831	297923	296324	282488	281442	284743	283238	282488	810665	758808
R134a	295501	289933	292581	317831	297924	296325	282488	281442	284745	283238	282488	810698	758840
R134a	295503	289935	292583	317831	297926	296327	282488	281442	284748	283238	282488	810758	758896
R134a	295506	289938	292587	317831	297930	296330	282488	281442	284753	283239	282488	810869	759000

APPENDIX A3 RESULTS

A3.6: Radial Turbine Simulations No. 02

Fluid\$	h_03rel	h_03ss	h_04	h_1	h_2	h_2s	h_3	h_3s	h_3ss	h_4	h_4s	P_01	P_02
	[J/kg]	[J/kg]	[J/kg]	[J/kg]	[J/kg]	[J/kg]	[J/kg]	[J/kg]	[J/kg]	[J/kg]	[J/kg]	[Pa]	[Pa]
R134a	295514	289945	292594	317831	297937	296338	282488	281442	284765	283240	282488	811098	759215
R134a	295531	289961	292611	317831	297954	296355	282490	281442	284791	283242	282490	811633	759717
R134a	295579	290005	292659	317831	298003	296403	282493	281442	284865	283249	282493	813123	761116
R134a	295755	290166	292835	317831	298178	296579	282505	281441	285136	283273	282505	818601	766256
R134a	296800	291126	293881	317831	299224	297624	282577	281434	286744	283418	282577	851894	797500
n-butane	653765	643228	648180	696489	658402	655342	630158	628261	633185	631498	630158	1.01E+06	929851
n-butane	653765	643228	648180	696489	658402	655342	630159	628262	633185	631499	630159	1.01E+06	929839
n-butane	653766	643228	648180	696489	658402	655342	630159	628262	633186	631499	630159	1.01E+06	929841
n-butane	653766	643228	648180	696489	658402	655342	630159	628262	633186	631499	630159	1.01E+06	929843
n-butane	653766	643228	648180	696489	658402	655342	630159	628262	633186	631499	630159	1.01E+06	929847
n-butane	653766	643229	648181	696489	658402	655342	630159	628262	633186	631499	630159	1.01E+06	929854
n-butane	653767	643229	648181	696489	658403	655343	630159	628262	633187	631499	630159	1.01E+06	929864
n-butane	653767	643230	648182	696489	658403	655343	630159	628262	633188	631499	630159	1.01E+06	929882
n-butane	653769	643231	648183	696489	658405	655345	630159	628262	633191	631499	630159	1.01E+06	929917
n-butane	653772	643234	648186	696489	658408	655348	630159	628262	633195	631500	630159	1.01E+06	929987
n-butane	653779	643241	648194	696489	658415	655355	630159	628262	633206	631501	630159	1.01E+06	930152
n-butane	653799	643259	648214	696489	658435	655375	630161	628262	633237	631503	630161	1.01E+06	930610
n-butane	653799	643259	648214	696489	658435	655375	630161	628262	633237	631503	630161	1.01E+06	930610
n-butane	653799	643259	648214	696489	658435	655375	630161	628262	633237	631503	630161	1.01E+06	930610
isobutane	606031	596417	601233	642727	610013	607385	579377	577236	588354	581002	579377	1.01E+06	937995
isobutane	606031	596417	601234	642727	610013	607385	579377	577236	588355	581002	579377	1.01E+06	937997
isobutane	606031	596417	601234	642727	610013	607385	579377	577236	588355	581002	579377	1.01E+06	937999
isobutane	606031	596417	601234	642727	610013	607385	579377	577236	588355	581002	579377	1.01E+06	938003

APPENDIX A3 RESULTS

A3.6: Radial Turbine Simulations No. 02

Fluid\$	h_03rel	h_03ss	h_04	h_1	h_2	h_2s	h_3	h_3s	h_3ss	h_4	h_4s	P_01	P_02
	[J/kg]	[J/kg]	[J/kg]	[J/kg]	[J/kg]	[J/kg]	[J/kg]	[J/kg]	[J/kg]	[J/kg]	[J/kg]	[Pa]	[Pa]
isobutane	606032	596417	601234	642727	610014	607385	579377	577236	588355	581003	579377	1.01E+06	938008
isobutane	606032	596417	601234	642727	610014	607386	579377	577236	588356	581003	579377	1.01E+06	938016
isobutane	606032	596418	601235	642727	610015	607386	579377	577236	588357	581003	579377	1.01E+06	938030
isobutane	606033	596419	601236	642727	610016	607387	579377	577236	588358	581003	579377	1.01E+06	938053
isobutane	606035	596421	601238	642727	610017	607389	579377	577236	588361	581003	579377	1.01E+06	938098
isobutane	606039	596424	601242	642727	610021	607393	579378	577236	588367	581004	579378	1.01E+06	938190
isobutane	606048	596432	601250	642727	610030	607402	579378	577236	588381	581005	579378	1.01E+06	938406
isobutane	606073	596455	601275	642727	610055	607427	579380	577235	588419	581008	579380	1.01E+06	939005
isobutane	606164	596538	601366	642727	610146	607517	579386	577235	588558	581021	579386	1.01E+06	941203
isobutane	606703	597032	601905	642727	610685	608057	579423	577232	589388	581095	579423	1.03E+06	954378

APPENDIX A3 RESULTS

A3.6: Radial Turbine Simulations No. 02

Fluid\$	P_02rel	P_03	P_03rel	Rr	R_s	c_1	c_2	c_3	c_4	eta_ts	eta_tt	Ma_1	Ma_2
	[Pa]	[Pa]	[Pa]	[-]	[-]	[m/s]	[m/s]	[m/s]	[m/s]	[-]	[-]	[-]	[-]
R245fa	290841	184255	216018	0.2247	0.35	0.6204	199.5	29.25	28.14	0.7631	0.9324	0.00482	1.453
R245fa	290842	184256	216018	0.2247	0.35	0.7122	199.5	29.25	28.14	0.7631	0.9324	0.005533	1.453
R245fa	290843	184256	216019	0.2247	0.35	0.826	199.5	29.25	28.14	0.7631	0.9324	0.006417	1.453
R245fa	290845	184258	216021	0.2247	0.35	0.9694	199.5	29.26	28.15	0.7631	0.9324	0.007531	1.453
R245fa	290848	184259	216023	0.2247	0.35	1.154	199.5	29.26	28.15	0.7631	0.9324	0.008963	1.453
R245fa	290853	184262	216026	0.2247	0.35	1.396	199.5	29.27	28.16	0.7631	0.9324	0.01085	1.453
R245fa	290861	184267	216032	0.2248	0.35	1.723	199.5	29.29	28.18	0.7632	0.9324	0.01339	1.453
R245fa	290875	184276	216042	0.2248	0.35	2.181	199.5	29.32	28.2	0.7632	0.9324	0.01695	1.453
R245fa	290902	184291	216060	0.2249	0.35	2.849	199.5	29.37	28.26	0.7632	0.9324	0.02213	1.453
R245fa	290957	184324	216098	0.225	0.35	3.878	199.5	29.48	28.36	0.7632	0.9324	0.03013	1.453
R245fa	291085	184399	216186	0.2253	0.35	5.584	199.5	29.73	28.61	0.7633	0.9324	0.04338	1.453
R245fa	291441	184610	216432	0.2261	0.35	8.724	199.5	30.44	29.28	0.7636	0.9323	0.06778	1.453
R245fa	292748	185384	217334	0.2292	0.35	15.51	199.5	32.85	31.61	0.7646	0.9321	0.1205	1.453
R245fa	300636	190047	222768	0.2472	0.35	34.9	199.5	44.61	42.92	0.7708	0.9308	0.2711	1.454
R134a	391794	271464	305041	0.4367	0.35	0.9074	199.5	142.1	136.7	0.7631	0.9051	0.005508	1.214
R134a	391798	271466	305044	0.4367	0.35	1.042	199.5	142.1	136.7	0.7631	0.9051	0.006322	1.214
R134a	391801	271468	305046	0.4367	0.35	1.208	199.5	142.1	136.7	0.7631	0.9051	0.007333	1.214
R134a	391805	271471	305049	0.4367	0.35	1.418	199.5	142.1	136.7	0.7631	0.9051	0.008606	1.214
R134a	391811	271475	305054	0.4367	0.35	1.687	199.5	142.1	136.7	0.7632	0.9051	0.01024	1.214
R134a	391822	271482	305061	0.4367	0.35	2.042	199.5	142.1	136.7	0.7632	0.9051	0.01239	1.214
R134a	391838	271493	305074	0.4368	0.35	2.521	199.5	142.1	136.7	0.7632	0.9051	0.0153	1.214
R134a	391868	271512	305095	0.4368	0.35	3.19	199.5	142.1	136.7	0.7632	0.9051	0.01936	1.214
R134a	391924	271548	305135	0.4369	0.35	4.167	199.5	142.1	136.7	0.7632	0.9051	0.02529	1.214

APPENDIX A3 RESULTS

A3.6: Radial Turbine Simulations No. 02

Fluid\$	P_02rel	P_03	P_03rel	Rr	R_s	c_1	c_2	c_3	c_4	eta_ts	eta_tt	Ma_1	Ma_2
	[Pa]	[Pa]	[Pa]	[-]	[-]	[m/s]	[m/s]	[m/s]	[m/s]	[-]	[-]	[-]	[-]
R134a	392039	271623	305219	0.4371	0.35	5.671	199.5	142.2	136.8	0.7633	0.905	0.03442	1.214
R134a	392306	271798	305413	0.4376	0.35	8.166	199.5	142.3	136.9	0.7635	0.905	0.04957	1.214
R134a	393053	272284	305956	0.4389	0.35	12.76	199.5	142.6	137.2	0.7641	0.9049	0.07745	1.214
R134a	395797	274072	307946	0.4437	0.35	22.68	199.5	143.7	138.3	0.7663	0.9044	0.1377	1.214
R134a	412479	284920	320024	0.4722	0.35	51.04	199.5	150.4	144.7	0.7797	0.9016	0.3098	1.213
n-butane	423617	278343	318145	0.4258	0.35	0.5855	276	189.9	182.7	0.7631	0.907	0.00306	1.338
n-butane	423612	278340	318142	0.4258	0.35	0.6721	276	189.8	182.7	0.7631	0.907	0.003512	1.338
n-butane	423613	278340	318142	0.4258	0.35	0.7795	276	189.8	182.7	0.7631	0.907	0.004074	1.338
n-butane	423614	278341	318143	0.4258	0.35	0.9148	276	189.9	182.7	0.7631	0.907	0.004781	1.338
n-butane	423616	278342	318144	0.4258	0.35	1.089	276	189.9	182.7	0.7631	0.907	0.00569	1.338
n-butane	423618	278344	318146	0.4258	0.35	1.317	276	189.9	182.7	0.7631	0.907	0.006884	1.338
n-butane	423623	278346	318149	0.4258	0.35	1.626	276	189.9	182.7	0.7631	0.907	0.008499	1.338
n-butane	423631	278351	318155	0.4258	0.35	2.058	276	189.9	182.7	0.7631	0.907	0.01076	1.338
n-butane	423646	278361	318165	0.4258	0.35	2.688	276	189.9	182.7	0.7632	0.907	0.01405	1.338
n-butane	423678	278380	318187	0.4259	0.35	3.659	276	189.9	182.7	0.7632	0.907	0.01912	1.338
n-butane	423751	278424	318238	0.426	0.35	5.269	276	189.9	182.7	0.7632	0.907	0.02754	1.338
n-butane	423955	278548	318379	0.4263	0.35	8.233	276	190	182.8	0.7634	0.907	0.04303	1.338
n-butane	423955	278548	318379	0.4263	0.35	8.233	276	190	182.8	0.7634	0.907	0.04303	1.338
n-butane	423955	278548	318379	0.4263	0.35	8.233	276	190	182.8	0.7634	0.907	0.04303	1.338
isobutane	462455	312772	352563	0.4836	0.35	0.6517	255.8	209.1	201.2	0.7631	0.896	0.003487	1.271
isobutane	462456	312773	352564	0.4836	0.35	0.7482	255.8	209.1	201.2	0.7631	0.896	0.004002	1.271
isobutane	462457	312774	352564	0.4836	0.35	0.8677	255.8	209.1	201.2	0.7631	0.896	0.004642	1.271
isobutane	462459	312775	352566	0.4836	0.35	1.018	255.8	209.1	201.2	0.7631	0.896	0.005448	1.271

APPENDIX A3 RESULTS

A3.6: Radial Turbine Simulations No. 02

Fluid\$	P_02rel	P_03	P_03rel	Rr	R_s	c_1	c_2	c_3	c_4	eta_ts	eta_tt	Ma_1	Ma_2
	[Pa]	[Pa]	[Pa]	[-]	[-]	[m/s]	[m/s]	[m/s]	[m/s]	[-]	[-]	[-]	[-]
isobutane	462461	312776	352567	0.4836	0.35	1.212	255.8	209.1	201.2	0.7631	0.896	0.006483	1.271
isobutane	462465	312779	352570	0.4836	0.35	1.466	255.8	209.1	201.2	0.7631	0.896	0.007845	1.271
isobutane	462472	312783	352575	0.4836	0.35	1.81	255.8	209.1	201.2	0.7631	0.896	0.009685	1.271
isobutane	462483	312790	352583	0.4836	0.35	2.291	255.8	209.1	201.2	0.7632	0.896	0.01226	1.271
isobutane	462505	312804	352598	0.4837	0.35	2.993	255.8	209.1	201.2	0.7632	0.896	0.01601	1.271
isobutane	462549	312831	352629	0.4837	0.35	4.073	255.8	209.1	201.2	0.7632	0.896	0.02179	1.271
isobutane	462653	312896	352701	0.4839	0.35	5.866	255.8	209.2	201.2	0.7633	0.896	0.03138	1.271
isobutane	462941	313076	352903	0.4842	0.35	9.165	255.8	209.3	201.3	0.7635	0.8959	0.04903	1.271
isobutane	463998	313735	353644	0.4856	0.35	16.29	255.8	209.7	201.7	0.7641	0.8958	0.08716	1.271
isobutane	470328	317681	358073	0.4938	0.35	36.66	255.8	212	204	0.7682	0.8949	0.1961	1.271

APPENDIX A3 RESULTS

A3.6: Radial Turbine Simulations No. 02

Fluid\$	Ma_2rel	Ma_3	Ma_3rel	Ma_4	N_blades	rpm	PSI	PHI	L_d	d_1	d_1	d_2	d_2
	[-]	[-]	[-]	[-]		[-/min]	[-]	[-]	[m]	[m]	[mm]	[m]	[mm]
R245fa	0.5439	0.2124	0.5943	0.2044	61.1	16252	1.55	0.2	0.18	0.21	210	0.15	150
R245fa	0.5439	0.2124	0.5943	0.2044	61.1	17412	1.55	0.2	0.168	0.196	196	0.14	140
R245fa	0.5439	0.2125	0.5943	0.2044	61.1	18752	1.55	0.2	0.156	0.182	182	0.13	130
R245fa	0.5439	0.2125	0.5943	0.2044	61.1	20315	1.55	0.2	0.144	0.168	168	0.12	120
R245fa	0.5439	0.2125	0.5944	0.2045	61.1	22161	1.55	0.2	0.132	0.154	154	0.11	110
R245fa	0.5439	0.2126	0.5944	0.2045	61.1	24377	1.55	0.2	0.12	0.14	140	0.1	100
R245fa	0.5439	0.2127	0.5944	0.2046	61.1	27086	1.55	0.2	0.108	0.126	126	0.09	90
R245fa	0.5439	0.2129	0.5945	0.2048	61.1	30472	1.55	0.2	0.096	0.112	112	0.08	80
R245fa	0.5439	0.2133	0.5946	0.2052	61.1	34825	1.55	0.2	0.084	0.098	98	0.07	70
R245fa	0.5439	0.2141	0.5949	0.206	61.1	40629	1.55	0.2	0.072	0.084	84	0.06	60
R245fa	0.5439	0.216	0.5956	0.2078	61.1	48755	1.55	0.2	0.06	0.07	70	0.05	50
R245fa	0.5439	0.2211	0.5974	0.2127	61.1	60944	1.55	0.2	0.048	0.056	56	0.04	40
R245fa	0.5439	0.2386	0.6042	0.2295	61.1	81258	1.55	0.2	0.036	0.042	42	0.03	30
R245fa	0.5441	0.324	0.6426	0.3116	61.1	121887	1.55	0.2	0.024	0.028	28	0.02	20
R134a	0.4546	0.8767	0.9955	0.8422	61.1	16252	1.55	0.2	0.18	0.21	210	0.15	150
R134a	0.4546	0.8767	0.9955	0.8422	61.1	17412	1.55	0.2	0.168	0.196	196	0.14	140
R134a	0.4546	0.8767	0.9955	0.8422	61.1	18752	1.55	0.2	0.156	0.182	182	0.13	130
R134a	0.4546	0.8767	0.9955	0.8422	61.1	20315	1.55	0.2	0.144	0.168	168	0.12	120
R134a	0.4546	0.8768	0.9955	0.8422	61.1	22161	1.55	0.2	0.132	0.154	154	0.11	110
R134a	0.4546	0.8768	0.9956	0.8422	61.1	24377	1.55	0.2	0.12	0.14	140	0.1	100
R134a	0.4546	0.8768	0.9956	0.8423	61.1	27086	1.55	0.2	0.108	0.126	126	0.09	90
R134a	0.4546	0.8769	0.9957	0.8424	61.1	30472	1.55	0.2	0.096	0.112	112	0.08	80
R134a	0.4546	0.8771	0.9958	0.8425	61.1	34825	1.55	0.2	0.084	0.098	98	0.07	70

APPENDIX A3 RESULTS

A3.6: Radial Turbine Simulations No. 02

Fluid\$	Ma_2rel	Ma_3	Ma_3rel	Ma_4	N_blades	rpm	PSI	PHI	L_d	d_1	d_1	d_2	d_2
	[-]	[-]	[-]	[-]		[-/min]	[-]	[-]	[m]	[m]	[mm]	[m]	[mm]
R134a	0.4546	0.8774	0.9961	0.8428	61.1	40629	1.55	0.2	0.072	0.084	84	0.06	60
R134a	0.4546	0.878	0.9967	0.8434	61.1	48755	1.55	0.2	0.06	0.07	70	0.05	50
R134a	0.4546	0.88	0.9984	0.8453	61.1	60944	1.55	0.2	0.048	0.056	56	0.04	40
R134a	0.4545	0.887	1.005	0.852	61.1	81258	1.55	0.2	0.036	0.042	42	0.03	30
R134a	0.4542	0.9277	1.041	0.891	61.1	121887	1.55	0.2	0.024	0.028	28	0.02	20
n-butane	0.5008	0.9142	1.046	0.8782	61.1	22478	1.55	0.2	0.18	0.21	210	0.15	150
n-butane	0.5008	0.9142	1.046	0.8782	61.1	24084	1.55	0.2	0.168	0.196	196	0.14	140
n-butane	0.5008	0.9142	1.046	0.8782	61.1	25936	1.55	0.2	0.156	0.182	182	0.13	130
n-butane	0.5008	0.9142	1.046	0.8782	61.1	28098	1.55	0.2	0.144	0.168	168	0.12	120
n-butane	0.5008	0.9142	1.046	0.8782	61.1	30652	1.55	0.2	0.132	0.154	154	0.11	110
n-butane	0.5008	0.9142	1.046	0.8782	61.1	33717	1.55	0.2	0.12	0.14	140	0.1	100
n-butane	0.5008	0.9142	1.046	0.8782	61.1	37463	1.55	0.2	0.108	0.126	126	0.09	90
n-butane	0.5008	0.9142	1.046	0.8782	61.1	42146	1.55	0.2	0.096	0.112	112	0.08	80
n-butane	0.5008	0.9142	1.046	0.8782	61.1	48167	1.55	0.2	0.084	0.098	98	0.07	70
n-butane	0.5009	0.9143	1.046	0.8783	61.1	56195	1.55	0.2	0.072	0.084	84	0.06	60
n-butane	0.5009	0.9145	1.047	0.8785	61.1	67434	1.55	0.2	0.06	0.07	70	0.05	50
n-butane	0.5009	0.915	1.047	0.8789	61.1	84293	1.55	0.2	0.048	0.056	56	0.04	40
n-butane	0.5009	0.915	1.047	0.8789	61.1	84293	1.55	0.2	0.048	0.056	56	0.04	40
n-butane	0.5009	0.915	1.047	0.8789	61.1	84293	1.55	0.2	0.048	0.056	56	0.04	40
isobutane	0.4757	1.029	1.136	0.9876	61.1	20832	1.55	0.2	0.18	0.21	210	0.15	150
isobutane	0.4757	1.029	1.136	0.9876	61.1	22320	1.55	0.2	0.168	0.196	196	0.14	140
isobutane	0.4757	1.029	1.136	0.9876	61.1	24037	1.55	0.2	0.156	0.182	182	0.13	130
isobutane	0.4757	1.029	1.136	0.9876	61.1	26040	1.55	0.2	0.144	0.168	168	0.12	120

APPENDIX A3 RESULTS

A3.6: Radial Turbine Simulations No. 02

Fluid\$	Ma_2rel	Ma_3	Ma_3rel	Ma_4	N_blades	rpm	PSI	PHI	L_d	d_1	d_1	d_2	d_2
	[-]	[-]	[-]	[-]		[-/min]	[-]	[-]	[m]	[m]	[mm]	[m]	[mm]
isobutane	0.4757	1.029	1.136	0.9876	61.1	28408	1.55	0.2	0.132	0.154	154	0.11	110
isobutane	0.4757	1.029	1.136	0.9876	61.1	31248	1.55	0.2	0.12	0.14	140	0.1	100
isobutane	0.4757	1.029	1.136	0.9876	61.1	34720	1.55	0.2	0.108	0.126	126	0.09	90
isobutane	0.4757	1.029	1.136	0.9877	61.1	39060	1.55	0.2	0.096	0.112	112	0.08	80
isobutane	0.4757	1.029	1.136	0.9877	61.1	44640	1.55	0.2	0.084	0.098	98	0.07	70
isobutane	0.4757	1.029	1.136	0.9878	61.1	52081	1.55	0.2	0.072	0.084	84	0.06	60
isobutane	0.4757	1.029	1.136	0.988	61.1	62497	1.55	0.2	0.06	0.07	70	0.05	50
isobutane	0.4757	1.03	1.137	0.9885	61.1	78121	1.55	0.2	0.048	0.056	56	0.04	40
isobutane	0.4757	1.032	1.139	0.9904	61.1	104161	1.55	0.2	0.036	0.042	42	0.03	30
isobutane	0.4759	1.043	1.149	1.002	61.1	156242	1.55	0.2	0.024	0.028	28	0.02	20

APPENDIX A3 RESULTS

A3.6: Radial Turbine Simulations No. 02

Fluid\$	d_3	d_4	alpha_1	alpha_2	alpha_3	alpha_4	beta_2	beta_3	b_1	b_2	b_3	b_4
	[m]	[m]	[deg]	[deg]	[deg]	[deg]	[deg]	[deg]	[m]	[m]	[m]	[m]
R245fa	0.09	0.135	0	82.65	0	0	70.02	69.39	0.0225	0.0225	0.03162	0.01343
R245fa	0.084	0.126	0	82.65	0	0	70.02	69.39	0.021	0.021	0.02951	0.01343
R245fa	0.078	0.117	0	82.65	0	0	70.02	69.38	0.0195	0.0195	0.02741	0.01343
R245fa	0.072	0.108	0	82.65	0	0	70.02	69.38	0.018	0.018	0.0253	0.01343
R245fa	0.066	0.099	0	82.65	0	0	70.02	69.38	0.0165	0.0165	0.02319	0.01343
R245fa	0.06	0.09	0	82.65	0	0	70.02	69.37	0.015	0.015	0.02108	0.01343
R245fa	0.054	0.081	0	82.65	0	0	70.02	69.36	0.0135	0.0135	0.01897	0.01343
R245fa	0.048	0.072	0	82.65	0	0	70.02	69.34	0.012	0.012	0.01686	0.01343
R245fa	0.042	0.063	0	82.65	0	0	70.02	69.31	0.0105	0.0105	0.01476	0.01343
R245fa	0.036	0.054	0	82.65	0	0	70.02	69.23	0.009	0.009	0.01265	0.01343
R245fa	0.03	0.045	0	82.65	0	0	70.02	69.06	0.0075	0.0075	0.01054	0.01343
R245fa	0.024	0.036	0	82.65	0	0	70.02	68.6	0.006	0.006	0.008432	0.01343
R245fa	0.018	0.027	0	82.65	0	0	70.02	67.03	0.0045	0.0045	0.006324	0.01343
R245fa	0.012	0.018	0	82.65	0	0	70.02	59.94	0.003	0.003	0.004216	0.01343
R134a	0.09	0.135	0	82.65	0	0	70.02	28.34	0.0225	0.0225	0.03162	0.01343
R134a	0.084	0.126	0	82.65	0	0	70.02	28.34	0.021	0.021	0.02951	0.01343
R134a	0.078	0.117	0	82.65	0	0	70.02	28.34	0.0195	0.0195	0.02741	0.01343
R134a	0.072	0.108	0	82.65	0	0	70.02	28.34	0.018	0.018	0.0253	0.01343
R134a	0.066	0.099	0	82.65	0	0	70.02	28.34	0.0165	0.0165	0.02319	0.01343
R134a	0.06	0.09	0	82.65	0	0	70.02	28.34	0.015	0.015	0.02108	0.01343
R134a	0.054	0.081	0	82.65	0	0	70.02	28.34	0.0135	0.0135	0.01897	0.01343
R134a	0.048	0.072	0	82.65	0	0	70.02	28.34	0.012	0.012	0.01686	0.01343
R134a	0.042	0.063	0	82.65	0	0	70.02	28.33	0.0105	0.0105	0.01476	0.01343

APPENDIX A3 RESULTS

A3.6: Radial Turbine Simulations No. 02

Fluid\$	d_3	d_4	alpha_1	alpha_2	alpha_3	alpha_4	beta_2	beta_3	b_1	b_2	b_3	b_4
	[m]	[m]	[deg]	[deg]	[deg]	[deg]	[deg]	[deg]	[m]	[m]	[m]	[m]
R134a	0.036	0.054	0	82.65	0	0	70.02	28.33	0.009	0.009	0.01265	0.01343
R134a	0.03	0.045	0	82.65	0	0	70.02	28.31	0.0075	0.0075	0.01054	0.01343
R134a	0.024	0.036	0	82.65	0	0	70.02	28.25	0.006	0.006	0.008432	0.01343
R134a	0.018	0.027	0	82.65	0	0	70.02	28.06	0.0045	0.0045	0.006324	0.01343
R134a	0.012	0.018	0	82.65	0	0	70.02	27.01	0.003	0.003	0.004216	0.01343
n-butane	0.09	0.135	0	82.65	0	0	70.02	29.18	0.0225	0.0225	0.03162	0.01343
n-butane	0.084	0.126	0	82.65	0	0	70.02	29.18	0.021	0.021	0.02951	0.01343
n-butane	0.078	0.117	0	82.65	0	0	70.02	29.18	0.0195	0.0195	0.02741	0.01343
n-butane	0.072	0.108	0	82.65	0	0	70.02	29.18	0.018	0.018	0.0253	0.01343
n-butane	0.066	0.099	0	82.65	0	0	70.02	29.18	0.0165	0.0165	0.02319	0.01343
n-butane	0.06	0.09	0	82.65	0	0	70.02	29.18	0.015	0.015	0.02108	0.01343
n-butane	0.054	0.081	0	82.65	0	0	70.02	29.18	0.0135	0.0135	0.01897	0.01343
n-butane	0.048	0.072	0	82.65	0	0	70.02	29.17	0.012	0.012	0.01686	0.01343
n-butane	0.042	0.063	0	82.65	0	0	70.02	29.17	0.0105	0.0105	0.01476	0.01343
n-butane	0.036	0.054	0	82.65	0	0	70.02	29.17	0.009	0.009	0.01265	0.01343
n-butane	0.03	0.045	0	82.65	0	0	70.02	29.17	0.0075	0.0075	0.01054	0.01343
n-butane	0.024	0.036	0	82.65	0	0	70.02	29.15	0.006	0.006	0.008432	0.01343
n-butane	0.024	0.036	0	82.65	0	0	70.02	29.15	0.006	0.006	0.008432	0.01343
n-butane	0.024	0.036	0	82.65	0	0	70.02	29.15	0.006	0.006	0.008432	0.01343
isobutane	0.09	0.135	0	82.65	0	0	70.02	25.16	0.0225	0.0225	0.03162	0.01343
isobutane	0.084	0.126	0	82.65	0	0	70.02	25.16	0.021	0.021	0.02951	0.01343
isobutane	0.078	0.117	0	82.65	0	0	70.02	25.16	0.0195	0.0195	0.02741	0.01343
isobutane	0.072	0.108	0	82.65	0	0	70.02	25.16	0.018	0.018	0.0253	0.01343

APPENDIX A3 RESULTS

A3.6: Radial Turbine Simulations No. 02

Fluid\$	d_3	d_4	alpha_1	alpha_2	alpha_3	alpha_4	beta_2	beta_3	b_1	b_2	b_3	b_4
	[m]	[m]	[deg]	[deg]	[deg]	[deg]	[deg]	[deg]	[m]	[m]	[m]	[m]
isobutane	0.066	0.099	0	82.65	0	0	70.02	25.16	0.0165	0.0165	0.02319	0.01343
isobutane	0.06	0.09	0	82.65	0	0	70.02	25.16	0.015	0.015	0.02108	0.01343
isobutane	0.054	0.081	0	82.65	0	0	70.02	25.16	0.0135	0.0135	0.01897	0.01343
isobutane	0.048	0.072	0	82.65	0	0	70.02	25.16	0.012	0.012	0.01686	0.01343
isobutane	0.042	0.063	0	82.65	0	0	70.02	25.16	0.0105	0.0105	0.01476	0.01343
isobutane	0.036	0.054	0	82.65	0	0	70.02	25.16	0.009	0.009	0.01265	0.01343
isobutane	0.03	0.045	0	82.65	0	0	70.02	25.15	0.0075	0.0075	0.01054	0.01343
isobutane	0.024	0.036	0	82.65	0	0	70.02	25.14	0.006	0.006	0.008432	0.01343
isobutane	0.018	0.027	0	82.65	0	0	70.02	25.1	0.0045	0.0045	0.006324	0.01343
isobutane	0.012	0.018	0	82.65	0	0	70.02	24.85	0.003	0.003	0.004216	0.01343

APPENDIX A3 RESULTS

A3.7: Radial Turbine Simulations No. 03

Fluid\$	m_dot	P_1	P_2	P_3	P_4	T_1	T_2	T_3	T_4	h_01	h_02	h_02rel	h_03
	[kg/s]	[Pa]	[Pa]	[Pa]	[Pa]	[C]	[C]	[C]	[C]	[J/kg]	[J/kg]	[J/kg]	[J/kg]
R245fa	0.396	810600	250080	180000	180000	80.99	48.67	40.64	40.67	462357	462357	445237	437104
R245fa	0.396	810600	250080	180000	180000	80.99	48.67	40.64	40.67	462357	462357	445237	437104
R245fa	0.396	810600	250080	180000	180000	80.99	48.67	40.64	40.67	462357	462357	445237	437104
R245fa	0.396	810600	250080	180000	180000	80.99	48.67	40.64	40.67	462357	462357	445237	437104
R245fa	0.396	810600	250080	180000	180000	80.99	48.67	40.64	40.67	462357	462357	445237	437104
R245fa	0.396	810600	250080	180000	180000	80.99	48.67	40.64	40.67	462357	462357	445237	437104
R245fa	0.396	810600	250080	180000	180000	80.99	48.67	40.64	40.67	462357	462357	445237	437104
R245fa	0.396	810600	250080	180000	180000	80.99	48.67	40.64	40.67	462357	462357	445237	437104
R245fa	0.396	810600	250080	180000	180000	80.99	48.67	40.64	40.67	462357	462357	445237	437104
R245fa	0.396	810600	250080	180000	180000	80.99	48.67	40.64	40.67	462357	462357	445237	437104
R245fa	0.396	810600	250080	180000	180000	80.99	48.67	40.64	40.67	462357	462357	445237	437104
R245fa	0.396	810600	250080	180000	180000	80.99	48.67	40.64	40.67	462357	462357	445237	437104
R245fa	0.396	810600	250080	180000	180000	80.99	48.67	40.64	40.67	462357	462357	445237	437104
R245fa	0.396	810600	250080	180000	180000	80.99	48.67	40.64	40.67	462357	462357	445237	437104
R245fa	0.396	810600	250080	180000	180000	80.99	48.67	40.64	40.67	462357	462357	445237	437104
R134a	0.396	810600	350969	180000	180000	80.99	53.84	33.69	34.55	317831	317831	300712	292579
R134a	0.396	810600	350969	180000	180000	80.99	53.84	33.69	34.55	317831	317831	300712	292579
R134a	0.396	810600	350969	180000	180000	80.99	53.84	33.69	34.55	317831	317831	300712	292579
R134a	0.396	810600	350969	180000	180000	80.99	53.84	33.69	34.55	317831	317831	300712	292579
R134a	0.396	810600	350969	180000	180000	80.99	53.84	33.69	34.55	317831	317831	300712	292579
R134a	0.396	810600	350969	180000	180000	80.99	53.84	33.69	34.55	317831	317831	300712	292579
R134a	0.396	810600	350969	180000	180000	80.99	53.84	33.69	34.55	317831	317831	300712	292579
R134a	0.396	810600	350969	180000	180000	80.99	53.84	33.69	34.55	317831	317831	300712	292579
R134a	0.396	810600	350969	180000	180000	80.99	53.84	33.69	34.55	317831	317831	300712	292579
R134a	0.396	810600	350969	180000	180000	80.99	53.84	33.69	34.55	317831	317831	300712	292579
R134a	0.396	810600	350969	180000	180000	80.99	53.84	33.69	34.55	317831	317831	300712	292579
R134a	0.396	810600	350969	180000	180000	80.99	53.84	33.69	34.55	317831	317831	300712	292579
R134a	0.396	810600	350969	180000	180000	80.99	53.84	33.69	34.55	317831	317831	300712	292579

APPENDIX A3 RESULTS

A3.7: Radial Turbine Simulations No. 03

Fluid\$	m_dot	P_1	P_2	P_3	P_4	T_1	T_2	T_3	T_4	h_01	h_02	h_02rel	h_03
	[kg/s]	[Pa]	[Pa]	[Pa]	[Pa]	[C]	[C]	[C]	[C]	[J/kg]	[J/kg]	[J/kg]	[J/kg]
R134a	0.396	810600	350969	180000	180000	80.99	53.84	33.69	34.55	317831	317831	300712	292579
R134a	0.396	810600	350969	180000	180000	80.99	53.84	33.69	34.55	317831	317831	300712	292579
R134a	0.396	810600	350969	180000	180000	80.99	53.84	33.69	34.55	317831	317831	300712	292579
R134a	0.396	810600	350969	180000	180000	80.99	53.84	33.69	34.55	317831	317831	300712	292579
R134a	0.396	810600	350969	180000	180000	80.99	53.84	33.69	34.55	317831	317831	300712	292579
n-butane	0.207	1.01E+06	372911	180000	180000	80.03	48.65	28.86	29.61	696489	696489	663739	648180
n-butane	0.207	1.01E+06	372911	180000	180000	80.03	48.65	28.86	29.61	696489	696489	663739	648180
n-butane	0.207	1.01E+06	372911	180000	180000	80.03	48.65	28.86	29.61	696489	696489	663739	648180
n-butane	0.207	1.01E+06	372911	180000	180000	80.03	48.65	28.86	29.61	696489	696489	663739	648180
n-butane	0.207	1.01E+06	372911	180000	180000	80.03	48.65	28.86	29.61	696489	696489	663739	648180
n-butane	0.207	1.01E+06	372911	180000	180000	80.03	48.65	28.86	29.61	696489	696489	663739	648180
n-butane	0.207	1.01E+06	372911	180000	180000	80.03	48.65	28.86	29.61	696489	696489	663739	648180
n-butane	0.207	1.01E+06	372911	180000	180000	80.03	48.65	28.86	29.61	696489	696489	663739	648180
n-butane	0.207	1.01E+06	372911	180000	180000	80.03	48.65	28.86	29.61	696489	696489	663739	648180
n-butane	0.207	1.01E+06	372911	180000	180000	80.03	48.65	28.86	29.61	696489	696489	663739	648180
n-butane	0.207	1.01E+06	372911	180000	180000	80.03	48.65	28.86	29.61	696489	696489	663739	648180
n-butane	0.207	1.01E+06	372911	180000	180000	80.03	48.65	28.86	29.61	696489	696489	663739	648180
n-butane	0.207	1.01E+06	372911	180000	180000	80.03	48.65	28.86	29.61	696489	696489	663739	648180
n-butane	0.207	1.01E+06	372911	180000	180000	80.03	48.65	28.86	29.61	696489	696489	663739	648180
n-butane	0.207	1.01E+06	372911	180000	180000	80.03	48.65	28.86	29.61	696489	696489	663739	648180
n-butane	0.207	1.01E+06	372911	180000	180000	80.03	48.65	28.86	29.61	696489	696489	663739	648180
isobutane	0.241	1.01E+06	412422	180000	180000	66.82	38.13	15.33	16.29	642727	642727	614597	601233
isobutane	0.241	1.01E+06	412422	180000	180000	66.82	38.13	15.33	16.29	642727	642727	614597	601233
isobutane	0.241	1.01E+06	412422	180000	180000	66.82	38.13	15.33	16.29	642727	642727	614597	601233
isobutane	0.241	1.01E+06	412422	180000	180000	66.82	38.13	15.33	16.29	642727	642727	614597	601233

APPENDIX A3 RESULTS

A3.7: Radial Turbine Simulations No. 03

Fluid\$	m_dot	P_1	P_2	P_3	P_4	T_1	T_2	T_3	T_4	h_01	h_02	h_02rel	h_03
	[kg/s]	[Pa]	[Pa]	[Pa]	[Pa]	[C]	[C]	[C]	[C]	[J/kg]	[J/kg]	[J/kg]	[J/kg]
isobutane	0.241	1.01E+06	412422	180000	180000	66.82	38.13	15.33	16.29	642727	642727	614597	601233
isobutane	0.241	1.01E+06	412422	180000	180000	66.82	38.13	15.33	16.29	642727	642727	614597	601233
isobutane	0.241	1.01E+06	412422	180000	180000	66.82	38.13	15.33	16.29	642727	642727	614597	601233
isobutane	0.241	1.01E+06	412422	180000	180000	66.82	38.13	15.33	16.29	642727	642727	614597	601233
isobutane	0.241	1.01E+06	412422	180000	180000	66.82	38.13	15.33	16.29	642727	642727	614597	601233
isobutane	0.241	1.01E+06	412422	180000	180000	66.82	38.13	15.33	16.29	642727	642727	614597	601233
isobutane	0.241	1.01E+06	412422	180000	180000	66.82	38.13	15.33	16.29	642727	642727	614597	601233
isobutane	0.241	1.01E+06	412422	180000	180000	66.82	38.13	15.33	16.29	642727	642727	614597	601233
isobutane	0.241	1.01E+06	412422	180000	180000	66.82	38.13	15.33	16.29	642727	642727	614597	601233
isobutane	0.241	1.01E+06	412422	180000	180000	66.82	38.13	15.33	16.29	642727	642727	614597	601233

APPENDIX A3 RESULTS

A3.7: Radial Turbine Simulations No. 03

Fluid\$	h_03rel	h_03ss	h_04	h_1	h_2	h_2s	h_3	h_3s	h_3ss	h_4	h_4s	P_01	P_02
	[J/kg]	[J/kg]	[J/kg]	[J/kg]	[J/kg]	[J/kg]	[J/kg]	[J/kg]	[J/kg]	[J/kg]	[J/kg]	[Pa]	[Pa]
R134a	295499	289931	292579	317831	297922	296323	282487	281442	284741	283238	282487	810629	758775
R134a	295499	289931	292579	317831	297922	296323	282487	281442	284741	283238	282487	810629	758775
R134a	295499	289931	292579	317831	297922	296323	282487	281442	284741	283238	282487	810629	758775
R134a	295499	289931	292579	317831	297922	296323	282487	281442	284741	283238	282487	810629	758775
R134a	295499	289931	292579	317831	297922	296323	282487	281442	284741	283238	282487	810629	758775
n-butane	653765	643228	648180	696489	658401	655341	630158	628262	633185	631498	630158	1.01E+06	929842
n-butane	653765	643228	648180	696489	658401	655341	630159	628262	633185	631499	630159	1.01E+06	929836
n-butane	653765	643228	648180	696489	658401	655341	630159	628262	633185	631499	630159	1.01E+06	929836
n-butane	653765	643228	648180	696489	658401	655341	630159	628262	633185	631499	630159	1.01E+06	929836
n-butane	653765	643228	648180	696489	658401	655341	630159	628262	633185	631499	630159	1.01E+06	929836
n-butane	653765	643228	648180	696489	658401	655341	630159	628262	633185	631499	630159	1.01E+06	929836
n-butane	653765	643228	648180	696489	658401	655341	630159	628262	633185	631499	630159	1.01E+06	929836
n-butane	653765	643228	648180	696489	658401	655341	630159	628262	633185	631499	630159	1.01E+06	929836
n-butane	653765	643228	648180	696489	658401	655341	630159	628262	633185	631499	630159	1.01E+06	929836
n-butane	653765	643228	648180	696489	658401	655341	630159	628262	633185	631499	630159	1.01E+06	929836
n-butane	653765	643228	648180	696489	658401	655341	630159	628262	633185	631499	630159	1.01E+06	929836
n-butane	653765	643228	648180	696489	658401	655341	630159	628262	633185	631499	630159	1.01E+06	929836
n-butane	653765	643228	648180	696489	658401	655341	630159	628262	633185	631499	630159	1.01E+06	929836
n-butane	653765	643228	648180	696489	658401	655341	630159	628262	633185	631499	630159	1.01E+06	929836
n-butane	653765	643228	648180	696489	658401	655341	630159	628262	633185	631499	630159	1.01E+06	929836
isobutane	606031	596417	601233	642727	610013	607385	579377	577236	588354	581002	579377	1.01E+06	937994
isobutane	606031	596417	601233	642727	610013	607385	579377	577236	588354	581002	579377	1.01E+06	937994
isobutane	606031	596417	601233	642727	610013	607385	579377	577236	588354	581002	579377	1.01E+06	937994
isobutane	606031	596417	601233	642727	610013	607385	579377	577236	588354	581002	579377	1.01E+06	937994

APPENDIX A3 RESULTS

A3.7: Radial Turbine Simulations No. 03

Fluid\$	h_03rel	h_03ss	h_04	h_1	h_2	h_2s	h_3	h_3s	h_3ss	h_4	h_4s	P_01	P_02
	[J/kg]	[J/kg]	[J/kg]	[J/kg]	[J/kg]	[J/kg]	[J/kg]	[J/kg]	[J/kg]	[J/kg]	[J/kg]	[Pa]	[Pa]
isobutane	606031	596417	601233	642727	610013	607385	579377	577236	588354	581002	579377	1.01E+06	937994
isobutane	606031	596417	601233	642727	610013	607385	579377	577236	588354	581002	579377	1.01E+06	937994
isobutane	606031	596417	601233	642727	610013	607385	579377	577236	588354	581002	579377	1.01E+06	937994
isobutane	606031	596417	601233	642727	610013	607385	579377	577236	588354	581002	579377	1.01E+06	937994
isobutane	606031	596417	601233	642727	610013	607385	579377	577236	588354	581002	579377	1.01E+06	937994
isobutane	606031	596417	601233	642727	610013	607385	579377	577236	588354	581002	579377	1.01E+06	937994
isobutane	606031	596417	601233	642727	610013	607385	579377	577236	588354	581002	579377	1.01E+06	937994
isobutane	606031	596417	601233	642727	610013	607385	579377	577236	588354	581002	579377	1.01E+06	937994
isobutane	606031	596417	601233	642727	610013	607385	579377	577236	588354	581002	579377	1.01E+06	937994
isobutane	606031	596417	601233	642727	610013	607385	579377	577236	588354	581002	579377	1.01E+06	937994
isobutane	606031	596417	601233	642727	610013	607385	579377	577236	588354	581002	579377	1.01E+06	937994

APPENDIX A3 RESULTS

A3.7: Radial Turbine Simulations No. 03

Fluid\$	P_02rel	P_03	P_03rel	Rr	R_s	c_1	c_2	c_3	c_4	eta_ts	eta_tt	Ma_1	Ma_2
	[Pa]	[Pa]	[Pa]	[-]	[-]	[m/s]	[m/s]	[m/s]	[m/s]	[-]	[-]	[-]	[-]
R245fa	290845	184257	216020	0.2247	0.35	0.9396	199.5	29.25	28.14	0.7631	0.9324	0.0073	1.453
R245fa	290845	184257	216020	0.2247	0.35	0.9396	199.5	29.25	28.14	0.7631	0.9324	0.0073	1.453
R245fa	290845	184257	216020	0.2247	0.35	0.9396	199.5	29.25	28.14	0.7631	0.9324	0.0073	1.453
R245fa	290845	184257	216020	0.2247	0.35	0.9396	199.5	29.25	28.14	0.7631	0.9324	0.0073	1.453
R245fa	290845	184257	216020	0.2247	0.35	0.9396	199.5	29.25	28.14	0.7631	0.9324	0.0073	1.453
R245fa	290845	184257	216020	0.2247	0.35	0.9396	199.5	29.25	28.14	0.7631	0.9324	0.0073	1.453
R245fa	290845	184257	216020	0.2247	0.35	0.9396	199.5	29.25	28.14	0.7631	0.9324	0.0073	1.453
R245fa	290845	184257	216020	0.2247	0.35	0.9396	199.5	29.25	28.14	0.7631	0.9324	0.0073	1.453
R245fa	290845	184257	216020	0.2247	0.35	0.9396	199.5	29.25	28.14	0.7631	0.9324	0.0073	1.453
R245fa	290845	184257	216020	0.2247	0.35	0.9396	199.5	29.25	28.14	0.7631	0.9324	0.0073	1.453
R245fa	290845	184257	216020	0.2247	0.35	0.9396	199.5	29.25	28.14	0.7631	0.9324	0.0073	1.453
R245fa	290845	184257	216020	0.2247	0.35	0.9396	199.5	29.25	28.14	0.7631	0.9324	0.0073	1.453
R245fa	290845	184257	216020	0.2247	0.35	0.9396	199.5	29.25	28.14	0.7631	0.9324	0.0073	1.453
R245fa	290845	184257	216020	0.2247	0.35	0.9396	199.5	29.25	28.14	0.7631	0.9324	0.0073	1.453
R245fa	290845	184257	216020	0.2247	0.35	0.9396	199.5	29.25	28.14	0.7631	0.9324	0.0073	1.453
R134a	391801	271468	305046	0.4367	0.35	1.374	199.5	142.1	136.7	0.7631	0.9051	0.008341	1.214
R134a	391804	271470	305048	0.4367	0.35	1.374	199.5	142.1	136.7	0.7631	0.9051	0.008341	1.214
R134a	391804	271470	305048	0.4367	0.35	1.374	199.5	142.1	136.7	0.7631	0.9051	0.008341	1.214
R134a	391804	271470	305048	0.4367	0.35	1.374	199.5	142.1	136.7	0.7631	0.9051	0.008341	1.214
R134a	391804	271470	305048	0.4367	0.35	1.374	199.5	142.1	136.7	0.7631	0.9051	0.008341	1.214
R134a	391804	271470	305048	0.4367	0.35	1.374	199.5	142.1	136.7	0.7631	0.9051	0.008341	1.214
R134a	391804	271470	305048	0.4367	0.35	1.374	199.5	142.1	136.7	0.7631	0.9051	0.008341	1.214
R134a	391804	271470	305048	0.4367	0.35	1.374	199.5	142.1	136.7	0.7631	0.9051	0.008341	1.214
R134a	391804	271470	305048	0.4367	0.35	1.374	199.5	142.1	136.7	0.7631	0.9051	0.008341	1.214
R134a	391804	271470	305048	0.4367	0.35	1.374	199.5	142.1	136.7	0.7631	0.9051	0.008341	1.214
R134a	391804	271470	305048	0.4367	0.35	1.374	199.5	142.1	136.7	0.7631	0.9051	0.008341	1.214
R134a	391804	271470	305048	0.4367	0.35	1.374	199.5	142.1	136.7	0.7631	0.9051	0.008341	1.214
R134a	391804	271470	305048	0.4367	0.35	1.374	199.5	142.1	136.7	0.7631	0.9051	0.008341	1.214
R134a	391804	271470	305048	0.4367	0.35	1.374	199.5	142.1	136.7	0.7631	0.9051	0.008341	1.214

APPENDIX A3 RESULTS

A3.7: Radial Turbine Simulations No. 03

Fluid\$	P_02rel	P_03	P_03rel	Rr	R_s	c_1	c_2	c_3	c_4	eta_ts	eta_tt	Ma_1	Ma_2
	[Pa]	[Pa]	[Pa]	[-]	[-]	[m/s]	[m/s]	[m/s]	[m/s]	[-]	[-]	[-]	[-]
R134a	391804	271470	305048	0.4367	0.35	1.374	199.5	142.1	136.7	0.7631	0.9051	0.008341	1.214
R134a	391804	271470	305048	0.4367	0.35	1.374	199.5	142.1	136.7	0.7631	0.9051	0.008341	1.214
R134a	391804	271470	305048	0.4367	0.35	1.374	199.5	142.1	136.7	0.7631	0.9051	0.008341	1.214
R134a	391804	271470	305048	0.4367	0.35	1.374	199.5	142.1	136.7	0.7631	0.9051	0.008341	1.214
R134a	391804	271470	305048	0.4367	0.35	1.374	199.5	142.1	136.7	0.7631	0.9051	0.008341	1.214
n-butane	423613	278340	318142	0.4258	0.35	0.4635	276	189.8	182.7	0.7631	0.907	0.002422	1.338
n-butane	423611	278339	318141	0.4258	0.35	0.4635	276	189.8	182.7	0.7631	0.907	0.002422	1.338
n-butane	423611	278339	318141	0.4258	0.35	0.4635	276	189.8	182.7	0.7631	0.907	0.002422	1.338
n-butane	423611	278339	318141	0.4258	0.35	0.4635	276	189.8	182.7	0.7631	0.907	0.002422	1.338
n-butane	423611	278339	318141	0.4258	0.35	0.4635	276	189.8	182.7	0.7631	0.907	0.002422	1.338
n-butane	423611	278339	318141	0.4258	0.35	0.4635	276	189.8	182.7	0.7631	0.907	0.002422	1.338
n-butane	423611	278339	318141	0.4258	0.35	0.4635	276	189.8	182.7	0.7631	0.907	0.002422	1.338
n-butane	423611	278339	318141	0.4258	0.35	0.4635	276	189.8	182.7	0.7631	0.907	0.002422	1.338
n-butane	423611	278339	318141	0.4258	0.35	0.4635	276	189.8	182.7	0.7631	0.907	0.002422	1.338
n-butane	423611	278339	318141	0.4258	0.35	0.4635	276	189.8	182.7	0.7631	0.907	0.002422	1.338
n-butane	423611	278339	318141	0.4258	0.35	0.4635	276	189.8	182.7	0.7631	0.907	0.002422	1.338
n-butane	423611	278339	318141	0.4258	0.35	0.4635	276	189.8	182.7	0.7631	0.907	0.002422	1.338
n-butane	423611	278339	318141	0.4258	0.35	0.4635	276	189.8	182.7	0.7631	0.907	0.002422	1.338
n-butane	423611	278339	318141	0.4258	0.35	0.4635	276	189.8	182.7	0.7631	0.907	0.002422	1.338
n-butane	423611	278339	318141	0.4258	0.35	0.4635	276	189.8	182.7	0.7631	0.907	0.002422	1.338
isobutane	462454	312772	352563	0.4836	0.35	0.6007	255.8	209.1	201.2	0.7631	0.896	0.003214	1.271
isobutane	462455	312772	352563	0.4836	0.35	0.6007	255.8	209.1	201.2	0.7631	0.896	0.003214	1.271
isobutane	462455	312772	352563	0.4836	0.35	0.6007	255.8	209.1	201.2	0.7631	0.896	0.003214	1.271
isobutane	462455	312772	352563	0.4836	0.35	0.6007	255.8	209.1	201.2	0.7631	0.896	0.003214	1.271

APPENDIX A3 RESULTS

A3.7: Radial Turbine Simulations No. 03

Fluid\$	P_02rel	P_03	P_03rel	Rr	R_s	c_1	c_2	c_3	c_4	eta_ts	eta_tt	Ma_1	Ma_2
	[Pa]	[Pa]	[Pa]	[-]	[-]	[m/s]	[m/s]	[m/s]	[m/s]	[-]	[-]	[-]	[-]
isobutane	462455	312772	352563	0.4836	0.35	0.6007	255.8	209.1	201.2	0.7631	0.896	0.003214	1.271
isobutane	462455	312772	352563	0.4836	0.35	0.6007	255.8	209.1	201.2	0.7631	0.896	0.003214	1.271
isobutane	462455	312772	352563	0.4836	0.35	0.6007	255.8	209.1	201.2	0.7631	0.896	0.003214	1.271
isobutane	462455	312772	352563	0.4836	0.35	0.6007	255.8	209.1	201.2	0.7631	0.896	0.003214	1.271
isobutane	462455	312772	352563	0.4836	0.35	0.6007	255.8	209.1	201.2	0.7631	0.896	0.003214	1.271
isobutane	462455	312772	352563	0.4836	0.35	0.6007	255.8	209.1	201.2	0.7631	0.896	0.003214	1.271
isobutane	462455	312772	352563	0.4836	0.35	0.6007	255.8	209.1	201.2	0.7631	0.896	0.003214	1.271
isobutane	462455	312772	352563	0.4836	0.35	0.6007	255.8	209.1	201.2	0.7631	0.896	0.003214	1.271
isobutane	462455	312772	352563	0.4836	0.35	0.6007	255.8	209.1	201.2	0.7631	0.896	0.003214	1.271
isobutane	462455	312772	352563	0.4836	0.35	0.6007	255.8	209.1	201.2	0.7631	0.896	0.003214	1.271

APPENDIX A3 RESULTS

A3.7: Radial Turbine Simulations No. 03

Fluid\$	Ma_2rel	Ma_3	Ma_3rel	Ma_4	N_blades	rpm	PSI	PHI	L_d	d_1	d_2	d_3	d_4
	[-]	[-]	[-]	[-]		[-/min]	[-]	[-]	[m]	[m]	[m]	[m]	[m]
R245fa	0.5439	0.2125	0.5943	0.2044	61.1	20000	1.55	0.2	0.1463	0.1706	0.1219	0.07313	0.1097
R245fa	0.5439	0.2125	0.5943	0.2044	61.1	20000	1.55	0.2	0.1463	0.1706	0.1219	0.07313	0.1097
R245fa	0.5439	0.2125	0.5943	0.2044	61.1	20000	1.55	0.2	0.1463	0.1706	0.1219	0.07313	0.1097
R245fa	0.5439	0.2125	0.5943	0.2044	61.1	20000	1.55	0.2	0.1463	0.1706	0.1219	0.07313	0.1097
R245fa	0.5439	0.2125	0.5943	0.2044	61.1	20000	1.55	0.2	0.1463	0.1706	0.1219	0.07313	0.1097
R245fa	0.5439	0.2125	0.5943	0.2044	61.1	20000	1.55	0.2	0.1463	0.1706	0.1219	0.07313	0.1097
R245fa	0.5439	0.2125	0.5943	0.2044	61.1	20000	1.55	0.2	0.1463	0.1706	0.1219	0.07313	0.1097
R245fa	0.5439	0.2125	0.5943	0.2044	61.1	20000	1.55	0.2	0.1463	0.1706	0.1219	0.07313	0.1097
R245fa	0.5439	0.2125	0.5943	0.2044	61.1	20000	1.55	0.2	0.1463	0.1706	0.1219	0.07313	0.1097
R245fa	0.5439	0.2125	0.5943	0.2044	61.1	20000	1.55	0.2	0.1463	0.1706	0.1219	0.07313	0.1097
R245fa	0.5439	0.2125	0.5943	0.2044	61.1	20000	1.55	0.2	0.1463	0.1706	0.1219	0.07313	0.1097
R245fa	0.5439	0.2125	0.5943	0.2044	61.1	20000	1.55	0.2	0.1463	0.1706	0.1219	0.07313	0.1097
R245fa	0.5439	0.2125	0.5943	0.2044	61.1	20000	1.55	0.2	0.1463	0.1706	0.1219	0.07313	0.1097
R245fa	0.5439	0.2125	0.5943	0.2044	61.1	20000	1.55	0.2	0.1463	0.1706	0.1219	0.07313	0.1097
R245fa	0.5439	0.2125	0.5943	0.2044	61.1	20000	1.55	0.2	0.1463	0.1706	0.1219	0.07313	0.1097
R134a	0.4546	0.8767	0.9955	0.8422	61.1	20000	1.55	0.2	0.1463	0.1706	0.1219	0.07313	0.1097
R134a	0.4546	0.8767	0.9955	0.8422	61.1	20000	1.55	0.2	0.1463	0.1706	0.1219	0.07313	0.1097
R134a	0.4546	0.8767	0.9955	0.8422	61.1	20000	1.55	0.2	0.1463	0.1706	0.1219	0.07313	0.1097
R134a	0.4546	0.8767	0.9955	0.8422	61.1	20000	1.55	0.2	0.1463	0.1706	0.1219	0.07313	0.1097
R134a	0.4546	0.8767	0.9955	0.8422	61.1	20000	1.55	0.2	0.1463	0.1706	0.1219	0.07313	0.1097
R134a	0.4546	0.8767	0.9955	0.8422	61.1	20000	1.55	0.2	0.1463	0.1706	0.1219	0.07313	0.1097
R134a	0.4546	0.8767	0.9955	0.8422	61.1	20000	1.55	0.2	0.1463	0.1706	0.1219	0.07313	0.1097
R134a	0.4546	0.8767	0.9955	0.8422	61.1	20000	1.55	0.2	0.1463	0.1706	0.1219	0.07313	0.1097
R134a	0.4546	0.8767	0.9955	0.8422	61.1	20000	1.55	0.2	0.1463	0.1706	0.1219	0.07313	0.1097
R134a	0.4546	0.8767	0.9955	0.8422	61.1	20000	1.55	0.2	0.1463	0.1706	0.1219	0.07313	0.1097
R134a	0.4546	0.8767	0.9955	0.8422	61.1	20000	1.55	0.2	0.1463	0.1706	0.1219	0.07313	0.1097

APPENDIX A3 RESULTS

A3.7: Radial Turbine Simulations No. 03

Fluid\$	Ma_2rel	Ma_3	Ma_3rel	Ma_4	N_blades	rpm	PSI	PHI	L_d	d_1	d_2	d_3	d_4
	[-]	[-]	[-]	[-]		[-/min]	[-]	[-]	[m]	[m]	[m]	[m]	[m]
R134a	0.4546	0.8767	0.9955	0.8422	61.1	20000	1.55	0.2	0.1463	0.1706	0.1219	0.07313	0.1097
R134a	0.4546	0.8767	0.9955	0.8422	61.1	20000	1.55	0.2	0.1463	0.1706	0.1219	0.07313	0.1097
R134a	0.4546	0.8767	0.9955	0.8422	61.1	20000	1.55	0.2	0.1463	0.1706	0.1219	0.07313	0.1097
R134a	0.4546	0.8767	0.9955	0.8422	61.1	20000	1.55	0.2	0.1463	0.1706	0.1219	0.07313	0.1097
R134a	0.4546	0.8767	0.9955	0.8422	61.1	20000	1.55	0.2	0.1463	0.1706	0.1219	0.07313	0.1097
n-butane	0.5008	0.9142	1.046	0.8782	61.1	20000	1.55	0.2	0.2023	0.236	0.1686	0.1012	0.1517
n-butane	0.5008	0.9142	1.046	0.8782	61.1	20000	1.55	0.2	0.2023	0.236	0.1686	0.1012	0.1517
n-butane	0.5008	0.9142	1.046	0.8782	61.1	20000	1.55	0.2	0.2023	0.236	0.1686	0.1012	0.1517
n-butane	0.5008	0.9142	1.046	0.8782	61.1	20000	1.55	0.2	0.2023	0.236	0.1686	0.1012	0.1517
n-butane	0.5008	0.9142	1.046	0.8782	61.1	20000	1.55	0.2	0.2023	0.236	0.1686	0.1012	0.1517
n-butane	0.5008	0.9142	1.046	0.8782	61.1	20000	1.55	0.2	0.2023	0.236	0.1686	0.1012	0.1517
n-butane	0.5008	0.9142	1.046	0.8782	61.1	20000	1.55	0.2	0.2023	0.236	0.1686	0.1012	0.1517
n-butane	0.5008	0.9142	1.046	0.8782	61.1	20000	1.55	0.2	0.2023	0.236	0.1686	0.1012	0.1517
n-butane	0.5008	0.9142	1.046	0.8782	61.1	20000	1.55	0.2	0.2023	0.236	0.1686	0.1012	0.1517
n-butane	0.5008	0.9142	1.046	0.8782	61.1	20000	1.55	0.2	0.2023	0.236	0.1686	0.1012	0.1517
n-butane	0.5008	0.9142	1.046	0.8782	61.1	20000	1.55	0.2	0.2023	0.236	0.1686	0.1012	0.1517
n-butane	0.5008	0.9142	1.046	0.8782	61.1	20000	1.55	0.2	0.2023	0.236	0.1686	0.1012	0.1517
n-butane	0.5008	0.9142	1.046	0.8782	61.1	20000	1.55	0.2	0.2023	0.236	0.1686	0.1012	0.1517
n-butane	0.5008	0.9142	1.046	0.8782	61.1	20000	1.55	0.2	0.2023	0.236	0.1686	0.1012	0.1517
n-butane	0.5008	0.9142	1.046	0.8782	61.1	20000	1.55	0.2	0.2023	0.236	0.1686	0.1012	0.1517
n-butane	0.5008	0.9142	1.046	0.8782	61.1	20000	1.55	0.2	0.2023	0.236	0.1686	0.1012	0.1517
isobutane	0.4757	1.029	1.136	0.9876	61.1	20000	1.55	0.2	0.1875	0.2187	0.1562	0.09375	0.1406
isobutane	0.4757	1.029	1.136	0.9876	61.1	20000	1.55	0.2	0.1875	0.2187	0.1562	0.09375	0.1406
isobutane	0.4757	1.029	1.136	0.9876	61.1	20000	1.55	0.2	0.1875	0.2187	0.1562	0.09375	0.1406
isobutane	0.4757	1.029	1.136	0.9876	61.1	20000	1.55	0.2	0.1875	0.2187	0.1562	0.09375	0.1406

APPENDIX A3 RESULTS

A3.7: Radial Turbine Simulations No. 03

Fluid\$	Ma_2rel	Ma_3	Ma_3rel	Ma_4	N_blades	rpm	PSI	PHI	L_d	d_1	d_2	d_3	d_4
	[-]	[-]	[-]	[-]		[-/min]	[-]	[-]	[m]	[m]	[m]	[m]	[m]
isobutane	0.4757	1.029	1.136	0.9876	61.1	20000	1.55	0.2	0.1875	0.2187	0.1562	0.09375	0.1406
isobutane	0.4757	1.029	1.136	0.9876	61.1	20000	1.55	0.2	0.1875	0.2187	0.1562	0.09375	0.1406
isobutane	0.4757	1.029	1.136	0.9876	61.1	20000	1.55	0.2	0.1875	0.2187	0.1562	0.09375	0.1406
isobutane	0.4757	1.029	1.136	0.9876	61.1	20000	1.55	0.2	0.1875	0.2187	0.1562	0.09375	0.1406
isobutane	0.4757	1.029	1.136	0.9876	61.1	20000	1.55	0.2	0.1875	0.2187	0.1562	0.09375	0.1406
isobutane	0.4757	1.029	1.136	0.9876	61.1	20000	1.55	0.2	0.1875	0.2187	0.1562	0.09375	0.1406
isobutane	0.4757	1.029	1.136	0.9876	61.1	20000	1.55	0.2	0.1875	0.2187	0.1562	0.09375	0.1406
isobutane	0.4757	1.029	1.136	0.9876	61.1	20000	1.55	0.2	0.1875	0.2187	0.1562	0.09375	0.1406
isobutane	0.4757	1.029	1.136	0.9876	61.1	20000	1.55	0.2	0.1875	0.2187	0.1562	0.09375	0.1406
isobutane	0.4757	1.029	1.136	0.9876	61.1	20000	1.55	0.2	0.1875	0.2187	0.1562	0.09375	0.1406

APPENDIX A3 RESULTS

A3.7: Radial Turbine Simulations No. 03

Fluid\$	alpha_1	alpha_2	alpha_3	alpha_4	beta_2	beta_3	b_1	b_2	b_3	b_4	u_2	u_3	w_2	w_3
	[deg]	[deg]	[deg]	[deg]	[deg]	[deg]	[m]	[m]	[m]	[m]	[m/s]	[m/s]	[m/s]	[m/s]
R245fa	0	82.65	0	0	70.02	69.38	0.01828	0.01828	0.0257	0.01343	127.6	76.58	74.7	81.82
R245fa	0	82.65	0	0	70.02	69.38	0.01828	0.01828	0.0257	0.01343	127.6	76.58	74.7	81.82
R245fa	0	82.65	0	0	70.02	69.38	0.01828	0.01828	0.0257	0.01343	127.6	76.58	74.7	81.82
R245fa	0	82.65	0	0	70.02	69.38	0.01828	0.01828	0.0257	0.01343	127.6	76.58	74.7	81.82
R245fa	0	82.65	0	0	70.02	69.38	0.01828	0.01828	0.0257	0.01343	127.6	76.58	74.7	81.82
R245fa	0	82.65	0	0	70.02	69.38	0.01828	0.01828	0.0257	0.01343	127.6	76.58	74.7	81.82
R245fa	0	82.65	0	0	70.02	69.38	0.01828	0.01828	0.0257	0.01343	127.6	76.58	74.7	81.82
R245fa	0	82.65	0	0	70.02	69.38	0.01828	0.01828	0.0257	0.01343	127.6	76.58	74.7	81.82
R245fa	0	82.65	0	0	70.02	69.38	0.01828	0.01828	0.0257	0.01343	127.6	76.58	74.7	81.82
R245fa	0	82.65	0	0	70.02	69.38	0.01828	0.01828	0.0257	0.01343	127.6	76.58	74.7	81.82
R245fa	0	82.65	0	0	70.02	69.38	0.01828	0.01828	0.0257	0.01343	127.6	76.58	74.7	81.82
R245fa	0	82.65	0	0	70.02	69.38	0.01828	0.01828	0.0257	0.01343	127.6	76.58	74.7	81.82
R245fa	0	82.65	0	0	70.02	69.38	0.01828	0.01828	0.0257	0.01343	127.6	76.58	74.7	81.82
R245fa	0	82.65	0	0	70.02	69.38	0.01828	0.01828	0.0257	0.01343	127.6	76.58	74.7	81.82
R245fa	0	82.65	0	0	70.02	69.38	0.01828	0.01828	0.0257	0.01343	127.6	76.58	74.7	81.82
R134a	0	82.65	0	0	70.02	28.34	0.01828	0.01828	0.0257	0.01343	127.6	76.58	74.7	161.3
R134a	0	82.65	0	0	70.02	28.34	0.01828	0.01828	0.0257	0.01343	127.6	76.58	74.7	161.3
R134a	0	82.65	0	0	70.02	28.34	0.01828	0.01828	0.0257	0.01343	127.6	76.58	74.7	161.3
R134a	0	82.65	0	0	70.02	28.34	0.01828	0.01828	0.0257	0.01343	127.6	76.58	74.7	161.3
R134a	0	82.65	0	0	70.02	28.34	0.01828	0.01828	0.0257	0.01343	127.6	76.58	74.7	161.3
R134a	0	82.65	0	0	70.02	28.34	0.01828	0.01828	0.0257	0.01343	127.6	76.58	74.7	161.3
R134a	0	82.65	0	0	70.02	28.34	0.01828	0.01828	0.0257	0.01343	127.6	76.58	74.7	161.3
R134a	0	82.65	0	0	70.02	28.34	0.01828	0.01828	0.0257	0.01343	127.6	76.58	74.7	161.3
R134a	0	82.65	0	0	70.02	28.34	0.01828	0.01828	0.0257	0.01343	127.6	76.58	74.7	161.3
R134a	0	82.65	0	0	70.02	28.34	0.01828	0.01828	0.0257	0.01343	127.6	76.58	74.7	161.3
R134a	0	82.65	0	0	70.02	28.34	0.01828	0.01828	0.0257	0.01343	127.6	76.58	74.7	161.3
R134a	0	82.65	0	0	70.02	28.34	0.01828	0.01828	0.0257	0.01343	127.6	76.58	74.7	161.3
R134a	0	82.65	0	0	70.02	28.34	0.01828	0.01828	0.0257	0.01343	127.6	76.58	74.7	161.3

APPENDIX A3 RESULTS

A3.7: Radial Turbine Simulations No. 03

Fluid\$	alpha_1	alpha_2	alpha_3	alpha_4	beta_2	beta_3	b_1	b_2	b_3	b_4	u_2	u_3	w_2	w_3
	[deg]	[deg]	[deg]	[deg]	[deg]	[deg]	[m]	[m]	[m]	[m]	[m/s]	[m/s]	[m/s]	[m/s]
R134a	0	82.65	0	0	70.02	28.34	0.01828	0.01828	0.0257	0.01343	127.6	76.58	74.7	161.3
R134a	0	82.65	0	0	70.02	28.34	0.01828	0.01828	0.0257	0.01343	127.6	76.58	74.7	161.3
R134a	0	82.65	0	0	70.02	28.34	0.01828	0.01828	0.0257	0.01343	127.6	76.58	74.7	161.3
R134a	0	82.65	0	0	70.02	28.34	0.01828	0.01828	0.0257	0.01343	127.6	76.58	74.7	161.3
R134a	0	82.65	0	0	70.02	28.34	0.01828	0.01828	0.0257	0.01343	127.6	76.58	74.7	161.3
n-butane	0	82.65	0	0	70.02	29.18	0.02529	0.02529	0.03554	0.01343	176.5	105.9	103.3	217.3
n-butane	0	82.65	0	0	70.02	29.18	0.02529	0.02529	0.03554	0.01343	176.5	105.9	103.3	217.3
n-butane	0	82.65	0	0	70.02	29.18	0.02529	0.02529	0.03554	0.01343	176.5	105.9	103.3	217.3
n-butane	0	82.65	0	0	70.02	29.18	0.02529	0.02529	0.03554	0.01343	176.5	105.9	103.3	217.3
n-butane	0	82.65	0	0	70.02	29.18	0.02529	0.02529	0.03554	0.01343	176.5	105.9	103.3	217.3
n-butane	0	82.65	0	0	70.02	29.18	0.02529	0.02529	0.03554	0.01343	176.5	105.9	103.3	217.3
n-butane	0	82.65	0	0	70.02	29.18	0.02529	0.02529	0.03554	0.01343	176.5	105.9	103.3	217.3
n-butane	0	82.65	0	0	70.02	29.18	0.02529	0.02529	0.03554	0.01343	176.5	105.9	103.3	217.3
n-butane	0	82.65	0	0	70.02	29.18	0.02529	0.02529	0.03554	0.01343	176.5	105.9	103.3	217.3
n-butane	0	82.65	0	0	70.02	29.18	0.02529	0.02529	0.03554	0.01343	176.5	105.9	103.3	217.3
n-butane	0	82.65	0	0	70.02	29.18	0.02529	0.02529	0.03554	0.01343	176.5	105.9	103.3	217.3
n-butane	0	82.65	0	0	70.02	29.18	0.02529	0.02529	0.03554	0.01343	176.5	105.9	103.3	217.3
n-butane	0	82.65	0	0	70.02	29.18	0.02529	0.02529	0.03554	0.01343	176.5	105.9	103.3	217.3
n-butane	0	82.65	0	0	70.02	29.18	0.02529	0.02529	0.03554	0.01343	176.5	105.9	103.3	217.3
n-butane	0	82.65	0	0	70.02	29.18	0.02529	0.02529	0.03554	0.01343	176.5	105.9	103.3	217.3
isobutane	0	82.65	0	0	70.02	25.16	0.02344	0.02344	0.03294	0.01343	163.6	98.17	95.75	230.9
isobutane	0	82.65	0	0	70.02	25.16	0.02344	0.02344	0.03294	0.01343	163.6	98.17	95.75	230.9
isobutane	0	82.65	0	0	70.02	25.16	0.02344	0.02344	0.03294	0.01343	163.6	98.17	95.75	230.9
isobutane	0	82.65	0	0	70.02	25.16	0.02344	0.02344	0.03294	0.01343	163.6	98.17	95.75	230.9

APPENDIX A3 RESULTS

A3.7: Radial Turbine Simulations No. 03

Fluid\$	alpha_1	alpha_2	alpha_3	alpha_4	beta_2	beta_3	b_1	b_2	b_3	b_4	u_2	u_3	w_2	w_3
	[deg]	[deg]	[deg]	[deg]	[deg]	[deg]	[m]	[m]	[m]	[m]	[m/s]	[m/s]	[m/s]	[m/s]
isobutane	0	82.65	0	0	70.02	25.16	0.02344	0.02344	0.03294	0.01343	163.6	98.17	95.75	230.9
isobutane	0	82.65	0	0	70.02	25.16	0.02344	0.02344	0.03294	0.01343	163.6	98.17	95.75	230.9
isobutane	0	82.65	0	0	70.02	25.16	0.02344	0.02344	0.03294	0.01343	163.6	98.17	95.75	230.9
isobutane	0	82.65	0	0	70.02	25.16	0.02344	0.02344	0.03294	0.01343	163.6	98.17	95.75	230.9
isobutane	0	82.65	0	0	70.02	25.16	0.02344	0.02344	0.03294	0.01343	163.6	98.17	95.75	230.9
isobutane	0	82.65	0	0	70.02	25.16	0.02344	0.02344	0.03294	0.01343	163.6	98.17	95.75	230.9
isobutane	0	82.65	0	0	70.02	25.16	0.02344	0.02344	0.03294	0.01343	163.6	98.17	95.75	230.9
isobutane	0	82.65	0	0	70.02	25.16	0.02344	0.02344	0.03294	0.01343	163.6	98.17	95.75	230.9
isobutane	0	82.65	0	0	70.02	25.16	0.02344	0.02344	0.03294	0.01343	163.6	98.17	95.75	230.9
isobutane	0	82.65	0	0	70.02	25.16	0.02344	0.02344	0.03294	0.01343	163.6	98.17	95.75	230.9

APPENDIX A3 RESULTS

A3.9: Axial Turbine Preliminary Simulations

Working Fluid	m_dot [kg/s]	P_3 [Pa]	T_3 [C]	T_1 [C]	P_1 [Pa]	rpm [-/min]	d_1 [m]
R245fa	2	354638	61.29	80.99	810600	20764	0.04543
R245fa	1.5	354638	58.32	80.99	810600	29749	0.03661
R245fa	1	354638	52.69	80.99	810600	49385	0.02701
R245fa	0.95	354638	51.83	80.99	810600	52655	0.02599
R245fa	0.925	354638	51.38	80.99	810600	54440	0.02548
R245fa	0.9125	354638	51.14	80.99	810600	55374	0.02522
R245fa	0.91	354638	51.09	80.99	810600	55564	0.02517
R245fa	0.909	354638	51.07	80.99	810600	55640	0.02515
R245fa	0.9085	NO CONVERGENCE BELOW THIS					
Working Fluid	m_dot [kg/s]	P_3 [Pa]	T_3 [C]	T_1 [C]	P_1 [Pa]	rpm [-/min]	d_1 [m]
R134a	2	354638	65.13	80.99	810600	17169	0.05494
R134a	1.5	354638	61.96	80.99	810600	24599	0.04428
R134a	1	354638	55.84	80.99	810600	40835	0.03267
R134a	0.9	354638	53.85	80.99	810600	46584	0.03018
R134a	0.8	354638	51.41	80.99	810600	53973	0.02763
R134a	0.7	354638	48.33	80.99	810600	63777	0.025
R134a	0.6	354638	44.33	80.99	810600	77330	0.02227
R134a	0.5	354638	38.91	80.99	810600	97123	0.01942
R134a	0.45	354638	35.43	80.99	810600	110795	0.01795
R134a	0.4	354638	31.19	80.99	810600	128369	0.01643
R134a	0.3	354638	19.32	80.99	810600	183922	0.01324
R134a	0.25	354638	10.66	80.99	810600	230999	0.01155
R134a	0.24	354638	8.603	80.99	810600	243092	0.0112
R134a	0.23	354638	6.425	80.99	810600	256375	0.01085
R134a	0.229	354638	6.2	80.99	810600	257775	0.01081
R134a	0.228	354638	5.973	80.99	810600	259189	0.01078
R134a	0.227	354638	5.745	80.99	810600	260617	0.01074
R134a	0.226	354638	5.516	80.99	810600	262060	0.01071
R134a	0.225	NO CONVERGENCE BELOW THIS					

APPENDIX A3 RESULTS

A3.9: Axial Turbine Preliminary Simulations

Working Fluid	m_dot [kg/s]	P_3 [Pa]	T_3 [C]	T_1 [C]	P_1 [Pa]	rpm [-/min]	d_1 [m]
n-butane	2	354638	60.66	80.03	1010000	15454	0.06104
n-butane	1.5	354638	58.38	80.03	1010000	22141	0.04919
n-butane	1	354638	53.98	80.03	1010000	36755	0.03629
n-butane	0.9	354638	52.56	80.03	1010000	41929	0.03354
n-butane	0.8	354638	50.8	80.03	1010000	48580	0.0307
n-butane	0.7	354638	48.6	80.03	1010000	57404	0.02777
n-butane	0.6	354638	45.73	80.03	1010000	69603	0.02474
n-butane	0.5	354638	41.87	80.03	1010000	87419	0.02158
n-butane	0.45	354638	39.38	80.03	1010000	99725	0.01994
n-butane	0.44	354638	38.83	80.03	1010000	102566	0.01961
n-butane	0.43	354638	38.25	80.03	1010000	105556	0.01927
n-butane	0.42	354638	37.65	80.03	1010000	108707	0.01893
	0.419	NO CONVERGENCE BELOW THIS					
Working Fluid	m_dot [kg/s]	P_3 [Pa]	T_3 [C]	T_1 [C]	P_1 [Pa]	rpm [-/min]	d_1 [m]
isobutane	2	354638	46.94	66.82	1010000	15804	0.05968
isobutane	1.5	354638	44.57	66.82	1010000	22644	0.0481
isobutane	1	354638	39.99	66.82	1010000	37589	0.03549
isobutane	0.9	354638	38.51	66.82	1010000	42880	0.03279
isobutane	0.8	354638	36.69	66.82	1010000	49682	0.03002
isobutane	0.7	354638	34.41	66.82	1010000	58707	0.02716
isobutane	0.6	354638	31.45	66.82	1010000	71182	0.02419
isobutane	0.5	354638	27.48	66.82	1010000	89402	0.0211
isobutane	0.49	354638	27.01	66.82	1010000	91688	0.02078
isobutane	0.48	354638	26.52	66.82	1010000	94082	0.02046
isobutane	0.47	354638	26.01	66.82	1010000	96591	0.02014
isobutane	0.46	354638	25.48	66.82	1010000	99223	0.01982
isobutane	0.459	354638	25.43	66.82	1010000	99493	0.01979
	0.458	NO CONVERGENCE BELOW THIS					

APPENDIX A3 RESULTS

A3.9: Axial Turbine Simulations

WF\$	m_dot	P_1	P_2	P_3	T_1	T_2	T_3	eta_ts	eta_tt	PR	rpm	d	b	R_s
	[kg/s]	[Pa]	[Pa]	[Pa]	[C]	[C]	[C]	[-]	[-]		[-/min]	[m]	[m]	
R245fa	2.061	810600	356544	355000	80.99	62.67	61.58	0.8397	0.92	1.777	20000	0.04646	0.006969	0.1133
R134a	1.77	810600	356633	355000	80.99	65.28	63.91	0.8348	0.9196	1.896	20000	0.05013	0.00752	0.1204
n-butane	1.627	1010000	355929	355000	80.03	59.83	59.11	0.863	0.9222	2.226	20000	0.05229	0.007843	0.08103
isobutane	1.657	1010000	355998	355000	66.82	46.23	45.48	0.8632	0.9223	2.211	20000	0.05182	0.007773	0.08094

WF\$	alpha_1	alpha_2	alpha_3	beta_2	beta_3	C_1	C_2	C_3	U	W_2	W_3
	[deg]	[deg]	[deg]	[deg]	[deg]	[m/s]	[m/s]	[m/s]	[m/s]	[m/s]	[m/s]
R245fa	0	38.88	0	15.97	27.49	44.76	138.2	107.5	55.95	111.9	121.2
R134a	0	40.33	0	16.76	28.71	48.3	144.6	110.2	60.37	115.1	125.7
n-butane	0	32.01	0	12.51	21.96	50.37	184.1	156.1	62.97	159.9	168.3
isobutane	0	31.99	0	12.5	21.95	49.92	182.6	154.9	62.41	158.6	167

WF\$	Ma_1	Ma_2	Ma_3	Ma_2rel	Ma_3rel	P_01	P_02	P_03	T_01	T_02	T_03
						[Pa]	[Pa]	[Pa]			
R245fa	0.3478	1.001	0.7809	0.8103	0.8803	857366	590655	482513	83.25	76.95	70.1
R134a	0.2932	0.862	0.6586	0.6863	0.7509	847482	528134	446961	82.61	78.51	71.6
n-butane	0.2633	0.8666	0.7358	0.7527	0.7934	1.04E+06	522515	468284	81.34	71.41	67.39
isobutane	0.2671	0.8772	0.7451	0.7621	0.8033	1.04E+06	528046	471890	68.15	58.17	54.03

APPENDIX A3 RESULTS

A3.10 Experimental Test Results Template

The following template was prepared for capturing measurements from the experiments.

Test Cycle Ref (Date & Time)	Measurement Point	Pressure Reading		Temperature Reading
	Evaporator-Turbine			
	Turbine-Condenser			
	Condenser-Feed pump			
	Feed pump-Evaporator			
		Voltage Reading	Amperage Reading	Rotational Speed
	DC Generator			

APPENDIX A4 PUBLICATIONS

Journal Papers

- A4.1 Situmbeko S.M. and Inambao F.L., Small Scale Axial Turbine Preliminary Design and Modelling, International Journal of Engineering Research & Technology (IJERT), ISSN: 2278-0181, Vol. 5 Issue 07, July-2016, pp 683-690.
- A4.2 Situmbeko S.M. and Inambao F.L., Economic and environmental analyses of a 10 kWe low temperature solar thermal power plant, International Journal of Research in Engineering & Advanced Technology (IJREAT), ISSN: 2320 – 8791 (Impact Factor: 2.317), www.ijreat.org, Volume 3, Issue 6, Dec 2015 – Jan 2016, pp 1-12.
- A4.3 Situmbeko S.M. and Inambao F.L., ORC condenser heat exchanger design and modelling, International Journal of Engineering Research & Technology (IJERT), ISSN: 2278-0181, Vol. 4 Issue 08, August 2015, pp 279-286.
- A4.4 Situmbeko S.M. and Inambao F.L., Heat exchanger modelling for solar organic Rankine cycle, International Journal of Thermal and Environmental Engineering (IJTEE), Volume 9, No. 1, 2015, pp 7-16.
- A4.5 Situmbeko S.M., Kumar K.L. and Inambao F.L., Modeling of a solar air heater with sensible thermal storage and natural draft, International Journal of Engineering Research & Technology (IJERT), ISSN 2278-0181, Volume. 3, Issue. 09, September 2014, pp 624-634.
- A4.6 Situmbeko S.M. and Inambao F.L., System and component modelling of a low temperature solar thermal energy conversion cycle, Journal of Energy in Southern Africa, ISSN 1021 447X, Vol. 24 No 4, November 2013, pp 51-62.
- A4.7 Situmbeko S.M. and Inambao F.L., Low temperature solar thermal energy conversion, Energize, South Africa, June 2010, pp 21-24.

Conference Papers

- A4.8. Situmbeko S.M., Inambao F.L. (2016). Economic and Environmental Analysis of Renewable Energy Systems, Proceeding of the LeNSes Conference, September 28-30, 2016, Cape Town, South Africa, Paper ID 1095, pp 35-42.
- A4.9. Situmbeko S.M. and Inambao F.L., Review of designs for low temperature organic Rankine cycle expanders, presented to the Botswana Institution of Engineers (BIE) 14th Biennial Conference, Gaborone, Botswana, October 2015.
- A4.10 Situmbeko S.M. and Inambao F.L., Low temperature thermal power concept case study, Botswana Institution of Engineers (BIE) 13th Biennial Conference, Gaborone, Botswana, October 2013.
- A4.11 Situmbeko S.M. and Kumar K.L., Solar air heater with sensible thermal storage, Botswana Institution of Engineers (BIE) 13th Biennial Conference, Gaborone, Botswana, October 2013.
- A4.12 Situmbeko S.M. and Inambao F.L., Mathematical modelling and computer simulation of a solar

APPENDIX A4 PUBLICATIONS

- field for a low temperature organic Rankine cycle (ORC), 1st Southern African Solar Energy Conference (SASEC 2012) Stellenbosch, South Africa, 21-23 May 2012.
- A4.13 Situmbeko S.M. and Inambao F.L., Mathematical modeling and simulation of a low temperature solar thermal energy conversion system, International Solar Energy Society – Solar World Congress (ISES–SWC 2011), Kassel, Germany, 28 August - 2 September 2011.
- A4.14 Situmbeko S.M. and Inambao F.L., Low temperature solar thermal energy conversion, Domestic Use of Energy (DUE) Conference; Cape Peninsula University of Technology, Cape Town, South Africa, March 29 - 31, 2010.

Small Scale Axial Turbine Preliminary Design and Modelling

Shadreck M. Situmbeko

University of Botswana, Gaborone, Botswana;
University of KwaZulu-Natal, Durban, RSA;

Freddie L. Inambao

University of KwaZulu-Natal,
Durban, RSA;

Abstract- Purpose: This paper presents the preliminary design and modelling of an axial turbine suitable for use in a small to medium level, low temperature, solar thermal, organic Rankine cycle (ORC). The work involves thermodynamic and geometrical design and analyses. Empirical loss correlations are used to account for the different kinds of losses. The engineering equation solver (EES) is used to perform the thermodynamic analysis. 2D and 3D computational fluid dynamics (CFD) simulation and the aerofoil design are not done at this stage as they require specialized CFD software. The work is meant to contribute towards the development of optimal cost-effective turbine expanders suitable for small to medium sized operation at low to medium temperatures. There is not sufficient evidence to show that significant research and development work has been done with regard to turbomachinery design and development for small to medium size low temperature organic Rankine cycle (ORC) systems. Most turbine manufacturers and developers put more emphasis on larger scale models in the Megawatts (MW) ranges while most researchers who have shown interest in micro-scale operations in the low temperature applications have concentrated their efforts more on thermodynamic studies regarding the power cycle, and on the proper rules for the selection of the working fluids, with special attention to the power plant efficiency; others have made attempts at adaptation and modification of other equipment, especially positive displacement machines, for use as ORC expanders. A turbine design suitable for small scale and low temperature operation based on the ORC thermodynamic cycle is required because the operating conditions such as speed, flow rate, pressure ratio, etc. are quite different from those of conventional steam and gas turbines; also the properties of the organic fluids used as working fluids are different from those of the conventional steam or fossil-fuel-gas mixtures.

Keywords: ORC thermodynamic cycle, preliminary design and modelling, thermodynamic and geometrical design, EES

Paper type: Research Paper

Nomenclature

Roman symbols

b	blade height
c_p	isobaric specific heat capacity
d	mean diameter
e	internal energy per unit mass of the medium
\bar{G}	gravitational acceleration, electromagnetic acceleration, etc.
h	specific (static) enthalpy (J/kg)
I	rothalpy
\bar{I}	identity matrix equals the kronecker unit tensor
k	kinetic energy per unit mass of the medium

\dot{m}	mass flow rate (\dot{m} in EES code)
P	pressure
PR	pressure ratio
\bar{Q}	conductive heat flux
r	mean blade radius (m)
R_r	rotor degree of reaction (also R_s in EES code)
R_n	nozzle degree of reaction
s	entropy
t	time
T	temperature
U	blade velocity (m/s)
\bar{U}	fluid velocity vector
V	absolute fluid velocity (m/s)
V_a	axial component of velocity V
V_u	tangential component of velocity V
W	relative velocity of fluid flow to moving blades (m/s)
W_s	specific shaft work
\dot{w}	specific shaft work
\dot{W}_t	shaft work; turbine work

Greek symbols

α	absolute flow angle
β	relative flow angle
∂	partial differential operator
Φ	flow coefficient
η_{tt}	total-to-total efficiency (η_{tt} in EES code)
η_{ts}	total-to-static efficiency (η_{ts} in EES code)
θ	tangential (circumferential) component
ρ	specific mass; density
$\bar{\tau}$	stress tensor
ω	shaft angular velocity (rad/s)
Ψ	work coefficient (also blade loading)

mathematical operators

∇	gradient operator
----------	-------------------

numbers

1	inlet to machine; inlet to nozzle blades
2	outlet from machine; inlet to rotor blades
3	outlet from rotor blades
01	stagnation state at station 1
02	stagnation state at station 2
02 _{rel}	relative stagnation state at station 2
03 _{rel}	relative stagnation state at station 3
2'	static state at station 2 after an isentropic expansion in the nozzle

- 3' static state at station 3 after an isentropic expansion through entire stage
- 3'' static state at station 3 after an isentropic expansion in the rotor blades only
- 03' relative stagnation state at station 3 after an isentropic expansion through entire stage

I. INTRODUCTION

In this paper we present work done on the research and development of a turbine suitable for a low temperature solar thermal conversion cycle based on the organic Rankine cycle (ORC). The turbine is the single most critical component in a thermal conversion cycle. The ideal solution should be characterized by maximum efficiency, small footprint, and minimum shaft speed (Cooper *et al*, 2010). Although the research considered all the three possible architectures: single stage radial turbine – cantilever type; single stage radial turbine – Ninety Degrees In-Flow Radial turbine (90° IFR); and single stage axial turbine, this paper only presents findings on the latter.

The turbine design process can be broken down into three stages:

- Preliminary Design (PD);
- Meanline/Streamline (1D/2D) Analysis and Optimization
- Profiling, 3D Blade Design, 3D Modelling and Analysis

Preliminary Design involves finding the optimal flow path, number of stages and distribution of geometrical parameters (heights and angles) based on the given thermodynamic conditions at turbine inlet and outlet. This process can further be subdivided into two tasks:

- initial enthalpy drop distribution: this entails determining the optimal number of stages and appropriately distributing the enthalpy drop between them and finding the first approximation of flow path geometry paths; and
- adjusting design calculations (inverse calculation task): this entails calculation of turbine main performance characteristics as well as exact thermodynamic and kinetic parameters basing on initial enthalpy drop distribution results.

Initial design parameters are the inlet working fluid conditions (pressure, temperature, and enthalpy), outlet pressure, mass flow rate and rotational speed.

To fully develop a final working turbine model, the following factors are of paramount importance:

- manufacturing and material specifications of the rotor and nozzle;
- structural and aerodynamic design of the rotor and nozzle; and
- specifications of the inlet and outlet parameters such as pressures and temperatures.

II. THEORY OF TURBOMACHINERY

Fluid dynamics and hence turbomachinery theory is based on three fundamental principles of conservation of mass (continuity), conservation of momentum and conservation of energy, represented by the following equations [2]:

conservation of mass (continuity):

$$\frac{\partial \rho}{\partial t} + \nabla \cdot (\rho \bar{U}) = 0 \tag{1}$$

conservation of momentum:

$$\frac{\partial \rho \bar{U}}{\partial t} + \nabla \cdot (\rho \bar{U} \bar{U} + \bar{P} \bar{I} - \bar{\tau}) - \rho \bar{G} = 0 \tag{2}$$

conservation of energy:

$$\frac{\partial \rho(e+k)}{\partial t} + \nabla \cdot (\rho \bar{U} (e + \frac{p}{\rho} + k) - \bar{\tau} \cdot \bar{U} + \bar{Q}) - \rho \bar{G} \cdot \bar{U} = 0 \tag{3}$$

The work done by a turbomachine can be represented by the Euler turbine equation which can be written as (Ingram, 2009):

$$\dot{W}_t = \dot{m} \omega (r_2 \bar{V}_{\theta 2} - r_1 \bar{V}_{\theta 1}) \tag{4}$$

where \dot{m} is the mass flow rate, ω is the shaft angular velocity, r is the mean blade radius, \bar{V} is the working fluid flow velocity, while subscripts 1, 2 and θ represent the inlet and outlet to the machine, and tangential (circumferential) component respectively.

Velocity Triangles and Mollier diagrams are used to aid the analysis of the turbomachinery; typically the velocity triangle is a representation of the equation $\bar{V} = \bar{U} + \bar{W}$ at each station, that is, entry to nozzle, and entry and exit to rotor; where V is absolute fluid velocity, U is blade velocity and W is relative velocity of fluid flow to moving blades; refer to figure 1:

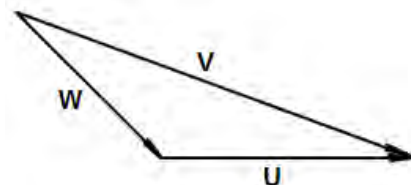


Figure 1: velocity diagram

The Mollier diagram is a plot of enthalpy against entropy for a process in which one property usually pressure or temperature is kept constant [4]; pertaining to turbine expansion process, the mollier diagram aids in visualizing the isentropic and real expansion processes as well as the stagnation and static states of the working fluid; figure 2 shows a typical expansion process on a mollier diagram.

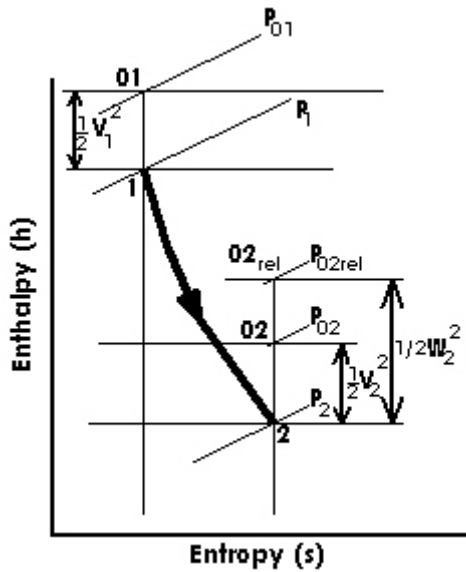


Figure 2: mollier diagram showing a typical expansion process

Stagnation state is represented by state parameters designated as P_0 for stagnation pressure, T_0 for stagnation temperature, and h_0 for stagnation enthalpy; stagnation pressure is a pressure at a state corresponding to zero velocity, a stagnation state, which is representative of an adiabatic throttling process. The throttling process is a representation of flow through inlets, nozzles, stationary turbomachinery blades, and the use of stagnation pressure as a measure of loss is a practice that has widespread application. Stagnation pressure is a key variable in propulsion and power systems.

The stagnation pressure at a given state is defined by the enthalpy equation:

$$h_0 = h + \frac{v^2}{2} \quad (5)$$

where: h_0 is the stagnation enthalpy (J/kg); h is the static enthalpy (J/kg); and V is the fluid speed (m/s)

Rothalpy is a function/property that remains constant throughout a rotating machine, that is, in an adiabatic irreversible process relative to the rotating component [5]. It is defined by the equation:

$$I = h + \frac{W^2}{2} - \frac{U^2}{2} \quad (6)$$

where h is static enthalpy, W is the relative velocity of the fluid, and U is the blade speed.

Thus rothalpy (rotational enthalpy) is conserved between two stations in a rotating reference in any turbomachinery:

$$I_2 = I_3 \quad (7)$$

Stagnation enthalpy is conserved between two points in a fluid flow stream in a non-rotating reference system:

$$h_{01} = h_{02} \quad (8)$$

The degree of reaction is expressed as the relative pressure or enthalpy drop in the nozzle or rotor blades to that of the stage:

Rotor degree of reaction:

$$R_r = \frac{\text{static enthalpy drop in rotor}}{\text{stagnation enthalpy drop in stage}} \quad (9)$$

Nozzle degree of reaction:

$$R_n = \frac{\text{static enthalpy drop in nozzle}}{\text{stagnation enthalpy drop in stage}} \quad (10)$$

III. AXIAL FLOW TURBINE MODEL

Description

The fluid flow in an axial turbine is essentially in a direction parallel to the axis of rotation of the machine. Axial turbines usually have several stages such that each stage only handles a moderate pressure or enthalpy drop. Figure 3 shows a single stage axial turbine rotor.



Figure 3: single stage axial turbine rotor

For a single stage the diameter will usually be the same at the turbine inlet and outlet and as such the blade speed remains constant along a flow path; and a combined velocity triangle can be drawn as shown in figure 4.

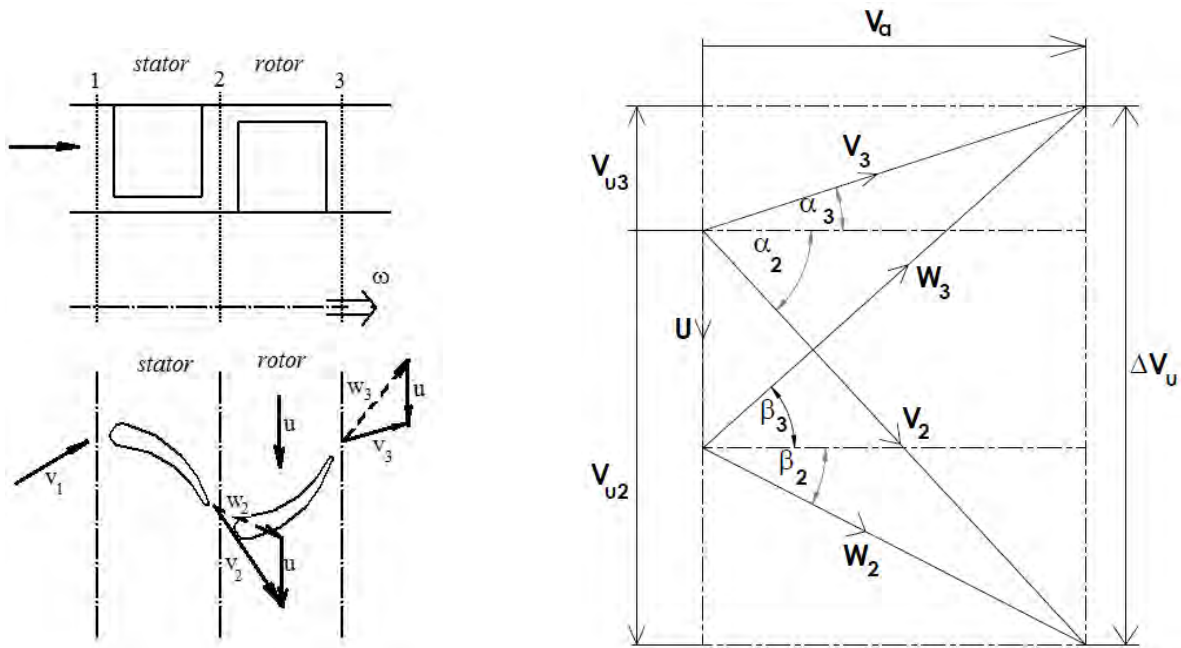


Figure 4: blade arrangement and velocity triangles

Mathematical Model

With reference to figures 4 and 5 the following set of equations can be written for the single stage axial turbine:

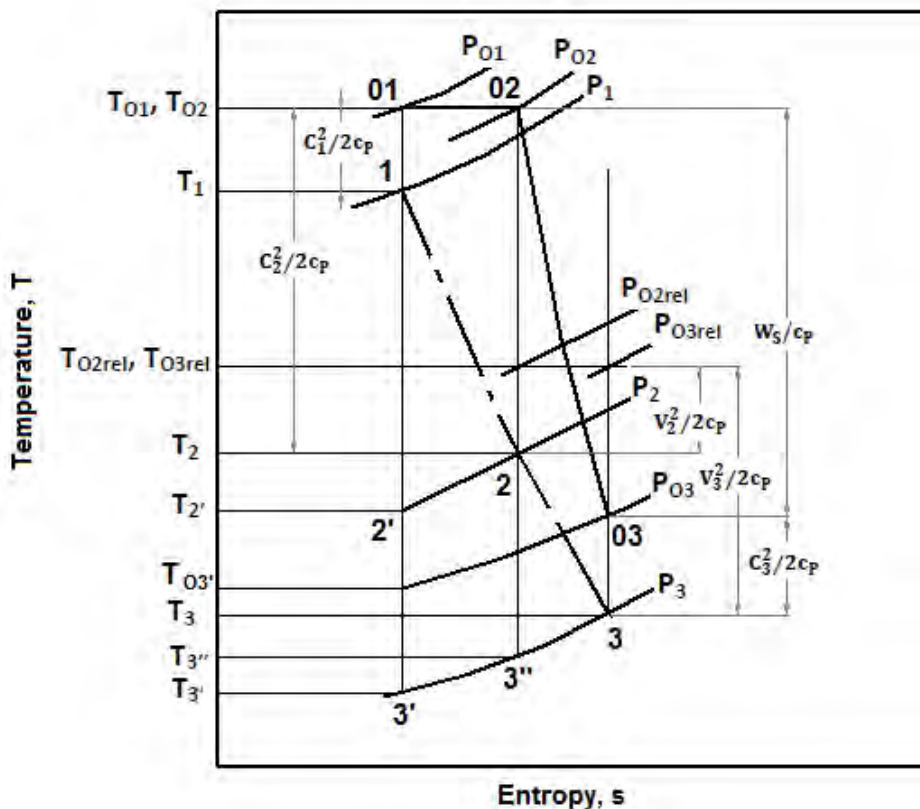


Figure 5: Mollier diagram for an axial turbine stage [6]

The work output per unit mass flow is given by:

$$\dot{w} = U \cdot (V_{u2} + V_{u3}) = U \cdot V_a \cdot (\tan\alpha_2 + \tan\alpha_3) = U \cdot V_a \cdot (\tan\beta_2 + \tan\beta_3) \quad (11)$$

The blade-loading coefficient is used to express work capacity of the stage. It is defined as the ratio of the specific work of the stage to the square of the blade velocity:

$$\Psi = \frac{\dot{w}}{U^2} \quad (12)$$

The flow coefficient, ϕ , is the ratio of the axial component of the inlet flow velocity to the blade speed:

$$\phi = \frac{V_a}{U} \tag{13}$$

Computer Simulations

Simulations were performed using the engineering equation solver (EES), (Klein, 2014); Soderberg’s loss correlations were used (Dixon, 1998). As no convergence could be attained with the given mass flow rates, i.e. from the evaporator model, (Situmbeko and Inambao, 2015), the first simulation was to determine the lowest feasible mass flow rates for all the working fluids by varying the mas flow rates from 0.1 to 2 kg/s; the results showed 0.459 kg/s (instead of 0.241) for isobutene, 0.420 kg/s (instead of 0.207) for n-butane, 0.226 kg/s (instead of 0.396) for R134a and 0.909 kg/s (instead of 0.396) for R245fa. Using these new figures the input conditions are modified and then the simulations progressed; the revised inlet conditions are shown in the following table 1:

Table 1: axial turbine model – revised inlet conditions

Working Fluid	Mass flow rate	Inlet Pressure	Inlet Temperature
	[kg/s]	[Pa]	[C]
R245fa	0.909	810600	80.99
R134a	0.226	810600	80.99
n-butane	0.420	1010000	80.03
isobutane	0.459	1010000	66.82

Three sets of simulations were conducted:

Simulation 1: Rotor exit static pressure was varied within the feasible pressure range and the results are shown in figures 6 and 7; convergence for R245fa could only be attained for pressures 350 to 360 kPa; however, since this range happened to yield higher total-to-total efficiencies, see figure 8, the rotor exit pressure was set constant at 355 kPa for the remainder of the simulations.

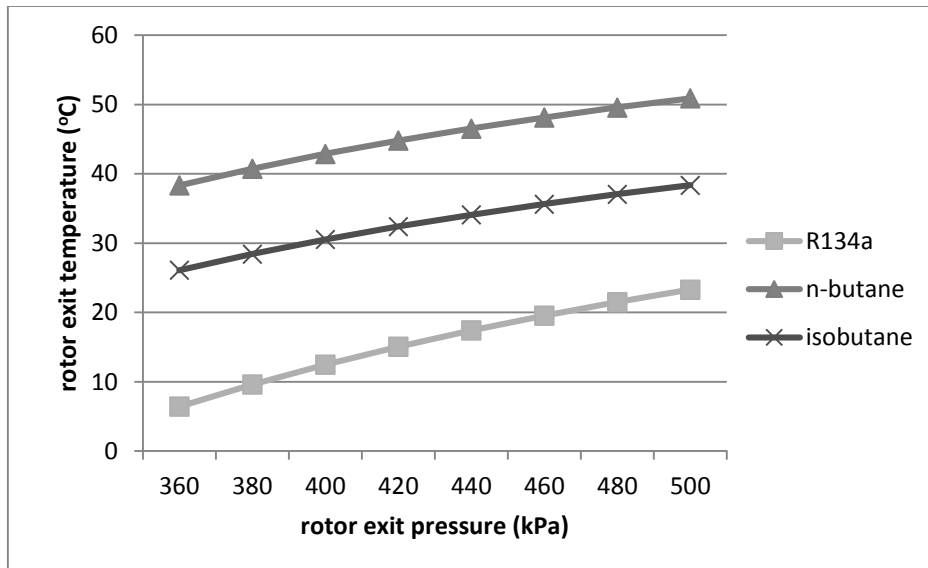


Figure 6: axial turbine model rotor exit - temperature versus pressure

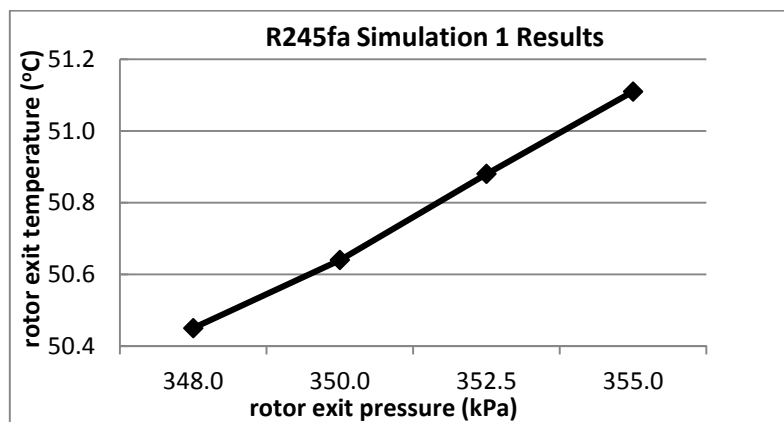


Figure 7: axial turbine model rotor exit - temperature versus pressure for R245fa

Note: The results for n-butane and isobutene appear superimposed in figure 8, although the results for isobutene are slightly superior.

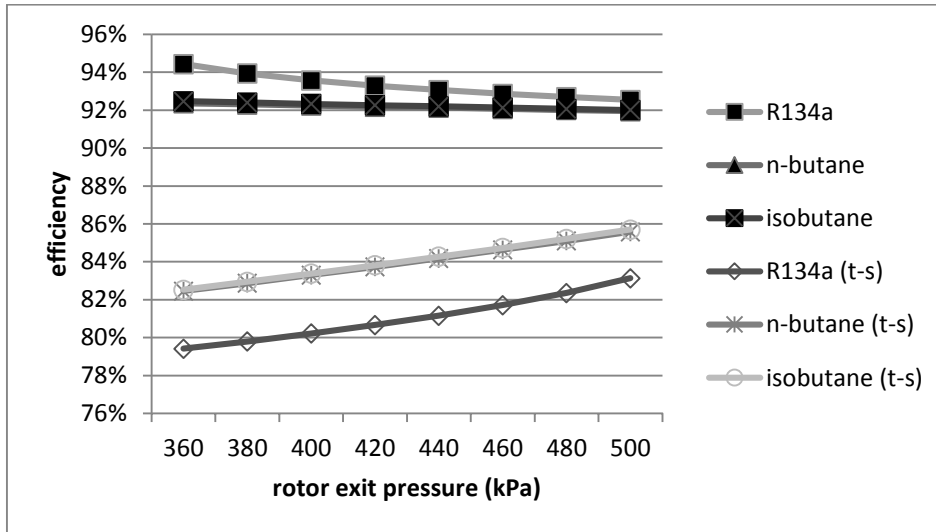


Figure 8: axial turbine model efficiency versus rotor exit pressure (t-s is for total-to-static; other series are for total-to-total)

With the rotor exit pressure set constant at 355 kPa, the rotor diameter was varied from 26 mm to 160 mm as a way to optimize the machine speed to a lower acceptable level. Results of these simulations are shown in figure 9; from the results it can be seen that any speed between 5000 rpm and

15000 rpm could be considered acceptable; however the speed was set at 20000 rpm as had been done with the radial turbine model (results will be presented in a separate publication). The final optimal results are shown in table 2 and velocity triangles of figures 10 to 13.

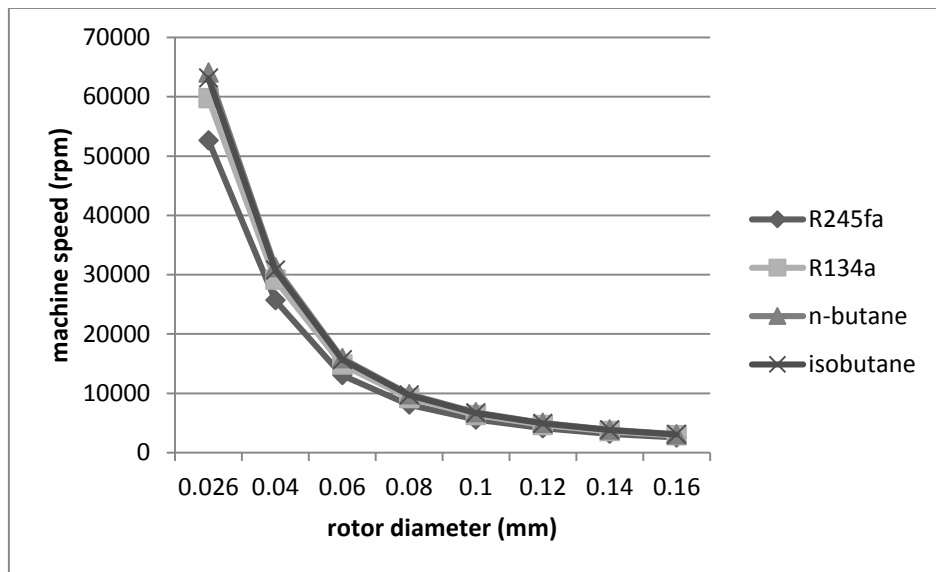


Figure 9: axial turbine model – machine speed versus rotor diameter

Table 2: axial turbine model simulation results

WFS	m dot	P ₁	P ₂	P ₃	T ₁	T ₂	T ₃	eta _{ts}	eta _{tt}	PR
	[kg/s]	[Pa]	[Pa]	[Pa]	[C]	[C]	[C]	[-]	[-]	
R245fa	2.061	810600	356544	355000	80.99	62.67	61.58	0.8397	0.92	1.777
R134a	1.77	810600	356633	355000	80.99	65.28	63.91	0.8348	0.9196	1.896
n-butane	1.627	1010000	355929	355000	80.03	59.83	59.11	0.863	0.9222	2.226
isobutane	1.657	1010000	355998	355000	66.82	46.23	45.48	0.8632	0.9223	2.211

WFS	C ₁	C ₂	C ₃	U	W ₂	W ₃	Ma ₁	Ma ₂	Ma ₃	Ma _{2rel}	Ma _{3rel}
	[m/s]	[m/s]	[m/s]	[m/s]	[m/s]	[m/s]					
R245fa	44.76	138.2	107.5	55.95	111.9	121.2	0.3478	1.001	0.7809	0.81	0.8803
R134a	48.3	144.6	110.2	60.37	115.1	125.7	0.2932	0.862	0.6586	0.686	0.7509
n-butane	50.37	184.1	156.1	62.97	159.9	168.3	0.2633	0.8666	0.7358	0.753	0.7934
isobutane	49.92	182.6	154.9	62.41	158.6	167	0.2671	0.8772	0.7451	0.762	0.8033

WFS	rpm	d	b	R _s	alpha ₁	alpha ₂	alpha ₃	beta ₂	beta ₃
	[-/min]	[m]	[m]		[deg]	[deg]	[deg]	[deg]	[deg]
R245fa	20000	0.04646	0.00697	0.1133	0	38.88	0	15.97	27.49
R134a	20000	0.05013	0.00752	0.1204	0	40.33	0	16.76	28.71
n-butane	20000	0.05229	0.00784	0.08103	0	32.01	0	12.51	21.96
isobutane	20000	0.05182	0.00777	0.08094	0	31.99	0	12.5	21.95

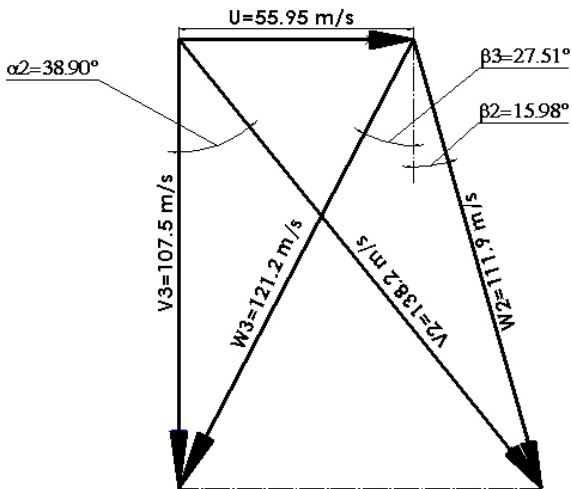


Figure 10: axial turbine velocity triangles for R245fa

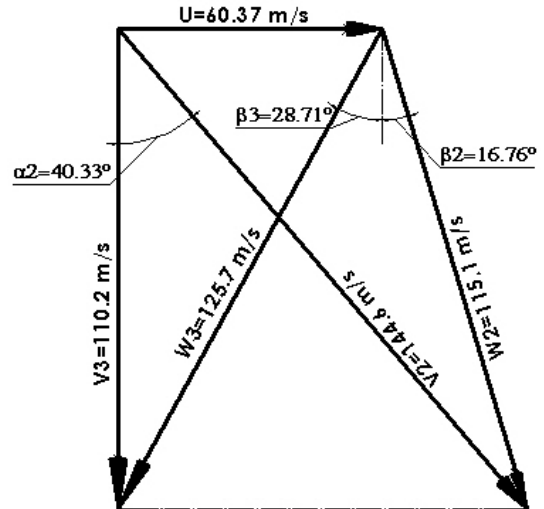


Figure 11: axial turbine velocity triangles for R134a

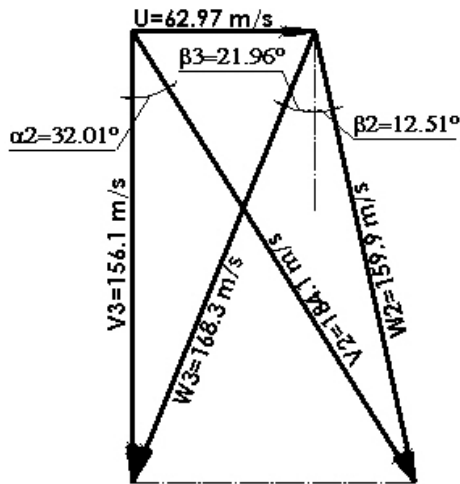


Figure 12: axial turbine velocity triangles for n-butane

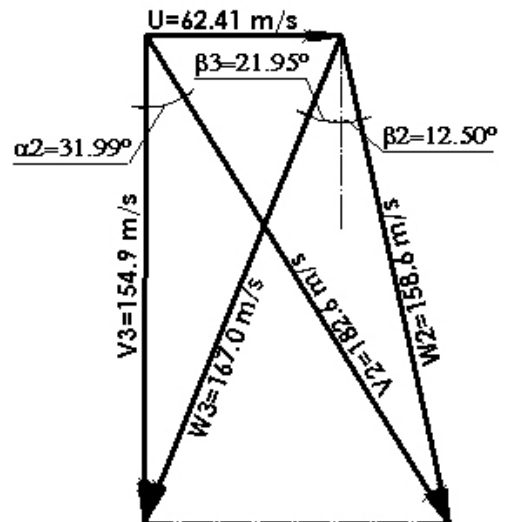


Figure 13: axial turbines velocity triangles for isobutene

IV. DISCUSSIONS AND CONCLUSIONS

The paper has presented the preliminary design models for axial turbines suitable for a 10 kWe low temperature organic Rankine cycle. The preliminary design has been presented in terms of geometric parameters of flow angles, blade diameters and heights; the preliminary design also includes thermodynamic parameters of stagnation and static pressures, temperatures and enthalpy's; the thermodynamic analyses were conducted within the cycle temperature ranges of the evaporator and condenser. Although the presented design models are not complete, this work has shown that small turbines for low temperature cycles are a feasible design option. The turbine preliminary design parameters for the 10 kWe turbine model after parametric optimization are listed in the table 2.

Efficiency: in terms of total-to-total efficiency all the four working fluids performed well of course with varying pressure ratios, mass flow rates and turbines sizes; however when all these factors are taken into account: R245fa requires the least pressure ratio, higher mass flow are and smaller turbine size. R134a performs second best in terms of smaller pressure ratio and smaller turbine size with a remarkable lower (than R245fa) mass flow rate. The performance of the other remaining two working fluids, isobutane and n-butane, is almost a tie, with isobutane having a slighter edge.

In terms of Mach numbers, the flow changes from subsonic to transonic status for all four working fluids but does not extend beyond the sonic stage. This implies that a more detailed study of the blade is required to determine whether the flow passages need to transition from convergent to divergent at any point in the flow passages.

To fully complete the turbine design task it is necessary to employ CFD and FEA analysis and modelling of the detailed blade and nozzle geometry and flow profile design. This would be followed by providing material and manufacturing specifications for prototype construction and testing. AxSTREAM software suite by SoftInWay Inc. is a good package for turbine CFD modelling.

REFERENCES

- [1] Cooper, D., Baines, N., Sharp, N. (2010), *Organic Rankine cycle Turbine For Exhaust Energy Recovery In A Heavy Truck Engine*, Concepts ETI, Inc.
- [2] http://web.stanford.edu/~cantwell/AA200_Course_Material/AA200_Course_Notes/AA200_Ch_06_The_Conservation_equations.pdf, accessed August 14, 2014
- [3] Ingram, G. (2009), *Basic Concepts in Turbomachinery*, Ventus Publishing ApS, ISBN 978-87-7681-435-9.
- [4] <http://dictionary.reference.com/browse/mollier+diagram>; accessed February 10, 2015.
- [5] http://www.answers.com/Q/What_is_the_rothalpy; accessed February 10, 2015.
- [6] Dekker, M (2003), *Chapter 7 Axial Flow and Radial Flow Gas Turbines*, in *Turbomachinery Design and Theory*, accessed at http://www.himech.files.wordpress.com/2010/02/dke672_ch7.pdf
- [7] Klein S.A., and Alvarado F.L. (2014) *Engineering Equation Solver for Microsoft Windows Operating Systems*, F-Chart Software, Middleton, USA.
- [8] Dixon S.L. (1978, 1998), *Fluid mechanics and thermodynamics of turbomachinery*, Elsevier Butterworth-Heinemann, 30 Corporate Drive, Suite 400, Burlington, MA 01803, USA, Linacre House, Jordan Hill, Oxford OX2 8DP, UK, ISBN: 0-7506-7870-4, pp 98-100
- [9] Situmbeko, S.M. and Inambao, F.L. (2015), *Heat Exchanger Modelling for Solar Organic Rankine Cycle*, Int. J. of Thermal & Environmental Engineering, Vol. 9 No. 1; pp 7-16

Economic And Environmental Analyses Of A 10kwe Low Temperature Solar Thermal Power Plant

Shadreck M. Situmbeko, Freddie L. Inambao

University of KwaZulu-Natal, Durban, RSA;

Abstract

This aspect of the study is meant for the evaluation of the economic and environmental performance of the 10 kWe low temperature solar thermal energy conversion plant. It is part of a study to evaluate the feasibility of low temperature solar thermal energy conversion system based on the organic Rankine cycle (ORC) as a viable means of generating clean and environmentally sustainable electricity. The study was conducted at University of KwaZulu-Natal (UKZN), Durban, South Africa. The study is presented in two sections; the first being on the economic analysis and the second on the environmental analysis. The Cost-Benefit Analysis is used for the economic analysis and its output is in the form of Net Present Value (NPV) and Rate on Investment (ROI); the Life Cycle Analysis (LCA) method is used for the environmental analysis and its output is in the form of Carbon Pay Back Period (CPBP) and Carbon Intensity. Two other parameters are determined and may aid in assessing both the economic and the environmental performances and they are Energy Pay Back Period and Energy Intensity.

1. Introduction

Economic and environmental positivity's emanating from wider access to clean energy have been deliberated at length by several researchers and other personalities; they include improved standards of living (cleaner indoor environments, HVAC, lighting, cooking, food storage, telecommunication and entertainment) and improved industrial production (employment, production of consumer and industrial goods); environmental benefits include reductions in carbon emissions (normalising or reduced global warming, reduction in climate change, and less ozone layer depletion), reductions in exposure to radioactive radiation, and reduced degradation of local environments (low air pollution, low water pollution).

The analysis in this paper will attempt to qualitatively and quantitatively establish the environmental and economic performance of the 10kW low temperature solar thermal power concept plant.

2. 10kW Concept Plant Design

The plant consists of a solar field, pumps and field piping, storage tank, a complete IT10 ORC plant supplied by Infinity Turbine and a cooling tower. A schematic representation of the concept plant is shown in figure 1.

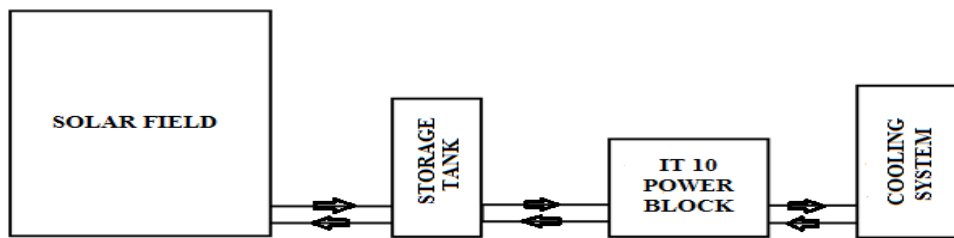


Figure 1: schematic representation of the final concept plant

The land requirement maybe calculated accurately taking into account geographical position of the field, shading, aperture area of the collectors and their orientation together with an analysis of the thermal losses from the field piping; however, as a general rule of thumb the size of land can usually be estimated by multiplying the total aperture area of the solar collectors by a factor of 2 to 3.5 [1]. For this concept plant with 180 solar collectors of 1840x1650 mm size, the area maybe estimated as $180 \times 1.84 \times 1.65 \times 2.5$ giving 1366.2 m². Allowing for spacing between the two fields, figure 12.2, and taking into account the space for the storage tank, cooling system and the IT10 ORC unit, a rough estimate of 1500m² of a piece of land 50m in length and 30m in width is considered adequate; a suitable remotely located, unused or disused cheap land would be attractive for this work; cost of the land estimated ZAR 50,000 to ZAR 100,000.

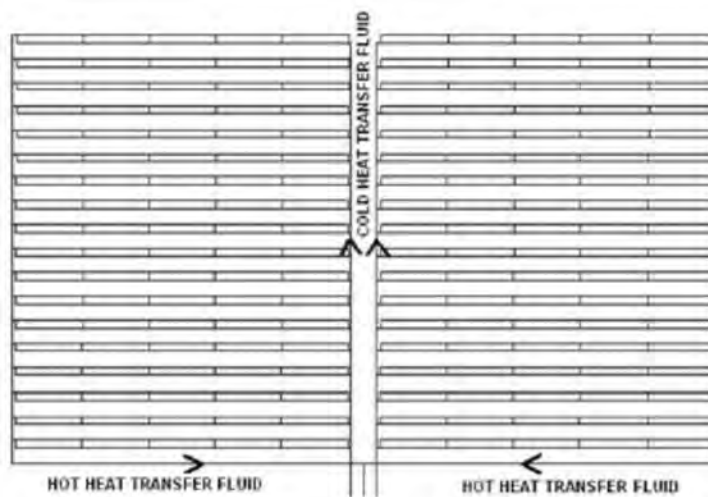


Figure 2: Layout for 180 solar collectors of the 10kWe solar field

Cost of the solar collectors: ZAR 1 260 000.00 (Solardome: SPX 3.0 Vertical: Solar Heating Collectors, Product code: SHC-S-SPX3.0-H, 1840 x 1650 x 76mm; price per collector Incl. Tax: R7, 000.00)

Cooling system: a small, compact, mechanical draught, dry cooling tower with a 44 gpm (gallons per minute) capacity is considered appropriate for this level of operation; more accurate design, modelling and optimized system can be developed. The cost is estimated as USD25-USD40 per gpm as initial investment and about USD6-USD10 per year per gpm as energy cost of operation. Cost of cooling system: USD 1500.00 \approx ZAR 20 000 (September 11, 2015) [2].

Pumping system: the pump cost required is for the solar field; the ORC unit comes complete with a feed pump while that for the cooling system is included in the cooling system cost estimates; solar field pump cost estimate: ZAR 5000. A combined pumping operational cost estimate will be adopted in the economic analysis \approx ZAR 12000 per year.

Field piping: high pressure, heat resistant, water flow pipe (PVC, flexible rubber hose, etc.) cost about USD 0.25 per meter; about 1500 meters required. Cost: USD 375 \approx ZAR 5000 [3].

Frame structure support for solar collectors (2000m of 30x30x4mm galvanised steel angle iron): estimate ZAR 100 000

Cost of ORC unit: USD 51 500 \approx ZAR 600 000

Working fluid: 58 kg of R134a (or 245fa); ZAR 4000 for 60 kg R134a.

Storage with pumping accessories: estimated ZAR 10,000.

Table 1 Cost Compilation for the 10 kWe Solar Thermal Power Plant

Component	Unit Price	Quantity	Sub-Total
Land		50 m x 30 m	100 000
Solar Collectors	7 000	180	1260000
Cooling Tower		01	20 000
Pumps		03	5000
Storage		01	10 000
Field Piping		PVC/Rubber Hose/PERT	5000
Frame Structure		30x30x4 mm Galvanised Steel	100 000
IT10 ORC Unit		01	600 000
Working Fluid: R134a		58kg	4000
Labour			100000
Total			ZAR 2 214 000

The price of electricity would normally be determined during the bidding process. For this analysis however tariffs obtained from the eThekweni Single-Phase Tariffs will be used; that is R1.3146/kWh [4]

3. Economic Analysis

Cost-benefit analysts typically use one of several metrics - or a combination of them - to report their findings. The benefit-cost ratio, return on investment and net present value report the results of a cost-benefit analysis by comparing discounted costs with discounted benefits.

Benefit-Cost Ratio (BCR): directly compares benefits and costs. To calculate the BCR, divide total discounted benefits by total discounted costs.

$$BCR = \frac{\text{Total Discounted Benefits}}{\text{Total Discounted Costs}} \quad [1]$$

Return on Investment (ROI): compares the *net benefit* (total discounted benefits minus total discounted costs) to costs. To calculate the ROI, first calculate the net benefits and then divide the net benefits by the total costs; expressed as a percentage.

$$ROI = \frac{(\text{Total Discounted Benefits} - \text{Total Discounted Costs})}{\text{Total Discounted Costs}}; (\%) \quad [2]$$

Net Present Value (NPV): reflects the net benefits of a project in ‘dollar’ terms. To calculate NPV, subtract the total discounted costs from the total discounted benefits.

$$NPV = \text{Total Discounted Benefits} - \text{Total Discounted Costs} \quad [3]$$

The formula for the NPV is as shown:

$$NPV = -I_{TOTAL} + \sum_{i=0}^n \frac{B}{(1+d)^n} \quad [4]$$

Where:

I_{TOTAL} = total investment cost
 B = yearly benefits of the 10kW solar plant
 d = discount rate
 n = number of years

The yearly benefits can be measured in several terms, i.e. avoided electricity costs, avoided wood fuel usage etc. To simplify the matter we adopt the former.

In this model we use a simplified equation for the NPV after ‘n’ years:

$$NPV = -I_{TOTAL} + \frac{B}{d} \left(1 - \frac{1}{(1+d)^n} \right) \quad [5]$$

The value of the discount rate is taken from analogous case studies. It has assumed value of 5%.

Energy Pay Back Period (EPBP): The energy benefit can be determined by Energy Pay Back Period (EPBP) which is given by the equation:

$$EPBP = \frac{\text{Energy consumed by power plant (kWh)}}{\text{Energy produced by power plant per year (kWh)}} \quad [6]$$

Energy Intensity: This energy benefit may also be represented by the energy intensity given by the equation:

$$\text{Energy Intensity} = \frac{\text{Total Input Energy (kWh)}}{\text{Life Time Electricity Production (kWh)}} \quad [7]$$

4. Environmental Analysis

The environmental analysis was done based on the **Life Cycle Analysis (LCA)** method which is a ‘cradle to grave’ analysis of environmental impacts, net energy and cost [5]. The following, figure 2, shows an LCA schematic representation of a solar power plant.

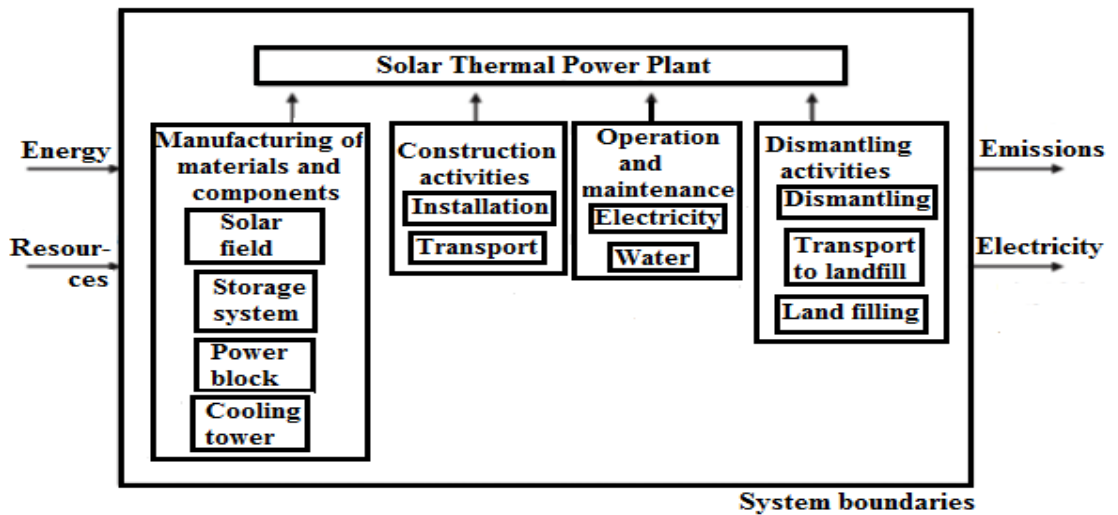


Figure 2: Life cycle of a solar thermal power plant

The environmental performance can be indicated by the Carbon Intensity and the Carbon Pay Back Period

Carbon Pay Back Period (CPBP): is a measure of how long a CO2 mitigating process needs to run to compensate the CO2 emitted to the atmosphere during the life cycle stage. The formula used is:

$$CPBP = \frac{\text{Life Cycle CO}_2 \text{ emission}}{\text{Gross CO}_2 \text{ emission avoided per year}} \times 365 \quad [8]$$

Carbon intensity: is the carbon emission associated with the manufacturing, operation and decommissioning of the power plant per unit of electricity produced over the life time. It is given by the equation:

$$\text{CO}_2 \text{ Intensity} = \frac{\text{Life Cycle CO}_2 \text{ emission (g of CO}_2\text{)}}{\text{Life time electricity generation (kWh)}} \quad [9]$$

5. Calculations

Notes regarding data used to perform analyses:

- Power Cost Calculations: price of electricity = 136c/kWh; increase in price per year = 15%; discounted rate = 5% [4]
- R134a is very attractive as a refrigerant because it has zero ozone depleting potential as well as a low direct global warming potential (GWP). [6]
- IT10 unit: 181 kg (un-crated); without proper data we assume the IT10 unit consists 90% steel and associated alloys; 2.5% copper; 2.5% aluminium and associated alloys; 2.5% rubber hoses; and 2.5% other metals.
- Power generated and Emissions Avoided: emissions avoided (Eskom average Emission Factor 1.015 kg CO₂-eqt/kWh)*power generated from IT10 plant per annum =30000kWh/annum: 30450 kg CO₂-eqt/annum. [7]
- Pump power estimated at 1% of produced power [8]: emissions 304 kg CO₂/annum; power 300 kWh/annum.

Table 2 shows the breakdown of cycle component prices under the current scenario where the power block is imported from Infinity Turbine and priced at R&D rates:

Table 2 cycle component prices

Component	Unit Price	Quantity	Sub-Total
Land		50 m x 30 m	100 000
Solar Collectors	7 000	180	126000 0
Cooling Tower		1	20 000
Pumps		3	5000
Storage		1	20 000
Field Piping		PVC/Rubber Hose/PERT	5000

Frame Structure		30x30x4 mm Galvanised Steel	100 000
IT10 ORC Unit		1	600 000
Working Fluid: R134a		58kg	4000
Labour			100000
Total			2 214 000

The NPV computations are done using Ms Excel spreadsheet. The results are shown in table 3.

Table 3 NPV computations

Year	Year	System Cost	Annual Cash Flow (ZAR)	NPV of Annual Cash Flow (ZAR)	Cumulative NPV (ZAR)
0	2015	-2 214 000	0.00	0.00	-2 214 000.00
1	2016		40392.00	38468.57	-2 175 531.43
2	2017		46450.80	42132.24	-2 133 399.18
3	2018		53418.42	46144.84	-2 087 254.34
4	2019		61431.18	50539.59	-2 036 714.76
5	2020		70645.86	55352.88	-1 981 361.88
6	2021		81242.74	60624.58	-1 920 737.29
7	2022		93429.15	66398.35	-1 854 338.94
8	2023		107443.52	72722.01	-1 781 616.94
9	2024		123560.05	79647.91	-1 701 969.03
10	2025		142094.06	87233.43	-1 614 735.60
11	2026		163408.17	95541.37	-1 519 194.23
12	2027		187919.39	104640.55	-1 414 553.68
13	2028		216107.30	114606.32	-1 299 947.36
14	2029		248523.40	125521.20	-1 174 426.16
15	2030		285801.91	137475.60	-1 036 950.55
16	2031		328672.19	150568.52	-886 382.03
17	2032		377973.02	164908.38	-721 473.66
18	2033		434668.98	180613.94	-540 859.72
19	2034		499869.32	197815.26	-343 044.45
20	2035		574849.72	216654.81	-126 389.64

Sensitivity analyses are also performed based on the assumption that the turbine unit and solar collectors are locally made at half prices (and cheap land is available) and the results are shown in table 4.

Table 5 shows computations for environmental analysis.

The two main references (databases) used as sources of information for embedded energy and carbon emissions are *Emission factors in kg CO₂-equivalent per unit* [9] and *Inventory of Carbon and Energy (ICE) Summary* [10].

6. Results

The results metrics are presented below:

Energy consumed by power plant (kWh) = 300 kWh/annum

Energy produced by power plant per year (kWh) = 30000kWh/annum

Total Output Energy (kWh) = 29700kWh/annum

Life Time Electricity Production (kWh) = X 20 years = 594000kWh

Table 4 NPV computations – Sensitivity Analysis:

Year	Year	System Cost	Annual Cash Flow (ZAR)	NPV of Annual Cash Flow (ZAR)	Cumulative NPV (ZAR)
0	2015	-1 234 000	0.00	0.00	-1 234 000.00
1	2016		40392.00	38468.57	-1 195 531.43
2	2017		46450.80	42132.24	-1 153 399.18
3	2018		53418.42	46144.84	-1 107 254.34
4	2019		61431.18	50539.59	-1 056 714.76
5	2020		70645.86	55352.88	-1 001 361.88
6	2021		81242.74	60624.58	-940 737.29
7	2022		93429.15	66398.35	-874 338.94
8	2023		107443.52	72722.01	-801 616.94
9	2024		123560.05	79647.91	-721 969.03
10	2025		142094.06	87233.43	-634 735.60
11	2026		163408.17	95541.37	-539 194.23
12	2027		187919.39	104640.55	-434 553.68
13	2028		216107.30	114606.32	-319 947.36
14	2029		248523.40	125521.20	-194 426.16
15	2030		285801.91	137475.60	-56 950.55
16	2031		328672.19	150568.52	93 617.97
17	2032		377973.02	164908.38	258 526.34
18	2033		434668.98	180613.94	439 140.28
19	2034		499869.32	197815.26	636 955.55
20	2035		574849.72	216654.81	853 610.36

Total embedded energy equals 635754.418 MJ or 176598.45 kWh

Gross CO₂ emission avoided per year = 30146kg

Life Cycle CO₂ emission = 35258.6 kg

Life Cycle CO₂ emission (g of CO₂) = 35 258 690 g

$$\text{Return on Investment (ROI)} = \frac{(126389.64)}{2214000} = -0.057$$

$$\text{Return on Investment (ROI) - Sensitivity Analysis} = \frac{853610.36}{2214000} = 0.386$$

Net Present Value (NPV): = ZAR-126 389.64 or ZAR (126 389.64)

Net Present Value (NPV) – Sensitivity Analysis: = ZAR 853 610.36

Table 5 environmental analysis:

Component	Description	Mass (kg)	Embedded Energy Index (MJ/kg)	Embedded Energy Content (MJ)	Embedded Carbon Emissions Index (kgCO ₂ eq/kg)	Embedded Carbon Emissions Content (kgCO ₂ eq)
IT10	Steel	162.9	24.4	3974.76	1.77	290
	Copper	4.525	50	226.25	2.77	12.5
	Aluminium	4.525	155	701.375	8.14	36.8
	Rubber hose	4.525	101.7	460.1925	3.18	14.4
	Others	4.525	-		4.4	19.9
Sub-Total				5362.5775		373.6
Solar Field	Galvanised steel 30x30x4 mm	3768	24.4	91939.2	1.77	6670
	0.5mm Galvanised steel casing	2200	24.4	53680	1.77	3894
	4mm Solar Glass	5720	15	85800	0.85	4862
	40mm Insulation	1400	45	63000	1.86	2604
	15mm Copper pipes	3263	50	163150	2.77	9038

	0.5mm Copper absorber	2500	50	125000	2.77	6925
	Rubber hose	60	101.7	6102	3.18	190
	Black paint	50 (546.48 m ²)	68 (/m ²)	37160.64	3	150
	Other		-			ignore
Sub-Total				625831.84		34333
Storage	Insulated & vented Tank					
	pumping energy – covered under operational energy and emissions					
Sub-Total						ignore
Cooling	mainly consists of pumping energy – covered under operational energy and emissions					
Sub-Total						ignore
Construction & Installation	Concrete (hard surface for equipment)	2m ³ (4800 kg)	0.95	4560	263/m ³	526
	Transport	100 km	-		0.26/km	26
Sub-Total				4560		552
TOTAL				635754.418		35258.6

Energy Pay Back Period (EPBP):

$$EPBP = \frac{\text{Energy consumed by power plant (kWh)}}{\text{Energy produced by power plant per year (kWh)}} = \frac{176598.45}{29700} = 5.95 \text{ years}$$

Energy Intensity:

$$\text{Energy Intensity} = \frac{\text{Total Input Energy (kWh)}}{\text{Life Time Electricity Production (kWh)}} = \frac{176598.45}{594000} = 0.2973$$

Carbon Pay Back Period (CPBP):

$$CPBP = \frac{\text{Life Cycle CO}_2 \text{ emission}}{\text{Gross CO}_2 \text{ emission avoided per year}} \times 365 = \frac{35258.6}{(30450-304)} \times 365 = 426.9 \text{ days}$$

Carbon intensity:

$$\text{CO}_2 \text{ Intensity} = \frac{\text{Life Cycle CO}_2 \text{ emissions (g of CO}_2\text{)}}{\text{Life time electricity generation (kWh)}} = \frac{35258.6 \times 1000}{594000} = 59.36 \text{ g/kWh}$$

7. Discussion and Conclusion

It is evident from the negative NPV value (ZAR–126 389.64) that under the current scenario the 10 kW Low Temperature Solar Thermal Concept Power Plant is not an attractive investment option, economically. This is mainly due to the higher initial capital requirements, resulting largely from the higher costs of the IT10 power block (ZAR600 000), which is charged at research and development (R&D) rates, and the Solar Field (ZAR 1 260 000 solar collectors only). Under an assumed scenario, where the power block and the solar collectors are designed and produced locally (solar water heater collectors have been developed and tested at the UKZN over the past few years [10.11], [10.12]), their costs could drop to 50% or lower, the NPV realised becomes positive (ZAR+853 610.36); commercially available larger turbine generators in the Megawatt range cost from USD450 to USD 950 per kW [13]; a similarly rated 10kW natural gas generator supplied locally by Bundu Power, Johannesburg, South Africa is priced at ZAR67 932.60 [14].

The energy payback period (EPBP) was obtained as six years; this is considered comparable with other similar technologies. A typical solar power system is reported to payback after about four years, a photovoltaic system between one-and-half and three-and-half years, while a small wind turbine could take between fifteen to fifty years [15], [16].

Carbon payback period (CPBP) on the other hand was computed as 426.9 days (1.17 years); this figure too is comparable with what has been obtained by other researchers such as 2.21 years obtained for a solar water heater by Marimuthu C. and Kirubakaran V. [17], and carbon payback periods (excluding transport) obtained as 6.0, 2.2, and 1.9 years respectively for PV system, solar thermal-individual and solar thermal-community by Croxford Ben and Scott Kat [18].

The results obtained here are considered partial or conservative because the scrap and recycling values of the materials or components following decommissioning has not been taken into account; this would reduce the embodied energy and emissions.

The implications of these analyses do indicate that the low temperature solar thermal concept plant has potential to be a net clean energy producer both cost effectively and environmentally beneficially.

References

- [1] Stine William B. and Geyer Michael, Power from the Sun, 2001, available at www.powerfromthesun.net/book.html
- [2] Lipták BG., *Cooling Tower Control*, in Control And Optimization of Unit Operations, in Process Control and Optimization, Instrument Engineers' Handbook, Fourth Edition, Volume II, Taylor And Francis, 2006, Pp 1794-1808
- [3] <http://www.alibaba.com/showroom/heat-resistant-water-pipe.html>

- [4] <http://businessstech.co.za/news/energy/88524/how-much-electricity-costs-in-south-africas-biggest-cities/>
- [5] Ref: ILCD Handbook: Analysing of existing Environmental Impact Assessment methodologies for use in Life Cycle Assessment First edition © European Union, 2010; europa.eu/; eplca.jrc.ec.europa.eu/uploads/ILCD-Handbook-LCIA-Background-analysis-online-12March2010.pdf
- [6] <http://www3.nd.edu/~enviro/design/r134a.pdf>
- [7] Letete T., et al., *Topic 3, Carbon Accounting for South Africa*, in Information on climate change in South Africa: greenhouse gas emissions and mitigation options, Energy Research Centre, available at www.erc.uct.ac.za/Information/Climate
- [8] Kroos Kenneth A., and Potter Merle C., *Thermodynamics for Engineers*, Cengage Learning, Timothy Anderson, ISBN-13: 978-1-133-11286-0, 2015, p282
- [9] http://www.winnipeg.ca/finance/findata/matmgt/documents/2012/682-2012/682-2012_Appendix_H-WSTP_South_End_Plant_Process_Selection_Report/Appendix%207.pdf
- [10] Hammond GP., and Jones CI., *Inventory of Carbon and Energy (ICE), Version 1.6a*, in Embodied Energy and Carbon in Construction Materials, Proc. Institution of Civil Engineers: Energy, University of Bath, UK, 2008, pp12-17 found at www.bath.ac.uk/mech-eng/sert/embodied/
- [11] Babulall M. et al, *Design of a Domestic Solar Water Heating System*, BSc Design and Research Project Thesis, University of KwaZulu-Natal, 2008.
- [12] Balwanth A. et al, *Design of a Solar Dryer System for Agricultural and Marine Products*, BSc Design and Research Project Thesis, University of KwaZulu-Natal, 2009.
- [13] Pauschert Dirk, *Study of Equipment Prices in the Power Sector*, Energy Sector Management Assistance Program (ESMAP) Technical Paper 122/09, International Bank for Reconstruction and Development, WORLD BANK GROUP, Washington, D.C. 20433, U.S.A., , 2009, p10 available at www.esmap.org/sites/esmap.org/files
- [14] <http://www.bundupower.co.za>
- [15] <http://www.solarserver.com/knowledge/lexicon/e/energy-payback-period.html>
- [16] <http://www.poplarnetwork.com/news/small-wind-turbine-what-payback-period>
- [17] Marimuthu C. and Kirubakaran V., *Carbon Payback Period and Energy Payback Period for Solar Water Heater*, International Research Journal of Environment Sciences, Vol. 3(2), 93-98, February (2014, ISSN 2319–1414, pp 93-98
- [18] Croxford Ben and Scott Kat, *Can PV or Solar Thermal Systems be Cost Effective Ways of Reducing CO₂ Emissions for Residential Buildings?*, Bartlett School of Graduate Studies, University College London, available at <http://discovery.ucl.ac.uk/2642/1/2642.pdf>

ORC Condenser Heat Exchanger Design and Modelling

Shadreck M. Situmbeko

University of Botswana, Gaborone, Botswana;
University of KwaZulu-Natal, Durban, RSA;

Freddie L. Inambao

University of KwaZulu-Natal,
Durban, RSA;

Abstract- The paper presents work done on the development of a condenser heat exchanger model suitable for incorporation into a low temperature solar thermal power cycle based on the organic Rankine cycle (ORC); it presents the mathematical and computer models of a flow of vapour over a bundle of horizontal tubes. Although the process of condensation finds application in a lot of industrial systems, the concept itself is still not yet well defined as a scientific notion and is still a subject of investigation; a number of empirical correlations that have been proposed are reviewed in this research and are to be evaluated against the results of experimental investigations. The working fluid is modelled from five organic fluids being R123, R134a, R245fa, n-butane and isobutene; the cooling liquid is placed on the tube side and consists of ethylene glycol at 50 % concentration. The condenser model is implemented on the engineering equation solver platform. The current study presents the preliminary results of the mathematical and computer analyses. The results are in the form of condensation heat transfer coefficients and rate of heat transfer for each tube in a vertical fire tube bundle.

Keywords: Condensation heat transfer coefficients, bundle of horizontal tubes, engineering equation solver

Nomenclature:

Roman Symbols

A	surface area at nominal diameter (m ²)
A _f	fin surface area (m ²)
A _r	tube surface area at the base of the fins (m ²)
D	tube diameter (m)
D _r	diameter at fin root (m)
F	a constant accounting for the effect of physical properties
h _{fg}	latent heat of condensation (J/kg)
g	gravitational acceleration (m/s ²)
h	heat transfer coefficient (W/m ² .K)
k	thermal conductivity of condensate (W/m ² .°C)
L _c	L _c is the characteristic length (m)
N	number of tubes
Nu	Nusselts' number
T	Temperature (°C)

Greek Symbols

η	fin efficiency
μ	dynamic viscosity (kg/m.s)
ρ	Density (kg/m ³)

Subscripts

G	vapour phase
i	inside
L	liquid phase
o	outside
sat	saturation state
w	tube wall

I. INTRODUCTION

Condensation is the heat transfer process by which a saturated vapour is converted into a saturated liquid by means of removing the latent heat of condensation; it occurs when the enthalpy of the vapour is reduced to the state of saturated liquid.

Condensation occurs through one or a combination of four basic mechanisms of drop-wise, film-wise, direct contact, and homogeneous [1]. Drop-wise refers to a situation whereby the vapour condenses as liquid drops at particular nucleation sites on the cooling surface and remains as drops until carried away by gravity or vapour shear; in film-wise condensation, the liquid drops coalesce into a continuous thin liquid film; and in direct contact condensation, the vapour condenses directly onto the coolant liquid that has been sprayed into the vapour; whilst in homogenous condensation the super-saturated vapour condenses in space away from any macroscopic surfaces similar to the formation of fog possibly on dust or other particles acting as nucleation sites [2]; refer to figure 1.

The majority of industrial condensation processes are considered to be based on the film-wise mode of condensation. In this research work the study of the condenser is particularly directed towards the development of a low temperature solar thermal power plant as depicted in figure 2, below:

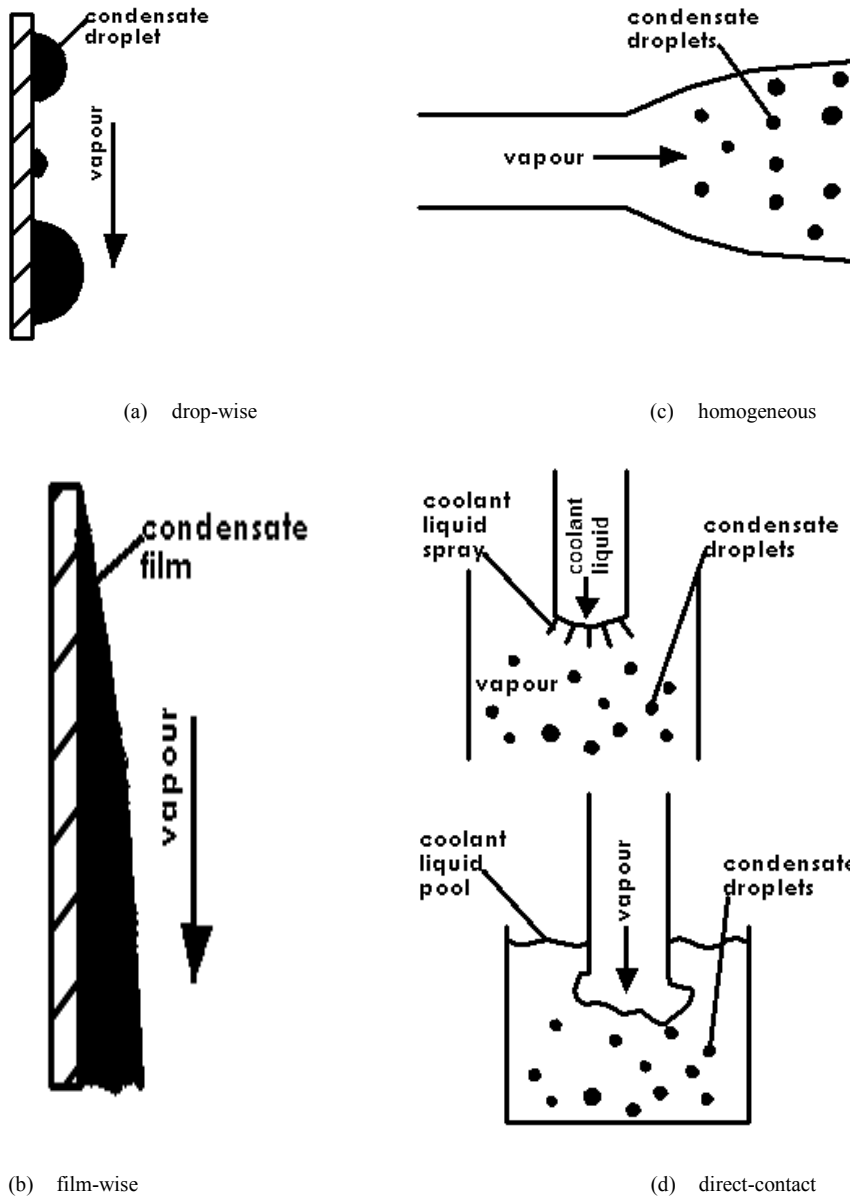


Figure 1: four condensation mechanisms

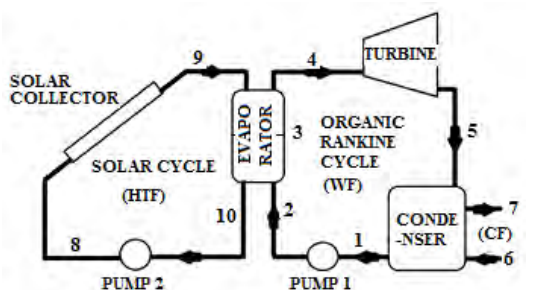


Figure 2: solar thermal power plant concept [3] (HTF: heat transfer fluid; WF: working fluid; CF: cooling fluid)

II. THE THEORY OF CONDENSATION

The theory of film condensation based on the Nusselt (1916) integral model for film condensation on a vertical plate and later extended to cover condensation on a horizontal bundle of tubes has been well documented by

Thome J.R. [1] and this theory forms the basis for the condenser model presented in this chapter; derivations of the formulae are considered outside the scope of this work and thus only the key equations are shown here.

Comparison of condensation heat transfer correlations for flow of refrigerants in horizontal smooth tube bundles has been presented by Santa Róbert [4].

A detailed comparison of condensation heat transfer correlations for different flow configurations including flow inside and outside of horizontal, vertical and inclined tubes has also been presented by Fang Xiande et al [5].

Two correlations can be identified for flow outside a single horizontal tube and these are the Nusselt (1916) and the Dhir and Lienhard (1971) correlations; these are similar in every respect and only differ in the prefix multiplier constant (number):

The correlation due to Nusselt (1916) is given as:

$$h=0.725 \left[\frac{\rho_L(\rho_L-\rho_G)gh_{fg}k_L^3}{\mu_L D_o (T_{sat}-T_w)} \right]^{\frac{1}{4}} \quad (1)$$

The correlation given by Dhir and Lienhard (1971) proposed the following average heat transfer coefficient:

$$h=0.729 \left[\frac{\rho_L(\rho_L-\rho_G)gh_{fg}k_L^3}{\mu_L D_o (T_{sat}-T_w)} \right]^{\frac{1}{4}} \quad (2)$$

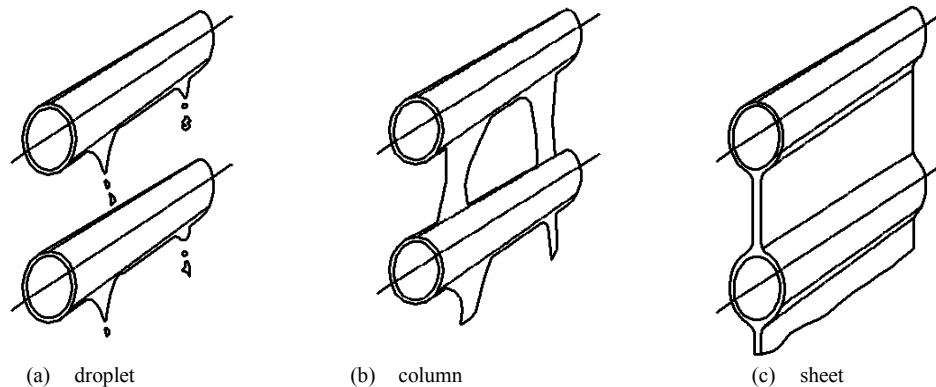


Figure 3: condensate inundation modes

Three correlations can be identified for flow outside a bundle of horizontal smooth tubes; these are Nusselt's (1949), Kern's (1958) and Eissenberg's (1972).

Nusselt's correlation gives the mean heat transfer coefficient as well as a coefficient for each of the tubes based on the coefficient for the first tube, as expressed by (1); the two equations for this correlation are as follows in (3) and (4):

$$\frac{\bar{h}}{h(N=1)} = N^{\frac{1}{4}} \quad (3)$$

$$\frac{h(N)}{h(N=1)} = N^{\frac{3}{4}} - (N-1)^{\frac{3}{4}} \quad (4)$$

Incropera and DeWitt (2002) also proposed a similar average heat transfer coefficient for vertically aligned horizontal tube bundles; their correlation, however, suggests using the Dhir and Lienhard (1971) correlation for the reference heat transfer coefficient, [7].

The correlation due to Kern (1958) gives:

$$\frac{\bar{h}}{h(N=1)} = N^{\frac{1}{6}} \quad (5)$$

$$\frac{h(N)}{h(N=1)} = N^{\frac{5}{6}} - (N-1)^{\frac{5}{6}} \quad (6)$$

The Butterworth and Eissenberg's (1972) correlations are only for the mean heat transfer coefficient and for a

The flow over a bundle is affected by condensate inundation; condensate inundation refers to the effect of condensate falling onto a tube from upper tubes in the tube bank. Condensate inundation modes include droplet, column and sheet; at higher inundation rates the inundation may progress into a spray mode which may involve side drainage, splashing and ripples on the lower tubes; see figure 3, below, [6].

staggered arrangement of vertical tubes; the correlations are expressed as, [8]; [9]:

$$\frac{Nu}{Re_G^{1/2}} = 0.416 \left[1 + \left(1 + 9.47 \frac{gD\mu_L h_{fg}}{u_G^2 k_L (T_{sat}-T_w)} \right)^{0.5} \right]^{0.5} \quad (7)$$

$$\frac{\bar{h}}{h(N=1)} = 0.6 + 0.42N^{\frac{1}{4}} \quad (8)$$

Beatty and Katz (1948) correlation provides for condensation on low-finned tubes and their correlation together with supporting equations is given as: [5].

$$h = 0.689F^{0.25} \left[\frac{A_r}{A} \frac{1}{D_r^{0.25}} + 1.3\eta \frac{A_f}{A} \frac{1}{L_c^{0.25}} \right] \quad (9)$$

$$F = \left(\frac{\rho_L^2 g k_L^3 h_{fg}}{\mu_L (T_{sat}-T_w)} \right) \quad (10)$$

$$L_c = \frac{\pi(D_o^2 - D_f^2)}{4D_o} \quad (11)$$

$$A = A_r + A_f(4d) \quad (12)$$

where η is the fin efficiency, A is the tube surface area at nominal diameter (m^2), A_r is the tube surface area at the base of the fins (m^2), A_f is the fin surface area (m^2), D_r is the diameter at fin root, F is a constant accounting for the effect of physical properties, and L_c is the characteristic length.

III. MATHEMATICAL MODELLING

The governing equations used in this model are as follows: The overall heat transfer coefficient for each tube is given by:

$$U[i]A_o = \frac{1}{\frac{1}{h_{CF}A_i} + \frac{R''_{fi}}{A_i} + \frac{\ln\left[\frac{D_o}{D_i}\right]}{2\pi k_w L_{tube}} + \frac{1}{h_{WF}[i]A_o} + \frac{R''_{fo}}{A_o}} \quad \text{for } i=1 \text{ to } N \quad (13)$$

where $h_{WF}[i]$ is determined from the correlations of section 3 and h_{CF} is determined from the Gnielinsk correlation given by:

$$\frac{h_{CF}D_i}{k_{CF}} = \frac{\frac{f_{CF}}{8}(Re_{DCF}-1000)Pr_{CF}}{1+12.7\left[\frac{f_{CF}}{8}\right]^{1/2}(Pr_{CF}^{2/3}-1)} \quad (14)$$

These are used to determine the heat transfer for each tube; total heat exchange is then given as:

$$Q_{COLUMN} = \sum_i^N Q[i] \quad (15)$$

$$Q_{TOTAL} = M * Q_{COLUMN}$$

Where N is the number of tubes in each column and M is the number of columns. The logarithmic mean temperature difference (LMTD) method is used together with the number of transfer units (NTU) method to determine the heat transfer for each tube.

The input conditions are taken as:

- The working fluid is any of: R123, R134a, R245fa, n-butane and isobutene;
- The cooling fluid is ethylene glycol at 50% concentration;
- $T_{WF} = 50^\circ\text{C}$ as the condensate temperature; $T_{CF,i} = 25^\circ\text{C}$ as the cooling fluid inlet temperature;
- Copper tubing is used for the tube bundles: inside diameter 16.5 mm, outside diameter 19 mm and length 2.85 m

Equations that are also useful in formulating the mathematical models are those obtained from Nusselt's Integral method and may be expressed as:

$$\Gamma = 1.924 \left[\frac{\Gamma^3 k_L^3 (T_{sat} - T_w)^3 (\rho_L - \rho_G) g}{h_{fg} \frac{3\mu_L}{\rho_L}} \right]^{1/4} \quad (16)$$

where Γ is the condensate mass flow rate on one side of the tube, per unit length of the tube, (kg/m.s); from this equation the overall heat transfer for a single tube can be expressed as:

$$\dot{Q} = 2\Gamma L_{tube} h_{fg} \quad (17)$$

where h_{fg} is the latent heat of condensation, (J/kg)

IV. COMPUTER SIMULATIONS

Four sets of simulations have been performed as follows:

- The first simulations are based on Nusselt's correlations for the heat transfer coefficient for the first tube, for the mean heat transfer coefficient for a column of N tubes, and the heat transfer coefficients for tubes 2 up to N.
- The second set of results use Nusselt's correlations for the first tube; and then uses Kern's method for the mean heat transfer coefficient as well as for the tubes 2 to N.
- The third set of simulations uses the Dhir and Lienhard correlation for the first tube and then uses the Nusselt's correlations for the mean and for tubes 2 to N.
- The fourth set uses the Dhir and Lienhard correlation for the first tube and then uses the Kern's method for the mean and for tubes 2 to N.

Working fluids used are R245fa, R134a, R123, n-butane and isobutene. The results are compiled for each working fluid and compared on the basis of the correlations.

The simulations were done for only the 10 kWe concept cycle plant; sizing is based on the thermal load of 84.2 kW_{th} determined from cycle efficiencies in the range 10-15% obtained from the initial system model thus giving an average cycle efficiency of 12.5% [3].

V. RESULTS

▪ Condensate Heat Transfer Coefficients

The results for the condensate heat transfer coefficients based on different correlations are shown in the charts of figures 4 to 7.

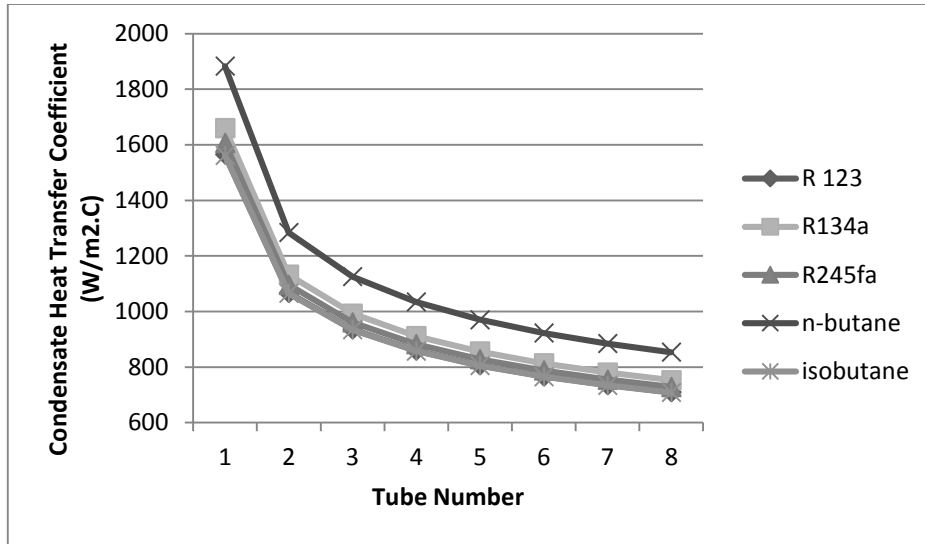


Figure 4: tube heat transfer coefficients based on Nusselts Correlations

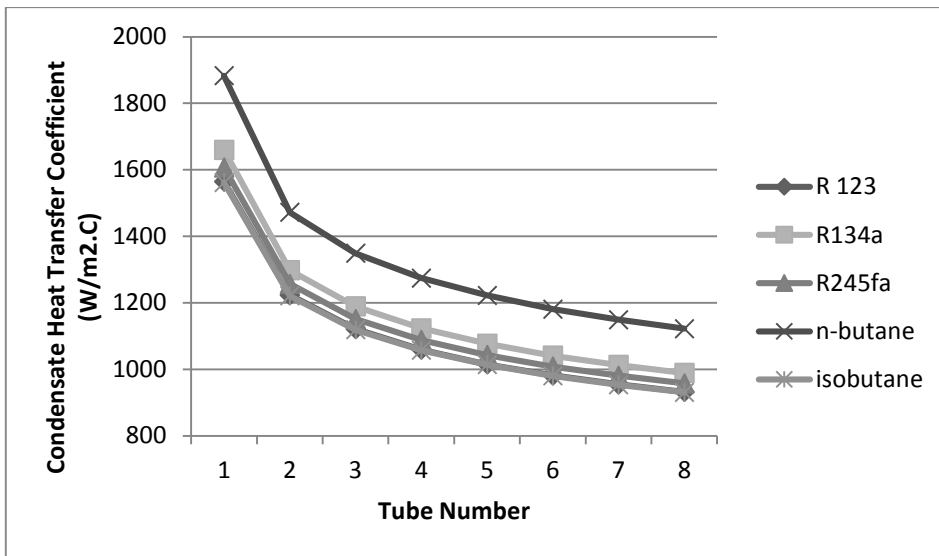


Figure 5: tube heat transfer coefficients based Nusselts and Kerns Correlations

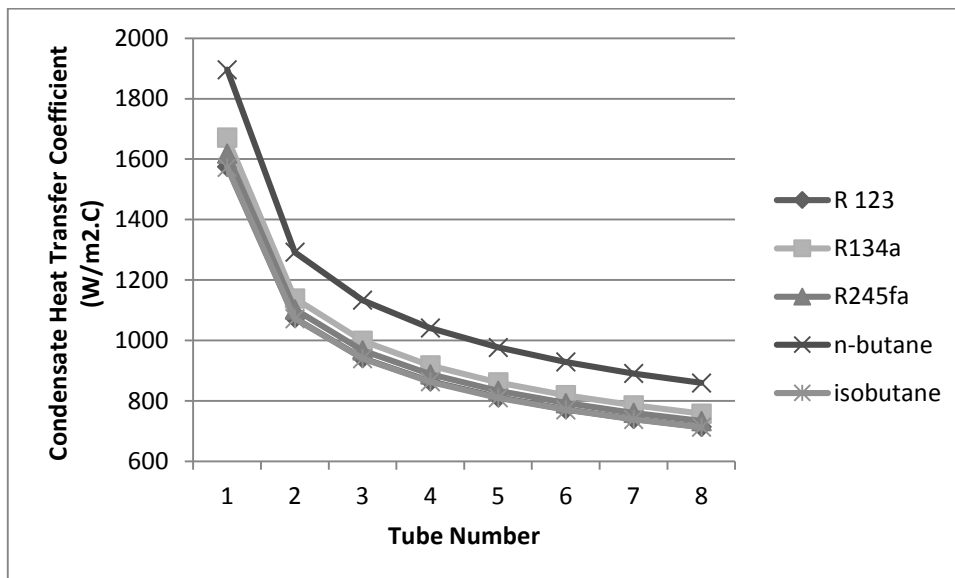


Figure 6: tube heat transfer coefficients based on Dhir and Lienhard, and Nusselts Correlations

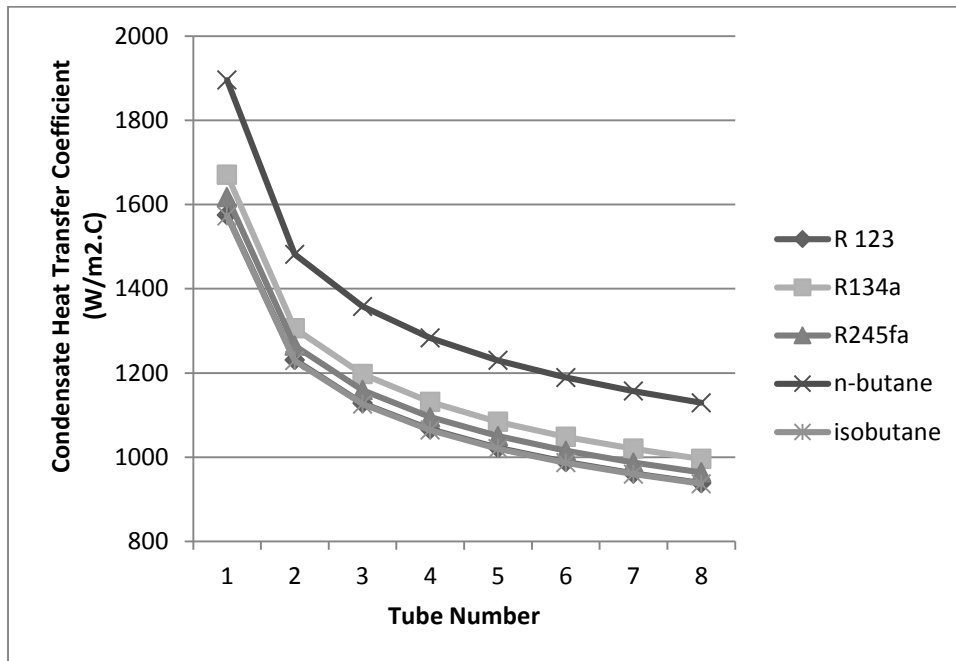


Figure 7: tube heat transfer coefficients based on Dhir and Lienhard, and Kerns Correlations

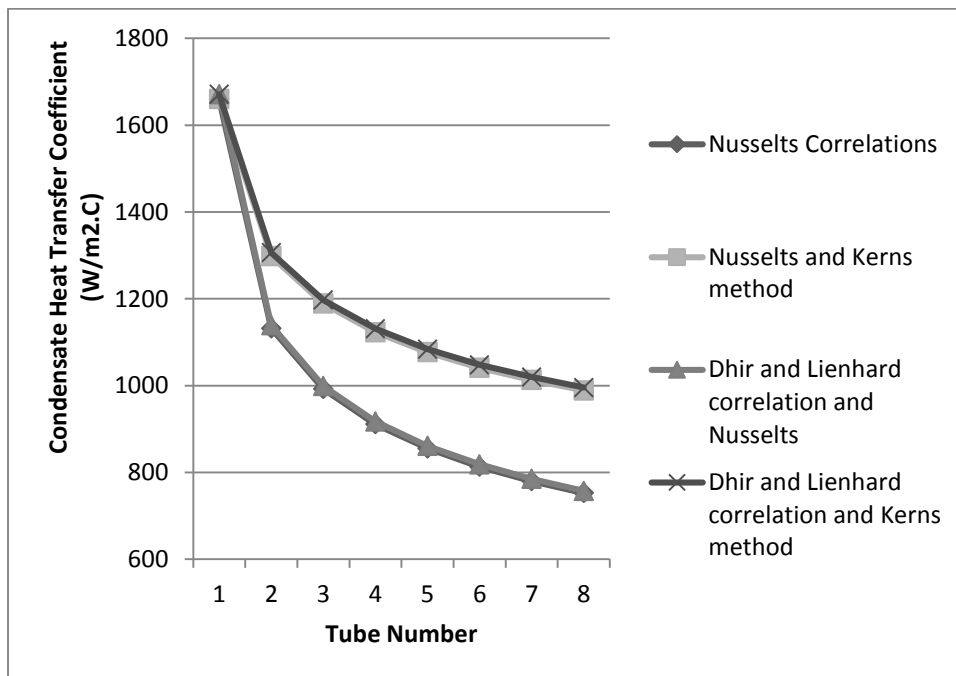


Figure 8: Condensate Heat Transfer Coefficient for R134a based on different combinations of Correlations

▪ Heat Transfer Rates

The total thermal loads per column data is captured for each working fluid and for each combination of correlations and the results are presented in the following table 1.

The overall heat exchanger thermal loads for each working fluid are shown in figure 9.

▪ Cooling Fluid Outlet Temperature

The average outlet temperatures of the ethylene glycol cooling fluid for each of the working fluids are shown in figure 10; the inlet temperature is assumed as 25°C whilst the condensation temperature is taken as 50°C.

TABLE 1: THERMAL LOADS PER COLUMN FOR EACH WORKING FLUID AND FOR EACH CORRELATIONS COMBINATION

WORKING FLUIDS	R 123	R134a	R245fa	n-butane	isobutane
CORRELATIONS	(W)	(W)	(W)	(W)	(W)
Nusselt's	14199	14585	14374	15402	14189
Nusselt's & Kerns	15470	15851	15643	16647	15461
Dhir and Lienhard & Nusselt's	14242	14628	14418	15444	14231
Dhir and Lienhard & Kern's	15512	15892	15685	16687	15502

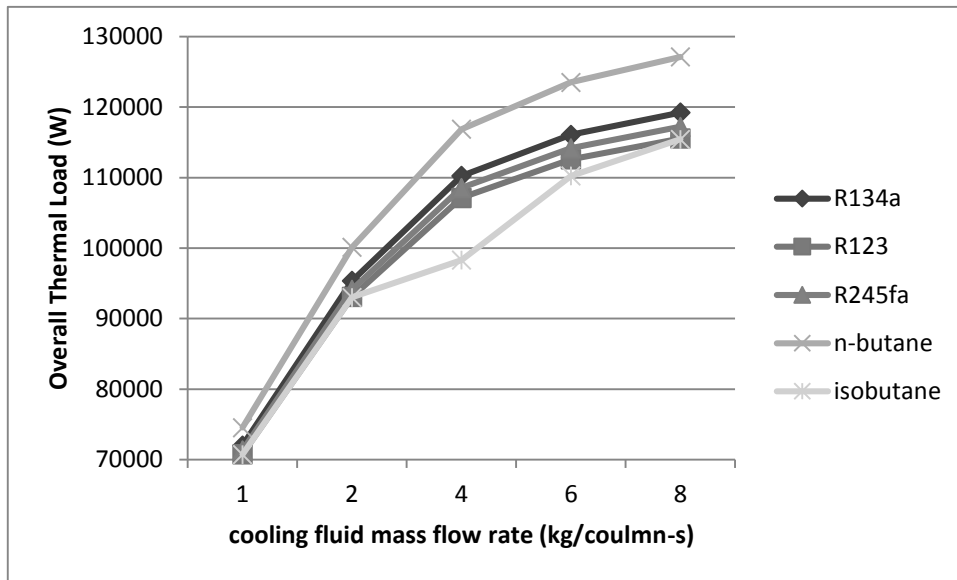


Figure 9: Overall Thermal Load versus cooling fluid column mass flow rate (based on Dhir and Lienhard, and Kerns Correlations)

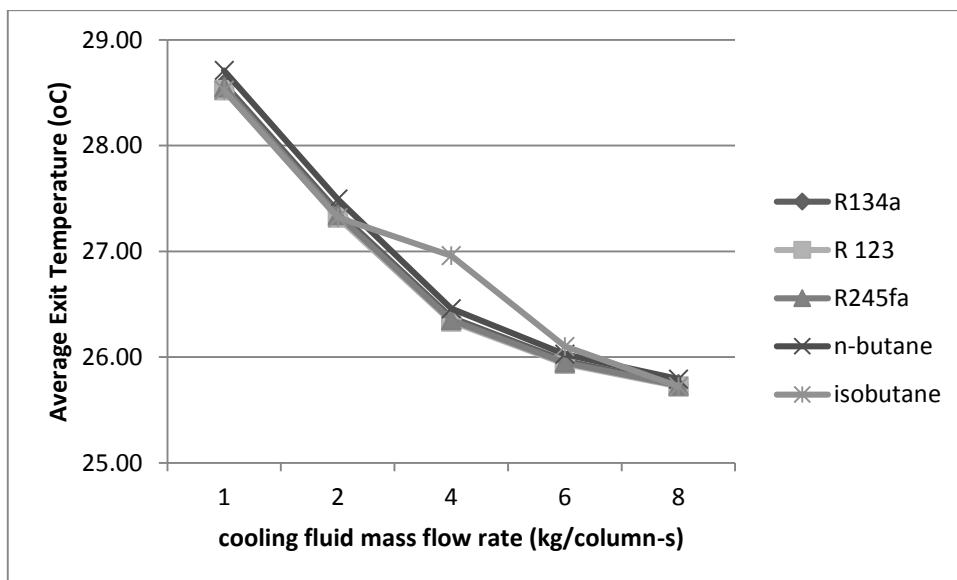


Figure 10: average cooling fluid exit temperature versus cooling fluid column mass flow rate (based on Dhir and Lienhard, and Kerns Correlations)

VI. DISCUSSIONS

Figure 4 to 7 show that for all combinations of correlations two observations can be made: condensate heat transfer coefficient varies from a high on the first tube to a minimum on the last tube; and condensate heat transfer coefficients are highest with n-butane, followed by R134a, R245fa, and are lowest for R123 and isobutene; plots of values for the latter two appear superimposed.

Figure 8 shows that Kerns method gives higher values of the condensate heat transfer coefficient, varying from about 900 to 1900 W/m².°C, as compared to the Nusselts correlation, where corresponding values vary from about 700 to 1900 W/m².°C. The heat transfer coefficient for the first tube is almost the same regardless of whether the Nusselts or the Dhir and Lienhard correlation is used.

In terms of thermal loads, table 1 and figure 9 show that n-butane gives the highest value followed by R134a, R245fa, and R123, with the lowest being obtained with isobutene.

The average outlet temperatures of the ethylene glycol cooling fluid for each of the working fluids, figure 10, show a continuous decline with increases in cooling fluid mass flow rate; also n-butane gives the highest outlet temperatures; all the other fluids show superimposed plots of the outlet temperatures; outlet temperatures vary from a maximum of about 28.5°C to a minimum of about 25.8°C.

VII. CONCLUSIONS

The paper has presented a condenser heat exchanger model suitable for incorporation into a low temperature solar thermal power cycle. The model consists of a flow of vapour over a bundle of horizontal tubes. The simulations have shown the effect of condensate inundation in reducing the heat transfer capacity of tubes low down in a column of horizontal tubes. The simulations have also shown that Nusselts correlations give more conservative values when compared to the Kerns method. All the working fluids depict similar device thermal exchange characteristics; n-

butane performs better than the other fluids whilst R123 and isobutene give the worst performance. Sizing of the heat exchanger is determined by the number of tube rows and columns; in this case, the simulations showed that 8 rows by 6 columns would be adequate for the given heat exchanger configuration and thermal load. These results are to be compared with the results of the on-going experiments.

ACKNOWLEDGMENTS

The authors would like to thank the Centre for Engineering Postgraduate Studies (CEPS) at University of KwaZulu-Natal for providing funds for certain aspects of the research as well as all colleagues, postgraduate students and staff of the section.

REFERENCES

- [1] Thome J.R. Engineering Data Book III; chapter 7: Condensation on External Surfaces, Laboratory of Heat and Mass Transfer, Swiss Federal Institute of Technology. Lausanne, Switzerland.
- [2] Thome J.R. Engineering Data Book III, Chapter 7, Fundamentals of Condensation on Tubes and Tube Bundles, Laboratory of Heat and Mass Transfer. Swiss Federal Institute of Technology. Lausanne, Switzerland.
- [3] Situmbeko SM., Inambao FL, Heat Exchanger Modelling for Solar Organic Rankine Cycle, paper accepted for publication in the International Journal of Thermal and Environmental Engineering, August, 2014
- [4] Sánta Róbert, The Analysis of Two-Phase Condensation Heat Transfer Models Based on the Comparison of the Boundary Condition in Acta Polytechnica Hungarica, Vol. 9, No. 6, 2012
- [5] Wei Xiaoyong, Fang Xiandel, and Shi Rongrong, A Comparative Study of Heat Transfer Coefficients for Film Condensation, Energy Science and Technology, Vol. 3, No. 1, 2012, pp. 1-9
- [6] <http://www.thermopedia.com/content/1210/>
- [7] Incropera FP, DeWitt DP. Fundamentals of heat and mass transfer (6th Ed.) Wiley.
- [8] Butterworth D. Developments in the design of shell and tube condenser. ASME; 1977. Paper 77-WA/HT-24.
- [9] Eissenberg DM. An investigation of the variable affecting steam condensation on the outside of a horizontal tube bundle. PhD thesis, University of Tennessee, Knoxville; 1972.
- [10] Klein S.A., and Alvarado F.L. Engineering Equation Solver for Microsoft Windows Operating Systems. F-Chart Software, Middleton, USA. 2013.

Heat Exchanger Modelling for Solar Organic Rankine Cycle

S.M. Situmbeko*, F.L. Inambao

University of KwaZulu-Natal, Durban, South Africa

Abstract

The paper presents work done on the development of a heat exchanger model suitable for incorporation into a low temperature solar thermal power cycle. In particular it presents the mathematical model comprising heat transfer, mass transfer, and convective heat transfer coefficients, and velocity and pressure drop correlations for single and two phase flows. The preliminary evaporator model is based on a counter flow double pipe configuration; the flow boiling process incorporates both convective and nucleate boiling. The shell side heat transfer fluid consists of ethylene glycol at 50 % concentration; the tube side fluid flow is modelled on four candidate working fluids pre-selected from previous stages of the research study. The evaporator model is implemented on the engineering equation solver platform; following on the computer simulation results a further proposal is made for conversion of the model design into a feasible shell-and-tube heat exchanger. The outputs of the model study are in the form of the rate of heat exchange, size and type of the heat exchanger, whilst ensuring that the pressure drops and fluid velocities are within acceptable limits.

Keywords: *low temperature solar thermal, convective and nucleate boiling, engineering equation solver.*

1. Introduction

The paper presents research done on the design of heat exchangers for the low temperature solar thermal conversion system based on the organic Rankine cycle (ORC). Figure 1 shows the general configuration of the basic ORC cycle; the cycle constitutes three major components that involve thermal energy exchanges, being the solar collector, the evaporator and the condenser; a solar thermal conversion cycle may incorporate other types of heat exchangers such as a preheater, a superheater and a recuperator. This paper presents the development of a design model for an evaporator heat exchanger.

The evaporator heat exchanger, also known as a boiler or vapouriser, entails two types of heat exchanges, sensible and latent heat exchanges, the processes 2-3 and 3-4 respectively shown in the Temperature-entropy (T-s) diagram of figure 2. In figure 2, $T_{H,i}$ is the temperature of the heat transfer fluid at the entrance to the heat exchanger; it can also be considered equal to the solar thermal storage temperature, assuming minimum thermal losses in the piping connecting the two

components; $T_{H,o}$ is the return temperature of the heat transfer fluid after the heat exchange process; $T_{H,s}$ is an arbitrary temperature along the heat transfer fluid flow stream that corresponds to the commencement of phase change along the working fluid flow stream; point 3 is otherwise also referred to as the pinch point.

2. Description of Model

In this part of the modelling process we develop a more detailed model of the evaporator. Specifying the heat exchanger type, materials as well as operating parameters. This information is helpful in the eventual specification of the heat exchanger to be incorporated in the solar power cycle.

The evaporator model is developed as two co-joined heat exchangers, the preheater for the sensible heating of the working fluid from the sub-cooled liquid state to the saturated liquid state and the vapouriser for the latent heating of the working liquid from the saturated liquid state to the saturated vapour state; the working fluids selected are those with near-to-isentropic turbine expansion thus not requiring superheating.

* Corresponding author. Tel.: +27710570753

Fax: +27 31 260 1233; E-mail: ssitumbeko@yahoo.com

© 2015 International Association for Sharing Knowledge and Sustainability

DOI: 10.5383/ijtee.09.01.002

The evaporator heat exchanger is initially modelled as a double pipe counter current flow heat exchanger as shown in the following figure 3; other operating parameters are also listed in table 1. In figure 3, numbers 2, 3 and 4 refer to fluid flow positions as in figures 1 and 2.

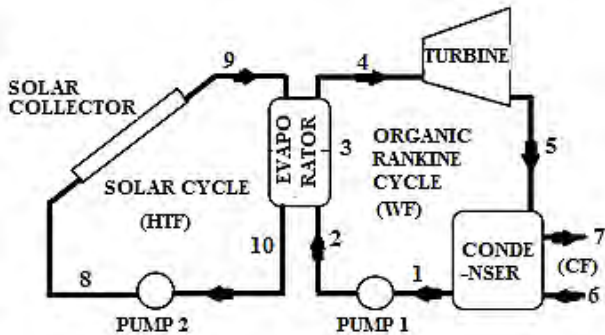


Figure 1: Heat cycle diagram [1]

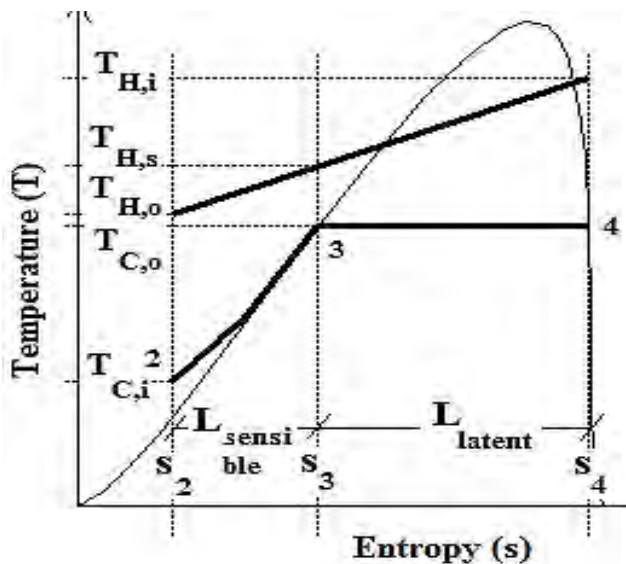


Figure 2: Temperature-Entropy diagram

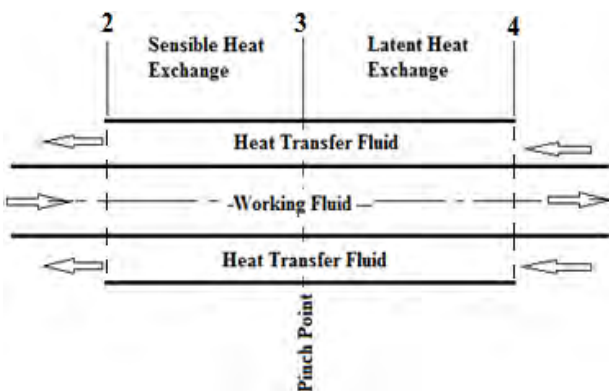


Figure 3: Evaporator heat exchanger model

The flow is assumed vertical; with the flow directions of the hot fluid (heat transfer fluid) being top-to-down in the outer pipe and that of the cold fluid (working fluid) being down-to-top in the inner pipe (refer to flow directions shown in figure 1). The complete list of model parameters is as shown in table 1 below:

Table 1: double pipe heat exchanger parameters

heat exchanger type	double pipe
flow configuration	counter flow
Thermal load required	4.2, 16.8, 84.2 kW _{th}
Heat transfer fluid (hot stream)	ethylene glycol (50% concentration)
Working fluid (cold stream)	any of:- (i) n-butane; (ii) isobutene; (iii) R245fa; (iv) R123
tube inside diameter	20 mm (tube material: copper alloy)
tube outside diameter	23 mm (tube material: copper alloy)
shell inside diameter	34 mm (determined after parametric simulations)
heat transfer fluid mass flow rate	Varying to acceptable velocity and pressure drop
working fluid mass flow rate	varying depending on thermal load and limits for velocity and pressure drop
cooling fluid mass flow rate	varying depending on thermal load and limits for velocity and pressure drop
heat transfer fluid inlet temperature	90 °C (from solar field model)
working fluid inlet temperature	40°C
cooling fluid inlet temperature	25°C
high cycle pressure	10 atmosphere; varying to conform with heat source temperature limit
low cycle pressure	3.5 atmosphere

Heat transfer fluid used is ethylene glycol (not simply water) because the solar energy systems are located outdoors and may not be operational at night thus requiring freeze protection and/or drainage capabilities.

3. Mathematical Model

The evaporator was initially modelled in the first pass system model simply as a change in enthalpy as shown below: [1]

$$\dot{Q} = \dot{m}_w (h_3 - h_2) \quad (1)$$

Where:

\dot{Q} is the rate of heat transfer from the heat transfer fluid to the working fluid in the evaporator, (W);

\dot{m}_w is the mass flow rate of the working fluid passing through the evaporator, (kg/s);

h_3 is the enthalpy of the working fluid exiting the evaporator, (J/kg-K); and

h_2 is the enthalpy of the working fluid entering the evaporator, (J/kg-K).

In this study the mathematical model is developed as two co-joined models with common parameters at the interface, the pinch point. The model is based on the following heat exchange diagram, figure 4:

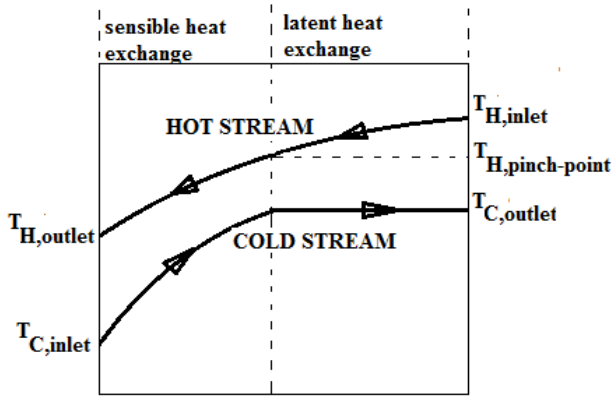


Figure 4: Heat transfer diagram

3.1 Sensible Heat Exchange Model

Heat transfer between the two streams can be expressed by equations 2, 3 and 4 as follows: [2]

$$Q_S = U_{S,o} A_{S,o} \Delta T_{S,LM} \quad (2)$$

where:

Q_S is the heat transfer per unit time in the preheater section of the heat exchanger (W);

$A_{S,o}$ is the heat transfer area on the outer surface of the inner pipe in the preheater section of the heat exchanger (m^2);

$U_{S,o}$ is the overall heat transfer coefficient on the outer surface of the inner pipe in the preheater section of the heat exchanger (W/m^2); and

$\Delta T_{S,LM}$ is the logarithmic mean temperature difference in the preheater section of the heat exchanger, ($^{\circ}C$).

$$Q_S = \dot{m}_H C p_H (T_{H,pinch-point} - T_{H,outlet}) \quad (3)$$

$$Q_S = \dot{m}_C C p_C (T_{C,outlet} - T_{C,inlet}) \quad (4)$$

where:

\dot{m}_H is the mass flow rate of the hot stream (kg/s);

\dot{m}_C is the mass flow rate of the cold stream (kg/s);

$C p_H$ is the specific heat capacity of the hot stream fluid ($J/kg\cdot^{\circ}C$);

$C p_C$ is the specific heat capacity of the cold stream fluid ($J/kg\cdot^{\circ}C$); and

the temperatures are as shown in figure 4.

The convective heat transfer coefficients are obtained using either the Dittus-Boelter or the Sieder and Tate correlations; the EES code checks for validity and chooses the appropriate one from the two. [3]

The Dittus-Boelter correlation is given by:

$$Nu_D = 0.023 Re_D^{0.8} Pr^n \quad (5)$$

where:

Nu_D is the Nusselt number (dimensionless);

Re_D is the Reynolds number (dimensionless); and

Pr is the Prandtl number (dimensionless);

$n=0.4$ when fluid is being heated; and
 $n=0.3$ when fluid is being cooled.

This correlation is valid for:

$$\left[\begin{array}{l} 0.7 \lesssim Pr \lesssim 160 \\ Re_D \gtrsim 10000 \\ \frac{L}{D} \gtrsim 10 \end{array} \right]$$

The Sieder and Tate correlation is given by:

$$Nu_D = 0.027 Re_D^{4/5} Pr^{1/3} \left(\frac{\mu}{\mu_s} \right)^{0.14} \quad (6)$$

where:

μ is the fluid viscosity at the bulk fluid temperature ($kg/s\cdot m$); and

μ_s is the fluid viscosity at the heat-transfer boundary surface temperature ($kg/s\cdot m$).

This correlation is valid for:

$$\left[\begin{array}{l} 0.7 \lesssim Pr \lesssim 16700 \\ Re_D \gtrsim 10000 \\ \frac{L}{D} \gtrsim 10 \end{array} \right]$$

The fouling resistances are obtained from the EES program database [4]

R''_{fo} =FoulingFactor('Ethylene glycol solution')

R''_{fi_S} =FoulingFactor('Refrigerant liquids')

R''_{fi_L} =FoulingFactor('R fr g r rs')

The same fouling factors are used in the latent heat exchanger model in section 3.2.

3.2 Latent Heat exchange Model

In the latent section the model is segmented on account of the varying quality of the cold stream from saturated liquid to saturated vapour.

Each segment is thus modelled as:

$$Q_L[i] = U_{L,o}[i] A_{L,o}[i] \Delta T_{L,LM}[i] \quad (7)$$

$$Q_L[i] = \dot{m}_H C p_H [i] (T_{L,H}[i+1] - T_{L,H}[i]) \quad (8)$$

$$Q_L[i] = \dot{m}_C h_{fg} (x[i+1] - x[i]) \quad (9)$$

where $U, A, \Delta T, C, H, C$ and \dot{m} have the same meanings and units as in section 3.1; while L stands for latent, x for quality of the vapour (0 for saturated liquid and 1 for saturated vapour); d_i is the internal diameter of the pipe.

The segmentation is made as in figure 5:

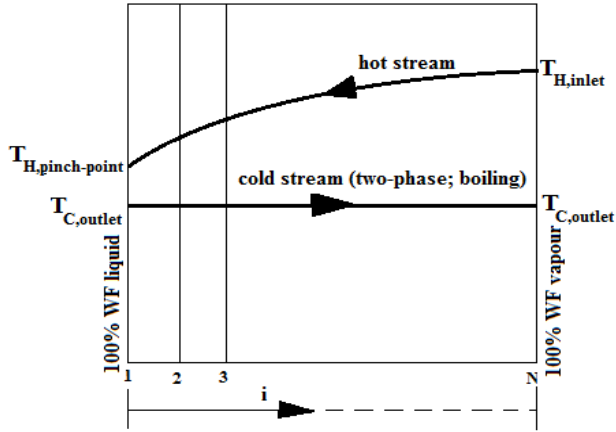


Figure 5: latent heat transfer diagram (showing segmentation direction)

The convective heat transfer coefficients for the latent heat exchange section are obtained using the Gnielinsk correlation for the hot stream and the Steiner and Taborek for the boiling stream (cold stream). Note that the Steiner and Taborek correlation also employs the Gnielinsk correlation; thus the Gnielinski correlation is given here in its general format hence the mention of liquid and vapour components.

The Gnielinsk correlation is given by:

$$\frac{h_{Lt} d_i}{k_L} = \frac{(f_L/8)(Re_{Lt}-1000)Pr_L}{1+12.7(f_L/8)^{1/2}(Pr_L^{2/3}-1)} \quad (10)$$

and the Fanning friction factor, f_L , for the liquid is:

$$f_L = [0.7904 \ln(Re_{Lt}) - 1.64]^{-2} \quad (11)$$

This expression is valid when $4000 < Re_{Lt} < 5000000$ and $0.5 < Pr_L < 2000$ for single-phase flows. The total mass velocity of liquid plus vapour is used for evaluating the liquid Reynolds number, so that:

$$Re_{Lt} = \frac{\dot{m} d_i}{\mu_L} \quad (12)$$

where:

h_{Lt} is the local liquid-phase forced convection coefficient based on the total flow as liquid ($W/m^2 \cdot ^\circ C$);

d_i is internal diameter of the pipe (m);

k_L is the local liquid-phase conductivity ($W/m \cdot ^\circ C$);

Pr_L is the local liquid-phase Prandtl number (-);

Re_{Lt} is the local liquid-phase Reynolds number (-);

\dot{m} is the total mass flow rate (of liquid and vapour) (kg/s); and;

μ_L is the liquid-phase viscosity at the bulk fluid temperature (kg/s-m);

The Steiner and Taborek (1992) comprehensive evaporation model for flow boiling in vertical tubes based on an asymptotic approach using an exponent equal to 3 is given by: [5]

$$h_{tp} = \left[(h_{nb,o} F_{nb})^3 + (h_{Lt} F_{tp})^3 \right]^{1/3} \quad (13)$$

where:

h_{tp} is the total boiling coefficient ($W/m^2 \cdot ^\circ C$);

$h_{nb,o}$ is the local nucleate pool boiling coefficient at a reference heat flux q_o at the reduced pressure $pr=0.1$, ($W/m^2 \cdot ^\circ C$);

F_{nb} is the nucleate correction factor (but not a boiling suppression factor);

h_{Lt} is the local liquid-phase forced convection coefficient based on the total flow as liquid and is obtained with the Gnielinski (1976) correlation, ($W/m^2 \cdot ^\circ C$); and

F_{tp} is the two-phase multiplier that accounts for enhancement of liquid convection by the higher velocity of a two-phase flow of a liquid in a channel.

The standard nucleate boiling coefficients for the Steiner-Taborek flow boiling correlation $h_{nb,o}$ are provided in a table (not included in this paper) for the majority of working liquids at the following standard conditions: a reduced pressure of $pr = 0.1$, a mean surface roughness of $R_{p,o} = 1 \mu m$ and the heat flux q_o equal to the value listed for each fluid. The values in this table have been calculated using the Gorenflo correlation (1993).

Some liquids are not listed in the database (table); for these, any suitable correlation may be used; in this case we used the method due to Cooper(1984), [6] to calculate the local nucleate pool boiling coefficients at reduced pressure, $pr=0.1$, surface roughness, $R_{p,o} = 1 \mu m$, and q_o equal $20000 W/m^2$, as the case is for the majority of refrigerants in the table due to Gorenflo.

The Cooper model is given by:

$$h_{nb,o} = 55 pr^{(0.12-0.4343 \ln(Rp))} (-0.4343 \ln(pr))^{-0.55} * M^{-0.5} q_o^{0.67} \quad (14)$$

where 'r' is the reduced pressure, 'R' is the surface roughness, 'M' is the mass flux.

3.3 Pressure Drop Correlations

Pressure drop in a fluid circuit results from a number of sources such as circuit components, ducting, and accessories such as headers, manifolds and nozzles. Circuit components may be tanks, collectors, heat exchangers etc. As the fluid has to be circulated through the circuit, it therefore means the pumping power required is associated with the pressure drop; and since pumping power has an economic factor on the circuit design, pressure drop in a heat exchanger becomes a design constraint or factor that has to be considered in heat exchanger designs.

The pressure drop in a heat exchanger is a combination of four types namely: (a) frictional losses consisting of skin friction, form drag and internal contractions and expansions; (b) momentum effects due to fluid density changes; (c) gravity effects due to changes in elevation between inlet and outlet; and (d) inlet and outlet losses due to sudden contraction and expansion at the inlet and outlet.

3.3.1 Single Phase Flow Pressure Drop Correlations [7]

The tube side pressure drop is given as:

$$\Delta P_t = \frac{f G_t^2 L n}{2g \rho_t d_i \Phi_t} \quad (15)$$

where:

- f is the friction factor;
- G_t is the mass velocity of the fluid (kg/s-m²);
- L is the length of the tube, (m);
- g is the acceleration due to gravity, = 9.8 m/s²;
- ρ_t is the density of the fluid (kg/m³);
- d_i is the inside diameter of the tube, (m);
- n is the number of tube passes;
- ΔP_t is the pressure drop, (Pa); and

$$\Phi_t \text{ is the dimensionless viscosity ratio; } \Phi_t = \left(\frac{\mu_\infty}{\mu_s}\right)^{0.14};$$

where μ_∞ the viscosity of the fluid at the bulk temperature; and μ_s is the viscosity of the fluid at the film temperature.

In a multi-pass exchanger, in addition to frictional loss there is also a pressure drop referred to as return loss and expressed as:

$$\Delta P_r = 4n \left(\frac{V^2}{2g}\right) \rho_t \quad (16)$$

where:

- n is the number of tube passes; and
- V is the linear velocity of the tube fluid (m/s).

Thus the total tube-side pressure drop is given as:

$$\Delta P_T = \Delta P_t + \Delta P_r \quad (17)$$

For the shell side if we assume an unbaffled layout, the pressure drop is given as:

$$\Delta P_s = \frac{f_s G_s^2 L N}{2g \rho_s D_H \Phi_s} \quad (18)$$

where:

- L is the shell length, (m);
- N is the number of shell passes;
- ρ_s is the shell fluid density, (kg/m³);
- G_s is the shell-side mass velocity, (kg/m²-s);
- D_H is the hydraulic diameter of the shell, (m); and
- Φ_s is viscosity correction factor for shell-side fluid;

$$\Phi_s = \left(\frac{\mu_\infty}{\mu_s}\right)^{0.14} \quad (19)$$

3.3.2 Two Phase Flow Pressure Drop Correlations[8]

The total pressure drop in a two-phase flow can be calculated as follows:

$$\Delta p = \Delta p_s + \Delta p_f + \Delta p_m + \Delta p_g \quad (20)$$

For the tube side flow the friction pressure drop can be presented as:

$$\Delta p_f = \Delta p_{f,lo} \varphi^2_{lo} = f_{lo} \frac{2L}{D_h} \frac{G^2}{g_c \rho_l} \varphi^2_{lo} \text{ or } \Delta p_f = \Delta p_{f,vo} \varphi^2_{vo} = f_{vo} \frac{2L}{D_h} \frac{G^2}{g_c \rho_v} \varphi^2_{vo} \quad (21)$$

where f_{lo} and f_{vo} represent the single-phase Fanning friction factor (the total mass flow rate as liquid or vapour, respectively, f_{lo} equal to $16/Re_{lo}$ for $Re_{lo} = GD_H/\mu_l < 2000$, and $f_{lo} = 0.079(Re_{lo})^{-0.25}$ for $Re_{lo} > 2000$). The pressure drop two phase friction Δp_f and φ^2_{vo} are determined from some correlations such as Friedel, Chisholm, and Lockhart-Martinelli.

The momentum pressure drop can be calculated by integrating the momentum balance equation, thus obtaining:

$$\Delta p_m = \frac{G^2}{g_c} \left[\left(\frac{x^2}{\alpha \rho_v} + \frac{(1-x)^2}{(1-\alpha)\rho_l} \right)_{z=z2} - \left(\frac{x^2}{\alpha \rho_v} + \frac{(1-x)^2}{(1-\alpha)\rho_l} \right)_{z=z1} \right] \quad (22)$$

where 'α' represents the dryness fraction (g phase).

Finally, the pressure drop caused by the gravity (hydrostatic) effect is:

$$\Delta p_g = \pm \frac{g}{g_c} \sin \theta \int_0^L [\alpha \rho_v + (1 - \alpha)\rho_l] dz \quad (23)$$

where the negative sign (i.e., the pressure recovery) stands for a downward flow in an inclined or vertical fluid flow.

3.3.3 Allowable pressure drop and velocities

Allowable pressure drop for both streams. This is a very important parameter for heat exchanger design. Generally, for liquids, a value of 0.5–0.7 kg/cm² (49.03–68.65 kPa) is permitted per shell. A higher pressure drop is usually warranted for viscous liquids, especially in the tube-side. For gases, the allowed value is generally 0.05–0.2 kg/cm² (4.903–19.61 kPa), with 0.1 kg/cm² (9.807 kPa) being typical. The velocity limits are: [9], [10]

$$0.5 \leq V_s \leq 2 \text{ (/s)}$$

$$1 \leq V_t \leq 3 \text{ (/s)}$$

4. Computer Simulations

Simulations are performed on the EES platform [11]; the simulation code consists of two sub-codes, one for the preheater and another for the vapouriser.

The simulations were done for each of the four candidate working fluids and for each of the three thermal loads of 4.2 kW_{th}, 16.8 kW_{th} and 84.2 kW_{th} respectively representing cycles with power outputs of 0.5 kW_e, 2 kW_e and 10 kW_e; the thermal loads were determined from cycle efficiencies in the range 10-15% obtained from the initial system model thus giving an average cycle efficiency of 12.5%. [1]

Parametric simulations were done in two runs; in the first run, the shell diameter (outer pipe) was varied from an initial assumed value of 0.026m in increments of 0.002m until acceptable pressure drops and velocities were attained at 0.034m. In the second set the shell diameter was kept constant at 0.034m with tube diameters maintained at 0.020 and 0.023 m respectively for inside and outside; while the glycol mass flow rate was varied from 0.5-5 kg/s in increments of 0.5 kg/s. Output parameters were mass flow rate for the working fluid, heat exchanger area and length, pressure drops and velocities, temperatures and overall heat transfer coefficients. It is also important to note that the high cycle operational pressure was constrained for each working fluid by the thermodynamic requirement that the saturation temperature must lie below the heat source temperature, 90°C; as shown in table 2; these values were determined in preliminary trial runs where the pressure was varied; the initial value of 10 atmospheres was determined from comparisons with typical operating conditions for similar cycles (10 to 30 atmospheres)[12], [13], and also with higher pressure steam cycles operating in the 100 to 300 atmospheres. [14], [15].

Table 2: high cycle pressure and saturation temperature

Working Fluid	Saturation Pressure (kPa)	Saturation Temperature (°C)
n-butane	1010	80.03
isobutane	1010	66.82
R123	506.6	81.35
R245fa	810.6	80.99

5. Results

The complete set of results is shown in the appendix. Table 3 shows the most optimal results in terms of minimum heat exchanger size that satisfies the velocity and pressure drop requirements; the results are presented for each of the three thermal loads and for each of the four working fluids. In cases where the selection requirements are not met the closest option has been selected; this is especially so with the 84.2 kW_{th} thermal load.

Other results are shown in plots in figures 6 to 14. The plots in figures 6, 7, 8, 9, 10 and 12 show the variation of shell side pressure drop and heat exchanger length with shell side mass flow rate; figure 11 shows the variation of tube side pressure drop with shell side mass flow rate. Finally figures 13 and 14, show the variation of tube side fluid velocity and mass flow rate with thermal load.

Table 3: Summarised Heat Exchanger Design Data

Working Fluid Parameter	Thermal Load (kW _{th})	n-butane	isobutane	R123	R245fa
		Total Heat Exchanger Length (m)	8.758	4.114	10.901
Total Shell Side Pressure Drop (kPa)	16.8	27.398	11.423	34.02	32.020
Total Tube Side Pressure Drop (kPa)	84.2	171.41	48.790	186.02	240.57
Maximum Shell Side Velocity (m/s)	4.2	3.980	1.880	4.960	4.740
Maximum Tube Side Velocity (m/s)	16.8	12.530	5.250	15.970	14.640
	84.2	267.74	76.510	430.48	375.82
	4.2	0.002	0.001	0.004	0.003
	16.8	0.058	0.032	0.131	0.108
	84.2	6.354	2.428	12.206	14.219
	4.2	1.993	1.993	1.993	1.993
	16.8	1.993	1.993	1.993	1.993
	84.2	3.985	3.985	4.982	3.985
	4.2	0.066	0.078	0.053	0.054
	16.8	0.263	0.312	0.214	0.216
	84.2	1.317	1.566	1.070	1.080

5.1 Thermal Load: 4.2kW_{th}

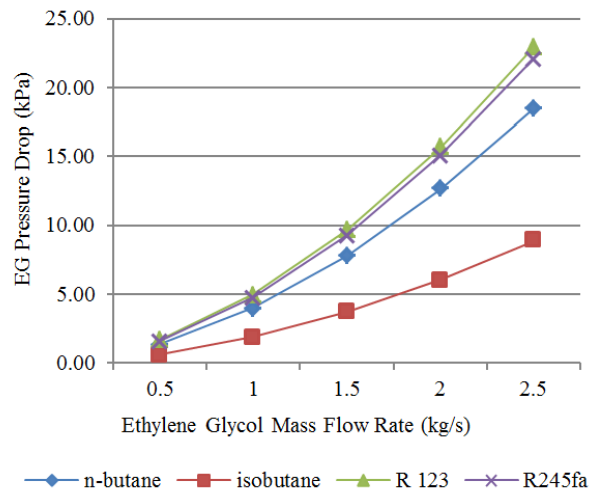


Figure 6: variation of shell side pressure drop with shell side mass flow rate for 4.2 kW_{th} thermal load

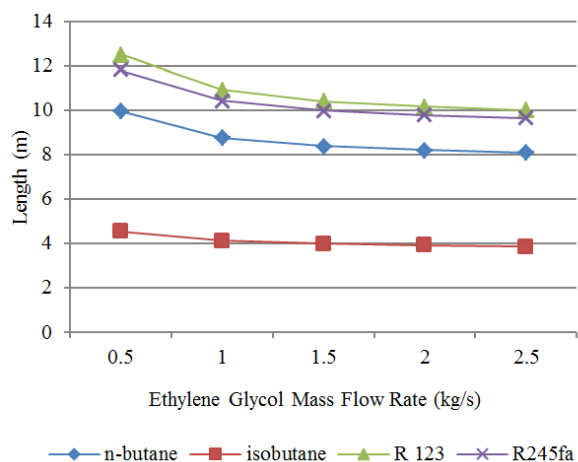


Figure 7: variation of heat exchanger length with shell side mass flow rate for 4.2 kW_{th} thermal load

5.2 Thermal Load: 16.8kWth

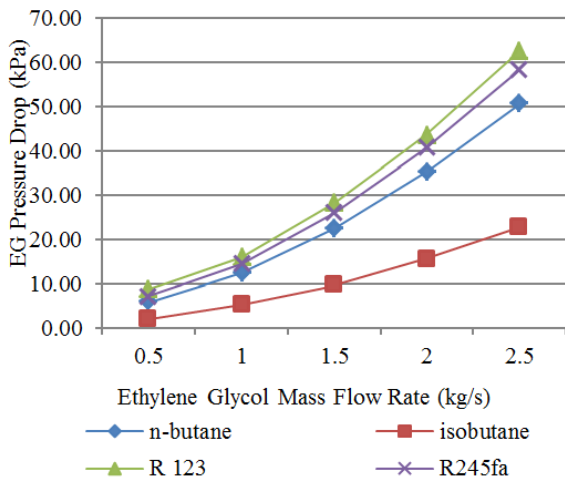


Figure 8: variation of shell side pressure drop with shell side mass flow rate for 16.8 kWth thermal load

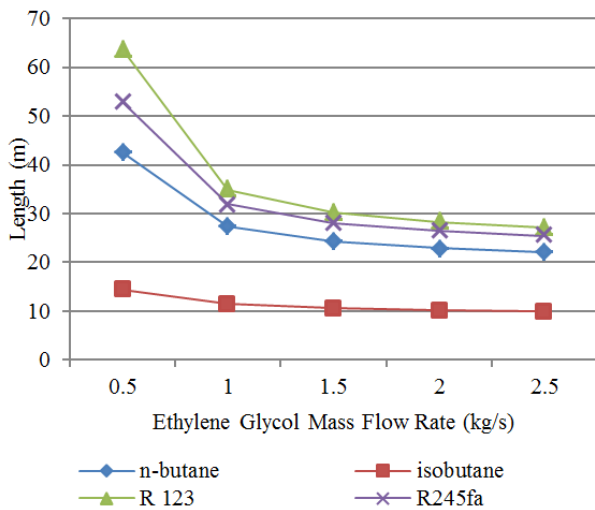


Figure 9: variation of heat exchanger length with shell side mass flow rate for 16.8 kWth thermal load

5.3 Thermal Load: 84.2kWth

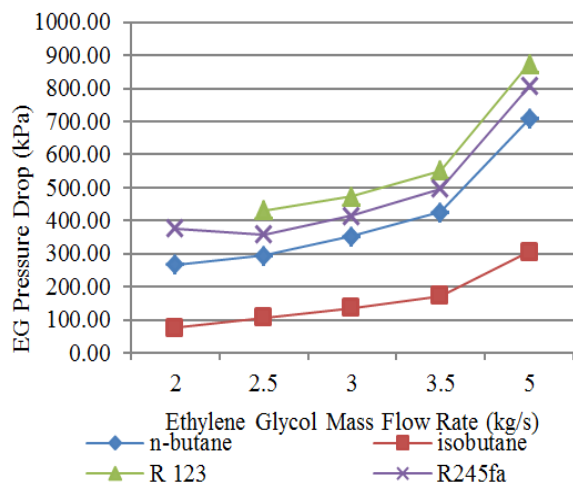


Figure 10: variation of shell side pressure drop with shell side mass flow rate for 84.2 kWth thermal load

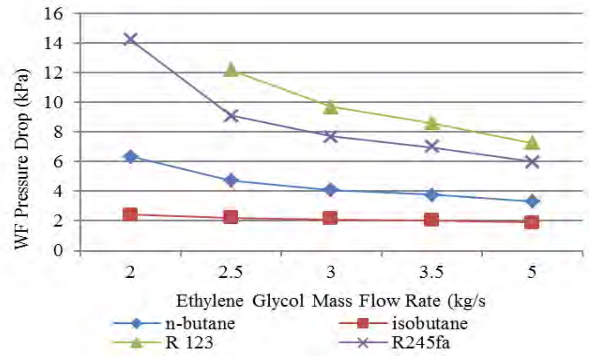


Figure 11: variation of tube side pressure drop with shell side mass flow rate for 84.2 kWth thermal load

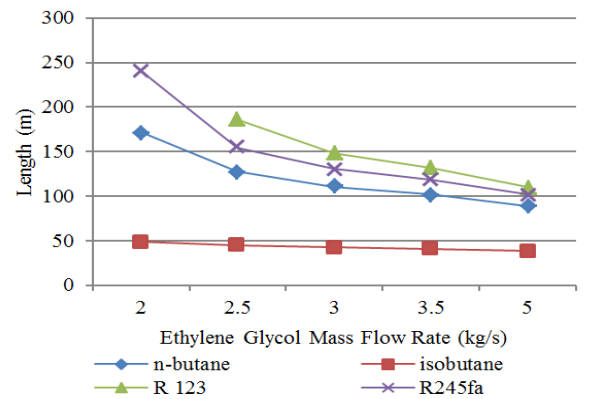


Figure 12: variation of heat exchanger length with shell side mass flow rate for 84.2 kWth thermal load

5.4 Other Results

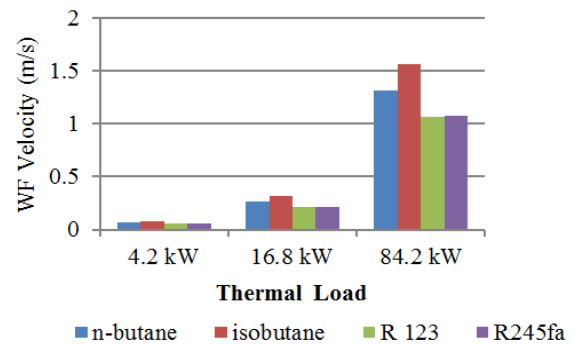


Figure 13: variation of tube side maximum velocity with working fluid type for all thermal loads

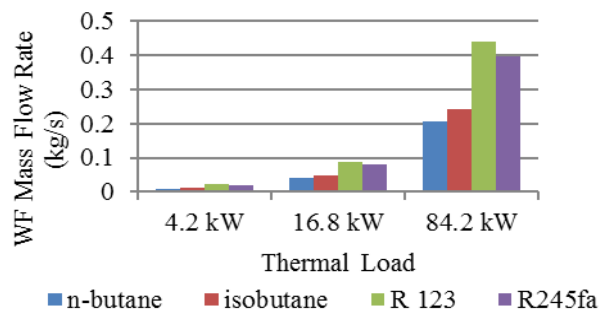


Figure 14: variation of tube mass flow rate with working fluid type for all thermal loads

6. Discussions

For thermal loads 4.2 and 16.8 kW_{th} the double pipe heat exchanger is adequate in terms of both material and manufacturing costs (size) and operational costs (pressure drop and velocity limits).

For the 84.2 kW_{th} thermal load there is need to reconfigure the heat exchanger into a shell and tube or plate heat exchanger. Assuming a tube length of 5m as acceptable a simple conversion to a single pass shell and single pass tube configuration is proposed as in table 4.

Table 4: Preliminary heat exchanger design configurations

Working Fluid	Preliminary Design Length (based on Double Pipe) [m]	Recommended Number of Tubes	Recommended Configuration
n-butane	171.41	35	1 shell pass & 1 tube pass; OR hairpin double pipe
Isobutane	48.79	10	1 shell pass & 1 tube pass; OR hairpin double pipe
R 123	186.02	38	1 shell pass & 1 tube pass; OR hairpin double pipe
R245fa	240.57	49	1 shell pass & 1 tube pass; OR hairpin double pipe

In terms of working fluid performance the optimal results are obtained with isobutene, followed by n-butane, and then R245fa, and finally R123. Simulations in the other cycle components such as the turbine and condenser will, however, consider all four candidate working fluids with the aim of selecting the overall optimal choice. The information obtained in this exercise will be used in evaluating performance of the heat exchanger in the Infinity IT10 mini turbine cycle validation process as well as evaluating the correlations used in the heat transfer models.

Further figures 6 to 9 show that a glycol mass flow rate of 2.5 kg/s is adequate for the two thermal loads of 4.2 and 16.8 kW_{th} for all four working fluids both in terms of shell side pressure drops and fluid velocities; the corresponding tube side pressure drops are found to be insignificant and fluid velocities very low as can be seen from figures 11 (only showing tube side pressure drops for 84.2 kW_{th}) and 13 respectively; the concern with extremely low tube side fluid velocities is that it may slow down or hinder optimal heat transfer. These results also show that for the two thermal loads the lowest cost of heat exchanger is that based on isobutene as the working fluid.

Figure 10 on the other hand shows that none of the models for the 84.2 kW_{th} meets the requirements for the shell side pressure drops; it also shows that the glycol mass flow rate must range from 2 to 5 kg/s in order to satisfy the thermal load. The models produced prohibitive pressure drops ranging from 250 to 900 kPa for the other three working fluids, other than isobutene and it was on the account of such excessive pumping requirements that table 4 was generated proposing a rethink of the heat exchanger models for this thermal load.

The mass flow rates for the working fluids determined by the parametric analyses for the three thermal loads are shown in figure 14; the actual figures are 0.010 kg/s, 0.041 kg/s and 0.207 kg/s respectively for 4.2, 16.8 and 84.2 kW_{th} for n-butane; the corresponding values for isobutene are 0.012, 0.048 and 0.241 kg/s; for R123 they are 0.022, 0.088 and 0.440 kg/s; and finally for R245fa they are 0.020, 0.079 and 0.396 kg/s. The lowest working fluid mass flow rates are attained with n-butane, followed by isobutene whilst R123 requires the highest mass flow rates followed by R245fa.

7. Conclusions and Recommendations

A heat exchanger model for the low temperature solar thermal organic Rankine cycle has been developed and evaluated on the EES platform. Parameters considered included heat exchanger size, pressure drop and fluid velocity on both the tube and shell sides. Reference values have been based on the tubular exchanger manufacturers association (TEMA) standards. Results have been analysed and discussed. The results have shown that models developed with isobutene as the working fluid are the most optimal from the four candidate working fluids tested. Further evaluations of the models and the correlations will be performed with the validation of the Infinity IT10 mini turbine ORC cycle.

Further the models developed satisfy the thermal loads, pressure drops and fluid velocities for the 4.2 and 16.8 kW_{th} loads. On account of very high pressure drops and therefore costly pumping requirements it has been proposed to redesign the heat exchanger model for the 84.2 kW_{th} to a multi-tube shell and tube heat exchanger.

It has also been established that a further conceptual investigation of two phase flow pressure drop be undertaken to fully appreciate its effect on the development of the heat exchanger models.

Acknowledgments

The authors would like to thank the Centre for Engineering Postgraduate Studies (CEPS) at University of KwaZulu-Natal for providing funds for certain aspects of the research as well as all colleagues, postgraduate students and staff of the section

References

- [1] Situmbeko S. M., Inambao F. L. Mathematical Modelling and Simulation of Low Temperature Solar Thermal Energy Conversion Systems. Proceedings of Solar World Congress. Kassel, Germany, 2011.
- [2] Thirumaleshwars M. Software Solutions to Problems of Heat Transfer, Heat Exchangers. ISBN 978-87-403-0578-4, Bookboon.com, 2013.
- [3] Incropera F.P. et al. Fundamentals of Heat and Mass Transfer. John Wiley & Sons. USA, 2007.
- [4] EES32\Userlib\HeatTransfer\FoulingFactors\FoulingFactor.lkt. 2013.
- [5] Thome J.R. Engineering Data Book III; chapter 10: Fundamentals of Evaporation in Plain Tubes, Laboratory of Heat and Mass Transfer. Swiss Federal Institute of Technology. Lausanne, Switzerland.
- [6] Thome J.R. Engineering Data Book III; chapter 9: Fundamentals of Boiling on Tubes and Tube Bundles, Laboratory of Heat and Mass Transfer, Swiss Federal Institute of Technology. Lausanne, Switzerland.

- [7] Website: slideshare.net/rijumoniboro/heat-exchangers-12606868
- [8] Website: [razifar.com/cariboost_files/Heat_20 Exchangeers.pdf](http://razifar.com/cariboost_files/Heat_20_Exchangeers.pdf)
- [9] Website: unix.ecs.umass.edu/~rlaurenc/Courses/che333/Reference/exchanger.pdf
- [10] Perry R.H. *Perry's Chemical Engineers' Handbook*. 7th Edition, McGraw-Hill, 1999
- [11] Klein S.A., and Alvarado F.L. *Engineering Equation Solver for Microsoft Windows Operating Systems*. F-Chart Software, Middleton, USA. 2013
- [12] Website: honeywell-refrigerants.com/Europe;honeywell-genetron-245a-orc-systems-brochure
- [13] Website: infinityturbine.com – ORC Waste Heat Turbine
- [14] Website: energy.siemens.com - power-generation steam turbines, SST-6000 Brochure, T_6000_Series_Datasheet.pdf
- [15] Website: energy.siemens.com, power-generation steam turbines, SST-300.pdf

Appendix: Simulation Results

Latent IIX Section 2 Overall Heat Transfer Coefficient	Latent IIX Section 1 Overall Heat Transfer Coefficient	Sensible IIX Overall Heat Transfer Coefficient	Working Fluid Boiling Temperature	Heat Transfer Fluid Pinch Point Temperature	Heat Transfer Fluid outlet Temperature	Working Fluid Velocity	Heat Transfer Fluid Maximum Velocity	Total IIX Tube Pressure Drop	Total IIX Shell Pressure Drop	Total IIX Length	Latent IIX Length	Sensible IIX Length	Latent Thermal Load	Sensible Thermal Load	Total Thermal Load	High Pressure	Heat Transfer Fluid Mass Flow Rate	Working Fluid Mass Flow Rate	Working Fluid
[Wm ² -C]	[Wm ² -C]	[Wm ² -C]	[C]	[C]	[C]	[m/s]	[m/s]	[kPa]	[kPa]	[m]	[m]	[m]	[W]	[W]	[W]	[kPa]	[kg/s]	[kg/s]	
1207	824.1	139.2	80.03	88.33	87.68	0.06569	0.9964	0.0019	1.35	9.927	4.729	5.198	3023	1177	4200	1.01E+06	0.5	0.01032	n-butano
1395	944.2	141.8	80.03	89.16	88.84	0.06569	1.993	0.0017	3.98	8.758	3.907	4.851	3023	1177	4200	1.01E+06	1	0.01032	n-butano
1475	994.5	142.8	80.03	89.44	89.23	0.06569	2.989	0.0016	7.78	8.383	3.643	4.74	3023	1177	4200	1.01E+06	1.5	0.01032	n-butano
1521	1023	143.3	80.03	89.58	89.42	0.06569	3.985	0.0016	12.65	8.196	3.511	4.685	3023	1177	4200	1.01E+06	2	0.01032	n-butano
1551	1041	143.7	80.03	89.67	89.54	0.06569	4.982	0.0015	18.53	8.082	3.43	4.652	3023	1177	4200	1.01E+06	2.5	0.01032	n-butano
1207	839.9	334.9	80.03	83.3	80.68	0.2628	0.9964	0.0899	5.86	42.52	29.41	13.11	12091	4709	16800	1.01E+06	0.5	0.04129	n-butano
1395	969.1	351.9	80.03	86.65	85.35	0.2628	1.993	0.0578	12.53	27.398	18.2	9.198	12091	4709	16800	1.01E+06	1	0.04129	n-butano
1475	1024	358.5	80.03	87.77	86.9	0.2628	2.989	0.0512	22.58	24.254	15.89	8.364	12091	4709	16800	1.01E+06	1.5	0.04129	n-butano
1521	1055	362	80.03	88.33	87.68	0.2628	3.985	0.0482	35.35	22.863	14.87	7.993	12091	4709	16800	1.01E+06	2	0.04129	n-butano
1551	1075	364.2	80.03	88.66	88.14	0.2628	4.982	0.0465	50.68	22.062	14.28	7.782	12091	4709	16800	1.01E+06	2.5	0.04129	n-butano
1521	1300	790	80.03	81.6	78.31	1.317	3.985	6.354	267.74	171.41	135.5	35.91	60599	23601	84200	1.01E+06	2	0.207	n-butano
1551	1324	802.2	80.03	83.29	80.66	1.317	4.982	4.717	294.54	127.29	99.81	27.48	60599	23601	84200	1.01E+06	2.5	0.207	n-butano
1572	1341	810.7	80.03	84.41	82.22	1.317	5.978	4.1027	353.76	110.72	86.59	24.13	60599	23601	84200	1.01E+06	3	0.207	n-butano
1588	1353	817	80.03	85.21	83.33	1.317	6.975	3.7671	427.29	101.7	79.44	22.26	60599	23601	84200	1.01E+06	3.5	0.207	n-butano
1619	1377	828.8	80.03	86.65	85.34	1.317	9.964	3.2975	706.91	89.04	69.45	19.59	60599	23601	84200	1.01E+06	5	0.207	n-butano
1207	746.2	107.4	81.35	88.24	87.68	0.05339	0.9964	0.0043	1.70	12.499	6.237	6.262	3175	1025	4200	506625	0.5	0.02192	R 123
1395	857.3	109	81.35	89.12	88.84	0.05339	1.993	0.0037	4.96	10.901	5.075	5.826	3175	1025	4200	506625	1	0.02192	R 123
1475	903.5	109.6	81.35	89.41	89.23	0.05339	2.989	0.0036	9.65	10.402	4.712	5.69	3175	1025	4200	506625	1.5	0.02192	R 123
1521	929.4	109.9	81.35	89.56	89.42	0.05339	3.985	0.0035	15.66	10.154	4.531	5.623	3175	1025	4200	506625	2	0.02192	R 123
1551	946.2	110.1	81.35	89.65	89.54	0.05339	4.982	0.0034	22.93	10.004	4.422	5.582	3175	1025	4200	506625	2.5	0.02192	R 123
1207	810.4	271.2	81.35	82.96	80.68	0.2136	0.9964	0.2396	8.77	63.68	46.4	17.28	12699	4101	16800	506625	0.5	0.0877	R 123
1395	925.1	282.3	81.35	86.49	85.35	0.2136	1.993	0.1312	15.97	34.93	24.04	10.89	12699	4101	16800	506625	1	0.0877	R 123
1475	974.4	286.5	81.35	87.66	86.9	0.2136	2.989	0.1138	28.19	30.299	20.51	9.789	12699	4101	16800	506625	1.5	0.0877	R 123
1521	1002	288.8	81.35	88.24	87.68	0.2136	3.985	0.1063	43.80	28.328	19.01	9.318	12699	4101	16800	506625	2	0.0877	R 123
1551	1020	290.2	81.35	88.59	88.14	0.2136	4.982	0.1022	62.52	27.225	18.17	9.055	12699	4101	16800	506625	2.5	0.0877	R 123
1551	1322	694.6	81.35	82.95	80.66	1.07	4.982	12.206	430.48	186.02	152.1	33.92	63647	20553	84200	506625	2.5	0.4395	R 123
1572	1339	701	81.35	84.12	82.22	1.07	5.978	9.73	473.84	148.3	120.3	28	63647	20553	84200	506625	3	0.4395	R 123
1588	1352	705.7	81.35	84.96	83.33	1.07	6.975	8.622	552.17	131.4	106.2	25.2	63647	20553	84200	506625	3.5	0.4395	R 123
1619	1375	714.6	81.35	86.48	85.34	1.07	9.964	7.241	876.56	110.41	88.84	21.57	63647	20553	84200	506625	5	0.4395	R 123
1207	827.9	117.6	80.99	88.34	87.68	0.05388	0.9964	0.0036	1.61	11.796	5.222	6.574	2994	1206	4200	810600	0.5	0.01975	R245fa
1395	950.9	119.5	80.99	89.17	88.84	0.05388	1.993	0.0032	4.74	10.418	4.284	6.134	2994	1206	4200	810600	1	0.01975	R245fa
1475	1002	120.2	80.99	89.45	89.23	0.05388	2.989	0.0031	9.26	9.982	3.987	5.995	2994	1206	4200	810600	1.5	0.01975	R245fa
1521	1031	120.6	80.99	89.59	89.42	0.05388	3.985	0.003	15.06	9.764	3.838	5.926	2994	1206	4200	810600	2	0.01975	R245fa
1551	1050	120.9	80.99	89.67	89.54	0.05388	4.982	0.0029	22.08	9.632	3.747	5.885	2994	1206	4200	810600	2.5	0.01975	R245fa
1207	824.2	292.4	80.99	83.36	80.68	0.2155	0.9964	0.1787	7.28	52.88	35.96	16.92	11977	4823	16800	810600	0.5	0.07898	R245fa
1395	959.7	305.3	80.99	86.68	85.35	0.2155	1.993	0.1081	14.64	32.02	20.59	11.43	11977	4823	16800	810600	1	0.07898	R245fa
1475	1017	310.2	80.99	87.79	86.9	0.2155	2.989	0.0948	26.15	28.1	17.74	10.36	11977	4823	16800	810600	1.5	0.07898	R245fa
1521	1050	312.9	80.99	88.34	87.68	0.2155	3.985	0.089	40.82	26.397	16.51	9.887	11977	4823	16800	810600	2	0.07898	R245fa
1551	1071	314.6	80.99	88.67	88.14	0.2155	4.982	0.0857	58.42	25.442	15.82	9.622	11977	4823	16800	810600	2.5	0.07898	R245fa
1521	1286	721.9	80.99	81.68	78.31	1.08	3.985	14.219	375.82	240.57	191.2	49.37	60030	24170	84200	810600	2	0.3958	R245fa
1551	1310	732.1	80.99	83.35	80.66	1.08	4.982	9.142	358.04	154.75	120.8	33.95	60030	24170	84200	810600	2.5	0.3958	R245fa
1572	1327	739.2	80.99	84.46	82.22	1.08	5.978	7.706	416.82	130.48	101.3	29.18	60030	24170	84200	810600	3	0.3958	R245fa
1588	1339	744.4	80.99	85.25	83.33	1.08	6.975	6.978	496.40	118.16	91.49	26.67	60030	24170	84200	810600	3.5	0.3958	R245fa
1619	1362	754.2	80.99	86.68	85.34	1.08	9.964	6.002	807.32	101.7	78.48	23.22	60030	24170	84200	810600	5	0.3958	R245fa

Modeling of a Solar Air Heater with Sensible Thermal Storage and Natural Draft

Shadreck M. Situmbeko

University of Botswana, Gaborone, Botswana;
University of KwaZulu-Natal, Durban, RSA;

Freddie L. Inambao

University of KwaZulu-Natal, Durban, RSA;

Kris L. Kumar

University of Botswana,
Gaborone, Botswana;

Abstract-The paper presents a novel system of employing reverse thermosyphon flow in order to create round-the-clock operation of a solar air heating system with a sensible thermal storage. In the proposed system, heating of air is achieved in the day through direct solar thermal heating; thereafter, heating is achieved in the night through reverse thermosyphon flow from the thermal storage; thus keeping the water-ethylene-glycol storage in motion at all times. The innovative technique has been shown to result in operating the solar air heater on a continuous basis over the 24 hours cycle. In doing so, it is also established that 50/50 water and glycol mixture is ideally suited to serve as the solar thermal energy storage and release medium. Basic principles of fluid dynamics and heat transfer are employed to study the flow of heat storage fluid in either direction in keeping with the thermal gradient during day and night. Conceptual framework is reinforced by solving the equations of motion through computer simulation on the one hand and designing and operating a prototype on the other. Both the computer simulation model and physical model establish the authenticity of the proposal. Optimization of some important operating parameters such as plate spacing, concentration of the water ethylene glycol heat transfer fluid and the draft height has also been undertaken.

Key words: reverse thermosyphon, solar air heating, sensible thermal storage, water-ethylene-glycol.

Nomenclature

Roman Symbols

A	area
a	ambient
c	cover
c_p	specific heat at uniform pressure
D	diameter
g	acceleration due to gravity
h	heat transfer coefficient
I	radiation
k	conductivity
L	length
l	longitudinal
L_{ins}	insulation thickness
m	mean
\dot{m}	mass flow rate

Nud	Nusselt number for flow in a pipe
Nup	Nusselt number for flow in between two flat plates
P	pressure
\dot{Q}	rate of heat transfer
Re	Reynold's number
T	temperature

Greek Symbols

α	absorptivity
Δ	delta (mathematical symbol)
ε	emissivity
θ	angle of inclination
μ	dynamic viscosity
ρ	density
τ	transmissivity

Abbreviations

abs	absorber
conv.	convection
I.D	internal diameter
ins	insulation
sol	solar
\dot{v}	volumetric flow rate

I. INTRODUCTION

This research has come about as an offshoot of a larger project on the research and development of a solar chimney, whose ultimate aim was to develop a working solar chimney plant to be constructed and installed for supplying power to a remote village in Botswana by 2016 [1]. The task was conducted as a consultancy cum joint-research by the authors from the University of Botswana (UB) with the then Botswana Technology Centre (BOTECH). The work was based on the research and development of a solar thermal storage model that could be integrated into the existing small 20 m height solar chimney plant at the BOTECH. A comprehensive survey was undertaken to study the literature and state of art of solar chimney research. It was soon realised that the major

problem was the inadequacy of solid storage devices in their inability to create a continuous thermal heating of air during day and night. It led the authors to conceive liquid storage systems, which are also more effective in terms of heat transfer and cost minimisation. The modelling process consisted of development of both mathematical (and computer simulations) and physical models. Finally, the paper presents a validation of the theoretical results by comparing with a sizable sample of experimental observations. A fair degree of agreement between the two is a pointer to the validity of the proposed model.

II. LITERATURE SURVEY

A comprehensive literature survey and consultations with industry and academia including a visit to University of Stellenbosch were undertaken; an abridged historical perspective is included here whereas other aspects including mathematical theories and empirical formulae are included in respective sections of the paper.

Solar collectors can typically be broadly classified as thermal collectors converting solar radiation into heat energy or photovoltaic converting solar radiation directly into electric energy. Tremendous strides have been made in the development of both types dating back to 1839 when the photovoltaic was first discovered [2] and 1767 when the solar thermal collector was first developed [3]. PVT for solar photovoltaic and thermal hybrid system is a technology convergence application combining the generation of electricity as well as space heating through air heating [4]. In this study we investigate a combined solar thermal air-and-water heating hybrid application; where the air is available immediately for use whilst the water is used as a storage medium available for space heating at later hours when solar radiation is not available.

III. SOLAR ENERGY SCENARIO IN BOTSWANA

The location of the study was Gaborone with coordinates $24^{\circ} 39' 29''$ S and $28^{\circ} 54' 44''$ E; Gaborone is a city in Botswana, Southern Africa. Botswana lies in the most favourable sunbelts; lying between latitudes 15° N, and 35° N, as also 15° S, and 35° S. These semi-arid regions are characterized by having the greatest amount of solar radiation, more than 90% of which comes as direct radiation because of the limited cloud coverage and rainfall. Moreover, there is usually over 3,000 hours of sunshine per year.

Gaborone has on average 74 days per year with temperatures above 32° C, 196 days per year with temperatures above 26° C and 51 days per year with temperatures below 7° C. There is on average one day per year with temperatures below 0° C. The average dew point peaks around January and February at 16° C and hits the lowest levels in July at 2° C. The average dew point in a given year is 10° C.

Solar radiation level at Gaborone is 14.6 MJ/m² in June and 26.2 MJ/m² in December, giving an average of 21 MJ/m²[5].

IV. THERMAL STORAGE MEDIUM

The result of the survey of thermal storage methods and media as well as a wide search and consulting strategy that included a visit to Stellenbosch University was that the most

appropriate storage system would have to be based on a sensible thermal storage employing a liquid such as water or more specifically a water-ethylene-glycol mixture as the storage media [6]. The selection was based on the comparison of several sensible thermal storage materials as represented in figure 1; the figure shows a comparison of thermal masses of various sensible storage materials and water appears to be most promising.

Further an analysis was undertaken of the following advantages and disadvantages associated with the use of water as a storage medium:

Advantages:

- (i) Water is most inexpensive, easy to handle, non-toxic, non-combustible and widely available.
 - (ii) Water has the highest specific heat and high density.
 - (iii) Heat exchangers are not necessary if water is used as the heat carrier in the collector.
 - (iv) Natural convection flows can be utilized when pumping energy is scarce.
 - (v) Simultaneous charging and discharging of the storage tank is possible.
 - (vi) Adjustment and control of a water system is easily variable and flexible.
- Disadvantages:
- (vii) Water might partially freeze at very low temperature or partially boil when very hot.
 - (ix) Water is highly corrosive to normally used materials.
 - (x) Working temperatures are limited to less than 100° C.
 - (xi) Water is difficult to stratify, if required.

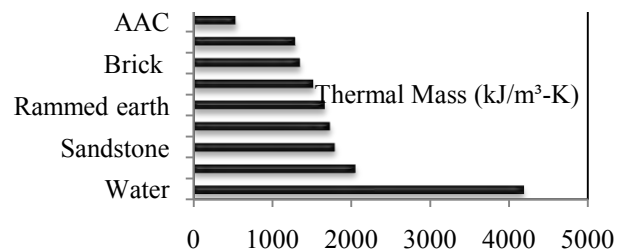


Fig. 1: Comparison of thermal masses of storage materials
(Note: AAC=Autoclaved Aerated Concrete; FC=Fibre Cement)

The thought of water-glycol mixture emerged from the fact that ethylene glycol is a good antifreeze agent and ethylene-water mixture has been tried successfully in cold climate. It is also noted that addition of ethylene to water does not result in loss of advantages of using water, except for nominal additional cost because, once added, the mixture remains circulating in the system. Water is a good candidate as per its advantages but in case the temperature drops too low, it may partially freeze and if the temperature rises too high, it may even become steam resulting in steam-lock; hence water-glycol is recommended.

It was also established that such a system would have to be passive, not employing any driving devices (such as pumps) requiring external power supply; as such it was envisaged that such a system would have to rely on thermosyphon flow and reverse-thermosyphon depending on the thermal gradient at a given instant.

V. CONCEPTUALISATION OF THE SYSTEM

Observation of existing tubular solar water heaters shows that the heated water rises up the inclined tubes and it is stored in the tank provided atop. It was also noted that it is often necessary to install a one-way valve in order to check the water from returning down. The authors studied the system closely and discovered that, during the process of solar heating, water cannot flow down but after the hot water is stored in the tank atop and solar heating has ceased, it tends to flow back. This phenomenon, called reversed thermosyphon, is the one which is desirable to heat the air during the part of the cycle when solar heating is not available.

In terms of fluid mechanics, reverse circulation in thermosyphon solar water heating systems refers to a type of flow whereby the heated water stored in the tank on account of lower density flows back to the solar collector and thereby loses heat to the ambient. Such thermal losses will normally be dictated by the differences between the temperatures of the collector-water, storage-water as well as the ambient and sky temperatures. It is to avoid the undesired reverse flow that conventional passive solar water heating systems usually have a non-return valve installed in the pipe connecting the top of the collector and the inlet to the tank; some other systems are designed or installed such that there is ample geometrical separation in the vertical heights of the top of the collector and the bottom of the tank; the separation is usually in the range of 200 to 500 mm [7]. In our system, the design is deliberately made to promote reverse thermosyphon in the non-solar hours by not incorporating a non-return valve and positioning the bottom level of the storage tank at or below the top of the collector.

The conceptualised model, therefore, consists of a standard solar collector with the lower and upper ends of the collector box removed; thus the collector doubles as a natural convection air heater as well as a water heater. The heated water is stored in the tank at the top of the collector as in figure 2. The overall dimensions of the collector are shown in figure 3.

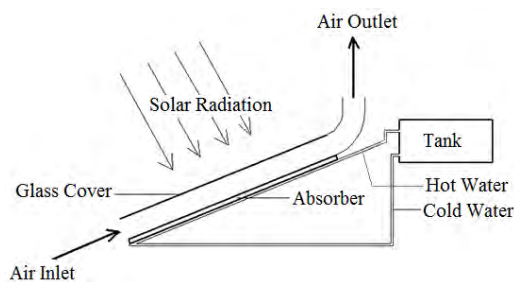


Fig. 2. Solar air heater with water as thermal storage medium

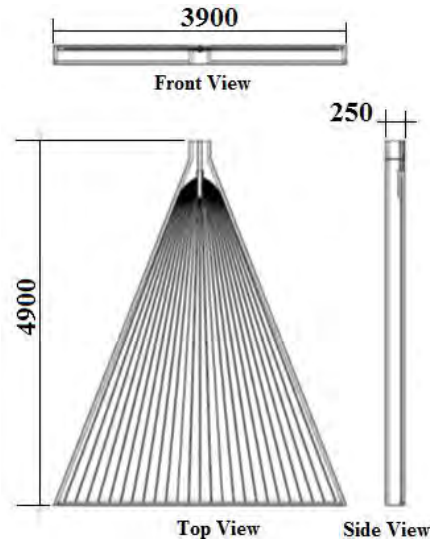


Fig. 3. Overall dimensions of the solar air heater (in mm)

The specification of the materials and their optical and thermal characteristics are shown in tables 1 and 2 as follows:

TABLE 1: MATERIAL CHARACTERISTICS OF THE COLLECTOR MODEL

absorber plate	1mm aluminium plate
riser pipes	I.D 6mm by 1mm copper pipe; number of riser pipes = 25.
insulation	40mm polyurethane foam
transparent cover	4mm solar grade glass
heat transfer fluid	water-ethylene glycol
size of storage tank	300 litres

TABLE 2: OPTICAL AND THERMAL CHARACTERISTICS OF THE COLLECTOR MODEL

absorber absorptivity	$\alpha_{abs} = 0.9$
absorber emissivity	$\epsilon_{abs} = 0.1$
cover emissivity	$\epsilon_c = 0.85$
cover transmissivity	$\tau_c = 0.9$
insulation conductivity	$k_{ins} = 0.023 \text{ W/m-K}$
wind convection coefficient	$h_{c-a} = 5.0 \text{ W/m}^2\text{-K}$
heat transfer fluid Nusselt number, heat transfer fluid flow determined to be laminar	$Nud_{wg} = (3.66 + 4.36)/2$
air flow Nusselt number	Nup_{air} - interpolated from a table [8] for laminar flow; for turbulent flow it is given by equation: $Nup = 0.0158 * Re_{air}^{0.8}$ where Re_{air} is Reynold's number

It is noted here that depending on the level of accuracy required the optical properties maybe modelled to vary with the solar radiation incident angle, such that that $\tau(\theta)$, $\alpha(\theta)$; [9].

IV. MATHEMATICAL MODEL OF THE SYSTEM

The mathematical model of the system is developed based on the segmented model of the air heater with water-glycol mixture as the storage material:

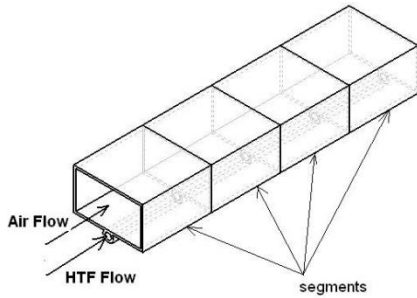


Fig.4. Segmented model (HTF (heat transfer fluid) refers to water-glycol mixture)

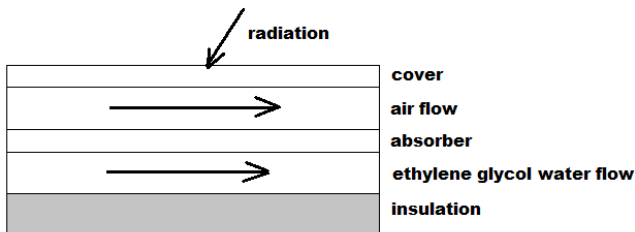


Figure 5: One segment model

Figure 6 shows the energy balance for the absorber segment. The energy balance is represented mathematically by equations 1 and 2.

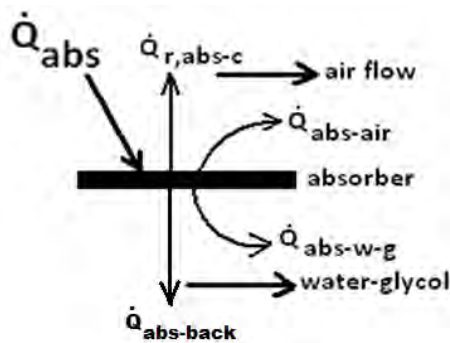


Fig.6. Absorber segment heat transfer model

$$\dot{Q}_{abs} = \dot{Q}_{abs-air} + \dot{Q}_{abs-wg} + \dot{Q}_{r,abs-c} + \dot{Q}_{abs-back} \quad (1)$$

$$\dot{Q}_{abs} = \tau_c * \alpha_{abs} * A_{abs} * I_{sol} \quad (2)$$

The energy balance for the cover segment is shown in figure 7 and is given by equations 3 to 8.

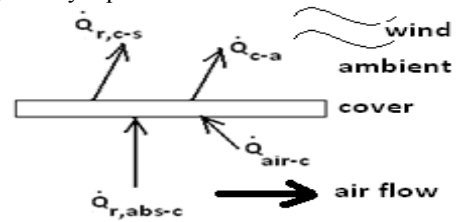


Fig. 7. Cover segment heat transfer model

$$\dot{Q}_{air-c} + \dot{Q}_{r,abs-c} = \dot{Q}_{c-a} + \dot{Q}_{r,c-sky} \quad (3)$$

$$\dot{Q}_{r,abs-c} = h_{r,abs-c} * A_c * (T_{abs} - T_c) \quad (4)$$

$$\dot{Q}_{air-c} = h_{air-c} * A_c * (T_{m,air} - T_c) \quad (5)$$

$$\dot{Q}_{r,c-sky} = \epsilon_c * \sigma * A_c * (T_c^4 - T_{sky}^4) \quad (6)$$

$$\dot{Q}_{c-a} = h_{c-a} * A_c * (T_c - T_a) \quad (7)$$

$$T_{sky} = 0.0552 * T_a^{1.5} \quad (8)$$

The energy balance on the air flow segment is represented by figure 8 and equations 9 to 13.

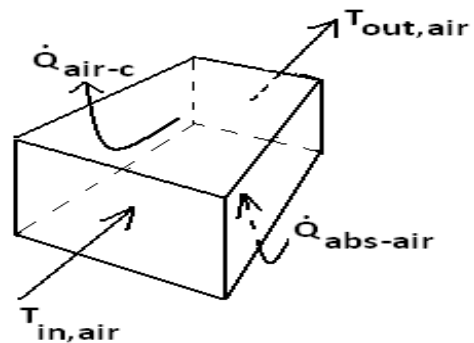


Fig.8. Air flow segment heat transfer model

$$\dot{Q}_{abs-air} - \dot{Q}_{air-c} = \dot{Q}_{air} \quad (9)$$

$$\dot{Q}_{abs-air} = h_{abs-air} * A_{abs} * (T_{abs} - T_{m,air}) \quad (10)$$

$$\dot{Q}_{air-c} = h_{air-c} * A_c * (T_{m,air} - T_c) \quad (11)$$

$$\dot{Q}_{air} = \dot{m}_{air} * c_{p,air} * (T_{out,air} - T_{in,air}) \quad (12)$$

$$h_{air-c} = h_{abs-air} \quad (13)$$

Figure 9 and equations 14 and 15 show the energy balance on the water-ethylene-glycol flow segment.

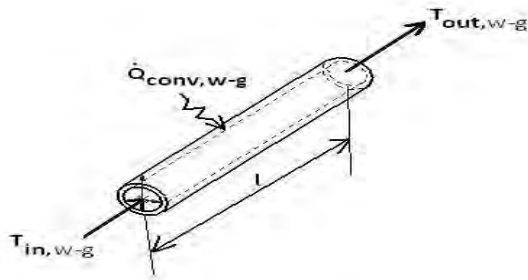


Fig.9. Water ethylene-glycol flow segment heat transfer model

$$\dot{Q}_{conv,wg} = \dot{m}_{wg} * c_{p,wg} * (T_{out,wg} - T_{in,wg}) \quad (14)$$

$$\dot{Q}_{conv,wg} = h_{abs-wg} * A_{l,wg} * (T_{abs} - T_{m,wg}) \quad (15)$$

The thermosyphon model is based on Poiseuille's Law for laminar flow and is shown in equations 16 and 17:

$$v \dot{Q} l = \pi \left(\frac{D}{2}\right)^4 * \frac{\Delta P}{8 \mu L} \quad (16)$$

$$\Delta P = g * \Delta \rho * L * \sin \theta \quad (17)$$

The total energy incident on the absorber, total energy transferred to the air, and total energy transferred to the heat transfer fluid are obtained by summations of the segment energies as in the following set of equations; number 18 below:

$$\begin{aligned} \dot{Q}_{abs} &= \sum_{i=1}^{i=N} \dot{Q}_{abs}(i) \\ \dot{Q}_{air} &= \sum_{i=1}^{i=N} \dot{Q}_{air}(i) \\ \dot{Q}_{w-g} &= \sum_{i=1}^{i=N} \dot{Q}_{w-g}(i) \end{aligned} \quad (18)$$

The draft required to promote air flow is represented by the Boussinesq approximation. In particular the air flow exit velocity is modeled by equation 19 as:

$$V_{Nn} = \sqrt{2gH \left(\frac{T_{air,Nn} - T_a}{T_a} \right)} \quad (19)$$

Where H is included as if there were a chimney, $T_{air,Nn}$ is the temperature of the air flow exiting the collector and T_a is the ambient temperature (also equals the temperature of the air flow entering the collector)

The thermal storage model consists of an energy balance consisting of Charging, Discharging and Thermal Losses. In this model thermal losses are assumed insignificant. That means during „Day Time Simulation“ the storage model assumes the „Charging Mode“ and during the „Night Time Simulation“, the „Discharging Mode“. Reverse thermosyphon

is assumed for the „Discharging Mode“. A further assumption made is that there is no stratification in the storage tank, that is, the storage has one uniform temperature.

The charging model is given by equations 20 and 21:

$$\dot{Q}_{tank} = \dot{m}_{wg} * C_{p,wg} * (T_{wg,out,Nn} - T_{tank}) \quad (20)$$

$$\dot{Q}_{tank} = m_{wg,tank} * C_{p,wg} * \left[\frac{T_{tank} - T_{wg,in,0}}{t_{cycle}} \right] \quad (21)$$

Where \dot{Q}_{tank} is the heat transfer rate to the thermal storage; \dot{m}_{wg} is the mass flow rate of the water ethylene glycol working fluid; $m_{wg,tank}$ is the mass of the water ethylene glycol in the storage tank; $C_{p,wg}$ is the specific heat capacity of the water ethylene glycol and t_{cycle} is the cycle time. The other parameters $T_{wg,out,Nn}$, $T_{wg,in,0}$ and T_{tank} are temperatures of the working fluid exiting the collector model and entering the storage tank, of the working fluid entering the collector model at the previous cycle (also the previous storage tank temperature) and the new storage tank temperature respectively.

The discharging model is given by the equations 22 and 23:

$$\dot{Q}_{tank} = \dot{m}_{wg} * C_{p,wg} * (T_{wg,out,0} - T_{tank}) \quad (22)$$

$$\dot{Q}_{tank} = m_{wg,tank} * C_{p,wg} * \left[\frac{T_{tank} - T_{wg,in,Nn}}{t_{cycle}} \right] \quad (23)$$

Where the reversed flow now means that $T_{wg,out,0}$ and $T_{wg,in,Nn}$, and are now temperatures of the working fluid exiting the collector model and entering the storage tank, and of the working fluid entering the collector model at the previous cycle (also the previous storage tank temperature) respectively.

The decision to use averaged figures was based on available climatic data which is based on hourly records as such it an hourly model-based solar radiation model was adopted for the computer simulations as follows:

The total hourly radiation can be estimated from the average daily radiation by using the following equation:

$$I_{sol} = H * r_t \quad (24)$$

The coefficient to convert total daily radiation to total hourly radiation is given by equation 25:

$$r_t = \frac{\pi}{24} (a + b \cos w) \frac{\cos w - \cos w_s}{\sin w_s - \frac{\pi w_s}{180} \cos w_s} \quad (25)$$

Where „w“ is the hour angle and „w_s“ is the sunset hour angle in degrees. The coefficients „a“ and „b“ are given by equations 26:

$$\begin{aligned} a &= 0.409 + 0.5016 \sin(w_s - 60) \\ b &= 0.6609 - 0.4767 \sin(w_s - 60) \end{aligned} \quad (26)$$

Two wind convection coefficients were considered for the study; however due to unavailability of wind speed data the simplification was made to use a constant wind coefficient value:

For the Wind Convection Coefficients, Duffie and Beckman[10] recommend using equation 27; that is, the greater of the two coefficients in the parenthesis:

$$h_w = \max \left[5, \frac{8.6V^{0.6}}{L^{0.4}} \right] \quad (27)$$

where V is wind speed and L is the cube root of the house volume.

Another wind coefficient is based on Jurges Equation [11]:

$$h_w = 2.8 + 3.8V; V < 5m/s \quad (28)$$

VII. COMPUTER MODEL AND SIMULATION STUDIES

The set of equations was compiled into an Engineering Equation Solver (EES) code. Computer simulations have been performed and the results are shown in section. [12]

VIII. VALIDATION OF THE THEORETICAL RESULTS

A prototype was designed and constructed and tested. The prototype was in the form of „a segment“ of the intended solar water heater as shown in figures 10 to 12 [13]. The prototype was considered adequate because the same segment could be placed in different orientations and the results compounded to represent the total heating system. Sample experiments, with limited orientations in order to represent the overall system adequately were conducted and data recorded. Comparison of the sample experimental results with those predicted theoretically showed fair agreement within the limits of experimental error. The theoretical computations were thus validated to the extent tested.



Fig.10. One panel test setup



Fig.11. Showing the Delta-T datalogger

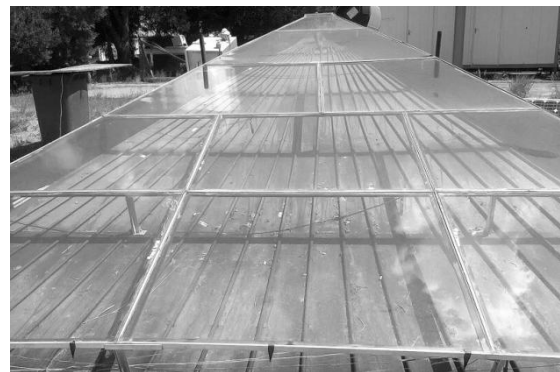


Fig. 12. Showing the riser pipes and instrumentation wiring

IX. RESULTS

The preliminary results are presented in the following charts of figures 13 to 18.

The first set of results was for testing the thermosyphon and reverse thermosyphon effects; this was done at plate spacing of 200mm and water ethylene glycol concentration of 50%; and simulations were performed for a 24 hours period. The results are shown in figures 13 and 14; figure 13 shows the temperature variation of the air and water at one hour intervals over a 24 hour cycle; figure 14 is a magnified view of figure 13 and only shows the part where the temperature in the storage tank becomes higher than the temperatures of both the absorber plate and of the heat transfer fluid flowing in the absorber runners thus depicting the reversal of energy transfer from solar hours to non-solar hours at 18 hours in the evening. Note that the air inlet temperature was equated to the hourly ambient air temperature data obtained from website <http://www.timeanddate.com/weather/botswana/gaborone/hourly> [14].

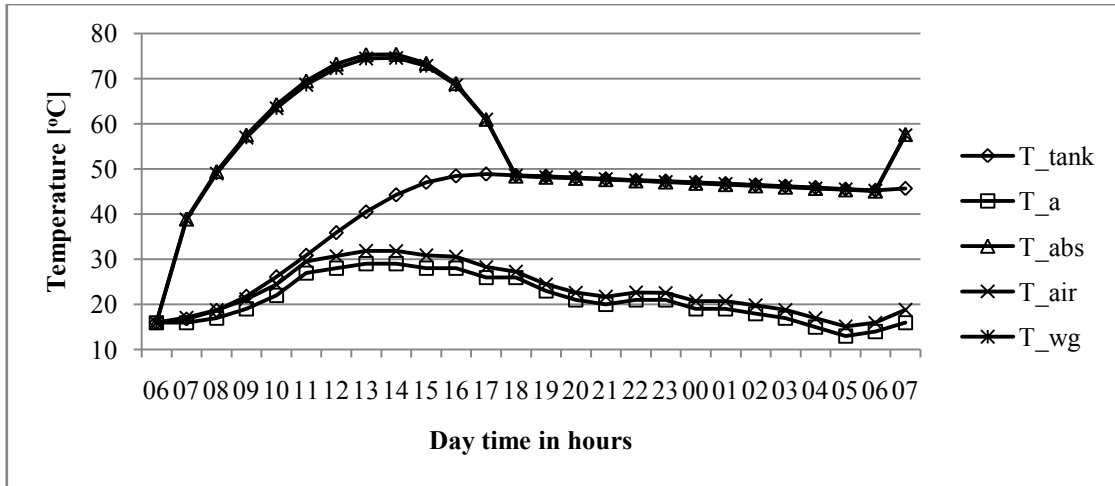


Fig. 13 Temperature Variation of Air and Water at One-Hour Intervals

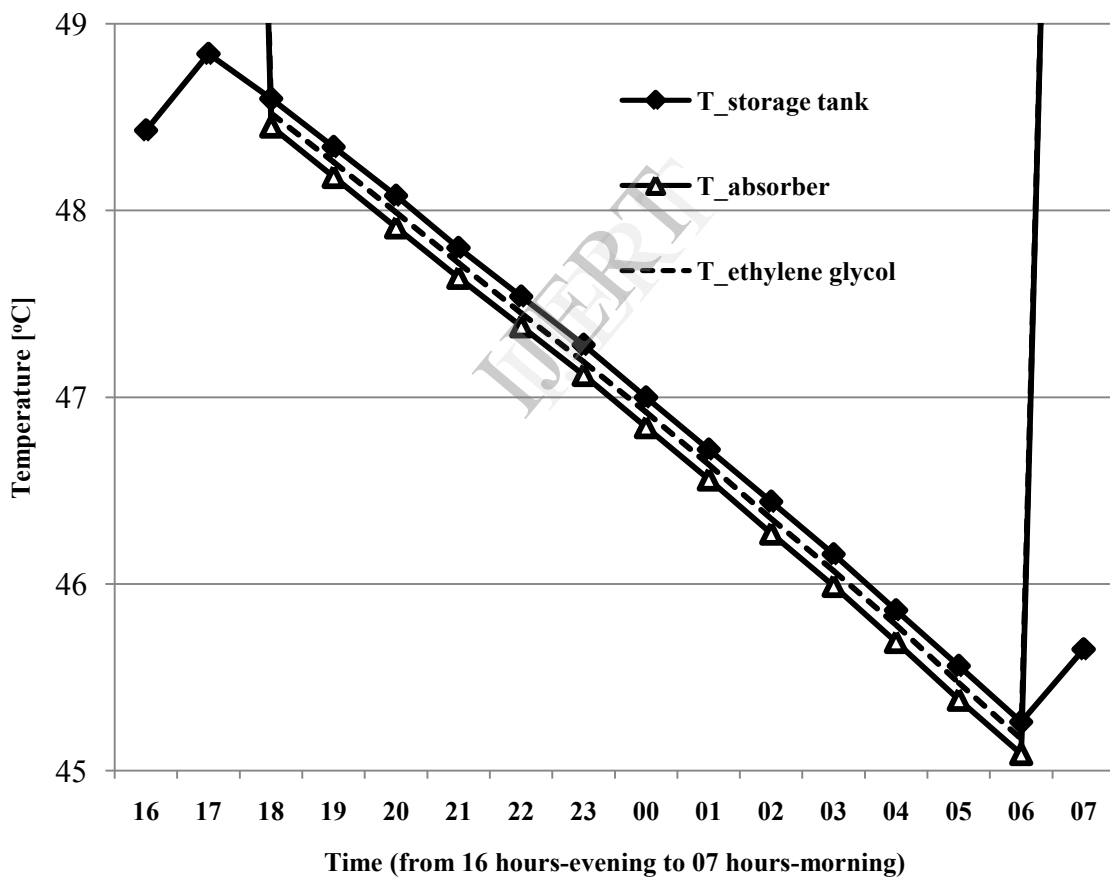


Fig. 14.Reversal of energy transfer from solar hours to non-solar hours

The second set of results is shown in figures15 and 16; this test is part of the optimization process to determine the optimal operating parameters. In this case the parameter being investigated is the plate spacing; the spacing is varied

from 5mm up to 1000mm. The percentage concentration of water ethylene glycol and the draft height are respectively maintained at 50% and 20m.

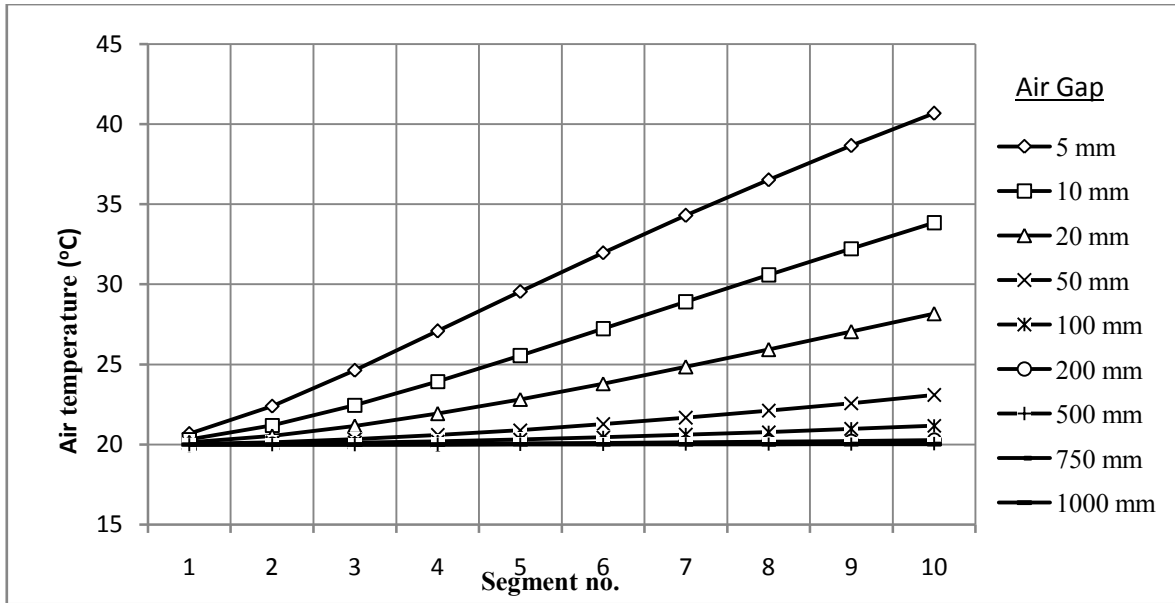


Fig.15.Segment air flow temperature profile for varying air gap

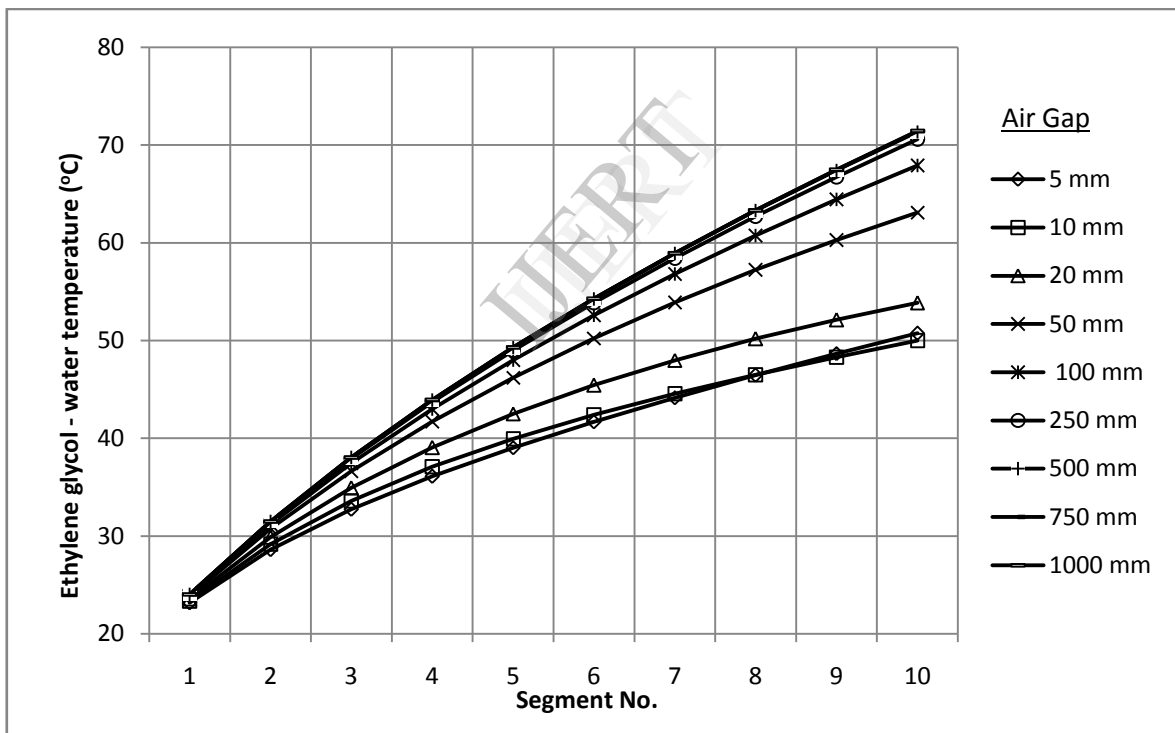


Fig.16.Segment water – ethylene glycol flow temperature profile for varying air gap

The third set of results are for optimising the concentration; the lower and upper limits of the concentration are set at 25% and 60% respectively as is

normally the practice ; the plate spacing for the results shown in figure 17 is maintained constant at 5mm and the draft height at 20m.

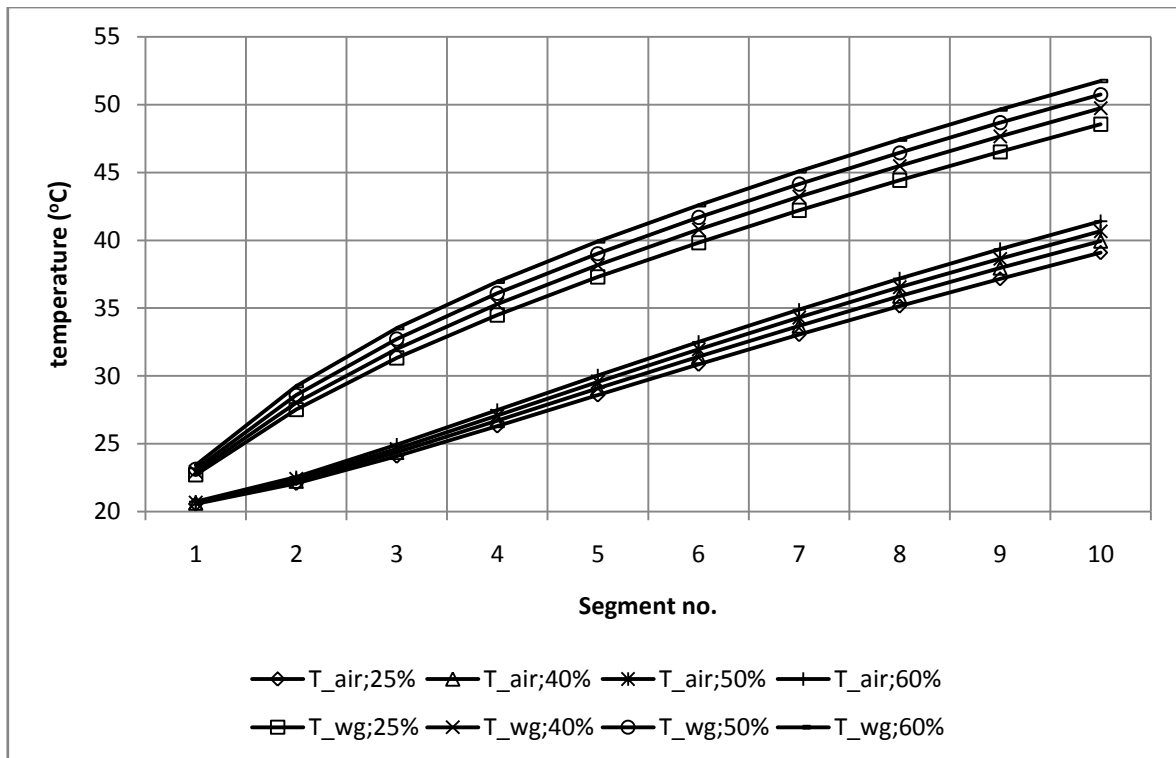


Fig.17.Segment air and water-glycol temperature profiles for varying concentration

Similar results have been obtained for other plate spacing's namely 50mm and 500mm are shown in figure 18. The spacing and concentration were kept constant at 20mm and 40% respectively.

The next results are for optimization of the draft height. The draft height was varied from 1m to 20m and the results

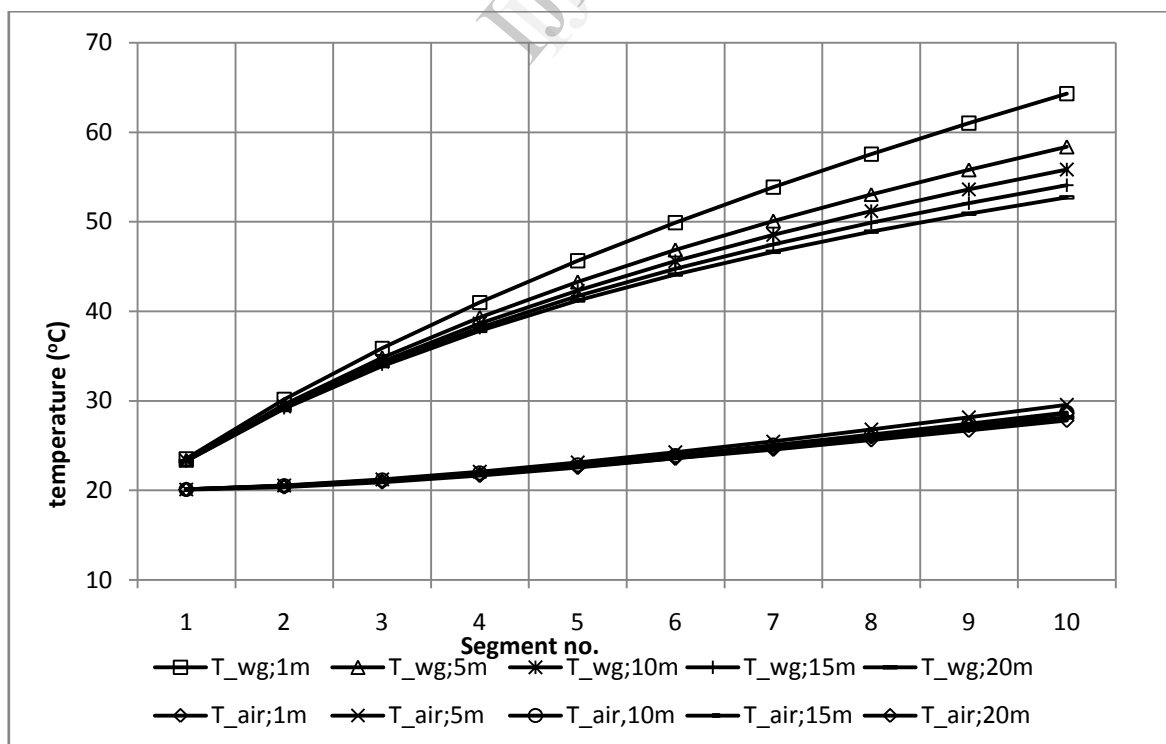


Fig. 18.Segment air and water-glycol temperature profiles for varying draft height

X. ANALYSIS AND DISCUSSION

The performance of the storage model is shown in figures 12 and 13.

- Air heating is maintained as indicated by the continuously higher temperature of air above the ambient temperature;
- Storage build-up shown by the continuous build-up of the storage or tank temperature; and
- Reversal of energy transfer between the storage/tank and the water ethylene glycol in the collector as shown by the temperature profiles crossing-over from the solar hours to the non-solar hours; this is shown in the magnified sector of figure 12 in figure 13 below where the tank temperature is now the highest followed by the temperature of the water ethylene-glycol in the collector and finally by the absorber temperature.

The optimisation aspect of the research is shown in figures 14 to 17. Air temperatures at different segments with varying air gaps are shown in figure 14. Temperatures with the minimum possible air gap of 5 mm were the highest as expected. Increase in air gap results in lower temperature at all segment numbers. Likewise, temperature at different segments for ethylene-glycol mixture and varying air gaps are shown in figure 15. The water ethylene glycol temperature profiles are higher at higher air gap values than at lower air gap values. Segment air and water-glycol temperature profiles for varying concentration for 5 mm air gap are plotted together in figure 16. It is observed that the temperature of air is generally lower than the temperature of water ethylene-glycol. This is possibly due to higher thermal conductivity of water; the same trend was observed with 50 mm air gap and 500 mm air gap. The temperature profiles for both flow streams are higher with higher concentration levels of the heat storage fluid. Figure 17 shows that the temperature profile for the air flow attains maximum values at the draft height of 5m and reduces when the draft height is lower or higher than 5m; this phenomenon requires further scrutiny.

XI. ECONOMIC CONSIDERATIONS

The economic analysis can be presented in two formats: as a financial analysis using the cost-benefit analysis metrics of benefit-cost ratio (BCR), return on investment (ROI), and net present value (NPV); or in a descriptive manner outlining the local relevance of the research. In this particular case it is found that the local context far outweighs any financial analysis that maybe conducted is more driven by the higher energy poverty currently being experienced in the sub-region. More information is required in order to undertake a financial benefit analysis: in particular the total investment cost, I_{TOTAL} , of the solar air heater is a sum of costs of all its components: $C_{COLLECTOR}$, cost of solar collector, $C_{STORAGE}$, cost of storage tank, C_{HTF} , cost heat transfer fluid (HTF) and C_{PIPING} , cost of piping.

$$I_{TOTAL} = C_{COLLECTOR} + C_{STORAGE} + C_{HTF} + C_{PIPING} \quad (29)$$

This information together with monetized benefits of the project maybe used to determine each of the following:

Benefit-Cost Ratio:

$$BCR = \frac{\text{Total Discounted Benefits}}{\text{Total Discounted Costs}} \quad (30)$$

Return on Investment; (%):

$$ROI = \frac{(\text{Total Discounted Benefits} - \text{Total Discounted Costs})}{\text{Total Discounted Costs}} \quad (31)$$

Net Present Value:

$$NPV = \text{Total Discounted Benefits} - \text{Total Discounted Costs} \quad (32)$$

These will be undertaken in a future study; for now it suffices to say: The concept of affordable solar thermal storage has been identified as one critical factor that could promote the adoption of solar energy usage; solar energy resource, despite being one of the best globally, remains largely untapped. Access to electricity in the Southern African sub-region is very low except for a few countries as shown in fig. 19 below. Only three countries have access to electricity significantly above the average for Sub Saharan Africa which is 17%, Mauritius, South Africa and Zimbabwe. [15]

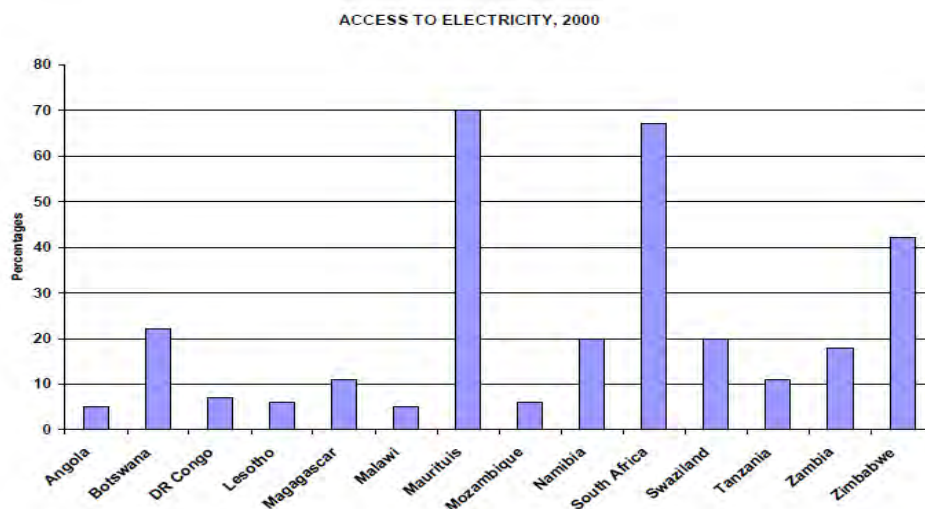


Fig. 19. Access to electricity by country in Southern Africa

XII. CONCLUSIONS

This work involved designing a novel method of simultaneously heating air for space heating or any other suitable application while at the same time heating a liquid sensible storage media for use during non-solar hours. It was initiated as an off-shoot project of an updraft solar chimney project for electricity generation; however upon an extensive survey as well as a detailed review of the solar chimney project it was found not to be viable, at least in the time being until more innovative and cost effective structural materials and construction methods are developed. The storage model was however considered adequate for other applications such as space heating, crop drying etc. A concept was developed followed by mathematical models and computer simulations; and finally a prototype was constructed. Preliminary trials were conducted on the prototype; however, due to the dissolution of the client company extensive trials remain outstanding.

Maximum temperatures attained were 75.3°C, 74.6°C, 48.8°C and 31.9°C respectively for the absorber, heat transfer fluid in the collector, heat transfer fluid in the storage tank, and air flow at the exit of the collector; the ambient temperature varied from 13°C to 29°C.

The results show a gradual growth in the storage temperature as indicative of the technical viability of the developed process. The results have also shown the reverse-thermosyphon effect through the reversal of the direction of the heat transfer from the storage to the air flow path during the non-solar hours. The varying in performance for different values of the variable parameters indicates the need for further optimization of the model. For the given storage design, the best performance parameters for both air heating and storage fluid heating maybe summarised as plate spacing of 5mm, glycol-water concentration of 60% and draft height of 5m. Further studies are recommended on optimisation and optimum design and extensive testing of the solar air heater systems with natural draft. A through economic analysis is also outstanding but the project is generally acceptable based on the need to develop clean energy technologies that also yield environmental benefits and encourage tapping into the abundant solar energy resources.

ACKNOWLEDGEMENTS

The Consultants wish to acknowledge the contribution of several other colleagues from the University of Botswana, the University of KwaZulu-Natal, University of Stellenbosch and the Botswana Technology Centre (BOTECH), who have tendered valuable suggestions and interacted with the Consultants during the progress of the work and in the formal presentations at BOTECH.

REFERENCES

- [1] <http://www.botec.bw/index.php/botec-projects/energy/the-solar-chimney> accessed July 29, 2013
- [2] <http://inventors.about.com/od/timelines/a/Photovoltaics.htm>
- [3] <http://exploringgreentech.com/solar-energy/history-of-solar-energy/>
- [4] <http://solarwall.com/media/images-main/2-products/brochure/SolarDuctSpec.pdf>
- [5] http://weather.uk.msn.com/monthly_averages.aspx?wealocations=wc:BCXX0001
- [6] Sharma Atuletal, Review on thermal energy storage with phase change materials and applications: *Renewable and Sustainable Energy Reviews 13 (2009) pp 318-345*
- [7] Morrison G.L., Reverse Circulation in Thermosyphon Solar Water Heaters, *Solar Energy Vol. 36, No. 4, pp. 377-379, 1986*
- [8] Incropera P Frank et al, 2007: *Fundamentals of Heat and Mass Transfer*; John Wiley & Sons; USA, ISBN *978-0-471-45728-2
- [9] <http://www.jgsee.kmutt.ac.th/exell/Solar/FlatPlate.rtf>
- [10] Duffie J.A., Beckman W.A., "Solar Engineering of Thermal Processes" 2nd Ed., John Wiley & Son, Inc., USA, 1991 ISBN 0-471-51056-4 p281
- [11] Rabadiya A.V., Kirar R., Comparative Analysis of Wind Loss Coefficient (Wind Heat Transfer Coefficient) For Solar Flat Plate Collector; in *International Journal of Emerging Technology and Advanced Engineering Website*; (ISSN 2250-2459, Volume 2, Issue 9, September 2012) 463; www.ijetae.com
- [12] Klein S.A., Alvarado F.L., EES, Engineering Equation Solver for Microsoft Windows Operating Systems, F-Chart Software, Middleton, WI 53562, USA, 1992-98
- [13] Situmbeko S.M., Kumar K.L., BOTECH Solar Thermal Storage Model Final Report, 2013.
- [14] <http://www.timeanddate.com/weather/botswana/gaborone/hourly> (2012)
- [15] <http://www.afrepren.org/project/gnesd/esdsi/erc.pdf>



Sponsored by the
Department of Science
& Technology
and
GIZ



This journal is accredited by the South African Department of Higher Education and Training for university subsidy purposes. It is abstracted and indexed in Environment Abstract, Index to South African Periodicals, and the Nexus Database System.

The journal has also been selected into the Science Citation Index Expanded by Thomson Reuters, and coverage begins from Volume 19 No 1. It is also on the Scientific Electronic Library Online (SciELO) SA platform and is managed by the Academy of Science of South Africa (ASSAf).

Editor

Richard Drummond

Editorial board

Mr J A Basson *Energy consultant*

Professor K F Bennett *Energy Research Centre, University of Cape Town*

Professor A A Eberhard *Graduate School of Business, University of Cape Town*

Dr S Lennon *Managing Director (Resources & Strategy Division), Eskom*

Mr P W Schaberg *Sasol Technology (Pty) Ltd*

Administration and subscriptions

Ms Fazlin Harribi

Annual subscriptions (four issues)

Individuals (Africa): R160 (single copy R51)

Individuals (beyond Africa): US\$109 (single copy US\$39)

Corporate (Africa): R321 (single copy R103)

Corporate (beyond Africa): US\$218 (single copy US\$77)

Cost includes VAT and airmail postage.

Cheques should be made payable to the University of Cape Town and sent to the address given below.

Enquiries may be directed to:

The Editor, Journal of Energy in Southern Africa,
Energy Research Centre, University of Cape Town,
Private Bag, Rondebosch 7701, South Africa

Tel: +27 (021) 650 3894 Fax: +27 (021) 650 2830

E-mail: Richard.Drummond@uct.ac.za

Website: www.erc.uct.ac.za

It is the policy of the Journal to publish papers covering the technical, economic, policy, environmental and social aspects of energy research and development carried out in, or relevant to, Southern Africa. Only previously unpublished work will be accepted; conference papers delivered but not published elsewhere are also welcomed. Short comments, not exceeding 500 words, on articles appearing in the Journal are invited. Relevant items of general interest, news, statistics, technical notes, reviews and research results will also be included, as will announcements of recent publications, reviews, conferences, seminars and meetings.

Those wishing to submit contributions should refer to the guidelines given on the inside back cover.

The Editorial Committee does not accept responsibility for viewpoints or opinions expressed here, or the correctness of facts and figures.

© Energy Research Centre ISSN 1021 447X

JOURNAL OF ENERGY

IN SOUTHERN AFRICA

Volume 24 Number 4 • November 2013

CONTENTS

- 2 A cost-benefit analysis of concentrator photovoltaic technology use in South Africa: A case study
Mario du Preez, Justin Beukes and Ernest van Dyk
- 12 A possible design and justification for a biogas plant at Nyazura Adventist High School, Rusape, Zimbabwe
Patrick Mukumba, Golden Makaka, Sampson Mamphweli and Shepherd Misi
- 22 Critical factors to be considered when planning the implementation of environmental improvements and energy saving
Juliane Barbosa dos Santos and Charbel José Chiappetta Jabbour
- 30 Emissions analysis from combustion of eco-fuel briquettes for domestic applications
Tsietsi J Pilusa, Robert Huberts and Edison Muzenda
- 37 Experimental study on natural convection greenhouse drying of papad
Mahesh Kumar
- 44 Dirt analysis on the performance of an engine cooling system
Yashvir Singh and Nishant Kr. Singh
- 51 System and component modelling of a low temperature solar thermal energy conversion cycle
Shadreck M Situmbeko and Freddie L Inambao
- 63 Modelling influence of temperature on daily peak electricity demand in South Africa
Delson Chikobvu and Caston Sigauke
- 71 Performance analysis of an air humidifier integrated gas turbine with film air cooling of turbine blade
Alok K Mahapatra and B E Sanjay
- 82 Details of authors
- 86 Index to Volume 24: February–November 2013

System and component modelling of a low temperature solar thermal energy conversion cycle

Shadreck M Situmbeko

Freddie L Inambao

University of KwaZulu-Natal, Howard College, Mechanical Engineering, Durban, South Africa

Abstract

Solar thermal energy (STE) technology refers to the conversion of solar energy to readily usable energy forms. The most important component of a STE technology is the collectors; these absorb the shorter wavelength solar energy (400-700nm) and convert it into usable, longer wavelength (about 10 times as long) heat energy. Depending on the quality (temperature and intensity) of the resulting thermal energy, further conversions to other energy forms such as electrical power may follow. Currently some high temperature STE technologies for electricity production have attained technical maturity; technologies such as parabolic dish (commercially available), parabolic trough and power tower are only hindered by unfavourable market factors including high maintenance and operating costs. Low temperature STEs have so far been restricted to water and space heating; however, owing to their lower running costs and almost maintenance free operation, although operating at lower efficiencies, may hold a key to future wider usage of solar energy. Low temperature STE conversion technology typically uses flat plate and low concentrating collectors such as parabolic troughs to harness solar energy for conversion to mechanical and/or electrical energy. These collector systems are relatively cheaper, simpler in construction and easier to operate due to the absence of complex solar tracking equipment. Low temperature STEs operate within temperatures ranges below 300°C. This research work is geared towards developing feasible low temperature STE conversion technology for electrical power generation. Preliminary small-scale concept plants have been designed at 500Wp and 10KWp. Mathematical models of the plant systems have been developed and simulated on the EES (Engineering Equation Solver) platform. Fourteen

candidate working fluids and three cycle configurations have been analysed with the models. The analyses included a logic model selector through which an optimal conversion cycle configuration and working fluid mix was established. This was followed by detailed plant component modelling; the detailed component model for the solar field was completed and was based on 2-dimensional segmented thermal network, heat transfer and thermo fluid dynamics analyses. Input data such as solar insolation, ambient temperature and wind speed were obtained from the national meteorology databases. Detailed models of the other cycle components are to follow in next stage of the research. This paper presents findings of the system and solar field component.

Keywords: low temperature solar thermal energy, mathematical model, EES computer simulations, working fluids, cycle configuration, component and system models

1. Introduction

Most naturally occurring energies such as light energy from the sun, chemical energy in fossil and biomass fuels, mechanical energy in hydro-streams of rivers and oceans, in tidal waves, and in wind etc., thermal energy in geothermal resources, and nuclear energy in nuclear fuels are present not in a readily usable form and sometimes presents a technical burden if an attempt is made to transport it in its natural form. Energy conversion systems allow us to transform the natural energy to conveniently usable, storable and transportable forms. This paper looks at the conversion of low temperature solar thermal energy to electrical energy.

STE technology refers to the conversion of shorter wavelength solar energy (400-700nm) to longer wavelength (about 10 times as long) heat energy. The most important component of a STE technology is the collectors which absorb and convert solar energy into electrical power, for example.

Currently some high temperature solar thermal energy (HTSTE) technologies for electricity production have attained technical maturity and are only hindered by unfavourable market factors including high maintenance and operating costs. Examples of HTSTE technologies include parabolic dish, parabolic trough, and power tower systems (Groenendaal, 2002).

Low temperature solar thermal energy (LTSTE) technologies have so far been restricted to water and space heating with little or no emphasis on power generation. Examples of applications include:

- Evaporation ponds for extraction of sea water salt;
- Concentrating brine solutions in leach mining and removing dissolved solids from waste streams;
- Domestic and process water heating;
- Preheating of ventilation air; and
- Crop drying as in drying of coffee beans and marigolds.

However, owing to their lower running costs and almost maintenance free operation, LTSTE technologies, although operating at lower efficiencies, may hold a key to future wider usage of solar energy.

Current research on LTSTE for power generation include solar thermal organic Rankine cycle, solar thermal Kalina cycle, Solar Chimney and SNAP (Groenendaal, 2002). Figure 1 shows schematic illustrations of the Solar Chimney, SNAP Plants, Organic Rankine and Kalina Cycles.

2. Feasibility study for development of low temperature solar thermal energy

LTSTE conversion technology typically uses flat plate and low concentrating collectors such as par-

abolic troughs to harness solar energy for conversion to mechanical and/or electrical energy. These collector systems are relatively cheaper, simpler in construction and easier to operate due to the absence of complex solar tracking equipment found in HTSTE systems. LTSTE operate within temperatures ranges below 300°C.

Figures 2 and 3 show two possible experimental setups. The general layout consists of the solar collector, heat exchangers, turbine-generator, pumps and piping. The first concept sketch shows the first experimental setup whereby the heat transfer fluid is pumped through the solar collector where it is heated and is then passed through the evaporator where heat is transferred to the working fluid. In the second experimental setup, as shown in the second concept sketch, the working fluid is directly heated and evaporated by a solar collector. Whereas the first setup has the advantage of eliminating one heat exchanger, the evaporator, and reducing the required piping, it presents other design challenges; for instance the solar collector must have the required corrosion resistance and be able to withstand higher pressures associated with the working fluid.

Preliminary small-scale concept plants have been designed at 500Wp and 10kWp, where the smaller model is intended as a laboratory experiment and the larger as a field experiment. The aim of this laboratory test is to get an insight in the experimental test setup and results recording and analyses as well as to implement any needed improvements. The field experimental setup will involve the 10kWp Low Temperature Solar Energy Conversion Model.

Designing the cycle involves optimally sizing its main components so as to attain the intended output. The main cycle components are the evaporator and condenser heat exchangers, and the turbine and pumps work devices, the solar collectors array and the generator. The other design aspect involves sizing the duct network so as to minimise both pressure and heat losses and determining the quantities

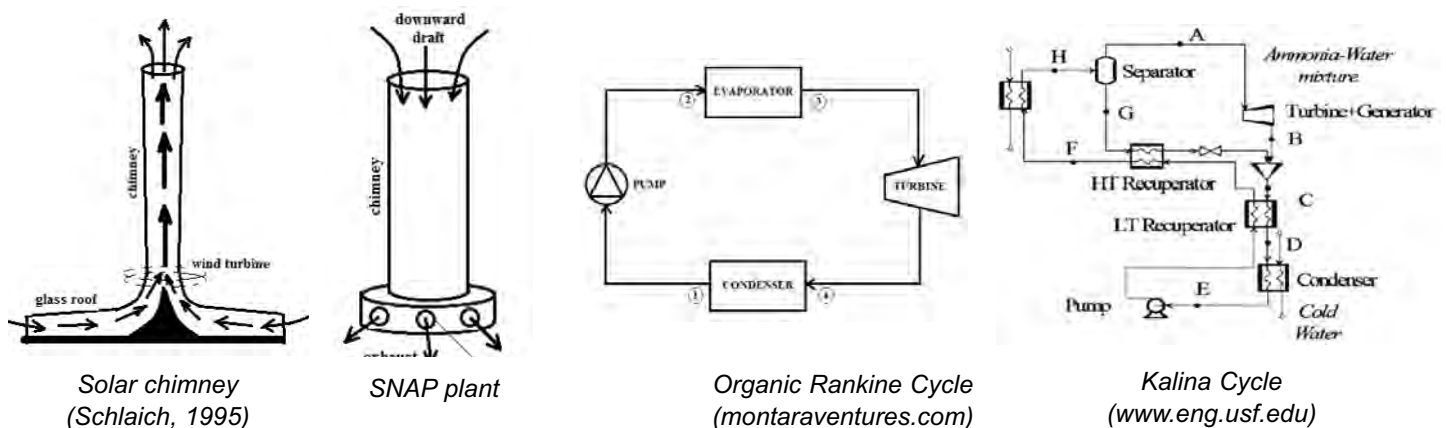


Figure 1: Examples of low temperature solar thermal energy technologies

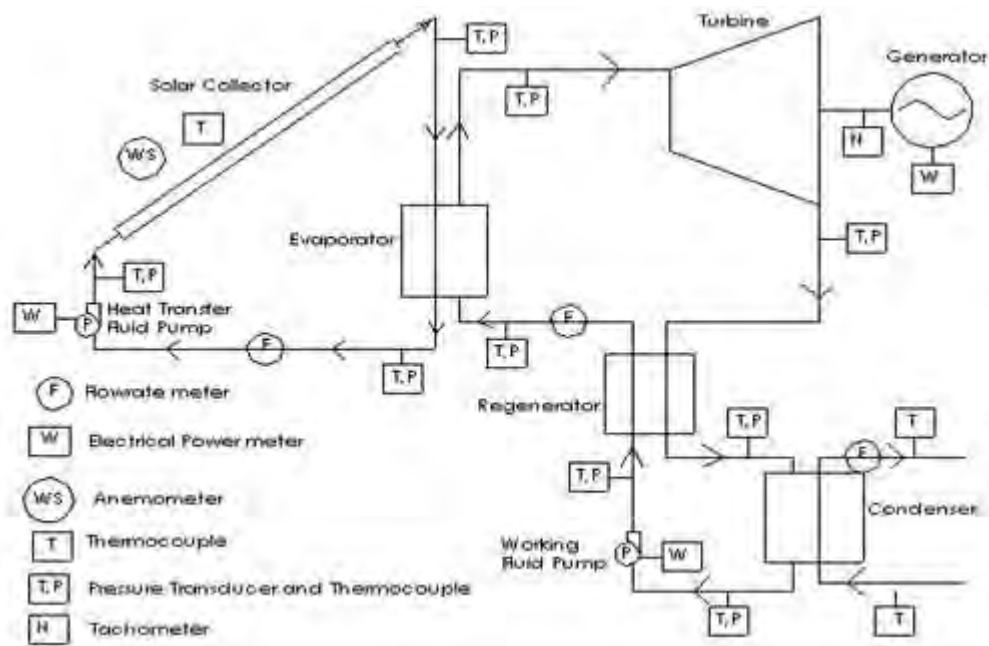


Figure 2: Experimental setup concept 1

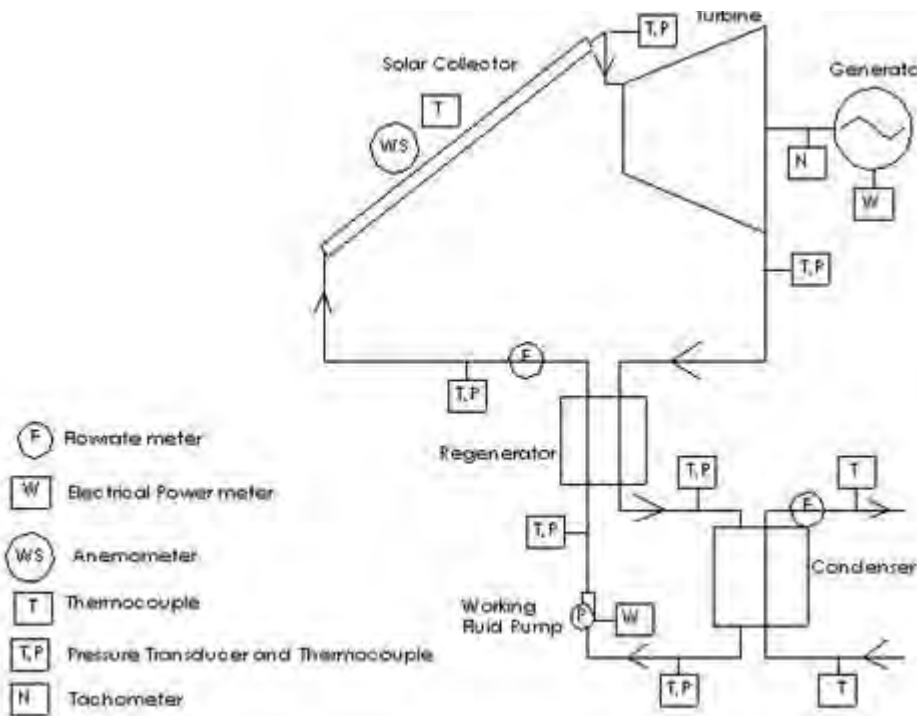


Figure 3: Experimental setup concept 2

of both the working and heat transfer fluids as well as specifying the type of insulation.

The solar field is an important aspect of this design as it involves not only determining the size of the field but also the layout of the solar collectors array.

The preliminary array design is based on the Solardome SA Solar Collector size 1840 x 1650 mm, giving area of 3.04 m² (www.solardome.co.za). The efficiencies of flat plate collector from Thermomax Industries (www.thermotechs.com)

range from 35 to 50 % for domestic hot water with mean temperature $T_m \approx 55^\circ\text{C}$. Where T_m is the average temperature of fluid in the collector and is given by:

$$T_m = \frac{T_{in} + T_{out}}{2} \quad (1)$$

where T_{in} and T_{out} are respectively the solar collector inlet and outlet temperatures. The range of efficiencies for Rankine cycle operating at low to medium temperatures ranges from 9.9 to 14.1%

(Nishith, 2009). Taking averages the overall system efficiency could be taken as 5.1%. Thus the solar thermal energy available should be about 9.8kW_{Th} for the laboratory model and 196kW_{Th} for the field model. Durban Insolation data averages $4.328\text{ kWh/m}^2/\text{day}$ (www.gaisma.com). First approximations of the corresponding solar fields are shown in Table 1 and preliminary solar array layouts are shown in Figures 4 .

Table 1: First pass size estimates of the solar arrays

Parameter	Lab. model (solar collector)	Field model (solar collector)	Units
Output power	0.5	10	kW
ORC mean efficiency	12	12	%
Solar mean efficiency	42.5	42.5	%
Input power	9.80	196.08	kW
Durban insolation $\text{kWh/m}^2/\text{day}$	4.328	4.328	
Incident area	27	545	m^2
Solar collector area	3.04	3.04	m^2
No. of solar collectors	9	179	

3. Mathematical modelling

Mathematical models of the plant systems have been developed and simulated on the EES (Engineering Equation Solver) platform. Fourteen candidate working fluids and three cycle configurations have been analysed with the models. The analyses include a logic model selector through which an optimal conversion cycle configuration and working fluid mix is established.

3.1 First pass mathematical modelling (Situmbeko, 2011)

The first pass model gives an initial insight into the performance of the proposed energy conversion system design. This first pass model output together

with the more detailed specifications of components for the proposed system design will yield a more detailed model with more realistic performance parameters that can now be incorporated in the design, development and validation of the physical model. In this work a more generalized model is first proposed as in Figure 6. This is then further customized to the thermo-physical properties of the different proposed working fluids. In particular a mathematical logic model is incorporated to assign an appropriate cycle configuration to each proposed working fluid.

The first pass model makes a number of assumptions such as:

- pumping and expansion efficiencies are assumed as $\eta_{\text{pump}} = 0.65$, $\eta_{\text{turbine}} = 0.85$
- modelling of heat exchangers at this stage is only performed as a thermal process to determine required input thermal energy and required exhaust thermal energy (detailed heat exchanger modelling will be done at a later stage)
- thermal losses in the cycle components and ducting are negligible;
- pressure head losses in the heat exchangers are negligible; and
- no work and no heat transfer occur in the valves, etc.

Three types of models can be identified with low temperature thermal cycles depending on the nature of the working fluid. Based on the fluids' T-s (temperature versus entropy) saturation curves these three types of energy conversion systems are: the conventional Rankine cycle, Rankine cycle with a recuperator and Rankine cycle with a superheater as shown in Figure 7. A summary of results of computer simulations of the first pass model is shown in Table 2.

3.2 Detailed component models: Solar field collector modelling

Detail modelling of a solar collector requires knowledge of the geometrical measurements and thermal

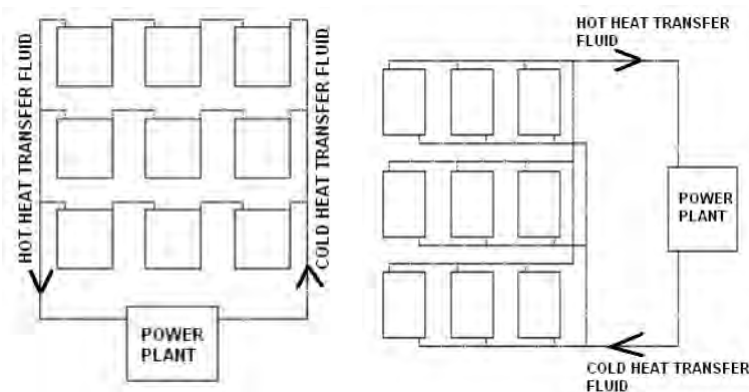


Figure 4: Two layouts options for 500 Wp solar field (requires 9 solar collectors with two layout options)

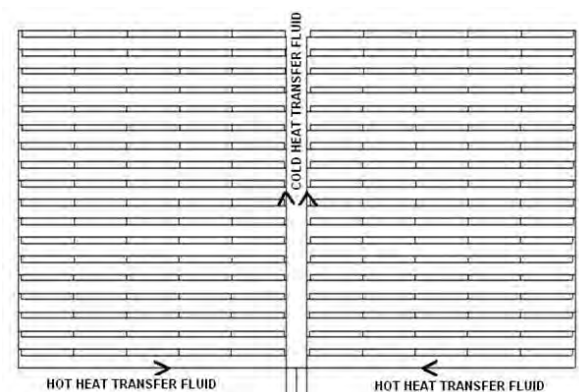


Figure 5: Possible layout for 10kWp solar field (requires 180 solar collectors)

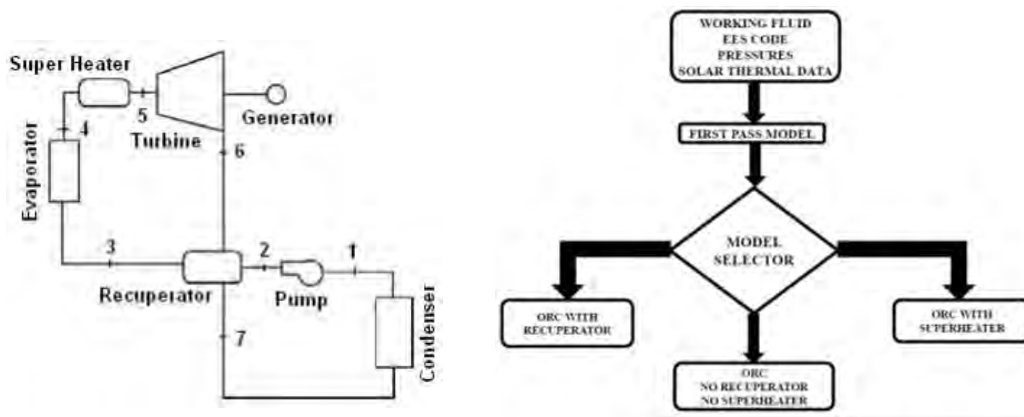


Figure 6: General configuration of a LTST technology and a Model Logic Selector

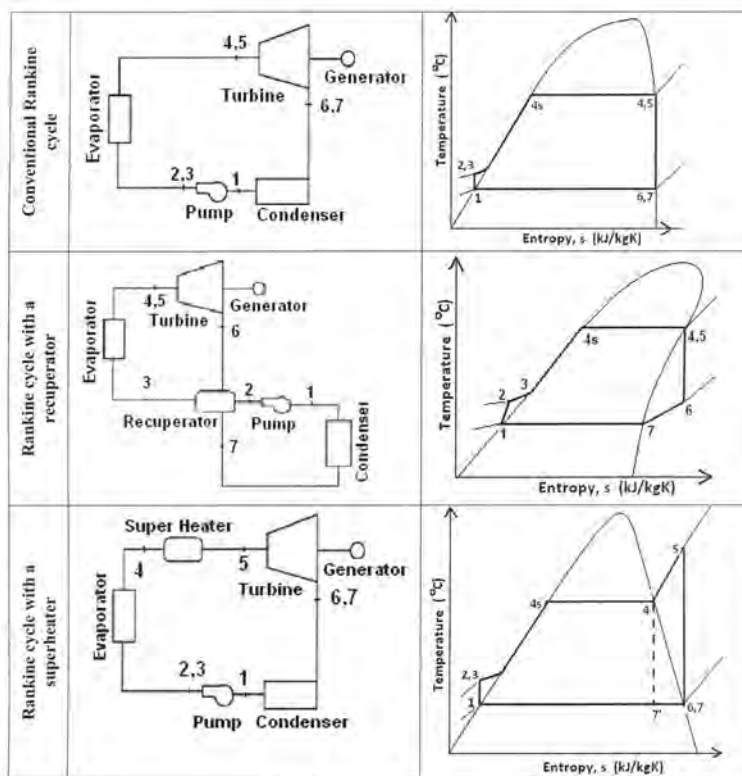


Figure 7: Three configuration options

properties of materials used in the construction. The process is based on carrying out an energy balance which can be either steady state or transient. A transient model is more useful when the solar data can be measured and fed synchronously to the simulation model.

Figure 8 shows the cross-section of a One-Riser-Pipe Solar Thermal Collector that was used to develop the energy balance represented in equations 2 to 6 below.

For the glass cover:

$$Q_{store,C} = Q_{in,C} - Q_{conu,C \rightarrow a} - Q_{rad,C \rightarrow a} + Q_{conu,A \rightarrow C} + Q_{rad,A \rightarrow C} \quad (2)$$

For the absorber plate:

$$Q_{store,A} = Q_{in,A} - Q_{conu,A \rightarrow C} - Q_{rad,A \rightarrow C} - Q_{cond,A \rightarrow F} - Q_{cond,A \rightarrow a} \quad (3)$$

For the heat transfer fluid:

$$Q_{cond,A \rightarrow F} = Q_{cond,F \rightarrow a} + C_{th} \quad (4)$$

For the storage tank:

$$Q_{store,T} = Q_{th} - Q_{cond,T \rightarrow a} \quad (5)$$

Thermal efficiency:

$$\eta_{th} = \frac{\int Q_{th} dt}{A_c \int G dt} \quad (6)$$

Table 2. Thermal efficiencies of different Organic Rankine Cycle configurations and different working fluids

Model type	Working fluid	Q_dot_r evaporato (kW)	Q_dot_ recuperator (kW)	Q_dot_ superheater (kW)	Power (kW)	eta_therm (%)
Rankine with recuperator no superheater	n-pentane	4.07	0.40	0	0.50	12.04
Conventional Rankine no recuperator no superheater	Benzene	4.68	0	0	0.53	11.11
Conventional rankine no recuperator no superheater	n-butane	4.56	0	0	0.54	11.60
Rankine with recuperator no superheater	n-hexane	3.75	0.61	0	0.46	12.10
Conventional Rankine no recuperator no superheater	Isobutene	4.31	0	0	0.52	11.72
Conventional Rankine no recuperator no superheater	R141b	2.60	0	0	0.30	11.30
Rankine with recuperator no superheater	Is pentane	3.90	0.38	0	0.49	12.20
Conventional Rankine no recuperator no superheater	R245fa	2.30	0	0	0.24	10.38
Rankine with recuperator no superheater	R113	1.64	0.16	0	0.20	11.89
Conventional Rankine no recuperator no superheater	R123	2.02	0	0	0.23	11.02
Rankine with superheater no recuperator	R22	2.50	0	0.21	0.33	12.01
Rankine with recuperator no superheater	Toluene	4.09	0.45	0	0.49	11.75
Rankine with superheater no recuperator	R134a	2.41	0	0.08	0.28	10.99
Rankine with superheater no recuperator	Water	23.29	0	2.57	2.80	10.81

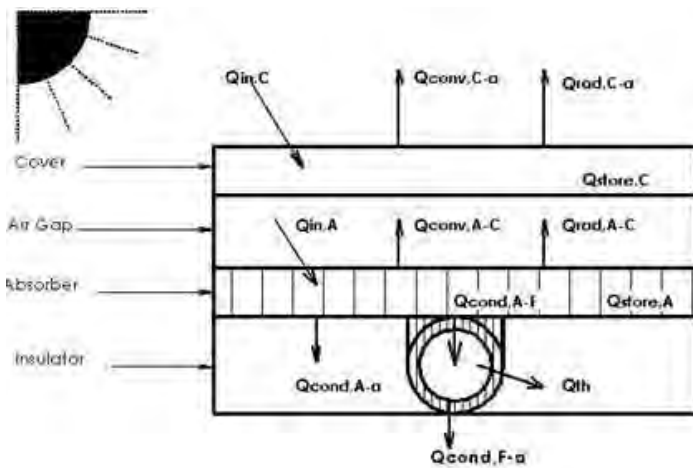


Figure 8: One pipe solar collector model

For the air gap the correlation used to determine the convective heat transfer coefficient is that given by Hollands et al (Duffie, 1991); for inclined parallel plates with a tilt angle of 0-75° which is given as:

$$Nu = 1 + 1.44 \left[1 - \frac{1708(\sin 1.8\beta)^{1.6}}{Ra \cos \beta} \right] \left[1 - \frac{1708}{Ra \cos \beta} \right]^+ + \left[\left(\frac{Ra \cos \beta}{5830} \right)^{1/3} - 1 \right]^+ \quad (7)$$

where the meaning of the + exponent is that only positive values of the terms in the square brackets are to be used (i.e., use zero if the term is negative); and the Nusselt number Nu and the Rayleigh number Ra are given by:

$$Nu = \frac{hL}{k} \quad \text{and} \quad Ra = \frac{g\beta' \Delta T L^3}{\nu\alpha} \quad (8)$$

where:

- h = heat transfer coefficient,
- L = plate spacing
- k = thermal conductivity

g = gravitational constant
 β = volumetric coefficient of expansion (for an ideal gas, $\beta=1/T$)
 ΔT = temperature difference between plates
 ν = kinematic viscosity
 α = thermal diffusivity

For laminar flow in circular pipes the correlation used is that given by Incropera (2007):

$$Nu_D \equiv \frac{hD}{k} = 4.36 \quad (9)$$

for uniform surface heat flux

$$Nu_D \equiv \frac{hD}{k} = 3.66 \quad (10)$$

for constant surface temperature

For this case the transfer to the heat transfer fluid lies in between the two conditions and therefore the Nusselt number used is the average of the two.

For the Wind Convection Coefficients, Duffie (1991) recommend using:

$$h_w = \max\left[5, \frac{9.6V^{0.6}}{L^{0.4}}\right] \quad (11)$$

where V (m/s) is wind speed and L (m) is the cube root of the house volume.

The average hourly radiation can be estimated from the total daily radiation by using the following equation (Silva, 2011):

$$I = Hr_t \quad (12)$$

The coefficient to convert total daily radiation, H (Wh/m²-day) to average hourly radiation I (W/m²) is given by:

$$r_t = \frac{\pi}{24} (a + b \cos w) \frac{\cos w - \cos w_s}{\sin w_s - \frac{\pi w_s \cos w_s}{180}} \quad (13)$$

where w is the hour angle and w_s is the sunset hour angle in degrees. The coefficients a and b are given by:

$$\begin{aligned}
 a &= 0.409 + 0.5016 \sin(w_s - 60) \\
 b &= 0.6609 - 0.4767 \sin(w_s - 60)
 \end{aligned} \quad (14)$$

The model also requires inputs of ambient temperatures; these are included in Table 3.

Transient conditions

Considering the steady-state model above, corresponding transient models can be developed. These are however not used in the current model as the transiency is modelled into the time step segmented model.

Table 3: Hourly ambient temperatures for the modelled day (www.weather.com)

Time	Temp. (°C)	Time	Temp. (°C)	Time	Temp. (°C)
5am	20	1pm	26	9pm	23
6am	20	2pm	27	10pm	22
7am	20	3pm	26	11pm	21
8am	20	4pm	26	12am	21
9am	22	5pm	26	1am	21
10am	23	6pm	24	2am	20
11am	25	7pm	24	3am	20
12pm	25	8pm	23	4am	20

Storage model

The thermal storage model consists of an energy balance consisting of charging, discharging and thermal losses. In this model, however, only charging has been considered. The discharging and thermal losses will be considered at the time of coupling the solar cycle sub-model to the thermal conversion cycle sub-model. The charging model is given by the equations:

$$\begin{aligned}
 \dot{Q}_{tank} &= \dot{m}_{wg} * Cp_{wg} * (T_{wg,out,30} - T_{tank}) \\
 \dot{Q}_{tank} &= m_{wg,tank} * Cp_{wg} * \left[\frac{T_{tank} - T_{wg,in,1}}{t_{cycle}} \right] \quad (15)
 \end{aligned}$$

where:

\dot{Q}_{tank} (J/s) is the heat transfer rate to the thermal storage;

\dot{m}_{wg} (kg/s) is the mass flow rate of the water ethylene glycol working fluid;

$m_{wg,tank}$ (kg) is the mass of the water ethylene glycol in the storage tank;

Cp_{wg} (J/kg-K) is the specific heat capacity of the water ethylene glycol;

t_{cycle} (s) is the cycle time for the current cycle;

$T_{wg,out,30}$ (°C) is the temperature of the working fluid exiting the collector model and entering the storage tank for the current cycle;

$T_{wg,in,1}$ (°C) is the temperature of the working fluid entering the collector model at the previous cycle (it is also the temperature of the storage tank at previous cycle); and

T_{tank} (°C) is the new storage tank temperature for the current cycle.

4 Computer simulations

4.1 Description of the computer model

The model consists of a code written in EES. EES has the advantage that apart from its flexible solver capabilities it also already contains thermodynamic properties of most working fluids and materials including the ethylene glycol water mixture used in this model and the air contained in the air gap. The thermodynamic properties include density, specific

heat, thermal conductivity, viscosity, etc.

The code is arranged in the following format:

- Main Program: Calls the two procedures NusseltNumber and HourCycle; and outputs thermal storage data.
- SubProgram SegmentedModel: calculates the energy balance for each cycle; calls the I_sol
- Function I_sol: calculates the hour solar radiation
- Procedure NusseltNumber: calculates the Nusselt number for each segment of the air gap.
- Procedure HourCycle: compiles energy data for all cycles in each hour

4.2 Model validation

The model was run for the selected hourly ambient temperatures of the typical March-April day as in Table 3. The model calculated the hourly total radiation as in equations 12 to 14. Two tests were done for the 9-solar-collectors field and the 180-solar-collectors field. The model used was a one pipe model; thus it was assumed for the 9 solar collectors that three one-pipe solar collectors were connected in series and for the 180 solar collectors that eighteen one-pipe solar collectors were connected in series. The geometrical sizes and thermal properties of the single riser pipe solar collectors model are given in Table 4.

5. Results of computer models and simulations

The results of the solar model computer simulations are presented in the following charts:

5.1 Computer solar radiation model

Figure 9 shows the computed hour radiation values. The computed solar radiation is highest at noon and is almost symmetrically reducing to zero on

sides, the forenoon and the afternoon. The peak at noon is 613.2 W/m². The simplified model seems adequate for design purposes. In actual situations the model would have to take into account other weather parameters such as cloud cover, wind and precipitation. The solar radiation curve closely follows the fourth order polynomial:

$$y = 0.296x^4 - 8.306x^3 + 59.70x^2 - 21.82x - 27.03$$

5.2 Temperature modelling results

Figure 10 shows the temperature profiles along the segments of the collectors. T_p is the temperature profile for the absorber plate and T_wg is the temperature profile for the water ethylene glycol working fluid. The numbers enclosed in the parentheses represent the number of the one-pipe-model collectors as they are connected in series. These results are for a one cycle pass with no storage model connected.

Figure 11 shows the energy profiles along the segments of the collectors. Q_dot_wg is the heat transfer profile to the working fluid and Q_dot_loss represents the thermal losses from the collector at each segment. Similarly these results are for a one cycle pass with no storage model connected.

The rate of heat gain by the working fluid decreases along linear segments of the collector whilst the rate of heat losses from the collector increases along the linear segments of the collector.

Figure 12 shows results for the 180-solar collector single pipe field model. The computer model consists of 18 one-pipe models connected in series to represent the 180-solar collector field.

There is a steady build-up of temperature for all components along the model segments and banks.

Table 4: Description of the simulated model

Length of absorber plate	2.0 m for entire collector; 200mm for each segment model
Width of absorber plate	1.0m for entire collector; 125mm for the one-pipe model
Diameter of riser pipe	6mm internal diameter
Material of absorber plate	1mm Aluminium plate
Material of riser pipe	I.D 6mmX1mm Copper Pipe
Material of insulation	40mm Polyurethane Form
Material of transparent cover	4mm Solar Grade Glass
Transmissivity of cover	0.9
Absorptance of absorber	0.9
Emissivity of absorber	0.1
Emissivity of glass	0.85
Heat transfer fluid	Ethylene glycol water; 50% concentration
Number of thermal model segments	10 for each collector; the model collector consists of a one-pipe absorber plate 2.0m length X 125mm width
Size of storage tank	300 litres for the 9 solar collectors (i.e. for the entire solar field); or 12.5 litres for one-pipe model

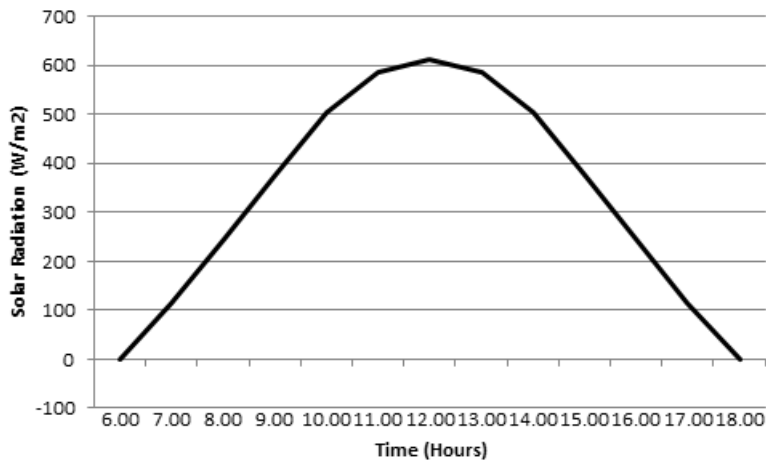


Figure 9: Simulated hourly solar radiation values

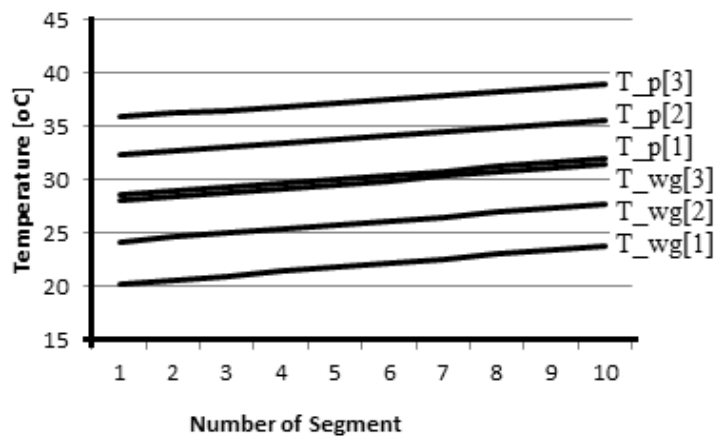


Figure 10: Plot of temperature profiles versus segment numbers

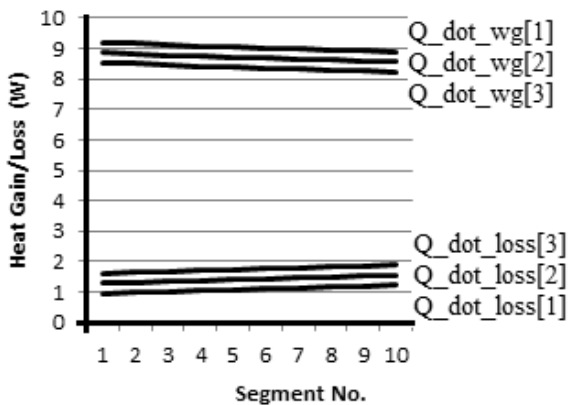


Figure 11: Energy gains and losses profiles versus segments

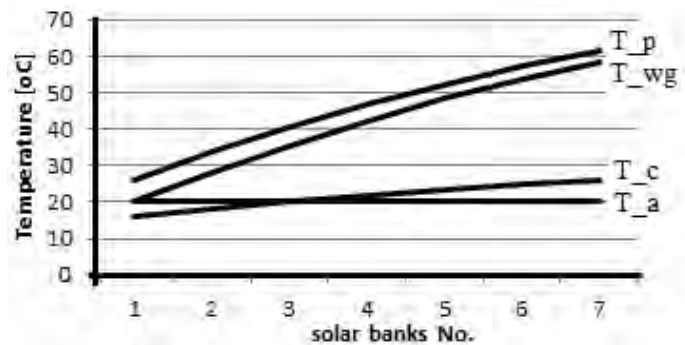


Figure 12: Temperature profile along solar banks; 180-collector model

The temperature is highest in the absorber plate and lowest in the transparent cover; also the rate of temperature increase is lowest in the transparent cover. The rate of temperature increase closely follows the same profile in both the absorber and in the working fluid.

Curve fit results yielded the following second

order polynomials:

$$T_p: y = -0.320x^2 + 8.483x + 17.93$$

$$T_{wg}: y = -0.334x^2 + 9.080x + 11.32$$

$$T_c: y = -0.087x^2 + 2.367x + 13.87$$

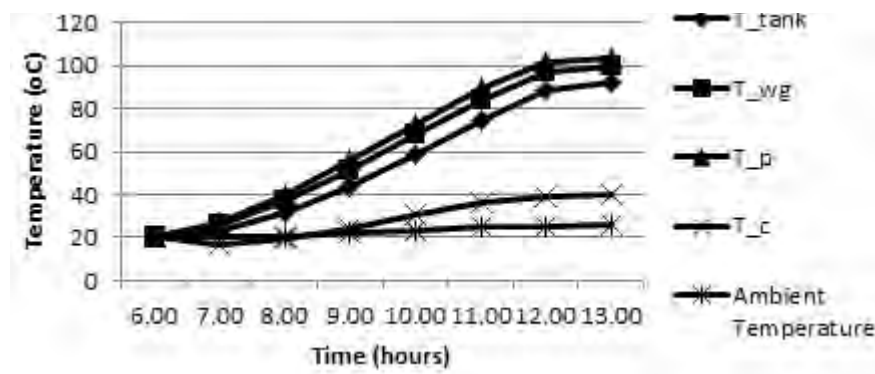


Figure 13: Hourly temperature profiles

Figure 13 shows the hourly temperature profiles. These simulations consists of several cycles (114 cycles calculated) to make an hour. The temperature measurement is taken at the end of the hour. These simulations include a thermal storage represented by the tank temperature T_{tank} .

The absorber plate attains the highest temperature followed by the working fluid (water ethylene glycol) at the exit of the solar field and in the tank storage. The three temperature profiles follow each other closely and build-up slowly from morning to a high about noon. The absorber increases temperature from ambient temperature of 20°C to slightly over 100°C about noon; the water ethylene glycol attains a maximum of slightly below 100°C and about 90°C at the exit of the solar collector and in the storage tank respectively. This is desirable for heat transfer to continue flowing from the absorber to the working fluid.

The transparent cover has a much lower temperature ranging from ambient temperature to about 40°C. This ensures lower thermal losses.

Curve fitting gave the following results:

$$T_p: y = -0.460x^3 + 6.007x^2 - 8.466x + 23.20$$

$$T_{wg}: y = -0.439x^3 + 5.955x^2 - 10.06x + 24.93$$

$$T_{\text{tank}}: y = -0.403x^3 + 5.831x^2 - 12.62x + 27.75$$

$$T_c: y = -0.258x^3 + 3.694x^2 - 11.48x + 27.65$$

$$T_{\text{ambient}}: y = 0.988x + 18.17$$

5.3 Energy modelling results

Figures 14 and 15 show useful heat gains and thermal losses.

The levels of heat transfer to the working fluid in the storage tank increases with time from the lowest values in the morning (7am) to the highest values in mid-morning (11am) and then decreases with time attaining lower values at noon and 1pm respectively.

The levels of heat transfer also decrease within each hour, being higher at the beginning of the hour than at the end; this, however, could be due to the hourly radiation level being assumed constant.

The level of thermal losses increases with time from the lowest at the start of the modelling time (7am) to the highest and the end of the modelling time (1pm). Sky losses are the highest ranging from about 50% to 100%.

Figure 16 shows average hourly thermal efficiency. The thermal efficiencies are highest near the commencement of the modelling period (7am, 8am and 9am are highest; the lowest efficiencies are at 1pm followed by 12pm).

The average efficiency has a high of 56% at 8pm and a low of 35% at 1pm; the regression analysis yielded the following curve fit:

$$y = 0.055x^3 - 1.321x^2 + 4.265x + 51.42.$$

6. Discussions and conclusions

Preliminary small-scale concept plants, 500Wp and 10kWp, have been presented, modelled and computer-simulated. The first pass modelling used 14 candidate organic fluids and three optional plant configurations which gave thermal efficiencies ranging from 10.38% to 12.20%; the highest being Isopentane and organic Rankine with recuperator and the lowest being R245fa with conventional organic Rankine cycle.

The solar field modelling has been done with Ethylene Glycol Water (50% concentration) as the heat transfer fluid. The model included simulations of hourly solar insolation values, and solar collector and storage tank energy balances.

The general trend exhibited by the temperature profiles for the absorber, ethylene glycol water and transparent cover along the flow direction of the heat transfer fluid is that of a second order polynomial continuously increasing but with a diminishing gradient.

The hourly temperature profiles for the absorber, transparent cover, heat transfer fluid at

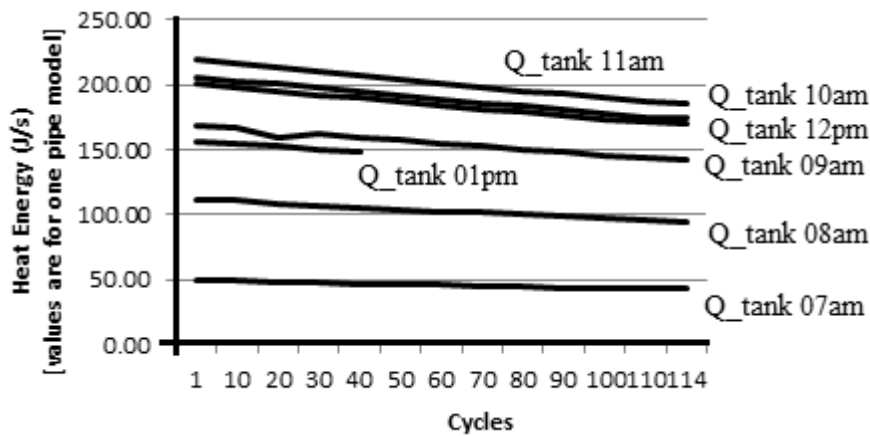


Figure 14: Heat energy rates for storage

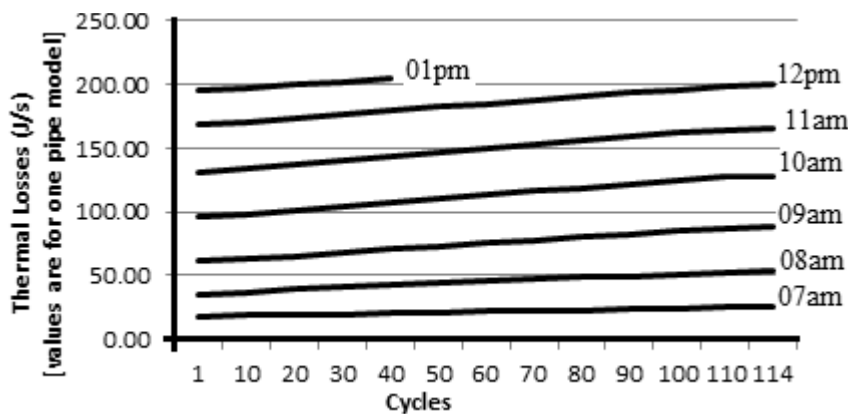


Figure 15: Thermal losses

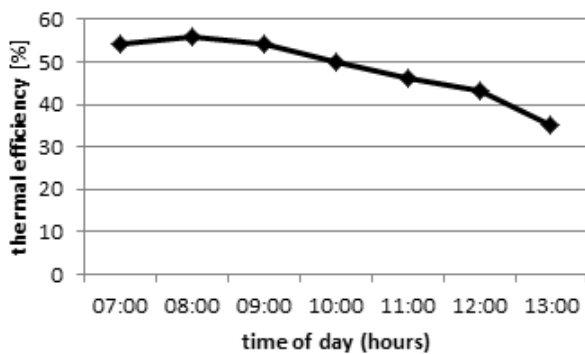


Figure 16: Average hourly thermal efficiency

collector exit, and heat transfer fluid in the storage tank, on the other hand exhibited a third order polynomial character starting with a lower gradient, developing into a steep gradient and then slowing down to a lower gradient.

The hourly efficiency curve also exhibited a third order polynomial profile starting with higher values and tailing down to lower values.

By regression one is able to mathematically determine the totals and averages for futures analyses.

A simple analysis of the 9-collector model shows the thermal energy output being less than the

approximated requirements. These will be adjusted in the full simulations once the models of the other components have been finalised.

The main limitation in the simulations was the lower number of permissible variables of the academic commercial version of the software and the low computing speed to the extent that some simulation cycles had to be broken down to allow for manual entering of data midway through the simulations.

The valuable insights gained from these simulations will provide a solid basis for the final concepts designs and physical validations.

References

- Duffie J.A., and Beckman W.A., (1991). Solar Engineering of Thermal Processes, 2nd Ed., John Wiley & Son, USA, p281.
- Engineering Equation Solver (EES).
- Groenendaal B.J., (2002). ECN project number 7.7372: Solar Thermal Power Technologies.
- Incropera F.P. et al, (2007) Fundamentals of Heat and Mass Transfer; John Wiley & Sons, USA.
- Nishith B. D. and Santanu B., (2009). Process integration of organic Rankine cycle, Energy Journal, Vol. 34 pp 1674–1686.
- Schlaich J. and Robinson M., (1995). Principle of a

Solar Chimney: Solar Chimney, Axel Menges GmbH.

Situmbeko S. M., Inambao F. L., (2011). Mathematical Modelling and Simulation of Low Temperature Solar Thermal Energy Conversion Systems, Proceedings ISES Solar World Congress, Kassel, Germany.

Silva M R. et al, (2011). Interactive Tool to Teach Solar Parabolic Trough Concepts; Proceedings ISES, SWC, Kassel, German, September 2011.

Website: www.weather.com/weather/hourbyhour/graph/SFXX0011?begHour=2&begDay=95#hhView (accessed April 03, 2012).

Website: <http://www.ienergyinc.com/> (accessed November 5, 2013).

Website: www.nrel.gov/csp/troughnet/power_plant_systems.html http://www.nrel.gov/csp/troughnet/power_plant_systems.html (accessed November 5, 2013).

Website: www.brightsourceenergy.com/technology (accessed November 5, 2013).

Website: www.montaraventures.com/energy/wp-content/uploads/2008/05/rankine-cycle-diagram.jpg (accessed January 13, 2010).

Website: www.eng.usf.edu/~hchen4/Kalina%20Cycle.htm (accessed April 04, 2012).

Website: www.solardome.co.za/documents/file/25-solar-dome-sa-pricelist.html (accessed March 12, 2012).

Website: www.thermotechs.com/Downloads/Thermomax%20Handbook.pdf (accessed March 12, 2012).

Website: www.gaisma.com/en/location/durban.html (accessed March 12, 2012).

Received 23 May 2012; revised 4 October 2013

Low temperature solar thermal energy conversion

by S M Situmbeko, University of Botswana, and F L Inambao, University of Kwazulu-Natal, South Africa

Solar thermal energy conversion for power generation for both low and high temperature systems is an active area of research aimed mainly at addressing environmental and climate change concerns, but also as a possible complimentary avenue of tackling the current power supply deficits in Southern Africa.

Low temperature solar thermal energy conversion research is still in its infancy but gaining momentum. This is partly due to its immense potential for utilizing waste heat to raise plant efficiency and its viability for small scale operations. The technology typically uses flat plate collectors, which are relatively cheap and easy to operate. Use for power generation requires modifications to the conventional energy conversion cycles. Research is currently on-going to develop low temperature thermal conversion technologies; examples would be the patented Kalina and the Organic Rankine cycles. This project will focus on the Rankine cycle, modified to suit low temperature operation, using a working fluid that attains phase change at low temperatures.

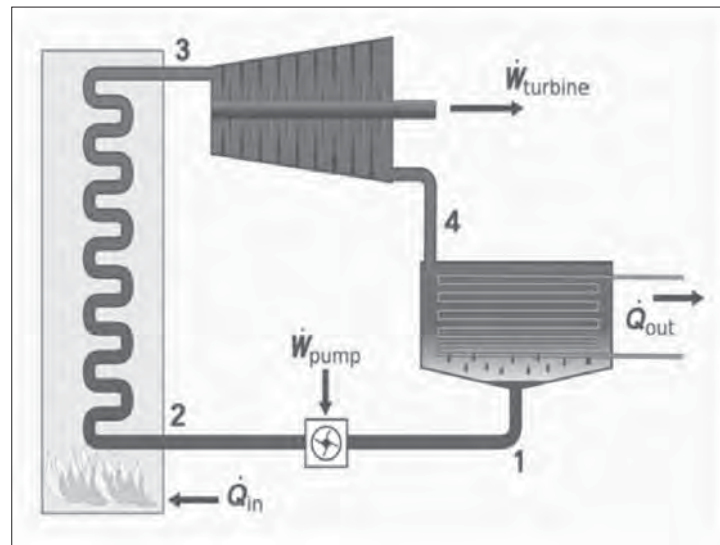


Fig. 1: Rankine cycle schematic representation [1].

Low temperature thermal energy conversion

This refers to the use of low temperature heat to generate electrical energy. Most thermal-energy based electrical generating systems use high temperatures to generate steam used to drive a turbine. About 80% of electrical energy used is produced using a thermodynamic cycle known as the Rankine cycle. A schematic representation of the Rankine cycle is shown in Fig. 1.

Fig. 2 is a TS (Temperature-Entropy) diagram of a Rankine cycle operating between 0,06 and 50 bar.

Several forms of energy are used in this cycle ranging from fossils such as coal, oil and natural gas to nuclear, solar thermal and geothermal energies.

In this paper we present a preliminary concept for use of low temperature solar energy in a Rankine cycle to generate electrical energy.

Research objectives

The main objectives of the current research are:

- To evaluate the suitability of various thermal-mechanical conversion cycles for low temperature solar thermal energy conversion applications.
- To develop and optimise a hypothetical computer model of a solar thermal

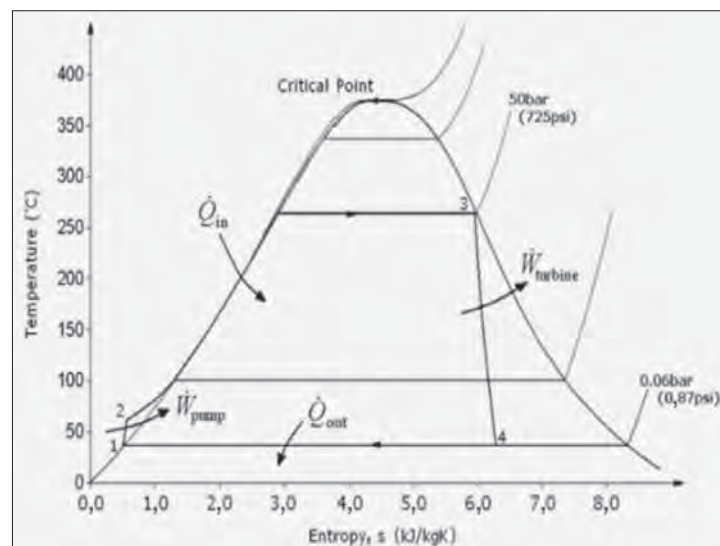


Fig. 2: Ts diagram of a typical rankine cycle [2].

energy conversion adapted Rankine cycle based on thermodynamics, fluid mechanics and heat transfer principles.

- To investigate the thermo-mechanical efficiency and overall economic and environmental performance of a low temperature solar thermal energy conversion system based on the adapted Rankine cycle.

- To investigate the performance of various working fluids including their blends in an adapted Rankine cycle.
- To review the design and performance of the major cycle components of a low temperature solar thermal energy conversion plant and carry out an optimization of their energy efficiencies, economic and environmental performances.

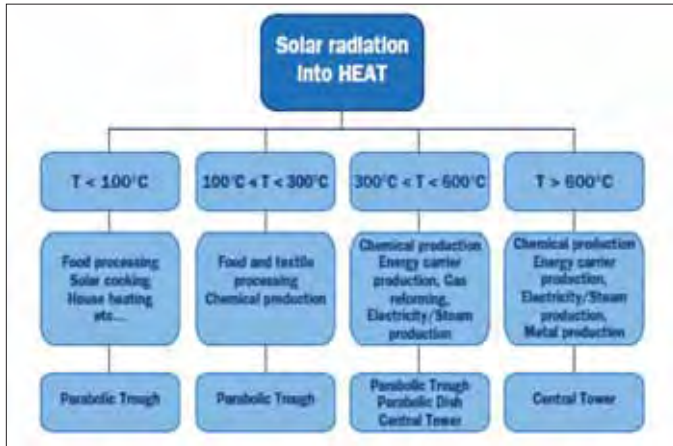


Fig. 3: Concentrated solar heat applications [3].

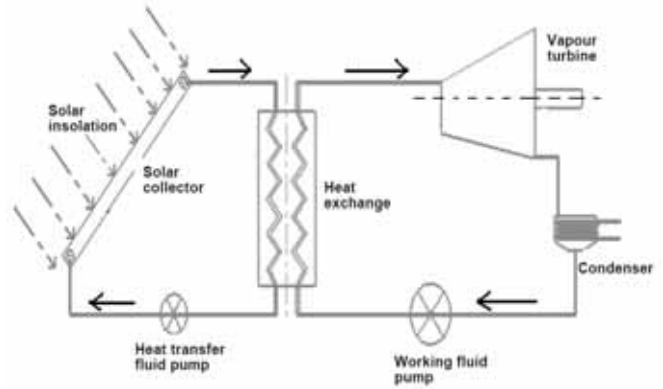


Fig. 4: Concept design of a low temperature solar thermal conversion power plant.

- To design, construct and install a concept plant of a solar thermal energy conversion adapted Rankine cycle.
- To propose a final working design suitable for a small scale power generating plant based on the findings of the project.

Methodology

Field and laboratory validations will be conducted on experimental models based on a final concept design. Supplementary validation based on physical simulations and laboratory testing will also be designed and effected at various stages of the experimental research. Different data will be measured at different points of the cycles (Fig. 4).

Low temperature power cycles

Research is currently on-going to develop low temperature thermal conversion technologies; examples include the patented Kalina cycle and the Organic Rankine cycle. In order for the Rankine cycle to be effectively incorporated into a low temperature thermal system, the working fluid usually water must be substituted with another working fluid that has a lower boiling point. Some liquids have a dry property and as such do not need to be "dry saturated". Generally the desirable properties for a working fluid include low cost, non corrosiveness, thermal stability, and high cycle and turbine efficiencies.

Possible liquids that could be used in the place of water include organic liquids, refrigerants, ammonia, toluene and fully fluorinated benzene ring fluids, or any feasible mixture of these [3]. Pentene isomers are organic fluids with boiling points ranging from 9 to 36°C; Ammonia is an inorganic compound with a boiling point of -33°C. Alternatively some dry fluids with boiling temperatures above that of water such as Toluene (a paint thinner) with a boiling point of 106°C, could be used and this may have some thermodynamic benefits.

Organic Rankine cycle

An organic Rankine cycle (ORC) is a Rankine cycle in which an organic fluid replaces water as the working fluid, enabling the use of lower temperature heat sources. Efficiency is lower but the cost of collecting the heat energy is also significantly lower.

Low temperature solar thermal

Low temperature solar thermal uses solar heat sources; in particular flat plate solar collectors. Fig. 3. shows the different ranges of solar thermal from low to high temperature. The low range normally covers temperatures below 300°C, medium range 300 to 600°C, while high is above 600°C. With central tower technology, temperatures more than 1000°C can be easily sustained.

Concept design

A theoretical model of the Rankine cycle based on low temperature solar thermal heat has been developed.

The system consists of two cycles: a solar thermal cycle and a Rankine cycle, with a heat exchanger providing the interface. Currently, mathematical modeling of the system is being undertaken. This will be followed by experimental research to determine correlation of the theoretical model. For this purpose a 10 kW vapour turbine is being sourced. This forms the basis for detail design of both the Rankine cycle as well as the solar thermal cycle.

Solar thermal cycle design

The main components on this cycle are the solar collectors, the pump and the heat exchanger. These are connected by insulated ducting. Solar collector design entails selecting an appropriate type of collector, in this case flat plate collectors, and sizing, based on European Standards EN12975 parts 1 and 2 (or on equivalent SABS standards). The heat transfer fluid is water mixed with antifreeze. The power from the solar collector may be determined by the equation:

$$P = A * (n_0 * G - a_1 * (T_m - T_a) - a_2 * (T_m - T_a)^2) \text{ [W]}$$

where:

G = solar irradiation [W/m²]

T_a = ambient air temperature [°C]

T_m = collector mean temperature [°C]

A = collector area (corresponding to the efficiency parameters) [m²]

n_0 = Zero-loss efficiency

a_1 = 1st order heat loss coefficient

a_2 = 2nd order heat loss coefficient

Using these parameters, the collector efficiency can be determined:

$$n = n_0 - a_1(T_m - T_a)/G - a_2(T_m - T_a)^2/G$$

The design for the heat exchanger, pump and ducting will be based on the design thermal loading resulting from the Rankine cycle as well as the solar collectors. A shell and tube heat exchanger in the countercurrent flow configuration was selected. The overall governing equation for shell and tube heat exchangers is:

$$Q_T = UAF(LMTD)$$

where:

Q_T = the total heat load to be transferred

U = the overall heat transfer coefficient referred to area A

A = any convenient heat transfer area

F = the temperature correction factor

$LMTD$ is the logarithmic mean temperature difference for the purely countercurrent flow configuration.

This equation is supported by the two heat transfer equations for the hot and cold fluids:

$$Q_H = m_H C_{pH} (T_{inH} - T_{outH})$$

$$Q_C = m_C C_{pC} (T_{outC} - T_{inC})$$

where:

Q = heat transferred in joules per unit time

m = mass flow rate

T = temperature

CP = specific heat capacity of fluid

Subscript "H" = hot fluid

Subscript "C" = cold fluid [5]

Rankine cycle design

The main components include the turbine, the condenser, the pump and the heat exchanger. The 10 kW turbine kit includes the evaporator, turbine generator, direct drive PM generator, water cooled condenser and feed-water pump.

Fluid mechanics design

Another aspect being considered is the optimisation of the fluid flow. Duct sizing is such that laminar flow is achieved; this is for reduced frictional losses. Flow in the heat exchanger is designed for turbulent flow so as to achieve effective heat transfer. Other factors such as fouling and erosion also need to be considered.

Overview of similar design concept

The design concept is based on ocean thermal energy conversion (OTEC), a power generation method where heat energy associated with temperature differences between the warm surface water and cold deep water of the ocean is converted into electricity [8 – 11]. Commercial OTEC plants must be located in an environment that is stable enough for efficient system operation. The temperature of the warm surface seawater must differ about $\Delta T = 20^\circ\text{C}$ from that of cold deep water. Most countries with adequate ocean-thermal resources have natural ocean thermal gradient of $\Delta T = 18 - 22^\circ\text{C}$. The available temperature differential of 20°C may well be called a "technology limit" [13].

The proposed conceptual design of approximately 10 kW seeks to address some short comings of the OTEC system. The advantages of the system lie more in eliminating of technological risks such as the elimination of underwater transmission cable and deep-water mooring technologies, and the lowering of operations and maintenance costs. The reduced pump power requirement, would in turn require smaller heat exchangers. Costs of both warm-water and cold-water pipes of larger diameters and lengths are to be reduced to minimum.

The above factors, i.e. heat exchanger, piping and added short construction period appear to have by far the most significant impact on reducing total system capital cost. This will result in a gross power almost equal to net power due to reduced requirements on piping and losses such as transmission and pumping.

A 10 kW pilot plant: University of Kwazulu-Natal experience and experimental research

The system is designed as an off-grid facility to achieve higher energy conversion

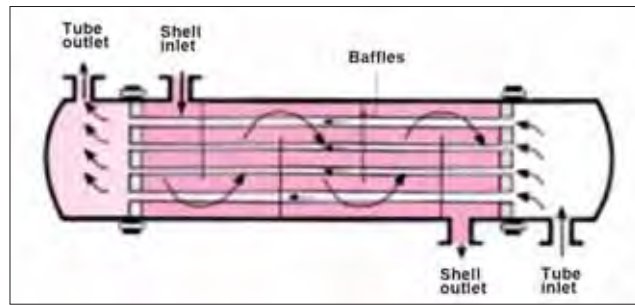


Fig. 5: One pass counter-current flow shell and tube heater exchanger [6].

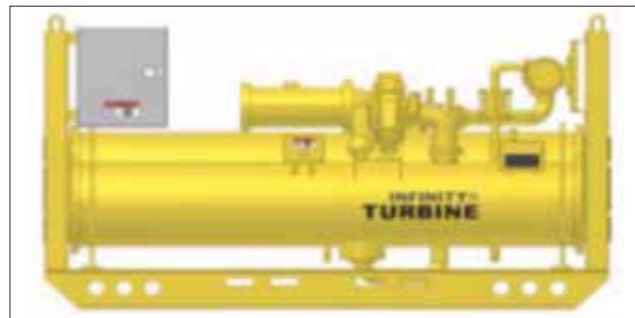


Fig. 6: Infinity vapour turbine [7].

efficiencies. Solar water heater collectors have been developed and tested at the UKZN over the past few years. On clear day, with an ambient temperature of about 25°C , the average temperature of the solar water collector was 60°C [15]. Another added advantage to the facility will be the introduction of solar air heater with an average air temperature of 75°C [16]. The typical low-cost solar-thermal collectors are expected to increase the turbine inlet temperature of the working fluid (Ammonia). The system will have a natural "land" thermal gradient of over 40°C , thus breaking the "technology limit".

Analysis of results

Among the analyses that will be conducted will be thermodynamic analysis, heat and mass transfer analyses, economic and environmental (including carbon emissions) analyses. Heat and mass transfer optimisation will be conducted to determine to what extent achieving an optimal flow process could enhance cycle efficiencies and minimise heat losses. Economic and environment analyses are not the main focus of this research. Nevertheless these will be conducted to satisfy inquisition. The economic aspects will attempt to determine cost savings as well as payback periods that would be attained as a result of improvements in energy efficiencies of plants or households from the use of low temperature solar thermal (or waste heat) to generate power. On the other hand environmental review will examine to what extent the process could yield carbon emissions offsets and how the process could be applied to available emissions trade mechanisms.

References

[1] <http://montaraventures.com/energy/wp-content/uploads/2008/05/rankine-cycle-diagram.jpg> (accessed 13/01/2010).

- [2] http://en.wikipedia.org/wiki/File:Rankine_cycle_Is.png (accessed 07/01/2010).
- [3] European Commission; Concentrated Solar Thermal Energy, EUR 20898, European Communities, Luxembourg, 2004, ISBN 92-894-6353-8.
- [4] www.powerfromthesun.net/chapter1/Chapter1.htm (accessed 05/01/2010).
- [5] R W Serth; Process heat transfer: principles and applications, Elsevier Ltd., Oxford, UK, 2007, ISBN 978-0-12-373588-1.
- [6] F P Incropera, D P De Witt; Fundamentals of heat and mass transfer, John Wiley & Sons, Inc. New York, 2002, ISBN 0-471-38650-2.
- [7] www.infinityturbine.com/pdf/IT10_brochure.pdf (accessed 20/01/2010).
- [8] W H Avery, C Wu. Renewable energy from the ocean- A guide, Oxford University Press: 1994.
- [9] T Dylan. Ocean thermal energy conversion: current overview and future outlook. Renewable Energy 1995;6(3):367-73.
- [10] D E Cavrot. "Economics of ocean thermal energy conversion", (OTEC). Renewable Energy 1993;3(8):891-6.
- [11] D E Lennard. "The viability and best locations for ocean thermal energy conversion systems around the world". World renewable energy congress climate change. Energy and Environment 1995;6(3):359-65.
- [12] www.nrel.gov/otec/achievements.html (accessed 20/02/2010).
- [13] www.nrel.gov/otec/design_location.html (accessed 20/02/2010).
- [14] N Yamada, et al. "Performance simulation of solar-boosted ocean thermal energy conversion plant". Renewable Energy 34 (2009) 1752-1758.
- [15] M Babulali, N Seumangal L Khuzwayo and J Betterton, "Design of a Domestic Solar Water Heating System", BSc Design and Research Project Thesis, University of Kwazulu-Natal, 2008.
- [16] A Balwanth, J S Joseph, P Naidoo and D Munien, "Design of a Solar Dryer System for Agricultural and Marine Products", BSc Design and Research Project Thesis, University of Kwazulu-Natal, 2009.
- [17] B D Nishith and B Santanu, "Process integration of organic Rankine cycle", Energy Journal Vol 34 (2009) pp1674-1686.

Contact Prof. F Inambao,
University of KZN, Tel 031 260-8530,
inambaof@ukzn.co.za ❖

DISTRIBUTED ENERGY RESOURCES AND INDEPENDENT POWER PRODUCERS – A REVIEW OF POLICIES IN AFRICA

Shadreck M Situmbeko,
 University of Botswana,
 Private Bag UB0061, Gaborone, Botswana
 situmbeko@mopipi.ub.bw; ssitumbeko@yahoo.com

ABSTRACT

Distributed Energy Resources (DER) deployment and participation of Independent Power Producers (IPP’s) in the African energy market provide a key to accelerating renewables deployment, diversification of the energy mix and improved access to modern and clean energy. DER deployment has experienced steady growth over the years while more and more power is now being provided by IPP’s. Policies are required to enhance this positive change in the energy market and indeed this has been the case in countries where policy development has received adequate attention. The paper explores this subject area further and provides scenarios in two countries, South Africa and Botswana.

KEY WORDS

Distributed Energy Resources, Independent Power Producers, renewables, energy mix, policy development

1. Introduction

There is evidence of growth in the number of countries developing policies and targets regarding energy and especially renewable energy; there is also an increase in the diversity of these policies. Table 1 shows a comparison in the global coverage of regions with renewable energy policies in the years 2004, 2013 and 2015.

Table 1

global policy development coverage for 2004, 2013 and 2015 [1]

Policies	Start 2004	2013	2014
Countries with policy targets	48	144	164
States/provinces/countries with feed-in policies	34	106	108
States/provinces/countries with RPS/quota policies	11	99	98
Countries with tendering/ public competitive bidding	n/a	55	60

Countries with heat obligation/mandate	n/a	19	21
States/provinces/countries with biofuels mandates	10	63	64

There are a number of factors responsible for this scenario, chief among them being:

- Shift in the business models; and
- Changes in the energy mix.

1.1 Shift in the business models:

The shift in the business models is mainly due to the trend to shift towards competition models and the admission of distributed energy resources in the energy systems. The basic structure of an electricity system is depicted in figure 3, comprising of a wholesale sector in the form of generation and transmission, and a retail sector in the form of a distribution network.

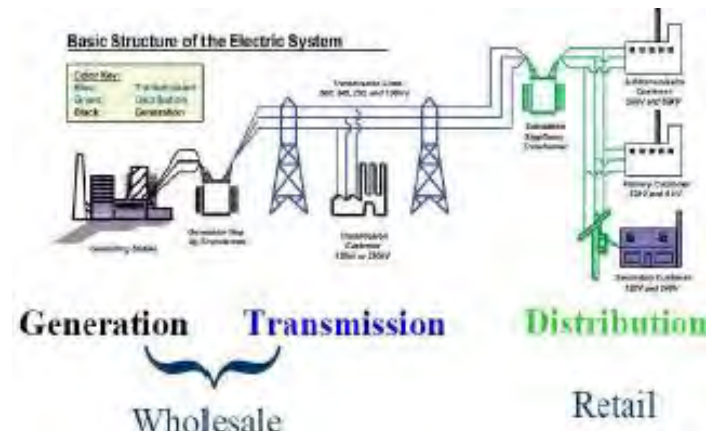


Figure 3: Basic electricity system [2]

The traditional business model consists mainly of vertically-integrated electric utilities, quite often national parastatals running a monopolistic business. This type of model is represented in figure 4.

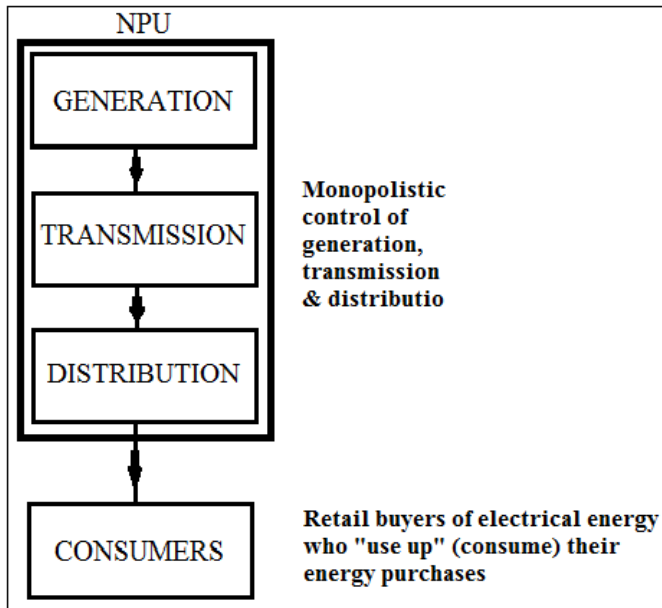


Figure 4: Traditional vertically-integrated electric utility [2]; (NPU= National Power Utility)

A move towards competition means adopting one of the three business models:

- Liberalized generation only (this is the most common format in Africa);
- Liberalized generation and transmission; or
- Liberalized generation, transmission and distribution

The three competition models are shown in figures 5, 6, and 7 respectively.

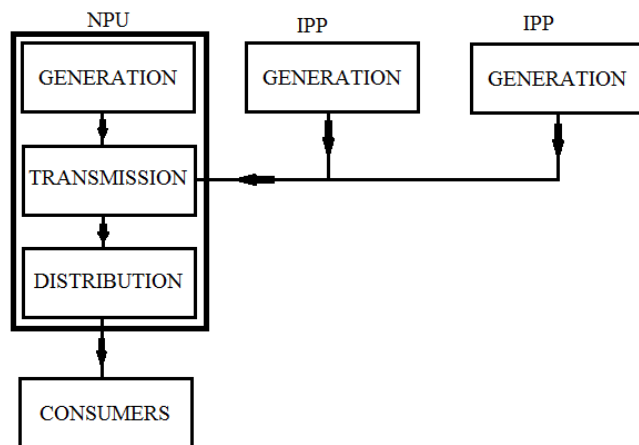


Figure 5: Generation Competition Only
 IPP=Independent Power Producer
 NPU= National Power Utility

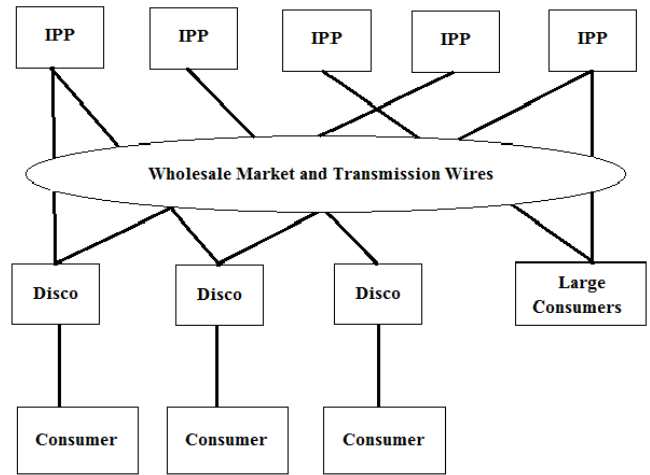


Figure 6: Wholesale Competition Only [2]
 IPP=Independent Power Producer
 DisCo=Distribution Company

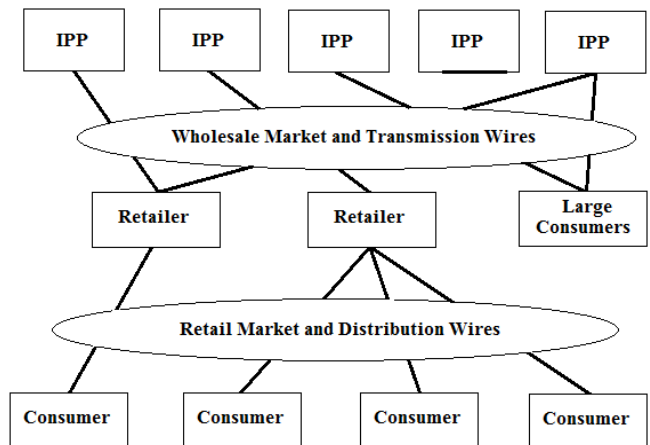


Figure 7: Both Wholesale and Retail Competition [2]

The incorporation of distributed energy resources in the energy mix is depicted in figure 8 and this gives rise to what are commonly referred to as prosumer, participants in the energy system that are both producers and consumers.

1.2 Changes in the energy mix:

Increasingly the energy sources are getting more and more diversified with unprecedented increases in renewable energy entrants. In 2014 alone, about 58.5% of net additional global power capacity came from renewables and by the yearend it is estimated that 27.7% of the global power generating capacity comprised of renewables, projected to contribute an estimated 22.8% to global electricity, with wind, solar PV, and hydro power taking center-stage in the market. These developments have compelled policy makers in some jurisdictions to stipulate that utilities update their business models and grid infrastructure. [1]

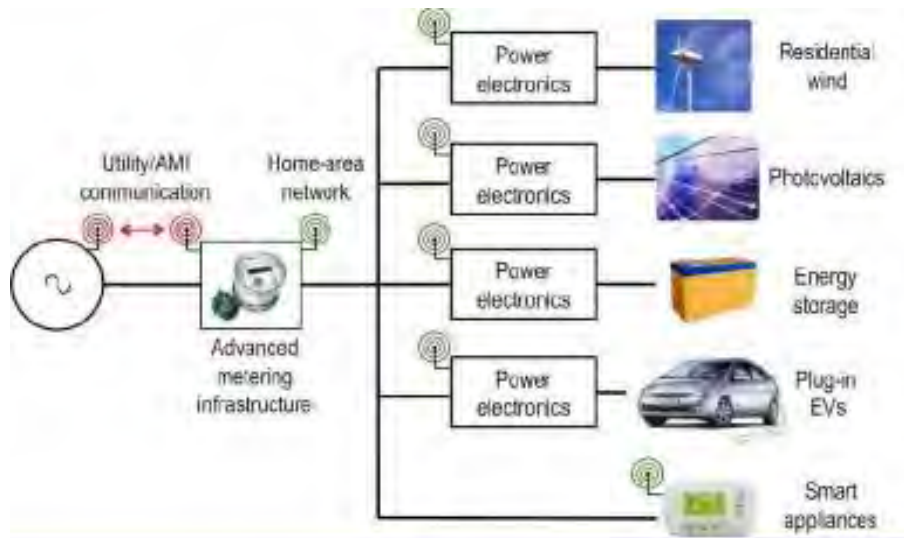


Figure 8: Consumer-Owned Distributed Energy Resource Possibilities [2]

2. Issues Requiring Policy and Regulatory Intervention [3]

- **Financial & Regulatory:** policies are required to determine a fair share of costs and incentives in a rational and transparent manner taking into account the interests and concerns of all stakeholders; costs should be borne by those who cause them and incentives should be based on well-defined objectives and regularly reviewed in accordance with the market conditions.
- **Market Development & Deployment:** there is need to setup interconnection rules and establish an appropriate regulatory body; appropriate and reasonable data sharing mechanisms need to be put in place. The participation of larger utilities in the market should be fair, equitable, non-prejudiced, and overseen and approved by an appropriate regulatory body. Deployment procedures should also cater for social acceptance of distributed energy systems.
- **Consumer Issues:** consumer protection policies should be reviewed regularly and updated as necessary. At any rate, consumers must be provided with a clear platform to resolve their grievances. There is need to develop standards for data protection, access, and disclosure consistent with national requirements.
- **Safety, Reliability & System Planning:** Due to changes from conventional centralised systems to a distributed power system there must be regulations, standards, procedures and practices for the planning, operation and reliability of transmission and distribution networks as well as for the safety and protection of the public, first responders, and electric utility workers, and of the assets of utilities and customers; deployment of

distributed energy resources should not compromise infrastructure security or cybersecurity.

3. Policy Development in Africa [4]

Clean energy has attained higher deployment levels in sub-Saharan Africa in recent years; for instance by the second half of 2015, investments in renewables, excluding large hydro, had reached 25 billion dollars; while in 2014 clean energy capacity almost doubled on the previous year. These developments are providing opportunities to these developing countries to deal with problems of low electrification and requirements for cleaner and modern energy provisions. Regarding policy development in Africa the following is noted for the year 2015:

- In many countries, policies and power sector reforms are slow to materialize, and investments in clean energy are rather lower.
- South Africa's, with its globally-significant REIPPP auctions, was the best performer regarding policy development.
- A number of countries have developed renewable energy market policies; notable among them being: Uganda, which ran the first tenders under its GET FiT scheme; Tanzania, which augmented its small power producer program to introduce similar competitively-allocated FiTs; and Mozambique, which in 2015 started implementing its 2014 FIT program.
- Nigeria and Cote d'Ivoire were the best performers with power sector reforms, reflecting

the more advanced stages of sector liberalization in those countries; as with the previous year, it was also noted that these reforms were as yet to translate into significant clean energy investment.

- Botswana, the DRC and Sierra Leone recorded low performances for their scant policy environments.
- Low liberalization of the energy markets and the failure to attract investments in clean energy maybe attributed to the tendency of many governments to artificially suppress power prices; this has been noted to be the case even in countries with low cost power sources such as hydro plants. Only 5 out of 19 Climatescope Africa countries have cost reflective tariffs [4]. Some of the reasons for this situation are that feed-in tariffs—for instance in Ghana, Nigeria and Kenya—have been slow to become operational or attract investors; governments and utilities have been slow to adopt new technologies, such as smart grids and bidirectional flow technologies, that have benefits of reducing costs; and the low capacities of grids to allow additions of utility scale distributed energy resources, as well as the perceived complexity of handling their variable output.

4. Policy Development in South Africa [5]

4.1 Overview

The electricity supply industry in South Africa is essentially based on a vertically integrated model with the state owned electricity utility ESKOM dominating the sector. ESKOM supplies about 96% of South Africa's electrical power with municipalities providing about 1 % and independent power producers 3% [5]. The company is the only transmission licensee while distribution is shared with the municipalities. Electricity is mainly generated from coal-fired power stations, a nuclear power station at Koeberg, two gas turbine facilities, two conventional hydroelectric plants, and two hydroelectric pumped-storage stations [6]. ESKOM has so far signed power purchase agreements with more than 20 independent power producers supplying about 1000 megawatts into the national grid [7].

4.2 Policy Development [8]

- Electricity Regulation Act of 2006 requires that all grid-connected and commercially-operated small-scale embedded generators must be licensed or registered by the Energy Regulator; this also applies to zero or net consumption customers providing they are connected to the grid.

- Policy developments in South Africa maybe summed up as follows: renewable energy finance subsidy (REFS) up to 2009, renewable energy feed-in tariff (REFIT) 2009 - 2011, and renewable energy independent power producer procurement programme (REIPPPP) after 2011.
- REIPPPP only made provisions for large (>5MW) and small-scale photovoltaic (>1MW) producers; thus excluding most rooftop systems.
- National Energy Regulator of South Africa (NERSA) is in the course of preparing the small scale embedded generation regulatory rules; Department of Energy (DoE) has indicated that it hopes to finalise the regulations early in 2016.

5. Policy Development in Botswana

5.1 Overview

- The Energy Supply Act of Botswana was amended in 2007 as a way of facilitating the involvement of Independent Power Producers (IPP's) in electricity generation. [9]
- Botswana Power Corporation (BPC) is the state-owned national power utility responsible for power generation, transmission and distribution; it is configured on the vertically-integrated utility model; and currently there are not specific plans to unbundle the utility functions.
- BPC operates the 132 MW Morupole A and the 600 MW Morupole B coal fired power plants as well as the 70 MW Matshelagabedi diesel peaking plant; it also operates the 1.3 MW grid-connected Phakalane SolarPV plant.
- The 90 MW Orapa dual fuel (gas and diesel) plant is the only IPP operated plant. It is operated by Karoo Sustainable Energy (KSE), the only IPP appointed by the BPC to date.
- Since November, 2015 the government is in the process of securing IPP's to develop an additional 300MW expansion of Morupole B.
- The government has also issued an Expression Of Interest (EOI) for a scalable 100 MW Solar Power Plant at Jwaneng. The plant would be constructed, operated, maintained and decommissioned at the end of its economic life by an IPP.

5.2 National Energy Policy for Botswana (Draft) [10]

The draft policy expresses the overall policy goal for the energy sector as “to provide affordable, environmentally friendly and sustainable energy services in order to promote social and economic development”. Sources of information for the draft policy included the following in addition to consultations with various stakeholders:

- Botswana’s Vision 2016,
- National Development Plan (NDP 10),
- Botswana Energy Master Plan (BEMP),
- Biomass Energy Strategy

In 2011, it was announced that Botswana would introduce renewable energy feed-in tariffs for electricity generation in 2012. Under this arrangement IPP’s would be paid for generating electricity for the country’s national grid. The size of projects under this scheme was limited to below 5MW; all projects with capacities above 5MW would be implemented through power purchase agreements with the state-owned Botswana Power Corporation. The renewable energy mix was expected to also include generation from biogas and biodiesel. Companies from Mauritius, China and South Africa had shown interest in the scheme.

Conclusion

The study has noted that several changes in energy systems globally are responsible for the drive for policy developments. There has been significant renewable energy deployment in Africa but that more progress is hampered by lack of strong policy support. South Africa has scored great successes with its REIPPPP but is still lacking on support for small scale distributed energy resource deployment mechanisms. Botswana is making progress with policy development but still far

from achieving significant distributed energy resource deployment.

References

- [1] Renewables 2015- Global Status Report, REN21, UNEP, 15 Rue de Milan, F-75441 Paris CEDEX 09, France, found at www.ren21.net/gsr.
- [2] Lecture slides by Daniel Kirschen for Kirschen/Strbac Chapter 1, with edits by Leigh Tesfatsion.
- [3] . Critical Consumer Issues Forum: Policy Considerations Related to Distributed Energy Resources, Katrina@CCIForum.com, www.CCIForum.com, July 2013
- [4] ClimateScope 2015: The Clean Energy Country Competitiveness Index found at <http://global-climatescope.org/en/region/africa/> accessed 08/03/2016.
- [5] Government Gazette, 19 December 2008 found at http://www.eskom.co.za/CustomerCare/TariffsAndCharges/Documents/18671_not13981.pdf accessed 18/08/2016.
- [6] <https://www.mbendi.com/indy/powr/af/sa/p0005.htm> accessed 19/08/2016.
- [7] <https://www.enca.com/south-africa/eskom-signs-deals-private-power-supplies> accessed 19/08/2016.
- [8] Eberhard A etal, South Africa’s Renewable Energy IPP Procurement Program- Success Factors and Lessons, © 2014 Public-Private Infrastructure Advisory Facility (PPIAF), 1818 H Street, NW, Washington, DC, 20433, www.ppiaf.org, E-mail: ppiaf@ppiaf.org, May 2014
- [9] [http://www.gov.bw/Global/MMWER/electricity%20supply%20act%2073-01%20\(2\).pdf](http://www.gov.bw/Global/MMWER/electricity%20supply%20act%2073-01%20(2).pdf)
- [10] Mzezewa C.T., Technical Report: National Energy Policy For Botswana –Final Draft, AECOM International Development, Gaborone, Botswana, March 2009, USAID Contract No. 690-M-00-04-00309-00 (GS 10F-0277P)

Review of Designs for Low Temperature Organic Rankine Cycle Expanders

Shadreck M. Situmbeko and Freddie L Inambao
University of KwaZulu Natal, Durban, South Africa
email : ssitumbeko@yahoo.com

Abstract

In general, expanders used in thermal energy conversion cycles can be divided into two main categories: positive displacement machines, also known as volumetric machines, denoted as the static type, and turbomachines, also known as velocity type machines, denoted as the dynamic type. Positive displacement expanders rely on the static forces of a fluid expanding in an enclosed chamber; the pressure is developed and the work done essentially as a result of static forces; the fluid is forced into or out of a chamber by changing the volume of the chamber. Positive displacement expanders can be further classified into rotating machines such as screws, vanes and gears, and alternating machines such as pistons, diaphragm and membrane types. Turbomachinery expanders extract energy from a fluid as a result of dynamic interactions or inertial forces (acceleration, deceleration, and turning) between the device and the fluid; energy is added by increasing or decreasing the inertia of the fluid as it passes through open passages inside the machine; turbomachines essentially consist of a collection of blades, buckets, flow channels, or passages arranged around an axis of rotation to form a rotor. Research and development on small-scale thermal energy conversion systems, typically less than 100 kWe, has to a larger extent been limited by the unavailability of suitable expanders; this is directly related to the perceived higher costs of development or adaptation of dedicated larger scale turbines for use in small scale systems owing to anticipated lower production volumes. Some of the technical challenges associated with the scaling-down of the existing larger turbine designs are: (i) the performance of turbomachines is normally associated with the machine blade tip speed [power output is given as:

$\dot{W} = \dot{m}(U_2 C_{U2} - U_3 C_{U3})$, where U is the blade tip speed, $\left(U = \frac{2\pi NR}{60}\right)$]; thus as the radius R decreases, the case for smaller turbines, there is need for the rotational speed N to increase; however, this requirement for higher rotational speed presents a technical challenge in terms of dynamic and bearing loads [1]; (ii) single stage expansion is more suited for low temperature energy conversion or small scale systems; this normally requires a higher pressure ratio, a more typical characteristic of positive displacement expanders; turbomachines are normally designed to spread the high pressure ratio over several stages and as such inherently have a lower pressure ratio per (single) stage; the higher rotational speeds and intrinsically less robust design of turbomachines make them more prone to damage resulting from expansion of wet (mixed phase) working fluids; this is not the case with volumetric expanders owing to their rugged design and their low rotational speeds. These considerations have led to expander developers and users to focus more on adaptation of similarly small-scale volumetric machines; these adaptation efforts are outlined in this Review Paper.

Keywords

positive displacement, volumetric, expanders, turbomachines, adaptation.

1. Introduction

The expander is a major and most expensive component of an energy conversion system producing shaft power or electricity. Most thermal energy conversion systems are based on the steam turbine design using either steam or other working fluids such as refrigerants or organics.

Expanders can be categorised as velocity expanders (e.g. axial or radial turbines) or volume expanders (e.g. screw expanders, scroll expanders or reciprocal piston expanders). Table 1 shows a summarised result of the survey of suppliers for organic Rankine cycle (ORC) expanders for small to medium sized operations:

Table 1: suppliers of ORC expanders

Manufacturer	Company Website	Product Type	Minimum Expander	Prices
Infinity Turbine LLC USA	www.infinityturbine.com	Turbine expander	Model IT01 (1kWe) Model IT10 (10kWe)	Turbine only US\$10,000
Green Energy, Australia	www.geaust.com.au	Turbine expander	Model SG10 (10kWe)	-
ORMAT Tech., Inc. USA	www.ormat.com	Screw expander	50kWe	-
ELECTRATHERM, USA	www.electratherm.com	Screw expander	50kWe	-
ENEFTECH, Switzerland	www.eneftech.com	Scroll expander	010GRE-01 (5kWe or 10kWe)	CHP unit cost €55,000
Freepower, UK	www.freepower.co.uk	Scroll expander	6kWe	-

2. Adaptations and Modifications

Numerous attempts have been made to convert some fluid machines, particularly of the compressor types, into ORC expanders; some of such machines are rotary vane type compressors, rotary screw compressors, scroll type compressors, piston type compressors and swash plate type compressors. More specific examples of equipment that have been modified to operate as ORC expanders include the rotating plate expander adapted from the BOSCH pneumatic drill, the inverted scroll compressor adapted from the LG Electronics model HQ028P and the adapted pneumatic wrench, model VS02YU1260T [8]; the wankel engine has also been suggested for use as an expander [9].

The following subsections present a survey of devices that can be modified and used as expanders:

2.1 Rotary Vane Type Compressor [10], [11]

The vane type compressor relies on trapping volumes of the refrigerant gas between the eccentric rotor, a fixed cylindrical body and a vane(s); the vane maybe fixed or may rotate with the rotor; the eccentricity of the rotor ensures suction, compression and discharge of the gas between the intake and exhaust ports; the vane or vanes undergo a radially reciprocating motion as the rotor revolves in the body. In order to employ this device as an expander, the flow of the gas is reversed. In the single and fixed vane model as shown in figure 1, the reference point of rotation coincides with the centre of the fixed bore.

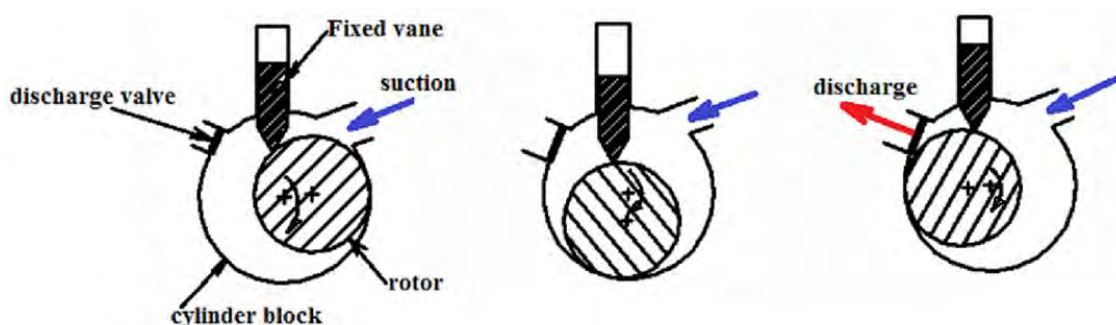


Figure 1: single (fixed) vane type compressor

In the multi-vane type compressor, as shown in figure 2, the vanes are not fixed but rather rotate together with the rotor inside the bore; the rotor rotates about its centre which is eccentric to the

centre of the bore hence permitting the radial reciprocating motion of the vanes.

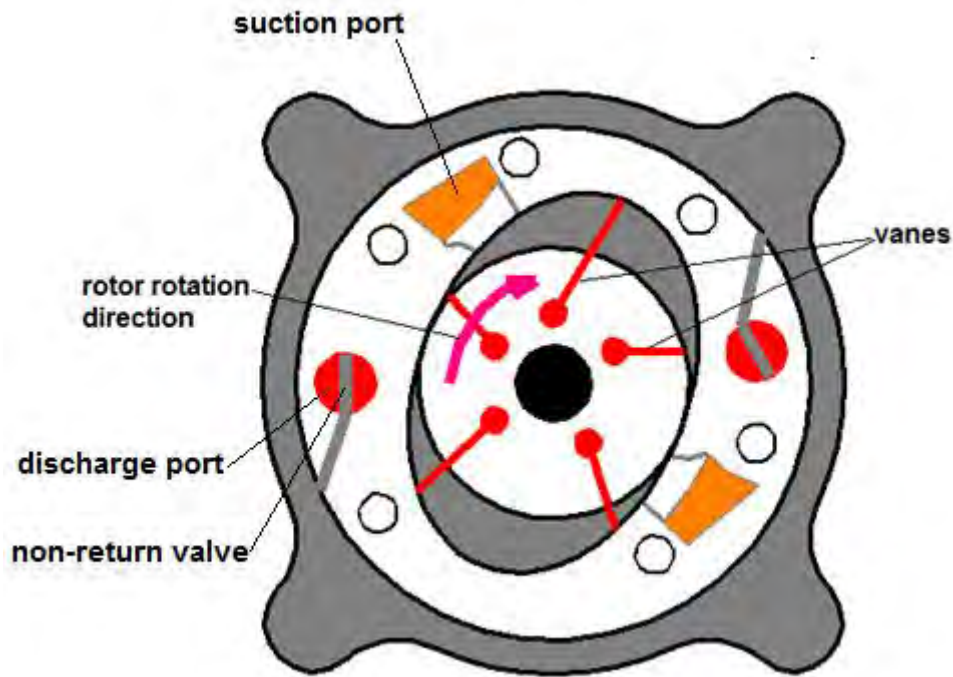


Figure 2: multi-vane type compressor

2.2 Rotary Screw Compressors [10]

Rotary screw compressors can be either single or twin screw type; the single screw type consists of a single helical screw and one or two planet wheels or gate rotors. The single screw is housed in a

cylindrical casing that has a discharge port at one end and a suction port at the other end. Power input to the screw is through the gate rotors that are usually driven by an electric motor. Figure 3 below is a simplified layout of a single screw rotary compressor.

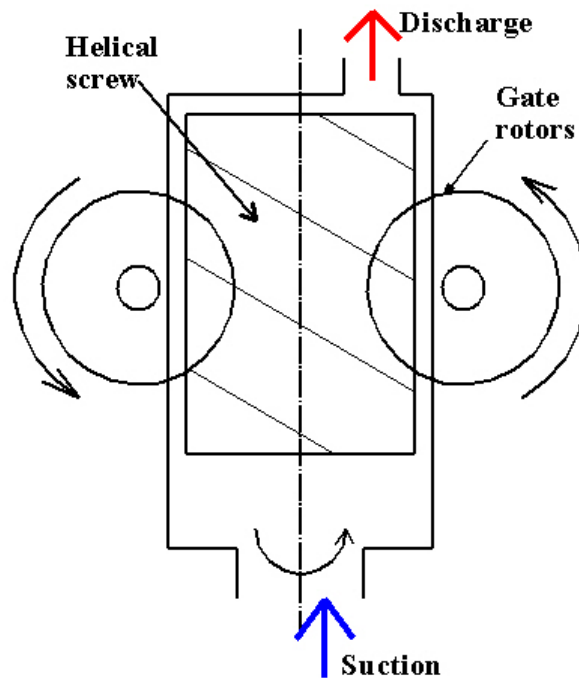


Figure 3: single screw rotary compressor

The twin-screw rotary compressor, depicted in figures 4 and 5, consists of two mating helically grooved rotors, a male rotor that drives the other,

female rotor. The male rotor has lobes, while the female rotor has flutes or gullies. The meshing and

un-meshing of the lobe-gully combination creates the suction and compression of the gas.

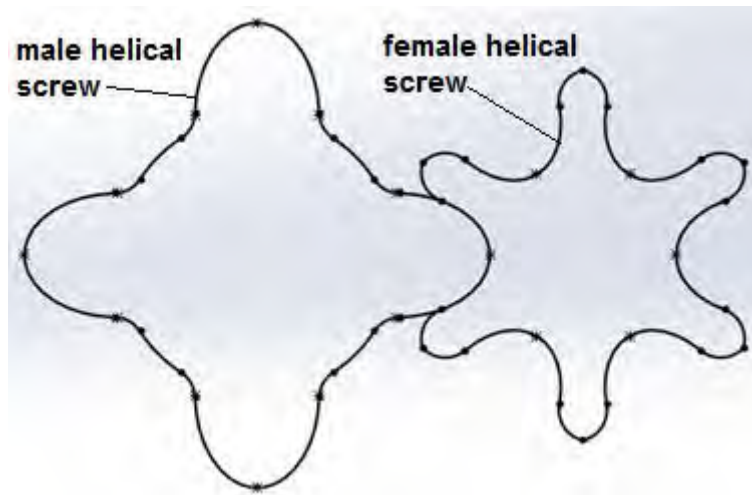


Figure 4: twin-screw compressor with 4 male lobes and 6 female gullies



Figure 5: rotary twin screw compressor

The rotary screw compressors maybe modified into an expander by reversing the direction of flow of the gas.

2.3 Scroll Type Compressors [12]

The operation of the scroll type compressor relies on two mating, spiral shaped scrolls (spirals); one is fixed while the other orbits in a rotary motion; the relative motion between the scrolls pinches and traps two pockets of the refrigerant gas at the periphery inlet ports; the two pockets of gas are

then compressed to an intermediate pressure whilst being continuously driven to the centre; at the centre the two pockets reach discharge pressure and are simultaneously released to the discharge port; figure 6 shows the three stages of the compression process. When used as an expander the flow is reversed; higher pressure gas is charged into the centre port whereby it drives the mobile scroll while flowing towards the periphery port; in the process expanding and thus losing pressure.

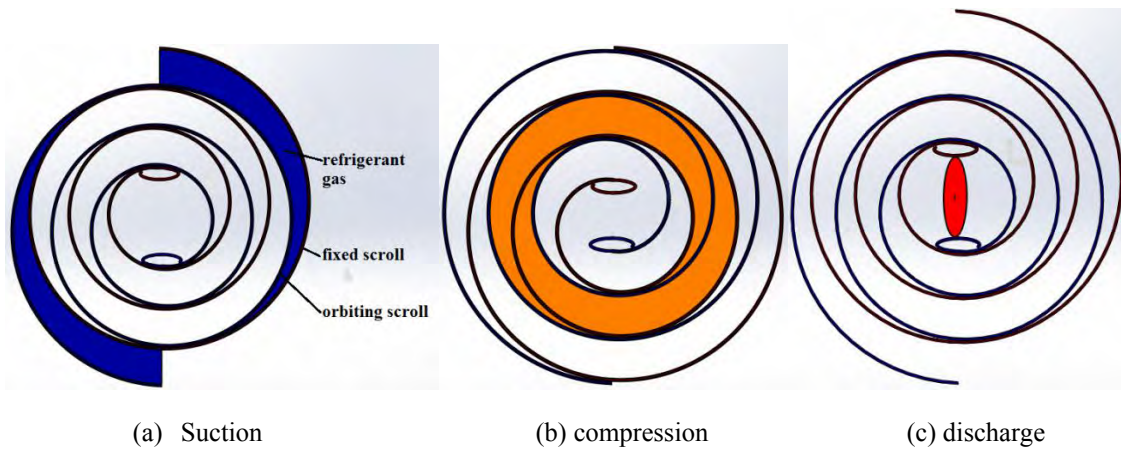


Figure 6: scroll compressor showing three stages of suction, compression and discharge

2.4 Piston Type Compressors

The piston type compressor uses the constant motion of pistons to pump and compress a fluid

such as air or refrigerant; one-way valves guide the fluid into a cylinder chamber, where the fluid is compressed; see figure 7.

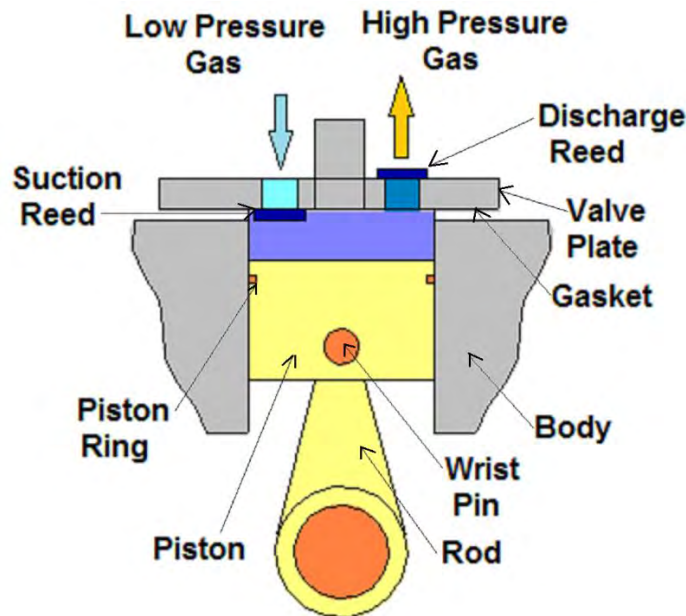


Figure 7: piston type compressor

2.5 Swash Plate Compressor

A swash plate compressor or commonly referred to as an axial piston pump is a positive displacement machine that has a number of pistons in a circular array within a cylinder block; it converts reciprocating motion of a disk plate into rotary motion of a shaft or vice-versa. It consists of a disk attached or mounted at an oblique angle to a shaft; as the shaft rotates, the edge of the disk describes a

path that oscillates along the shaft's axis; this oscillatory motion is converted into linear motion by pistons that act like cam followers pressing against the disk surface near its periphery. Thus this device finds applications either as a compressor or as an axial piston engine [13]; and may be adapted into a suitable ORC expander (engine). Figure 8 shows a schematic representation of a swash plate compressor.

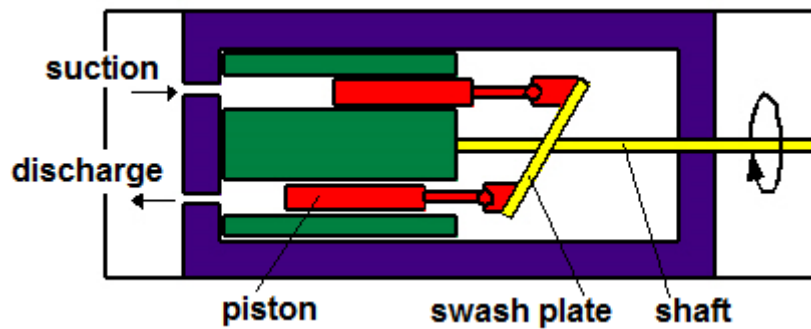


Figure 8: swash plate compressor

3. Discussions and Conclusions

The paper has examined positive displacement machines that can be used as expanders in small to medium scale ORC systems; and has described, though not in detail, the required modifications.

The most common type of expander used in small scale ORC systems are those based on the positive displacement type; this is attributed to their simplicity and low cost. Volumetric expanders are widely applied for large scale power generation systems and have achieved high turbine efficiency and high reliability. Factors that influence the type of expander adopted in a power generation cycle are shaft speed, mass flow rate, nominal power range, specific cost and operating conditions in general; operating conditions refer to inlet and outlet pressures (pressure ratio), temperatures and quality of working fluid at the end of the expansion process, mass and volumetric flow rates and nominal shaft speed.

The two positive displacement expanders that have been successfully developed and widely applied are the scroll type and the twin-screw expanders; this is mainly due to their smooth and low noise operation with minimum vibrations and compactness, with minimum number of moving parts. The reciprocation motion in the other types such as the vane type, reciprocating piston and swash plate limits their applications to very low speeds. Scroll type expanders are mainly confined to light applications with lower pressure ratio, lower speed and lower power rating, typically below 30 kWe) in order to avoid excessive leakages; the rotary twin screw type is aptly adapted to handle relatively higher pressures, speeds and power ratings owing to their robustness [14], [15].

4. Way Forward

Two models based on the velocity expander type, being radial inflow turbine and axial turbine models have been designed and are presented in further texts of this research.

Acknowledgments

The authors would like to express gratitude to the Centre for Engineering Postgraduate Studies (CEPS) at University of KwaZulu-Natal for the financial support rendered to this research.

References

- [1] Sylvain Quoilin, Experimental Study and Modelling of a Low Temperature Rankine Cycle for Small Scale Cogeneration, University of Liege, Aerospace And Mechanical Engineering Department, Thermodynamics Laboratory, May 2007
- [2] Infinity Turbine LLC USA website found at www.infinityturbine.com
- [3] Green Energy, Australia website found at www.geaust.com.au
- [4] ORMAT Tech., Inc. USA website found at www.ormat.com
- [5] ELECTRATHERM, USA website found at www.electratherm.com
- [6] ENEFTECH, Switzerland website found at www.eneftech.com
- [7] Freepower, UK website found at www.freepower.co.uk
- [8] Mikielewicz1 D. etal. Experiences from Operation of Different Expansion Devices in Domestic Micro ORC, Gdansk University of Technology, Department of Energy and Industrial Apparatus, ul. Narutowicza 11/12, 80-233 Gdańsk, Poland
- [9] Ming Tu, Gangyan Li, and Jian Hu, "Modeling of Waste Heat Recovery System and Effects at Different Engine Operating Conditions," Advances in Mechanical Engineering, vol. 2014, Article ID

739760, 10 pages, 2014. doi:10.1155/2014/739760;
found at

<http://www.hindawi.com/journals/ame/2014/739760/>

[10] Lesson 20: Rotary, Positive Displacement Type Compressors, Version 1 ME, IIT Kharagpur, found at

<http://nptel.ac.in/courses/112105129/pdf/R&AC%20Lecture%2020.pdf>

[11] Vane Type Compressor – Toyota Industries Corporation website found at <http://www.toyota-industries.com/product/auto/compressor/kind02.html>

[12] Scroll Type Compressor – Toyota Industries Corporation website found at <http://www.toyota-industries.com/product/auto/compressor/kind03.html>

[13] Swash Plate Type Compressor – Toyota Industries Corporation website found at <http://www.toyota-industries.com/product/auto/compressor/kind01.html>

[14]http://www.geothermal-energy.org/pdf/IGAstandard/NZGW/2013/Wong_Final.pdf

[15]<http://kth.diva-portal.org/smash/get/diva2:410363/FULLTEXT01>

Low Temperature Thermal Power Concept Case Study

Shadreck M. Situmbeko and Freddie L. Inambao
 University of KwaZulu-Natal, Durban, South Africa

ssitumbeko@yahoo.com; Shadreck Situmbeko <209542168@ukzn.ac.za>; inambaof@ukzn.ac.za

Abstract

Conventional thermal based electrical generating systems utilise high temperature heat energy to generate steam that is in turn used to drive a steam turbine. About 80% of electrical energy used in the world is produced from high temperature heat using a thermodynamic cycle known as the Rankine cycle [website en.wikipedia.org 2013]. In a Rankine cycle heat is applied externally to a closed cycle; water is normally used as the working fluid; typical temperatures are in the above 500°C range. The usual energy sources are fossil fuels (coal, oil and natural gas), nuclear, biomass and landfill gas, and concentrated solar thermal. However, there is abundant untapped low temperature thermal resources in the form of geothermal, non-concentrated solar radiation, oceanic thermal and process industries waste heat considered not suitable for conventional thermal power plants. Low temperature energy conversion cycles are to a larger extent still a subject of research. Examples of such cycles include Organic Rankine Cycle, Kalina Cycle and Variable Phase Cycle. In this study we present an ORC concept plant based on non-concentrated solar thermal. We also explore a number of candidate working fluids. Computer simulated results are presented for the proposed non-concentrated solar thermal conversion plant.

Keywords

Organic Rankine Cycle, Low Temperature Thermal, Working Fluid, Non-Concentrated Solar Thermal, Computer Simulated.

1. Introduction

Low temperature energy sources include geothermal, solar thermal, oceanic thermal and process industries waste heat; figure 1 is a map

showing global solar radiation resources whilst table 1 shows world geothermal resources.

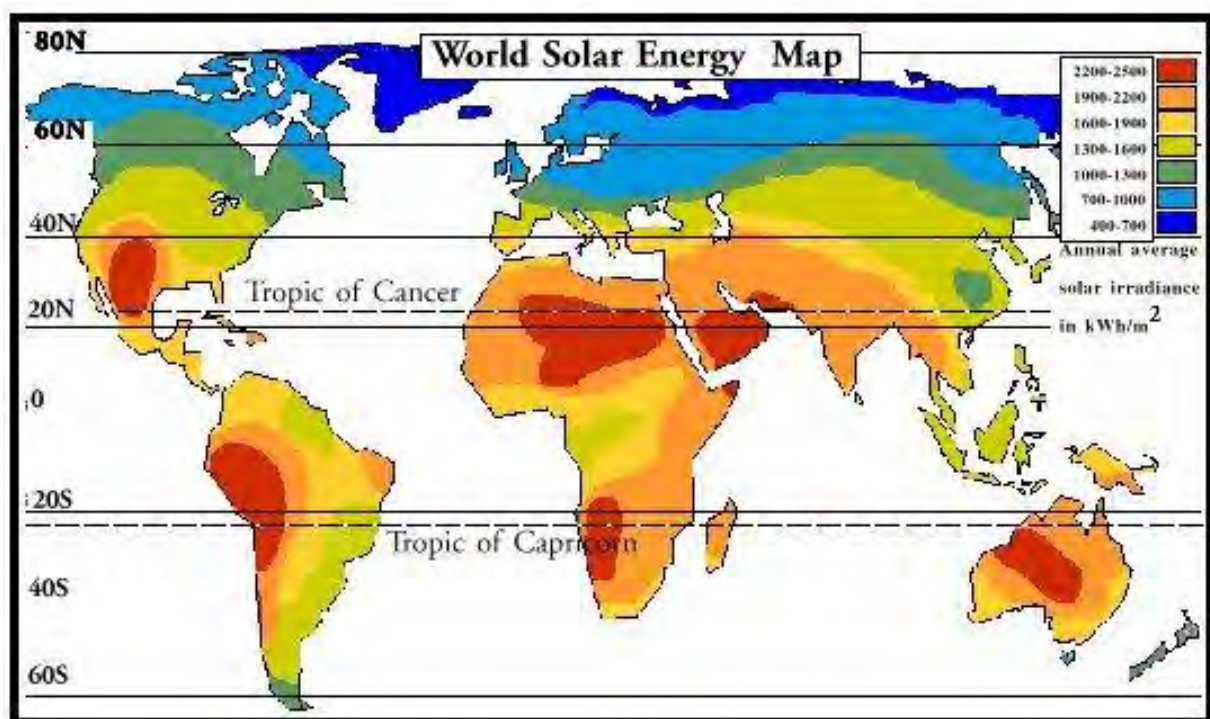


Figure 1. Global Solar Radiation Resources
 [website: alternative-energy-resources.net (2008)]

Table 1: Global Geothermal Resources [website: geothermal-energy.org (2013)]

Region	High-temperature resources suitable for electricity generation		Low-temperature resources suitable for direct use in million TJ/yr. of heat (lower limit)
	Conventional technology in TWh/yr. of electricity	Conventional and binary technology in TWh/yr. of electricity	
Europe	1830	3700	> 370
Asia	2970	5900	> 320
Africa	1220	2400	> 240
North America	1330	2700	> 120
Latin America	2800	5600	> 240
Oceania	1050	2100	> 110
World potential	11 200	22 400	> 1400

The extent of available global oceanic energy can be inferred from the fact that oceans cover more than 70% of the earth’s surface, making them the world’s largest solar collectors [website: renewableenergyworld.com (2013)]. The energy potential of the oceans may be used as thermal energy due to the temperature gradient from the surface to the larger depths or as mechanical energy from the tides and waves.

Waste heat is another low temperature thermal source and is normally a by-product of many industrial processes including thermal power stations and transportation technologies such as automobiles, locomotives, ships and aircrafts. Such waste heat normally has to be disposed of to the atmosphere or to a naturally occurring water body such as a lake, river or sea. Harnessing such waste heat can improve thermal efficiencies of such industrial processes and yield cost savings and optimisation of operational scales.

Low temperature solar thermal energy refers to temperatures typically in the below 300°C range. The figure below shows different temperature ranges for solar thermal energy from low to high temperature.

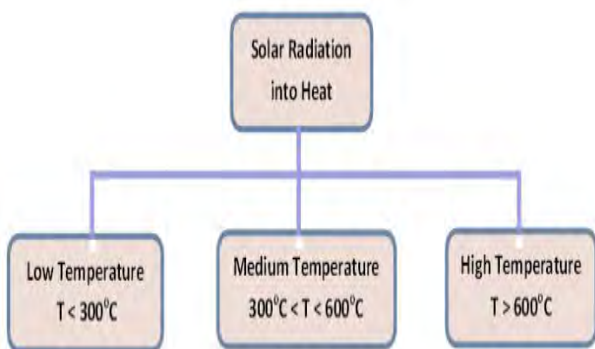


Figure 2. Solar Thermal Energy Temperature Ranges

Collection and concentration, where applicable, of solar radiation is achieved by using a solar collector

system; conversion of solar radiation to heat energy and its transference to a heat transfer fluid is accomplished by an absorber or receiver. The heat transfer fluid passes its heat to a working fluid in a thermodynamic cycle via a heat exchanger. The thermodynamic cycle subsequently converts the heat energy to mechanical energy (work) in a turbine; a generator coupled to this turbine further converts the mechanical energy to electrical energy. Low concentration ratios or no concentration at all yields low temperature solar thermal. Although use of low temperature solar thermal energy, such as with flat plate and evacuated tube collectors, for power generation gives lower energy conversion efficiencies it has the benefits of simplicity of design layout, and low operation and maintenance costs; its application can normally be justified in that it takes advantage of availability of cost effective large solar collecting surfaces such as in low densely populated semi-arid and arid areas as well as oceanic areas. This situation is also more suited for power generation in remote locations as well as for distributed grid connected power in that electricity is produced nearer to the point of consumption thus reducing transportation costs and losses.

Several low temperature energy conversion technologies have been researched and continue to be an active area of research. Developed technologies include the Organic Rankine Cycle (ORC), the Kalina Cycle and the Variable Phase Cycle.

The efficiency of a heat engine is constrained by the maximum possible efficiency of an ideal cycle known as the Carnot cycle; this constraint is dependent on the temperature difference between the heat source and the heat sink and is given by the second law of thermodynamics. The figure below is a p-v diagram of the Carnot cycle. [website: oberlin.edu (2013)]

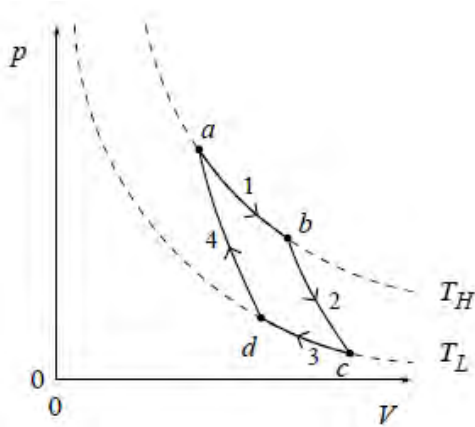


Figure 3. P-V diagram of the Carnot Cycle.

The efficiency of the Carnot cycle is given by:

$$\eta_{carnot} = \frac{T_H - T_L}{T_H} \quad (1)$$

where

- η_{carnot} : Carnot efficiency
- T_H : high temperature energy reservoir
- T_L : low temperature energy sink

Given limitations imposed by the Carnot efficiency the challenge is to optimise cycle efficiency based on other aspects. In particular it is necessary to minimise thermal losses through appropriate geometrical design and material selection for the insulation, glazing and absorber; also through reduction of frictional losses in the piping and optimization of working and heat transfer fluids matching with working temperature ranges.

The Organic Rankine Cycle (ORC) is in every sense the same as the conventional Rankine Cycle save for the fact that an organic fluid or a refrigerant is employed as a working fluid in place

of water and steam. This allows use of low temperature heat sources such as non-concentrated solar thermal, low temperature geothermal, oceanic thermal and waste heat to generate a low temperature vapour that in turn drives a vapour turbine. This is the cycle used in this research. Figure 4 shows the ORC configuration for a geothermal application.

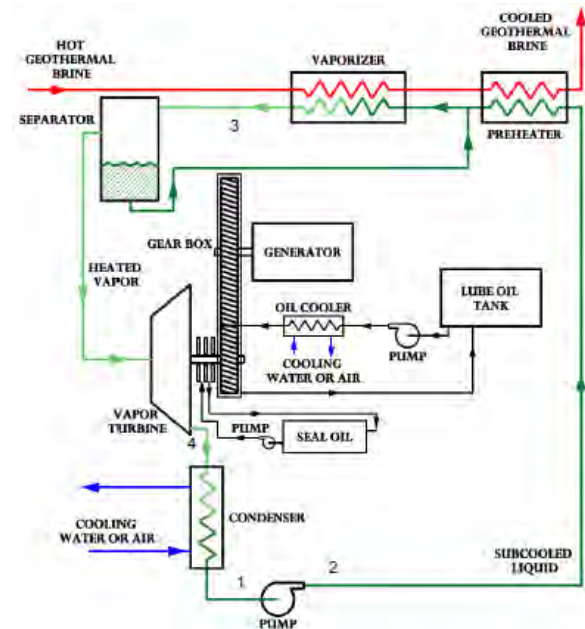


Figure 4. Organic Rankine Cycle [Geothermal_Resources_Council_2009_Poster]

2. Methodology

2.1 Solar Field Design

A solar field is initially proposed on the estimated power output of 10kW as shown in figures 5 and 6.

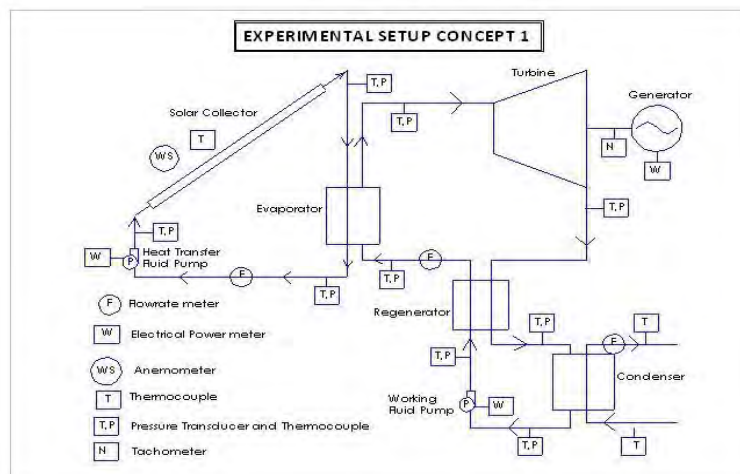


Figure 5. Concept Plant Setup for Solar Thermal ORC

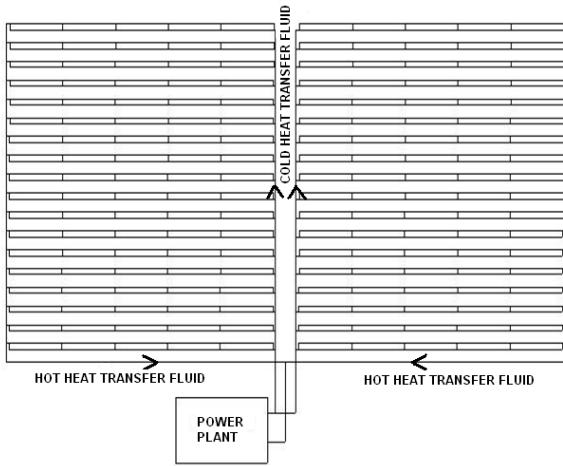


Figure 6. Proposed 10kWp Solar Field for ORC

Developing a detailed mathematical model of a solar collector requires knowledge of the geometrical measurements, and optical and thermal properties of materials used in the construction. The process is based on carrying out an energy balance which maybe steady state or transient. A transient model is more useful when the solar data can be measured and fed synchronously to the simulation model. A segmented model technique has been adopted in this study and an EES code written to establish the temperature profiles as well as thermal performance of the collector.

The figure shows the cross-section of a solar thermal collector with heat transfer balances for each component.

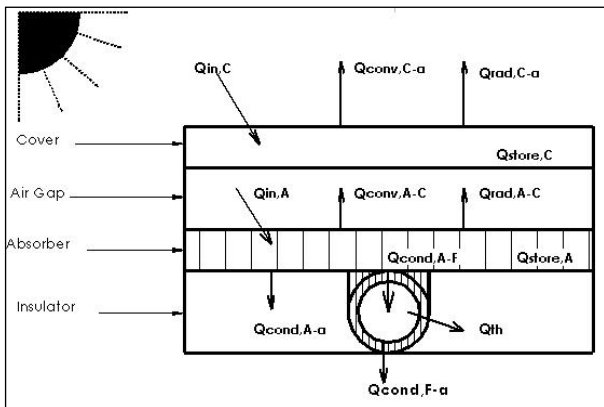


Figure 7. Solar Collector Heat Balance Layout

for the glass cover

$$Q_{store,C} = Q_{in,C} - Q_{conv,C \rightarrow a} - Q_{rad,C \rightarrow a} + Q_{conv,A \rightarrow C} + Q_{rad,A \rightarrow C} \quad (2)$$

for the absorber plate

$$Q_{store,A} = Q_{in,A} - Q_{conv,A \rightarrow C} - Q_{rad,A \rightarrow C} - Q_{cond,A \rightarrow F} + Q_{cond,A \rightarrow a} \quad (3)$$

for the heat transfer fluid

$$Q_{cond,A \rightarrow F} = Q_{cond,F \rightarrow a} + Q_{th} \quad (4)$$

for the storage tank

$$Q_{store,T} = Q_{th} - Q_{cond,T \rightarrow a} \quad (5)$$

thermal efficiency

$$\eta_{th} = \frac{\int Q_{th} dt}{A_c \int G dt} \quad (6)$$

2.2 ORC Optimization

Three ORC configurations are possible based on the working fluids' Temperature-Entropy (T-s) diagrams as follows:

- conventional rankine cycle,
- rankine cycle with a recuperator and
- rankine cycle with a superheater

In order to develop a generalized model that can be simulated using a computer program, a common configuration is indicated here from which the three models are generated:

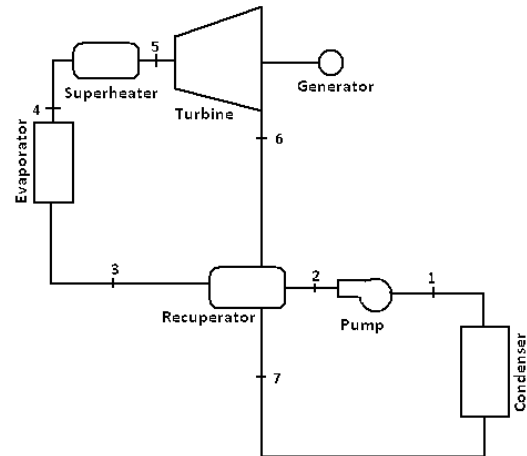


Figure 8. Common Configuration of the Organic Rankine Cycle

The mathematical models of the cycle components are given by:

Pump:

$$\frac{\dot{W}_{pump}}{\dot{m}} = (h_2 - h_1) \quad (7)$$

$$\approx \frac{v_1 \Delta P}{\eta_{pump}} \approx \frac{P_2 - P_1}{\eta_{pump}}$$

Turbine:

$$\frac{\dot{W}_{turbine}}{\dot{m}} = (h_5 - h_6) \quad (8)$$

$$= (h_5 - h_{6s}) \eta_{turbine}$$

Evaporator:
$$\frac{\dot{Q}_{evap}}{\dot{m}} = (h_4 - h_3) \quad (9)$$

Condenser:
$$\frac{\dot{Q}_{cond}}{\dot{m}} = (h_7 - h_1) \quad (10)$$

Recuperator cold stream:
$$\frac{\dot{Q}_{recu}}{\dot{m}} = (h_3 - h_2) \quad (11)$$

Recuperator hot stream:
$$\frac{\dot{Q}_{recu}}{\dot{m}} = (h_6 - h_7) \quad (12)$$

Superheater:
$$\frac{\dot{Q}_{superheater}}{\dot{m}} = (h_5 - h_4) \quad (13)$$

Thermal efficiency:
$$\eta_{therm} = \frac{\dot{W}_{turbine} - \dot{W}_{pump}}{\dot{Q}_{in}} \quad (14)$$

$$\approx \frac{\dot{W}_{turbine}}{\dot{Q}_{in}}$$

Where
$$\dot{Q}_{in} = \dot{Q}_{evap} + \dot{Q}_{superheater} \quad (15)$$

and in cases where there is no superheating as simply

$$\dot{Q}_{in} = \dot{Q}_{evap} \quad (16)$$

When implementing the model on the computer model an optimization scheme is included that equates either the superheating or the recuperating process or both to zero depending on the expansion characteristics of the working fluid. The optimization scheme is presented mathematically below.

$$If \frac{[s_{high} - s_{low}]}{s_{low}} < \delta \quad (17)$$

then the Isentropic Curve Model is selected; otherwise

$$If s_{high} > s_{low} \quad (18)$$

then the Positive Saturation Curve Model is selected; or

$$If s_{low} > s_{high} \quad (19)$$

then the Negative Saturation Curve Model is selected.

where s_{low} and s_{high} are the entropies of the dry saturated working fluid at the lower and higher cycle pressures respectively, and the value of the deviation δ is such that its limit approaches zero; mathematically $\delta \rightarrow 0$ and in the computer model a smaller acceptable value such as 5% is assigned δ .

2.3 Solar Irradiance Modelling

Several methods have been developed including Linear Models, Polynomial Models, Angular Models, and Other Models [Koray Ulgen & Arif Hepbasli (2004)]. The method used here is based on the Angular Models as proposed by Duffie J.A. and Beckman W.A. (1991).

The total hourly radiation can be estimated from the average daily radiation by using the following equation:

$$I = Hr_t \quad (20)$$

The coefficient to convert total daily radiation to total hourly radiation is given by:

$$r_t = \frac{\pi}{24} (a + b \cos w) \frac{\cos w - \cos w_s}{\sin w_s - \frac{\pi w_s}{180} \cos w_s} \quad (21)$$

Where w is the hour angle and w_s is the sunset hour angle in degrees. The coefficients a and b are given by:

$$\begin{aligned} a &= 0.409 + 0.5016 \sin(w_s - 60) \\ b &= 0.6609 - 0.4767 \sin(w_s - 60) \end{aligned} \quad (22)$$

3. Results

Chart 1 shows results for the 180 solar collector single-pipe field model. The solar field shown in figure 6 consists of two solar banks; each solar bank consists of 18 solar arrays; and each array consists of 5 solar collectors. The computer model consists of 18 one-pipe models connected in series to represent the 180 solar collector field. There is a steady build-up of temperature for all components along the model segments and banks. The temperature is highest in the absorber plate and lowest in the transparent cover; also the rate of temperature increase is lowest in the transparent cover. The rate of temperature increase closely follows the same profile in both the absorber and in the working fluid.

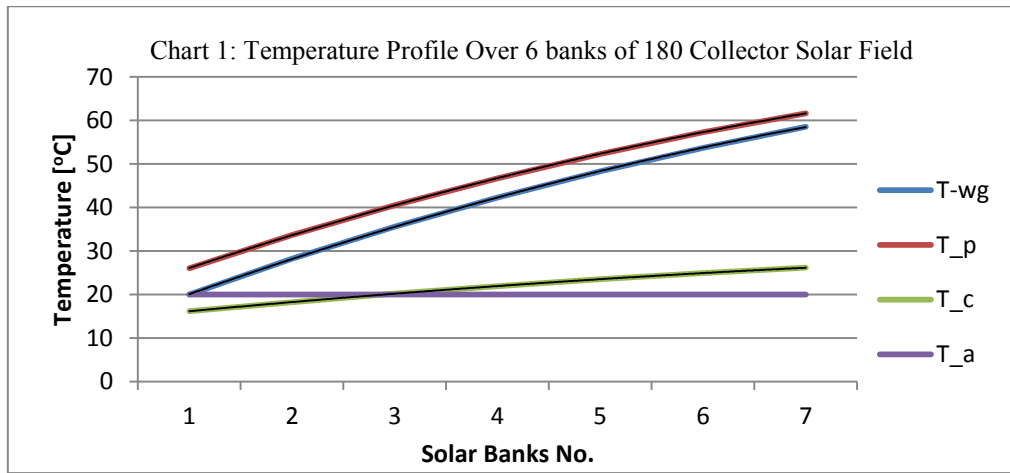
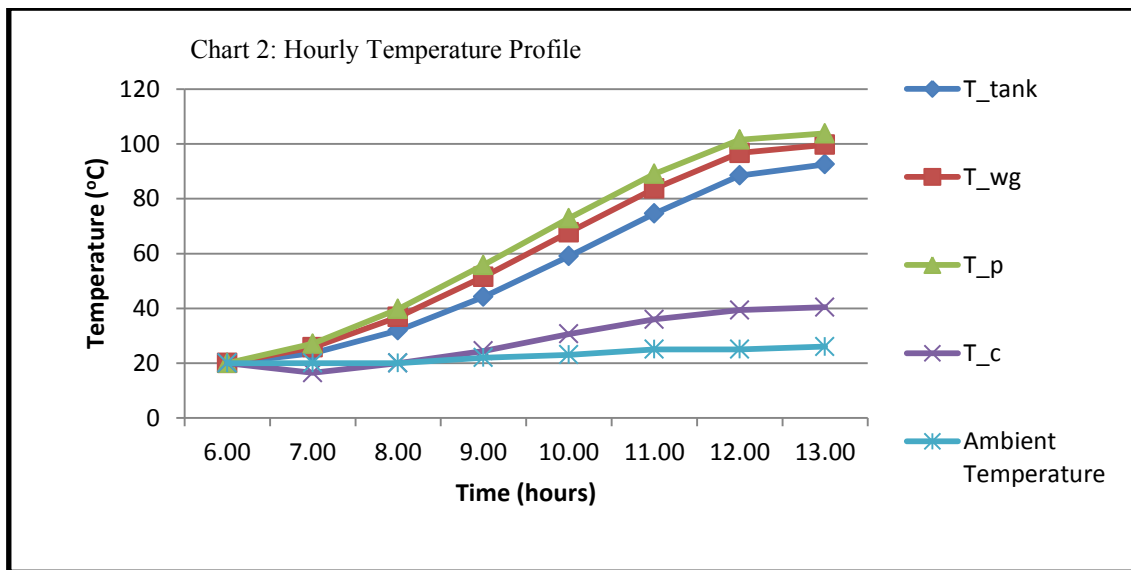


Chart 2 shows the hourly temperature profiles. These simulations consist of several cycles (114 cycles calculated) to make an hour. The temperature measurement is taken at the end of the hour. These simulations include a thermal storage represented by the tank temperature T_{tank}. The absorber plate attains the highest temperature followed by the working fluid (water ethylene glycol) at the exit of the solar field and into the tank storage. The three temperature profiles follow each other closely and build-up slowly from morning to

a high about noon. The absorber increases temperature from ambient temperature of 20°C to slightly over 100°C about noon; the water ethylene glycol attains maxima of slightly below 100°C and about 90°C at the exit of the solar collector and in the storage tank respectively. This is desirable for heat transfer to continue flowing from the absorber to the working fluid. The transparent cover has a much lower temperature ranging from ambient temperature to about 40°C. This ensures lower thermal losses.



Summarised results from the ORC computer simulations are shown in the following Table 2.

Table 2 ORC Computer Simulations Results

Working Fluid	Model Type	Low Temp [T _{low}]	High Temp [T _{high}]	Carnot Efficiency [η_{therm}]	Thermal Efficiency [η_{therm}]	Low Pressure Entropy [S _{low}]	High Pressure Entropy [S _{high}]
		[C]	[C]	[%]	[%]	[kJ/kg·K]	[kJ/kg·K]
Benzene	ORC with No Recuperator and No Superheater	80.07	142.7	15.06	11.11	1.176	1.151
n-butane	ORC with No Recuperator and No Superheater	-0.521	50.26	15.70	11.6	2.473	2.439
n-hexane	ORC with Recuperator; No Superheater	69.28	131.3	15.33	12.1	1.462	1.44
n-pentane	ORC with Recuperator; No Superheater	35.87	92.74	15.54	12.04	1.361	1.334
Isobutane	ORC with No Recuperator and No Superheater	-11.67	37.74	15.89	11.72	2.355	2.321
Isopentane	ORC with Recuperator; No Superheater	27.86	83.77	15.66	12.2	-0.4098	-0.4366
Toluene	ORC with Recuperator; No Superheater	110.4	178.3	15.04	11.75	1.053	1.032
R22	ORC with Superheater; No Recuperator	-40.81	29.52	23.24	12.01	1.849	1.825
R113	ORC with Recuperator; No Superheater	47.61	105.7	15.33	11.89	0.7788	0.7684
R123	ORC with No Recuperator and No Superheater	27.79	80.82	14.98	11.02	1.698	1.685
R134a	ORC with Superheater; No Recuperator	-26.09	24.08	16.88	10.99	0.9712	0.9516
R141b	ORC with No Recuperator and No Superheater	32.07	86.89	15.23	11.3	1.036	1.019
R245fa	ORC with No Recuperator and No Superheater	15.19	62.85	14.18	10.38	1.784	1.77
Water	ORC with Superheater; No Recuperator	99.97	271.8	31.53	10.81	7.483	7.355

The final choice of a working fluid will be influenced apart from the thermal performance indicated in table 2 by other factors including thermophysical properties, meeting environmental regulations and cost.

In terms of thermophysical properties an ideal working fluid should have “favourable thermodynamic properties, non-corrosive to mechanical components and safe (including nontoxic, non-flammable and environmentally benign). The desired thermodynamic properties are a boiling point somewhat below the target

temperature, a high heat of vaporization, a moderate density in liquid form, a relatively high density in gaseous form, and a high critical temperature.” [website: wikipedia.org. (2013)]. Table 3 lists the melting and boiling temperatures as well as the critical points (temperature and pressure) of the candidate working fluids. Table 4 lists the Global Warming Potential (GWP) and the Ozone Depletion Potential (ODP) of the working fluids. The GWP and ODP must also be taken into account in the selection of the working fluids.

Table 3 Comparison of Working Fluids Thermal Properties and ORC Thermal Requirements

Working Fluid	Melting Temp	Boiling Temp	Critical Temp	Critical Pressure
	[°C]	[°C]	[°C]	[MPa]
Benzene	5.5	80	289	4.74
n-butane	-138	-0.5	152	3.796
n-hexane	-95	69	234.5	3.02
n-pentane	-130	36	196.7	3.36
Isobutane	-133 to -33	-12	134.6	3.65
Isopentane	-160	28	187.25	3.38
Toluene	-95	111	318.64	4.109
R22	-175.42	-41	96.2	4.936
R113	-35	48	214.1	3.39
R123	-107	28	183.8	3.66
R134a	-103.3	-26	101.06	4.059
R141b	-103.5	32	204.15	4.25
R245fa		15.3	154.05	3.65

Table 4 Global Warming Potential and Ozone Depletion Potential of Working Fluids

Working Fluid	Molecular Formula	Global Warming Potential over 100 Years (GWP~100)	Ozone Depletion Potential (ODP)
Benzene	C ₆ H ₆	0	0
n-butane	C ₄ H ₁₀	20	0
n-hexane	C ₆ H ₁₄	20	0
n-pentane	C ₅ H ₁₂	11	0
Isobutane	C ₄ H ₁₀	20	0
Isopentane	C ₅ H ₁₂	11	0
Toluene	C ₇ H ₈	2.7	0
R22	CHClF ₂	1500	0.05
R113	C ₂ Cl ₃ F ₃	6000	0.8
R123	C ₂ HCl ₂ F ₃	90	0.02
R134a	CH ₂ FCF ₃	1300	0
R141b	C ₂ H ₃ Cl ₂ F	0.09	0.11
R245fa	C ₃ H ₃ F ₅	820	0

Ozone Depletion Potential: Reference is R11 (i.e. ODP for R11=1)

Global Warming Potential: Reference is CO₂ (i.e. GWP for CO₂=1)

4. Conclusions

The paper has explored the feasibility of tapping low temperature thermal energy for generation of power based on non-concentrated solar collecting system and the organic Rankine cycle. A concept plant has been proposed and computer simulations for both the solar field and the thermal cycle have been developed on its basis.

From two models the following can be inferred: temperatures attained in the solar field model storage reached a high of about 90°C; that means temperature T[5] in the ORC model is constrained to below this temperature.

From the ORC optimisation model it has been shown that potential working fluids and cycle configurations can be attained. Particularly in terms

of performance on all accounts other than cost (and safety), the optimal working fluids are Isopentane, n-hexane, n-pentane, R141b and Benzene; when the simplicity of cycle configuration (based on the T-s diagrams) is taken into account Benzene and R141b perform the best.

References

- [1]http://en.wikipedia.org/wiki/Electricity_generation accessed July 4, 2013
- [2]<http://www.earthlyissues.com/images/0013energysol.jpg> accessed June 14, 2013
- [3]http://www.geothermal-energy.org/geothermal_energy/what_is_geothermal_energy.html accessed July 4, 2013
- [4]<http://www.renewableenergyworld.com/rea/tech/ocean-energy> accessed June 14, 2013
- [5] Shuba V. Raghavan et al. (2010) Chapter 6: Solar Thermal Applications, In: *Harnessing Solar Energy-Options for India*. Editors: Payal Dhar and Radha HS. Center for Study of Science, Technology and Policy (CSTEP), Bangalore, India, pp. 91-102.
- [6]<http://www.oberlin.edu/physics/dstyler/P111/Carnot.pdf> accessed June 14, 2013
- [7] <http://www.findthatdoc.com/search-66008087-hPDF/download-documents-geothermal-resources-council-2009-poster-pdf.htm> accessed July 4, 2013
- [8] Koray Ulgen & Arif Hepbasli (2004): *Solar Radiation Models. Part 2: Comparison and Developing New Models*, Energy Sources, 26:5, 521-530
- [9] Duffie J.A., Beckman W.A., 1991: *Solar Engineering of Thermal Processes*, 2nd Ed., John Wiley & Son, Inc., USA, ISBN 0-471-51056-4
- [10]<http://en.wikipedia.org/wiki/Refrigerant> accessed July 14, 2013
- [11]http://www.engineeringtoolbox.com/Refrigerants-Environment-Properties-d_1220.html accessed July 17, 2013
- [12]<http://www.inventec.dehon.com/documents/pdf/cbac1510bfe289ca8669fe2fac5691f6.pdf> accessed July 17, 2013
- [13]<http://www.inventec.dehon.com/documents/pdf/a7532692d1e9257a2949c15e65311b7c.pdf> accessed July 17, 2013
- [14]<http://www.inventec.dehon.com/documents/pdf/98c2926bb0802baf7716d316ea8eed25.pdf> accessed July 17, 2013
- [15]<http://www.hc-sc.gc.ca/ewh-semt/pubs/contaminants/psl1-lsp1/benzene/index-eng.php> accessed July 17, 2013

Solar Air Heater with Sensible Thermal Storage

Shadreck M. Situmbeko and Kris L. Kumar,
University of Botswana, Gaborone, Botswana
situmbeko@yahoo.com , situmbeko@mopipi.ub.bw

Abstract

This research was conducted in collaboration with the Botswana Technology Centre (BOTECH) which has since been incorporated into a new research and development institution. The research was conceived as an offshoot of another project, the Solar Chimney, whose ultimate aim was to have a working short solar chimney constructed and installed in a remote village in Botswana by 2016 [website botec.bw (2013)]. This particular research is on the development of an appropriate solar thermal storage that could be incorporated into the Solar Chimney design. A number of concepts have been considered both in terms of geometrical design and storage media. The proposed thermal storage model is based on a sensible thermal storage technology employing water ethylene-glycol at 50% concentration and employs thermosyphon and reverse thermosyphon in the charging and discharging modes respectively. Computer simulations over a period of more than 24 hours have been performed. A physical prototype has also been constructed and testing is currently being undertaken. The proposed storage concept is also likely to find application in other solar thermal technologies that require thermal storage for effective operation; such applications as space heating and ventilation for comfort in residential buildings, crop drying in agriculture, etc.

Keywords:

solar thermal storage, sensible, water ethylene-glycol, (reverse-) thermosyphon, (dis-) charging

1. Introduction

Concerns over global warming and climate change associated with reliance on fossil fuels as well as energy supply deficits and increases in fuel prices have generated more interest and investment potentials in renewable energies' research and development. One emphasis in this regard has been on development of effective and reliable energy storage technologies; most renewable energies such as wind, sun and tides are available intermittently and must be stored in order to be released later when required for use. This would also optimise system performance and cost by reducing the mismatch between supply and demand. In the case of solar energy, for instance, it is available from the sun only when the sun shines and only a relatively smaller amount passes through to the earth's surface on hazy days. If we are to harness and employ solar energy during day and night, we need to be able to store a great deal of energy for later use.

2. Thermal Storage

Most energy storage technologies can be classified among any of the following storage systems: mechanical energy storage, electrical energy storage, thermal energy storage and thermochemical energy storage systems. Thermal

energy storage can be further subdivided into sensible thermal, latent thermal or chemical-thermal or a combination of these. (Atul Sharma, etal (2009)).

Currently the greatest potential for thermal storage appears to be for 'latent heat' storage materials also called Phase Change Materials (PCMs). The results of latest research show that 'molten salt' materials and technologies are the most promising for high efficiency solar storage and retrieval. In particular molten nitrate salt has been identified as a practical thermal energy storage system for Concentrated Solar Power (CSP) at temperatures above 300°C, with hours-long storage, and has proven reliable at commercial scales (NREL Technical Report (2011)). Such systems are, however, quite costly and therefore not optimally suited to low cost, low temperature and small to medium sized storage systems.

A comparative study of the properties of all possible sensible heat storage materials shows that water is the most promising 'specific heat' storage medium in view of its very high heat capacity and hence very large energy storage capacity with minimum volume. Addition of glycol to water in a predetermined ratio could enhance the merit of using water. Properties of Propylene Glycol, chemical formula C₃H₈O₂, reveal that its density is 1036 kg/m³, melting point -59°C and boiling point

188.2°C. The boiling point is much higher than that of water. Its thermal conductivity is 0.34 W/m-K. Glycol is miscible with water in all proportions and the density remains almost the same. It is neither flammable nor toxic or reactive.

To effectively compare sensible heat storage media it is necessary to look at their thermal masses. Thermal mass refers to the thermal inertia or thermal storage capacity of materials. Properties required for good thermal mass are high specific heat and high density. Table 1 presents the thermal masses of typical materials used for thermal storage. The data shows that water is by far the best medium compared to all other materials like concrete, sandstone, rammed earth, bricks, etc. Water is also the cheapest of all materials. The only problem with water is its poor thermal conductivity. Water can be used if the system design induces convection currents to compensate for lack of conductivity.

Table 1 Thermal Mass of Different Materials (website: wikipedia.org (2012))

Material	Thermal Mass (Volumetric Heat Capacity, kJ/m ³ -K)
Water	4186
Concrete	2060
Sandstone	1800
Compressed earth blocks	1740
Rammed earth	1673

FC sheet (compressed)	1530
Brick	1360
Earth wall (adobe)	1300
AAC	550

The storage model proposed in this research is thus based on ‘flowing water-glycol’ as the main medium for solar thermal storage.

3. Model Design

3.1 Development of the Storage Model Concept

In order to adequately address energy storage problems it is necessary to initially conceive what fraction of energy collected is for immediate use and what fraction has to be stored in the storage medium. Figure 1 shows the storage concept that was conceived for this research. It shows that a lot more energy, say 67 %, needs to be captured and stored during the day than what is utilized during that period or else there would be no energy available for later use.

The storage concept and the storage media based on a convective water-glycol system were further developed into the model design shown in figure 2.

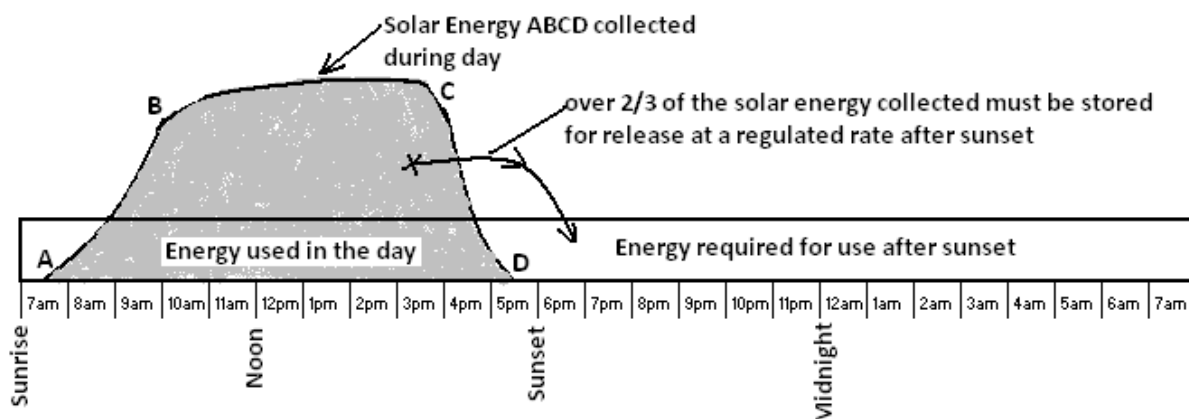


Figure 1 : Concept Sketch of Solar Energy Storage and Release

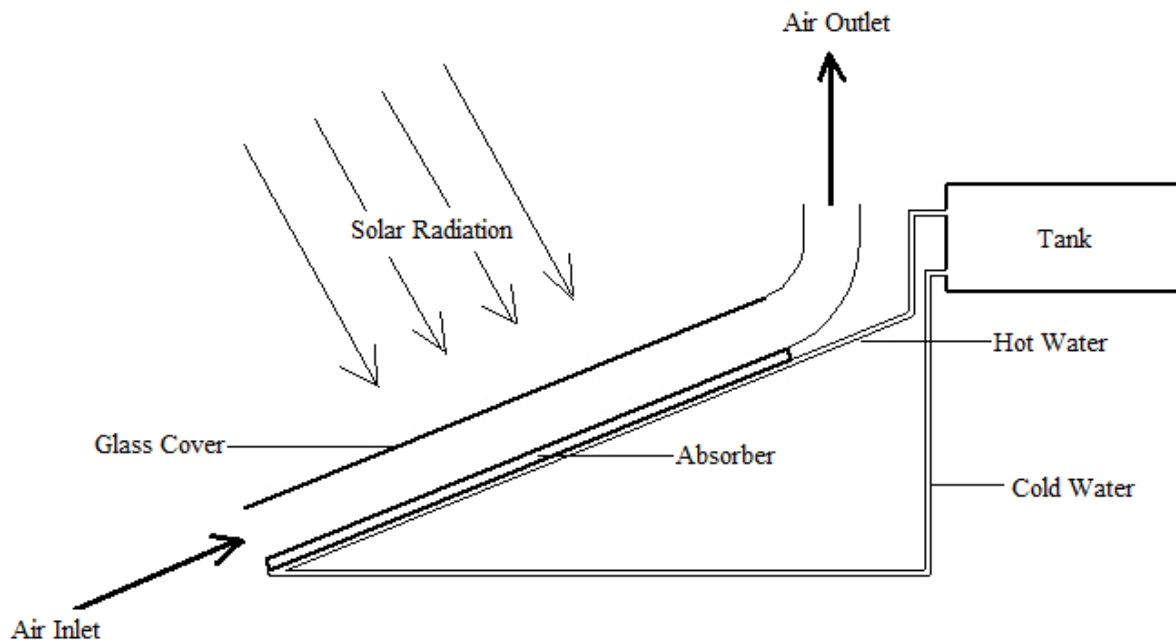


Figure 2: Solar Air Heater with a Water Thermal Storage

The design for the collector in this model had some geometrical constraints, emanating from the requirement that the developed storage model be adaptable for incorporation into the main stream research, the updraft solar chimney, hence the trapezoidal shape as depicted in figure 3, whereby the solar field is shown consisting of eight equal panels. In this design each panel consists of twenty five riser pipes. In the actual physical validation process only one panel would be constructed and tested. It was envisaged that the testing in different positions of the circular test setup could be simulated physically by simply placing the one panel in different locations of the circular test field as depicted in figure 4.

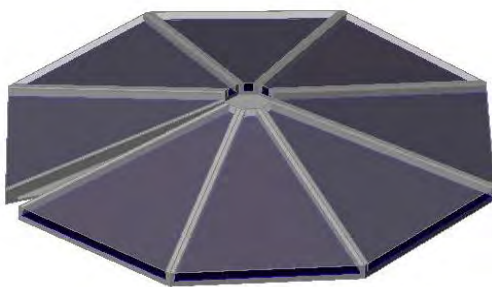


Figure 3: Final Storage Model Concept Design; 8 Panels Assembled

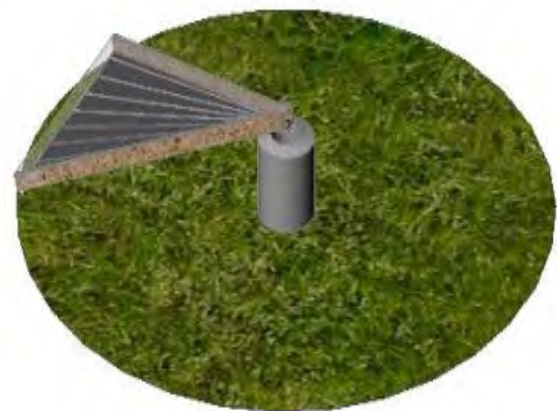


Figure 4: One Panel Test Setup

3.2 Mathematical Model

The mathematical model presented in this section is a set of heat transfer and fluid flow relations (equations) specific to the one pipe computer model and it is these that will form the basis for implementation of the computer simulations.

3.2.1 One Riser Pipe Model

The computer model is based on a one riser pipe model. The assumption made is that the one riser pipe model is representative of the thermal, temperature and flow profiles of the other riser pipes. The one pipe model is geometrically presented in figure 5 below. [dimensions are in mm]

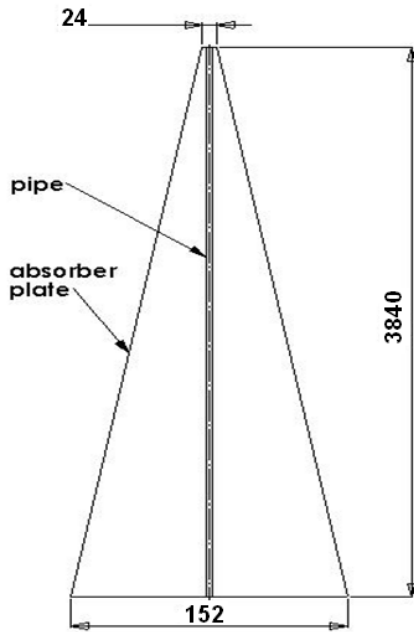


Figure 5: One Riser Pipe Model

The modeling technique adopted is the segmented model. When this is evaluated over a time period it simulates the transient condition or time dependence of the model. This technique has been adopted based on the fact that input data is not available as continuous functions of time but rather as discretized time-based data.

A 2-dimensional heat transfer model is adopted for the development of the computer programs; the assumption made is that heat transfer is only in the radial direction (x-axis), that is, in the direction of the air and heat transfer fluid flows, and in the vertical direction (y-axis), that is, in the direction of the solar radiation. The radial vertical surfaces (z-axis; not shown) are assumed adiabatic. (see figure 6)

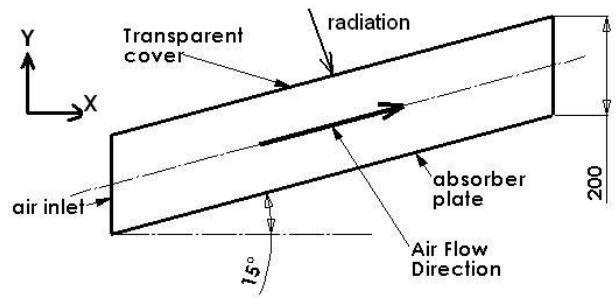


Figure 6: 2D Heat Transfer Model

- The segmented modeling technique requires that the one pipe model is divided into smaller sub-elements connected in series as shown in figure 7.
-

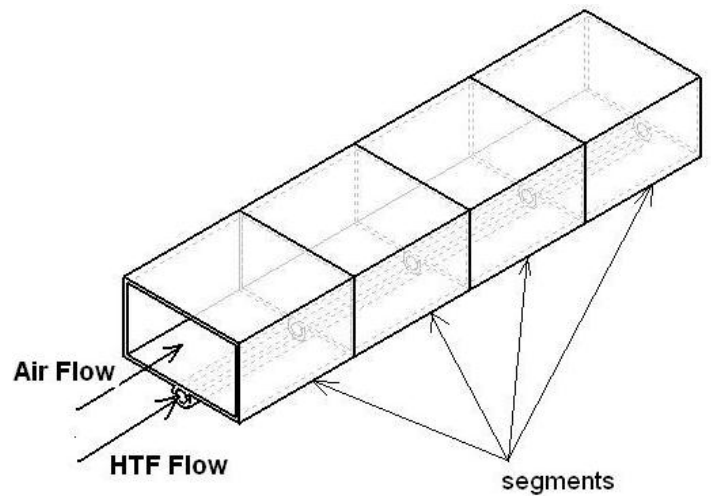


Figure 7: Segmented Model; HTF (Heat Transfer Fluid) refers to Ethylene-Glycol Water

- Further each segment is broken down into individual thermal components for the development of thermal gains and losses, heat transfer and storage capacity balances (see figure 8).

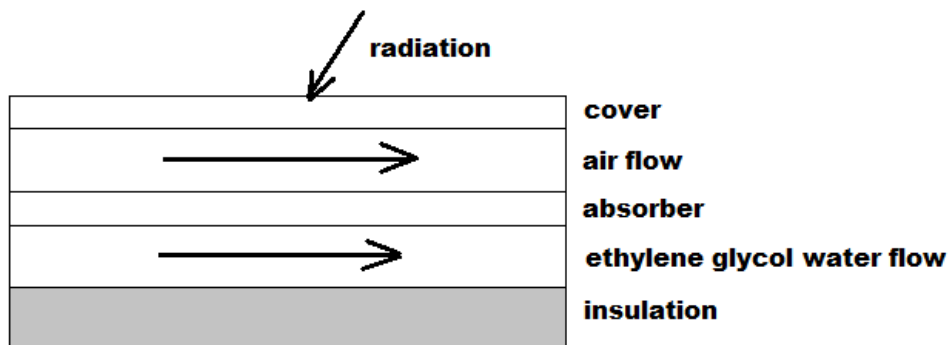


Figure 8: One Segment Model

The mathematical models are developed for each thermal component of the modeled segment. Output data from one segment form input data to the next

segment. Also included here are models for the solar radiation, thermosyphon process and thermal storage.

Figure 9 shows the energy balance for the absorber segment. The energy balance is represented mathematically by equations 1 and 2.

$$\dot{Q}_{abs} = \dot{Q}_{abs-air} + \dot{Q}_{abs-wg} + \dot{Q}_{r,abs-c} + \dot{Q}_{abs-back} \quad (1)$$

$$\dot{Q}_{abs} = \tau_c * \alpha_{abs} * A_{abs} * I_{sol} \quad (2)$$

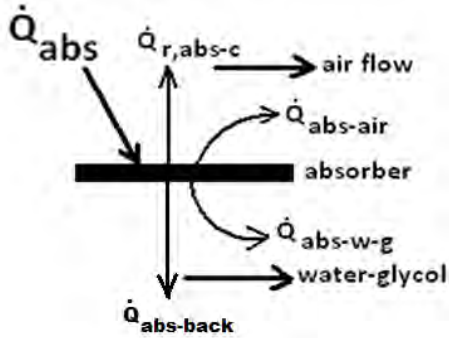


Figure 9: Absorber Segment Heat Transfer Model

The energy balance for the cover segment is shown in figure 10 and is given by equation 3.

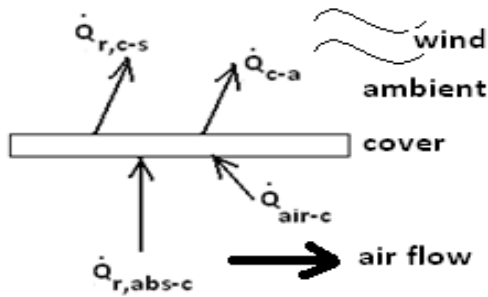


Figure 10: Cover Segment Heat Transfer Model

$$\dot{Q}_{air-c} + \dot{Q}_{r,abs-c} = \dot{Q}_{c-a} + \dot{Q}_{r,c-sky} \quad (3)$$

The energy balance on the air flow segment is represented by figure 11 and equations 4 and 5.

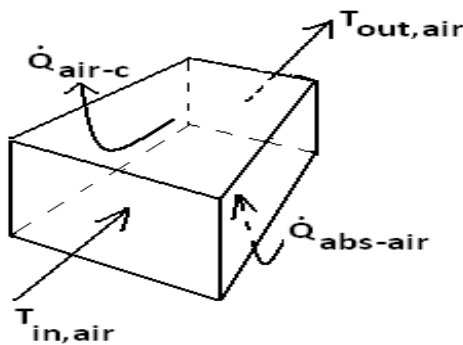


Figure 11: Air Flow Segment Heat Transfer Model

$$\dot{Q}_{abs-air} - \dot{Q}_{air-c} = \dot{Q}_{air} \quad (4)$$

$$\dot{Q}_{air} = \dot{m}_{air} * c_{p,air} * (T_{out,air} - T_{in,air}) \quad (5)$$

Figure 12 and equations 6 and 7 show the energy balance on the ethylene-glycol water flow segment.

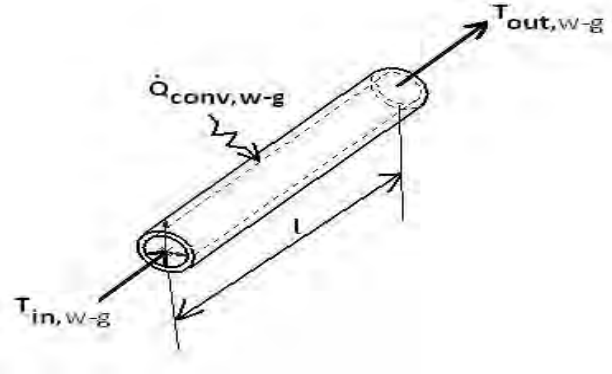


Figure 12: Ethylene-Glycol Water Flow Segment Heat Transfer Model

$$\dot{Q}_{conv,wg} = \dot{m}_{wg} * c_{p,wg} * (T_{out,wg} - T_{in,wg}) \quad (6)$$

$$\dot{Q}_{conv,wg} = h_{abs-wg} * A_{l,wg} * (T_{abs} - T_{m,wg}) \quad (7)$$

The total energy incident on the absorber, total energy transferred to the air, and total energy transferred to the heat transfer fluid are obtained by summations of the segment energies as in the following set of equations; number 8 below:

$$\dot{Q}_{abs} = \sum_{i=1}^{i=N} \dot{Q}_{abs}(i)$$

$$\dot{Q}_{air} = \sum_{i=1}^{i=N} \dot{Q}_{air}(i) \quad (8)$$

$$\dot{Q}_{w-g} = \sum_{i=1}^{i=N} \dot{Q}_{w-g}(i)$$

3.2.2 Thermosyphon Model

This is based on the Poiseuille's Law for Laminar flow which gives the volumetric flow rate and the buoyancy pressure difference as shown in equations 9 and 10:

$$v_{ol} = \pi \left(\frac{D}{2}\right)^4 * \frac{\Delta P}{8\mu L} \quad (9)$$

$$\Delta P = g * \Delta \rho * L * \sin \theta \quad (10)$$

3.2.3 Chimney Draft Model

The draft required to promote air flow is represented by the Boussinesq approximation. In particular the air flow exit velocity is modeled by equation 11 as:

$$V_{Nn} = \sqrt{2gH \left(\frac{T_{air,Nn} - T_a}{T_a}\right)} \quad (11)$$

Where H is included as if there were a chimney, $T_{air,Nn}$ is the temperature of the air flow exiting the collector and T_a is the ambient temperature (also equals the temperature of the air flow entering the collector)

3.2.4 Storage Tank Model

The thermal storage model consists of an energy balance consisting of Charging, Discharging and Thermal Losses. In this model thermal losses are assumed insignificant. That means during ‘Day Time Simulation’ the storage model assumes the ‘Charging Mode’ and during the ‘Night Time Simulation’, the ‘Discharging Mode’. Reverse thermosyphon is assumed for the ‘Discharging Mode’. A further assumption made is that there is no stratification in the storage tank, that is, the storage has one uniform temperature.

The charging model is given by equations 12 and 13:

$$\dot{Q}_{tank} = \dot{m}_{wg} * Cp_{wg} * (T_{wg,out,Nn} - T_{tank}) \quad (12)$$

$$\dot{Q}_{tank} = m_{wg,tank} * Cp_{wg} * \left[\frac{T_{tank} - T_{wg,in,0}}{t_{cycle}}\right] \quad (13)$$

Where \dot{Q}_{tank} is the heat transfer rate to the thermal storage; \dot{m}_{wg} is the mass flow rate of the water ethylene glycol working fluid; $m_{wg,tank}$ is the mass of the water ethylene glycol in the storage tank; Cp_{wg} is the specific heat capacity of the water ethylene glycol and t_{cycle} is the cycle time. The other parameters $T_{wg,out,Nn}$, $T_{wg,in,0}$ and T_{tank} are temperatures of the working fluid exiting the collector model and entering the storage tank, of the working fluid entering the collector model at the previous cycle (also the previous storage tank temperature) and the new storage tank temperature respectively.

The discharging model is given by the equations 14 and 15:

$$\dot{Q}_{tank} = \dot{m}_{wg} * Cp_{wg} * (T_{wg,out,0} - T_{tank}) \quad (14)$$

$$\dot{Q}_{tank} = m_{wg,tank} * Cp_{wg} * \left[\frac{T_{tank} - T_{wg,in,Nn}}{t_{cycle}}\right] \quad (15)$$

Where the reversed flow now means that $T_{wg,out,0}$ and $T_{wg,in,Nn}$, are now temperatures of the working fluid exiting the collector model and entering the storage tank, and of the working fluid entering the collector model at the previous cycle (also the previous storage tank temperature) respectively.

3.2.5 Solar Radiation Model

The total hourly radiation can be estimated from the average daily radiation by using the following equation:

$$I_{sol} = H * r_t \quad (16)$$

The coefficient to convert total daily radiation to total hourly radiation is given by equation 17:

$$r_t = \frac{\pi}{24} (a + b \cos w) \frac{\cos w - \cos w_s}{\sin w_s - \frac{\pi w_s}{180} \cos w_s} \quad (17)$$

Where ‘w’ is the hour angle and ‘w_s’ is the sunset hour angle in degrees. The coefficients ‘a’ and ‘b’ are given by equations 18:

$$\begin{aligned} a &= 0.409 + 0.5016 \sin(w_s - 60) \\ b &= 0.6609 - 0.4767 \sin(w_s - 60) \end{aligned} \quad (18)$$

3.3 Computer Simulations

The Computer Simulations are performed on the Engineering Equation Solver (EES) platform. The computer simulation developed consists of the following EES codes:

- One code for day time simulation,
- One code for night time simulation,
- One code for the solar model – to simulate the hourly solar radiation, and
- One code for lengths and areas calculations

4. Results

The simulations were run over a period of 24 hours, starting at 7am and ending at 6 am the following day. The computer code computed how many cycles to run in each hour. The input data was updated after each cycle as well as at the start of a new hour. The results for each cycle were saved. Summary and sampled results are shown here. Ambient temperatures were obtained for a typical April Day in Gaborone from website timeanddate.com (2012). Figures 13 and 14 show the hourly temperature and energy transfer rates for the simulated day. The temperatures shown for the air and ethylene glycol water flows are those at the exit flow’s exit from the collector. The energy rates are summations for the entire computer model as represented in equations 8.

5. Conclusions

The computer simulations have been presented using Engineering Equation Solver (EES) software.

The concept design of the solar storage model consisted of eight panels thus forming an octagon shape on the periphery rather than a circular one; with each panel consisting of twenty five riser pipes, a bottom header pipe and a top header pipe; with both header pipes connecting to a storage tank.

For the computer simulation a further simplification has been done thus only a one riser model has been considered. The computer simulation is based on a two dimensional heat transfer segmented model.

Mathematical models have been developed for this simplified one riser pipe, two dimensional heat transfer, segmented model. Models have also been

developed for the hourly solar radiation, thermosyphon and storage.

Results are presented in chart form. Figure 13 shows the hourly temperature plots for the exit air flow temperature, exit ethylene glycol water temperature, the storage temperature and the ambient temperature. The results are able to show growth in the thermal storage as well as the reversal of the heat transfer from solar hours to non-solar hours. Figure 14 shows the heat transfer rates at the end of each hour.

The simulations have shown the potential for implementation of the concept storage model based on ethylene glycol water heat transfer fluid at 50% concentration. Further simulations are recommended for other types or mixes of heat transfer fluid. Extended simulations covering several days are required in order to gain useful insight on the effectiveness of the proposed storage model. Further validations on other software platforms such as TRANSYS and CFD maybe necessary.

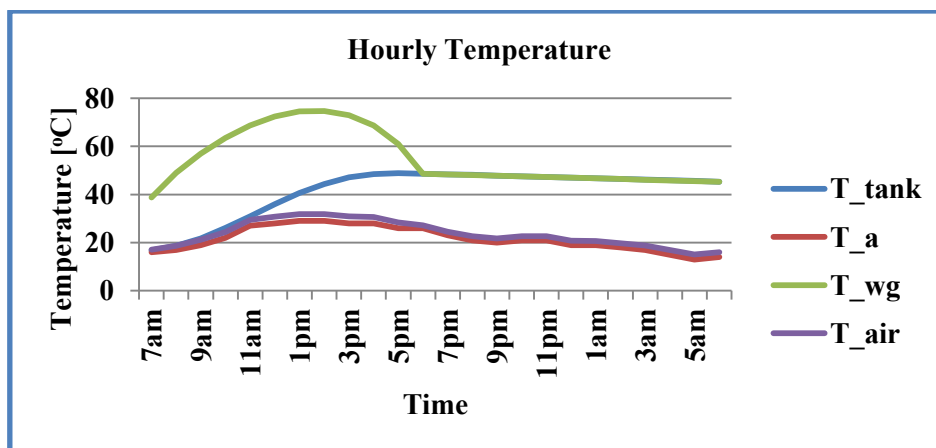


Figure 13: Hourly Temperatures

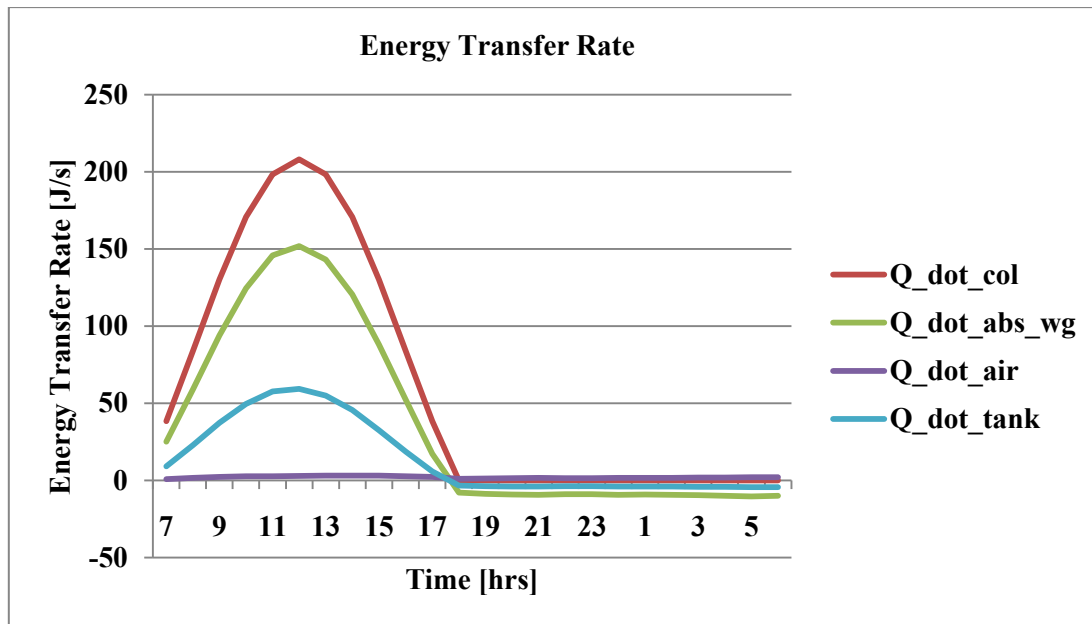


Figure 14: Energy Rates at End of each Hour

References

- [1] <http://www.botec.bw/index.php/botec-projects/energy/the-solar-chimney> accessed July 29, 2013
- [2] Atul Sharma, etal (2009) Review on thermal energy storage with phase change materials and applications in *Renewable and Sustainable Energy Reviews 13* (2009) 318–345
- [3] Glatzmaier G. (2011), Summary Report for Concentrated Solar Power Thermal Storage Workshop, *New Concepts and Materials for Thermal Energy Storage and Heat Transfer Fluids*, National Renewable Energy Laboratory Technical Report NREL/TP-5500-52134, Colorado, USA, p8.
- [4] http://en.wikipedia.org/wiki/Thermal_mass accessed 2012
- [5] <http://www.timeanddate.com/weather/botswana/gaborone/hourly> (2012)
- [6] BOTEC Solar Thermal Storage Model Final Report 2013

MATHEMATICAL MODELLING AND COMPUTER SIMULATION OF A SOLAR FIELD FOR A LOW TEMPERATURE ORGANIC RANKINE CYCLE (ORC)

SM Situmbeko¹ and FL Inambao²

1 University of KwaZulu Natal, Howard College, School of Mechanical Engineering, Durban, South Africa, 4041,
ssitumbeko@yahoo.com, cell 0825485101

2 University of KwaZulu Natal, Inambaof@ukzn.ac.za

Abstract

Low temperature solar thermal energy conversion refers to the use of low temperature and lower thermal intensity solar energy and the subsequent conversion to mechanical and/or electrical energy. Low temperature solar thermal typically operates below 300°C and employs lower concentrating or non-concentrating solar collectors. This research investigates the optimal conversion of lower temperature solar thermal energy to electrical power for use in remote and non-grid connected areas. Preliminary concept plant designs for 500 W and 10kW have been proposed. Outline cycle designs, and first pass mathematical and computer models have been presented to previous conferences, Domestic Use of Energy (DUE) Conference 2010 and International Solar Energy Society Solar World Congress (ISES SWC) 2011 respectively. The first pass model analysed a number of working fluids and different cycle configurations. The detailed mathematical models of the low temperature solar thermal field as well as the results obtained from the Engineering Equation Solver (EES) computer models are presented in this paper. These detailed models are based on 2-dimensional segmented heat transfer and thermofluids dynamics analyses. Input data has been obtained from meteorological databases and includes solar radiation, ambient temperature and wind speed.

Keywords: organic rankine cycle (orc), solar thermal, discretised model, thermal network, thermofluids dynamics

1. Introduction

Solar thermal energy conversion for power generation is an active area of research more so for low temperature systems. Currently some high temperature Solar Thermal Energy (HT-STE) technologies for electricity production have attained technical maturity; technologies such as the parabolic dish (commercially available), parabolic trough and power tower are only hindered by unfavourable market factors including high maintenance and operating costs and the exclusion of environmental burden in the costing of conventional systems. A number of power generation concept power plants based on high temperature thermal technology have been installed worldwide. [1]

Low temperature thermal energy resources have mainly been used for low heat applications such as water heating, space heating, crop drying etc. but not for electricity generation. Currently available technology is not suited for low temperature thermal power generation as it is unable to produce steam of the desired quality to run in the conventional thermal conversion cycle. There is however potential for research on low temperature thermal energy conversion as this would allow utilization not only of naturally occurring low temperature thermal resources such as low temperature geothermal, oceanic and non-concentrated solar but also waste heat, a product of many industrial processes including high temperature power generating plants running on fossils, nuclear and concentrated solar power. This realization has led to continued efforts on low temperature thermal energy research. Utilization of waste heat is also viewed as desirable owing to its potential to raise plant efficiencies. This also adds greater flexibility for remote and small scale power generation operations. Small scale power generation is also more suited to distributed energy systems, an area currently gaining attention and pursuit in global energy markets. Distributed energy systems are closer to the final users and as such result in reductions in electrical transport losses, operational and maintenance

costs, and environmental impact [2]. Low temperature solar thermal typically uses flat plate solar collectors; flat plate collectors are relatively cheaper and easier to operate and do not require complex sun tracking technologies. Low temperature in this regard refers to temperatures below 300°C, medium temperature from 300°C to 600°C, and high temperature to above 600°C.[3]

Use of low temperature thermal for power generation requires adjustments to the conventional energy conversion cycles such as replacement of the working fluid to enable vapourisation at lower temperatures. The replacement of water may also be desirable in some instances where there is scarcity of water for both the working and cooling cycles such as in arid environments. The Rankine cycle when operated with working fluids other than water is referred to as the Organic Rankine cycles.

This project focuses on the Organic Rankine cycle powered with low temperature solar thermal energy. Various working fluids such as R141b, n-hexane, n-pentane and R22 being investigated as part of this research have thus far shown positive results from preliminary mathematical models and computer simulations. Further considerations will be placed on aspects of heat transfer and fluid flow losses.

2. Concept Plants for Development of Low Temp STE

The next two figures show two possible experimental setups. The figures show the general layout of the solar collector, heat exchangers, turbine-generator, pumps and piping. Figure 1(a) shows the first experimental setup whereby the heat transfer fluid is pumped through the solar collector where it is heated and is then passed through the evaporator where heat is transferred to the working fluid. In figure (b) the second experimental setup, as shown, the working fluid is directly heated and evaporated by a solar collector. Whereas the second setup has the advantage of eliminating one heat exchanger, the evaporator, and reducing the required piping, it presents other design challenges; for instance the solar collector must have the required corrosion resistance and be able to withstand higher pressures associated with the working fluid.

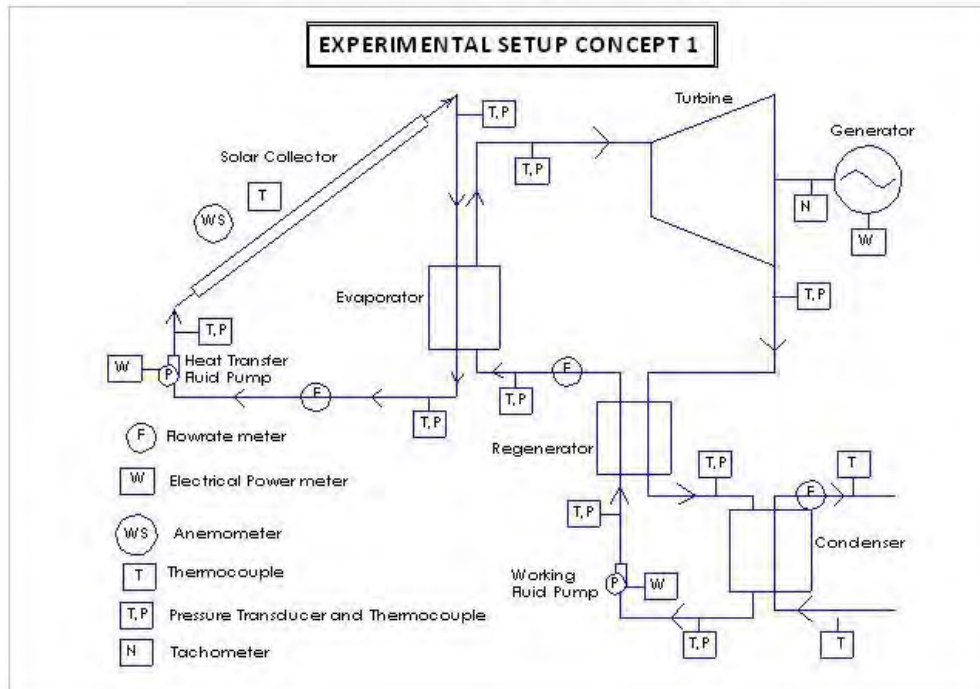


Figure 1(a): Experimental Setup Concept 1

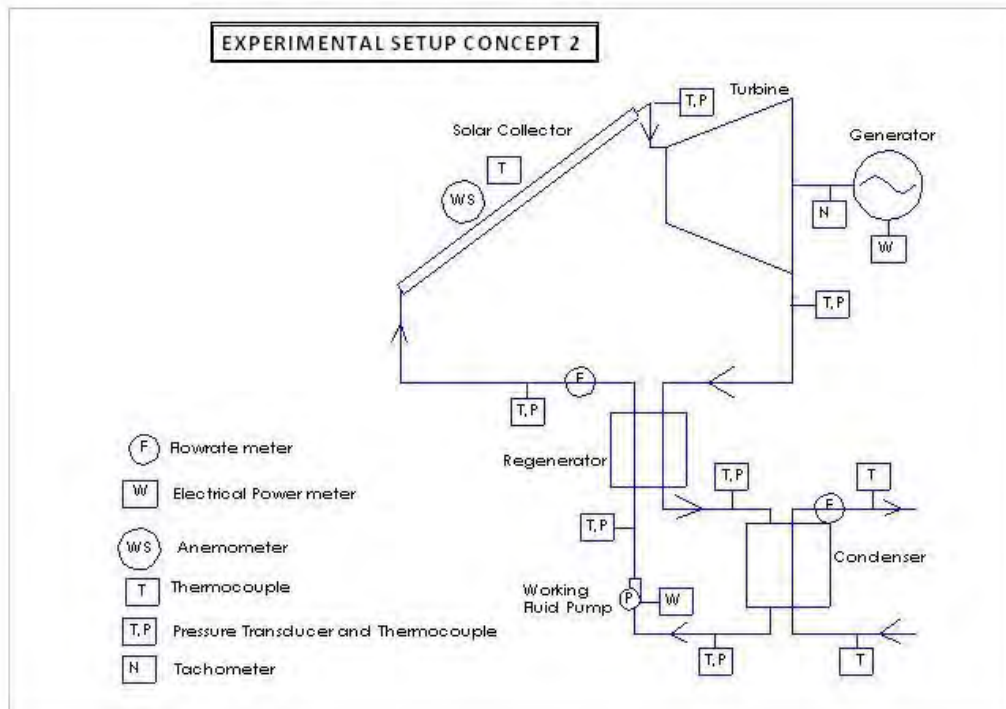


Figure 1(b): Experimental Setup Concept 2

Preliminary small-scale concept plants have been designed at 500Wp and 10Kwp. The smaller model is intended as a laboratory experiment and the larger as a field experiment. The aim of this laboratory test is to get an insight in the experimental test setup and results recording and analyses; and implement any needed improvements. The field experimental setup will involve the 10kWp Low Temperature Solar Energy Conversion Model.

Design involves optimally sizing the cycle main components so as to attain the intended output. The main cycle components are the evaporator and condenser heat exchangers, and the turbine and pumps work devices, the solar collectors array and the generator. The other design aspect involves sizing the duct network so as to minimise both pressure and heat losses and determining the quantities of both the working and heat transfer fluids as well as specifying the type of insulation.

The solar field is an important aspect of this design as it involves not only determining the size of the field but also the layout of the solar collectors array.

The preliminary array design is based on the Solardome SA solar collector of size 1840 x 1650 mm, giving an area of 3.04 m²[4]. The efficiencies of flat plate collector from Thermomax Industries [5] range from 35 to 50 % for domestic hot water with mean temperature $T_m \approx 55^\circ\text{C}$. Where T_m is the average temperature of fluid in the collector and is given by:

$$T_m = \frac{T_{in} + T_{out}}{2}$$

where T_{in} and T_{out} are respectively the solar inlet and outlet temperatures.

The range of efficiencies for Organic Rankine Cycle operating at low to medium temperatures ranges from 9.9 to 14.1% [6],[7]. Taking averages the overall system efficiency could be taken as 5.1%; [i.e. $\frac{35\%+50\%}{2} * \frac{9.9\%+14.1\%}{2} = 5.1\%$]. Thus the solar thermal energy available should be about 9.8kW_{th} for the laboratory model and 196kW_{th} for the field model. Durban Insolation data averages 4.328 kWh/m²/day which gives 180W/m² for the 24 hours' day or 360W/m² for a 12 sun-hours' day [8].

The table shows the first pass size estimates of the solar arrays:

Parameter	Laboratory Model [solar collector]	Field Model [solar collector]	Units
Output power	0.5	10	kW
ORC mean efficiency	12	12	%
Solar mean efficiency	42.5	42.5	%
Input power	9.80	196.08	kW
Durban Insolation	4.328	4.328	kWh/m ² /day
Incident Area	27	545	m ²
Solar Collector Area	3.04	3.04	m ²
No. of Solar Collectors	9	179	

Table 1: Estimated Solar Field Sizes

Based on the foregoing estimates, the preliminary solar arrays are designed as shown in the following figure 2(a) and figure 2(b):

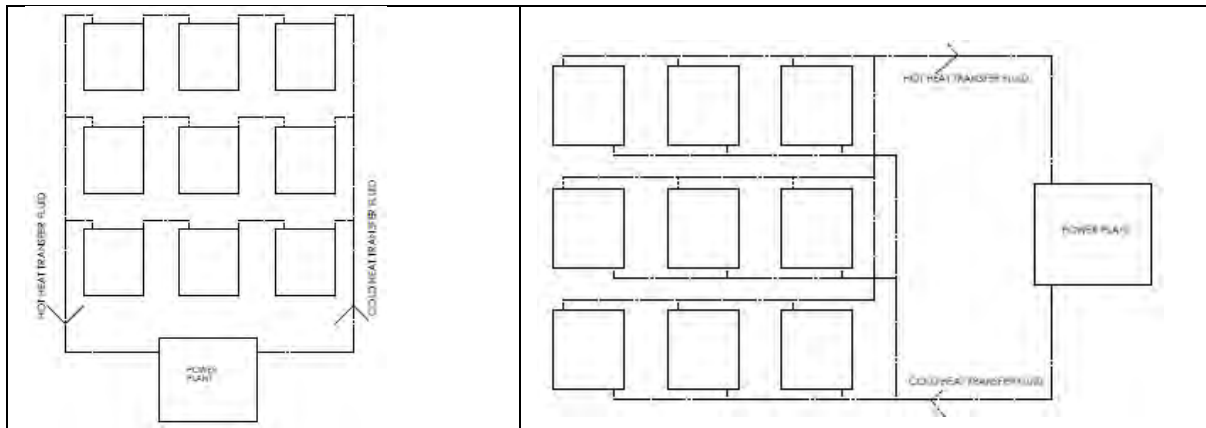


Figure 2(a): 500W Layout requiring 9 solar collectors

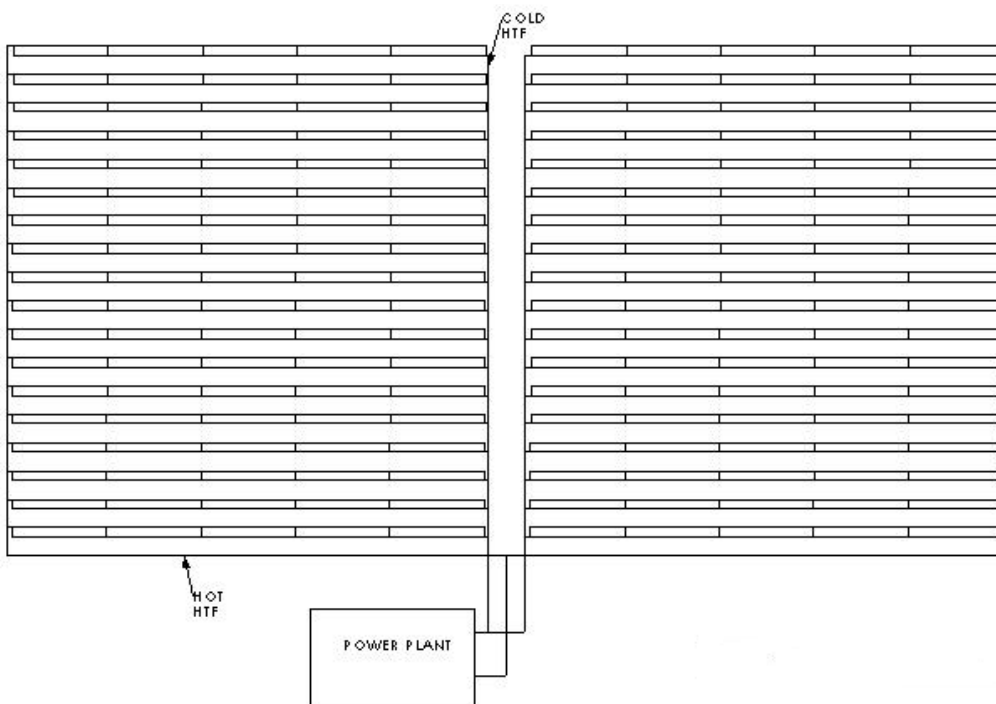


Figure 2(b): 10kW Layout requiring 180 solar collectors

3. First Pass System Model

The first pass model of the plant system was developed and simulated on the EES (Engineering Equation Solver) platform [9]. Fourteen candidate working fluids and three cycle configurations were analysed. The model incorporated a logic model selector through which an optimal conversion cycle configuration and working fluid mix was established. The figure 3 shows the flow diagram of the model. The results of the analyses of the 14 working fluids are shown in the table 2 [7].

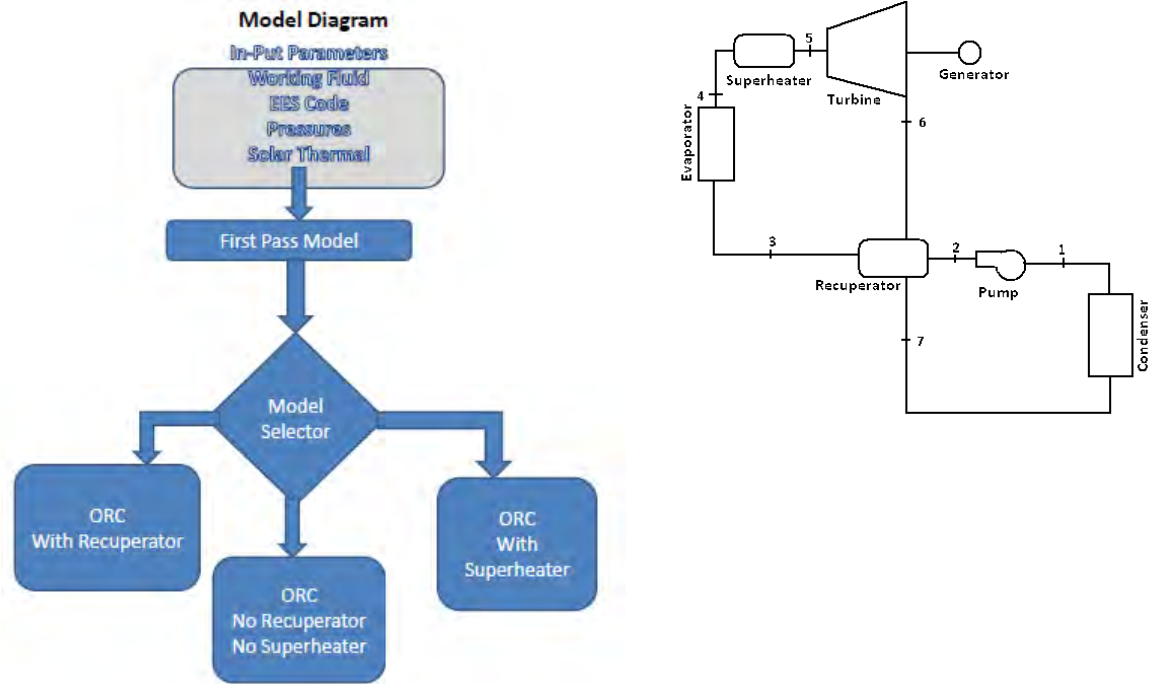


Figure 3: First Pass Model Flow Diagram and General Configuration of the Organic Rankine Cycle

Model Type	Working Fluid	Q_dot_evaporator [kW]	Q_dot_recuperator [kW]	Q_dot_superheater [kW]	Power [kW]	eta_therm [%]
ORC with Recuperator; No Superheater	n-pentane	4.067	0.4041	0	0.4997	12.04
ORC with No Recuperator and No Superheater	Benzene	4.68	0	0	0.5272	11.11
ORC with No Recuperator and No Superheater	n-butane	4.558	0	0	0.539	11.6
ORC with Recuperator; No Superheater	n-hexane	3.753	0.6134	0	0.4641	12.1
ORC with No Recuperator and No Superheater	Isobutane	4.306	0	0	0.5151	11.72
ORC with No Recuperator and No Superheater	R141b	2.6	0	0	0.2987	11.3
ORC with Recuperator; No Superheater	Isopentane	3.901	0.376	0	0.4859	12.2
ORC with No Recuperator and No Superheater	R245fa	2.301	0	0	0.2432	10.38

Table 2: Thermal Efficiencies of Different Organic Rankine Cycle Configurations and Different Working Fluids

Model Type	Working Fluid	Q_dot_evaporator	Q_dot_recuperator	Q_dot_superheater	Power	eta_therm
		[kW]	[kW]	[kW]	[kW]	[%]
ORC with Recuperator; No Superheater	R113	1.64	0.156	0	0.1991	11.89
ORC with No Recuperator and No Superheater	R123	2.021	0	0	0.2268	11.02
ORC with Superheater; No Recuperator	R22	2.496	0	0.2123	0.3296	12.01
ORC with Recuperator; No Superheater	Toluene	4.094	0.4495	0	0.489	11.75
ORC with Superheater; No Recuperator	R134a	2.413	0	0.08032	0.2784	10.99
ORC with Superheater; No Recuperator	Water	23.29	0	2.569	2.803	10.81

(Table 2: continued)

Working Fluid	T[1]	T[2]	T[3]	T[4]	T[5]	T[6]	T[7]
	[C]	[C]	[C]	[C]	[C]	[C]	[C]
n-pentane	35.87	36.17	52.94	92.74	92.74	58.26	35.87
Benzene	80.07	80.33	80.33	142.7	142.7	96.87	96.87
n-butane	-0.521	-0.133	-0.133	50.26	50.26	10.38	10.38
n-hexane	69.28	69.58	94.75	131.3	131.3	100.5	69.28
Isobutane	-11.67	-11.25	-11.25	37.74	37.74	-2.53	-2.53
R141b	32.07	32.5	32.5	86.89	86.89	41.03	41.03
Isopentane	27.86	28.16	44.35	83.77	83.77	49.15	27.86
R245fa	15.19	15.43	15.43	62.79	62.85	26.24	26.24
R113	47.61	48.04	64.22	105.7	105.7	69.54	47.61
R123	27.79	28.11	28.11	80.82	80.82	40.66	40.66
R22	-40.81	-39.14	-39.14	0.1148	29.52	31.19	31.19
Toluene	110.4	110.6	132.6	178.3	178.3	139.8	110.4
R134a	-26.09	-25.87	-25.87	15.71	24.08	-19.9	-19.9
Water	99.97	100.1	100.1	151.8	271.8	124.5	124.5

(Table 2: continued)

4. Solar Collector Models

4.1. First Pass Models

The first pass model simply represented this by the governing equation of Hottel-Whillier [10] given as:

$$Q_u = A_c F_R [\tau \alpha G - U(T_{in} - T_a)] \quad (1)$$

where A_c (m^2) is the solar collector field aperture area, F_R is the heat removal factor, τ is the cover glazing transmittance, α is the absorber absorptance and U is the overall heat loss coefficient of the solar collector field. Operational conditions are solar insolation G , heat transfer fluid inlet temperature T_{in} and ambient temperature T_a .

4.2. Detailed Solar Field Model

The detailed models are developed in a two stage format as Solar Collector and Solar Field Models. The solar collector model develops a steady state and/or transient model of a single collector based on the equations of Continuity, Momentum and Energy. The Solar Field Model links individual collector models into Collector Banks, Banks into Arrays and finally the whole lot of the arrays form the Field Model, taking into cognizance at every stage the input and output parameters to determine performance of the solar field.

4.3. Solar Collector Model

Detail modelling of a solar collector requires knowledge of the geometrical measurements and thermal properties of materials used in the construction. The process is based on carrying out an energy balance which maybe steady state or transient. A transient model is more useful when the solar data can be measured and fed synchronously to the simulation model. A segmented model technique will be adopted and an EES code written to establish the temperature profile as well as thermal performance of the collector.

The figure shows the cross-section of a Solar Thermal Collector with Heat Transfer for each component.

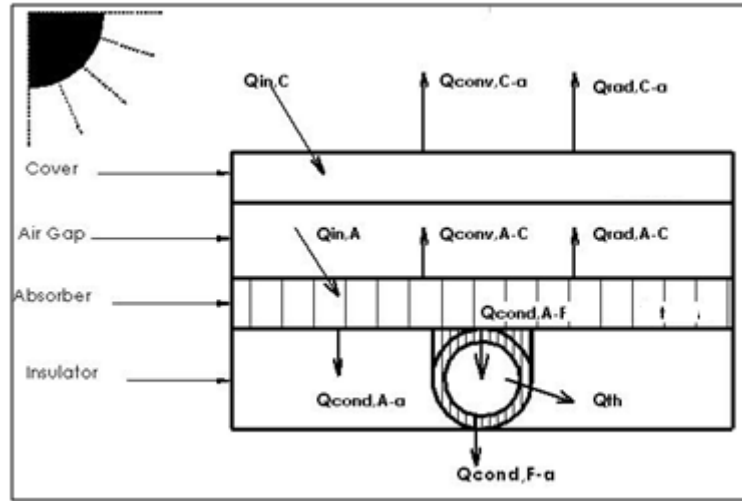


Figure 4: Solar Collector Heat Balance Layout

$$\text{For the glass cover: } Q_{store,C} = Q_{in,C} - Q_{conv,C \rightarrow a} - Q_{rad,C \rightarrow a} + Q_{conv,A \rightarrow C} + Q_{rad,A \rightarrow C} \quad (2)$$

$$\text{For the absorber plate: } Q_{store,A} = Q_{in,A} - Q_{conv,A \rightarrow C} - Q_{rad,A \rightarrow C} - Q_{cond,A \rightarrow F} - Q_{cond,A \rightarrow a} \quad (3)$$

$$\text{For the fluid: } Q_{cond,A \rightarrow F} = Q_{cond,F \rightarrow a} + Q_{th} \quad (4)$$

$$\text{For the storage tank: } Q_{store,T} = Q_{th} - Q_{cond,T \rightarrow a} \quad (5)$$

$$\eta_{th} = \frac{\int Q_{th} dt}{A_c \int G dt} \quad (6)$$

The one pipe model is assumed in developing the mathematical model. EES code for one pipe model is being developed. Preliminary results for one pass of water-glycol heat transfer fluid through the one pipe model are shown below. The model has been set to 10 segments and for the trial run the collector size has been set to 2.0m length and 1.0m width.

Figure 5 shows the temperature profiles along the segments of the collectors. T_p is the temperature profile for the absorber plate and T_{wg} is the temperature profile for the water ethylene glycol working fluid. The numbers enclosed in the parentheses represent the number of the one pipe model as they are connected in series. These results are for a one cycle pass with no storage model connected.

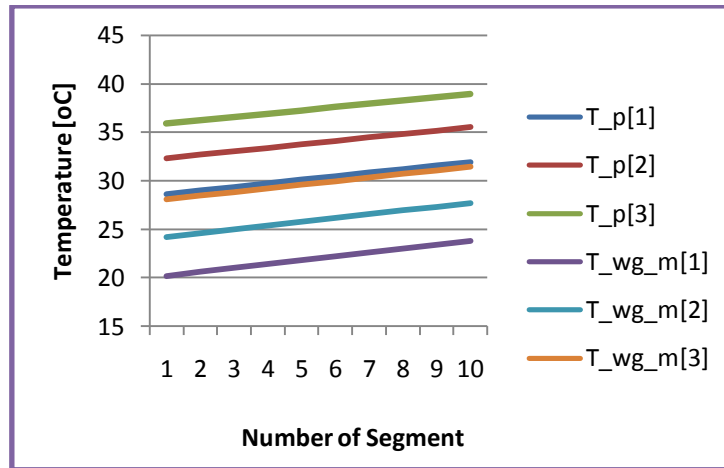


Figure 5: Temperature vs Segment Number

Figure 6 shows the energy profiles along the segments of the collectors. Q_{dot_wg} is the heat transfer profile to the working fluid and Q_{dot_loss} represents the thermal losses from the collector at each segment. Similarly these results are for a one cycle pass with no storage model connected. The rate of heat gain by the working fluid decreases along linear segments of the collector whilst the rate of heat losses from the collector increases along the linear segments of the collector.

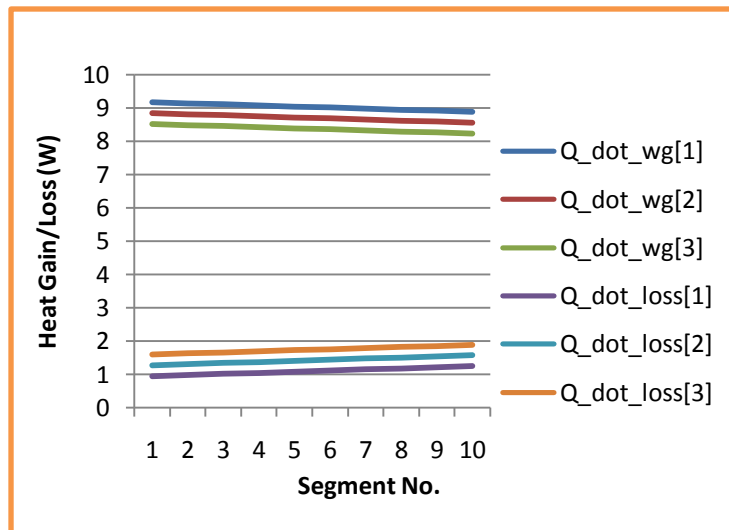


Figure 6: Energy Gain/Loss Per Segment

Figure 7 shows results for the 180 solar collector single pipe field model. The computer model consists of 18 one-pipe models connected in series to represent the 180 solar collector field. There is a steady build up of temperature for all components along the model segments and banks. The temperature is highest in the absorber plate and lowest in the transparent cover; also the rate of temperature increase is lowest in the transparent cover. The rate of temperature increase closely follows the same profile in both the absorber and in the working fluid.

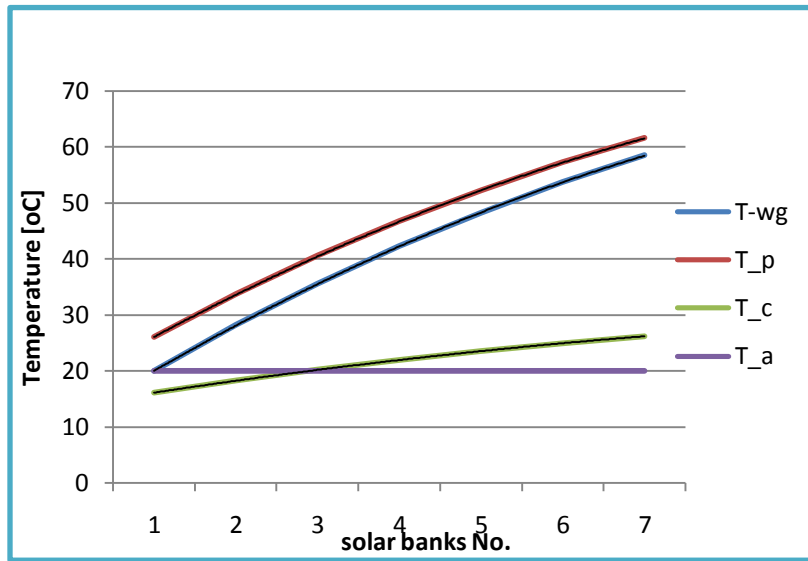


Figure 7: Temperature Profile Over 6 banks of 180 Collector Solar Field

Figure 8 shows the hourly temperature profiles. These simulations consisted of several cycles (114 cycles calculated) to make an hour. The temperature measurement is taken at the end of the hour. These simulations include a thermal storage represented by the tank temperature T_{tank} .

The absorber plate attains the highest temperature followed by the working fluid (water ethylene glycol) at the exit of the solar field and in the tank storage. The three temperature profiles follow each other closely and build-up slowly from morning to a high about noon. The absorber increases temperature from ambient temperature of 20°C to slightly over 100°C about noon; the water ethylene glycol attains maxima of slightly below 100°C and about 90°C at the exit of the solar collector and in the storage tank respectively. This is desirable for heat transfer to continue flowing from the absorber to the working fluid.

The transparent cover has a much lower temperature ranging from ambient temperature to about 40°C . This ensures lower thermal losses.

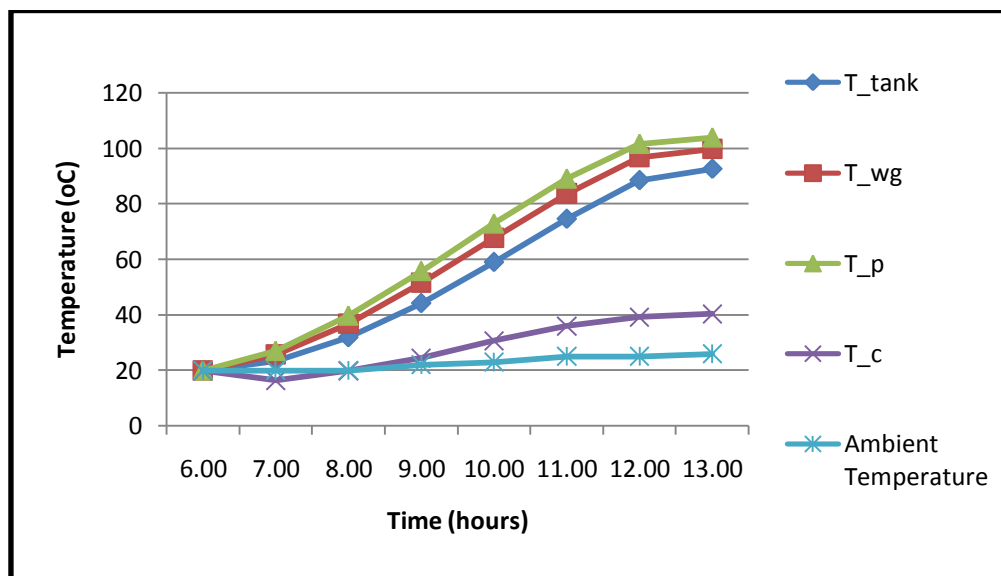


Figure 8: Hourly Temperature Profile

Figure 9 shows average hourly thermal efficiencies. The thermal efficiencies are highest near the commencement of the modelling period (7am, 8am and 9am are highest; the lowest efficiencies are at 1pm followed by 12pm). The average efficiency has a high of 56% at 8pm and a low of 35% at 1pm.

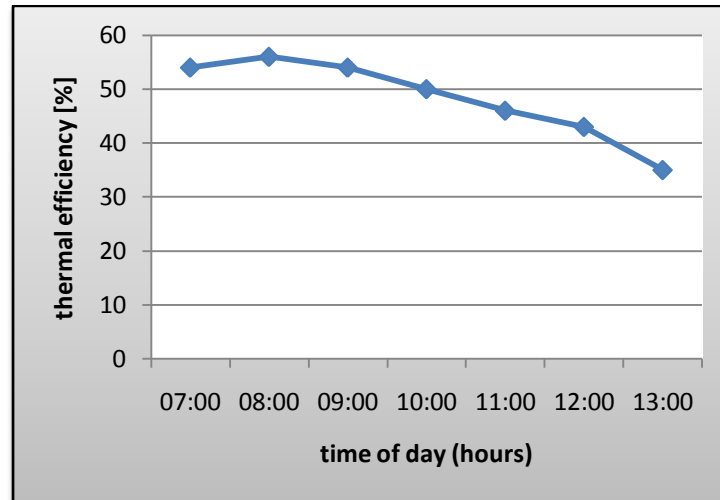


Figure 9: Average Hourly Thermal Efficiency

4. Conclusions

Preliminary small scale concept plants, 500Wp and 10kWp, have been presented, modelled and computer simulated. The first pass modelling using 14 candidate organic fluids and three optional plant configurations gave thermal efficiencies ranging from 10.38% to 12.20%; the highest being Isopentane and Organic Rankine Cycle with Recuperator and the lowest being R245fa with conventional Organic Rankine Cycle.

The solar field modelling has been done with Ethylene Glycol Water (50% concentration) as the heat transfer fluid. The model included simulations of hourly solar insolation values, and solar collector and storage tank energy balances.

The general trend exhibited by the temperature profiles for the absorber, ethylene glycol water and transparent cover along the flow direction of the heat transfer fluid is that of continuously increasing but with a diminishing gradient.

The hourly temperature profiles for the absorber, transparent cover, heat transfer fluid at collector exit, and heat transfer fluid in the storage tank also continuously increases starting with a lower gradient, developing into a steep gradient and then slowing down to a lower gradient. The hourly efficiency curve starts with higher values and tailing down to lower values.

A simple analysis of the 9 collector model shows the thermal energy output being less than the approximated requirements; this outcome will be considered in the final design of the physical model.

Acknowledgements

Acknowledgements are in order to the co-author and research supervisor Dr. Inambao, the Centre for Engineering Postgraduate Studies (CEPS) represented by Professor N.M Ijumba and all supporting staff and colleagues.

References

- [1] http://www.solarpaces.org/Library/CSP_Documents/Concentrated-Solar-Thermal-Power-Plants-2005.pdf accessed March 8, 2012
- [2] http://cdn.intechopen.com/pdfs/12089/InTech-Micro_gas_turbines.pdf accessed March 8, 2012
- [3] European Commission; Concentrated Solar Thermal Energy, EUR 20898, European Communities, Luxembourg, 2004, ISBN 92-894-6353-8
- [4] <http://www.solardome.co.za/documents/file/25-solardome-sa-priclelist.html> accessed March 12, 2012

- [5] <http://thermotechs.com/Downloads/Thermomax%20Handbook.pdf> accessed March 12, 2012
- [6] Nishith B. D, Santanu B., *Process integration of organic Rankine cycle*, Energy Journal, Vol 34 (2009) pp1674–1686
- [7] Situmbeko S. M., Inambao F. L. Mathematical Modelling and Simulation of Low Temperature Solar Thermal Energy Conversion Systems, Proceedings ISES Solar World Congress, Kassel, Germany, September 2011.
- [8] <http://www.gaisma.com/en/location/durban.html> accessed March 12, 2012
- [9] Engineering Equation Solver (EES)
- [10] Duffie J.A., Beckman W.A., “Solar Engineering of Thermal Processes” 2nd Ed., John Wiley & Son, Inc., USA, 1991 ISBN 0-471-51056-4 p281

MATHEMATICAL MODELING AND SIMULATION OF A LOW TEMPERATURE SOLAR THERMAL ENERGY CONVERSION SYSTEM

Situmbeko S.M., Inambao F.L.
University of KwaZulu-Natal, Durban (South Africa)

Abstract

Research and development work on Low Temperature Energy Conversion has great potential for harnessing waste heat and low energy density solar radiation. This has implications on improving plant thermal efficiencies and promoting recovery and utilization of waste energy otherwise conventionally regarded unusable. A low temperature solar thermal system typically uses flat plate and low concentrating collectors such as parabolic troughs. Such collectors are relatively simpler in construction, easier to operate owing to the absence of complex solar tracking equipment and therefore more suited to remote and rural outposts. Such systems operate within temperatures ranges below 300°C. This calls for changes to the conventional conversion systems and necessitates substituting the heat transfer and working fluids; a subject currently invoking immense research interests. This paper presents a mathematical model based on such a concept plant. The mathematical model is developed from in-depth analyses of energy balances and thermo-fluid dynamics at component, subsystem and system levels. Simulations are carried out by employing a combination of various computer software's such as EEE (Engineering Equation Solver), F-chart and Polysun. Different configurations are considered by varying heat transfer fluids, working fluids and plant layouts. Results of the simulations are presented in the final paper. These results will inform the physical investigations that are to follow in the next stage of the research.

Keywords: Low temperature, energy conversion, solar thermal, heat transfer fluid, working fluid, mathematical model, simulation

1. Introduction

Solar energy technology has great potential but its full development is hampered by some major drawbacks. Solar energy conversion technologies have lower efficiencies and higher costs when compared with other energy sources and technologies; solar radiation has a relatively low energy density thus requiring large harvesting fields. Table 1 shows energy conversion efficiencies of some common conversion systems and the chart shows levelized electricity costs from different sources/ technologies.

Table 1. Energy Conversion Efficiencies [1]

Conversion Process – Electricity Generation	Efficiency
Gas turbine	up to 40%
Gas turbine plus steam turbine (combined cycle)	up to 60%
Water turbine	up to 90% (practically achieved)
Wind turbine	up to 59% (theoretical limit)
Solar cell	6%-40% (technology dependent, 15% most often, 85%-90% theoretical limit)
Fuel cell	up to 85%
*Solar – Thermal CSP	
*Solar – Thermal ORC	3 – 25 %

* added to table from other sources

Figure A.1. Levelized Cost of Electricity for Various Technologies in 2015 (2010\$)

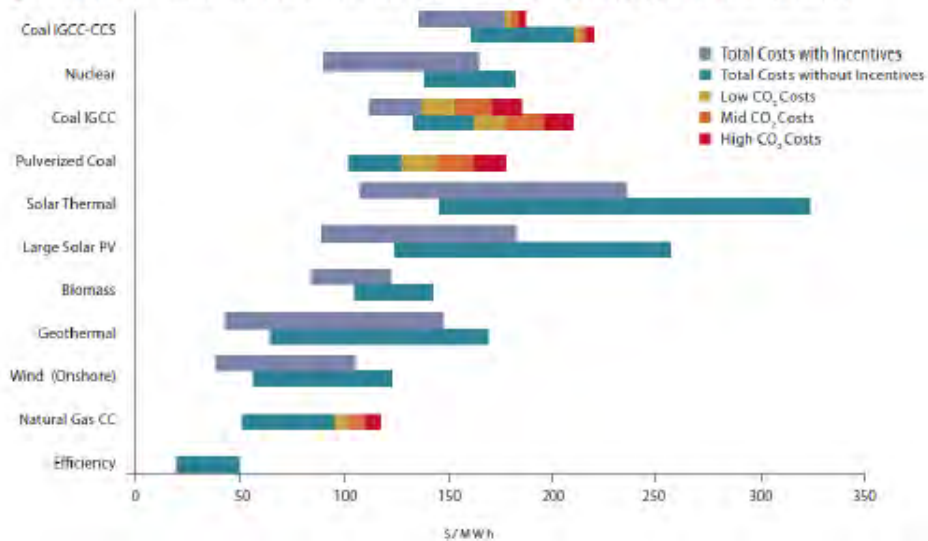


Figure 1. Levelized Cost of Electricity for Various Technologies [2]

The solar radiation measured just outside the earth’s atmosphere, the solar constant, averages 1365 W/m^2 . Ignoring clouds, the average insolation for the Earth is approximately 250 watts per square meter ($6 \text{ (kW}\cdot\text{h/m}^2\text{)/day}$), taking into account the lower radiation intensity in early morning and evening, and its near-absence at night. [3]

Solar energy technologies include moderate temperature systems for space heating (including swimming pool and domestic hot water), moderate to high temperatures for industrial processes, high temperature for electricity generation (commonly referred to as Concentrated Solar Power), Photovoltaic and Oceanic Thermal Energy Conversion for electricity generation.

So if we can avoid high costs by developing simple conversion devices with minimum number of components and still be able to harness this low energy density resource the technology potential might have a prospect of improvement. Researchers and developers of ORC generally agree on the need to maintaining simplicity and low cost through keeping the number of plant devices few. Low temperature operation allows cheaper and safer operating conditions; thus adoption of a single stage small (micro) expander removes the usual complexity associated with conventional power plants. Another plus to this technology is that if adopted for harnessing waste heat it still has an infinitesimal incremental effect onto the overall plant energy efficiency with considerably lower associated cost increase.

This paper proposes an appropriate mathematical modeling and computer simulation scheme for a low temperature solar thermal energy conversion system. The analysis covers a wide range of candidate working fluids and different optimal cycle configurations. The results of this model will be incorporated in a physical model to be build and validated as part of the ongoing research.

2. First Pass Mathematical Modeling

The modeling has been done in two parts; the first part, which is presented in this section, being the first pass model gives an initial insight into the performance of the proposed energy conversion system design. The output of this first model forms an input into the second part, the detailed model, not included in this paper. This first pass model output together with the more detailed specifications of components for the proposed system design will yield a

more detailed model with more realistic performance parameters that can now be incorporated in the design, development and validation of the physical model.

In this work a more generalized model is first proposed. This is then further customized to the thermo-physical properties of the different proposed working fluids. In particular a mathematical logic model is incorporated to assign an appropriate cycle configuration to each proposed working fluid.

2.1 Thermal Cycle

The first pass model serves to provide a first performance indicator which can then be improved in subsequent models as more details of the system, subsystems and components are generated.

The first pass model makes a number of assumptions such as:

- the pumping and expansion are adiabatic
- the thermal losses in the cycle components and ducting are negligible.
- the pressure head losses in the heat exchangers are negligible.
- no work and no heat transfer occurs in the valves, etc.

Three types of models can be identified with low temperature thermal cycles depending on the nature of the working fluid. Based on the fluids' T-s saturation curves these three types of energy conversion systems are: the conventional rankine cycle, the rankine cycle with a recuperator and the rankine cycle with a superheater. In order to develop a generalized model that can be simulated using a computer program, a general configuration is indicated here from which the three models will be generated.

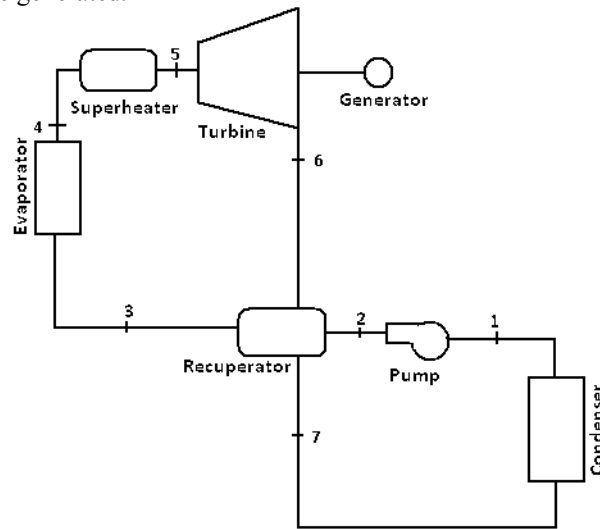


Figure 2. General Configuration of the Organic Rankine Cycle

In order to come up with any of the three configurations the two states representing the input and output of any device that is to be excluded in the model are merged as shown in figure 3.

Description of T-s curve	T-s curve Diagram	Recommended Cycle configuration
Isentropic Vapour Saturation Curve		<p style="text-align: center;"><u>Model 1: Conventional Rankine</u></p>
Positive Vapour Saturation Curve		<p style="text-align: center;"><u>Model 2: Rankine with Recuperator</u></p>
Negative Vapour Saturation Curve		<p style="text-align: center;"><u>Model 3: Rankine with Superheater</u></p>

Figure 3. Different Model Configurations of the Organic Rankine Cycle

2.1.1 Isentropic Vapour Saturation Curve

With the Isentropic saturation curve the process diagram includes only the turbine, pump, evaporator and condenser. The vapour remains a saturated vapour during expansion process from the higher temperature and higher pressure at the turbine entry to the lower temperature and lower pressure at the turbine exit; there is no risk of damage to the turbine blades due to formation of liquid droplets and there is no excessive residual heat in the vapour at the turbine exhaust.

The four processes making up the thermal energy conversion cycle and identified by numbers in the cycle diagram are:

Process 1-2: The working fluid is pumped from low to high pressure, as the fluid is a liquid at this stage the pump requires little input energy.

Process 3-4: The high pressure liquid enters a boiler where it is heated at constant pressure by an external heat source to become a dry saturated vapor. Note that states 2 and 3 are merged as there is no recuperating device.

Process 5-6: The dry saturated vapor expands through a turbine, generating power. This decreases the temperature and pressure of the vapor. Note also here, that states 4 and 5 are merged as there is no superheating device.

Process 7-1: The dry saturated turbine exhaust vapor then enters a condenser where it is condensed at a constant pressure and temperature to become a saturated liquid. The pressure and temperature of the condenser is fixed by the temperature of the cooling coils as the fluid is undergoing a phase-change. States 6 and 7 coincide due to the absence of a recuperator.

The mathematical models for the four processes are derived from the energy and mass balance for a control volume.

$$\text{Pump:} \quad \frac{\dot{W}_{pump}}{\dot{m}} = (h_2 - h_1) \approx \frac{v_1 \Delta P}{\eta_{pump}} \approx \frac{P_2 - P_1}{\eta_{pump}} \quad (2.1)$$

$$\text{Turbine:} \quad \frac{\dot{W}_{turbine}}{\dot{m}} = (h_5 - h_6) = (h_5 - h_{6s}) \times \eta_{turbine} \quad (2.2)$$

In a real Rankine cycle, the compression by the pump and the expansion in the turbine are not isentropic. In other words, these processes are non-reversible and entropy is increased during the two processes. This increases the power required by the pump and decreases the power generated by the turbine. The models take this into account by incorporating the isentropic efficiencies.

$$\text{Evaporator:} \quad \frac{\dot{Q}_{evap}}{\dot{m}} = (h_4 - h_3) \quad (2.3)$$

$$\text{Condenser:} \quad \frac{\dot{Q}_{cond}}{\dot{m}} = (h_7 - h_1) \quad (2.4)$$

2.1.2 Positive Vapour Saturation Curve

In some cases, the vapour exiting the turbine attains the lower pressure in a superheated state. This imposes a larger cooling load on the condenser and consequently reduces the cycle thermal efficiency. In order to overcome this a recuperator is added to the system to provide preheating through heat exchange between the vapor exiting the turbine and the working fluid before it enters the evaporator and thus reduce the cooling load on the condenser as well as the heating load on the evaporator. The recuperator is applicable when the organic fluid is of the "dry expansion" type, namely a fluid where the expansion in the turbine is done in the dry superheated zone and the expanded vapor contains heat that has to be extracted prior to the condensing stage. The recuperated Organic Rankine cycle is typically 10-15% more efficient than the simple Organic Rankine cycle.

In addition to the four processes of the Isentropic Saturation Curve we now have two additional processes taking place in the Recuperator as follows:

Process 2-3: The high pressure working liquid from the pump is preheated in the recuperator to a higher temperature before it enters the evaporator.

Process 6-7: The superheated low pressure dry vapor exiting the turbine enters a recuperator where it loses some heat at constant pressure to become a saturated dry vapour before entering the condenser.

$$\text{Recuperator – Cold Stream: } \frac{\dot{Q}_{recu}}{\dot{m}} = (h_3 - h_2) \quad (2.5)$$

$$\text{Recuperator – Hot Stream: } \frac{\dot{Q}_{recu}}{\dot{m}} = (h_6 - h_7) \quad (2.6)$$

2.1.3 Negative Vapour Saturation Curve

These types of organic fluids are referred to as “wet” or as having a negative Isentropic Vapour saturation curve; these liquids resemble much the curve for water. If the working fluid is fed into the turbine in a dry saturated state, it ends as a mixture of liquid and vapour upon expansion. This is undesirable as the formation of liquid droplets tend to cause pitting erosion on the turbine blades and gradually reduce the efficiency of the turbine. This problem is overcome by superheating the vapour before it enters the turbine so that it ends in a dry saturated vapour after expansion.

Thus in addition to the four processes of the Isentropic Saturation Curve we now have one additional process taking place in the Superheater:

Process 4-5: The high pressure dry saturated vapour from the evaporator is further heated at constant pressure in the superheater to a higher temperature superheated state. The superheated state is designed to coincide with the end state after expansion resulting in a dry saturated state at the lower pressure assuming ideal (isentropic) expansion.

$$\text{Superheater: } \frac{\dot{Q}_{superheater}}{\dot{m}} = (h_5 - h_4) \quad (2.7)$$

The reason for assuming a dry saturated end state under isentropic expansion is that due to the fact that at this state the performance of the superheater is not yet ascertained (will also deteriorate with operation) and that it is safer to assume it lower, fixing the real end state at dry saturated state risks ending the expansion in a wet state.

The final equation in the thermal model defines the thermodynamic efficiency of the cycle as the ratio of net power output to heat input. As the work required by the pump is often around 1% of the turbine work output, equation 5 can be simplified.

$$\text{Thermal efficiency: } \eta_{therm} = \frac{W_{turbine} - W_{pump}}{\dot{Q}_{in}} \approx \frac{W_{turbine}}{\dot{Q}_{in}} \quad (2.8)$$

Where \dot{Q}_{in} is defined as $\dot{Q}_{in} = \dot{Q}_{evap} + \dot{Q}_{superheater}$ and in cases where there is no superheating as simply $\dot{Q}_{in} = \dot{Q}_{evap}$

2.2 Solar Cycle

The first pass mathematical model of the solar thermal cycle is governed by the Hottel-Whillier equation. [4]

$$Q_u = A_C F_R [\tau \alpha G - U(T_{in} - T_a)] \quad (2.9)$$

where A_C (m^2) is the solar collector field aperture area, F_R is the heat removal factor, τ is the cover glazing transmittance, α is the absorber absorptance and U is the overall heat loss coefficient of the solar collector field. Operational conditions are solar insolation G , heat transfer fluid inlet temperature T_{in} and ambient temperature T_a .

2.3 Model Type Selection

This is incorporated by first selecting an acceptable difference between the entropy values of the working fluid dry saturated vapour at the lower and higher pressures that would be considered as Isentropic. The model then proceeds, for all cases not satisfying this requirement, to determine which entropy is larger; if the lower pressure entropy is larger the working fluid falls into the negative vapour saturation curve and if the higher pressure entropy is larger, the positive vapour saturation curve. Mathematically the model selection is expressed as:

$$\text{If } \frac{[s_{high}-s_{low}]}{s_{low}} < \delta \text{ then Isentropic Curve Model is selected} \quad (2.10)$$

Otherwise

$$\text{If } s_{high} > s_{low} \text{ , Positive Saturation Curve Model is selected or} \quad (2.11)$$

$$\text{If } s_{low} > s_{high} \text{ , Negative Saturation Curve Model is selected}$$

3. Computer Simulation

Engineering Equation Solver (EES) software is used to develop the computer simulation code. The EES code consists of the Solar Model and Model Selection Procedures in addition to the main Thermal Model code.

A lookup table listing the working fluids to be analysed is called up during the running of the code. A parametric table is included to define the type of output data required.

EES software has inbuilt thermophysical properties of several working fluids as well as other materials. It also allows the user to incorporate properties of materials not included in the initial software.

4. Results

The results from the computer simulations are shown in tables 2 and 3 appended to this paper. The results shown here do not include the Solar Model code which is yet to be incorporated.

6. Conclusion

Fourteen working fluids have been tested with the model. The model assigned six working fluids (Benzene, n-butane, Isobutane, R141b, R245fa, R123) to Model 1, Conventional Rankine, five working fluids (n-pentane, n-hexane, Isopentane, R113, Toluene) to Model 2, Rankine with Recuperator, and three working fluids (R22, R134a, Water) to Model 3, Rankine with Superheater. Water is included as a control since it is well established that water requires superheating. The thermal efficiencies vary from 10.38% for R245fa (Conventional Rankine) to 12.04% for n-pentane (Rankine with Recuperator). The model requires further improvement to include error reporting for results that are outside the feasible solutions. Particularly, with heat exchangers, the working fluid may not attain certain temperatures with low temperatures energy sources. For instance the high pressure temperatures reported for certain working fluids such as 271.8°C for water, 178.3°C for Toluene, 142.7°C for Benzene and 131.3°C for n-hexane may not be feasible with flat plate collectors.

In concluding, the mathematical model was successfully developed into EES code and computer simulations conducted with fourteen different working fluids. Three models were developed to optimize the energy cycle performance based on thermodynamic properties of the working fluids. These models will be further developed into detailed models. The results will be presented in future reports. This model has shown that low temperature solar thermal energy conversion is feasible and potential for further development.

7. References

- [1] http://en.wikipedia.org/wiki/Energy_conversion_efficiency accessed August 14, 2011
- [2] http://www.ucsusa.org/assets/documents/clean_energy/Appendix-Key-Assumptions-Levelized-Costs.pdf accessed August 10, 2011.
- [3] <http://en.wikipedia.org/wiki/Insolation> accessed August 10, 2011
- [4] Duffie J.A., Beckman W.A., "Solar Engineering of Thermal Processes" 2nd Ed., John Wiley & Son, Inc., USA, 1991 ISBN 0-471-51056-4 p281
- [5] Engineering Equation Solver (EES) software

Table 2. Thermal Efficiencies of Different Organic Rankine Cycle Configurations and Different Working Fluids

Model Type	Working Fluid	Q_dot_evaporator	Q_dot_recuperator	Q_dot_superheater	Power	eta_therm	s_high_s	s_low_s
		[kW]	[kW]	[kW]	[kW]	[%]	[kJ/kg.K]	[kJ/kg.K]
Rankine with Recuperator No Superheater	n-pentane	4.067	0.4041	0	0.4997	12.04	1.334	1.235
Conventional Rankine No Recuperator No Superheater	Benzene	4.68	0	0	0.5272	11.11	1.151	1.12
Conventional Rankine No Recuperator No Superheater	n-butane	4.558	0	0	0.539	11.6	2.439	2.408
Rankine with Recuperator No Superheater	n-hexane	3.753	0.6134	0	0.4641	12.1	1.44	1.29
Conventional Rankine No Recuperator No Superheater	Isobutane	4.306	0	0	0.5151	11.72	2.321	2.3
Conventional Rankine No Recuperator No Superheater	R141b	2.6	0	0	0.2987	11.3	1.019	1.013
Rankine with Recuperator No Superheater	Isopentane	3.901	0.376	0	0.4859	12.2	-0.4366	-0.5304
Conventional Rankine No Recuperator No Superheater	R245fa	2.301	0	0	0.2432	10.38	1.77	1.75
Rankine with Recuperator No Superheater	R113	1.64	0.156	0	0.1991	11.89	0.7684	0.7317
Conventional Rankine No Recuperator No Superheater	R123	2.021	0	0	0.2268	11.02	1.685	1.668
Rankine with Superheater No Recuperator	R22	2.496	0	0.2123	0.3296	12.01	1.751	1.825
Rankine with Recuperator No Superheater	Toluene	4.094	0.4495	0	0.489	11.75	1.032	0.9404
Rankine with Superheater No Recuperator	R134a	2.413	0	0.08032	0.2784	10.99	0.9242	0.9516
Rankine with Superheater No Recuperator	Water	23.29	0	2.569	2.803	10.81	6.822	7.355

Table 3. Other Parameters for Different Organic Rankine Cycle Configurations and Different Working Fluids

Working Fluid	T[1]	T[2]	T[3]	T[4]	T[5]	T[6]	T[7]	h[1]	h[2]	h[3]	h[4]	h[5]	h[6]	h[7]
	[C]	[C]	[C]	[C]	[C]	[C]	[C]	[kJ/kg]	[kJ/kg]	[kJ/kg]	[kJ/kg]	[kJ/kg]	[kJ/kg]	[kJ/kg]
n-pentane	35.87	36.17	52.94	92.74	92.74	58.26	35.87	23.38	24.39	64.8	471.5	471.5	421.5	381.1
Benzene	80.07	80.33	80.33	142.7	142.7	96.87	96.87	3E-05	0.7541	0.7541	468.7	468.7	416	416
n-butane	-	-	-	-	-	-	-	-	-	-	-	-	-	-
	0.521	0.133	0.133	50.26	50.26	10.38	10.38	199	200	200	655.8	655.8	601.9	601.9
n-hexane	69.28	69.58	94.75	131.3	131.3	100.5	69.28	104.5	105.5	166.8	542.2	542.2	495.8	434.4
Isobutane	-	-	-	-	-	-	-	-	-	-	-	-	-	-
	11.67	11.25	11.25	37.74	37.74	-2.53	-2.53	173.7	174.8	174.8	605.3	605.3	553.8	553.8
R141b	32.07	32.5	32.5	86.89	86.89	41.03	41.03	75.69	76.19	76.19	336.1	336.1	306.3	306.3
Isopentane	27.86	28.16	44.35	83.77	83.77	49.15	27.86	-343.5	-342.5	-304.9	85.18	85.18	36.59	-1.005
R245fa	15.19	15.43	15.43	62.79	62.85	26.24	26.24	219.6	220	220	450.1	450.1	425.8	425.8
R113	47.61	48.04	64.22	105.7	105.7	69.54	47.61	77.59	77.99	93.6	257.6	257.6	237.7	222.1
R123	27.79	28.11	28.11	80.82	80.82	40.66	40.66	229.1	229.5	229.5	431.6	431.6	408.9	408.9
R22	-	-	-	-	-	-	-	-	-	-	-	-	-	-
	40.81	39.14	39.14	0.1148	29.52	31.19	31.19	155.2	155.6	155.6	405.2	426.5	393.5	393.5
Toluene	110.4	110.6	132.6	178.3	178.3	139.8	110.4	-0.425	0.3616	45.31	454.7	454.7	405.8	360.9
R134a	-	-	-	-	-	-	-	-	-	-	-	-	-	-
	26.09	25.87	25.87	15.71	24.08	-19.9	-19.9	17.63	18.08	18.08	259.4	267.4	239.6	239.6
Water	99.97	100.1	100.1	151.8	271.8	124.5	124.5	419	419.6	419.6	2749	3005	2725	2725

Table 3. continued

Working Fluid	s[1]	s[2]	s[3]	s[4]	s[5]	s[6]	s[7]
	[kJ/kg·K]	[kJ/kg·K]	[kJ/kg·K]	[kJ/kg·K]	[kJ/kg·K]	[kJ/kg·K]	[kJ/kg·K]
n-pentane	0.07778	0.07892	0.2061	1.334	1.334	1.361	1.235
Benzene	1.09E-07	0.000747	0.000747	1.151	1.151	1.176	1.176
n-butane	0.9964	0.9977	0.9977	2.439	2.439	2.473	2.473
n-hexane	0.3267	0.3278	0.5004	1.44	1.44	1.462	1.29
Isobutane	0.9021	0.9035	0.9035	2.321	2.321	2.355	2.355
R141b	0.2812	0.2828	0.2828	1.019	1.019	1.036	1.036
Isopentane	-1.668	-1.667	-1.546	-0.4366	-0.4366	-0.4098	-0.5304
R245fa	1.07	1.07	1.07	1.77	1.77	1.784	1.784
R113	0.2813	0.2826	0.3298	0.7684	0.7684	0.7788	0.7317
R123	1.101	1.102	1.102	1.685	1.685	1.698	1.698
R22	0.8241	0.8248	0.8248	1.751	1.825	1.849	1.849
Toluene	-0.00111	-0.00039	0.1135	1.032	1.032	1.053	0.9404
R134a	0.07331	0.07394	0.07394	0.9242	0.9516	0.9712	0.9712
Water	1.307	1.307	1.307	6.822	7.355	7.483	7.483

LOW TEMPERATURE SOLAR THERMAL ENERGY CONVERSION

SM Situmbeko¹ and FL Inambao²

¹University of Botswana, Gaborone, Botswana

²University of Kwazulu Natal, Durban, South Africa

ABSTRACT

Solar thermal energy conversion for power generation for both low and high temperature systems is an active area of research aimed mainly at addressing environmental and climate change concerns but also as a possible complimentary avenue of tackling the current power supply deficits in Southern Africa. A number of high temperature thermal power generation concept power plants have been installed worldwide. Low temperature thermal energy conversion research, however, is still at an infancy stage but quickly gaining momentum. This is partly due to its immense potential for utilizing waste heat and thus raising plant efficiency as well as its viability for remote and small scale operations. Low temperature solar thermal typically uses flat plate solar collectors; flat plate collectors are relatively cheaper and easier to operate; its use is currently mainly limited to water heating and space heating. Use of low temperature thermal for power generation requires modifications to the conventional energy conversion cycles to enable conversion at lower temperatures. Several thermal-mechanical conversion cycles have been developed e.g. Diesel, Otto, Rankine, Brayton, Kalina. However, majority of these have been developed for high temperature systems. Research is currently on-going to develop low temperature thermal conversion technologies; examples would be the patented Kalina and the Organic Rankine cycles. This project will focus on the Rankine cycle. The Rankine cycle will be modified to suit low temperature operation. One aspect will be to switch to a working fluid that attains phase change at low temperatures.

Keywords:

Solar thermal, energy conversion, low temperature, waste heat, Rankine cycle, phase change.

1. INTRODUCTION

Low temperature thermal energy conversion refers to the use of low temperature heat to generate mainly electrical energy. Most thermal-energy based electrical generating systems use high temperature heat energy to generate steam that is in turn used to drive a turbine. About 80% of electrical energy used in the world is produced from high temperature heat using a thermodynamic cycle known as the Rankine cycle. In a Rankine cycle heat is applied externally to a closed cycle; water is normally used as the working fluid. A schematic representation of the Rankine cycle is shown in Figure 1.

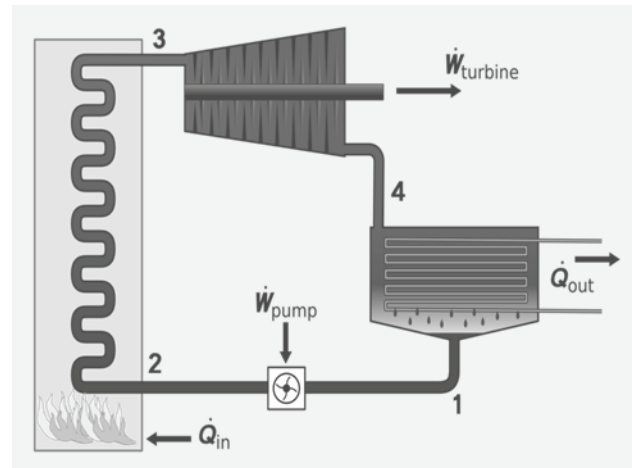


Figure 1: Rankine Cycle schematic representation [1]

External heat \dot{Q}_{in} is applied to the boiler where it heats up a working fluid, that has been pumped from low pressure to high pressure, \dot{W}_{pump} , to produce a dry saturated vapour. The dry saturated vapour at high temperature and high pressure is directed onto turbine blades where it expands thus generating mechanical power, $\dot{W}_{turbine}$, losing thermal energy, both temperature and pressure drop, in the process. The wet vapour then enters a condenser where it is cooled further by losing heat, \dot{Q}_{out} , to become a saturated liquid which is then pumped again to raise its pressure and hence completing the cycle. Figure 2 is a TS (Temperature-Entropy) diagram of a Rankine cycle operating between 0.06bar and 50bar.

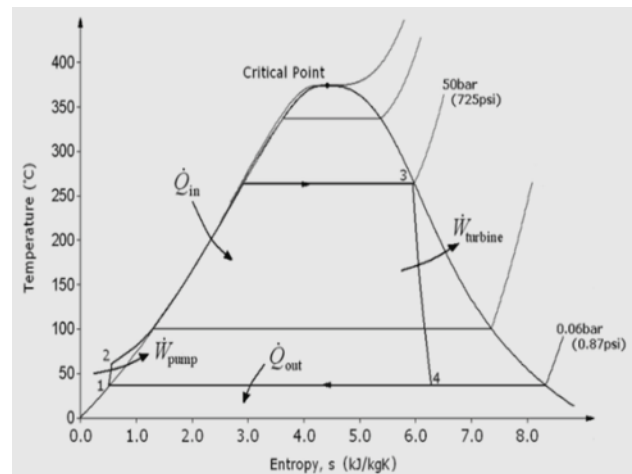


Figure 2: Ts diagram of a typical Rankine cycle [2]

Several forms of energy are used in this cycle ranging from fossils such as coal, oil and natural gas to nuclear, solar thermal and geothermal energies.

In this paper we present a preliminary concept for use of low temperature solar energy in a Rankine cycle to generate electrical energy. The motivation for generating electricity from low temperature heat comes from the fact that a lot of what is currently classified as waste heat including the heat exhausted from the numerous high temperature power plants (Q_{out} in Figure 1) could be harnessed thus improving conversion and operating efficiencies of plants. Also other sources of low temperature heat such as solar, geothermal and ocean thermal energy could become viable generators of electricity.

2. OBJECTIVES

Outlines the main objectives of the current research:

- 2.1 To evaluate the suitability of various thermal-mechanical conversion cycles for low temperature solar thermal energy conversion applications.
- 2.2 To develop and optimize a hypothetical computer model of a solar thermal energy conversion adapted Rankine cycle based on thermodynamic, fluid mechanics and heat transfer principles.
- 2.3 To investigate the thermo-mechanical efficiency and overall economic and environmental performance of a low temperature solar thermal energy conversion system based on the adapted Rankine cycle.
- 2.4 To investigate the performance of various working fluids including their blends in an adapted Rankine cycle.
- 2.5 To review the design and performance of the major cycle components of a low temperature solar thermal energy conversion plant and carry out an optimization of their energy efficiencies, economic and environmental performances.
- 2.6 To design, construct and install a concept plant of a solar thermal energy conversion adapted Rankine cycle.
- 2.7 To propose a final working design suitable for a small scale power generating plant based on the findings of the project.

3. METHODOLOGY

Field and Laboratory Validations will be conducted on Experimental Models based on a final concept design. Supplementary Validation based on physical simulations and laboratory testing will also be designed and effected at various stages of the experimental research. Different

data will be measured at different points of the cycles (Figure 6).

Temperature, pressure and fluid flow rates will be measured at:

- Inlet and Outlet to solar collector
- Inlet and Outlet to heat exchanger on flow lines
- Inlet and outlet to turbine
- Inlet and outlet to condenser

Ambient temperature, direct and global solar insolation will also be measured at the site of the solar collectors.

Also to be measured will be the energy output of the turbine i.e. the power output at the generator end.

Several measuring equipment will be required for this purpose and it will include: Digital Data Loggers, Storage Modules, Thermocouples, Fluid Flow Meters, Pressure Meters and Energy Meters, Pyranometer and Pyrheliometer.

4. LOW TEMPERATURE POWER CYCLES

Research is currently on-going to develop low temperature thermal conversion technologies; examples include the patented Kalina cycle and the Organic Rankine cycle. Use of low temperature thermal for power generation requires that modifications are done to the conventional energy conversion cycles to enable operation at low temperatures. In order for the Rankine cycle to be effectively incorporated into a low temperature thermal energy conversion system, the working fluid usually water must be substituted with another working fluid that has a lower boiling point so that it is able to vapourise to a dry (saturated-) vapour at low temperatures. Some liquids have a dry property and as such do not need to be 'dry saturated'. Generally the desirable properties for a working fluid include low cost, non corrosiveness, thermal stability, and high cycle and turbine efficiencies.

Possible liquids that could be used in the place of water include organic liquids, refrigerants, ammonia, toluene and fully fluorinated benzene ring fluids, or any feasible mixture of these [3]. Pentene isomers are organic fluids with boiling points ranging from 9°C to 36°C; Ammonia is an inorganic compound with a boiling point of -33°C.

Alternatively some dry fluids with boiling temperatures above that of water such as Toluene (a paint thinner) with a boiling point of 106°C, could be used and this may have some thermodynamic benefits.

4.1 ORGANIC RANKINE CYCLE

The term organic Rankine cycle (ORC) is used to refer to a Rankine cycle in which an organic fluid replaces water as the working fluid. Such a cycle enables us to utilize lower temperature heat sources. The efficiency is lower due to the low temperature range the cycle operates in but

the cost of collecting the heat energy is also significantly lower.

4.2 LOW TEMPERATURE SOLAR THERMAL

Low temperature solar thermal uses low temperature solar heat; in particular it uses flat plate solar collectors; flat plate collectors are relatively cheaper and easier to operate.

Figure 3 shows the different ranges of solar thermal from low to high temperature. The low temperature range normally covers temperatures below 300°C, medium temperatures 300°C to 600°C, while high temperatures are those above 600°C. With the Central Tower technology, temperatures more than 1000°C can be easily sustained.

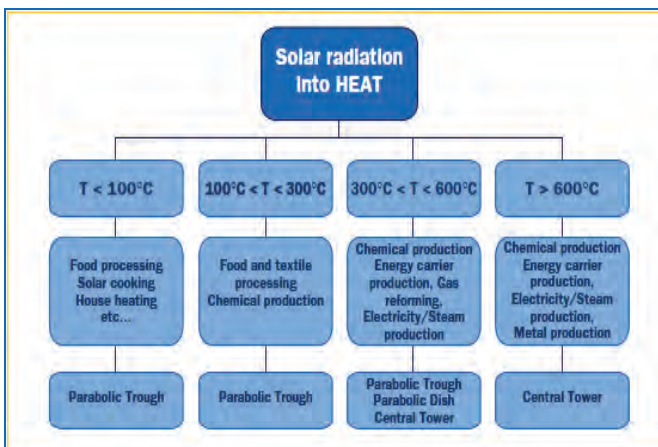


Figure 3: Concentrated Solar Heat Applications [3]

4.3 SOLAR COLLECTORS

Solar collectors form the key component of any solar energy technology. The solar collector functions to intercept incoming solar radiation and convert it into a useable form of energy that can be applied to meet a specific demand. Solar collectors are broadly classified as concentrating or non-concentrating. Non-concentrating collectors maybe treated as collectors with a concentration ratio $A_{in}/A_{abs} = 1$. Concentration ratio is defined as the ratio A_{in}/A_{abs} , where A_{in} is the area of the incident solar radiation and A_{abs} is the area of the absorber. High concentration ratios are obtained by making A_{in} large than A_{abs} .

Flat-plate thermal solar collectors are the most commonly used type of solar collector. Their construction and operation are simple. A large plate of blackened material is oriented in such a manner that the solar energy that falls on the plate is absorbed and converted to thermal energy thereby heating the plate. Tubes or ducting are provided to remove heat from the plate, transferring it to a liquid or gas, and carrying it away to the load. One (or more) transparent (glass or plastic) plates are often placed in front of the absorber plate to reduce heat loss to the atmosphere. Likewise, opaque insulation is placed around

the backside of the absorber plate for the same purpose. Operating temperatures up to 125°C are typical.

Flat plate collectors have the advantage of absorbing not only the energy coming directly from the disc of the sun (beam normal insolation) but also the solar energy that has been diffused into the sky and that is reflected from the ground. Flat plate thermal collectors are seldom tracked to follow the sun's daily path across the sky, however, their fixed mounting usually provides a tilt toward the north (or south if in the northern hemisphere) to minimize the angle between the sun's rays and the surface at noontime. Tilting flat-plate collectors toward the north provides a higher rate of energy at noontime and more total energy over the entire day. Figure 4 shows an installation of flat-plate thermal collectors.



Figure 4: Flat-plate thermal solar collectors for providing hot water. (photo courtesy of DOE/NREL, Warren Gretz)

When higher temperatures are required, concentrating solar collectors are used. Solar energy falling on a large reflective surface is reflected onto a smaller area before it is converted into heat. This is done so that the surface absorbing the concentrated energy is smaller than the surface capturing the energy and therefore can attain higher temperatures before heat loss due to radiation and convection wastes the energy that has been collected. Most concentrating collectors can only concentrate the parallel insolation coming directly from the sun's disk (beam normal insolation), and must follow (track) the sun's path across the sky. Four types of solar concentrators are in common use; parabolic troughs, parabolic dishes, central receivers and Fresnel lenses. Figure 5 shows the first three of these concepts schematically.

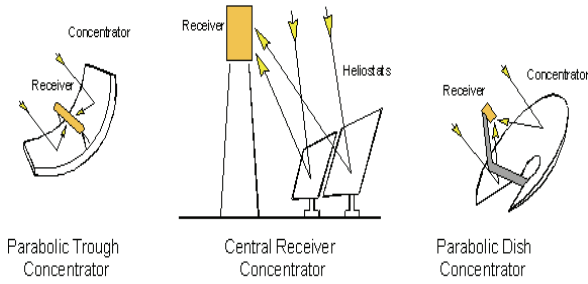


Figure 5: Three commonly used reflecting schemes for concentrating solar energy to attain high temperatures

A Fresnel lens concentrator uses *refraction* rather than reflection to concentrate the solar energy incident on the lens surface to a point. These lenses are used in photovoltaic concentrators. [4]

5. CONCEPT DESIGN

A theoretical model of the Rankine cycle based on low temperature solar thermal heat has been developed. This is shown in Figure 5 below.

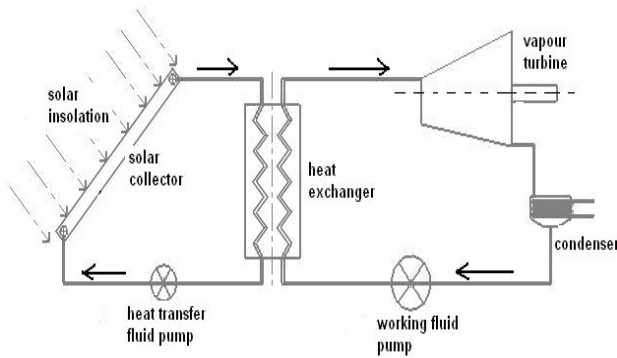


Figure 6: Concept design of a low temperature solar thermal conversion power plant

The system consists of two cycles: a solar thermal cycle and a rankine cycle, with a heat exchanger providing the interface.

Currently, mathematical modeling of the system is being undertaken. This will be followed by experimental research to determine correlation of the theoretical model. For this purpose a 10 kilowatt IT10 Vapour Turbine from Infinity Turbine is being sourced. This, therefore, forms the basis for detail design of both the rankine cycle as well as the solar thermal cycle.

5.1 SOLAR THERMAL CYCLE DESIGN

The main components on this cycle are the solar collectors, the pump and the heat exchanger. These are connected by insulated ducting.

Solar collector design entails selecting an appropriate type of collector, in this case flat plate collectors, and sizing.

Sizing of flat plate collectors is based on European Standards EN12975 parts 1 and 2 (or on equivalent SABS standards). The heat transfer fluid is water mixed with antifreeze.

Thus, the power from the solar collector may be determined by the equation:

$$P = A*(n_0*G - a_1*(T_m - T_a) - a_2*(T_m - T_a)^2) \text{ [W]} \quad [1]$$

where:

- G = solar irradiation [W/m²]
- T_a = ambient air temperature [°C]
- T_m = collector mean temperature [°C]
- A = collector area (corresponding to the efficiency parameters) [m²]
- n₀ = Zero-loss efficiency
- a₁ = 1st order heat loss coefficient
- a₂ = 2nd order heat loss coefficient

Using these parameters, the collector efficiency can be expressed:

$$\eta = n_0 - a_1(T_m - T_a)/G - a_2(T_m - T_a)^2/G \quad [2]$$

The design for the heat exchanger, pump and ducting will be based on the design thermal loading resulting from the Rankine cycle as well as the solar collectors.

The type of heat exchanger selected for this application is the shell and tube heat exchanger in the countercurrent flow configuration. The overall governing equation for shell and tube heat exchangers is:

$$Q_T = UAF(LMTD) \quad [3]$$

where:

- Q_T is the total heat load to be transferred
- U is the overall heat transfer coefficient referred to area A
- A is any convenient heat transfer area
- F is the temperature correction factor
- LMTD is the logarithmic mean temperature difference for the purely countercurrent flow configuration.

This equation is supported by the two heat transfer equations for the hot and cold fluids thus:

$$Q_H = m_H C_{PH} (T_{inH} - T_{outH}) \quad [4]$$

$$Q_C = m_C C_{PC} (T_{outC} - T_{inC}) \quad [5]$$

where:

- Q = heat transferred in joules per unit time
- m = mass flow rate
- T = temperature
- CP = specific heat capacity of fluid

Subscript 'H' = hot fluid
Subscript 'C' = cold fluid [5]

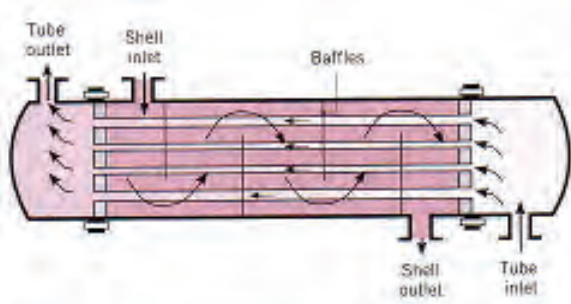


Figure 7: One pass counter-current flow shell and tube heat exchanger (Incropera) [6]

5.2 RANKINE CYCLE DESIGN

The main components on the power cycle include the turbine, the condenser, the pump and the heat exchanger. The 10 kilowatt IT10 Vapour Turbine kit includes the evaporator, turbine generator, direct drive PM generator, water cooled condenser and feedwater pump.

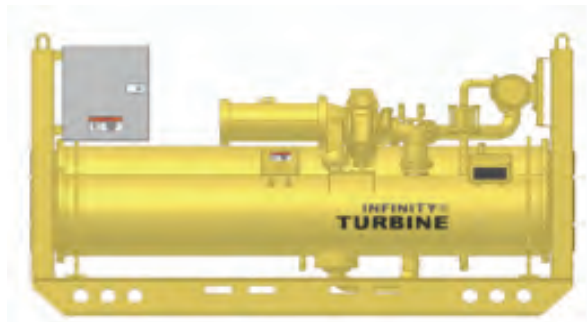


Figure 8: Infinity vapour turbine [7]

5.3 FLUID MECHANICS DESIGN

Another aspect being considered is the optimization of the fluid flow. Duct sizing is such that laminar flow is achieved; this is for reduced frictional losses. Flow in the heat exchanger is being designed for turbulent flow so as to achieve effective heat transfer.

This will be determined by use of the Reynolds Number as in equation 6 below.

$$Re = \rho V l / \mu \quad [6]$$

where: ρ is density, V is Velocity, l is characteristic Length and μ is viscosity.

The critical values of the Reynolds number for fully developed flow in the ducting of diameter D , are:

laminar flow occurs when $Re_D < 2300$ and
turbulent flow occurs when $Re_D > 4000$

'transition' flows (i.e. combination of laminar and turbulent flows) occur between 2300 and 4000.

Other factors such as fouling and erosion also need to be considered.

6. OVERVIEW OF SIMILAR DESIGN CONCEPT

The design concept presented in this paper is based on based on Ocean thermal energy conversion (OTEC), a power generation method wherein the heat energy associated with temperature difference between the warm surface water and cold deep water of the ocean is converted into electricity [8 - 11]. Considerable research has been conducted through numerous theoretical and experimental studies. The latest achievements in OTEC Technology are as follows:

In 1979, the first 50-kilowatt (electric) (kWe) closed-cycle OTEC demonstration plant went up at NELHA. This "Mini-OTEC" was mounted on a converted U.S. Navy barge moored approximately 2 kilometers off Keahole Point. The plant used cold-water pipe to produce 52 kWe of gross power and 15 kWe net power.

In 1981, Japan demonstrated a shore-based, 100 kWe closed-cycle plant in the Republic of Nauru in Pacific Ocean. This plant employed cold-water pipe laid on the sea bed to a depth of 580 meters and produced 31.5 of net power during continuous operating tests.

In May 1993, an open-cycle OTEC plant at Keahole Point, Hawaii, produced 50 000 watts of electricity during a net power-producing experiment [12].

Commercial OTEC plants must be located in an environment that is stable enough for efficient system operation. The temperature of the warm surface seawater must differ about $\Delta T = 20^\circ\text{C}$ from that of cold deep water that is no more than about 1000 meters. Most less-developed countries with adequate Ocean-thermal resources have natural ocean thermal gradient of $\Delta T = 18 - 22^\circ\text{C}$ at approximately 25 km distance from resource to shore and 10 km or less for Islands. The available temperature amounting to only 20°C may well be called a "technology limit" [13].

Performance simulation of solar-boosted ocean thermal energy conversion plant (SOTEC) was studied by Noboru, Y., et. This OTEC system uses solar-thermal energy as a secondary heat source at Kumejima Island in southern part of Japan. The results show that the proposed SOTEC plant ($\eta_{\text{net}} = 6.3\%$) can potentially enhance the annual mean net thermal efficiency up to a value that is approximately 1.5 times higher than that of the conventional OTEC plant ($\eta_{\text{net}} = 2.3\%$) if a single-glazed flat-plate collector of 5000 m² effective area is installed to boost the temperature of the warm sea water by 20K [14].

In the offshore plant the length the thickness of both warm water and cold-water piping (CWP) results in higher capital costs of the subsystem and cost of electricity. The increase in power systems costs for

onshore application results from the increased pump power requirement, which in turn means larger heat exchangers. The system requires expensive advanced underwater transmission cable or deep-water mooring technologies. Higher operating and maintenance costs further increases the capital costs of the facility.

The proposed conceptual design of approximately 10 kW seeks to address some short comings of the OTEC system. The advantages of the system lie more in eliminating of technological risks such as the elimination of underwater transmission cable and deep-water mooring technologies, and the lowering of operations and maintenance costs. The reduced pump power requirement, would in turn require smaller heat exchangers. Costs of both warm-water and cold-water pipes of larger diameters and lengths are to be reduced to minimum.

The above factors, i.e. heat exchanger, piping and added short construction period appear to have by far the most significant impact on reducing total system capital cost. This will result in a gross power almost equal to net power due to reduced requirements on piping and losses such as transmission and pumping.

7. A 10-kW PILOT PLANT: UNIVERSITY OF KWAZULU-NATAL EXPERIENCE AND EXPERIMENTAL RESEARCH

The low temperature solar thermal conversion system is designed as an off-grid facility to achieve higher energy conversion efficiencies. Being a land-based facility, it will not require sophisticated mooring, lengthy power cables, or more extensive maintenance associated with open-ocean environments. The system will use solar-thermal energy as a primary heat source. Solar water heater collectors have been developed and tested at the University of KwaZulu-Natal over the past few years. On clear day, with an ambient temperature of about 25°C, the average temperature of the solar water collector was 60°C [15]. Another added advantage to the facility will be the introduction of solar air heater with an average air temperature of 75°C [16]. The typical low-cost solar-thermal collectors are expected to increase the turbine inlet temperature of the working fluid (Ammonia). The system will have a natural "land" thermal gradient of over $\Delta T = 40^\circ\text{C}$, thus breaking the "technology limit".

In this phase of the research a demonstration prototype of the Adapted Rankine cycle will be implemented on the basis of the design concept of sections 5 to 7 above, using an organic fluid as a working fluid and employing low to medium temperature flat solar thermal collectors.

8. ANALYSIS OF RESULTS

Among the analyses that will be conducted will be thermodynamic analysis, heat and mass transfer analyses, economic and environmental (including carbon emissions) analyses.

Thermodynamic analyses will also included standard plots such as pressure versus volume (P-V) and temperature versus entropy (T-S); these are the two types of charts generally used to analyze a thermodynamic power cycle. The area under a process curve on a p-V diagram is equal to the work performed by the system during the process. The area under a process curve on a T-s diagram is related to the amount of heat transferred to the system. Heat and mass transfer optimization will be conducted to determine to what extent achieving an optimal flow process could enhance cycle efficiencies and minimize heat losses.

Economic and Environment analyses are not the main focus of this research. Nevertheless these will be conducted to satisfy inquisition. The economic aspects will attempt to determine cost savings as well as payback periods that would be attained as a result of improvements in energy efficiencies of plants or households from the use of low temperature solar thermal (or waste heat) to generate power. On the other hand environmental review will examine to what extent the process could yield carbon emissions offsets and how the process could be applied to available emissions trade mechanisms.

9. CONCLUSION AND FURTHER WORK

The research proposal has presented a design concept of the modified Rankine cycle based on low temperature solar thermal energy conversion. The research only focuses on low temperature solar. High temperature solar thermal concept plants have been demonstrated through installations at Mojave desert California, USA (354 MWe initial installed capacity), and in Spain at Andalusia and also near Seville. In 2003 a total of 2.7 GWe demonstration projects had been planned.

The main difference between low temperature- and high temperature thermal energy conversion systems lies in the heat sources and working fluids; with the high temperature systems, usually operating on water and steam, and the low temperature schemes on a variety of fluids ranging from organic fluids to refrigerants. Water and steam if used on the low temperature applications the wet steam will usually cause pitting and erosion on the turbine blades, resulting in losses in efficiency and high maintenance costs. Progress is being made with regard to research on low temperature thermal energy conversion; particularly energy sources targeted include Ocean Thermal Energy Conversion (OTEC), GeoThermal Energy Conversion (GeoTEC), waste heat, biomass, and Solar Thermal Energy Conversion (SoTEC), as well as combinations of these such as Solar assisted Ocean Thermal Energy Conversion (SOTEC). Nishith and Santanu have documented mathematically simulated performance data (computed with Refprop software) for various working fluids operated on low heat sources with maximum and condensation temperatures of the cycle assumed to be 120°C and 40°C. Thermal cycle efficiencies ranged from 9.9 – 14.1 % for the basic cycle; 11.5 – 14.6 % with regeneration; 11.4 – 15.1% with

turbine bleeding; and 12.8 – 15.3 % for combined regeneration and turbine bleeding [17].

10. REFERENCES

1. <http://montaraventures.com/energy/wp-content/uploads/2008/05/rankine-cycle-diagram.jpg> (accessed 13/01/2010).
2. http://en.wikipedia.org/wiki/File:Rankine_cycle_Ts.png (accessed 07/01/2010).
3. European Commission; Concentrated Solar Thermal Energy, EUR 20898, European Communities, Luxembourg, 2004, ISBN 92-894-6353-8.
4. <http://www.powerfromthesun.net/chapter1/Chapter1.htm> (accessed 05/01/2010).
5. Serth RW; *Process heat transfer: principles and applications*, Elsevier Ltd., Oxford, UK, 2007, ISBN 978-0-12-373588-1.
6. Incropera FP, De Witt DP; *Fundamentals of heat and mass transfer*, John Wiley & Sons, Inc. New York, 2002, ISBN 0-471-38650-2.
7. http://www.infinityturbine.com/pdf/IT10_brochure.pdf (accessed 20/01/2010).
8. Avery WH, Wu C. Renewable energy from the ocean- A guide to Oxford: Oxford University Press: 1994.
9. Dylan T. Ocean thermal energy conversion: current overview and future outlook. *Renewable Energy* 1995;6(3):367-73.
10. Cavrot DE. Economics of ocean thermal energy conversion (OTEC). *Renewable Energy* 1993;3(8):891-6.
11. Lennard DE. The viability and best locations for ocean thermal energy conversion systems around the world, *Renewable Energy*. World renewable energy congress climate change. *Energy and Environment* 1995;6(3):359-65.
12. <http://www.nrel.gov/otec/achievements.html> (accessed 20/02/2010).
13. http://www.nrel.gov/otec/design_location.html (accessed 20/02/2010).
14. Yamada N. et al. Performance simulation of solar-boosted ocean thermal energy conversion plant, *Renewable Energy* 34 (2009) 1752-1758.
15. Babulall M, seumangal N, Khuzwayo L, Betterton J, Design of a Domestic Solar Water Heating System, BSc Design and Research Project Thesis, University of KwaZulu-Natal, 2008.
16. Balwanth A, Joseph JS, Naidoo P, Munien D, Design of a Solar Dryer System for Agricultural and Marine Products, BSc Design and Research Project Thesis, University of KwaZulu-Natal, 2009.
17. Nishith B. D, Santanu B., *Process integration of organic Rankine cycle*, *Energy Journal*, Vol 34 (2009) pp1674–1686.

11. AUTHORS

Principal Author: Shadreck M. Situmeko holds MSc Degree (Design) from Loughborough University, UK. He is currently a Lecturer at University of Botswana.

situmbeko@mopipi.ub.bw

Co-author: Dr Freddie Inambao holds a PhD in Technical Sciences from Volgograd State Technical University. He has worked for University of Zambia, University of Botswana, University of Durban Westville, and now at the University of Kwazulu-Natal as a Senior Lecturer following the merger. He has authored and co-authored over 28 technical papers, publications and presentations covering Alternative Energy Systems, Energy Management, Internal Combustion Engines, Fuels, Pumps and Thermodynamics.



inambaof@ukzn.ac.za

Presenter: The paper is presented by Dr Freddie Inambao.

